UNIVERSITY OF SOUTHAMPTON

HYDROELASTIC MODELLING FOR THE PREDICTION OF WAVE INDUCED LOADS ON BULK CARRIERS

by

Spyridon Evgenios Hirdaris

Thesis submitted for the requirements of the degree of
Doctor of Philosophy

FACULTY OF ENGINEERING AND APPLIED SCIENCES
SCHOOL OF ENGINEERING SCIENCES
DEPARTMENT OF SHIP SCIENCE

June 2002

Dedicated to:

Master Cpt. Evgenios Hirdaris,
Andromachi Hirdaris,
Mike Sotirakos
&
Theodoros Koulouris

In grateful love and appreciation

Τα πρώτα μου χρόνια τ'αξέχαστα τα'ζησα
κοντά στ'ακρογιάλι,
στη θάλασσα εκεί τη ρηχή και την ήμερη,
στη θάλασσα εκεί την πλατιά, τη μεγάλη.

Και κάθε φορά που μπροστά μου η πρωτάνθιστη
ζωούλα προβάλλει
και βλέπω τα ονείρατα και ακούω τα μιλήματα
των πρώτων μου χρόνων κοντά στ'ακρογιάλι,

στενάζεις, καρδιά μου, το ίδιο αναστένασμα.
Να ζούσα και πάλι
στη θάλασσα εκεί τη ρηχή και την ήμερη,
στη θάλασσα εκεί την πλατιά, τη μεγάλη.

Κ. Παλαμάς

I spent my first, memorable years
Near the sea,
That sea, shallow and calm
A sea so wide, so large

And every time life blooms
In front of my eyes
And I see the dreams and I hear the voices
Of my first years near the sea,

You sigh, my heart, as you have always sighed
If only I could live again
Near that shallow and calm sea,
A sea so wide, so large.

C. Palamas
(Translation: Olga Sari)

UNIVERSITY OF SOUTHAMPTON

ABSTRACT

FACULTY OF ENGINEERING AND APPLIED SCIENCE
DEPARTMENT OF SHIP SCIENCE

Doctor of Philosophy

HYDROELASTIC MODELLING FOR THE PREDICTION OF WAVE INDUCED LOADS ON BULK CARRIERS

By: Spyridon Evgenios Hirdaris

The relatively high rates of bulk carrier casualties in recent years make this vessel type a suitable example for investigating the influence of hydroelastic modelling on the fluid-structure interactions and subsequent loads and responses in waves as opposed to the empirical and quasi-static methods which are traditionally used. Two- and three-dimensional fluid-flexible structure interaction models, due to their different degree of complexity and associated data requirements, can be used at different stages of the design process when estimating wave-induced loads, namely preliminary and detailed design stages respectively.

For the purposes of the current investigation, therefore, two- and three-dimensional hydroelasticity theories are applied to predict and compare the steady state dynamic behaviour of a bulk carrier hull, based on OBO MV Derbyshire, in regular waves. Both symmetric and antisymmetric motions and distortions are incorporated in these investigations.

Problems encountered during the structural modelling stage, for all idealisations, are briefly outlined, with particular emphasis to modelling hatch openings shear center and warping. Whilst the three-dimensional finite element model consists entirely of shell elements, representing all the major external and internal structural components, the two-dimensional simulation is implemented by means of Timoshenko beam-like finite element and difference discretisations. In vacuo dynamic characteristics (natural frequencies, mode shapes, modal stresses shear forces and bending moments) are discussed and compared for all models, again with special emphasis upon identifying the influences of hatch openings, shear center and warping on the antisymmetric dynamics of the structure. For the wet analysis the fluid structure interaction is carried out using two-dimensional (Timoshenko beam and strip theories) and three-dimensional (finite element idealisation and potential flow analysis based on pulsating source distribution over the mean wetted surface) analyses. Comparisons are made between responses, such as vertical, horizontal and torsional moments, shear forces as well as direct stresses predicted by two- and three-dimensional models in regular waves for a range of headings, speeds and ship- to wave-length aspect ratios.

It is shown that whereas for symmetric motion the behaviour of two- and three-dimensional idealisations are in remarkably good agreement some deviations arise in the antisymmetric plane, mainly due to the fact that the weakness of the two dimensional beam idelisation to simulate realistically the warping induced dynamics of the hull girder.

LIST OF CONTENTS

Appendix 1

- Scantlings for OBO MV Derbyshire
- Sectional data for OBO MV Derbyshire
- Sectional data for closed ship
- Sectional data for open ship
- General arrangement plan for OBO MV Derbyshire
- Shipshape lines plan for OBO MV Derbyshire
- Simplified mid ship section for OBO MV Derbyshire

Appendix 2

- The finite difference method
- The finite element method in 2D & 3D hydroelasticity analyses
- The finite element method as a measure of dynamic strength
- Mass matrix entries for a typical Przemieniecki finite element

Appendix 3

- 1st Conference Publication

Appendix 4

- 2nd Conference Publication

Appendix 5

- Journal publication

LIST OF FIGURES

LIST OF TABLES

NOMENCLATURE

A. General

- The most important meanings of a given symbol in the document are given in this section. The occasional meaning is not given here.
- Symbols are also defined where they appear in the text.
- Overdots signify differentiation with respect to time.
- Primes signify differentiation with respect to space.
- Subindices m and n refer to mode numbers.
- Subindices R and D refer to rigid and flexible degrees of freedom.

B. Latin Characters

A, A_{mi},	Area of a cross section
A_{rk}	Hydrodynamic coefficient of the generalised added mass
A_{rr}	Diagonal terms of the hydrodynamic added mass matrix
A_w	Immersed cross-sectional area
a	unit wave amplitude
$[a]$	Generalised mass matrix
$[B]$	Damping matrix
$B(x)$	Buoyancy distribution functional
B_{rk}	Hydrodynamic coefficient of the generalised added damping
B_{rr}	Diagonal hydrodynamic damping terms
$[b]$	Generalised damping matrix
$b(x)$	Buoyancy distribution
C	Torsional rigidity
C_{rk}	Hydrodynamic coefficient of the generalised added stiffness
C_w	Warping rigidity
$[C]$	Elemental displacements coefficient matrix
$[c]$	Generalised stiffness matrix
$[D]$	Elasticity matrix
$[\overline{D}]$	Matrix of the mode shape vectors

$\{\overline{D}_r\}$	Mode shape of the r^{th} principal mode
ds	Incremental length of a plate
E	Young's modulus
EI	Flexural rigidity
e	Element
F,f	Force
G	Shear modulus
$\{G\}$	Generalised gravitational force vector
GJ	Torsional stiffness
g	Acceleration of gravity
$H_r(t)$	r^{th} generalised radiation force
I	Moment of inertia
I_C	Moment of inertia passing trough the center of gravity of a section
I_S	Moment of inertia passing trough the shear center of a section
I_W,$I_{\Omega\Omega}$	Sectorial moment of inertia
I_y	Horizontal moment of inertia
I_z	Vertical moment of inertia
J	Torsional constant
[J]	Jacobean matrix
$[K]$	Stiffness matrix
K_e	Elemental stiffness matrix
K	Shear deflection constant
kAG	Shear rigidity
L	Length
L_{OA}	Length over all
L_{BP}	Length between perpendiculars
M(x)	Longitudinal bending moment distribution
$[M]$	Mass matrix
M_e	Elemental mass matrix
M_r	Modal bending moment
M_{xr}	Torsional modal moment

M_x^{tot}	Total torsional modal moment
M_{yr}	Vertical modal bending moment
M_y^{tot}	Total vertical modal bending moment
M_{zr}	Horizontal modal bending moment
M_s	Saint Venant's moment
M_Ω	Bimoment
m_i	sectional mass
$N(x)$	Shape function
$\vec{n}$	Local normal vector
$\{p_D\}$	Principal coordinate vector of the m-6 flexible distortions
P_i	Point load
p_r	Principal coordinate corresponding to the rth mode shape
$\{p_R\}$	Principal coordinate vector of the 6 rigid body modes
$p(x)$	Net force
q_r	Shear flow of a section
r	Radius of gyration
$R_r(t)$	r^{th} generalised restoring force
$S(x)$	Shear force functional
S_{deck}	Section modulus at deck
S_e	Elemental surface
S_{keel}	Section modulus at keel
s	Coordinate around the perimeter of a ship's section
T	Draft
T_e	Elemental kinetic energy
T_{rk}	Radiation term
T_s	Saint Venant's torque
T_{tot}	total torque
T_w	warping torque
t	thickness
t_{fb}	Thickness of fictitious bulkhead
$\overline{U}$	Forward speed

$\{U\}$	Vector of the nodal displacements
$\hat{U}$	Nodal displacements of finite element model
u_i	Rigid body degrees of freedom for a ship (I = 1,6)
V_e	Elemental volume
V_y	Horizontal shear force
V_z	Vertical shear force
v	Horizontal translation
w	Vertical translation
w_r	Mode shape
X,x	Longitudinal Cartesian coordinates axes
Y,y	Horizontal Cartesian coordinates axes
Z,z	Vertical Cartesian coordinates axes
$\{Z\}$	Generalised fluid force vector
$\bar{z}$	Distance between shear and gravity centers

C. Greek Characters

$[\alpha]$	Direct nodal displacements matrix
$[\beta]$	Nodal displacements matrix
$\{\Delta\}$	Generalised concentrated force vector
Δx	Increment
$\{\delta\}$	Viscous displacement
$\{\varepsilon\}$	Strain displacement
η	Vertical spatial integration variable
θ_r	Rotational degree of freedom
θ_x	Rotation about x -axis
θ_y	Rotation about y -axis
θ_z	Rotation about z -axis
κ	Wave number
λ	Eigenvalue
μ	Mass per unit length

ν	Poisson ratio
ν_r	Structural damping coefficient
$\Xi_{Dr}(t)$	Generalised exciting force
$\Xi_{0r}(t)$	Generalised Froude-Kriloff exciting force
$\Xi_r(t)$	Generalised diffraction force
ξ	Horizontal spatial integration variable
Π_e	Potential energy of an element
ρ	Density
σ_x	Wet direct stress
σ_{xr}	Modal direct stress
τ	Shear stress
τ_w	Shear warping induced stress
Φ	Parasitic term of velocity potential
$\overline{\Phi}$	Steady term of velocity potential
Φ_D	Velocity potential due to diffraction forces
Φ_0	Velocity potential due to radiation
ϕ_r	Rotation
ϕ	Angle of twist
χ	Heading
$\chi(\ )$	Warping function
Ω	Sectorial coordinate
Ω_f	Fluid domain
Ω_s	Structural domain
ω	Incident wave frequency
ω_r	Modal natural frequency
ω_e	Encounter frequency

D. Mathematical operators

Adj	Adjoint matrix
Cos	Cosine

$\in$	Belongs to
Im	Imaginary part of a compex number
N	Set of Physical numbers
Re	Real part of a complex number
$\Re$	Langrangean functional
$\neq$	Different than
∞	Infinity
$\times$	Product
$\bullet$	Dot product
$\cap$	Intersection of sets representing two different domains
∇	Gradient (Hamiltonean) operator
∇^2	Laplacean operator
[ ]	Matrix
$[\,]^T$	Transposed matrix
[I]	Unit matrix
Σ	Summation
$\{\ \}$	Vector
$\int_a^b f(x)dx$	Integration of a function f(x) from limit a to limit b with respect to x
$\oint f(x)dx$	Cyclic integration of a function f(x) with respect to x
$d^{(n)}f(x)/dx^{(n)}$	n^{th} grade of derivation of a function f(x) with respect to x
$\partial^{(n)}f(x)/\partial x^{(n)}$	n^{th} grade of partial derivation of a function f(x) with respect to x
$\lim_{\Delta x \to 0} f(x)$	Lemma of a function f(x)

E. Abbreviations

ABS	American Bereau of Shipping
APDL	ANSYS Parametric Design Language
BIMCO	Baltic International Maritime Council

BMT	British Maritime Technology
BSRA	British Ship Research Association
BV	Berrau Veritas
CG	Centre of Gravity
DNV	Det Norske Veritas
FD	Finite Difference
FEA	Finite Element Analysis
FSI	Fluid-structure interaction
GL	German Lloyd
HB	Horizontal Bending
HBM	Horizontal Bending Moment
HSF	Horizontal Shear Force
IACS	International Association of Classification Societies
IMO	International Maritime Organisation
ISSC	International Ship Structures Committee
RAO	Response Amplitude Operators
SC	Shear Centre
T	Torsion
TM	Torsion Moment
VB	Vertical Bending
VBM	Vertical Bending Moment
VSF	Vertical Shear Force

ACKNOWLEDGEMENTS

'God' thank you for giving me the strength and patience to do it even at those moments that everything seemed dull and impossible.

I would like to thank and express my gratitude to:

My supervisor Prof. P. Temarel for teaching me life and science over the last three years. Prof. W.G. Price for being encouraging, keeping some interest in my work and validating my scientific publications. My parents Evgenios and Andromachi Hirdaris as well as Demetrios and Athena Papadatos and my best friend Mike Sotirakos for standing by me over the last 7 years. CETEC consultants Ltd. and especially Mr. A. Marchant and Mr. M. Pollard for giving me the chance to work on a hi-tech six month industrial placement. BMTSeaTech and Mr. A. Cooper for acknowledging the quality of my work and giving me employment. Prof. A.W. Lees of the University of Wales Swansea for standing by me as good friend and exceptional teacher over the last six years. Dr. J. Barton encouraging me and supporting me in the good and difficult moments over the last three years. Dr. M.A. Salas Insuza for helping me at the first difficult steps of my PhD.

Last but not least I would like to thank Tulla and Colin Green, I.S. Sidiropoulos, I. Sidiropoulos, G. Tsolis, A. Logothetis, K. Papanagiotou, R. Speht, N. Vassilakis and N. Polemikos for their moral support; A. Aggio, E. Amoiridou, D. Kakaraki, R. Ouzouni for being my 'muses' for certain periods of time over the last four years as well as my fellow research students and members of staff of the fluid-structure interaction research group. Especially my office mate Paolo Manganelli, for contributing to this work in various ways.

Chapter 1

Introduction

1.1 Introduction

Floating structures such as offshore oil production systems, low speed conventional ships and high speed monohull or multihull vessels are affected by several types of dynamic loads including environmental actions, such as wind and waves, the latter being considered as the most important source of motions and structural responses in a seaway. It is only fair then to say that engineering analyses for the prediction of the seaway induced dynamic responses of such structures demands a realistic formulation of the fluid-structure interaction (FSI) domain via integration of hydrodynamics, structural mechanics and use of novel modelling techniques. The degree of interaction between the structural response and the hydrodynamic loads determines the practical solution in each of the structural and fluid domains respectively and provides valuable information with regards to the assessment of the global strength of the floating structure. According to the degree of structural response problem areas can be divided between those where the ship can be treated as a rigid body and those for which its inherent flexibility significantly affects the degree of dynamic response.

In recent decades the treatment of ships as rigid bodies responding to waves has continued to be largely in use and the prediction of seaway induced dynamic loads has been approached by two distinct procedures namely hydrodynamic analysis and quasi-static structural safety assessment. In both these approaches bodily motions imply that the structure is a rigid body experiencing neither strains nor stresses. However, concepts such as mode shapes, natural and resonance frequencies, fatigue, etc are not encompassed by the rigidity restriction. Although the traditional methodologies have been successful to a certain extent and are continuously

striving to improve [1.1,1.2] they still do not prevent catastrophes happening as a result of excessive wave excited hull responses of ships in rough seas [1.3,1.4,1.5].

Traditionally, the study of the hydrodynamic behaviour of a moving floating structure in water has been divided into three distinct subjects namely manoeuvering, seakeeping and strength analysis. The first one relates to the deterministic behaviour of a rigid ship in calm water when it is subject to external actions caused by forced motion of the rudder or stabilizer fins or by selective use of propellers and thrusters. On the other hand, seakeeping theory determines the responses of a rigid ship, moving in regular sinusoidal waves or random seaway, while strength analysis is used to determine the loading experienced by the structure under static or quasi-static conditions.

Hydroelasticity theory provides an alternative. In its two- or three-dimensional form it is unified in the sense that it subsumes the principles of structural theory and naval hydrodynamics (conventional seakeeping and strength) by studying the behaviour of a flexible body moving through a liquid [1.6,1.7]. The two-stage approach of *dry* (or *in vacuo*) and *wet* analyses assesses the dynamic strength of a floating structure travelling at arbitrary heading in regular waves or irregular seaways via direct evaluation of its dynamic loads and responses. When applied to a ship hull it may be used within the concepts of linearity to determine the inherent stresses, motions and distortions under the actions of external loading arising from the seaway, rotation of the propeller, etc. This methodology becomes particularly important for ships like bulk carriers, LNG carriers and tankers, which are large, slender, beam-like and inherently flexible structures operating in a random dynamic and definitely not quasi-static environment.

1.2 Bulk carrier – A problematic ship

The excessive cracking, catastrophic failures and disappearances of bulkers in recent years have created a worrying and unhealthy picture of ship failure and casualty statistics [1.1,1.2,1.3,1.4,1.5]. This statement is of utmost importance considering that the bulk carrier industry today is recognised as the workhorse of the world's merchant fleet.

The carriage of cargoes in 'bulk' first emerged as a major and rapidly expanding shipping sector following the Second World War. Important industries involved in the manufacture of steel, aluminum and fertilisers looked to foreign suppliers for raw materials. As a consequence, a large number of bulk carriers has been built up to service the trade, the principal dry bulk cargoes being the 'major bulk' commodities associated with the raw material trades such as iron ore, coal, grain, phosphates and bauxite [1.4].

Following this revolution, bulk carriers today comprise 33% of the world's merchant fleet. Of these 72% are Handysize, 19% Panamax and 9% Capesize. The age of the current fleet is between 10 and 15 years [1.4]. Casualty statistics for the period between 1990 and 1997, as assessed by the Baltic and International Maritime Council (BIMCO), indicate that 25 bulk carriers, totaling 1,847,174 DWT, and 572 lives were lost. Of these casualties 40% correspond to Handysize, 12% to Panamax and 48% to Capesize ship types [1.8]. Since the beginning of the eighties, according to Lloyd's Register of Shipping, more than 57 bulk carriers have been lost at sea and a further 61 incurred damage to such an extent that their loss was narrowly averted [1.9]. Although these statistics provide just a general overview of the situation a number of points should be noted:

- The rate of known or possible structural failures increased dramatically between 1989 and 1994, 1991 being the worst year with 11 ships lost and 14 occurrences of serious structural failure (see figure 1.1) [1.9] ;
- The average age of ships lost in this period was 17.5 years (see figure 1.2) [1.9];
- The majority of the casualties occurred midway between special surveys with the peak at 18 years of age;
- The number of losses for vessels carrying steel or iron may be considered rather high as these products account only for 7% of the dry bulk trade [1.9].

Research undertaken by the International Maritime Organisation (IMO) and the International Association of Classification Societies (IACS) suggests that some of the possible causes for 90% of the losses could be hull girder failure, loss of stability and loss of reserve buoyancy [1.4]. Briefly the first is related to the cargo distribution and loading, the second to the structural loss of stability of the ship's cell and the third to the bad quality of ship to shore

communication. Under these circumstances IACS and some of the leading classification societies have taken measures related to the operational and design aspects of the problem. Amongst the main initiatives were the introduction of the 'unified bulk carrier design requirements' (URS/Z standards) and the 'enchanged survey program' according to which ship-owner, operator, surveyor and governmental bodies have to subscribe to certain design and survey specifications [1.4]. IMO in the 65th maritime safety session (MSC 65) has set up a correspondence group to asses single skin bulkers in terms of subdivision, transverse watertight bulkheads and survey requirements. In the same note these regulations were reinforced even further by the 1996 committee (MSC67) as well as the new Safety for Life at Sea (SOLAS) amendments. Lloyds Register of Shipping and other leading classification societies recognized as a result of the rising casualties in 1991 that the rules for bulk carriers need to be reviewed. This culminated in rule changes for side frames and brackets, transverse bulkheads and coatings [1.4,1.8].

However there still remains 10% unexplained disasters, which could be attributed to structural failure, although concrete evidence is hard to procure. The prediction of seaway induced dynamic loads by means of hydroelasticity theory could be able to shed light in explaining those.

1.3 Objectives of the current investigation

The influence of structural configurations, such as large deck openings and side skin, encountered in bulkers, containerships and LNG carriers, on predicting the global dynamic behaviour of these inherently flexible vessels in waves is of particular interest. This is due to the options available for structural modelling namely two-dimensional beam and three-dimensional finite element idealisations. Two-dimensional idealisations offer a fast and efficient means of simulating the dynamic behaviour in waves, whilst three-dimensional models are time and effort consuming, even when a relatively simple idealisation is used. The high rate of bulk carrier casualties in recent years (see figures 1.1,1.2 and section 1.2) makes this vessel type a suitable example for investigating the influence of hydroelastic modelling on the fluid-structure interactions and subsequent loads and responses in waves.

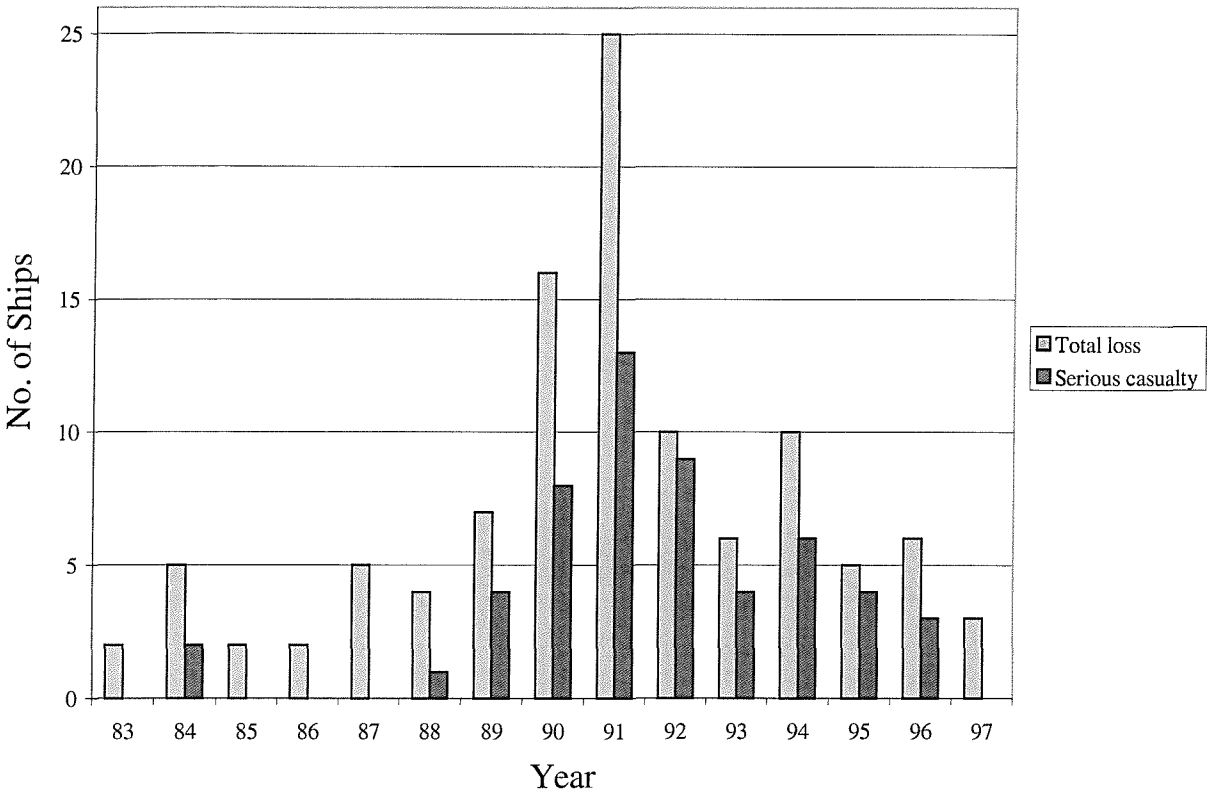

Fig. 1.1 Rate of Bulk Carrier Casualties per year between 1980 & 1997 [1.8]

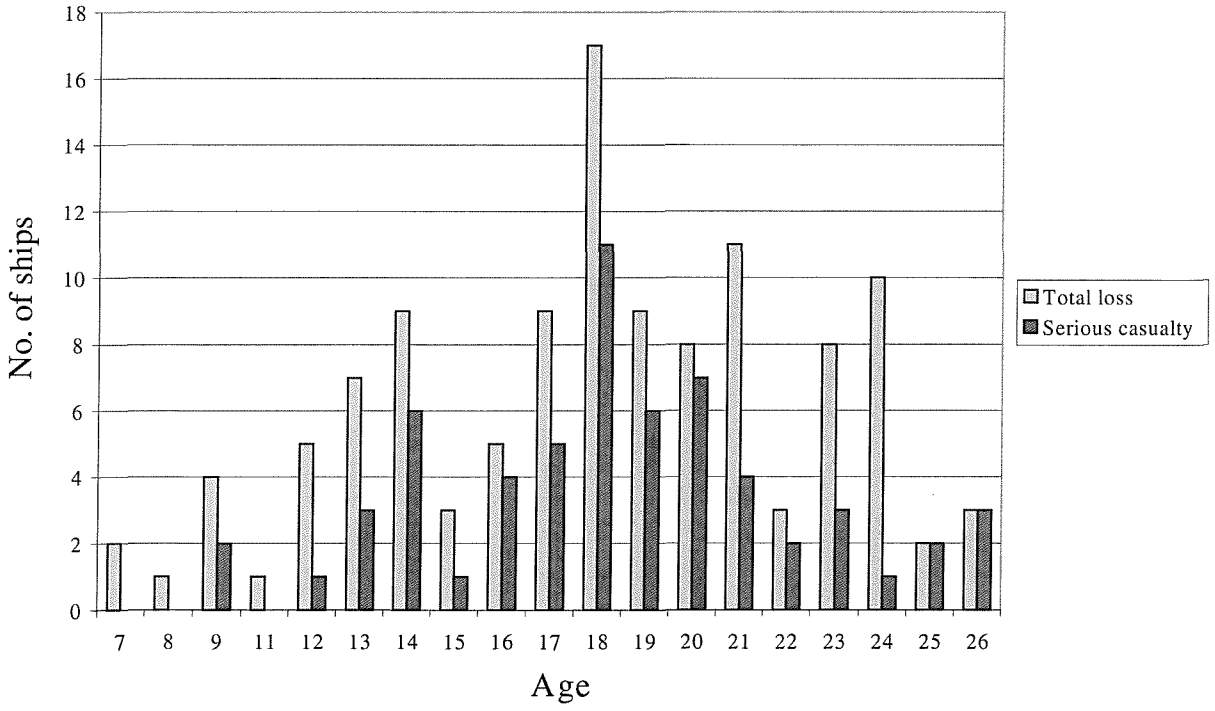

Fig. 1.2 Age of serious casualties between 1983 and 1997 [1.8]

In the current investigation two- and three-dimensional hydroelastic fluid-structure interaction (FSI) models are used to predict and compare the steady state dynamic behaviour of a bulk carrier hull, having similar structure to that of OBO-MV Derbyshire, in regular waves. The modelling levels, options and procedures available to the naval architect when assessing the steady state dynamic behaviour of long slender monohulls with large deck openings are explicitly highlighted. Both symmetric and antisymmetric motions and distortions are incorporated in the analyses which along the lines of the unified hydroelasticity theory [1.6,1.7] is divided in two parts, namely dry and wet.

In the dry analyses two- and three-dimensional idealisations are used to determine the symmetric and antisymmetric in vacuo dynamic characteristics of the bulker. Three-dimensional finite element models, using shell- or brick-type elements, are compared against two-dimensional Timoshenko beam models simulated by means of either finite element or finite difference schemes discretised in equal or unequal spaces. For the wet analysis the flexible fluid-structure interaction (FSI) is carried out using models with varying details for structural and hydrodynamic properties. A unified two-dimensional FSI model (combining Timoshenko beam and strip theory) is compared against alternative three-dimensional (beam and shell finite element idealisations combined with potential flow analysis based on pulsating source distribution over the mean wetted surface) unified hydroelastic idealisations. Special emphasis is paid upon identifying the influences of hatch openings, shear center and warping rigidity on the antisymmetric dynamics of the structure and for this reason the in vacuo dynamics and steady state hydroelastic behaviour of an open-deck and a closed-deck ship structures are explicitly outlined. The differences and similarities between the different levels and approaches of modelling are ascertained via comparison of a wide range of dynamic characteristics.

Accordingly, the current investigation not only consists of a novel hydroelastic modelling application but also highlights that two- and three-dimensional fluid-structure interaction models, due to their different degree of complexity and associated data requirements, could have different uses in design. The former could be, in general, suitable for the concept (preliminary) design stage, where the performance of design variants can be assessed using

acceptable engineering approximations. The latter could be, in general, far more suitable in predicting or confirming the dynamic performance of a detailed design. This notwithstanding the present investigation assesses the degree of confidence that can be placed on hydroelastic predictions obtained from two-dimensional models by comparison to three- dimensional models where structural features, such as deck openings, double bottoms, transverse bulkheads, hopper spaces etc, are modelled more explicitly.

1.4 Thesis Outline

The present chapter serves as general introduction. It sets up the objectives of this theses and highlights the importance of predicting the seaway induced dynamic loads imposed upon long slender monohulls (e.g. bulkers, tankers, containerships etc) by means of the unified hydroelasticity theory.

Chapters 2 and 3 cover general and theoretical issues. The first one attempts an explicit literature review of the existent quasi-static, hydrodynamic and hydroelastic approaches that could be used for the prediction of seaway induced dynamic loads. The latter outlines the basic mathematical background related to two- and three-dimensional unified hydroelasticity theories.

In chapters 4 and 5 the in vacuo dynamic analysis of a bulker having similar mass and structural properties to those of OBO MV Derbyshire is carried out. Chapter 4 focuses on aspects associated with the derivation of the ship's structural properties as well as the characteristics and sensitivity of the alternative two- and three-dimensional finite discretisation models that could be used for the structural idealisation of long slender monohulls. Consequently, in chapter 5 the two- and three-dimensional dynamic characteristics of the dry hull (natural frequencies, mode shapes, generalised masses, vertical and horizontal bending moments as well as torsional moments) are outlined and compared for all models. Analogies between alternative discretisation schemes are discussed with special emphasis upon identifying the influences of hatch openings, shear center and warping on the antisymmetric dynamics of the structure. In an attempt to further validate the latter two fictitious ship idealisations corresponding to a closed- and open-deck vessels are also studied.

Chapter 6 discusses issues related to the two- and three-dimensional hydroelastic analyses/modelling of the bulker in regular waves. The fluid-structure interaction is carried out using two-dimensional (Timoshenko beam and strip theories) and three-dimensional (finite element idealisation and potential flow analysis over the mean wetted surface) unified hydroelastic models. In the three-dimensional wet analysis a composite pulsating source distribution (Green's function) technique is employed over the panelised port half of the hull's mean wetted surface in order to evaluate the generalised fluid actions. In both cases, the generalised equations of motion are solved in the frequency domain in terms of principal coordinates. These describe the coupled rigid and flexible responses of the vessel in regular seas. Comparisons of steady state symmetric and antisymmetric wave induced dynamic loads predicted by two- and three-dimensional models for the bulker in regular waves for alternative headings, wave- to ship-length aspect ratios, damping and speed levels are presented. The effects of alternative structural considerations (closed- and open-deck ships) on the steady-state wave induced dynamics of the structure are also demonstrated. After a brief frequency response analyses the steady state seaway induced dynamic loads predicted by two- and three-dimensional models in regular waves for alternative operational conditions (speed, wave- to ship-length aspect ratios, damping) and structural configurations (open- and closed-deck ships) are outlined.

Finally, in chapter 7 conclusions are drawn and recommendations for future research are presented. Detailed lists of the structural properties (scantlings, sectional properties, masses) of the vessel are included in appendix 1. Appendix 2 includes some additional information related to the background of finite difference and finite element methodologies used in this project. The last three appendices include the conference and journal papers published by the author throughout the current investigation.

1.5 References

[1.1] Report of ISSC: Committee II.1 on quasi-static response, 13th International Ship and Offshore Structures Congress, Trondheim, Norway, (1997).

[1.2] Report of ISSC: Committee II.1 on quasi-static response, 14th International ship and offshore structures congress, Nagasaki, Japan, (2000).

[1.3] IACS: Bulk carriers – guidance and information on bulk cargo loading and discharging to reduce the likelihood of over-stressing the hull structure, IACS publications, London, (1997).

[1.4] Mathiesen, T.C.: Safety of new and existing bulk carriers, International association of classification societies studies and conclusions, RINA International Conference on the Design and Operation of Bulk Carriers, 23-27, London, (1998).

[1.5] Bishop, R.E.D., Price, W.G., and Temarel, P.: A theory on the loss of MV OBO Derbyshire, Trans. RINA, 127:169-186, (1991).

[1.6] Bishop, R.E.D. and Price, W.G.: Hydroelasticity of Ships, Cambridge University Press, UK, (1979).

[1.7] Bishop, R.E.D, Price, W.G. and Wu, Y.: A general linear hydroelasticity theory of floating structures moving in a seaway, Phil. Trans. Royal Soc. London, A316: 375-426, (1986).

[1.8] BIMCO: Bulk carrier safety – the view and role of an industry organisation, RINA International Conference on the Design and Operation of Bulk Carriers, 1-12, London, (1998).

[1.9] Tustin, R.D.: Existing bulk carrier safety – on the evaluation of the foremost hold structure under conditions of hold flooding, RINA International Conference on the Design and Operation of Bulk Carriers, 48-68, London, (1998).

Chapter 2

Literature Review

2.1 Coupled field problems and engineering multiphysics – A general reference

In engineering applications the term *coupled problem* refers to a dynamic system that can be decomposed into physically heterogeneous components that exhibit mutual interaction. Often each of these components is idealised as a field operating in different continuum and therefore the equivalent term *coupled field* or *multiphysics* problems has been widely used in literature [2.1,2.2,2.3,2.4]. In practice the numerical simulation of the components of coupled problems encountered in alternative engineering fields has been achieved by following interdisciplinary procedures. These are investigated in most cases by approaches that exploit innovative modelling, numerical methods and problem decomposition rather than quasi-static methods and analytical tools. Following are four examples that illustrate the wide spectrum of such engineering problems:

- *Fluid-structure interaction* (FSI). A structure is immersed in a gas, fluid or soil medium. The system components are the structure and the external fluid or medium [2.1].
- *Control-structure interaction* (CSI). A flexible structure interacts with an active control system. The system components are the structure, the controller, the sensors and the actuators [2.2].
- *Flow in porous media* (FPM). A diffusing fluid phase, such as oil or pollutant, interacts with another fluid phase, such as injected water or gas, as it propagates through soil. The components are the two fluid phases and the soil medium [2.3].
- *Thermomechanical extrusion* of a metal or plastic in a fabrication process. The components are the thermal field, the extruded material and the constraining structure [2.4].

These alternative interaction domains have also different 'dimensionality': a surface in FSI, a discrete set (sensor/actuator locations) in CSI, the soil volume in FPM, both volume and surfaces in thermomechanical extrusion problems. Specific applications of the generic coupled problem classes noted above give rise to technology areas of interest in engineering. For instance, aeroelasticity is a specialization of FSI to aircraft flight whereas hydroelasticity is the corresponding counterpart for the estimation of seaway induced dynamic loads.

Inadvertently, from either scientific or engineering perspective efforts related with improving the understanding and innovation of such techniques dominate a vast area of scientific research. However, the purpose of the present chapter is not to review all of those but to highlight the existence and significance of FSI and particularly hydroelastic techniques as coupled engineering analyses tools useful for the design and safety of ship structures. Particular emphasis is paid upon the importance of the unified hydroelasticity theory as an alternative to quasi-static and traditional hydrodynamic methods used for the evaluation of seaway induced global dynamic loads and dynamic strength assessment of the hull girder.

2.2 FSI problems – Coupling the fluid and structural domains

The assessment of hydrodynamic loadings, motions, deformations, strength under static and dynamic loads is necessary in order to assess the performance, serviceability, reliability and safety of a marine vehicle in rough seas. Among all of these areas, many are related to fluid-structure interactions and therefore adequate understanding of such methodologies is crucial for research, innovation and application purposes. In FSI analysis the overall model consists of at least two very distinct physical domains, namely structural (Ω_s) and fluid (Ω_f). The degree of interaction between the structural response and the hydrodynamic loads determines the practical significance of the solution procedure followed. Along these lines the response of the system can be assessed within the frequency or time domains where the structure can be treated either as a rigid or flexible body. The finite element method (FEM) has been established as the preferred choice for modelling the structural domain. While frequency domain problems are restricted to linear and weakly non-linear problems, time domain simulations may also include highly non-linear effects even at the fluid-structure interface

level. The fundamental equations for the fluid-structure system may be stated in a weak form appropriate for the coupling of the two sub-domains as $\Omega_f \cap \Omega_s$.

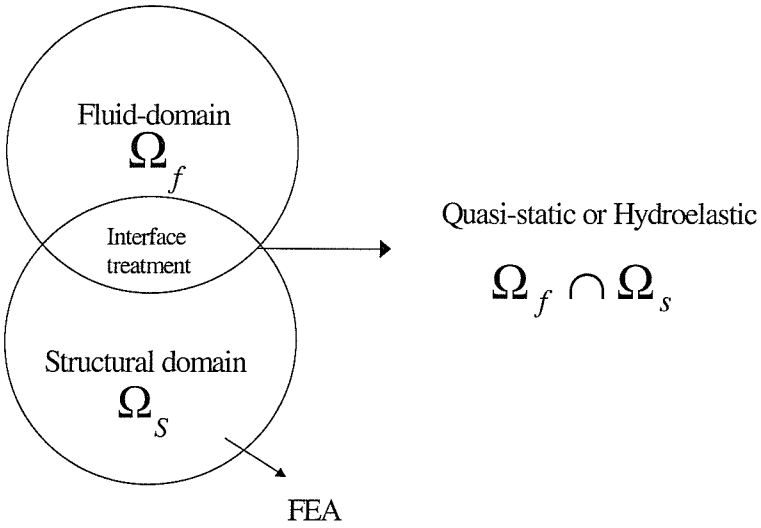

Fig. 2.1 FSI problems: coupling the structural and fluid domains

Particular emphasis is paid upon modelling the common interface treatment (e.g. free surface effects) [2.5] where the velocities are supposed to be continuous so that $\partial\Omega_f \cap \partial\Omega_s$. The equations have to be supplemented by appropriate constitutive relations, boundary and initial conditions which are highly dependant upon the flow and modelling assumptions (e.g. linearity assumption, viscous flow effects, condensation of degrees of freedom etc). For the simulation to be adequate the coupling of the two sub-domains should be accompanied by a dynamic simulation technique following the evolution of the system in time or its response within a frequency spectrum [2.5].

2.3 Traditional ship problems and the prediction of dynamic loads via FSI techniques

The adequate understanding and simulation of fluid-structure interaction problems becomes particularly important in naval, pleasure craft or shipping industry where the prediction of wave induced dynamic motions and loads is crucial both in design, safety and operational studies. The estimation of local motions and accelerations, the effect of breaking waves and green water on decks, slamming, sloshing, springing, wave induced bending moments,

torsional moments, shear forces and their effects on global ship strength are frequently met problems of practical design significance [2.6].

A ship traveling in a seaway is subject to a variety of loads arising from her weight, the waves (e.g. ship motions, slamming etc), machinery, propeller, wind, etc. It is convenient then to divide these loads into five categories [2.7]

- Static loads such as weight, static buoyancy;
- Thermal loads, arising from non-linear temperature gradients in the hull;
- Low frequency dynamic loads such as wave induced pressure variations on hull and inertia accelerations resulting from the mass or the cargo of the ship etc;
- High frequency dynamic loads namely:
    1. Hydrodynamic loads induced by propulsive devices on hull or appendages;
    2. Loads imparted to the hull by reciprocating or unbalanced rotating machinery;
    3. Hydroelastic loads resulting from interaction of appendages with the flow past the ship;
    4. Wave induced loads due to primarily short waves whose frequencies of encounter overlaps the lower encounter frequencies of hull vibration and which therefore may excite appreciable reasonable response known as springing (resonant hull vibration);
- Impact loads resulting from slamming or wave impact on the forefoot, bow flare and other parts of the hull structure including the effects of green water on deck, which may lead to whipping (transient hull vibration).

In addition to the above categories, there may be specialised operational loads, which may be dominant for some ships (e.g. ice loads, structural thermal loads imposed by special cargo, sloshing loads caused by movement of liquid in tanks, loads due to hull and explosion etc)

The most important classes of loads are the static ones resulting from the ship's weight and buoyancy and the low frequency dynamic loads, without this statement underestimating the significance of the rest depending on the situation. In any case stresses generated in the material and the resulting deformations must both be kept within acceptable limits, while each

element of the structure must play its part. From the consideration of these loads it is possible to distinguish three main structural design aspects namely longitudinal, transverse, torsional (combining longitudinal and transverse ship strength) and local strength. Consideration then of the overall structural behaviour of the hull under either still water or random sea-state conditions consists a measure of the strength of the vessel.

2.4 Empirical and quasi-static methods

The geometrical arrangement and resulting stress or deflection response patterns of a typical ship structure are such that it is usually convenient to divide the structure and its associated response into three components, labeled as primary, secondary and tertiary [2.7].

- Primary response is mainly the global hull response when the ship is bending and twisting under the external longitudinal distribution of vertical, lateral and twisting loads.
- Secondary response comprises of the stress and deflection of a single panel of stiffened plating, such as the panel of bottom structure contained between two adjacent transverse bulkheads. The loading of the panel is normal to its plane and the boundaries of the secondary panel are usually formed by other secondary panels (side shell and bulkheads).
- Tertiary response describes the out of plane deflection and associated stress of an individual panel of plating. The loading is normal to the panel and its boundaries are formed by the stiffeners of the secondary panel of which it is a part.

It is necessary to know the localised distribution of the loads or even the distribution of the resultants of the local loads depending upon the structural response being sought. Traditionally, the naval architects have restricted themselves to static or quasi-static considerations when dealing with the structural design of a beamlike ship moving in waves. Accordingly, the primary stress level which relates to the hull girder bending is often based upon a scenario whereby the ship, treated as a flexible structure, is either in still water (static) or is seated onto a trochoidal waveform so that the crest or trough is amidships and global balance exists between gravity and buoyancy forces (static balance methodology). Locally, net forces are generated give rise to shear force and bending moment distributions. The

secondary and tertiary levels of stresses are generally treated simply based upon the local hydrostatic pressure [2.7,2.8].

Today there are essentially two types of design methods for hull strength assessment. One is the traditional semi-empirical approach, normally applied in the rules, the other is rational design where the models used for loads, strength, and so on, account for physical behaviour from first principles [2.8,2.9,2.98,2.99,2.100,2.101,2.102]. Traditional design is based on deterministic analysis, however, fluctuations of loads, variability of material properties and uncertainty in analysis models, require a rational treatment of relevant uncertainties to be achieved through the adoption of a probabilistic design procedure allowing the evaluation of the probability of failure of structures. Whereas deterministic approaches are currently applied for the evaluation of symmetric dynamic loads (vertical bending moments and shear forces) semi-probabilistic and reliability based approaches are used for the evaluation of antisymmetric dynamic loads or the effects of fatigue on hull girder's strength [2.8,2.9].

It is important to stress that from the 1970's up to today the application of finite element structural analysis has been established as important technique used for the estimation of the quasi-static response and assessment of the hulls' girder strength [2.8,2.9]. As a result most of the research undertaken by the classification societies and international maritime bodies has been concentrated upon coupling the basic principles of this technique with quasi-static methodologies assembled within the context of general ship design. Lately, ABS, LR, BV, NK, DNV and GL have developed several computational systems namely SafeHull, Shipwright, Veristar, PrimeShip-ASSAS, NaticusHull and Poseidon ND respectively. All of these assist ship designers with the structural design requirements (scantling calculations) while they provide quasi-static global wave load calculations by means of two- or three-dimensional finite element analyses [2.8,2.9]. The considerations introduce two levels of analysis: a structural initial scantling procedure (phase A) and an integrated global strength verification procedure (phase B). The FEA models used are coarse mesh models of discrete elements and basically follow the arrangement of primary structure like decks, stringers, bulkheads, webs and girders. Stiffeners are then simplified as line elements and lumped to the nearest element's boundary. In this sense the global hull girder strength is preserved. To have

a better description of stress response in subsequent detailed assessments, primary supporting members and areas of interest are evaluated by a separate fine mesh of two- or three-dimensional form. The boundary displacements of these finer mesh analyses are referred back to the results of the corresponding three-dimensional coarse mesh analysis. Stress responses are verified against strength criteria of yielding, buckling, ultimate as well as fatigue strength. Since these criteria are the same in all cases and are applied to all structural components there is a unified safety level of the structure all over the ship.

As far as theoretical developments are concerned since 1985, important advancements have occurred in the field of ultimate strength of the hull girder, their main novelty residing upon the fact that they attempt to provide reliable evaluation of the ultimate strength of ship hulls under combined loads [2.97]. Simplified analytical methodologies together with numerically based evaluations and reliability-based approaches are widely suggested. A simple analytical expression for an interaction relation under combined vertical and horizontal bending moments is proposed by Mansour et al [2.10, 2.11]. This empirical relationship attempts to asses the structural safety of ships via evaluation of the reliability levels associated with hull girder, stiffened panels and non-stiffened plates failure modes. The developed methodology was applied to four ships: two cruisers, a double hull tanker and a container ship. Recommendations on target reliability levels useful for improving structural strength criteria are reported. Gordo and Soares have proposed a similar model [2.12] which has been used to evaluated the ultimate collapse of the mid-ship section of tankers and containerships under combined vertical and horizontal bending moment. The method has been applied to study five tankers and six containerships. A comprehensive and valuable contribution has been achieved by Paik et al [2.13]. This work suggests a relatively simple analytical formulation for the ultimate strength of long slender monohulls subjected to combined vertical, horizontal bending and shearing forces. Sets of interaction curves were determined empirically based on numerical results from the idealised structural unit method (ISUM) on 11 ships. Hu [2.14] proposed a simplified incremental approach for the prediction of the ultimate bending moment of ship hulls according to which strain measures are obtained through interpolation from a set of generic stress-strain curves generated via finite element analysis.

2.5 Hydrodynamic theories

Although at first instance the analysis of dynamic loads imposed upon the hull girder could be assessed by means of empirical and quasi-static methods (see section 2.4), the fact that in reality the ship structure operates in conditions determined by environmental factors should not be underestimated. According to this methodology, known as seakeeping analysis, in order to predict the motions in waves a ship is regarded as an unrestrained rigid body with six degrees of freedom. The three components of translation are known as surge, heave and sway. The three components of rotation are roll, pitch and yaw (see figure 2.2).

With the assumption of small unsteady motions, of the ship and the surrounding fluid, linear superposition can be applied. Thus, one considers separately the radiation problem, where the

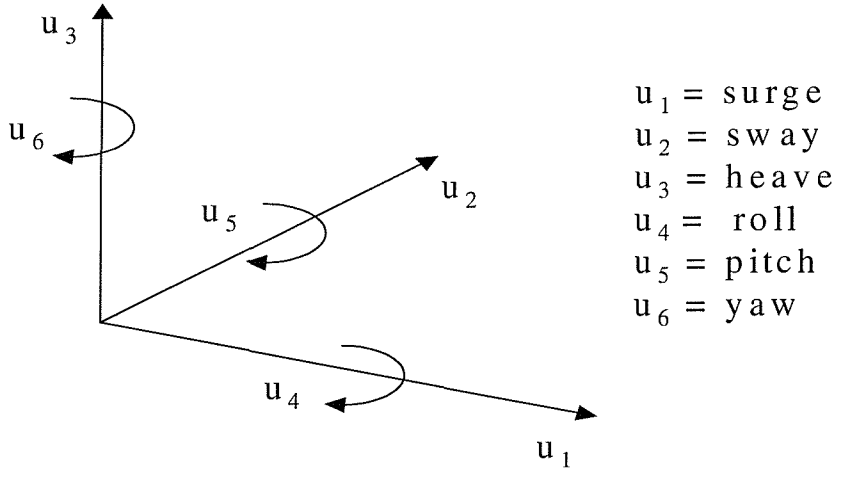

Fig. 2.2 Six degrees of freedom for motions

ship undergoes prescribed oscillatory motion in each of the six degrees of freedom in calm water, and the diffraction problem, due to incident waves act upon the ship in its equilibrium position. The investigation of the motions requires the formulation of the fluid-structure interaction, which in addition to hydrostatics (i.e. evaluation of hydrostatic restoring coefficients) contains hydrodynamics (i.e. the evaluation of added mass and damping coefficients) as well as the exciting force and moment. For an arbitrary shaped vessel the six equations of motion must be solved simultaneously. However, for the case of an unrestrained

ship with port/starboard symmetry the six equations may be uncoupled into two sets of three equations. The vertical plane or longitudinal motions (surge, heave and pitch) are uncoupled from the horizontal plane or transverse motions (sway, roll and yaw).

2.5.1 Early developments in rigid body hydrodynamics

The fundamental concepts related to the understanding of ship hydrodynamics were initiated by the end of the 19th century independently by W. Froude [2.15], his son R.E. Froude [2.16] and Kriloff [2.17,2.18]. The famous Froude-Kriloff hypothesis, i.e. the assumption that the hull does not disturb the pressure field of the incident waves is attributed to the genius of these notable scientists. Froude and Kriloff derived differential equations of motion for the inertial and restoring forces of the ship. Only the pressure field of the undisturbed incident waves was considered and the resultant force on the ship has become known as the Froude-Kriloff exciting force. The first significant step to account for the hydrodynamic disturbance due to a ship hull of realistic form was the steady state wave resistance theory of Mitchel [2.19]. He assumed that the ship is a thin body, that is, the beam is small compared to all other characteristic dimensions of its structure (length, draft and wavelength). Another major advancement in accounting for the ships' hydrodynamic disturbance was the classical work formulated by Lewis [2.20]. He studied the added mass associated with hull vibrations in structural modes. In his work the wave frequency is assumed to be sufficiently large such that the inertial effects are dominant and gravitational forces can be neglected. To simplify the analysis wave effects are ignored and a simple two-parameter conformal transformation for ship sections is suggested. Due to its simplicity the method is still in use for the formulation of ship-like section forms known as 'Lewis sections'. The first comprehensive analysis of the pitch and heave motions was made in two papers by Haskind [2.21,2.22]. In this work Greens' theorem was used to construct the velocity potential due to the presence of a ship hull and the necessary Green's function or source potential was derived. Like Mitchel [2.19], he used the thin-ship approximation to solve the resultant integral equation. A notable feature of Haskind's work is the decomposition of the velocity potential into a form, which includes separately the solution of the diffraction and radiation problems for each mode of oscillatory ship motion.

2.5.2 Two-dimensional hydrodynamics

This continuous research on ship hydrodynamics has led to the formulation of the so called 'strip theory' which calculates the inertia loads and the fluid actions due to the wave induced motions of a slender hull by subdividing it longitudinally into a number of transverse strips. Each strip has associated hydrodynamic properties (added mass and damping). The wave excitations experienced by the hull are composed of contributions from all the strips. In their classical form strip theories assume that the fluid can be presented by a velocity potential function, i.e. the fluid is assumed to be inviscid, homogeneous and the fluid motion is irrotational. They are also based on the Froude-Kriloff hypothesis, i.e. they assume that the presence of the hull has no effect on the waves. Generally speaking the method can be used to calculate the hydrodynamic actions upon a hull of 'Lewis' form [2.20]. Alternatively, hydrodynamic properties may be calculated via the multiparameter conformal mapping method where a number of points are used to define the form of each hull section [2.23,2.24].

The strip theory concept originated in the late 1950s with the work of Korvin-Kroukovsky and Jacobs [2.25,2.26]. It was further improved and validated by Gerritsma and Beukelman in 1964 [2.27]. Their research efforts provided a method for the estimation of symmetric responses. Later, improvements in formulating the two-dimensional hydrodynamic theory [2.28,2.29,2.30] enabled the inclusion of antisymmetric motions and led in early 1970s to the derivation of the well known strip theory of Salvesen, Tuck and Faltinsen [2.31] and Vugts [2.32]. In 1997 Faltinsen and Zhao developed a strip theory specifically for high Froude numbers [2.33]. Although this method is only valid at high Froude numbers it accounts for some three-dimensional properties of the flow and is commonly referred to as 2 ½ D strip theory.

Strip theories in their classical form assume potential flow analysis, they omit completely the potential of the steady flow disturbance and approximate the remaining unsteady potential in each longitudinal strip independently of the other strips along the vessel. Thus, the three-dimensional problem is reduced to a set of two-dimensional boundary value problems. Bending moments, shear forces and torsional loadings of the hull in waves are estimated by taking into account the time-varying distribution of hydrodynamic forces over the wetted

surface coupled with the distribution of the inertia reaction loads. The physical assumptions related to linear (small motions) strip theories are:

1. the ship is slender (i.e. the length is much greater than the beam or the draught and the beam is much less than the wavelength);
2. the speed is moderate so that there is no appreciable planning lift;
3. the ship hull sections are wall sided;
4. the flow velocities in the longitudinal direction are assumed to be smaller than those in the transverse plane. Since this happens when the forward speed is zero the theory is valid for low speeds and high frequencies.

Because of its high frequency nature strip theory provides accurate predictions only if the wavelength is small compared to the ships' length. In an attempt to overcome this limitation Newman and Tuck [2.34] developed the so called ordinary slender-body theory of ship motions. Although this is a low frequency theory assuming the wavelength of the incident waves to be the same magnitude as the ships' length, it provides unreliable results for increasing speeds and frequencies. This disadvantage appears due to the fact that the fundamental theory formulation assumes that the hydrostatic restoring forces and the Froude-Kriloff exciting forces are the dominant terms with the result that the leading order equations of motion are non-resonant.

In the context of slender body theory (whether ordinary or strip) it is desirable to avoid restrictive assumptions concerning the wavelength or the frequency of encounter. That objective has led Newman and Sclavounos [2.35,2.36] to the development of the unified slender body theory that embraces both long and short wavelengths. Kashiwagi describes more recent developments [2.37] of this method. In essence the theory generates the flow by means of singularities along the centerline of the ship. Despite its better theoretical foundation it appears not to give better results than the strip theory for real ship geometries.

2.5.3 Three-dimensional hydrodynamics

Whilst strip theory provides a way of determining the forces associated with the motion of the vessel and the Froude-Kriloff force allows for the calculation of the forces due to incident

waves, the calculation of the forces associated to the diffraction of the incident waves by the vessel remains difficult with a two-dimensional theory. Although strip theories have proven particularly reliable in predicting symmetric motions of beam-like ships the study of multihull vessels, offshore structures and high speed craft require a three-dimensional approach in order to evaluate the fluid effects adequately.

Probably the most common analysis technique for predicting ship motions after strip theory is the three-dimensional frequency domain singularity distribution method, also known as the Green Function Method (GFM). GFMs distribute panels on the mean wetted surface (usually for calm-water floating position neglecting dynamical trim, sinkage and the steady wave profile) or on a surface slightly inside the hull (desingularised approach). The velocity potential of each panel (Green's function) fulfils automatically the Laplace equation, the radiation condition, the body boundary condition (no net flow through the hull surface) and the free-surface condition (omitting the potential of the steady flow disturbance completely). One distinct advantage that the three-dimensional methods have over strip theories, is that the diffraction component of the wave exciting forces may be obtained directly from the solution rather than via the radiation forces. As with strip theory, however, three-dimensional GFMs used in design applications often include terms to augment the roll damping predicted by the potential flow method.

Initially, three-dimensional theoretical seakeeping studies were oriented towards analysing stationary offshore structures [2.38,2.39]. Almost the first three-dimensional analyses for a ship advancing at steady forward speed using a frequency domain panel method were accomplished in the early 1980s by Inglis and Price [2.40,2.41] and Guevel and Bougis [2.42]. Both of these research efforts follow quite similar approaches of dealing with the ship motion problem. They are based on the distribution of singularities of known strength on the mean wetted area of the hull surface. The strength of these singularities is determined by simply applying the condition that there should be no net flow through the hull surface. Hence the calculation of the source strength allows for the determination of the fluid pressure and forces acting on the moving hull. The use of the linearised equations of motion contributes towards the calculation of the vessel's response to regular waves of prescribed frequency. In

the Inglis and Price panel method the approach of a source (pulsating / translating) distribution was adopted to account for the effects of forward speed. Guevel and Bougis proposed two three-dimensional singularities models the first being based on mixed (sources and doublets) and the second on ordinary (sources only) distribution. In both methods the boundary condition must be satisfied at the center of each panel. The definition of the hull surface by a suitable number and distribution of quadrilateral panels therefore forms an important factor for their computational implementation. The various Green function methodologies suggested after the works of Inglis and Price and Guevel and Bougis differ primarily in the way the Green function is computed. For instance, Ba and Guilbaud [2.43] investigated an alternative method for the computation of the translating or translating pulsating Green's function. The formulation adopted is essentially the same as that of Guevel and Bougis but particular attention is paid on the efficient numerical integration of the terms in the Green's function. In any case Green function methods are useful tools for three dimensional seakeeping analyses although they are fundamentally restricted to simplifications in the treatment of the potential of the steady flow disturbance.

2.5.4 Time domain approaches

Despite the numerical improvements described before, the frequency domain Green's function remains relatively time consuming and difficult to evaluate. An alternative approach is to formulate the time domain initial value problem. The time dependant Green function that satisfies the linearised free surface boundary condition is simpler than the corresponding ones in the frequency domain. This is achieved by acknowledging the importance of free surface memory effects, i.e. by obtaining the velocity potential at each time step for the instantaneous, rather than the mean, wetted surface of the hull [2.44]. In this sense, non-linearities can be directly incorporated in the analysis but the computational effort to solve the problem does increase substantially.

Linearised time domain results have been available in the scientific literature for some time. Liapis and Beck [2.45,2.46], King et al [2.47,2.48] and Korsmeyer et al [2.49] have extensively reported on the general linearised problem with forward speed. Maskew et al [2.50], Nakos et al [2.51] and Kring et al [2.52] among others have studied the effects of non-

linearities. The extension from the forward speed problem to a more general body motion incorporating incident waves of large amplitude, but still with linear free surface effects, has been presented in literature by Lin et al [2.44,2.53] as well as Beck and Magee [2.54]. Bingham et al [2.55] described a three dimensional method employing the time dependent free surface Green function to calculate linearised radiation and diffraction forces on ships with steady forward speed. These forces were used to simulate ship motions in irregular head seas. Specific formulations allowed the calculation of the radiation forces due to impulsive accelerations, velocities and displacements. His predictions have been compared with experimental data and were found to be in good agreement. Magee [2.56] also used a three-dimensional time domain methodology to calculate the radiation and exciting forces at steady forward speed. Solving the equations of motion in the time domain permitted the calculation of incident wave and hydrostatic forces on the instantaneous body surface. Comparisons with frequency domain calculations and experimental results for a series 60 hull form were presented and found to be once more in good agreement.

2.6 Hydroelasticity theories

From the discussion so far becomes apparent that up to today the treatment of ships as rigid bodies responding to waves has continued to be largely in use following the traditional approach that the design process should be divided into the distinct procedures of hydrodynamic and quasi-static analyses. According to these methods, however, bodily motions imply that the structure experiences neither strains nor stresses. Also, concepts such as mode shapes, natural and resonant frequencies, fatigue, etc. are not encompassed by the rigidity restriction. Hence it is of utmost importance for the naval architect to assess the wave excited responses of a ship structure by describing its overall behaviour, from a dynamics point of view based on combining the structural and hydrodynamic theories.

The fact that floating structures are flexible has probably been intuitively accepted since ancient times. The assumption that ships are rigid structures is a relatively modern simplification in an attempt to bring some understanding into ship motions in waves. In technical literature, the idea that the ship is really a flexible structure and could be modelled as an elastic beam was considered in a paper by Inglis in 1929 [2.57].

Despite these early attempts, hydroelasticity of floating bodies is a relatively new subject. The term appeared for first time in technical literature in 1959 as the naval counterpart to aeroelasticity. Heller and Abramson [2.58] proposed the following definition: *'Hydroelasticity is concerned with the phenomena involving mutual interactions among inertial, hydrodynamic and elastic forces'*. Their definition recognises that significant differences exist between the two different fields with respect to the free surface effect, the fluid properties, the influence of cavitation and the relative speed between the vehicle and the fluid. Kalinowski and Chen and Pierucci [2.59,2.60] reviewed the methods developed to obtain the fluid actions and structural responses during the first two decades of the development of hydroelasticity. Later Zienkiewicz and Bettess [2.61] summarized the mathematical descriptions and numerical techniques for fluid-structure interactions using finite element methods. Although a considerable amount of work has been published in this field, most of it is concerned with the acoustic radiation and scattering, underwater free vibration and shock responses of submerged bodies in the absence of free surface and rigid boundaries.

2.6.1 Two-dimensional hydroelasticity theories

The study of hydroelasticity of ships traveling in waves did not gain significant momentum until the mid seventies when Bishop and Price established the basic principles of a theory for flexible beam-like hulls subject to steady state and transient (e.g. slamming) wave-induced loads, combining Timoshenko beam and strip theories [2.62]. The two-stage approach of *dry* or *in vacuo* and *wet* analyses leads to a direct evaluation of dynamic loads and responses (e.g. stresses, bending moments, shear forces, torsional moments) for a vessel traveling at arbitrary heading in regular waves and irregular seaways. This theory is unified in the sense that it incorporates rigid body motions (i.e. conventional seakeeping) as well as distortions.

The method was applied successfully to a variety of beamlike merchant and naval ships and its capability to simulate symmetric, antisymmetric and unsymmetric dynamic behaviour in waves was widely demonstrated in literature [2.63,2.64,2.65]. The concept of modal analysis has been successfully applied not only to describe steady state responses but also the

behaviour of transient responses due to slamming. Bishop et al [2.66] and later Belik et al [2.67] investigated the problem of transient responses due to slamming in regular head waves using impact and momentum slamming theories. Further work by Belik et al [2.68,2.69] accounted for transient responses due to slamming in irregular head waves. Time domain simulations of the behaviour of ships travelling in irregular head seaways agreed well with full scale measurements [2.70]. In addition to impact slamming theories, bow flare slamming was incorporated into the available modal approaches to analyse transient responses due to the effects of bottom and bow flare slamming on a destroyer [2.71].

In the early 1990s the analysis has been applied to investigate the excessive cracking and catastrophic failures observed in MV Derbyshire [2.72]. Such casualties have raised questions about the conventional, quasi-static and semi-empirical approaches employed by the classification societies in establishing the global strength of ship hulls. Further research on the assessment of the steady state or transient (e.g. slamming) dynamic loading induced pressures along the hulls of bulkers and tankers has proved that dynamic global responses occur anywhere in these hulls and not only at amidships. This phenomenon has been analysed and illustrated with particular reference to large stresses arising at the extremities of the hull, namely 15-20% of hull's length from either end [2.73,2.74,2.72,2.75].

Domnisoru and Domnisoru [2.76] extended the theory for symmetric motions and distortions of a monohull in head waves to account for slamming as well as hull geometry non-linearities. In this work a direct time integration of the equations of motion is used to obtain linear and non-linear responses in the time domain by accounting for the instantaneous waterline and applied external forces. The vertical bending moment values were compared with experimental measurements extracted form an elastic segmented model. For a significant number of headings it appears that linear predictions are closer to the experimental measurements by comparison to the predictions including non-linearities.

To overcome the limitations associated with two-dimensional hydroelasticity theories, assuming slender ship and moderate forward speed some modifications are necessary. Wu and Moan [2.77] employed the higher order strip theory (2 ½ D theory) (see section 2.5.2)

together with Vlasov beam idealisation to study the symmetric hydroelastic responses in head waves and irregular seas generated by ISSC wave spectra. Comparisons between time and frequency domain techniques have shown that the effects of non-linearities become particularly important at high speeds. Hermundstad et al [2.78] applied the linear part of this method to predict the symmetric responses of a catamaran structural model of which was modelled by means of beam and shell elements. His work has shown that the influence of the interactions between the hulls on the predicted responses is important. The comparisons with experimental results for a range of speeds and headings, however, has not been shown to be so good most probably due to the slender body assumption of the theory used.

Xia and Wang [2.79] presented a three-dimensional time domain linear hydroelasticity theory in which the radiation and diffraction potentials are decomposed into instantaneous and memory parts. This theory was then simplified in two dimensions using a beam idealisation (for the dry analysis) and a slender body strip theory (for the wet analysis). Only symmetric motions and distortions were considered. Predicted vertical bending moments and motions were found to be in good agreement with experimental measurements of an elastic warship and the S175 containership models in head waves and irregular seas. The non-linear time domain hydroelastic analysis by Xia et al [2.80] illustrates the importance of non linearities in hydrodynamic actions. The predicted bending moments for the S175 containership models show improved agreement with experimental measurements especially for the flared model.

2.6.2 Three-dimensional hydroelasticity theories

The beamlike hull idealisation is not suitable for structures such as multihull vessels, jack-up rigs, semi-submersibles etc. The three-dimensional hydroelasticity theory, by Bishop, Price and Wu, overcomes these limitations and is able to simulate the wave-induced dynamic behaviour of beam or non-beam like vessels in waves [2.81]. This analysis makes use of a three-dimensional finite element model of the structure (dry analysis) and a pulsating source distribution over its mean wetted surface (wet analysis). Because of the nature of the hydrodynamic coupling in the mathematical model, all principal coordinates are excited at each frequency with the dominant principal coordinate occurring at resonance. For example, at low wave frequencies, the principal coordinates associated with bodily motions are

dominant but the principal coordinates associated with distortions are also excited. The structure therefore continuously flexes in all seaways (i.e. a fatigue mechanism is always present for a vessel in random waves) and the dynamics of distortion are not confined to resonances. At higher frequencies (e.g. resonance) a principal coordinate with corresponding principal mode dominates with the other coordinates excited to a lesser degree. The excitation of coordinates is dependent on the mass and stiffness properties of the structure and hence on its natural or resonance frequencies when excited externally by waves or other implied loading (e.g. propeller). The principal mode shapes determine the magnitudes of the responses at a particular position within the structure whereas the principal coordinate describes the frequency content or time dependant nature of the response.

The theory has also been modified to allow for fluid viscous damping effects [2.82]. Ergin et al [2.83] developed an alternative time domain analysis to describe the effects of impulsively loading a flexible cylindrical shell in air whilst submerged. Time history effects were included in the mathematical model and iterative procedures were developed so that the time dependent response signals generated could be directly compared with experimental data. Studies incorporating the responses to transient excitation in irregular head and oblique waves were also carried out by Aksu et al [2.84] following the earlier two dimensional work on slamming by Belik at al [2.67]. Comparisons of responses derived from two- and three-dimensional hydroelasticity theories for a slender structure experiencing slamming in head waves showed good agreement [2.85]. However, as the dimensions of the vessel changed (i.e. the beam approached length) the two-dimensional slamming theory produced not so good results in contrast to the three-dimensional approach.

The theoretical predictions were validated by experiments for the case of (i) a SWATH, using crude and refined theoretical structural models [2.81,2.85, 2.86], (ii) the behaviour of a dry dock [2.87], (iii) a thin cylindrical shell representative of a submarine hull immersed below the free water surface [2.83] and (iv) a fast patrol boat traveling in rough seas [2.89]. Recent applications to trimarans showed also good agreement with flexible model experiments for wave induced loads, such as prying moment, for a range of speeds and headings [2.90,2.91].

Applications to non-slender, mono-hulled vessels, such as sailing yachts, demonstrated that the method is capable of simulating accurately the dynamic behaviour of such vessels and identifying correctly areas where structural problems may arise [2.92]. The analysis has also been applied to beamlike mono-hulls (without any significant deck openings), showing good agreement between wave-induced loads and responses predicted by two- and three-dimensional models [2.93].

As in the case of two-dimensional hydroelasticity simulations the unified three-dimensional theory may be considered as the reference point of several other research efforts of similar scope. Fathi et al [2.94] carried out a hydroelastic analysis of containers. The results for the surge pressure mode showed a way to obtain external hydrodynamic coefficients for use in computing the internal surging motions of the cargo. Of the main theoretical advances may be considered the work of Xia and Wu [2.95] who developed a general form of the interface boundary condition for fluid-structure interaction, which takes into account the strain tensor field of the body surface. This boundary condition reduces to that provided by Bishop et al [2.81] when there is no shear force acting on the wetted surface and simplifies to that widely employed in strip theory for a slender ship in an ideal fluid. The method also provided the possibility to develop an alternative to that of Price and Wu [2.82] approach for the hydroelastic analysis of a three-dimensional body moving in a viscous fluid [2.95].

Du et al [2.96] developed a revised approach of the three dimensional hydroelastic analysis of a ship traveling in waves. They extended the theory of Bishop et al [2.81] using translating, pulsating source distribution over the mean wetted surface area of the vessel. This singularity satisfies a speed dependent linearised free surface boundary condition and it is therefore more rigorous in accounting for forward speed effects. The method was illustrated for a semi-ellipsoid and the S175 containership, whose structures were idealised using finite elements. The predicted motions and distortions in regular waves, indicate that the dynamic responses are affected by the steady flow particularly when the translating, pulsating source distribution is used.

2.7 Conclusions

In this chapter the significance of FSI and particularly hydroelastic techniques as coupled engineering analyses tools useful for the design and safety of ship structures has been highlighted. In principle all current dynamic response methodologies are striving to improve the accuracy of the predicted responses for mono- and multi-hull vessels via adequate representation of the physics of the FSI domain, the effects of forward speed and the hull geometry non-linearities (e.g. flare and transom). Along these lines, it appears that hydroelasticity theory, compared to quasi-static and hydrodynamic methods, provides a physically more accurate idealisation of the FSI system and, consequently, more rigorous analysis by which dynamic responses, such as stresses, bending and torsional moments in waves are obtained. Although, in general, two-dimensional hydrodynamic and hydroelastic theories appear to provide good predictions for mono-hulled vessels, future research could concentrate on the development of improved three-dimensional hydroelastic, numerically more rigorous solutions (by means of impulse response functions in the time domain or fast algorithms). Such techniques should be able to model more accurately the dynamic behaviour of mono- or multi-hulled vessels. There is also a clear necessity for further experimental investigations by means of flexible models and full-scale measurements able to inspire confidence in the analytical predictions of hydroelastic results.

2.8 References

[2.1] Païdoussis, M.P.: Fluid-structure interactions, slender structures and axial flow, Vol. 1, Academic Press, London, UK, (1999).

[2.2] Soong, T.T.: Active structural control theory and practice, Longman scientific and technical, Essex, UK, (1990).

[2.3] Bear, J.: Dynamics of fluids in porous media, America Elsevier publishers Co., New York, (1972).

[2.4] Ransing, R.S., Hardy, S.J. and Gethin, D.T.: How to undertake finite element based thermal analyses, NAFEMS, UK, (1999).

[2.5] Bergan, P.G., Nestegard, A, Skeie, G.: On the solution of fluid-structure interaction problems in the maritime industry, European conference on computational mechanics (ECCM), Munich, Germany, (1999).

[2.6] Faltisen, O.M.: Sea loads on ships and offshore structures, Cambridge ocean technology series, Cambridge university press, UK, (1990).

[2.7] The society of Naval Architects and Marine Engineers (SNAME): Principles of Naval Architecture, New Jersey, USA, (1989).

[2.8] Report of ISSC: Committee II.1 on quasi-static response, 13th International Ship and Offshore Structures Congress, Trondheim, Norway, (1997).

[2.9] Report of ISSC: Committee II.1 on quasi-static response, 14th International ship and offshore structures congress, Nagasaki, Japan, (2000).

[2.10] Mansour, A.E., Lin, Y.H. and Paik, J.K.: Ultimate strength of ships under combined vertical and horizontal moments, International conference for the practical design of ships and mobile units (PRADS), 2: 844-856,Seoul, Korea, (1995).

[2.11] Mansour, A.E., Wirshing, P.H., Lucket, M.D., Plumpton, A.M., Lin, Y.H.: Structural safety of ships, Trans. SNAME, 105:61-98, (1997).

[2.12] Gordo, J.M. and Soares, C.G.: Approximate assessment of the ultimate longitudinal strength of hull girder, Journal of Ship Research, 40:60-69, (1996).

[2.13] Paik, J.K., Thayamballi, A.K. and Jung, S.C.: A simple formulation for predicting the ultimate strength of ships, Trans. SNAME, 104:23-35, (1996).

[2.14] Hu, S.Z.: Prediction of ultimate bending moment of ship hull using a simplified approach, Proceedings of the 15th Canadian congress of applied mechanics, Victoria, B.C. Canada, (1995).

[2.15] Froude, W.: On the rolling of ships, Trans. INA, 2:180-229, (1861).

[2.16] Froude, R.E.: The non-uniform rolling of ships, Trans. INA, 37:293-325, (1896).

[2.17] Kriloff, A.: A new theory of the oscillations of a ship on waves, Trans. INA, 40:135-196, (1896).

[2.18] Kriloff, A.: A general theory of the oscillations of a ship on waves, Trans. INA, 40:135-196, (1898).

[2.19] Mitchel, J.H.: The wave resistance of a ship, Phil. Magazine, 45:106-123, (1898).

[2.20] Lewis, F.M.: The inertia of water surrounding a vibrating ship, Trans. SNAME, 27:1-20, (1929).

[2.21] Haskind, M.D.: The hydrodynamic theory of ship oscillations in rolling and pitching, Technical Research Bulletin of SNAME, 12:3-43, (1953a).

[2.22] Haskind, M.D.: The oscillation of a ship in still water, Technical Research Bulletin of SNAME, 12:23-34, (1953b)

[2.23] Von Kerczek, C. and Tuck, E.O.: The representation of ship hulls by conformal mapping functions, Journal of Ship Research, 13:284-298, (1969).

[2.24] Westlake, P.C. and Wilson, P.A.: A new conformal mapping technique for ship sections, International Shipbuilding Progress, 47:5-22, (2000).

[2.25] Korvin Kroukovski, B.V.: Investigation of ship motions in regular waves, Trans. SNAME, 63:386-435, (1955).

[2.26] Korvin Kroukovski, B.V. and Jacobs, W.R.: Pitching and heaving motions of a ship in regular waves, Trans. SNAME, 65:590-632, (1957).

[2.27] Gerritsma, J. and Beukerlman, W.: The distribution of the hydrodynamic forces on a heaving and pitching shipmodel in still water, Publication no. 22, Shipbuilding Lab., Delft university of Technology, Denmark, (1964).

[2.28] Grim, O.: A method for a more precise computation of heaving and pitching motions both in smooth water and in waves, Proceedings of the 3rd symposium on naval hydrodynamics, 1:483-518, Schevenigen, Netherlands, (1960).

[2.29] Timman, R. and Newman, J.N.: The coupled damping coefficients of symmetric ships, Journal of Ship Research, 5:34-55, (1962).

[2.30] Ogilvie, T.F.: Nonlinear high Froude number free surface problems, Journal of Engineering Mathematics, 1:215-235, (1967).

[2.31] Salvesen, N., Tuck, E.O. and Faltisen, O.: Ship motions and sea loads, Trans. SNAME, 78:250-287, (1970).

[2.32] Vugts, J.H.: The hydrodynamic forces and ship motions in oblique waves, The Netherlands ship research center (NSRC), Internal report, 150S, (1971).

[2.33] Faltisen, O. and Zhao, R.: Numerical prediction of ship motions at high forward speed, Phil. Trans. of R. Soc. Lond., 334:241-252, (1997).

[2.34] Newman, J.N. and Tuck, E.O.: Current progress in the slender-body theory of ship motions, Proceedings of the 5th symposium on naval hydrodynamics, 1:129-167, Washington D.C., USA, (1964).

[2.35] Newman, J.N.: The theory of ship motions, Advances In Applied Mechanics, 18:222-283, (1977).

[2.36] Newman, J.N. and Sclavounos, P.D.: The unified theory of ship motions, Proceedings of the 13th symposium on naval hydrodynamics, 1:129-167, Japan, (1980).

[2.37] Kashiiwagi, M.: Numerical seakeeping calculations based on slender ship theory, Ship Technology Research Bulletin (SNAME), 44: 167-192, (1997).

[2.38] Faltinsen, O.M. and Michelsen, F.C.: Motions of large structures in waves at zero Froude number, International symposium on the dynamics of marine vehicles and structures in waves, 1:91-106, Bishop et al editors, IMEch, London, UK, (1974).

[2.39] Garrison, C.J.: Hydrodynamic loading on large offshore structures and three-dimensional source distribution methods, Numerical methods in offshore engineering, John Willey, 87-140, (1978).

[2.40] Inglis, R.B. and Price, W.G.: Comparisons of calculated responses for arbitrary shaped bodies using two- and three-dimensional theories, International Shipbuilding Progress, 27:86-95, (1980).

[2.41] Inglis, R.B. and Price, W.G.: A three-dimensional ship motion theory – Comparison between theoretical predictions and experimental data of the hydrodynamic coefficients with forward speed, Trans. RINA, 124:141-157, (1982).

[2.42] Guevel, P. and Bougis, R.: Ship motions with forward speed in infinite depth, International Shipbuilding Progress, 29:20-33, (1982).

[2.43] Ba, M. and Guilbaud, M.: A fast method of evaluation for the translating and pulsating Green's function. Ship Technology Research Bulletin (SNAME), 42(2), (1995).

[2.44] Lin, W.M. and Yue, D.K.P.: Numerical solutions for large amplitude ship motions in the time domain, Proceedings of the 18th symposium of naval hydrodynamics, USA, (1990).

[2.45] Liapis, S.J. and Beck, R.F.: Seakeeping computations using time domain analysis, Proc. of the 4th International conference on numerical hydrodynamics, National academy of sciences, Washington, D.C., 34-54, (1985).

[2.46] Liapis, S.J.: Time domain analysis of ship motions, Report no. 302, Department. of Naval Architecture and Marine Engineering, University of Michigan, Ann Arbor, Michigan, USA, (1986).

[2.47] King, B.W.: Time domain analysis of wave exciting forces on ships and bodies, Technical report 306, Department. of Naval Architecture and Marine Engineering, University of Michigan, Ann Arbor, Michigan , USA, (1987).

[2.48] King, B.W., Beck, R.F. and Magee, A.R.: Seakeeping calculations with forward speed using time domain analysis, Proceedings of the 17th symposium on naval hydrodynamics, USA, (1988).

[2.49] Korsmeyer, F.T., Lee C.H., Newman, J.N. and Sclavounos, P.D.: The analysis of wave effects on tension leg platforms, Proceedings of the international conference on offshore mechanics and arctic engineering (OMAE), Huston, USA, (1988).

[2.50] Maskew, B., Tidd, D.M. and Fraser, J.S.: Prediction of non-linear hydrodynamic characteristics of complex vessels using a time domain approach, Proceedings of the 6th international conference on numerical ship hydrodynamics, USA, (1993).

[2.51] Nakos, D.E., Kring, D.E. and Sclavounos, P.D.: Rankine panel methods for time domain free surface flows, Proceedings of the 6th international conference on numerical ship hydrodynamics, USA, (1993).

[2.52] Kring, D.C., Huang, Y.F., Sclavounos, P.D., Vada, T. and Braathen, A.: Nonlinear ship motions and wave induced loads by Rankine panel method, Proceedings of the 21st symposium on naval hydrodynamics, Trondheim, Norway, (1996).

[2.53] Lin, W.M., Meinhold, M., Salvensen, N. and Yue, D.K.P.: Large amplitude motions and wave loads for ship design, Proceedings of the 20th symposium of naval hydrodynamics, Santa Barbara, California, (1994).

[2.54] Beck, R.F. and Magee, A.: Time domain analysis for predicting ship motions, International symposium on the dynamics of marine vehicles and structures in waves, Price W.G. et al editors, Elsevier Science Publishers, UK, (1991).

[2.55] Bingham, H.: Simulating ship motions in the time domain, PhD thesis, Massachusetts Institute of technology, Cambridge, Massachusetts, USA, (1994).

[2.56] Magee, A.R.: Seakeeping calculations using a time domain method, Proceedings of the 20th symposium of naval hydrodynamics, Santa Barbara, California, USA, (1994).

[2.57] Inglis, C.E.: Natural frequencies and modes of vibration in beams of non-uniform mass and section, Trans. INA, 2:145-166, (1929).

[2.58] Heller, S.R and Ambramson, H.N.: Hydroelasticity - a new naval science, Journal of the American Society of Naval Engineers, 71:205-209, (1959).

[2.59] Kalinowski, A.J.: Fluid structure interaction - shock and vibration computer programs, reviews and summaries; Naval Research Laboratory; 1:405-452, Washington. D.C., USA, (1975).

[2.60] Chen, J.H. and Pierucci, M.: Underwater fluid - structure interaction; Part I,II,III shock and vibration digest, (1977).

[2.61] Zienkiewicz, O.C. and Bettess, P.: Fluid structure interaction, symposium of ocean structures dynamics, Oregon State University, USA, (1982).

[2.62] Bishop, R.E.D. and Price, W.G.: Hydroelasticity of Ships, Cambridge University Press, UK, (1979).

[2.63] Bishop, R.E.D., Price, W.G. and Tam, P.K.Y.: A unified dynamic analysis of a ship response to waves, Trans. of RINA, 119:363-390, (1977).

[2.64] Bishop, R.E.D., Price, W.G. and Temarel, P.: Antisymmetric vibration of ship hulls, Trans. of RINA, 122:197-208, (1980).

[2.65] Bishop, R.E.D., Chalmers, D.W., Price, W.G. and Temarel, P.: The dynamic characteristics of unsymmetrical ship structures, Trans. RINA, 128:205 - 215, (1986).

[2.66] Bishop, R.E.D., Price, W.G. and Tam, P.K.Y.: On the dynamics of slamming, Trans. of RINA, 120:259-280, (1980).

[2.67] Belik, O., Bishop, R.E.D. and Price, W.G.: On the slamming response of ships to regular head waves, Trans. of RINA, 122:250-262, (1980).

[2.68] Belik, O., Bishop, R.E.D. and Price, W.G.: Comparison of slamming theories in the time simulation of ship responses in irregular waves, International Shipbuilding Progress, 29:173-187, (1982).

[2.69] Belik, O., Bishop, R.E.D. and Price, W.G.: A simulation of ship responses due to slamming in irregular head waves, Trans. of RINA, 125:237-253, (1983).

[2.70] Bishop, R.E.D., Clarke, J.D. and Price, W.G.: Comparison of full scale and predicted responses of two frigates in severe weather trial, Trans. RINA, 126:123-166, (1984).

[2.71] Belik, O., Bishop, R.E.D. and Price, W.G.: Influence of bottom and flare slamming on structural responses, Trans. RINA, 130:261-275, (1988).

[2.72] Bishop, R.E.D., Price, W.G., and Temarel, P.: A theory on the loss of MV OBO Derbyshire, Trans. RINA, 127:169-186, (1991).

[2.73] Bishop, R.E.D., Price, W.G., and Temarel, P.: A hypothesis concerning the disastrous failure of the Onomichi Maru, Trans. RINA, 127:169-186, (1985).

[2.74] Bishop, R.E.D., Huot, J.P., Price, W.G., and Temarel, P.: On the distribution of symmetric shearing force and bending moment in hulls, Trans. RINA, 128:205-215, (1984).

[2.75] Aksu, S., Price, W.G. and Temarel, P.: Loads and stress distributions on bulk carriers and tankers in various loading conditions, RINA international conference on Tankers and Bulkers-The way ahead, London, UK, (1992).

[2.76] Domnisoru, L. and Domnisoru, D.: The unified analysis of springing and whipping phenomena. Trans. RINA, 140:19-36, (1998).

[2.77] Wu, M.K. and Moan, T.: Linear and non-linear hydroelastic analysis of high speed vessels, Journal of Ship Research, 40:149-163, (1996).

[2.78] Hermundstad, O.A., Wu, M.K. and Moan, T.: Hydroelastic response analysis of a high speed monohull, Proceedings of the international conference on hydroelasticity in marine technology, Tordheim, Norway, (1994).

[2.79] Xia, J. and Wang, Z.: Time domain hydroelasticity theory of ships responding to waves, Journal of Ship Research, 41:286-300, (1997).

[2.80] Xia, J., Wang, Z. and Jensen, J.J.: Non-linear wave loads and ship responses by a time domain strip theory, Marine Structures, 11,101-123, (1998).

[2.81] Bishop, R.E.D, Price, W.G. and Wu, Y.: A general linear hydroelasticity theory of floating structures moving in a seaway, Phil. Trans. Royal Soc. London, A316: 375-426, (1986).

[2.82] Price, W.G. and Wu, Y.: The influence of non-linear fluid forces in the time domain responses of flexible SWATH ships excited by a seaway, Proceedings of the international conference on offshore mechanics and arctic engineering (OMAE), 2:125-135, (1989).

[2.83] Ergin, A., Price, W.G., Randall, R. and Temarel, P.: Dynamic characteristics of a submerged, flexible cylinder vibrating in finite water depths, Journal of ship Research, 36:154-167, (1992).

[2.84] Aksu, S., Price, W.G and Temarel, P.: A three-dimensional theory of ship slamming in irregular oblique seaways, International symposium on the dynamics of marine vehicles and structures in waves, Price W.G. et al editors, Elsevier Science Publishers, UK, (1991).

[2.85] Aksu, S., Price, W.G and Temarel, P.: A comparison of two-dimensional and three-dimensional hydroelasticity theories including the effects of slamming, Proceedings of IMechE, 205:3-15, (1991).

[2.86] Price, W.G., Temarel, P. and Keane, A.J.: Hydroelastic analysis of a SWATH in waves, In International Conference of Hydroelasticity in Marine Technology, 231-243, Trondheim, Norway, (1994).

[2.87] Qian, J.Y. and Li, Q.H.: The theoretical and experimental study on the hydroelastic behaviour of a SWATH travelling in waves, Proceedings of the second national conference on Marine Technology, China, (1996).

[2.88] Lundgen, J., Price, W.G. and Wu, Y.:A hydroelastic investigation into the behaviour of a floating dry dock in waves, Trans. RINA, 131:213-231, (1989).

[2.89] Aksu, S., Price, W.G., Suhrbier, K.R. and Temarel, P.: A comparative study of the dynamic behaviour of a fast patrol boat travelling in rough seas, Marine Structures, 6:421-441, (1993).

[2.90] Miao, S.H., Price, W.G. and Temarel, P.: The hydroelastic behaviour of multi hulls travelling in a seaway, Proceedings 3rd international conference for advances in marine structures, Dunfermline, (1997).

[2.91] Bingham, A.E., Hampshire, J.K., Miao, S.H. and Temarel, P.: Motions and loads of a trimaran travelling in regular waves, The 6th international conference on fast ship transportation, 2:167-176, Southampton, UK, (2001).

[2.92] Louarn, F.H. and Temarel, P.: An investigation of the structural dynamics of a racing yacht, Proceedings of the 14th Chesapeake sailing yacht symposium, 123-142, USA, (1999).

[2.93] Price, W.G., Salas Inzunza, M.A. and Temarel, P.: The dynamic behaviour of a monohull in oblique waves using two- and three-dimensional fluid-structure interaction models, Submitted to RINA, (2000).

[2.94] Fathi, D.E., Lee, C.H., and Newman, J.N.: Computation of wave induced motions on a flexible container, International conference on hydroelasticity in marine technology, Tordheim, Norway, (1994).

[2.95] Xia, J.A. and Wu, Y.S.: A general interface boundary condition of fluid-structure interaction, Ship Behaviour Research Bulletin, Vol. 2, (1993).

[2.96] Du, S.X., Wu, Y. and Price W.G.: Forward speed effect on the structural responses of a ship travelling in waves, Proceedings of the 2nd international conference of hydroelasticity in marine technology, 1:401-410, (1998).

[2.97] Faulkner, J.A., Clarke, C.S., Smith, C.S. and Faulkner, D.: The loss of HMS COBRA – A Reassesment, Trans. RINA, 127:125-152, (1985).

[2.98] Class LR, Rules for the classification of ships, Part 3 - Ship structures, Chapter 2 - Longitudinal strength, (2001).

[2.99] Class BV, Rules for the classification of ships, Part B-Hull and stability, Chapter 4 - Longitudinal strength of ocean going vessels, (2002).

[2.100] Class ABS, Rules for the classification of steel vessels, Part 3 - Hull construction and equipment (2002).

[2.101] Class DNV, Rules for the classification of ships, Part3 - Structures and equipment main class, Chapter 1 - Hull structural design for ships of length 100m or above (2002).

[2.102] Class GL, Rules for classification and construction, Part 1 - Seagoing ships, Chapter 1 - hull structures (2000).

Chapter 3

Theoretical Background

3.1 Introduction

The mathematical background related to the Bishop, Price et al two- and three-dimensional hydroelasticity theories has been well established in literature [3.1,3.2] and therefore, in this chapter only a brief description of the relevant basic formulations is presented. At first stage the principles of the two- and three-dimensional fluid-structure interaction models are outlined. Secondly, the hydroelastic formulations related to the evaluation of the steady state dynamic response and seaway induced dynamic loads are presented.

3.2 Fundamental hydrodynamic assumptions

In both two- and three-dimensional hydroelasticity theories the analysis of the wet structure is based upon the so-called potential flow theory assumptions according to which the fluid domain, extending to infinite depth, is treated as inviscid, incompressible and irrotational [2.1,2.2]. Accordingly, within the context of linearity (i.e. by assuming that unsteady motions of the fluid remain small) the potential function is decomposed into a 'steady' term $(\overline{\Phi})$ dependant (in calm water) on a constant forward speed $(\overline{U})$ and a 'parasitic' component (Φ) (see figure 3.1 and equation 3.1)

$$\Phi(X_0, Y_0, Z_0, t) = \overline{U}\ \overline{\Phi}(X, Y, Z) + \Phi(X, Y, Z)e^{i\omega_e t} \tag{3.1}$$

The time dependence of the fluid motion is dictated by the encounter frequency (ω_e) defined as:

$$\omega_e = \omega - \overline{U}\frac{\omega^2}{g}\cos\chi \tag{3.2}$$

where (ω) is the incident wave frequency and (χ) represents the angle (assumed constant), at which the boat is heading into waves (e.g. $\chi=180^0$ in head seas).

Throughout the fluid domain, the physical principle of mass conservation (continuity assumption) implies that the velocity potential (Φ) must satisfy Laplace's equation:

$$\nabla^2\Phi = 0 \tag{3.3}$$

A unique solution for the potential flow component is then provided via application of the linearised boundary conditions acting upon the body, on the free surface of the body and at infinite distances from the body. This is achieved with different methodology in two- and three-dimensional hydroelasticity theories (see sections 3.5 and 3.6).

3.3 Generalised response for two- and three-dimensional FSI domains

In both two- and three- dimensional hydroelasticity theories the total deflection of a ship hull undergoing total steady motion, at constant forward speed $(\overline{U})$, may be considered as the summation of still water and time dependent bodily motions and flexible distortions. The former refers to the flat water configuration of the hull acted upon gravity and buoyancy forces. The latter involves fluctuations which take place about the still water equilibrium condition due to motion of the ship at constant heading (χ) through regular waves. In such circumstances, it is convenient to describe the motion of the ship within a set of equilibrium axes (OXYZ) (where O denotes the origin)[3.1,3.2]. Such system refers to the hull geometry and it is assumed to be right handed so that OX (denoting the mass direction) and OY lay in the still water plane whilst OZ points vertically upwards (see figure 3.1).

The frame (OXYZ) is thought of as travelling with a forward speed $(\overline{U})$ along the OX direction. The linear equations of motion of the discretised structure can then be expressed in matrix form as:

$$[M]\{\ddot{U}\}+[B]\{\dot{U}\}+[K]\{U\}=\{P\}+\{F\}+\{g\} \tag{3.4}$$

where $[M],[B],[K]$ are known as the mass, structural damping and stiffness matrices respectively. Provided that they relate to the dry structure, they are symmetric real matrices

containing (n×n) submatrices composed of (6×6) corresponding to (n) nodes featuring six degrees of freedom each (see figures 2.2 and 3.1). Accordingly, the displacement vector at any point in the structure is defined as $\{U\}=\{u,v,w,\theta_x,\theta_y,\theta_z\}$ where u,v,w and $\theta_x,\theta_y,\theta_z$ denote translations and rotations with respect to the (X,Y,Z) directions respectively.

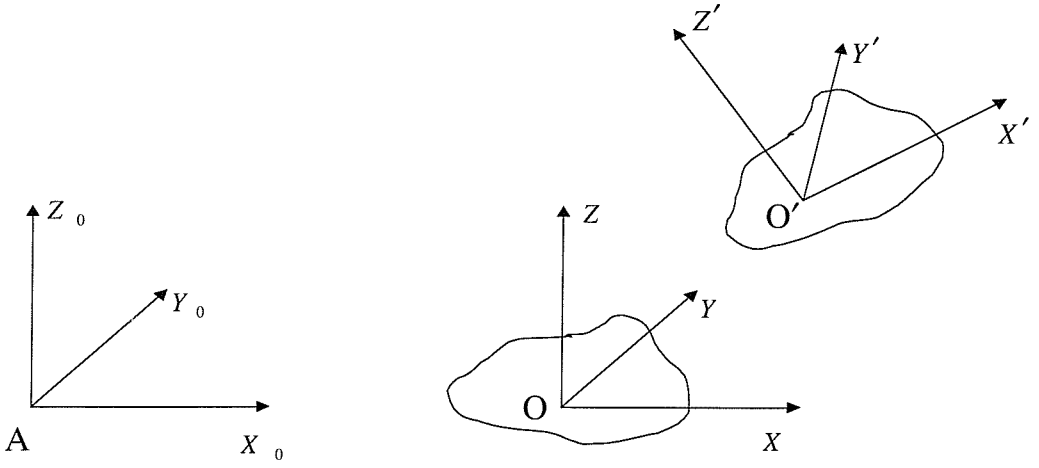

Fig. 3.1 Right-handed systems of axes to define the fluid actions and structural dynamic characteristics; ($AX_0Y_0Z_0$) = fixed space reference frame; (OXYZ) = equilibrium frame of reference moving with a ship whilst remaining parallel to ($AX_0Y_0Z_0$); (O′X′Y′Z′) = body fixed axis system such that it coincides with (OXYZ) in the absence of unsteady disturbance.

According to Rayleigh's theorem [3.3], the total motion of the structure, including rigid and flexible terms, may be expressed as an aggregate of displacements in its principal modes. It follows that the vector of nodal displacements may be written as:

$$\{U\}=\sum_{r=1}^{m} p_r(t)\{\overline{D}_r\} \tag{3.5}$$

or

$$\{U\}=[\overline{D}]\{p\} \tag{3.6}$$

in matrix form, where $[\overline{D}]$ is the matrix of the mode shape vectors; the vector $\{\overline{D}_r\}$ represents the r^{th} principal mode shape and the terms $p_r(t)$ form a set of time dependent principal coordinates. After substituting (3.6) into (3.4), premultiplying by $[\overline{D}]^T$ and applying orthogonality conditions governing the principal mode shapes [3.1,3.2] the generalised form of the equation of motion is expressed as:

$$[a]\{\ddot{p}\}+[b]\{\dot{p}\}+[c]\{p\}=\{Z\}+\{G\}+\{\Delta\} \tag{3.7}$$

where,

- $[a]=[\overline{D}]^T[M][\overline{D}]$ is the generalised mass matrix (diagonal);
- $[b]=[\overline{D}]^T[B][\overline{D}]$ is the generalised structural damping matrix (diagonal). In practice $b_{rr}=2\nu_r\omega_r a_{rr}$, where (ω_r) and (ν_r) are the r^{th} natural frequency and modal damping factor respectively;
- $[c]=[\overline{D}]^T[K][\overline{D}]$ is the generalised structural stiffness matrix(diagonal).Orthogonality conditions imply that $c_{rr}=\omega_r^2 a_{rr}$;
- $\{Z\}=[\overline{D}]^T[P]=\{Z_1,Z_2,....,Z_m\}$ is the generalised fluid force vector containing (m) terms corresponding to a set of (m) selected principal modes. These terms are obtained, in principle, from integration over the instantaneous wetted surface of the elements used to idealise the body;
- $\{\Delta\}=[\overline{D}]^T[F]$ is the generalised concentrated force vector (m×1).
- $\{G\}=[\overline{D}]^T[g]$ is the generalised gravitational force vector (m×1). Component terms are obtained from integration over the whole body.

The term 'generalised' relates to the notion that the principal mode shapes of the dry structure are used as generalised coordinates in the equation of motion of the structure. Assuming that the system is freely floating (i.e. no displacement condition is imposed) the principal coordinates fall into two categories namely $\{p\}=\{\{p_R\},\{p_D\}\}^T$ where $\{p_R\}=\{p_1,p_2,...,p_6\}$ refers to the six rigid body modes (3 translations and 3 rotations in space) and $\{p_D\}=\{p_7,...,p_m\}$ relates to (m-6) flexible distortions (see figure 2.2). The introduction of rigid body motions implies that equation (3.7) may be partitioned as:

$$\begin{bmatrix}[a_R] & 0\\ 0 & [a_D]\end{bmatrix}\begin{Bmatrix}\ddot{p}_R\\ \ddot{p}_D\end{Bmatrix}+\begin{bmatrix}0 & 0\\ 0 & [b_D]\end{bmatrix}\begin{Bmatrix}\dot{p}_R\\ \dot{p}_D\end{Bmatrix}+\begin{bmatrix}0 & 0\\ 0 & [c_D]\end{bmatrix}\begin{Bmatrix}p_R\\ p_D\end{Bmatrix}=\begin{Bmatrix}Z_R\\ Z_D\end{Bmatrix}+\begin{Bmatrix}G_R\\ G_D\end{Bmatrix}+\begin{Bmatrix}\Delta_R\\ \Delta_D\end{Bmatrix} \tag{3.8}$$

where $[a_R]$ and $[b_D]$ (considering the general formulation for damping) are symmetric, while $[a_D]$ and $[c_D]$ are diagonal square matrices. Seakeeping theory concentrates on the rigid motions given by:

$$[a_R]\{\ddot{p}_R\} = \{Z_R\} + \{G_R\} + \{\Delta_R\} \tag{3.9}$$

In this case $[a_R]$ is a 6×6 matrix. The six degrees of freedom are: surge (r=1), sway(r=2), heave(r=3), roll(r=4), pitch(r=5) and yaw(r=6). The matrix of the generalised masses is:

$$[a_R] = \begin{bmatrix} m & 0 & 0 & 0 & 0 & 0 \\ 0 & m & 0 & 0 & 0 & 0 \\ 0 & 0 & m & 0 & 0 & 0 \\ 0 & 0 & 0 & I_{44} & -I_{45} & -I_{46} \\ 0 & 0 & 0 & -I_{54} & I_{55} & -I_{56} \\ 0 & 0 & 0 & -I_{64} & -I_{65} & I_{66} \end{bmatrix}$$

where (m) is the mass of the structure and the quantities I_{44},I_{45},....etc. are the moments and products of inertia in the equilibrium axis system. Note that for a port starboard symmetric structure, $I_{45}=0=I_{56}$ but $I_{46}\neq 0$. This last argument shows that when rigid body modes are considered, matrix $[a]$ is no longer diagonal. Therefore in a more general form equation (3.7) can be expressed as:

$$\sum_{k=1}^{m}\left[a_{rk}\ddot{p}_k(t) + b_{rk}\dot{p}_k(t)\right] + c_{rr}p_r(t) = Z_r(t) + G_r + \Delta_r \tag{3.10}$$

The r^{th} generalised external fluid force may be expressed as

$$Z_r(t) = \Xi_r(t) + H_r(t) + R_r(t) + \overline{R}_r \tag{3.11}$$

The integration of the pressure components leading to equation (3.11) is carried out, in principle, over the instantaneous wetted surface which is taken as a time dependent variation about the mean wetted surface. The mathematical symbols used in the latest equation represent:

- $\Xi_r(t) = \Xi_{0r}(t) + \Xi_{Dr}(t)$ is the r^{th} generalised wave exciting force. The terms $\Xi_{0r}(t)$ and $\Xi_{Dr}(t)$ express the Froude-Kriloff (incident waves) and the diffraction forces and moments, respectively;

- $H_r(t) = -\sum_{k=1}^{m}\left[A_{rk}\ddot{p}_k(t) + B_{rk}\dot{p}_k(t)\right]$ is the r^{th} generalised radiation force generated by the motions and distortions of the structure. The terms (A_{rk}) and (B_{rk}) are in phase with acceleration and velocity respectively and express the generalised added mass and damping. Both are associated with the r^{th} mode but also account for the effect of coupling with a unit amplitude displacement in the k^{th} mode;
- $R_r(t) = -\sum_{k=1}^{m} C_{rk} p_k(t)$ describes the r^{th} generalised restoring force dependent on the fluid hydrostatic pressure field; (C_{rk}) is a restoring coefficient associated with the r^{th} mode, including coupling effects due to a unit amplitude displacement in the k^{th} mode;
- $\overline{R}_r$ represents the generalised contribution from hydrostatic effects (e.g. buoyancy forces) which is independent of all time varying motions.

Equation (3.10) may be rewritten as

$$\begin{aligned}
&\sum_{k=1}^{m}\left[a_{rk}\ddot{p}_k(t) + b_{rk}\dot{p}_k(t)\right] + \omega_r^2 a_{rr} p_r(t) \\
&= \Xi_r(t) + H_r(t) + R_r(t) + \overline{R}_r + G_r + \Delta_r \qquad \text{for r= 1,2,...,m.} \\
&= \Xi_r(t) - \sum_{k=1}^{m}\left[A_{rk}\ddot{p}_k(t) + B_{rk}\dot{p}_k(t)\right] - \sum_{k=1}^{m} C_{rk} p_k(t) + \overline{R}_r + G_r + \Delta_r
\end{aligned}$$

By assuming that no concentrated forces (Δ_r) are applied and extracting the steady state conditions $\left(\overline{R}_r + G_r = 0\right)$, one obtains:

$$c_{rr} p_r(t) + \sum_{k=1}^{m}\left[(a_{rk} + A_{rk})\ddot{p}_k(t) + (b_{rk} + B_{rk})\dot{p}_k(t) + C_{rk} p_k(t)\right] = \Xi_r(t), \text{ for r= 1,2,...,m.}$$

Transferring the hydrodynamic inertia, damping and restoring terms to the left hand side leads to the matrix form expression:

$$[[a]+[A]]\left\{\ddot{p}(t)\right\} + [[b]+[B]]\left\{\dot{p}(t)\right\} + [[c]+[C]]\{p(t)\} = \{\Xi(t)\} \qquad (3.12)$$

which corresponds to a Lagrangean equation of motion for a linear dynamic system. The system submatrices are made up of a structural submatrix specific to the dry hull (lower case) and a hydrodynamic submatrix (capital) whose elements are dependent on the encounter

frequency component (ω_e). Hence, equation (3.12) describes the **dynamic interaction between the fluid and the structure**.

3.4 Two-dimensional hydroelasticity

3.4.1 2D dry analysis

In two-dimensional hydroelasticity theory for the simulation of the *symmetric* in vacuo vibrations the hull is generally modelled as a non-uniform Timoshenko beam freely vibrating in vacuo in absence of any damping effects [3.1]. The typical Timoshenko's beam formulation has been updated by Bishop et al [3.1,3.4] to allow for warping effects which become significant in *antisymmetric* motion especially for hulls with large deck openings. An alternative beam model using a Vlasov beam idealisation was also investigated by Bishop et al [3.6] but it has not been applied to hydroelastic investigations.

Timoshenko's beam theory assumes that the rotation of the cross section is considered as the sum of the shearing angle and the rotation of the neutral axis [3.1]. Being concerned only with the extraction of the natural frequencies and principal modes and by excluding all forcing terms, damping terms, shear strain and bending rotation the equations of motion describing the horizontal bending of a *uniform* Timoshenko beamlike hull for the r^{th} principal distortion mode (where $u(x,t) = u_r(x)\sin\omega_r t$ and $\phi(x,t) = \phi_r(x)\sin\omega_r t$) takes the form:

$$EI\frac{d^4u_r(x)}{dx^4} + \omega_r^2\left[I_z + \frac{EI\mu}{kAG}\right]\frac{d^4u_r(x)}{dx^4} - \frac{EI\mu\bar{z}\omega_r^2}{kAG}\frac{d^2\phi_r(x)}{dx^2} - \mu\omega_r^2\left[u_r(x) - \bar{z}\phi_r(x)\right] + \frac{\mu I_z\omega_r^4}{kAG}\left[u_r(x) - \bar{z}\phi_r(x)\right] = 0 \tag{3.13}$$

where, (I_z) is the rotary inertia term; (G) is the shear modulus; (A) is the cross-sectional area; (k) is Timoshenko's shear coefficient which takes account of the shape of the cross-section. The terms (EI) and (kAG) are known as flexural and shear rigidity respectively while $(\bar{z})$ represents the distance between shear (S) and gravity (C) centers (see figure 3.2). Please note that equation (3.13) provided that $(\bar{z} = 0)$ and I_z is replaced by I_y (the vertical moment of inertia) expresses the vertical bending of a uniform Timoshenko beam. For torsion,

$$C\frac{d^2\phi_r(x)}{dx^2} - C_w\frac{d^4\phi_r(x)}{dx^4} + I_S\omega_r^2\phi_r(x) - \mu\bar{z}(x)\omega_r^2\phi_r(x) - \mu\bar{z}\omega_r^2 u_r(x) = 0 \quad (3.14)$$

where $I_s = I_c + \mu\bar{z}^{-2}$

In the above equations (I_s) and (I_c) are the moment of inertia per unit length passing through the shear and gravity centers of the cross section; C (=EJ) is the torsional rigidity; C_w(=EI_w) is the warping rigidity. The last two quantities are related to the torsional constant (J) and the sectorial moment of inertia (I_w) (expressing the warpage of the cross section) respectively (see figure 3.2). Apparently, equation (3.14) is not meaningful for in vacuo symmetric vibrations. It is also worthwhile noting that for the case of a non-uniform beam representing a monohull equations (3.13),(3.14) are expressed in form of partial derivatives, while the inertia, mass and rigidity components are functions varying along the length of the ship.

Since the functions $u_r(x)$ and $\phi_r(x)$ are related only to their derivatives (of even order) it is expected that solutions of the equations will have the general form $u_r(x) = u_r(x)e^{\lambda x}$ and $\phi_r(x) = \phi_r(x)e^{\lambda x}$ respectively. Thus, after formulating the characteristic function (polynomial of 8th order) applying Crammers' rule as well as the boundary conditions for a free-free beam structure (that is shear force, bending and twisting moments vanish as well as there is no warping constraints at the free ends of the structure) the following equations (3.15,3.16,3.17) are formulated

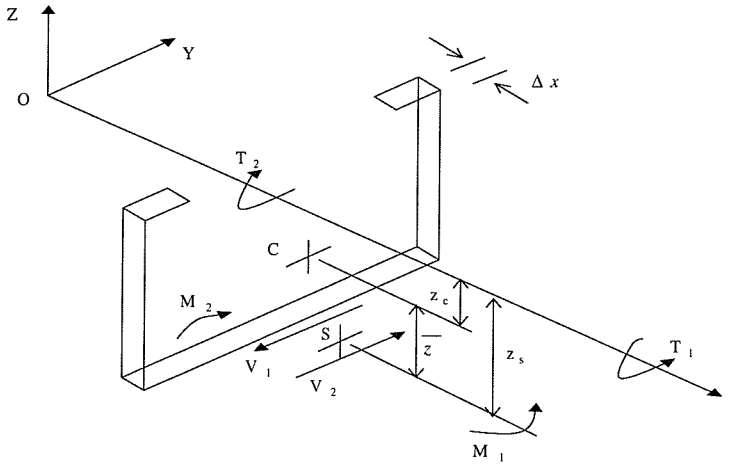

Fig.3.2 Transverse section of a hull showing the notations employed in antisymmetric dry analysis (C = centre of gravity; S= shear centre; M = horizontal bending moment, T = twisting moment).

$$u_r''(x)+\frac{\mu\omega_r^2}{kAG}\left[u_r(x)-\bar{z}\phi_r(x)\right]=0 \tag{3.15}$$

$$I_z\omega_r^2u_r'(x)+EI\left[u_r'''(x)+\frac{\mu\omega_r^2}{kAG}\left[u_r'(x)-\bar{z}\phi_r'(x)\right]\right]=0 \tag{3.16}$$

$$C\phi_r'(x)-C_w\phi_r'''(x)=0 \tag{3.17}$$

Equations (3.15) and (3.16) are related to symmetric bending (pure horizontal or pure vertical bending of the hull provided that $\bar{z}=0$) [3.1,3.4]. Equation (3.17) is related to pure torsion of the hull. These equations are coupled to simulate the in vacuo antisymmetric motion (coupled horizontal bending and twisting) of the hull [3.1,3.4]. It is worthwhile to mention that the current methodology does not account for the structural discontinuities that could occur between the open/closed parts of a ship's deck structure. Also although it accounts for the effects of warping no additional terms simulating the so-called warping restraint effects (bi-moment and warping torsional moment direct and shear stresses respectively) which are important for ship hulls with large deck openings are included. The implications of this omission are clearly discussed and demonstrated in chapters 4 and 5.

3.4.2 2D wet analysis

In two-dimensional hydroelasticity the unique solution of the potential flow component (see section 3.2) is achieved via implementation of the revised Salvensen, Tuck, Faltinsen [3.1] strip theory. This typical strip theory formulation operates under the two-dimensional potential flow analysis principles [3.1,3.7] according to which the velocity potentials of an oscillating strip should satisfy Laplace's equation along with:

1. the body boundary condition expressing the impermeability (i.e. that no fluid enters or leaves the body surface)

$$\frac{\partial\Phi}{\partial n}=0 \tag{3.18}$$

on the body surface, where $\partial/\partial n$ denotes differentiation along the normal to the body surface;

2. the linearised free surface (x=0) condition:

$$k\Phi+\frac{\partial\Phi}{\partial x}=0 \tag{3.19}$$

where k denotes the wave number;

3. the radiation condition at infinity ($x \rightarrow \infty$);
4. the no flow condition at infinite depth ($y \rightarrow \infty$).

After the evaluation of the free in vacuo modal characteristics of the Timoshenko beam-like hull (see section 3.5.1) the fluid action is applied in the form of external forces and is divided in two parts [3.1]:

1. the Froude-Kriloff contribution due to the incident wave which is undisturbed by the presence of the hull;
2. the dynamic contribution which includes the effects of wave diffraction.

Accordingly, the determination of the added mass and damping coefficients is reduced to a two-dimensional problem and the coefficients are determined for a number of sections along the ship (approximated using Lewis or multiparameter conformal transformations) swaying, heaving and rolling harmonically at the encounter frequency of the free surface [3.5]. As shown by Bishop et al [3.1,3.8] the hydrodynamic terms of equation (3.12) for the symmetric motions and distortions (i.e. heave and pitch) can be expressed as:

$$A_{rk} = \int_0^L \left[m(x)w_r(x)w_k(x) + \frac{\overline{U}^2}{\omega_e^2} m(x)w_r'(x)w_k'(x) + \right.$$
$$\left. \frac{\overline{U}}{\omega_e^2} N(x)\left\{ w_r'(x)w_k(x) - w_k'(x)w_r(x) \right\} \right] dx - \qquad (3.20)$$
$$\frac{\overline{U}^2}{\omega_e^2} \left| m(x)w_k(x)w_r'(x) \right|_0^L + \frac{U}{\omega_e^2} \left| N(x)w_k(x)w_r(x) \right|_0^L$$

for the fluid added mass;

$$B_{rk} = \int_0^L \left[N(x)w_r(x)w_k(x) + \right.$$
$$\left. \overline{U}m(x)\left\{ w_r(x)w_k'(x) - w_k(x)w_r'(x) \right\} \right] dx - \qquad (3.21)$$
$$\frac{\overline{U}^2}{\omega_e^2} \left| N(x)w_k(x)w_r'(x) \right|_0^L + -\overline{U} \left| m(x)w_k(x)w_r(x) \right|_0^L$$

for the fluid added damping;

$$C_{rk} = \rho g \int_0^L B(x) w_k(x) w_r(x) dx \tag{3.22}$$

for the fluid restoring component; and

$$\Xi_k = \int_0^L w_k(x) Z(x,t) dx \tag{3.23}$$

for the exciting wave forces vector.

In equations (3.20) to (3.23) the term $(\overline{U})$ represents the forward reference speed and $B(x)$ is the sectional beam. The sectional added mass $(m(x))$ and the sectional fluid damping $(N(x))$ depend not only on the position (x) along the length (L) of the ship but also on the encounter frequency (ω_e). The mode shapes $w_r(x)$ and $w_k(x)$ and their derivatives are obtained from the Timoshenko beam analysis. Finally, $Z(x,t)$ represents the generalised forcing vector at position x and is time dependent in accordance with the wave excitation. It is interesting to note that two-dimensional fluid properties depend on the particular two-dimensional hydrodynamic theory used. For instance equations (3.20) and (3.21) are those from theory developed by Salvesen at al [3.9]. In the two-dimensional theory of Gerritsma and Beulkerman [3.10] some speed dependant terms are not considered.

Expressions similar to equations (3.20) to (3.21) can be written for the antisymmetric motions (sway, roll and yaw). These equations are demonstrated by Price et al [3.1, 3.5] and they are not reproduced in this work due to length and complexity.

3.5 Three-dimensional hydroelasticity

3.5.1 3D dry analysis

In the dry analysis part of the generalised hydroelasticity theory a three-dimensional finite element modelling procedure is initially used to describe the dynamic behaviour of the structure in vacuo, in absence of any damping effects, as shown in the following equation:

$$[M]\{\ddot{U}\}+[K]\{U\}=0 \tag{3.24}$$

where $([M],[K])$ are the structural mass and stiffness matrices respectively and $\{U\}$ is the nodal displacement vector (see section 4.2.7). The trial solution $\{U\}=\{D\}e^{i\omega t}$ shows that non-trivial amplitude matrices $\{D\}$ exist provided the characteristic equation $\left|[K]-\omega^2[M]\right|=0$ is satisfied. Thus, the natural frequencies, the corresponding principal mode shapes of the structure as well as the dynamic characteristics (e.g. generalised masses, modal stresses etc) can be calculated.

By following the procedure highlighted in section 3.3 equation (3.24) is transformed into a set of uncoupled scalar equations corresponding to different vibration modes.

3.5.2 3D wet analysis

In the generalized hydroelasticity theory [3.2] the dynamics of a flexible body of arbitrary shape travelling in a seaway are described by means of a more complex hydrodynamic model. The fluid actions associated with the distorting three-dimensional wet structure are determined from a theoretical hydrodynamic model involving pulsating sources.

In three-dimensional hydroelasticity a unique solution of Laplace's equation requires that boundary conditions suited to the problem are specified on the free surface, at infinity from the body and on the body wetted surface. The formulation proposed by Newman [3.7] and adopted in seakeeping theory, has been generalised within the scope of hydroelasticity theory in order to admit flexible distortion related terms [3.2]. Furthermore, the problem has been simplified by means of linearisation of such boundary conditions whereby it is assumed that:

1. wave amplitudes remain small compared to the wave length;
2. the unsteady oscillations of the body and the surrounding flow are of small amplitude;

3. the perturbation of the steady flow due to the steady forward motion of the body is assumed negligible because the body is assumed to be thin or flat or, if genuinely three-dimensional, it is restricted to relatively low forward speeds.

The key relationships describing mathematically the required linearised boundary conditions could be summarised as follows [3.2]:

1. On the free surface (Z=0), the incident, diffraction and radiation potentials obey the kinematic boundary condition

$$\overline{U}^2 \frac{\partial^2 \Phi}{\partial X^2} - 2i\omega_e \overline{U} \frac{\partial \Phi}{\partial X} - \omega_e^2 \Phi + g \frac{\partial \Phi}{\partial Z} = 0 \qquad (3.25)$$

where $(\overline{U})$ is the constant forward speed of the body and *g* represents the acceleration of gravity.

2. Suitable kinematic bottom and far field radiation conditions ensure that the energy flux of waves associated with the disturbance from the floating body is directed away from it, to infinity (conservation of energy). This condition is implicitly fulfilled via the use of a Green's function [3.2,3.7].

3. The incident and diffracted potentials, at a point (X,Y,Z) on the instantaneous wetted surface of the body (S) obey:

$$\frac{\partial \Phi_0}{\partial n} = -\frac{\partial \Phi_D}{\partial n} \qquad (3.26)$$

where (n) indicates the direction of the outward normal to the instantaneous fluid surface.

4. The r^{th} radiation potential is governed by the generalised Timman-Newman relation [3.7,3.11], on the body's instantaneous wetted surface (S):

$$\frac{\partial \Phi_r}{\partial n} = \left[i\omega_e \vec{u}_r + \vec{\theta}_r \times \vec{W} - (\vec{u}_r . \nabla)\vec{W} \right] \cdot \vec{n} \qquad (3.27)$$

where vectors $(\vec{u}_r)$ and $(\vec{\theta}_r)$ represent, respectively, the translation and rotation fields associated with the r^{th} principal mode shape, in the body fixed coordinate system $(O'X'Y'Z')$.

The vector $(\vec{W}_r)$ represents the steady flow velocity relative to the moving equilibrium frame of reference (OXYZ) (see figure 3.1). Since the perturbation of the steady flow due to the steady forward motion of the body is assumed negligible the steady flow velocity vector can be expressed as: $\vec{W} = -\overrightarrow{U\vec{i}}$. Equation (3.27) then reduces to:

$$\frac{\partial \Phi_r}{\partial n} = i\omega_e(u_r n_1 + v_r n_2 + w_r n_3) + \frac{1}{2}\overline{U}\left[n_3\theta_r Y_r' - n_2\theta_r Z_r' \right] \qquad (3.28)$$

Here, (u_r, v_r, w_r) and (n_1, n_2, n_3) are, respectively, components of the local displacement vector; (θ_r) are rotations respectively associated with the r^{th} mode shape.

The conservation of energy condition is fulfilled implicitly via the implementation of a three-dimensional Green's function method representing the velocity potential $\Phi(X,Y,Z)$ at any point in the fluid. Any numerical solution **must** satisfy the first three key relationships describing the linearised boundary conditions summarised in the above discussion. The generalised Timman-Newman [3.7,3.11] relation on the body instantaneous wetted surface governs the source strengths associated with the radiation potential.

Green's function may take alternative forms each of which corresponds to a type of singularity, e.g. a source, be it pulsating, translating or both, a dipole or a mixed source-dipole distribution. For the sake of computational efficiency pulsating sources are implemented in the current analysis. Although this simplified approach overlooks the forward speed effect on the free surface engineering experience has proved that it provides reasonably good results even for higher speed monohulls and therefore could be considered as being acceptable approximation for low forward speed problems [3.12,3.13]. The accuracy of the solution based on a distribution of pulsating sources relies, especially, on the fact that the perturbation of the steady flow due to the steady forward motion of the body is assumed to be negligible. In the case of a genuinely three- dimensional body, this assumption requires that the steady velocity of the fluid relative to the body is small so that $\vec{W} = -\overrightarrow{U\vec{i}}$. Hence, the steady component of the total velocity potential, $(\overline{\Phi})$ (see equation 3.2) may be disregarded. From a physical viewpoint, this means that the *Kelvin* wave pattern, generated by relative forward motion in the fluid-body system, is neglected as the potential due to ship oscillations

dominates that due to forward ship motion [3.7]. Furthermore, assuming that the encounter frequency (ω_e) is high, the first two terms of equation (3.25) are one order of magnitude smaller that the others and vanish so that the free surface boundary condition (at Z = 0) condenses into:

$$\frac{\partial \Phi}{\partial Z} - \frac{\omega_e^2}{g}\Phi = 0 \tag{3.29}$$

Consequently, expression (3.28) remains as the only speed dependent relation making a problem suited to an efficient implementation of pulsating sources.

Further computational simplification is attained by the implementation of the so-called composite technique that relies on the hull port-starboard symmetry in such a way that the composite source strengths are solved only over the port side of the body surface for any wave-heading angle [3.2]. The numerical procedure used in order to find the source strengths and in turn the radiation and diffraction potentials entails the discretisation of the hull wetted surface into a number of quadrilateral panels. Conveniently, the corresponding finite elements on the mean wetted surface (linear shell elements) may be directly transposed into hydrodynamic panels capable of representing the three-dimensional unified hydrodynamic behaviour of the flexible floating body under consideration.

As shown by Bishop et al [3.2] the generalised hydrodynamic added mass (A_{rk}), damping (B_{rk}), radiation (T_{rk}) and restoring force coefficients (C_{rk}) are defined by the integrals of the solutions of potential flow over the wetted surface (S), with their elements as follows:

$$A_{rk} = \frac{\rho}{\omega_e^2}\mathrm{Re}\left[\iint_S \{n\}^T\{U_r\}\left(i\omega_e - \overline{U}\frac{\partial}{\partial X}\right)\Phi_k dS\right] \tag{3.30}$$

$$B_{rk} = -\frac{\rho}{\omega_e^2}\mathrm{Im}\left[\iint_S \{n\}^T\{U_r\}\left(i\omega_e - \overline{U}\frac{\partial}{\partial x}\right)\phi_k dS\right] \tag{3.31}$$

$$C_{rk} = -\rho g\iint_S \{n\}^T\{U_r\}w_k dS \tag{3.32}$$

for k = 1,2,...,m.

In equations (3.30-3.32) Re and Im indicate that real and imaginary parts are taken from a complex quantities in brackets while the component $\left[\iint_s \{n\}^T\{U_r\}\left(i\omega_e - \overline{U}\frac{\partial}{\partial X}\right)\Phi_k dS\right]$ expresses the radiation term (T_{rk}); ρ represents the fluid density; $\{n\}^T$ the transpose of the matrix representing the unit normal vector from the surface into the fluid; $\{U_r\}$ denotes the displacement vector of the relevant mode and $(\overline{U})$ the forward speed of the floating structure.

If a similar integration procedure is followed, the Froude-Kriloff (Ξ_{0r}) and diffraction (Ξ_{Dr}) forces expressing the total exciting forces ($\Xi = \Xi_{0r} + \Xi_{Dr}$) are define as:

$$\Xi_{0r} = \rho\int_s \{n\}^T\{U_r\}\omega_e\Phi_0 dS \tag{3.33}$$

$$\Xi_{Dr} = \rho\int_s \{n\}^T\{U_r\}\left(i\omega_e - \overline{U}\frac{\partial}{\partial X}\right)\Phi_D dS \tag{3.34}$$

3.6 Two- and three- dimensional steady state displacements and loadings

When the structure is floating, it is excited by the waves and executes a forced motion. For both two- and three-dimensional hydroelasticity in regular sinusoidal waves the exciting force $(\Xi(t))$ and the principal coordinates $(p(t))$ can be expressed as functions of the encounter frequency (ω_e):

$$\Xi(t) = \Xi e^{i\omega_e t} \tag{3.35}$$

$$p(t) = p e^{i\omega_e t} \tag{3.36}$$

By applying equations (3.35) and (3.36) in equation (3.12) it is possible to determine the principal coordinates as:

$$[I]\{p\} = \frac{Adj[D]}{|D|}[\Xi] \tag{3.37}$$

where $[D] = \left[-\omega_e^2[[a]+[A]] + i\omega_e[[b]+[B]] + [[c]+[C]]\right]$ and $[I]$ is the unit matrix.

According to Rayleigh's theorem [3.3], any distortion of the structure may be expressed as an aggregate of distortions in its principal modes. Hence, based on the knowledge of the principal coordinates determined by equation (3.37) as well as the principal mode shapes and modal bending moments, shear forces and torsional moments evaluated during the dry analyses the responses to regular wave excitation may be evaluated using modal summation. Considering, for example, nodal displacements:

$$\begin{aligned} u(x,y,z,t) &= \sum_{r=1}^{m} p_r(t)u_r(x,y,z) \\ v(x,y,z,t) &= \sum_{r=1}^{m} p_r(t)v_r(x,y,z) \\ w(x,y,z,t) &= \sum_{r=1}^{m} p_r(t)w(x,y,z) \end{aligned} \tag{3.38}$$

where (m) denotes the highest distortion mode admitted to the analysis; u,v,w denote the deflections and $p_r(t)$ represents the principal coordinate amplitudes of the r^{th} mode. The first six modes represent the rigid body modes namely, surge (r=1), sway (r=2), heave (r=3), roll(r=4), pitch (r=5), yaw(r=6). The incorporation of flexible distortions starts from the 7^{th} mode.

Additionally, any relevant response such as bending moments, shearing forces, twisting moments or stresses may be determined in a similar way using the appropriate characteristic function of the dry structure. For example the expression for moments is

$$M(x,y,z,t) = \sum_{r=7}^{m} p_r(t)M_r(x,y,z) \tag{3.39}$$

where (M) denotes any seaway induced bending moment load such as vertical, horizontal or torsional moment. The corresponding symmetric and antisymmetric internal actions (modal properties) of the dry structure (M_r) are obtained from suitable modal analysis (see chapter 5).

Stresses can be determined in a similar manner. For example, the longitudinal seaway induced direct stress is

$$\sigma_x(x,y,z,t) = \sum_{r=7}^{m} p_r(t)\sigma_{xr}(x,y,z) \tag{3.40}$$

where $\sigma_{xr}(x,y,z)$ represents the modal direct longitudinal stress for the r^{th} mode. In three-dimensional hydroelasticity theory, these modal stresses are obtained from nodal stresses available from a three-dimensional finite element model. By contrast, in the two-dimensional case the stresses have to be derived from modal bending moments. For instance, the modal stress at the hull-deck junction can be expressed as:

$$\sigma_{xr} = \frac{M_r}{S_{deck}} \tag{3.41}$$

where (M_r) is the modal bending moment and (S_{deck}) represents the section modulus, defined as the ratio of the appropriate second moment of area (I) over the distance from the neutral axis to the hull deck junction (c). It is interesting to note no contribution to these loadings arise from the rigid body modes (r=1,…,6). This is not the case with displacements, as given in equation (3.38). It is also worthwhile to emphasize that whereas in three-dimensional hydroelasticity symmetric and antisymmetric dynamic loads are computed all together (6 degrees of freedom rigid body model), two-dimensional methodology implies that surge motion is excluded (5 degrees of freedom rigid body model) with symmetric (Timoshenko beam) and antisymmetric (Timoshenko beam with warping) analyses carried out separately, being uncoupled within the context of port starboard symmetry and linearity.

3.7 Conclusions

A brief description of the mathematical background related to the Bishop, Price et al two- and three-dimensional hydroelasticity theories has been outlined. In principle both two- and three-dimensional hydroelastic FSI formulations appear to be capable of predicting the steady state seaway induced dynamic loads of long slender monohulls in regular waves from a unified analysis. Whereas in three-dimensional hydroelasticity symmetric and antisymmetric dynamic loads are computed all together (6 degrees of freedom rigid body model), two-dimensional methodology implies that surge motion is excluded (5 degrees of freedom rigid body model) with symmetric (Timoshenko beam) and antisymmetric (Timoshenko beam with warping) analyses carried out separately, being uncoupled within the context of linearity for hulls with port / starboard symmetry. Even at this early stage it is worthwhile to emphasize that the partial differential equation describing the in vacuo antisymmetric dynamics of the hull girder does not account either for the structural discontinuities that could occur between the

open/closed parts of a ship or for the effects of warping restraint. The importance of both these simplifications for the case of ships with large deck openings will be further discussed and demonstrated in the following chapters.

3.7 References

[3.1] Bishop, R.E.D. and Price, W.G.: Hydroelasticity of Ships, Cambridge University Press, UK, (1979).

[3.2] Bishop, R.E.D, Price, W.G. and Wu, Y.: A general linear hydroelasticity theory of floating structures moving in a seaway, Phil. Trans. Royal Soc. London, A316: 375-426, (1986).

[3.3] Rayleigh, Lord: The theory of sound, 2nd edition, Macmillan, UK, (1894).

[3.4] Bishop, R.E.D., Price, W.G. and Temarel, P.: Antisymmetric vibration of ship hulls, Trans. RINA, 122:209-226, (1980).

[3.5] Bishop, R.E.D., Price, W.G. and Temarel, P.: Hydrodynamic coefficients of some swaying and rolling cylinders of arbitrary shape, International Shipbuilding Progress, 27:54-65, (1980).

[3.6] Bishop, R.E.D., Price, W.G. and Cheng, Z.X,: On the structural dynamics of a Vlasov beam, Proc. R. Soc. Lon.,A338:49-73, (1983).

[3.7] Newman, J.N.: Marine Hydrodynamics, The MIT press, Cambridge, Massachusetts, USA, (1992).

[3.8] Bishop, R.E.D., Price, W.G. and Tam, P.K.Y.: A unified dynamic analysis of a ship response to waves, Trans. of RINA, 119:363-390, (1977).

[3.9] Salvesen, N., Tuck, E.O. and Faltisen, O.: Ship motions and sea loads, Trans. SNAME, 78:250-287, (1970).

[3.10] Gerritsma, J. and Beulkerman, W.: The distribution of the hydrodynamic forces on a heaving and pitching shipmodel in still water, Publication no. 22, Shipbuilding Lab., Delft university of Technology, Denmark, (1964).

[3.11] Timman, R. and Newman, J.N.: The coupled damping coefficients of symmetric ships, Journal of Ship Research, 5:34-55, (1962).

[3.12] Louarn, F.H. and Temarel, P.: An investigation of the structural dynamics of a racing yacht, Proceedings of the 14^{th} Chesapeake sailing yacht symposium, 123-142, USA, (1999).

[3.13] Price, W.G., Salas Inzunza, M.A. and Temarel, P.: The dynamic behaviour of a monohull in oblique waves using two- and three-dimensional fluid-structure interaction models, Submitted to RINA, (2000).

Chapter 4

Ship Structural Modelling

4.1 Introduction

The analysis of an engineering system requires its numerical idealisation into a form that can be solved via the development of a feasible model (pre-processing module), its solution (solution module) and the interpretation of the results (post-processing module). Accordingly, intuition and experience throughout the years have shown that the dynamic analysis of non-uniform slender mono-hull ship structures can be achieved by means of two- or three-dimensional numerical discretisation techniques which, due to their different degree of complexity and associated data requirements, could have different uses within the design process [4.1,4.2]. Two-dimensional idealisations offer a fast and efficient means of simulating the structural dynamic behaviour of mono-hull vessels for the preliminary design stage, where the performance of design variants can be assessed using acceptable engineering approximations to provide the relevant data for the vessel and its structure. Three-dimensional models although they are time and effort consuming, even when a relatively simple idealisation is used, are much more suitable in predicting/confirming the dynamic performance of a mono- or multi-hull vessel at the detailed design stage.

Finite difference (FD) and especially finite element analyses (FEA) methods, the latter due to their ability to model with reasonable ease and accuracy two- or three-dimensional arbitrary structural geometries, have dominated the approximation of such problems. The basic principles and mathematical background of these discretisation techniques have been well established in literature [4.1,4.2,4.3,4.4,4.5]. However, since they comprise a significant part of the dry analysis module of the unified hydroelasticity theories (see chapters 2,3), in this chapter some of the fundamental modelling assumptions and options available to the naval

architect in assessing the in vacuo dynamic strength of long slender monohulls (e.g. tankers, bulkers, containerships, etc) are firmly highlighted (see also appendix 2). A significant part of the discussion is focused upon the degree of confidence that can be placed on predictions obtained from two-dimensional beam models by comparison to three-dimensional models where special structural features, such as large deck openings, double bottoms, transverse bulkheads, hopper spaces etc, are modelled more explicitly. The guidelines issued have a general character and could be applied for the case of most slender monohull vessels with or without large deck openings (e.g. containerships, tankers, LNG carriers etc). However, special emphasis is attributed to the modelling difficulties associated with the in vacuo dynamic assessment of a bulk carrier hull representing a structure similar to that of OBO MV Derbyshire.

4.2 Preliminary considerations

4.2.1 The ship as a simple beam

When the motions and distortions of a ship under way in waves are to be investigated, it is necessary to model the hull suitably. For the case of long slender monohulls such as bulk carriers, tankers and containerships the hull has port/starboard symmetry and therefore symmetric and antisymmetric motions are considered separately, being uncoupled in linear theory. The symmetric response involves neither rolling nor twisting and therefore the hull is modelled as a free-free beam with motions investigated by means of the Bernoulli-Euler or Timoshenko theories [4.9] (see sections 2.6.1,3.4.1). Antisymmetric motions and distortions, by contrast, raise serious difficulty although they could provide significant insight with regards to the dynamic behaviour of the structure. These distortions involve coupled bending and twisting of the non-uniform beam like hull. In order to overcome this difficulty traditionally in two-dimensional hydroelasticity studies, the Timoshenko beam theory has been modified to admit the effects of torsion, including if desired, those associated aspects with warping which become particularly important for the case of beam-like vessels with large deck openings such as bulk carriers and containerships. The mathematics of the method have been well established in literature [4.9] and were briefly outlined in chapter 3 (see section 3.4.1). Before proceeding, however, it is important to highlight that the Bishop et al beam model is based on elastic beam mechanics and assumes that:

- primarily there is only one independent variable along the ship's longitudinal position. Thus loads and deflections have only a single value at any cross-section and the effects of shear lag are neglected;
- the hull girder remains elastic;
- the hull girder is prismatic (i.e. no discontinuities of the cross-section are allowed for);
- although the warping stiffness is allowed for in the mathematical model the beam idealisation assumes that the horizontal bending moment internal actions operate according to Saint-Venant's theory torsion. Thus the effects of axial stresses caused by out of plane (warping) deformations are neglected;
- the longitudinal strain due to bending varies linearly over the cross-section about a transverse axis of zero strain (neutral axis).

These fundamental engineering assumptions establish the basis of beam analyses presented in the current investigation. Due to effect of out of plane longitudinal deformations (known as warping) the assumption of pure torsion is not satisfied for open thin-walled sections if the beam has external supports, or it is non-prismatic or when the torsional moment varies along its length. In such cases the twisting resistance of the open sections is so small and the axial displacements are so large that the axial stress (σ_x) caused by *warping restraint* cannot be neglected. Warping induced shear stresses caused by torsion are usually very small, axial stresses may, however, sometimes be of concern [4.11]. More often it is the deformations which cause structural defect and they should be as small as possible especially at double bottom configurations. This is the case for a ship hull with large deck openings (e.g. containership) or hatch openings (e.g. bulker). These ship types are structurally subject to the distinctive features of a thin walled multi-cell beam that undergoes out of plane longitudinal deformations as a result of torsion induced structural behaviour. As it will be demonstrated (see chapter 5), warping has the effect of greatly reducing the torsional rigidity of the hull and this results in close coupling between bending and twisting distortions especially for open-deck beam-like ship structures where the distance between shear and gravity centres is significant (see figure 4.4). The simulation of the torsion induced vibrations could become even more complex because of the structural discontinuities (non-prismatic characteristics)

that appear at the common locations between the open and closed parts of the hull girder (see figures 4.4 and 4.6).

The theory of torsion for such structures has been summarised by Haslum et al as well as Vlasov [4.10,4.11] and it assumes that the stresses σ_y, σ_z, τ_{yz} are negligibly small so that the stress tensor has the form:

$$\begin{bmatrix} \sigma_x & \tau_{xy} & \tau_{xz} \\ \tau_{xy} & 0 & 0 \\ \tau_{xz} & 0 & 0 \end{bmatrix}$$

In literature it is made clear that the identification of such torsional problems is divided into two main categories, depending upon the boundary conditions at the ends of the beam element. One is called *free or St. Venant torsion* when the beam is completely free to warp and the other is called *flexural torsion, or warping restrained torsion* when warping of the ends is partly or completely prevented. These two approaches are of different significance and complexity depending upon whether the cross-section is open or closed.

To estimate the stresses due to a given torque, two activities are clearly necessary. First the torsional and warping stiffnesses have to be calculated, and secondly the relationship between shear stress and rate of twist has to be established.

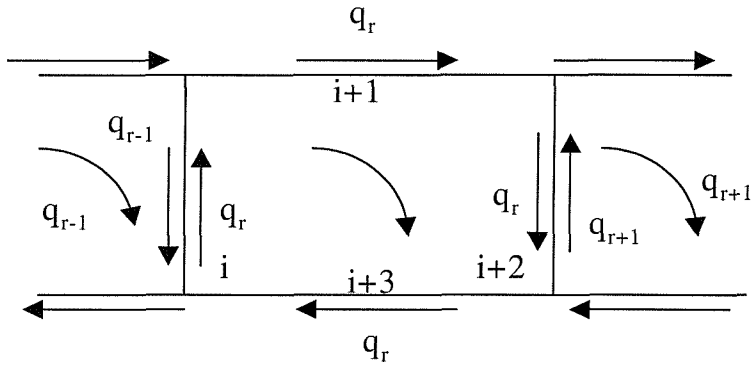

Fig. 4.1 Shear flow loops for a typical multi-cell section

The adoption of the multi-cell hybrid approach becomes particularly important at open deck spaces where the distance between the shear and gravity centers is significant and the

magnitude of warping against torsional stiffness reaches its absolute extremes (see figure 4.4) [4.1,4.12,4.13]. Since the problem is statically indeterminate (there is no known point in the cross-section on which the shear flow is zero), a method of analysis is to introduce a cut in each cell for the closed section to provide a free edge where an unknown shear flow is applied [4.10,4.13]. Hence, the unknown quantities are determined from the condition that no twisting of the section takes place, i.e. the angle of twist (ϕ) for each cell of the section should be zero (see figure 4.1). This condition provides for each cell an equation of the type:

$$\phi = \frac{1}{2A_m G}\int q\frac{ds}{t} = 0 \Rightarrow \oint\frac{qds}{t} = 0 \tag{4.1}$$

where A_m = area bounded by perimeter of the cell; q = shear flow ; s = coordinate around the perimeter; t = thickness of the wall section (i). All cells experience the same rate of twist namely

$$\phi' = \frac{T}{GJ} \tag{4.2}$$

where the torque carried $T = \sum_i T_i = 2\sum_i q_i A_{mi}$. After application of equation (4.1) to each cell the redundant quantities giving the shear flow at the cuts introduced can be calculated and therefore the unknown torsional stiffness (GJ) of the system may be evaluated.

For St. Venant torsion then the magnitude of the warping of the section is proportional to the angle of twist and the shape of the longitudinal cross section may be considered as property of the cross-section. This distribution is described by the so-called unit warping or sectorial coordinate (Ω). The longitudinal displacement, which is a function both of the longitudinal coordinate (z) and the position in the particular cross section, is written as a product of two functions:

$$w(z,s) = \phi'(z)\cdot\Omega \tag{4.3}$$

An attempt to restrain the warping will give longitudinal stresses (σ_{xr}) in the beam. The resultant of these stresses at any section is called the bimoment and is denoted by (M_Ω). The normal warping stresses are given by:

$$\sigma_{xr} = \frac{M_\Omega \times \Omega}{I_{\Omega\Omega}} \tag{4.4}$$

where $I_{\Omega\Omega} = \int_F \Omega^2 dF$ is the sectorial moment of inertia about the shear center for warping torsion. The similarity between this expression and that for an ordinary bending stress is quite remarkable. In ordinary bending the rate of change in longitudinal direction of the normal stresses is accompanied by shear stresses. In warping restrained torsion the longitudinal changes in (σ_{xr}) are accompanied by torsional shear stresses ($\tau_w = \tau_{xy} + \tau_{xz}$). Their result is the warping torque (T_w). Thus, the externally applied torque is now balanced by the summation of the two internal torques, (T_w) and (T_s), the latter being the resultant of the shear stresses (τ_s) (the only ones present due to St. Venant's torsion). Numerically,

$$T_s = GJ\phi \text{ and } T_W = -EI^0_{\Omega\Omega}\phi'' \tag{4.5}$$

where (E) is the Young's modulus and $\left(I^0_{\Omega\Omega}\right)$ is the mass sectorial moment of inertia ($I_{\Omega\Omega}$). The product $\left(EI^0_{\Omega\Omega}\right)$ is known as warping stiffness of the system. For those cases where warping is restrained, the response of a particular section also depends upon the twist (and the torque) at other sections. Thus the total torque (T_{tot}) is given by the summation:

$$T_{tot} = T_w + T_s = -EI^0_{\Omega\Omega}\phi'' + GI_t\phi \tag{4.6}$$

When the differential equation is solved, the warping is given by equation (4.3) and the total horizontal bending moment (M_{tot}) equals numerically to the summation of direct horizontal bending moment (M_s) and the bimoment (M_Ω) as shown below:

$$M_{tot} = M_s + M_\Omega = EIy'' - EI_{\Omega\Omega}\phi'' \tag{4.7}$$

where $\left(y''\right)$ represents the second derivative of the horizontal deflection.

4.2.2 Principles of numerical discretisation

In solving a structural problem, whatever the type of structure, excitation, the nature of the structure's material or the finite discretisation scheme (e.g. FEA or FD) there are three types of separate and distinct arguments that can be deployed and should be considered by the designer when selecting or formulating an appropriate numerical model [4.3,4.4] (see figure 4.2). These are known as:

- Equilibrium

Used to relate stress to applied forces whether there are applied forces or not. If the structure is excited dynamically then the 'inertia forces' can be inserted into the equations of equilibrium as if the problem was still static. If displacements are small then the equations of equilibrium are linear.

- Compatibility and conformity

These relate strains to displacements and are purely geometrical arguments that depend on the definition of strain and the type of deformation and geometry of the particular structure. For ships with significant structural discontinuities this could be significant modelling issue (see figure 4.4). For geometrically linear problems these assumptions are linear.

- Stress - Strain law

These 'constitutive relationships' are empirical and depend on experimental evidence. They may include thermal effects, and for ferrous materials the relationship may be elastoplastic. For many structural materials within their useful working range these laws may be taken as linear. Considering that both two- and three-dimensional unified hydroelasticity theories operate within the context of dynamic and hydrodynamic linearity the latest assumption is not of great concern.

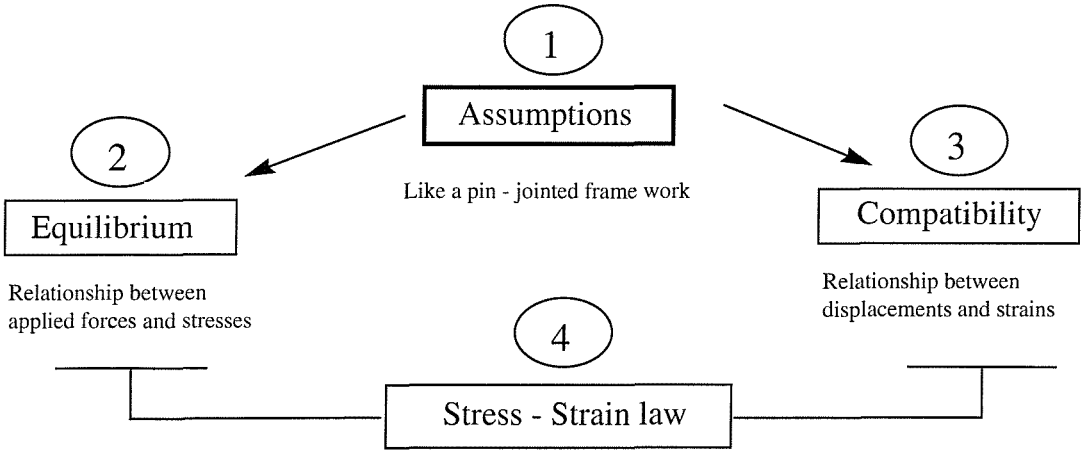

Fig. 4.2 Fundamental finite discretisation assumptions

4.3 Preprocessing

4.3.1 The bulker

The work presented in this project is based on a series of calculations related to a vessel having similar principal particulars to OBO MV Derbyshire. This was the last of six Bridge class ships built on the Tees and Haverton Hill Shipyard, subsidiary company of Swan Hunter. She was completed in 1976 and on or about the 9th of September 1980 she was lost with all hands in Typhoon Orchid in the western Pacific, south of Japan. Several formal investigations have been undertaken until recently in an attempt to explain the reasons of loss [4.6,4.7,4.8,4.51]. Definitely the historical facts and past reports related to the loss of this vessel are of interest and motivating from scientific point of view. Before proceeding, however, it is important to stress that it is not the purpose of the present investigation to solve or even suggest a solution to the Derbyshire problem but to gain insight of the dynamic strength and integrity of slender monohulls having similar features. The principal particulars of the bulker under consideration are given in table 4.1.

Length over all (m)	L_{OA}	294.1
Length between perpendiculars (m)	L_{BP}	281.94
Beam moulded (m)	B	44.2
Depth moulded (m)	D	24.99
Draft amidships (m)	T	17.4
Displacement (tonne)	∇	186,514
Block coefficient (m)	C_B	0.861

Table 4.1 Principal particulars for the bulker examined

4.3.2 Structural modelling procedure

For structures as large and complex as ships there are three levels of structural design namely *concept*, *preliminary* and *detailed*. *Concept* design deals with the topology of the structure; *detailed* design is concerned with local aspects such as joints, openings and reinforcements and *preliminary* design deals with the structural dimensions (scantlings) of all principal members. For the purposes of the current investigation at first instance a detailed lines plan was generated based on the information provided within the general arrangement plan (see appendix 1). The Wolfson Unit SHIPSHAPE v.32 software was used to generate a realistically possible Derbyshire-hull form with principal dimensions as those shown in table

4.1, block coefficient of the order of 0.861 and longitudinal center of gravity at 147.5m from the aft end of the vessel (see figure 4.3). This development was particularly useful for the generation of a globally realistic three-dimensional finite element model of the ship structure.

From this point on most of the work was concentrated upon estimating the scantlings of 46 sections that were considered adequate to simulate the major sectional characteristics of the vessel such as horizontal and vertical moments of inertia, center of gravity, shear center torsional constant, warping constant etc. The drawing plans of the detailed ORE/OIL mid-ship section together with past structural data along key hull positions provided by the British Ship Research Association (BSRA – today British Maritime Technology) [4.50] were used as reference points. As in most of such cases engineering intuition implies that the construction of a reliable equivalent hull form which would subsume most of these properties is vital in order to simulate realistically the global mass and stiffness characteristics of the ship. Along these lines an equivalent multi-cell hull of the mid-ship section (in the vicinity of a hatch opening) was generated at first instance with sufficient detail to model the topside tanks, hopper spaces and inner bottom using seven longitudinal girders and hopper spaces (see figure 4.6 and appendix 1). The material contributions of other longitudinal stiffeners and transverse frames were subsumed into the properties of the adjacent shell elements.

(a) (b)

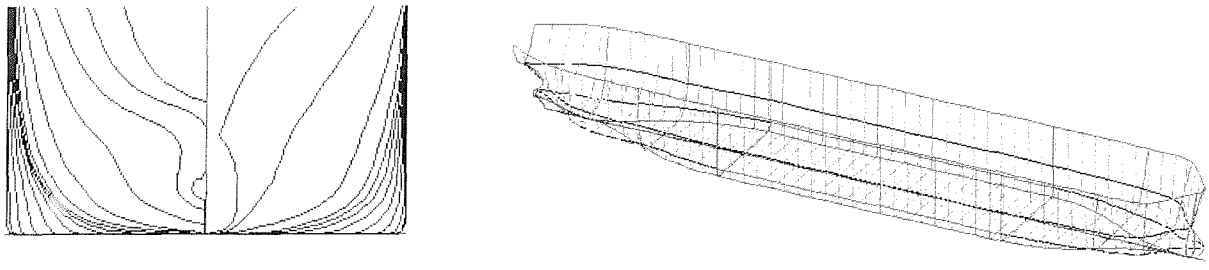

Fig.4.3 Body plan and three-dimensional view of the lines plan of MV Derbyshire (C_B = 0.861; LCB = 147.5m from A.P.)

For the remaining sections of the hull the scantlings were calculated on the basis of fitting realistic plate thickness so as to meet the data estimated by BSRA. For simplicity of modelling the superstructure as well as the stiffness of the hatch covers were not included.

Special attention was paid upon retaining the physical and structural properties at the hull extremities. Although some of the main steps followed in this modelling approach may be perceived as relatively crude, it is firmly believed that all elements necessary for an accurate idealisation of the dynamic behaviour of this vessel, in vertical bending and coupled horizontal bending and torsion, are adequately incorporated for the purposes of a global dynamic analysis.

A summary of the scantlings, mass and structural properties of the vessel are included in appendix 1. The lengthwise variation of structural and inertia properties for the beam models were calculated using the three-dimensional model, to allow for meaningful comparisons between the idealisations used. Properties such as mass, moments of inertia, second moments of area, effective shear areas, torsional stiffness (or torsional constant), warping stiffness (or sectorial second moment of area) were evaluated. The only difference between past applications and the current analysis, as far as the beam idealisation is concerned, is the saw-tooth variation of structural properties, clearly seen in figure 4.4, due to the deck openings. As explained before (see section 4.2.1), the multi-cell thin walled beam approach was used for the calculation of the shear center, the center of gravity, the torsional and the warping stiffness of the structure [4.6,4.7,4.14]. For the calculation of the shear center and center of gravity initially an in-house FORTRAN 77 algorithm namely SHEAR was used. This software provided results of the shear and gravity centers along the length of the ship via input of a pointer indicating the direction of the shear flows of each cell of the hull. The results were initially cross-checked with those provided by BSRA and then all four properties namely shear center, gravity center, torsional stiffness and warping stiffness were calculated by means of the software FEMAP v3.3 [4.15]. This is a finite element translator system, which includes a subroutine based on plane strain one-dimensional rod elements, calculating the sectional characteristics of closed or open single-cell or multi-cell sections. Further crosschecks were implemented via hand calculations on simplified equivalent mono-cell sections as well as by using the Germanister Lloyd Poseidon ND v2.0 suite [4.16]. This is an automatic ship scantling generation program calculating the sectional properties of a crudely modelled bulker, container or tanker hull forms. All results were found to be in good agreement.

In treating a ship's hull as a Timoshenko beam of varying cross-section, it has been shown by Bishop and Price [4.9] that the effect of shear rigidity is important in calculating the modal responses, especially for natural frequencies of the dry hull with increasing mode number. Generally speaking the accurate calculation of effective shear area factor is not well understood in antisymmetric dynamics of multi-cell structures where the orientation of shear flows cannot be defined from a unified mathematical model [4.17,4.18]. Thus, the effective shear area of ship's hull is usually adjusted empirically as a fraction of the (longitudinally effective) cross section area [4.19]. In the current analysis this fraction was adjusted empirically by comparing the natural frequencies obtained, for the two-noded symmetric and antisymmetric (horizontal bending dominated) mode shapes, from the three-dimensional shell and beam models. This resulted in 0.21 and 0.28 of the cross-section area being considered effective in shear for the symmetric and antisymmetric distortions, respectively (see figure 4.3). Similar methodology has been successfully followed in the past [4.26].

Following the derivation of the structural properties two- and three-dimensional models were used to simulate the bulk carrier hull. For the three-dimensional idealisation ANSYS 5.4 shell finite elements were used to incorporate major structural elements such as deck, side, inner/outer bottom, hopper spaces, bulkheads, major longitudinal girders etc [4.25]. Beam-like idealisations were implemented by using two-dimensional finite difference scheme as well as two- and three-dimensional ANSYS 5.4 uniaxial beam finite elements [4.25]. The theoretical concepts of the finite element and finite difference methods employed for these idealisations have been well established in literature [4.3,4.4] (see also appendix 2) and will not be repeated here. The following sections of the preprocessing module highlight the technicalities related to the generation of the two- and three-dimensional ship models.

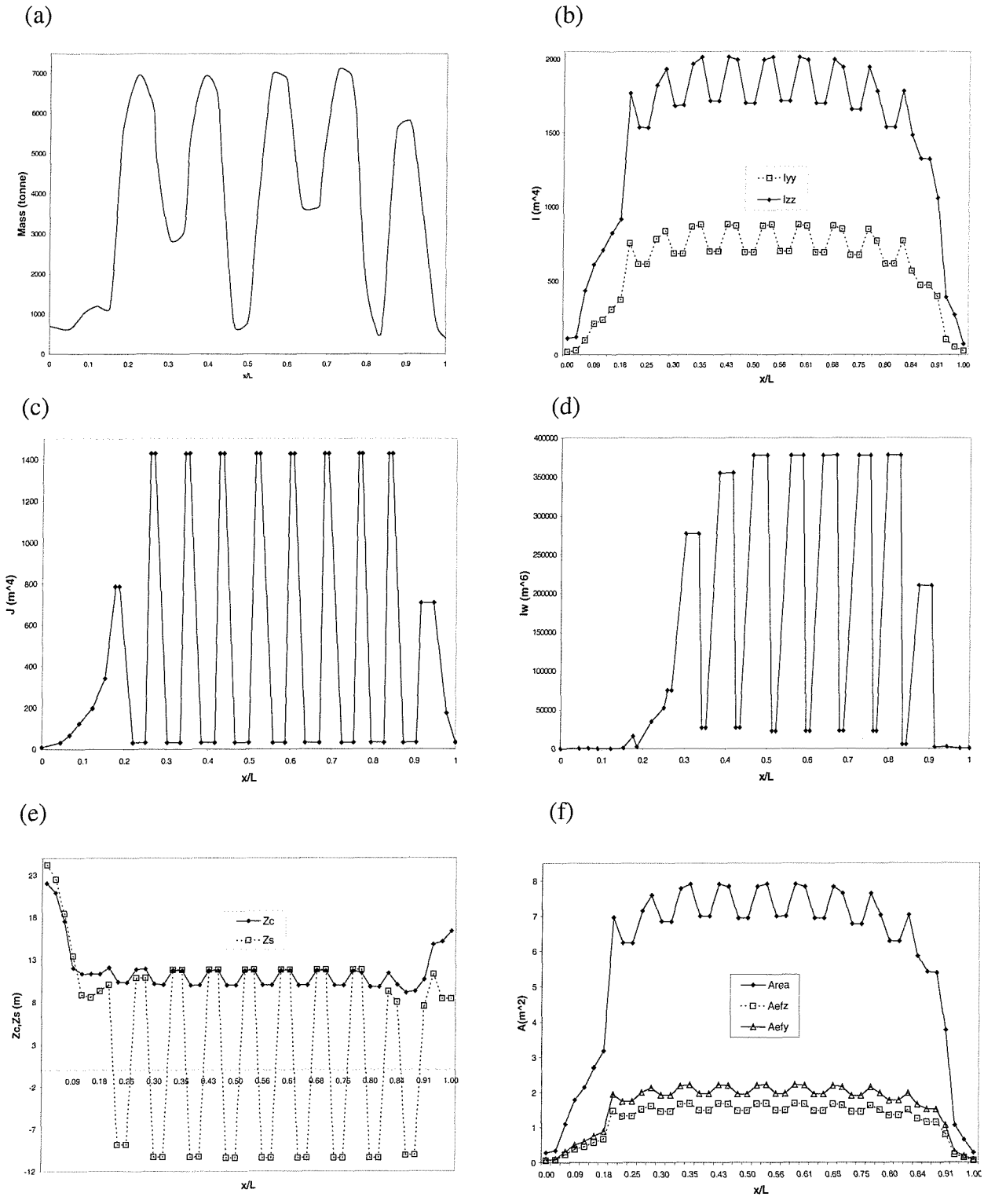

Fig.4.4 Variation of mass and structural properties along the bulk carrier: (a)Mass distribution (tonnes); (b) Moments of inertia I_{zz} and I_{yy} (m^4); (c) Torsional constant J (m^4); (d) Sectorial moment of inertia I_w (m^6); (e) distances of shear centre z_s and centre of gravity z_c from keel (m); (f) cross-section A and effective shear areas A_{efz} and A_{efy} (m^2).

4.3.3 The shell model

ANSYS software permits the selection of fifteen different SHELL elements, which may be used for thermal, axissymmetric, harmonic, plastic, dynamic, multilayer, elastic or strain analysis. Before proceeding it is important to highlight that for the majority of these elements the software is quite flexible in the sense that: (i) it allows small tolerance for out of plane loads and (ii) it accounts for the warpage of the element via computation of a factor defined as the component of the vector from the first to the fourth node (parallel to the element normal) over the shell thickness [4.25]. For the purposes of the current investigation the following possibilities were examined:

- SHELL 16 : structural shell with quadratic displacement field;
- SHELL 93 : elastic shell with quadratic displacement field;
- SHELL63 : elastic cell with linear displacement field;
- SHELL41: membrane shell with linear displacement filed.

SHELL 16 allows for inputting the structural properties of the model quite conveniently. It is functional though only for unidirectional analysis or calculations of thickness stress distributions. A quadratic displacement field is appropriate for the modelling of static bending problems because it yields correct first order bending strain and stress fields after differentiation. Yet in the instance of dynamic analysis mid-side nodes are not recommended since they result in an uneven mass distribution across the element. These points further crosses out the selection of SHELL 93.

On the contrary elements SHELL 63 and 41 should converge, provided the mesh is sufficiently fine, while they are more economical in terms of computational expense. Both may be used in either rectangular or triangular form depending on the warpage of the region topology they simulate. SHELL 41 has three degrees of freedom at each of its four nodes (translations in the nodal x,y,z, directions) and therefore it simulates adequately membrane (in-plane) stiffness only. SHELL 63 has six degrees of freedom per node (three translations and three rotations in and about the x,y,z-axes correspondingly). In both elements stress stiffening large deflection capabilities reinforced by a consistent tangent stiffness matrix are

included for use in large deflection (finite rotation) analyses. However, these FE capabilities were of no use for the purposes of the current investigations.

SHELL 63 was eventually selected since it is a more general-purpose element, although the ship structure behaves primarily as a membrane element allowing for the normal to plane loads (finite nodal rotations) to be excluded from the analysis. Its mathematical background is based on linear interpolation functions following the classical Ahmadian, Irons and Zienkiewicz isoparametric formulation (see figure 4.7) [4.3,4.4] given by:

$$\Phi = N_1\Phi_1 + N_2\Phi_2 + N_3\Phi_3 + N_4\Phi_4 \tag{4.8}$$

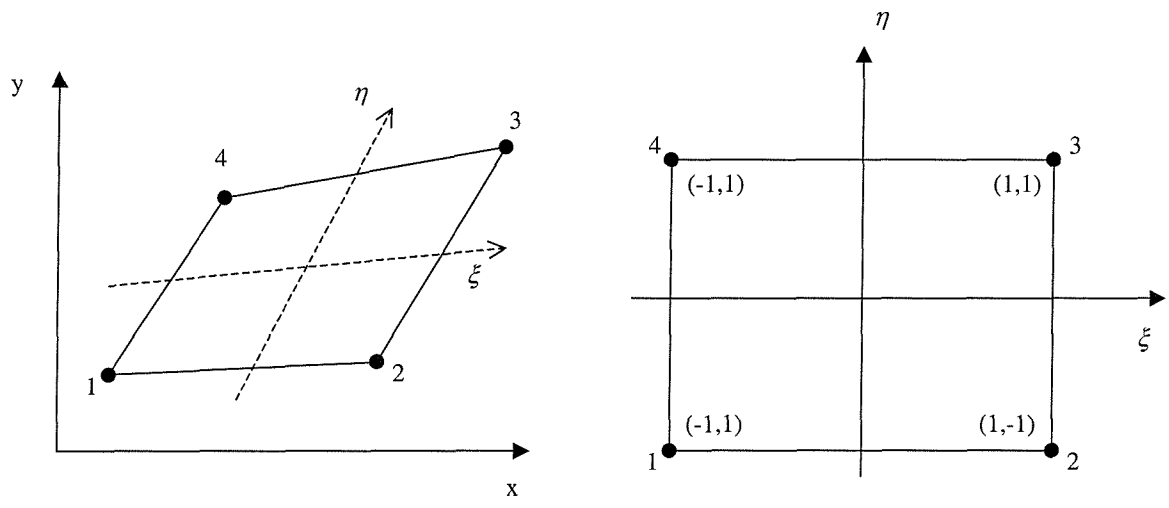

Fig. 4.5 Natural coordinate system used in SHELL63 quadrilateral elements

where the two dimensional C^0 shape functions describing the elemental geometry are found to be:

$$\begin{aligned} N_1 &= \frac{1}{4}(1-\xi)(1-\eta) \\ N_2 &= \frac{1}{4}(1+\xi)(1-\eta) \\ N_3 &= \frac{1}{4}(1+\xi)(1+\eta) \\ N_4 &= \frac{1}{4}(1-\xi)(1+\eta) \end{aligned} \tag{4.9}$$

where (ξ) and (η) are valid in the region (-1,1).

The elemental mass (M_e) and stiffness (K_e) matrices are presented in the form:

$$K_e = \int_{-1}^{1}\int_{-1}^{1}\int_{-1}^{1} B^T D B \det(J) d\xi_1 d\xi_2 d\xi_3 \tag{4.10}$$

$$M_e = \int_{-1}^{1}\int_{-1}^{1}\int_{-1}^{1} N^T \rho N \det(J) d\xi_1 d\xi_2 d\xi_3 \tag{4.11}$$

where (ρ) represents the mass density, (N) is the matrix of the shape functions and (B) is the matrix of shape function derivatives $\left[\frac{\partial N_j}{\partial x}, \frac{\partial N_j}{\partial y}, \frac{\partial N_j}{\partial z}\right]_{j=1}^{j=n\in N}$ also known as strain displacement matrix. Matrix (D) represents the elasticity or material properties of the structure. The Jacobean matrix (J) links the local to the global coordinates so that in three-dimensional space:

$$dV = \det(J)\, d\xi_1\, d\xi_2\, d\xi_3 \tag{4.12}$$

for

$$J = \begin{bmatrix} \frac{\partial x}{\partial \xi_1} & \frac{\partial y}{\partial \xi_1} & \frac{\partial z}{\partial \xi_1} \\ \frac{\partial x}{\partial \xi_2} & \frac{\partial y}{\partial \xi_2} & \frac{\partial z}{\partial \xi_2} \\ \frac{\partial x}{\partial \xi_3} & \frac{\partial y}{\partial \xi_3} & \frac{\partial z}{\partial \xi_3} \end{bmatrix}$$

The elasticity (or material property) matrix (D) under the isotropic plane stress elastic conditions is given as a function of Young's modulus (E) and Poisson's ration (ν) as shown below:

$$[D] = \frac{E}{1-\nu^2}\begin{bmatrix} 1 & \nu & 0 \\ \nu & 1 & 0 \\ 0 & 0 & \frac{1-\nu}{2} \end{bmatrix} \tag{4.13}$$

After the formulation of the connectivity matrix and provided that compatibility and equilibrium conditions are satisfied at each of the nodal points (see section 4.2.4) the global mass (M) and stiffness (K) matrices over a model comprising of (m) number of elements (e) are formulated as:

$$K = \sum_{m} K_e^m \tag{4.14}$$

$$M = \sum_{m} M_e^m \tag{4.15}$$

By following this idealisation the mid-ship section (in the vicinity of a hatch opening) was generated along the lines of the structural design practice demonstrated in section 4.2.3, in the first instance with sufficient detail to model the hopper tanks, topside tanks and inner bottom using seven longitudinal girders (see figure 4.6(a)). The midship section was, subsequently, incorporated into the parallel body and the idealisation was extended through the length of this vessel including transverse bulkheads and hatch openings where appropriate. Particular care was paid to the structural configurations at the stern and bow, including the bulbous bow. For simplicity of modelling the superstructure as well as the stiffness of the hatch covers were not included. The resultant model consists entirely of shell elements representing deck, side, inner/outer bottom, hopper, bulkhead plating (incorporating the adjacent transverse frames and longitudinal stiffeners) and inner bottom girders.

(a) (b)

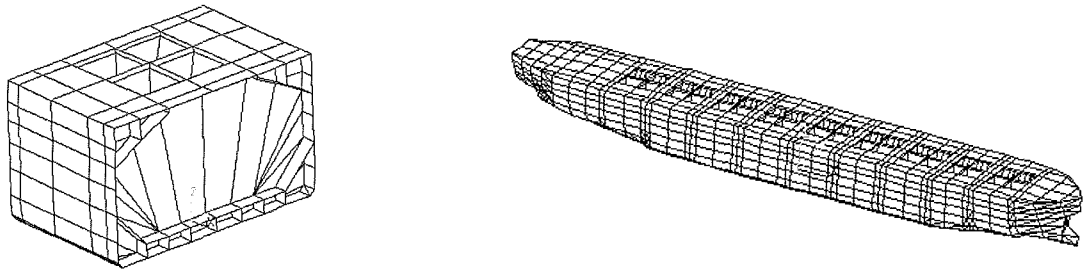

Fig.4.6 Finite element idealisation for model shell3d: (a) Transverse cross section in the parallel body; (b) Three-dimensional view of the entire vessel.

Corresponding triangular elements were used in areas of large curvature, such as the bilge and the side shell in the vicinities of bow and stern, where the warpage (due to the four nodes of the shell element not being on a flat plane) was outside acceptable limits. The final three-dimensional FE model, shown in figure 4.6(b), consists of 6439 nodes and 3673 shell elements and it is divided in the form of 46 sections along the ship. This facilitates the determination of the mass distribution along the vessel by manipulating the mass density of elements in a section, as well as the acquisition of properties required for the beam models

(see figure 4.4). This method was preferred to using lump mass elements so that relevant numerical problems during modal analysis can be avoided [4.27]. There is a wide dispute in literature on the advantages and disadvantages of the lumped parameter methods [4.28]. It is true, however, that in most of the finite element packages, including ANSYS, it is preferable to work with consistent rather lumped assembled mass matrix quantities. The crux of the matter is that with any mass matrix the product must yield the correct total force on an element according to Newton's second law of motion. Hence, to achieve convergence this kind of motion must be represented in a proper manner because it is the only motion experienced by an element. Consistent mass matrices are positive definite (i.e. the kinetic energy is positive for each displacement vector different than zero). A lumped mass matrix is positive, semi-definite or indefinite (if zero or negative masses respectively appear on the diagonal). These terms may or may not make some operations awkward, depending on the algorithm, while negative masses require some special treatment. Engineering experience has shown that consistent matrices are more accurate for flexural problems simulated by means of beams and shells [4.29]. Lumped matrices on the other hand are more important when the wave propagation over the wavelength is important. They may, however, lead to odd eigenforms [4.27].

The omission of transverse frames and longitudinal stiffeners from structural idealisations of mono- and multi-hull vessels has been dealt successfully in the past by incorporating *fictitious* bulkheads where appropriate [4.26,4.30,4.31]. Omission of such elements results in mode shapes containing localised distortions, which are not physically representative of the dynamic behaviour of the vessel (see figure 4.7).

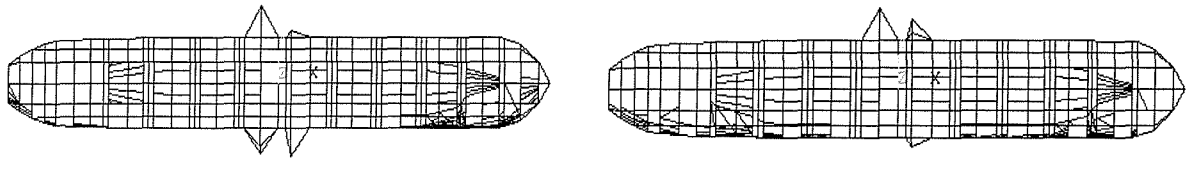

Fig.4.7 Localised deformations (spark effects) due to the lack of fictitious bulkheads

These *fictitious* bulkheads, of negligible mass and thickness, act as anchors, so to speak, to nodes of elements not otherwise connected to other elements in a direction normal to their plane. Adopting the same approach, transverse and longitudinal *fictitious* bulkheads were incorporated in the structural model shown in figures 4.6(a) and (b). The degree of refinement adopted in this model would have resulted in a large number of shell elements to idealise the transverse bulkheads. Consequently, the *fan* shape form, seen in figure 4.6(a), was adopted for both actual and fictitious transverse bulkheads used in the idealisation. Although modal analyses (see chapter 5) has **clearly** demonstrated the adequacy of this idealisation it is important to highlight that the high aspect ratio of these *fan* shape finite elements could slightly affect the computation of the polar mass moment of inertia of the bulkhead's transverse cross section. This is an expected modelling disadvantage that the designer should keep in mind in the sense that in three-dimensional shell FEA the total mass is simply apportioned amongst the nodes. Hence, the polar mass moment of inertia of the lumped masses of a typical quadrilateral element ($I_{c(e)}$) about its own centroidal axis (parallel to the longitudinal axis of the ship) is given by :

$$I_{c(e)} = (\text{number of nodes}) \times (\text{mass associated with each node}) \times (\text{distance of each node from the centroidal axis})^2$$

and therefore the polar mass moment of inertia of the element about the longitudinal axis of the cross-section $\left(I_c^{ij}\right)$ is given by:

$$I_c^{ij} = I_{c(e)} + m_{(e)} \times \left(r^{ij}\right)^2 \tag{4.16}$$

where $(m_{(e)})$ is the mass of the element and (r^{ij}) is the distance from the centroid of the element (i,j). Considering that elementary beam theory dictates [4.12] that the magnitude of the mass moment of inertia along a transverse section (i) of the ship should be:

$$I_c^i = \rho\left(I_{yy} + I_{zz}\right) \tag{4.17}$$

where (I_{yy}) and (I_{zz}) represent the vertical and horizontal moments of inertia for a cross-section, the effects of such inaccuracy could become evident when the antisymmetric modal actions (horizontal bending moments, torsional moments) of the shell model are compared against those produced by a beam finite idealisation (finite difference or finite element beam analysis). From engineering point of view adequate solution to such a problem could be attained by replacing the polar moment of inertia of the beam model by those of the shell model in order to eliminate differences when doing comparisons.

4.3.4 The beam models

A review of considerable number of Euler or Timoshenko beam finite elements used in dynamics problems [4.32,4.33,4.34,4.35], shows that they can be classified as simple or complex, with additional degrees of freedom and in some cases higher accuracy. Although in many cases it is possible to derive such elements by means of the isoparametric concept methodology briefly demonstrated in section 4.3.3, it is customary to follow the so called displacement or energy-based finite element formulation. This methodology is regarded as an extension of the well known displacement method of analysis [4.29] and it is used to derive all the ANSYS 5.4 beam finite element formulations used in the current investigation.

It is based on the idea of formulating force balanced equations and hence calculating the internal stress distributions by means of displacement models (polynomial functions of a conforming cubic or higher order) corresponding to the unknown joint displacements comprising a structure assembled by beam elements interconnected by structural joints. Accordingly, a function $(\{w\})$ characterising the internal displacements $(\{\delta\}^e)$ of an element (e) at any point is assumed to be uniquely determined by the nodal displacement of an element, i.e.

$$\{w\} = [\Phi]\{\delta\}^e \tag{4.18}$$

The internal strains $(\{\varepsilon\}^e)$ of the element (curvatures of a beam for instance) are defined in terms of the nodal [B] and elemental displacements $(\{\delta\}^e)$ as:

$$\{\varepsilon\}^e = [B]\{\delta\}^e \tag{4.19}$$

The internal stresses $(\{\sigma\}^e)$ are given by Hookes' law as:

$$\{\sigma\}^e = [D]\{\varepsilon\}^e \tag{4.20}$$

where [D] is the elasticity matrix. By applying the principle of virtual work (see appendix 2) and equating the internal and external work done during a viscous displacement $(\{\delta\}^e)$ results in:

$$\left(\{\delta\}^e\right)^T\{F\}^e = \iiint_V \left(\{\delta\}^e\right)^T \sigma dV \tag{4.21}$$

where $\{F\}^e$ represents the elemental force for an integration being carried out over a volume (V) of the element. Substitution of both the strain and virtual displacements into the latest equation results into the following mass and stiffness matrix formulae:

$$K_e = \left([C^{-1}]\right)^T \left(\int_V [\beta]^T [D][\beta] dV \right) [C^{-1}] \tag{4.22}$$

$$M_e = \left([C^{-1}]\right)^T \left(\int_V [\alpha]^T \rho [\alpha] dV \right) [C^{-1}] \tag{4.23}$$

The analogy of the above formulae to equations (4.10) and (4.11) respectively is quite obvious. The manipulations of the generalised displacement coefficient matrix ([C]) with the so called true strain of the nodal displacements matrix ([β]) (for the stiffness component K_e) and the direct representation of the displacement ([α]) (for the mass component M_e) replaces the shape functions. As per convention (ρ) represents the material density. The assembled stiffness and mass matrices are calculated by using equations (4.14), (4.15) respectively.

In literature the simplest beam element derived by following this approach is the one simulating a uniform Euler beam with 2 nodal points and 2 degrees of freedom (one translation and one rotation) per node (see figure 4.8).

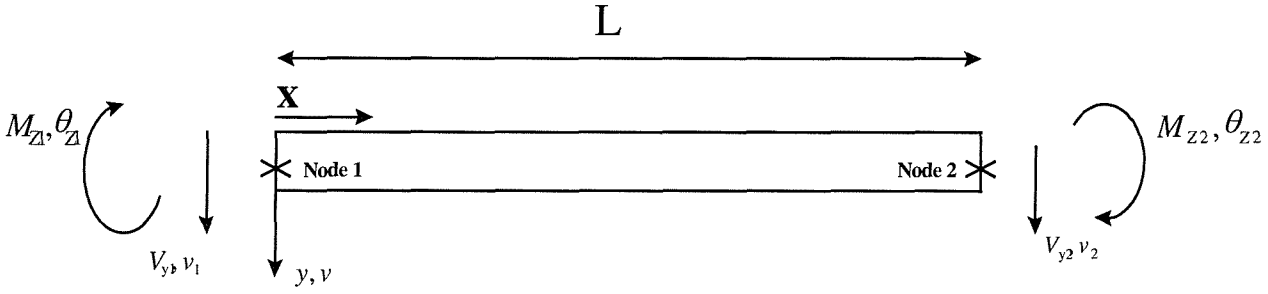

Fig. 4.8 The basic beam finite element (L: length, x: longitudinal direction, v_i translation θ_{zi}: rotation, V_{yi}: modal displacement, M_{zi}: modal moment).

By using a third degree polynomial ($y = a_0 + a_1x + a_2x^2 + a_3x^3$) and applying equations (4.33) and (4.34) [4.29,4.35] the stiffness and mass matrices of this element are derived as:

$$[K_e]_{axial} = \begin{bmatrix} 6 & 3L & -6 & 3L \\ 3L & 2L^2 & -3L & L^2 \\ -6 & -3L & 6 & -3L \\ 3L & L^2 & -3L & 2L^2 \end{bmatrix} \quad and \quad [M_e]_{axial} = \frac{mL}{420} \begin{bmatrix} 156 & 22L & 54 & -13L \\ 22L & 4L^2 & 13L & -3L^2 \\ 54 & 13L & 156 & -22L \\ -13L & -3L^2 & -22L & 4L^2 \end{bmatrix} \quad (4.24)$$

where (L) is the length of the beam element and (m) is the mass.

Przemieniecki [4.29,4.35] provides a more detailed derivation of the stiffness and mass matrices of a uniform Timoshenko beam via inclusion of the effects of rotary inertia and shear deformation in the following form:

$$[K_e]_{axial}^{shear} = \frac{EI}{L^3(1+\Phi)} \begin{bmatrix} 12 & 6L & -12 & 6L \\ 6L & L^2(4+\Phi) & -6L & L^2(2-\Phi) \\ -12 & -6L & 12 & -6L \\ 6L & L^2(2-\Phi) & -6L & L^2(4+\Phi) \end{bmatrix}$$

$$[M_e]_{axial}^{shear} = \frac{\rho AL}{(1+\Phi)^2} \begin{bmatrix} m_1 & m_2 & m_3 & m_4 \\ m_2 & m_5 & -m_4 & m_6 \\ m_3 & -m_4 & m_1 & -m_2 \\ m_4 & m_6 & -m_2 & m_5 \end{bmatrix} + \frac{\rho AL}{(1+\Phi)^2} \left(\frac{r}{L}\right)^2 \begin{bmatrix} m_7 & m_8 & -m_7 & m_8 \\ m_8 & m_9 & -m_8 & m_{10} \\ -m_7 & -m_8 & m_7 & -m_8 \\ m_8 & m_{10} & -m_8 & m_9 \end{bmatrix} \quad (4.25)$$

where (A) is the cross-sectional area of the beam, (I) represents the moment of inertia (vertical or horizontal), (E) is the Young's modulus of elasticity, $\Phi = \frac{12EI}{GkAL^2}$ (G : shear modulus) and the (m_i) coefficients are given as a function of (Φ) and (L) in the corresponding (4×4) matrices explicitly shown in appendix 2 . The effects of rotary inertia are accounted for by the quantity $I_z = \rho I$ by introducing the radius of gyration $r = \sqrt{\frac{I}{A}}$ and the constant (k) representing the effective shear area factor [4.27,4.18,4.19,4.29,4.35].

ANSYS 5.4 includes a number of beam and brick type Przemieniecki finite elements which may be implemented in either Euler or Timoshenko form by means of a term, namely shear deflection constant, defined as the ratio between the actual cross-sectional area over the effective shear area of the hull ($SDC = \frac{1}{k}$ where (k) is the shear deformation factor) [4.25].

Four alternative finite elements were considered for the purposes of the current investigation namely BEAM3, BEAM4, BEAM54, and BEAM44.

BEAM3 is a uniaxial element with tension, compression and bending capabilities. It has three degrees of freedom at each node, namely two translations along the x and y-axes and one rotation about the z-axis. Because of its flexibility characteristics it is capable of simulating in uncoupled form pure bending in either vertical or horizontal planes as well as axial distortion. The inclusion of flexural effects (longitudinal translation) gives to this element a more general form and makes it applicable for study cases where beams have a certain angular orientation (e.g. pin jointed frames). Hence, the terms of the stiffness and mass matrices of this element are of similar form to those presented in equations (4.24),(4.25) but include 2 additional degrees of freedom (1 per node) simulating the longitudinal translations (size 6×6). To be more precise the elemental stiffness $\left([K_e]_{BEAM3}\right)$ and mass $\left([M_e]_{BEAM3}\right)$ matrices are:

$$[K_e]_{BEAM3} = \begin{bmatrix} [K_e]_{flex} & 0 \\ 0 & [K_e]^{shear}_{axial} \end{bmatrix} \tag{4.26}$$

$$[M_e]_{BEAM3} = \begin{bmatrix} [M_e]_{flex} & 0 \\ 0 & [M_e]^{shear}_{axial} \end{bmatrix} \tag{4.27}$$

where $\left([K_e]^{shear}_{axial}\right)$ and $\left([M_e]^{shear}_{axial}\right)$ represent the axial stiffness and mass matrices of equation (4.36) and

$$[K_e]_{flex} = \begin{bmatrix} AE/L & -AE/L \\ -AE/L & AE/L \end{bmatrix} \text{ and } [M_e]_{flex} = \begin{bmatrix} 2 & 1 \\ 1 & 2 \end{bmatrix} \tag{4.28}$$

represent the flexural stiffness and mass matrices respectively.

BEAM4 is a uniaxial brick type element with tension, compression, torsion and bending capabilities. The element has six degrees of freedom per node and therefore the mass and stiffness matrices are of the order of (12×12). These are three translations in the nodal x, y, z directions and three corresponding rotations about the nodal x, y, z-axes. It is important to highlight that in this case the element stiffness and mass matrices are given by superimposing the axial, flexural as well as the torsion effects for which the effects of warping are not

considered at all. By following the same methodology adopted for BEAM3 formulation the $([K_e]_{BEAM4})$ and mass $([M_e]_{BEAM4})$ matrices of this element are:

$$[K_e]_{BEAM4} = \begin{bmatrix} [K_e]_{flex} & 0 & 0 & 0 \\ 0 & [K_e^{vert}]_{axial}^{shear} & 0 & 0 \\ 0 & 0 & [K_e^{horiz}]_{axial}^{shear} & 0 \\ 0 & 0 & 0 & [K_e]_{torsion} \end{bmatrix} \tag{4.29}$$

$$[M_e]_{BEAM4} = \begin{bmatrix} [M_e]_{flex} & 0 & 0 & 0 \\ 0 & [M_e^{vert}]_{axial}^{shear} & 0 & 0 \\ 0 & 0 & [M_e^{horiz}]_{axial}^{shear} & 0 \\ 0 & 0 & 0 & 0 \end{bmatrix} \tag{4.30}$$

where $([K_e]_{flex})$ and $([M_e]_{flex})$ represent mass and stiffness flexural effects given in equation (4.39); $\left([K_e^{vert}]_{axial}^{shear}\right)$, $\left([M_e^{vert}]_{axial}^{shear}\right)$ along with $\left([K_e^{horiz}]_{axial}^{shear}\right), \left([M_e^{horiz}]_{axial}^{shear}\right)$ represent the axial stiffness and mass matrices for vertical or horizontal motion respectively. The torsional stiffness $([K_e]_{torsion})$ matrix is:

$$[K_e]_{torsion} = \frac{GJ}{L}\begin{bmatrix} 1 & -1 \\ -1 & 1 \end{bmatrix} \tag{4.31}$$

BEAM54 and BEAM44 correspond to BEAM3 and BEAM4 elements respectively in tapered form. Both allow for different asymmetric geometry at the ends of the beam and permit the end nodes to be offset from the centroidal axis of the beam (eccentric elements). By all means the lack of distinction between the shear center and the center of gravity in BEAM4 and BEAM3 elements is a negative point but considering that (i) BEAM54 and BEAM44 cannot either simulate successfully the antisymmetric motion, (ii) their definition is 'uneconomic' (due to the number of constants that have to be input) and (iii) they do not include the effects of shear deformations in their mass element matrices, engineering judgement resulted in discounting them.

All the above elements have shortcomings in simulating the coupling between horizontal bending and torsion for a vessel with large deck openings where the effects of warping free

and warping restrained torsion become important (see equations 4.31 and section 4.2.1). In principle, the correct simulation of the torsional characteristics requires the development of a special stiffness matrix that can account for both warping and warping restraint. The finite difference beam idealisation appears to be more realistic in the sense that at least it acccounts for the effect of St. Venant's torsion (see sections 4.2.1 and chapter 3).

An ideal finite beam element should satisfy the governing differential equation of torsion and its stiffness matrix must reflect both St. Venant and warping torsional stiffness. In the author's knowledge two different approaches exist in literature and although they are not used in the current investigation they could form the basis of an alternative beam formulation able of simulating appropriately the antisymmetric in vacuo dynamics of ships with large deck openings.

Kwai [4.36] has demonstrated that a suitable element could be formulated by using a third-order polynomial to represent the twist. Accordingly, the torsion stiffness matrix consists of two parts corresponding to St. Venant torsional stiffness $\left([K_e]_J\right)$ and warping torsional stiffness $\left([K_e]_\omega\right)$. In this work it is suggested that by incorporating the first derivative of the rotation (Vlasov warping degree of freedom corresponding to the bi-moment M_Ω) in the representation of the angle of twist of the cross-section the torsion matrix can be expressed as:

$$[K_e]_{torsion} = [K_e]_J + [K_e]_\omega = \frac{GJ}{L}\begin{bmatrix} 6/5 & & & \\ L/10 & 2L^2/15 & \text{symmetric} & \\ -6/5 & L/10 & 6/5 & \\ L/10 & -L^2/30 & L/10 & 2L^2/15 \end{bmatrix} + \frac{EI_{\Omega\Omega}}{L^3}\begin{bmatrix} 12 & & & \\ 6L & 4L^2 & \text{symmetric} & \\ -12 & -6L & 12 & \\ 6L & 2L^2 & -6L & 4L^2 \end{bmatrix} \tag{4.32}$$

Along the same lines, Pedersen [4.37,4.38,4.39,4.40] suggested a consistent Przemieniecki family two-noded beam finite element having three translations, three rotations and one classical Vlasov warping degree of freedom plus possibly (N) degrees of freedom associated

with higher order generalised warping deformation modes. These higher order warping modes are generated from an eigenvalue problem associated with the homogeneous plane stress equilibrium condition for the individual beam cross-sections. The corresponding stiffness and mass matrices of this element can be found in the open literature [4.37,4.39] and are not included in the thesis due to length and complexity. Apart from the incorporation of higher order warping functions, which nevertheless do not appear to affect the eigen-solution [4.39], the novelty of this approach resides upon the incorporation of continuity conditions between the open and closed part of the hull. Such conditions reassure the compatibility of the beam discretisation and since they are in the main related to the solution rather with the formulation of the problem are further highlighted in section 4.3.3. Although, to the author's knowledge, Pedersen's beam approach has been widely applied for the case of containerships it could be even more beneficial for the case of bulkers where structural discontinuities (because of the existence of hatch openings) are rather important.

4.4 Solution

4.4.1 FD solution strategy

When the finite difference method of analysis is used for the evaluation of steady state linear dynamics of a continuum the designer should keep in mind that a reliable solution is highly dependant upon:

1. the discretisation methodology (e.g. equal or unequal intervals);
2. the engineering assumptions related to the implementation of the boundary conditions for the specific problem;
3. the convergence and stability of the numerical approach. In principle the better quality (convergence and stability) of the approximation should improve with increasing refinement in discretisation provided that equilibrium and compatibility conditions are satisfied at the appropriate nodal locations of the FD grid.

There are, of course, many ways of extracting the principal modes and natural frequencies of a non-uniform beam vibrating in flexure [4.42]. Perhaps one of the most useful in ship dynamics is the so-called Prohl-Myklestad method [4.43,4.44] which is familiar in vibration theory and can be made to cater for a Timoshenko beam analysis. Accordingly, Bishop et al implemented [4.9,4.41] this methodology to simulate the symmetric and antisymmetric in

vacuo vibration of a beam-like vibrating in vacuo in absence of any structural damping effects.

Since the mathematics of the method have been well established in literature, they will not be included in the present discussion (see appendix 2). In this methodology the ship is divided into a number of sections interconnected with massless rods each having a lumped mass in the middle. The remaining structural properties are situated in the middle (mass related properties) or the ends (structure related properties) of each section. The iteration starts by assuming that the boundary value derivatives (torsional moment, shear force, bending moment) are zero at the aft end. The corresponding boundary values at the forward end are calculated by using a recurrence formulae. The numerical procedure commences with an initial frequency and the determinant of the coefficients at the forward end is calculated for the corresponding eigenvalue. Subsequently, the frequency is incremented by a certain magnitude and the procedure is repeated until a change of sign occurs in the value of the determinant. The iteration continues until the required level of accuracy is achieved.

4.4.2 FEA solution strategy-The subspace reduction method

Opposite to the FD, FEA solution methodologies are not that sensitive to the implementation of boundary conditions unless the system is constrained. Discretisation and in extent convergence and stability are important issues which should be tackled accordingly.

Five alternative eigenvalue-eigenvector extraction procedures which exist under ANSYS software namely reduced, subspace, block Lanczos, unsymmetric eigensolver and damped eigensolver were examined. The mathematical procedures related to these alternative solution algorithms are well established in literature [4.2,4.3,4.4,4.25].

The unsymmetric method was immediately rejected since it is useful whenever the system matrices are unsymmetric such as in acoustic fluid-structure interaction problems using FLUID30 elements or in rotor dynamic problems when MATRIX27 elements are used. The damped method was also not examined since the system vibrates in vacuo.

The reduced eigenvalue extraction method was also rejected. Although it is considered as quite economical in a computational sense, looses in accuracy because a condensation of the system matrices is operated via Guyan reduction where the degrees of freedom of the model are decomposed into masters and slaves [4.2, 4.4,4.25]. For beam finite element models (with small number of degrees of freedom) the selection of masters and slaves is not that practical, while for three-dimensional models significant experience is required when selecting the dominant degrees of freedom of the model.

Block Lanczos and subspace iteration methods were both appropriate for the evaluation of steady state dynamics of beam and shell models. The first one is by default a good method for the rapid evaluation of natural frequencies of large symmetric eigenvalue problems although sometimes looses slightly in accuracy. The subspace method developed and so named by K.J. Bathe [4.45,4.46] was, therefore, selected. Although it requires higher computational time than the block Lanczos and reduced iterations, it is definitely accurate and reliable. It has excellent convergence ratio, since it operates under implicit double precision and it is robust and relatively easy to understand [4.4,4.47].

4.4.3 Problems related to the solution of FD and FEA beam models

All beam models (both FD and FE) used for the purposes of the current investigation do not account for the discontinuity of the structural properties (non-prismatic features of the hull girder) which appear at the common locations of the closed/open parts of the hull girder. Such simplification leads to violation of the compatibility discretisation conditions related to the antisymmetric dynamics of a hull girder with large deck openings (e.g. bulker or containership). The problem has been initially identified by Tonnesen [4.48] and implemented in Pedersen's beam formulation [4.37,4.38,4.39,4.40]. In this approach the application of orthogonality conditions leads to the derivation of discontinuity correction factors (s_1,s_2), introduced to ensure approximate numerical kinematic compatibility at the common nodal locations of two different (open/closed) cross sections. The first correction factor (s_1) relates the warping function of the left hand side of the cross section $\chi(x_i^-)$ to the warping function of the right hand side $\chi(x_i^+)$ so that:

$$\chi\left(x_i^+\right) = s_1^i \chi\left(x_i^-\right) \text{ for } s_1^i = \pm\sqrt{\frac{I_\Omega^- - \frac{\left(I_{z\Omega}^-\right)^2}{I_{zz}}}{I_\Omega^+ - \frac{\left(I_{z\Omega}^+\right)^2}{I_{zz}}}} \tag{4.33}$$

where (I_Ω) represents the sectorial moment of inertia, (I_{yy}) the horizontal moment of inertia and ($I_{y\Omega}$) their bi-product. The second correction factor (s_2) introduces a coupling between the bending slope about the vertical axis (θ) and the warping function (χ):

$$\theta\left(x_i^+\right) = s_2^i \theta\left(x_i^-\right) \text{ for, } s_2^i = \frac{I_{y\Omega}^- - s_1^i I_{y\Omega}^+}{I_{yy}} \tag{4.34}$$

The rotation about the longitudinal axes of the beam (ϕ') is assumed to behave adequately so that:

$$\phi'\left(x_i^+\right) = \phi'\left(x_i^-\right) \tag{4.35}$$

Due to the coupling between warping displacements and horizontal bending of the ship hull, for those cases where the warping restraint effects on the hull girder are considered, Pedersen suggests an adjoint relation between the bi-moments and bending moments at a discontinuity along the longitudinal axis. This relation is determined on the basis that the work of an internal direct stress distribution (σ_x) at the junction shall be the same on both sections for an arbitrary virtual displacement. That is:

$$\left(\int_{A_{left}} \sigma_x \delta u dA\right)_{x=x_i^-} = \left(\int_{A_{right}} \sigma_x \delta u dA\right)_{x=x_i^+} \tag{4.36}$$

Hence the horizontal bending moment (M_z), the bimoment (M_Ω) become:

$$M_{z\left(x_i^-\right)} = M_{z\left(x_i^+\right)} \tag{4.37}$$

$$M_{\Omega\left(x_i^-\right)} = s_1^i M_{\Omega\left(x_i^+\right)} - s_2^i M_z\left(x_i\right) \tag{4.38}$$

Additional static discontinuity conditions for the horizontal shear force (V_z) and the torsional moment (M_x) imply:

$$V_{y\left(x_i^-\right)} = V_{y\left(x_i^+\right)} \tag{4.39}$$

$$M_{x\left(x_i^-\right)} = M_{x\left(x_i^+\right)} + V_y(x_i)\left\{z_s\left(x_i^-\right) - z_s\left(x_i^+\right)\right\} \tag{4.40}$$

4.4.4 Normalisation and orthogonality properties

The magnitude of eigenvectors can be rendered unique by a process known as normalisation. This can be implemented in ANSYS interactive environment either via using the graphical user interface or by means of a macro script, which can easily be developed by means of APDL (Ansys Parametric Design Language) [4.25]. The latter approach was followed for the purposes of this project. Concisely the mathematical process could be stated as follows:

$$\{X\}^T[M]\{X\} = [m_r] \tag{4.41}$$

$$\{X\}^T[K]\{X\} = [k_r] \tag{4.42}$$

from which $\left[\omega_r^2\right] = [m_r]^{-1}[k_r]$, where $[m_r]$ and $[k_r]$ are often referred to as the modal mass and stiffness of mode (r). Since the eigenvector matrix is subject to an arbitrary scaling factor, the normalized modal mass and stiffness quantities apriori are not unique and therefore it is inadvisable to refer to the modal mass and stiffness of a particular mode without specifying the normalisation followed. Most eigenvalue extraction routines scale each vector so that its largest element has unit magnitude, but it is not universal. In any event the ratio of $[k_r]/[m_r]$ is unique and equal to the eigenvalue. Among the many scaling or normalisation processes, the so called *mass normalisation* has most relevance to modal testing [4.49] and for this reason could be used in hydroelasticity studies. According to this technique the mass normalised eigenvectors are written as (ϕ) and have the particular property that:

$$[\phi]^T[M][\phi] = [I] \Rightarrow [\phi]^T[K][\phi] = \overline{\omega}_r^2 \tag{4.43}$$

The relationship between the mass normalised mode shape (ϕ_r) for mode (r), and its more general form X_r is:

$$[\phi] = \{X\}\left[m_r^{-1/2}\right], \text{ where } m_r = \{X_r\}^T[M]\{X_r\} \tag{4.44}$$

One of the most significant consequences of symmetry of the stiffness and mass characteristics of the system is the orthogonality of natural modes. If ω_r and ω_s are the

eigenvalues corresponding to the eigenvectors X_r, X_s respectively then the orthogonality of the natural modes implies that,

$$[X_r]^T[M][X_s] = m_{rs} = \begin{cases} \neq 0, (r = s) \\ = 0, (r \neq s) \end{cases} \tag{4.45}$$

There are several ways of interpreting physically the orthogonality relationships. For the purposes of hydroelasticity studies, however, it is important to comprehend that they specify conditions experienced by the ship when this behaves as a conservative system which is subject neither to damping nor to external excitation.

The normalisation process is related to the fact that the identification of the model's orthogonal eigen-parameters is quite important since it provides the so-called *generalised mass* and *stiffness* values. There are a variety of terminologies in this area that is worth mentioning so that at least the different quantities can be identified, even if uniformity of terminology cannot be assured. Three terms are encountered in the literature namely modal mass (and stiffness); generalised mass and effective or equivalent mass [4.49]. There is confusion with regards to the significance of each of these terms and it is worthwhile to interpret the use of generalised mass and stiffness in hydroelasticity analysis as opposed to other terms. The modal mass is a quantity based on the eigenvector for mode (r) and the system's mass matrix. There is no unique value for its magnitude and it is directly related to the scaling method that is used to define the mode shape. This scaling is completely arbitrary and, therefore, the modal mass as well as the corresponding modal stiffness could be any value.

The mass normalised vector has dimensions of mass$^{-0.5}$. In the following equation (4.46) the effective mass and stiffness diagonals $\left[m_{jj}\right]_r$ can be related to the eigenvector elements (ϕ_{ij}) by the simple formulae:

$$\left[m_{jj}\right]_r = \left[\frac{1}{\phi_{jr}}\right]^2 \text{ and } \left[k_{jj}\right]_r = \left[\frac{\omega_r}{\phi_{jr}}\right]^2 \tag{4.46}$$

the first one having the units of mass.

It can be seen that since the mass normalised eigenvectors are unique and not subject to any arbitrary scaling factors these effective mass and stiffness properties are also unique and represent a useful description of the underlying behaviour of the structure point by point and mode by mode. Hence, they may be considered as universal and therefore equivalent to the so-called effective mass and stiffness terms for the (r^{th}) mode of vibration at the degree of freedom with the largest amplitude of response.

4.5 Post-processing

4.5.1 Evaluation of internal modal loads for beam models

The algorithm UCLMOD (see chapter 6) initially developed by Temarel [4.41] implements the Bishop and Price beam finite difference ship idealisation [4.9] and performs modal analysis automatically on the basis of simple beam theory [4.9,4.12] (see section 4.2.1). The process of evaluating the dry hull stresses, shear forces, bending and torsional moments for a beam-like monohull vibrating in vacuo in absence of any damping effects is considered therefore elementary and will not be reproduced in this section.

Along the same lines ANSYS beam finite elements (BEAM3, BEAM4) provide automatically the modal internal actions of the ship at post-processing level. Following the calculation of the eigenvalues and the nodal displacements $\left(\hat{U}\right)$ the stress tensors of an element (j) are calculated from the corresponding element strains (strain displacement matrix B) and the elasticity matrix (D) under plane stress conditions (see equation 4.24) as:

$$\sigma^m = D^m B^m(x,y,z)\hat{U} \tag{4.47}$$

Consequently, the remaining of the modal loads are calculated by using beam theory [4.4,4.12]. It is important to highlight once more that although the finite difference model accounts for the warping free effects of the hull girder none of the finite difference or element idealisation used incorporates the warping restraint and non-prismatic features of the hull (see sections 4.2.1, 4.4.3).

4.5.2 Evaluation of internal modal loads for the FE shell model

As in the case of the beam FE models equation (4.57) is used for the evaluation of the direct and shear stresses at each of the four nodal points of SHELL63 element. The software does not calculate the sectorial coordinate and therefore it does not provide any information related to the direct warping stresses, contributing to the bi-moment, nor the torsional shear stresses contributing to the warping induced torsional moment (see section 4.2.1). It is therefore apparent that as in the case of beam analyses ANSYS does not consider any of the warping restraint effects imposed upon the three-dimensional model.

Another modelling issue worthwhile to mention is that in principle, since the element stresses are calculated using derivatives of the displacements, the stresses obtained at a shell element edge (or face) when calculated in adjacent elements may differ substantially if a coarse finite element mesh is used. The stress differences at the element boundaries decrease as the finite element mesh is refined and the rate at which this decrease occurs is of course determined by the level of discretisation. This numerical feature is fundamental characteristic of the finite element method of analysis and direct consequence of the fact that although forces at individual elements and element boundaries balance out, stress equilibrium is not accurately satisfied at the differential level unless a very fine finite element discretisation is used. As the number of real and virtual displacement patterns is equal to the number of nodal degrees of freedom only an approximate solution in terms of satisfying the stress equilibrium at the differentiation level is obtained (while the compatibility and constitutive relations are firmly satisfied) (see figure 4.9). Improved values are found by averaging the stress values obtained at the nodes of the adjacent elements via an APDL macro at post processing level [4.4,4.25].

In contrast to beam finite element analysis ANSYS does not provide any of the bending and torsional moments nor the shear forces of the model. Those should be calculated at post-processing level by considering individually each of the 46 sections along the hull.

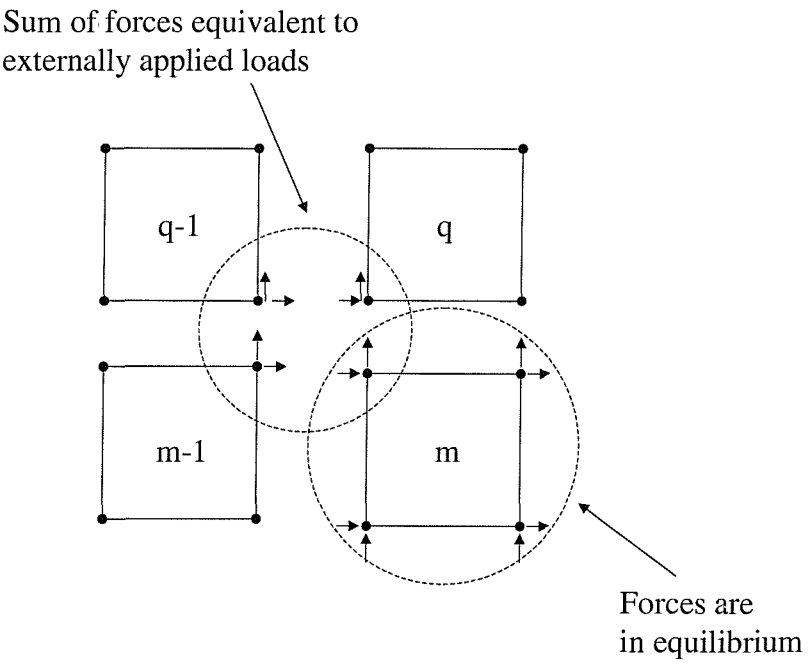

Fig. 4.9 Nodal point and element equilibrium in FEA

For a quadrilateral shell element (SHELL63 element) intersected by a cross-section having distance (x) from a ship's stern the globally transformed direct nodal stresses ($\sigma_x^{i,j}$) contribute to the modal vertical bending moment (M_y) and the horizontal bending moment (M_z). The nodal shear stresses ($\tau_{xz}^{i,j}$) contribute to the vertical shear force (V_z) and the St. Venant torsion moment (M_x). Finally, the shear stresses ($\tau_{xy}^{i,j}$) contribute to the horizontal shear force (V_y) as well as the St. Venant torsion moment (M_x). Assuming that the stress distribution is linear along the intersected length (L) of the k^{th} element the contributions to the internal actions are:

$$S_k = Lt\frac{\left(\tau_{xz}^{i} + \tau_{xz}^{j}\right)}{2} \tag{4.48}$$

$$M_k = Lt\left(\frac{\sigma_x^{i} + \sigma_x^{j}}{2}\right)\left(z_c - z_n\right) \tag{4.49}$$

$$Q_k = Lt\frac{\left(\tau_{xy}^{i} + \tau_{xy}^{j}\right)}{2} \tag{4.50}$$

$$N_k = Lt\frac{\left(\sigma_x^{i} + \sigma_x^{j}\right)}{2}y_c \tag{4.51}$$

$$L_k = S_k y_c - Q_k (z_c - z_n) \tag{4.52}$$

where (t) is the element thickness (assuming that the element has a uniform thickness), (y_c) and (z_c) are the element centre coordinates and (z_n) is the vertical position of the neutral axis (i.e. centroid) of the cross-section which lies on the ship centre line in the global system. In these equations the direct and shear stress components are assumed to represent the r^{th} (r=7,8,...etc) mode modal stresses. Thus the primary internal actions acting on a cross-section corresponding to the r^{th} symmetric mode are:

$$V_z = \sum_{k=1}^{m} S_k \tag{4.53}$$

$$M_y = \sum_{k=1}^{m} M_k \tag{4.54}$$

and to the r^{th} antisymmetric mode are:

$$V_y = \sum_{k=1}^{m} Q_k \tag{4.55}$$

$$M_z = \sum_{k=1}^{m} N_k \tag{4.56}$$

$$M_x = \sum_{k=1}^{m} L_k \tag{4.57}$$

where (m) is the total number of elements included in a cross-section.

If the analysis is extended to account for warping restraint effects, provided that the sectorial coordinate (ω) is given then for an individual element the following additional actions could be introduced:

$$S_k^* = Lt \frac{\left(\tau_{xz}^i \omega + \tau_{xz}^j \omega\right)}{2} \tag{4.58}$$

$$Q_k^* = Lt \frac{\left(\tau_{xy}^i \omega + \tau_{xy}^j \omega\right)}{2} \tag{4.59}$$

$$N_k^* = Lt \frac{\left(\sigma_x^i \omega + \sigma_x^j \omega\right)}{2} y_c \tag{4.60}$$

$$L_k^* = S_k^* y_c - Q_k^* (z_c - z_n) \tag{4.61}$$

By following this methodology the direct warping stresses ($\sigma_x^{i,j}$) contribute to the warping induced moment (bi-moment M_Ω) and the warping induced shear stresses ($\tau_{xy}^{i,j}$,$\tau_{xz}^{i,j}$) contribute to the warping induced torsional moment (M_x^*) so that:

$$M_\Omega = \sum_{k=1}^{m} N_k^* \tag{4.62}$$

$$M_x^* = \sum_{k=1}^{m} L_k^* \tag{4.63}$$

Hence, the total horizontal bending moment and torsional moment magnitudes are:

$$M_z^{tot} = M_z + M_\Omega \tag{4.64}$$

$$M_x^{tot} = M_x + M_x^* \tag{4.65}$$

Equations (4.64) and (4.65) are equivalent to equations (4.6) and (4.7). The methodology outlined in this section however is from modelling point of view superior in the sense that for ships with large deck openings (e.g. bulkers and containerships) because of the saw-tooth variation of the cross-sectional properties (see figure 4.4) the evaluation of the modal loads from the deflection differentials may lead to erroneous results.

4.6 Conclusions

This chapter focussed on the fundamental engineering assumptions and scientific principles related to the generation of two- and three-dimensional finite discretised models representing a ship having similar structural and inertial characteristics to those of OBO MV Derbyshire. From the discussion outlined the following general purpose modelling-guidelines have emerged:

- Finite discretisation techniques are useful engineering tools for the assessment of the global in vacuo dynamic behaviour of long slender monohulls.
- Engineering intuition and experience implies that irrespective of the finite discretisation technique used, the simulation methodology should comprise of three individual modules namely:
  1. *Pre-processing,* where the system is idealised geometrically into a form that can be solved by means of a feasible mathematical model representing adequately its

structural (scantlings and structural sectional properties) and dynamic characteristics (inertial structural properties);

2. *Solution,* where a numerical algorithm ensuring that boundary conditions are applied appropriately (especially when the FD method is used) while convergence, stability and compatibility conditions are not violated at the common nodal locations (especially when the hull is highly non-prismatic). The Prohl-Myklestad approach (for FD idealisations) and the subspace reduction method (for FEA simulations) are two general purpose techniques that could be adequately used;
3. *Post-processing*, where the modal actions are evaluated and the numerical results are interpreted so that modelling uncertainty is reduced via suitable model updating.

- Two- and three-dimensional idealisations due to their associated design variants and data requirements could have different uses in design. Two-dimensional beam idealisations could offer a fast and efficient means in simulating the structural dynamic behaviour of mono-hull vessels for the preliminary design stage. Three-dimensional models, although they are time and effort consuming, even when a relatively simple idealisation is used, are much more suitable in predicting/confirming the in vacuo dynamic performance of a mono- or multi-hull vessel at the detailed design stage. In any case the engineer should be able to judge and justify the limitations and advantages of each idelisation.
- The formulation of a unified beam model suitable for simulating the antisymmetric dynamic characteristics of an in vacuo vibrating hull is not that straight forward. For a non-prismatic ship (e.g. bulker or containership) the effects of warping free and warping restrained torsion along with suitable discontinuity conditions at the boundary nodes of each element should be incorporated in the beam model. None of the ANSYS beam finite elements outlined are able of simulating such effects and for the case of ships with large deck openings should be used only for the assessment of symmetric in vacuo vibrations. The Bishop Price et al finite difference scheme is slightly more advantageous in the sense that it is able of incorporating the effects of

warping free torsion. The engineer should realise the limitations of the latest idealisation when comparing the modal results with those of a suitable shell model.

- When a reasonably detailed shell finite element model of a ship structure is constructed, to avoid local deformation effects, appearing because of the omission of transverse frames and longitudinal stiffeners, fictitious bulkheads of negligible mass and thickness could be used to anchor the nodes of the elements in a direction normal to their plane. As it will be demonstrated in chapter 5 this methodology appeared to have worked well resulting in a model with a reasonably small number of elements and degrees of freedom.
- The ANSYS shell idealisation does not provide any of the stress variants (direct and shear warping stresses) related to the warping restrained dynamics of the ship structure. Ideally, for the adequate evaluation of the modal internal actions of ships with large deck openings (e.g. bulkers and containerships) such effects are important since the give rise to warping induced horizontal bending moments (bi-moments) and warping induced torsional moments. Despite this modelling disadvantage it is worthwhile to mention that comparison of the direct (and not warping induced) modal actions with those extracted from the Bishop Price finite difference idealisation could lead to significant conclusions with regards to the degree of confidence that can be placed on predictions obtained from two-dimensional beam models by comparison to three-dimensional models where special structural features, such as deck openings, double bottoms, transverse bulkheads hopper spaces etc, are modelled more explicitly.

Following these observations in the following chapter an extended modal analysis along the lines of the dry analysis module of two- and three-dimensional hydroelasticity theories is presented. The investigation is carried out by using two different types of idealisation. Namely, three-dimensional finite element models using shell-type (shell3d) and brick-type (beam3d) elements and two-dimensional beam models discretised by means of either finite element (beam2d), or equally (beamfde) and unequally (beamfd) discretised finite difference schemes.

MODEL	ABBREVIATIONS	DYNAMIC MODEL
2D beam FD or FEA	beamfd,beamfde,beam2d	Timoshenko beam
3D beam FEA	beam3d	Timoshenko beam
3D shell FEA	shell3d	Finite element plate model

Table 4.2. Outline of dry analyses

4.7 References

[4.1] Hughes, O.F., Ship structural design – A rationally based, Computer aided optimisation approach; The society of Naval Architects and Marine Engineers (SNAME), (1983).

[4.2] Meirovitch, L.; Principles and techniques of vibrations, Prentice Hall, New York, USA, (1994).

[4.3] Zienkiewicz, O.C., Taylor, R.L.: The finite element method, McGraw Hill, New York, USA, (1979).

[4.4] Bathe, K.J.: Finite element procedures, Prentice Hall, New Jersey, USA, (1996).

[4.5] Ferziger, J.H., Peric, M: Computational methods for fluid dynamics, Springer, Berlin, Germany, (1997).

[4.6] Bishop, R.E.D., Price, W.G. and Temarel, P.: A theory on the loss of MV OBO Derbyshire, Trans. RINA, 127:169-186, (1991).

[4.7] Bishop, R.E.D., Price, W.G. and Temarel, P.: Derbyshire - A design review, Report to Dept. of Transport, UK, (1984).

[4.8] Faulkner, D., An analytical assessment of the sinking of the MV Derbyshire; Trans. SNAME, 106:59-103, (1998).

[4.9] Bishop, R.E.D. and Price, W.G.: Hydroelasticity of Ships, Cambridge University Press, UK, (1979).

[4.10] Vlasov, V.Z.: Thin walled elastic beams, Israel program for scientific translation, Jerusalem, (1961).

[4.11] Haslum, K., Tonnessen, A.: Torsional analysis of ship hulls, European Shipbuilding, No. 5/6, (1972).

[4.12] Gere, J.M. and Timoshenko, S.: Mechanics of Materials; Third SI edition, Chapman and Hall, (1987).

[4.13] Paz, M.,Strehl, C.P. and Schrader, P. : Computer determination of the shear center of open and closed sections ; Journal of Computers and Structures, 6:117-125, (1976).

[4.14] Gilbert, D. and Ward, G.: Report on the computed structural properties for MV Derbyshire; British Ship Research Association (BSRA), (1983).

[4.15] Mathworks Inc.; FEMAP v.3.2, Finite element analysis system; Mathworks Inc., (1999).

[4.16] Germanischer Lloyd, POSEIDON Manual, V2.0, (1999).

[4.17] Cowper, C.R.: The shear coefficient in Timoshenko beam theory; Journal of Applied Mechanics, 33:335-340, (1997).

[4.18] Schramm, U., Kitis, L., Kang, W., Pilkey, W.D.: On the shear deformation coefficient in beam theory, Finite Elements in Analysis and Design, 16:141-162, (1994).

[4.19] Chalmers, D.W. and Price, W.G.: On the effective shear area of ship sections, Trans. RINA, 122: 245-252, (1980).

[4.20] Turner, M, Clough, R., Martin, H. and Topp, L.: Stiffness and deflection analysis of complex structures, Journal of Aerospace Science, 23:805-823, (1956).

[4.21] Courant, R.: Variational methods for the solution of problems of equilibrium and vibration, Bulletin of the American Mathematical Society, 49:1-43, (1943).

[4.22] McHerny, D.:A lattice method for the solution of plane stress problems, Journal of Institution of Civil Engineers, 21:59-82, (1943).

[4.23] Hrenikoff, A. Solution problems in elasticity by the framework method, Journal of Applied Mechanics, 8:169-175, (1941).

[4.24] Argyris, J, Kesley, S.: Energy theorems and structural analysis, Butterworth Scientific Publications, London, (1960).

[4.25] Swanson Ltd.: The ANSYS 5.6 users manual, (2000).

[4.26] Price, W.G., Salas Inzunza, M.A. and Temarel, P.: The dynamic behaviour of a mono-hull in oblique waves using two- and three-dimensional fluid-structure interaction models, Submitted to Trans. RINA, (2000).

[4.27] Price, W.G., Temarel, P. and Keane, A.J.: Hydroelastic analysis of a SWATH in waves, In International Conference of Hydroelasticity in Marine Technology, 231-243, Trondheim, Norway, (1994).

[4.28] Zienkiewicz, O.C., Kelly, D.W. and Battess, P.: The coupling of the finite element method and boundary solution procedures; International Journal for Numerical Methods in Engineering, 11: 355-375, (1977).

[4.29] Przemieniecki, J.S.: Theory of matrix structural analysis, McGraw Hill, New York, USA, (1970).

[4.30] Miao, S.H., Price, W.G. and Temarel, P.: The hydroelastic behaviour of multihulls travelling in a seaway, Proceedings of the 3rd International Conference Advances in Marine Structures, Dunfermline, (1997).

[4.31] Louarn, F.H. and Temarel, P.: An investigation of the structural dynamics of a racing yacht, In Proceedings of the 14th Chesapeake Sailing Yacht Symposium, 123-142, USA, (1999).

[4.32] Lees, A.W. and Thomas, D.L.: A unified Timoshenko beam finite element; Journal of Sound and Vibration, 80:335-366, (1981).

[4.33] Lees, A.W. and Hirdaris, S.E.: Models of beams and frames; 17th International modal analysis conference (IMAC), 1:1531-1537, Kissimmee, Florida, USA, (1999).

[4.34] Hirdaris, S.E. and Lees, A.W.: On the Identification of natural frequencies of thick portal frames; 7th International Conference on recent advances in Structural dynamics; Finite elements and applications; Vol. 2, pp. 887 - 899, Southampton, (2000).

[4.35] Hirdaris, S.E. Finite element modelling of free vibrating continuous systems; MSc Internal Report, University of Wales Swansea, Department of Mechanical Engineering, Wales, UK, (1998).

[4.36] Kwai, T.: The application of finite element methods to ship structures; Computers and Structures, 3:1175-1194, (1973).

[4.37] Gunnlaugsson, A.G. and Pedersen, P.T.: A finite element formulation for beams with thin walled cross-sections, Computers and Structures, 15:691-699, (1982).

[4.38] Pedersen, P.T.: A beam model for the torsional-bending response of ship hulls; Trans. RINA, 119:171-182, (1983).

[4.39] Pedersen, P.T.: Torsional response of containerships; Journal of Ship Research, 29:194-20, (1985).

[4.40] Pedersen, P.T.: Beam theories for torsional response of ship hulls; Journal of Ship Research, 35:254-265, (1991).

[4.41] Bishop, R.E.D., Price, W.G. and Temarel, P.: Antisymmetric vibration of ship hulls, Trans. of RINA, 122:197-208, (1980).

[4.42] Bishop, R.E.D, Gladwell, G.M.L. and Michaelson, S.: The matrix analysis of vibration, Cambridge University Press, UK, (1965).

[4.43] Myklestad, N.O.:A new method for calculating natural modes of uncoupled bending vibrations of airplane wings and other types of beams, Journal of Aerospace Science,11:153-162, (1944).

[4.44] Bishop, R.E.D.: Myklestad's method for non-uniform vibrating beams, Engineer, 202: 838-840 and 874-875, (1956).

[4.45] Bathe, K.J: Solution methods of large generalised eigenvalue problems in structural engineering, Report UC SESM 71-20, Civil Engineering Department, University of California, Berkeley, (1971).

[4.46] Bathe, K.J.: Convergence of subspace iteration, Formulations and numerical algorithms in finite element analysis (Bathe, K.J., Oden, J.T. and Wunderlich, W., eds.), M.I.T. Press, Cambridge, MA, 1:575-598, (1977).

[4.47] Bathe, K.J and Wilson, E.L.: Large eigenvalue problems in engineering analysis, ASCE Journal of Engineering Mechanics Division, 99:467-479, (1973).

[4.48] Tonnesen, A. and Haslum, K.: An analysis of torsion in ship hulls, European Shipbuilding, 5/6, (1972).

[4.49] Ewins, D.J.: Modal Testing, Research Studies Press Ltd., England, UK, (2000).

[4.50] Gilbert, D. and Ward, G.: Report on the computed structuiral properties for MV Derbyshire, British Ship Research Association (BSRA), (1983).

[4.51] Donaldson, Lord: Lord Donaldson's assessment (DERBYSHIRE), Cm 3128, London, HSMSO, December, ISBN-0-10-131282-2, (1995).

Chapter 5

Dry Analyses

5.1 Introduction

In this chapter two- and three-dimensional idealisations are implemented to determine the symmetric and antisymmetric in vacuo dynamic characteristics of a bulk carrier hull, representing a structure similar to that of OBO MV Derbyshire. Along the ship structural modelling guidelines outlined in chapter 4 the investigation is carried out by using two different types of idealisation. These are three-dimensional finite element models using shell-type (shell3d) and brick-type (beam3d) elements and two-dimensional beam models discretised by means of either finite element (beam2d), or equally (beamfde) and unequally (beamfd) discretised finite difference schemes (see table 4.2). The dynamic characteristics (i.e. natural frequencies, mode shapes, generalised masses, modal stresses, shear forces, bending and torsional moments) of all idealisations are outlined and the analogies between beam and shell finite discretisations are discussed. Special emphasis is paid upon identifying the influences of hatch openings, shear center and warping rigidity on the antisymmetric dynamics of the structure and for this reason the in vacuo dynamics of open- and closed-deck ship structures are also highlighted. It is shown that although in symmetric motion long slender mono-hulls behave like beam structures certain deviations from this behaviour are encountered in antisymmetric plane where the non-prismatic features of the hull girder appear to be of utmost importance.

5.2 Frequency parameter identification

The modal analysis issues outlined in the current and the following sections of this chapter are based on finite discretised models which are believed to represent realistically the general

particulars along with the mass and structural properties of OBO MV Derbyshire as shown in chapter 4.

Initial investigations [5.1,5.2] have led to a better understanding of the significance of uneven mass distribution as well as the stiffness and effective shear area effects along the hull. These studies were concentrated upon comparing the modal characteristics of shell3d with those of an equally spaced finite difference model (beamfde) for both symmetric and antisymmetric in *vacuo* vibrations (see appendices 4,5). At second stage the relation of modal characteristics of shell3d with those of an unequally spaced finite difference model (beamfd) for both symmetric and antisymmetric motion as well as beam2d and beam3d beam and brick type finite elements respectively (for the symmetric motion only) were explored. An overview of the natural frequencies and corresponding mode shapes, in ascending order, obtained for model shell3d are shown in figure 5.1. As this vessel is assumed to be port-starboard symmetric the principal mode shapes were classified as symmetric (vertical bending) and antisymmetric (coupled horizontal bending and torsion). The corresponding natural frequencies are shown in tables 5.1, 5.2 and tables 5.3, 5.4 for equal and unequal finite difference discretisation respectively in ascending form, including a brief description of the type of mode shape.

Two sets of natural frequencies were calculated for model shell3d, corresponding to thicknesses (t_{fb}=1mm and 5mm) for the fictitious bulkheads used. This methodology has led to better understanding of the influence of these bulkheads on the modal characteristics. It was observed that values of (t_{fb}<1mm) resulted in the emergence of localised distortions in the mode shapes obtained, whilst for values of (t_{fb}>5mm) eigenvector stiffening occurred. In other words 1mm is the minimum thickness that can be assigned to the fictitious bulkheads of this structural idealisation in order to obtain realistic mode shapes. The natural frequencies increase with increasing values of (t_{fb}), as can be seen from tables 5.1,5.2 due to increasing stiffness but not mass. Comparison of the finite element and finite difference calculations obtained when beamfde and beamfd discretisation practice is followed show some marginal differences in both symmetric and antisymmetric frequency domains which are increasing with increasing with modal complexity. This is clearly demonstrated via comparison of table

5.1 against 5.3 (symmetric) as well as table 5.2 against 5.4 (antisymmetric). Irrespective of the type of beam discretisation (equal or unequal) the effect of including rotary inertia and shear deformation is to decrease the natural frequency of the system. As explained in chapter 4 (see section 4.2.3) the estimation of the effective shear area factor is controlled arbitrarily and for the purposes of the current investigation the same effective shear area was used for both finite element and finite difference schemes based on the needs of the equally spaced finite difference model. This resulted in 0.23 and 0.28 of the cross-section area being considered effective in shear for the symmetric and antisymmetric distortions respectively. The same factors were used for the unequally spaced model in an attempt to assess the effects of discretisation methodology upon the bulkers in vacuo dynamic performance. For the first symmetric mode shape the natural frequency obtained from model shell3d (t_{fb}=1mm) is higher than the one calculated from all beam models. This trend is gradually changing for higher mode shapes. The finite difference appears to be always stiffer than the finite element approach when the unequal spacing discretisation scheme is followed (see tables 5.3,5.4). This is an expected numerical result which, in the main, could be attributed to the sensitivity of the finite difference scheme boundary conditions implied via the Prohl-Myklestad approach (see section 4.3.1). All finite element models predict a longitudinal mode shape, which is not included in the formulation of model beamfd. The antisymmetric natural frequencies calculated using model shell3d (t_{fb}=1mm) are lower than the corresponding predictions from model beamfde (accounting for the effects of warping) for its first two mode shapes, but higher for the remaining few, as can be seen from table 5.2. When unequal discretisation is used beamfd is always stiffer than shell3d. The antisymmetric dynamic behaviour of this vessel is driven by the influence of warping, i.e. the natural frequencies calculated from model beamfd ignoring the effects of warping (assuming zero warping stiffness) are very low and, in the main, dominated by torsion. In this respect, one should note that the maximum value for the warping stiffness (or sectorial second moment of area) corresponds to a minimum value of torsional stiffness (or torsional constant) and occurs at sections with hatch openings as can be seen from figure 4.4.

Model Mode type	beamfde k=0,I_z=0	beamfde	beam2d	beam3d	shell3d t_{fb} = 0.001m	shell3d t_{fb} = 0.005m
2 node VB	5.073	4.419	4.503	4.503	4.529	4.598
3 node VB	13.058	9.247	9.067	9.072	9.010	9.343
4 node VB	24.950	14.236	13.737	13.741	13.236	14.999
5 node VB	37.458	17.615	17.105	17.106	15.915	17.567
Longitudinal	-	-	17.824	17.831	17.932	18.208
6 node VB	61.332	25.019	23.986	23.989	24.586	25.250

Table 5.1 Natural frequencies (rad/s) for symmetric distortions of the dry hull (t_{fb} = thickness of fictitious bulkheads, VB = vertical bending,k = shear factor, I_z= rotary inertia).

Model Mode type (I_z, kA, $C_W \neq 0$)	beamfde $C_W \neq 0$ k=0.28	shell3d t_{bf} = 0.001m	shell3d t_{bf} = 0.005m	beamfde $C_W \neq 0$, k=0,I_z=0	beamfde $C_W = 0$, k=0.28
1 node HB – 1 node **T**	5.148	5.004	5.390	5.274	1.655
2 node **HB** - 2 node T	5.847	5.554	5.727	7.251	2.933
2 node HB – 2 node **T**	10.099	12.629	12.993	11.486	4.523
3 node **HB** – 3 node T	11.132	10.712	11.045	13.955	5.392
3 node HB – 3 node **T**	15.385	18.981	19.440	18.933	6.770
4 node **HB** – 4 node T	16.382	16.286	16.725	22.033	7.773

Table 5.2 Natural frequencies (rad/s) for antisymmetric distortions of the dry hull (HB = horizontal bending, **HB** = dominant HB, T = torsion, **T** = dominant T, C_w= warping stiffness, k = shear factor, I_z= rotary inertia).

model mode type	beamfd k=0,I_z=0	beamfd	beam2d	beam3d	shell3d t_{fb} = 0.001m
2 node VB	5.262	4.527	4.503	4.502	4.529
3 node VB	13.085	9.060	9.067	9.072	9.010
4 node VB	24.285	13.632	13.737	13.741	13.236
5 node VB	35.595	16.954	17.105	17.106	15.915
Longitudinal	-	-	17.824	17.831	17.932
6 node VB	57.078	23.363	23.986	23.989	24.586

Table 5.3 Natural frequencies (rad/s) for symmetric distortions of the dry hull (t_{fb} = thickness of fictitious bulkheads, VB = vertical bending, k = shear factor, I_z= rotary inertia).

Model Mode type (I_z, kA, $C_W \neq 0$)	beamfd $C_W \neq 0$	shell3d t_{bf} = 0.001m	beamfd $C_W \neq 0$, k=0,I_z=0	beamfd $C_w = 0$
1 node HB – 1 node **T**	5.992	5.004	6.173	1.797
2 node **HB** - 2 node T	6.261	5.554	7.742	3.189
2 node HB – 2 node **T**	10.995	12.629	13.323	4.622
3 node **HB** – 3 node T	12.656	10.712	16.432	5.856
3 node HB – 3 node **T**	16.047	18.981	23.749	7.077
4 node **HB** – 4 node **T**	17.086	16.286	24.605	8.080

Table 5.4 Natural frequencies (rad/s) for antisymmetric distortions of the dry hull (HB = horizontal bending, **HB** = dominant HB, T = torsion, **T** = dominant T, C_w = warping stiffness, k = shear factor, I_z= rotary inertia).

2 node VB
(ω_r = 4.529 rad/s)

1 node HB and 1 node **T**
(ω_r = 5.004 rad/s)

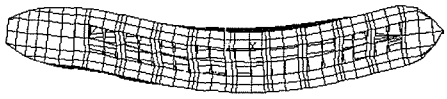

2 node **HB** and 2 node T
(ω_r = 5.554 rad/s)

3 node VB
(ω_r = 9.010 rad/s)

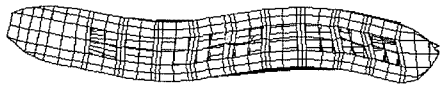

3 node **HB** and 3 node T
(ω_r = 10.712 rad/s)

2 node HB and 2 node **T**
(ω_r = 12.629 rad/s)

4 node VB
(ω_r = 13.236rad/s)

5 node VB
(ω_r = 15.915 rad/s)

4 node **HB** and 4 node T
(ω_r = 16.286 rad/s)

3 node HB and 3 node **T**
(ω_r = 18.981 rad/s)

Fig. 5.1 Principal mode shapes of model shell3d (VB: vertical bending; HB: horizontal bending; T: torsion, **HB**: dominant HB, **T**: dominant T).

5.3 Eigenvector identification

The vertical deflections, normalised to unit vertical displacement at the stern (near A.P.; keel centre line for model shell3d) are shown for all models in figure 5.2. There is good agreement between all symmetric mode shapes although the wavelength of the eigenvector for beamfde simulation remains unrealistically smooth due to the equally spaced discretisation and shell3d idealisation appears to provide more distorted results at higher modes. The latest probably appears because of the fact that the shell type idealisation provides more realistic description of the higher modal distortions possibly due to the inclusion of the local hull characteristics (e.g. double bottom) in the global dynamics of the structure.

Comparison of the first few antisymmetric mode shapes, normalised to unit horizontal displacement at the stern (near A.P.; keel centre line for model shell3d) are shown in figures 5.3,5.4. The mode shapes are represented by the horizontal displacement (at shear center) and the angle of twist for the finite difference beam idealisations (warping is considered). The horizontal displacements (v_k) and (v_d), at keel (centre line) and deck (junction of side and deck shells) respectively, are used for model shell3d. The corresponding angle of twist is calculated as $\tan^{-1}[(v_k-v_d)/D]$, where (D) represents the vertical distance between deck and keel. The horizontal deflections at keel and deck of model shell3d are very close to each other for horizontal bending dominated modes, (e.g. see figures 5.3(b) and 5.4(a)) but different for the torsion dominated modes although, in general, have the same characteristics (e.g. see figures 5.3(a) and (c) and 5.4(b)). This difference can sometimes result in horizontal deflections with different number of nodes for the keel and deck. In spite of these difficulties, the overall agreement between the mode shapes obtained from all models is good for the first few mode shapes.

In any case it is important to highlight that in both symmetric and antisymmetric planes the eigenvectors resulting from the equal beam discretisation (beamfde), in general, compare well with those of beamfd idealisation and in this sense they model realistically the in vacuo dynamics of the vessel.

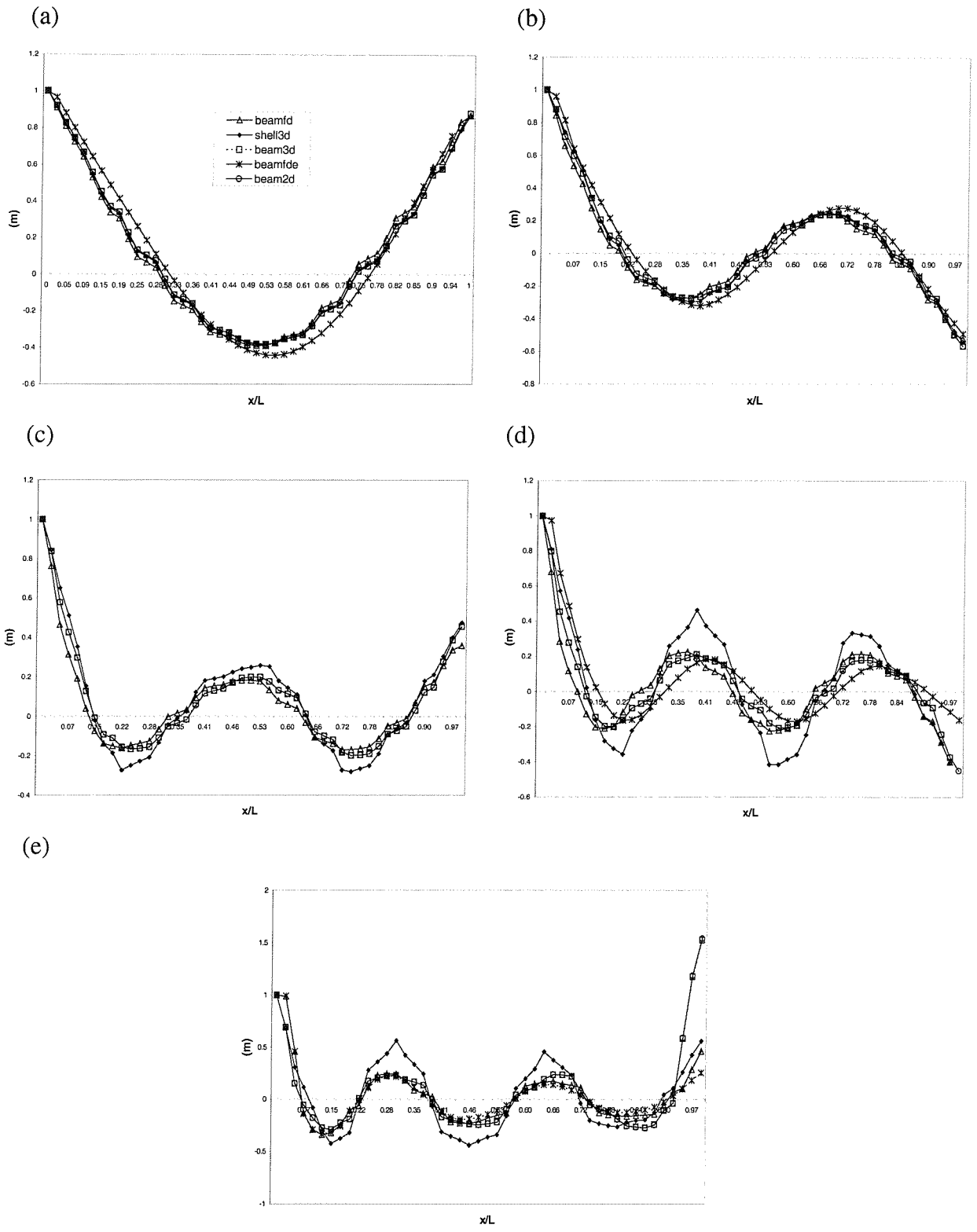

Fig. 5.2 Symmetric mode shapes for all models corresponding to (a)2 node, (b)3 node, (c)4 node, (d)5 node and (e) 6 node vertical deflections.

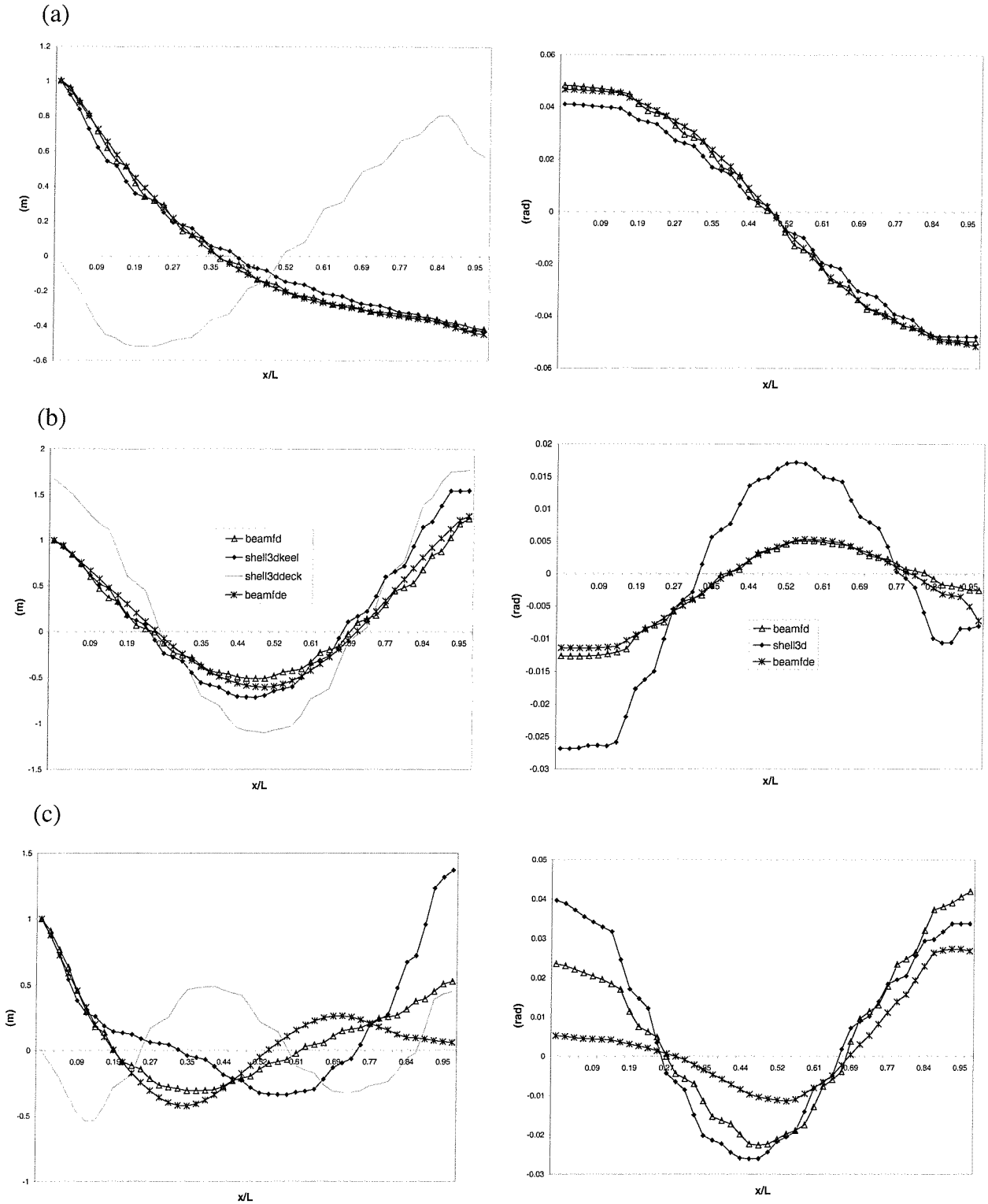

Fig. 5.3 Antisymmetric mode shapes, represented by the horizontal deflection (m) and twist angle (rad), obtained from models beamfde ($C_w \neq 0$), beamfd ($C_w \neq 0$) and shell3d (keel centre line and deck side junction) corresponding to: (a) 1 node HB 1 node **T**; (b) 2 node **HB** 2 node T; (c) 2 node HB 2 node **T** (HB: horizontal bending; T: torsion; **HB, T**: dominant HB,T).

(a)

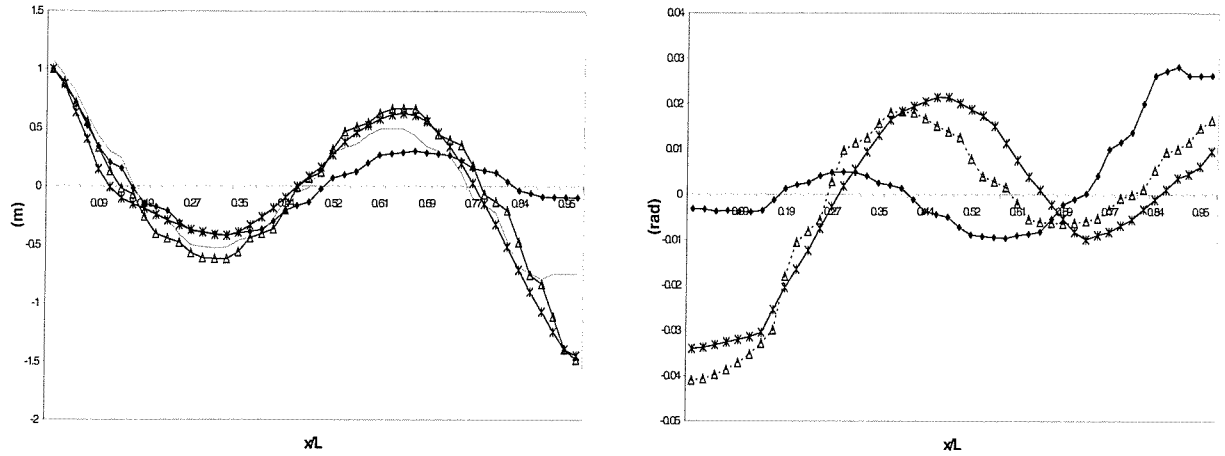

(b)

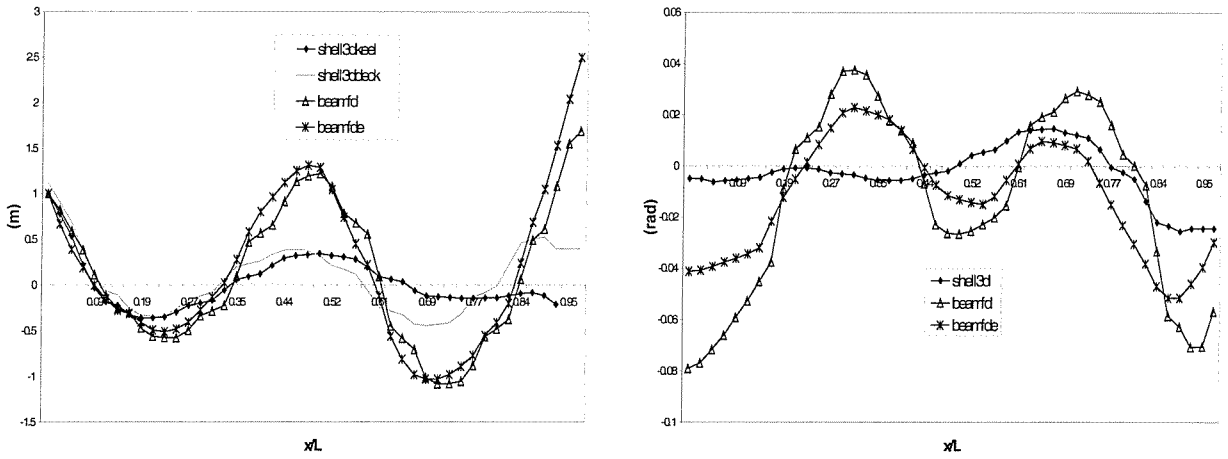

Fig. 5.4 Antisymmetric mode shapes, represented by the horizontal deflection (m) and twist angle (rad), obtained from models beamfde ($C_w \neq 0$), beamfd ($C_w \neq 0$) and shell3d (keel centre line and deck side junction) corresponding to: (a) 3 node **HB** 3 node T; (b) 3 node HB 3 node **T** (HB: horizontal bending; T: torsion; **HB, T**: dominant HB,T).

5.4 Generalised masses

For the purposes of the current investigation equation (4.56) was implemented into an ANSYS macro (see sections 4.3.4, 4.3.5) so that the generalised masses were evaluated for all finite element models and all symmetric and antisymmetric modes of vibration for unit deflection (vertical or horizontal) at stern. As it will be demonstrated two factors affect the generalised masses namely the length of each of the finite sections along the ship and the complexity of the distortions for the specific eigenvalue. It becomes obvious from table 5.5 that the generalised mass values of the finite elements (shell3d, beam2d and beam3d) and finite difference approximations are in good agreement when both equal or unequal spaces are used respectively. It is clear, however that equal spacing provides higher generalised masses for the lower modes of vibration (2,3 noded vertical bending) and lower generalised masses for higher modes (3,4,5 node vertical bending). The discrepancies in the generalised masses between the shell and beam (finite element and finite difference) idealisations is increased for the fifth and sixth modes. This is due to the fact that the shell model distorts differently to the beam models (see figure 5.3). Along the same lines the finite difference model deviates from the generalised mass values of the finite element beam idealisations and from the shell idealisation for five and six node vertical bending.

Mode description	Generalised mass (tonne-m^2)					
	shell3d	beam2d	beam3d	beamfd	beam3d (equal)	beamfde
2 node VB	19364	19772	19761	19648	25145	24834
3 node VB	8922	8805	8799	8591	12055	11082
4 node VB	6577	4788	4778	4308	5612	4492
5 node VB	10036	5054	5072	6268	3481	3940
6 node VB	8854	7400	7343	5868	6944	3984

Table 5.5 Symmetric motion generalised masses for alternative finite discretisation schemes

For the antisymmetric motion some discrepancies in the values between the shell and beam finite difference idealisations were found (see table 5.6). This was expected since the eigenvectors of the shell model deviate in magnitude from those of the beam finite difference approximation. For example, for the first torsion dominated mode (where very good agreement is achieved between the two numerical approximations) the generalised masses are in much better agreement than for the higher modes of vibration.

Mode description	Generalised mass (tonne-m^2)		
	shell3d	beamfd	beamfde
1 node HB – 1 node **T**	81577.10	84710.95	95683.54
2 node **HB** – 2 node T	53729.74	34277.81	40727.19
2 node HB – 2 node **T**	15313.22	25142.98	14116.81
3 node **HB** – 3 node T	40267.67	51104.78	37139.76
3 node HB – 3 node **T**	8287.68	13185.35	7447.02
4 node **HB** – 4 node T	18827.63	17879.12	15382.34

Table 5.6 Anti-symmetric motion generalised masses for alternative finite discretisation schemes.

5.4 Evaluation of internal modal loads

In hydroelasticity studies the evaluation of the modal direct stresses and bending moments is considered important since it leads to the estimations of the hydroelastic stresses and bending moments along the hull girder after the application of Rayleigh's theorem (see section 3.7). Although the calculations included in the current part of the analysis do not include the relevant hydrodynamic actions, they could provide (i) preliminary indication of the possible defects in the global behaviour of the hull girder (ii) information for the scantling assessment and reiteration process which is as significant for the feasibility and preliminary design stages.

Figures 5.5 and 5.6 demonstrate the distribution of global direct stresses (σ_x) along the hull for the flexible modes of vibration of shell3d. The illustration of the direct stress tensors by means of multi-dimensional contours provides an indication of the effects that global symmetric and antisymmetric vibration imposes upon the structure. For symmetric distortions (sagging, hogging) the bottom and especially deck side junction of the vessel appears to be vulnerable to high stresses (see figure 5.5). On the other hand antisymmetric and especially horizontal bending dominant modes (see figure 5.6) clearly indicate that the vessel although in vacuo experiences high stresses at the vicinities between the forward and aftward hatch openings with the bow and stern closed section decks respectively (transverse sections 7,8 and 41,42). Although this point could be further investigated in the wet analysis calculations at different wave headings and sea states, it is useful to note at this early stage that this particular occurrence could be a reason for concern under the imposition of fluid actions or green water

on decks leading to bow section fracture (and subsequently flooding). In any case it is quite interesting that, even at 'dry stage', the antisymmetric distortions raise such a point of speculation considering that traditionally they are not considered in the hull girder analysis. The antisymmetric direct stresses at the bottom of the structure are almost negligible.

The relation of modal internal actions predicted by shell3d model against all beam idealisations (beam2d, beam3d, and beamfd) for symmetric motions and the finite difference beam model (beamfd, beamfde) for antisymmetric motions was explored.

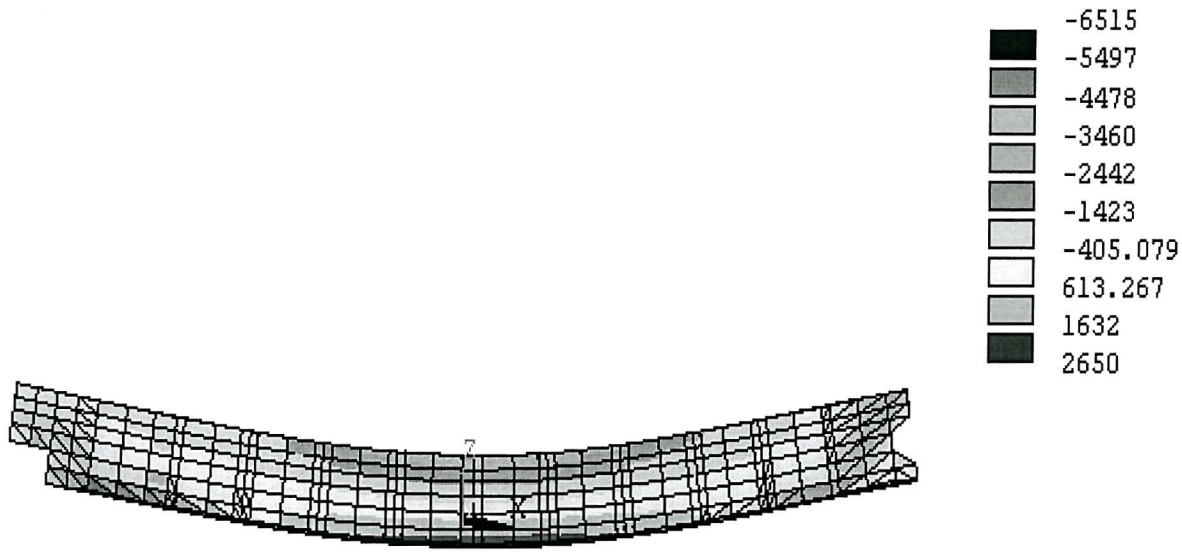

2 node VB
(ω_r=4.529 rad/s)

Fig. 5.5 Two-noded symmetric direct modal stresses (KN/m^2) for shell3d idealisation (VB: vertical bending)

(a)

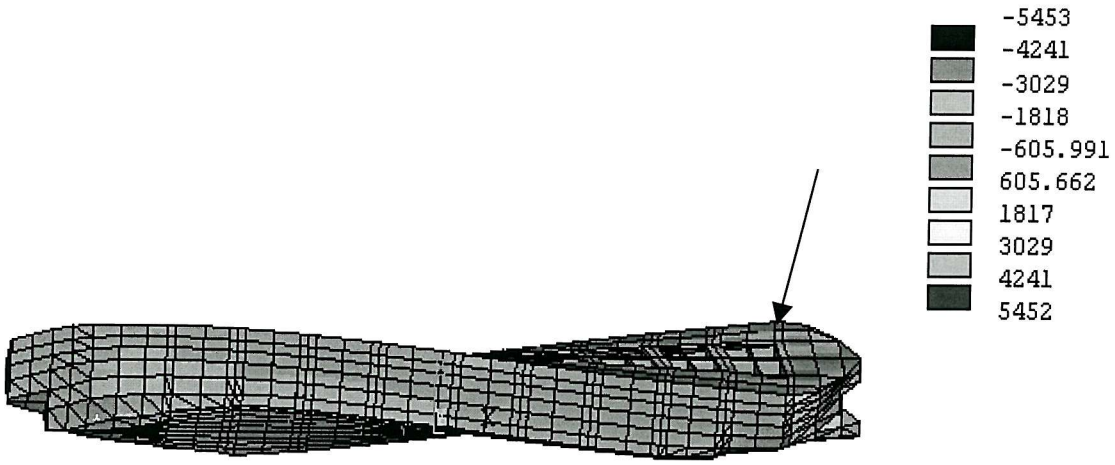

1 node HB and 1 node **T**
(ω_r=5.004 rad/s)

(b)

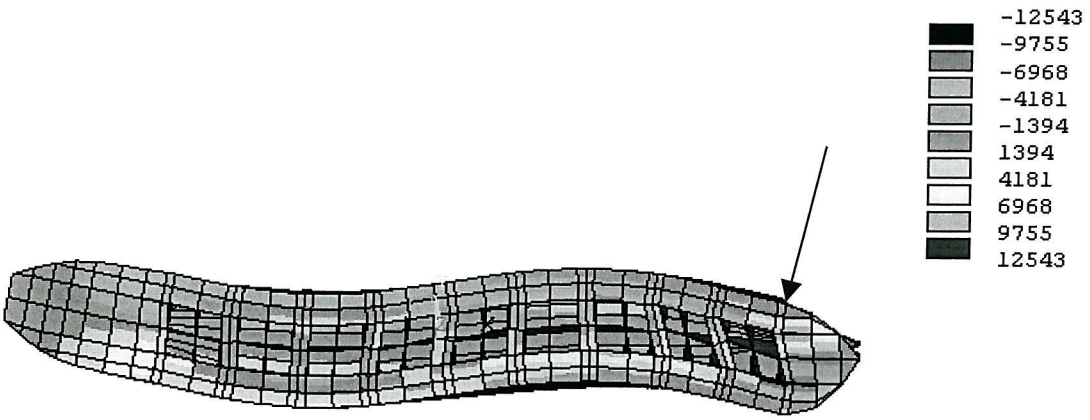

2 node **HB** and 2 node T
(ω_r=5.554 rad/s)

Fig. 5.6 Antisymmetric direct modal stresses (KN/m^2) for shell3d idealisation – arrows indicate possible critical areas (HB: horizontal bending, T: torsion, **HB,T**: dominant HB, T).

For the finite difference and the finite element two-dimensional beam models the modal shear force and bending moment values were readily available (see section 4.5.1). For the shell3d idealisation, however, the relevant modal actions at a particular station had to be appropriately defined by means of the corresponding internal actions. Modelling experience has shown that in the case of ships with large deck openings the simplified evaluation of modal loads from the product of the appropriate nodal direct stresses and the corresponding section modulus along the deck edge or the keel (for vertical or horizontal bending moments) as shown in equations (5.1),(5.2) should be avoided and the modelling approach outlined in section 4.5.2 should be followed.

$$\left(\text{HBM or VBM}\right)_{\text{deck}} = \sigma_{xr}^{\text{deck}} \times S_{\text{deck}} \tag{5.1}$$

$$\text{VBM}_{\text{keel}} = \sigma_{xr}^{\text{keel}} \times S_{\text{keel}} \tag{5.2}$$

To demonstrate the latter, the values of VBM and HBM calculated for the shell3d model were compared against those of all beam idealisations for the first two modes of symmetric vibration. As it is shown in figures 5.7(a),(b) the beam approximations are in remarkably good agreement. Maximum VBM magnitudes are obtained from model shell3d along the deck edge of the ship (where maximum direct stresses appear) and, consequently, minimum values appear along the double bottom centreline. Although this methodology provides some indication with regards to the significance of modal actions the saw-tooth variation of the bending moment curve for shell3d model, mapping the non-prismatic features of the hull girder, is not acceptable since it deviates form the traditional naval architecture rule implying its continuous distribution along the hull girder. Similar effects appear when the HBM of shell3d model at the second mode of antisymmetric vibration (horizontal bending dominant mode) is compared against that of beamfd idealisation (see figure 5.7(d)). For the first antisymmetric mode (torsion dominant) the results are rather disappointing since the shell idealisation does not provide any meaningful comparison against the corresponding values of beamfd model (see figure 5.7(c)). Neither of these modelling problems appear when the symmetric and antisymmetric modal actions are evaluated from the summation of the nodal stress at each of the elements of a cross-section (see section 4.5.2). From figures 5.8 and 5.9 becomes obvious that all compared modal vertical bending moments as well as shear forces, are in remarkably good agreement although with increasing modal complexity the predicted distortions from alternative models show some small differences. This fact clearly

demonstrates the beam-like behaviour of the bulk carrier in symmetric distortions. For the antisymmetric motion once more the results are particularly interesting. Shell3d and finite difference idealisations are not in such a good agreement, with the finite difference approximation overestimating the shell idealisation results (see figures 5.10,5.11,5.12). However, comparison of figure 5.7(c) against 5.10(a) and 5.7(d) against 5.10(b) clearly demonstrates the validity of the approach. Comparison of symmetric and antisymmetric dynamic loads of all idealisations against the equally spaced finite difference scheme (beamfde) has shown that as in the case of natural frequencies, generalised masses and eigenvectors the type of discretisation is not that significant for the first few modes of vibration (see figures 5.8,5.9,5.10,5.11,5.12).

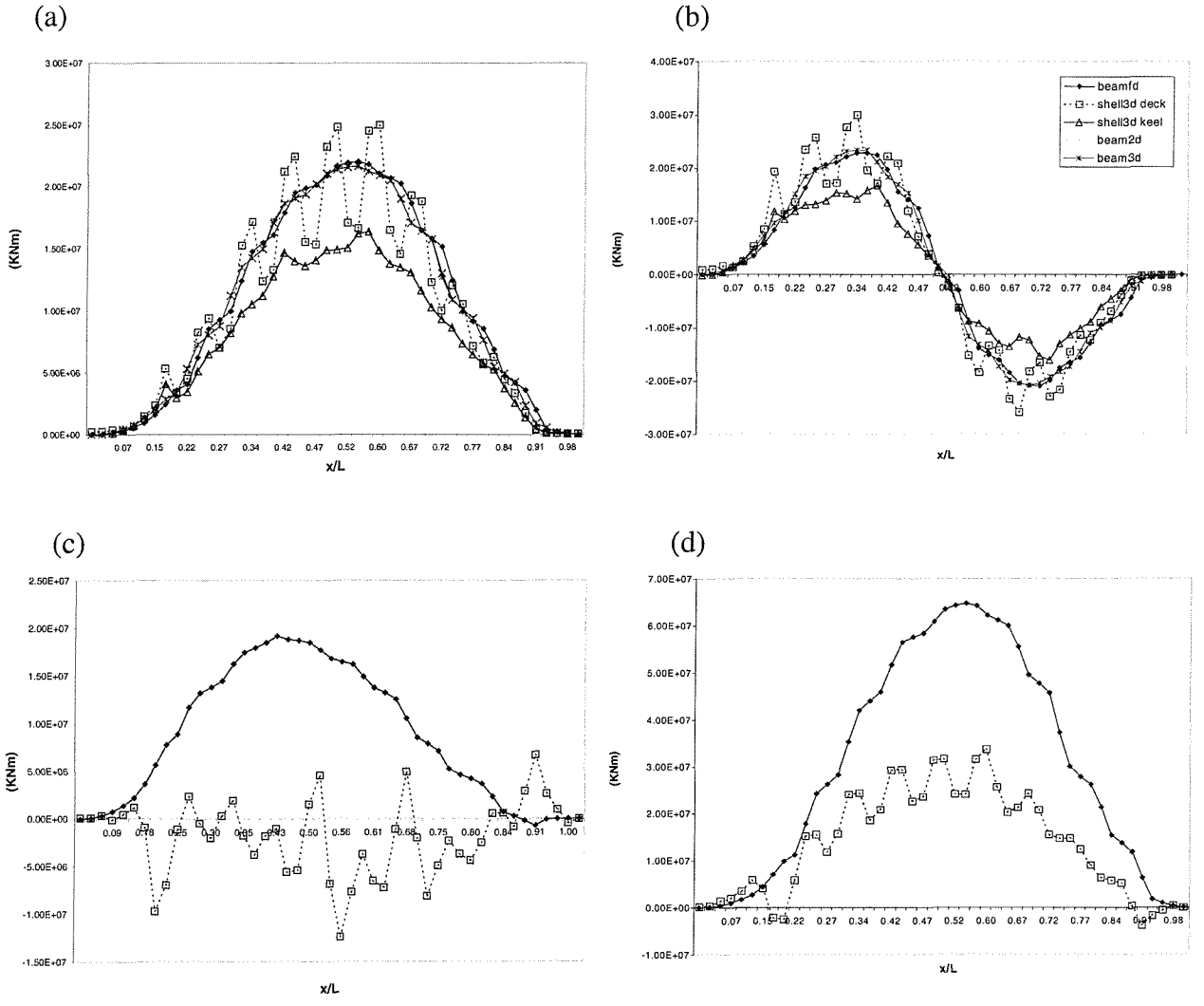

Fig.5.7: Vertical and horizontal modal bending moment variations (VBM, HBM) for all models when only the direct stresses along the deck edge or keel of the shell model are considered (a) 2 node VB; (b) 3 node VB; (c) 1 node **HB** 1 node T; (d) 2 node **HB** 2 node T; (VB: vertical bending, HB: horizontal bending, T: torsion, **HB,T**: dominant HB,T).

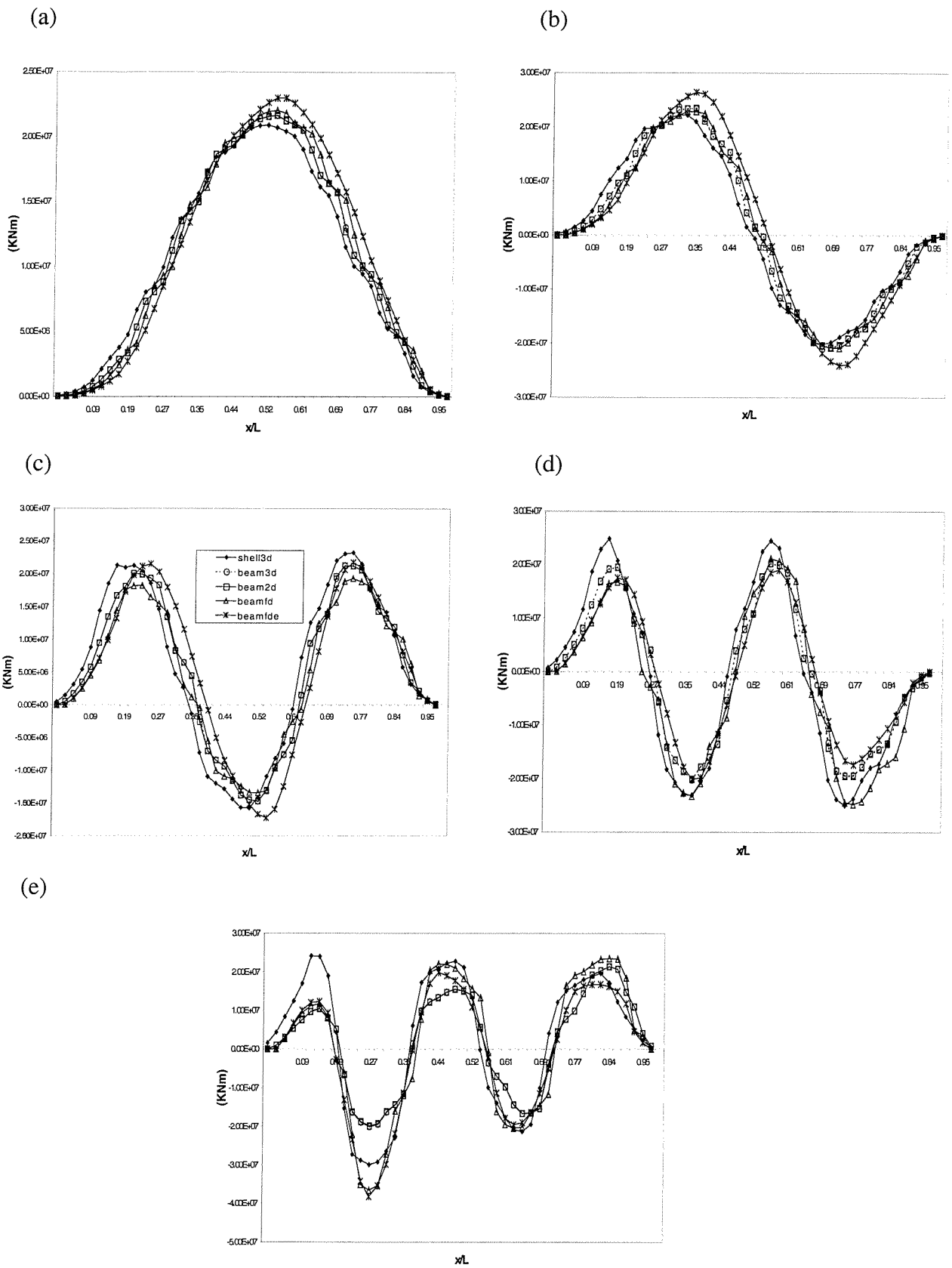

Fig. 5.8 Vertical bending moments (VBM) for all models corresponding to (a) 2 node, (b)3 node, (c)4 node, (d) 5 node and (e) 6 node vertical deflections.

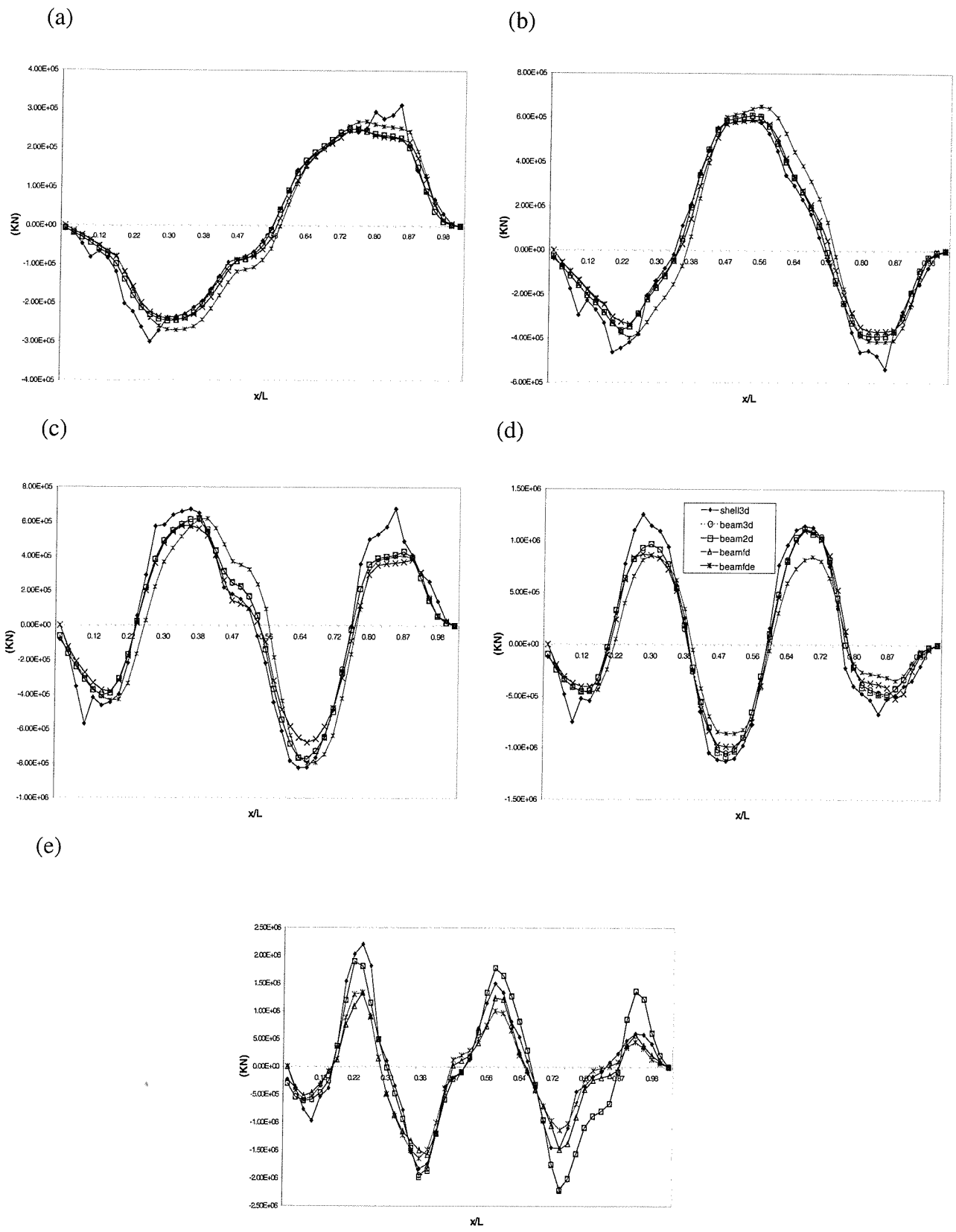

Fig. 5.9 Vertical shear forces (VSF) for all models corresponding to corresponding to (a) 2 node, (b) 3 node, (c)4 node, (d) 5 node and (e) 6 node vertical deflections.

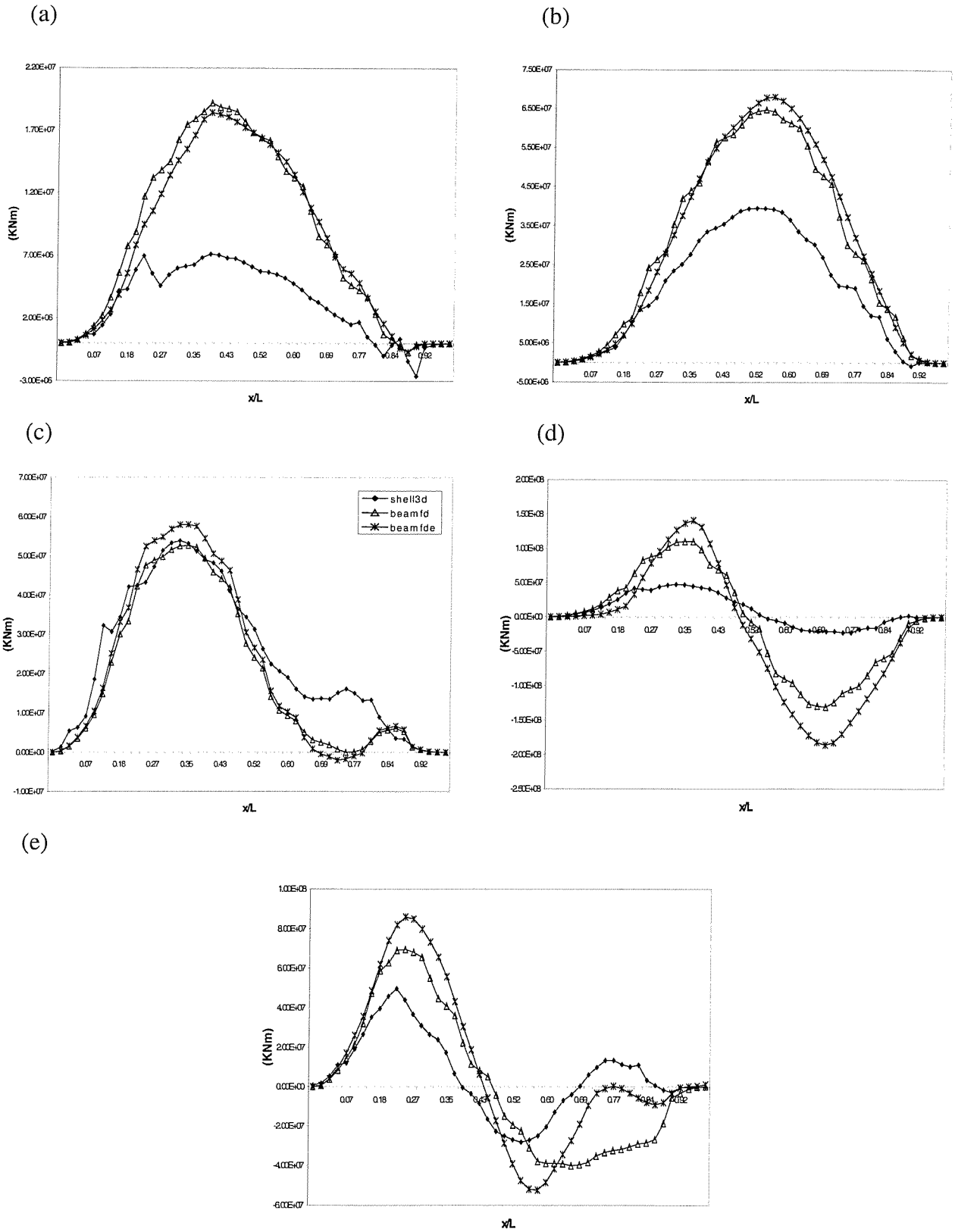

Fig. 5.10 Horizontal bending moments (HBM) corresponding to antisymmetric modes for finite difference and shell3d idealisations (a) 1 node HB 1 node **T**; (b) 2 node **HB** 2 node T; (c) 2 node HB 2 node **T**; (d) 3 node **HB** 3 node T; (e) 3 node HB 3 node **T** (HB: horizontal bending, T: torsion, **HB,T**: dominant HB,T).

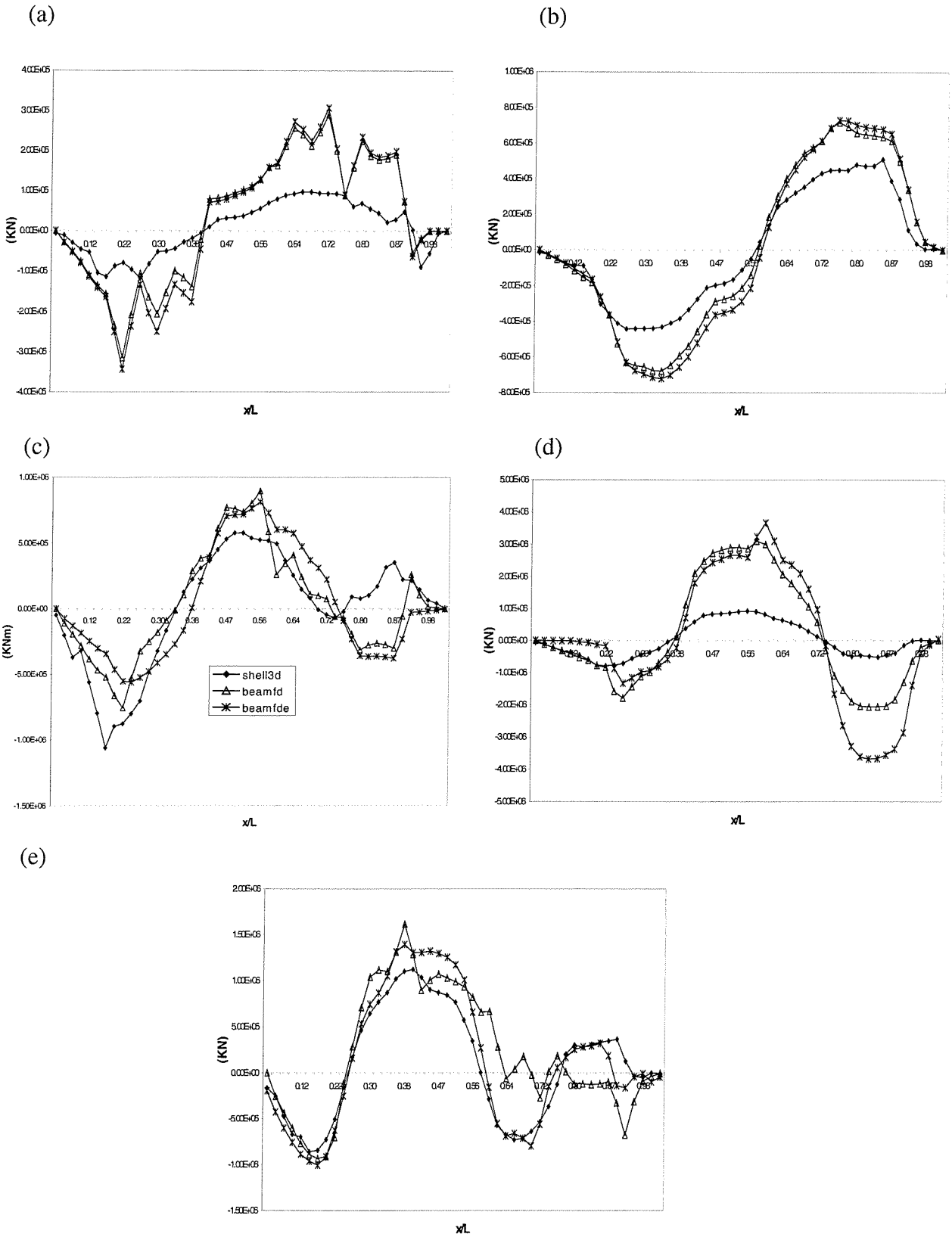

Fig. 5.11 Horizontal shear forces (HSF) corresponding to antisymmetric modes for finite difference and shell3d idealisations (a) 1 node HB 1 node **T**; (b) 2 node **HB** 2 node T; (c) 2 node HB 2 node **T**; (d) 3 node **HB** 3 node T; (e) 3 node HB 3 node **T** (HB: horizontal bending, T: torsion, **HB,T**: dominant HB,T).

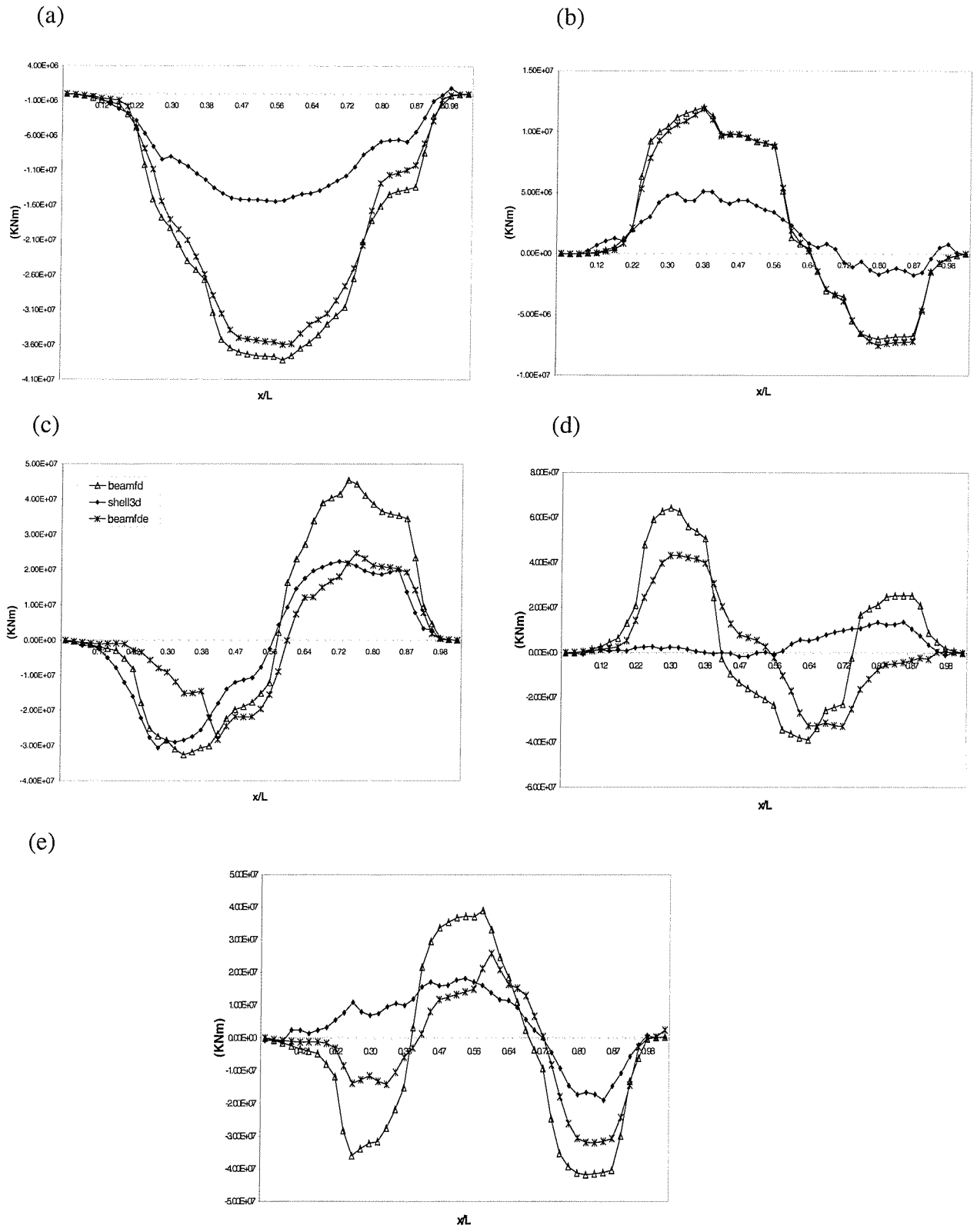

Fig.5.12 Torsional moments (TM) corresponding to antisymmetric modes for finite difference and shell3d idealisations (a) 1 node HB 1 node **T**; (b) 2 node **HB** 2 node T; (c) 2 node HB 2 node **T**; (d) 3 node **HB** 3 node T; (e) 3 node HB 3 node **T** (HB: horizontal bending, T: torsion, **HB,T**: dominant HB,T).

This discrepancy between the different types of idealisations in antisymmetric distortions definitely raises an interesting point for discussion. At first instance it is useful to state that although the slenderness ratio of the hull in the antisymmetric plane of vibration is relatively low (L/B=6.7) it should not be considered as a factor affecting the dynamic load deviations between beam and shell idealisations. Past work for the case of a mine-hunter having even lower corresponding length to beam ratio of the order of 4.7 [5.11] as well as the in vacuo dynamic analysis of the closed-deck and open-deck ship structures presented in section 5.7 validate in further this point. Although for the case of a bulk carrier the hull girder response analysis corresponds to that of a non-prismatic beam structure in hydroelasticity theory traditionally this problem has been treated by means of the Bishop Price et al updated Timoshenko beam formulation which does not account for the structural discontinuities of the hull [5.3] (see sections 3.5.1,4.3.4,4.4.3). In this approach the non-prismatic hull girder is divided by means of a finite difference scheme into individual prismatic segments, each corresponding to a portion of the hull girder for which the cross-section is constant, however short it may be. Even this formulation, however, is based on the traditional thin walled torsion theory which is derived for prismatic beams and in such beams the assumption that the cross-section does not change its shape is fulfilled satisfactorily.

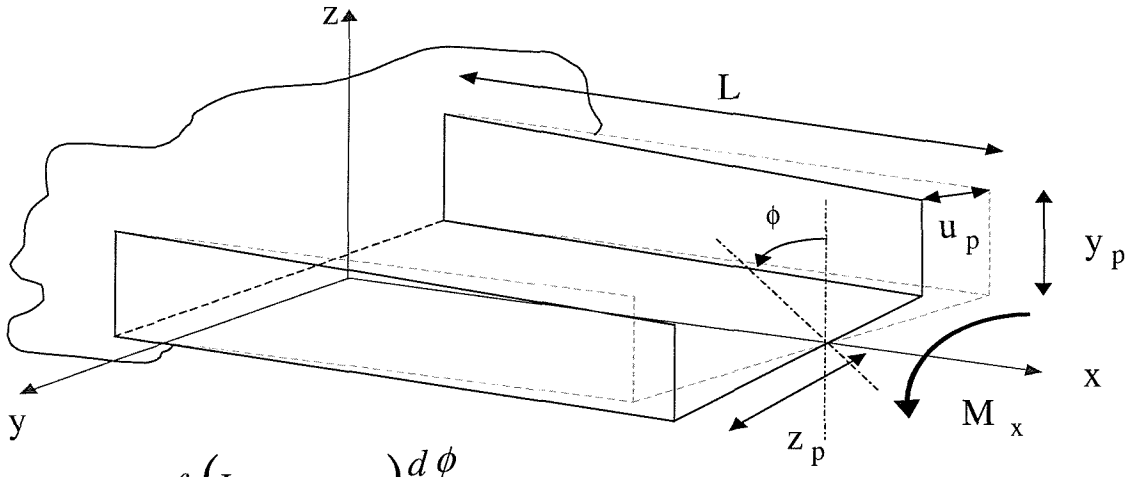

$$u_p = f(L, y_p, z_p)\frac{d\phi}{dx}$$

$$v_p = -\phi y_p$$

$$w_p = -\phi z_p$$

Fig. 5.13 Torsional deflection of a prismatic thin walled beam of open section

Thus, it is not the theory that is wrong but rather its application to beams that are markedly non-prismatic, leading to some deviations in the horizontal bending moment and shear force results and highly significant deviations in the torsion moment results obtained when a three-dimensional model is compared with a two-dimensional idealization. If each prismatic beam segment in the hull girder is acted in isolation its longitudinal warping and other responses would be as predicted by theory. But globally, when two segments which have completely different warping response in isolation (e.g. open, closed) are connected rigidly together, further information is required in order to achieve a geometric compatibility mapping the alternative warping functions at the common nodal points between two segments. In other words at the node joining two different segments the common value of the angle of twist produces two alternative and incompatible distributions of warping, implying a discontinuity of longitudinal displacement. At this point there is disadvantage of the numerical approach, which does not account for the discontinuity of the angle of twist rather than the warping at the node. The significance of the effects of departure of the two-dimensional approach from the realistic three-dimensional model would become much more apparent for cases of wholly closed (tanker like) or open (container like) ship structures (see section 5.7). A possible cure to the problem could be the imposition of Pedersen's correction factors [5.4,5.5,5.6,5.7] outlined in section 4.4.3.

5.6 Investigation of the effects of refinement

When a continuous system is discretised by means of a finite element or finite difference scheme it is customary to investigate the effects of refinement of the model for the purposes of convergence (see sections 4.2.2,4.4.1).

In the current investigation the idea of refinement of shell3d finite element idealisation (see figure 4.8) was immediately abandoned since the adopted modelling approach by means of *'fictitious'* bulkheads makes it particularly tedious and the educational version of ANSYS5.4, used for the purposes of this project, is restricted to the number of nodal points and elements [5.8] (see section 4.3.3). Some preliminary studies with uniform lightweight barge models of similar dimensions to MV Derbyshire have shown, however, that modal characteristics converge well with increasing discretisation level in both symmetric and uncoupled antisymmetric planes of vibration (see figure 5.14 and table 5.7). In this sense the shell3d finite element idealisation used so far may be considered as being adequate in simulating the global dynamic behavior of the structure and could be used as a reference point for further numerical convergence tests.

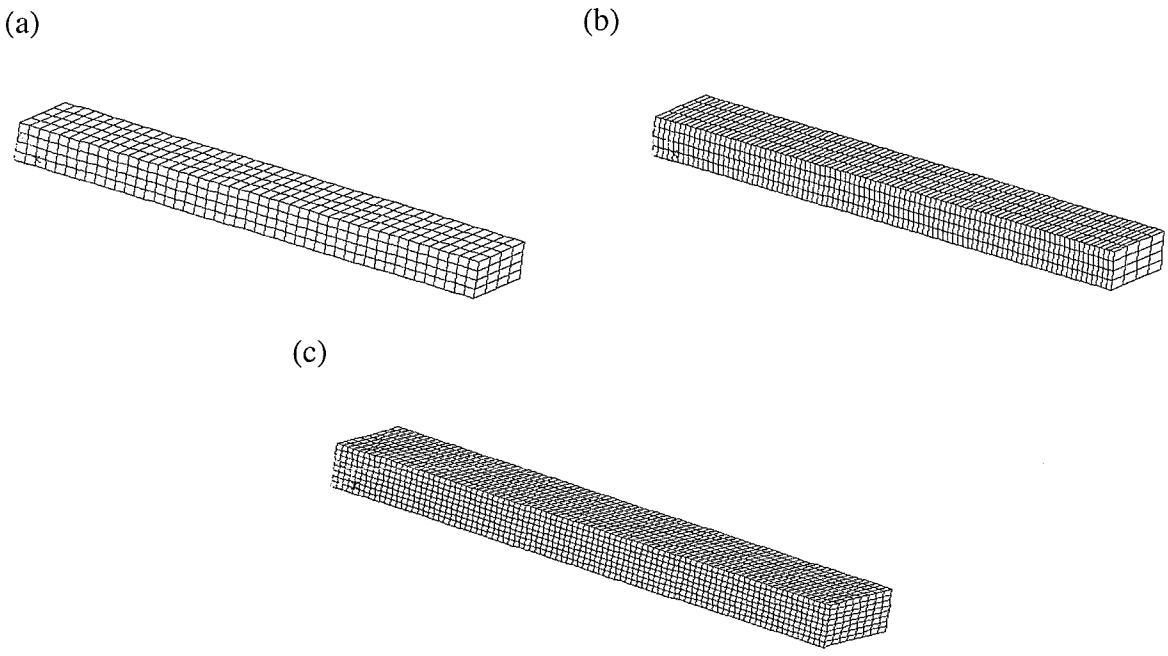

Fig. 5.14 Uniform lightweight barge models having similar dimensions to MV Derbyshire, ANSYS 5.4 SHELL63 idealisation (a) 2592 elements; (b) 5184 elements; (c) 10368 elements.

(a)

Element no. / Description	2592	5168	19200
2 node VB	2.349	2.356	2.356
3 node VB	5.133	5.152	5.158
4 node VB	7.778	8.061	8.073
5 node VB	9.927	10.536	10.562
Longitudinal	12.019	12.044	12.057
6 node VB	13.056	15.148	15.205

(b)

Element no. / Description	2592	5168	19200
2 node HB	3.763	3.769	3.776
1 node T	4.932	4.957	4.963
3 node HB	9.047	9.116	9.135
2 node T	9.424	9.694	9.726
4 node HB	15.111	15.387	15.400

Table 5.7 Demonstration of the effects of mesh refinement on barge models having similar dimensions to MV Derbyshire, ANSYS 5.4 SHELL63 idealisation, all frequencies in rad/s (a) symmetric motion; (b) antisymmetric motion.

Progressively the beam model was divided longitudinally to 46,92,184,368,736 and 1472 elements so that the convergence of beamfd, beam2d, beam3d simulations could be investigated for both symmetric (see tables 5.8,5.9,5.10) and antisymmetric motions (see tables 5.11,5.12,5.13). The structural and mass properties were distributed accordingly along the longitudinal sections of the hull.

In symmetric motion, as the level of the finite difference discretisation increases the natural frequencies become marginally higher. The difference in magnitude of eigenfrequencies between 46 and 1472 sections, however, is just 1.15% for the first mode of vibration raising to 3.56% for the six node vertical bending. Considering that (i) for such type of approximate studies the allowable numerical error lies within the range of 3 to 5% and (ii) the model converges well with respect to the shell idealisations, it is acceptable to state that the finite difference scheme employed provides excellent rate of convergence in symmetric motion and 46 sections are enough to approximate the problem. The finite element beam and brick like idealisations (beam2d, beam3d) have an

opposite convergence trend (i.e. natural frequencies are decreasing with increasing number of elements) but appear to be even more stable with their frequencies changing just by 0.026 and 0.024% respectively for the first mode of vibration.

In antisymmetric motion shell3d, beamfd and beam3d (with negligible warping) idealisations were compared. The finite difference scheme appears to converge rather slowly for this non-prismatic ship structure with its natural frequencies changing by the unacceptable percentage of 38% (for the first mode of vibration) between 46 and 1472 discretisation divisions. The coupling between torsion and horizontal bending in the finite difference scheme appears to be not so stable most probably due to the fact that the structural properties of the ship studied vary in saw-tooth (non-prismatic) manner (see figure 4.3). Some additional tests on barge structures with similar properties verified this speculation. From this analyses it became apparent that:

- for a barge structure having entirely closed decks the finite difference scheme is stable (see table 5.14);
- for a barge structure experiencing some form of structural discontinuities (e.g. deck 20% closed, 30% open, 10% closed, 30% open, 10%closed) the finite difference algorithm converges well only when the pure in vacuo horizontal bending dynamics of the beam are studied (see table 5.16). The structure does not converge well where the effects of torsion become significant, i.e. for pure torsion dynamics as well as coupled horizontal bending torsion antisymmetric analysis (see tables 5.15, 5.17).

The sensitivity of the vertical bending moment with increasing level of discretisation was also examined in an attempt to judge the reliability of the finite difference and element discretisations. No significant differences in the symmetric or antisymmetric mode shapes were observed. It was shown that although all the predicted bending moments for up to 736 elements provide the same bending moment results the finite difference scheme becomes particularly unstable providing higher bending moment (even at the first vertical bending mode) when 1472 finite difference sections are used to discretise the hull. Numerical instability does not appear in the finite element beam idealisations (see figure

5.15). In this sense it was concluded that 46 sections are adequate to identify the dynamic parameters of the system.

Element no.		46 elements			92 elements		
Description	shell3d	beamfd	beam2d	beam3d	beamfd	beam2d	beam3d
2 node VB	4.529	4.527	4.503	4.5029	4.555	4.502	4.5022
3 node VB	9.010	9.060	9.067	9.0720	9.148	9.0572	9.0572
4 node VB	13.236	13.632	13.737	13.7410	13.817	13.697	13.6970
5 node VB	15.915	16.954	17.105	17.1060	17.195	17.0368	17.0390
Longitudinal	17.932	-	17.824	17.8310	-	17.813	17.8190
6 node VB	24.586	23.363	23.986	23.9890	23.990	23.807	23.8060

Table 5.8 Demonstration of the effects of mesh refinement for MV Derbyshire (bulker structure), all frequencies in rad/s, symmetric motion, 46 sections versus 92 sections (shell3d versus beamfd, beam2d, beam3d).

Element no.		184 elements			368 elements		
Description	shell3d	beamfd	beam2d	beam3d	beamfd	beam2d	beam3d
2 node VB	4.529	4.568	4.5019	4.5019	4.575	4.5018	4.5018
3 node VB	9.010	9.186	9.0547	9.0546	9.204	9.054	9.0540
4 node VB	13.236	13.888	13.688	13.6880	13.918	13.686	13.6860
5 node VB	15.915	17.279	17.020	16.8900	17.313	17.016	16.8580
Longitudinal	17.932	-	17.814	17.8150	-	17.814	17.8140
6 node VB	24.586	24.180	23.761	23.7610	24.221	23.749	23.7490

Table 5.9 Demonstration of the effects of mesh refinement for MV Derbyshire (bulker structure), all frequencies in rad/s, symmetric motion, 182 sections versus 368 sections (shell3d versus beamfd, beam2d, beam3d).

Element no.		736 elements			1472 elements		
Description	shell3d	beamfd	beam2d	beam3d	beamfd	beam2d	beam3d
2 node VB	4.529	4.578	4.5018	4.5018	4.580	4.5018	4.50180
3 node VB	9.010	9.213	9.0541	9.0540	9.217	9.054	9.0540
4 node VB	13.236	13.939	13.685	13.685	13.938	13.685	13.6850
5 node VB	15.915	17.328	17.014	16.850	17.335	17.014	16.8480
Longitudinal	17.932	-	17.814	17.814	-	17.814	17.8140
6 node VB	24.586	24.221	23.746	23.746	24.226	23.746	23.7460

Table 5.10 Demonstration of the effects of mesh refinement for MV Derbyshire (bulker structure), all frequencies in rad/s, symmetric motion, 736 sections versus 1472 sections (shell3d versus beamfd, beam2d, beam3d).

Element no.		46 elements			92 elements		
Description (B-T)	shell3d	beamfd		beam3d	beamfd		beam3d
$C_w \neq 0$		$C_w \neq 0$	$C_w = 0$	$C_w = 0$	$C_w \neq 0$	$C_w = 0$	$C_w = 0$
1 – **1**	5.004	5.992	1.797	1.430	5.282	1.604	1.429
2 - 2	5.554	6.261	3.189	2.893	6.041	2.879	2.891
2– **2**	12.629	10.995	4.622	4.181	10.626	4.203	4.173
3 – 3	10.712	12.656	5.856	5.408	11.546	5.288	5.386
3 – **3**	18.981	16.047	7.077	6.968	15.647	6.942	6.966

Table 5.11 Demonstration of the effects of mesh refinement for MV Derbyshire (bulker structure), all frequencies in rad/s, antisymmetric motion, 46 sections versus 92 sections (shell3d versus beamfd, beam3d).

Element no.		184 elements			368 elements		
Description (B-T)	shell3d	beamfd		beam3d	beamfd		beam3d
$C_w \neq 0$		$C_w \neq 0$	$C_w = 0$	$C_w = 0$	$C_w \neq 0$	$C_w = 0$	$C_w = 0$
1 – **1**	5.004	4.836	1.530	1.428	5.580	1.496	1.428
2 - 2	5.554	5.995	2.753	2.890	5.926	2.695	2.890
2– **2**	12.629	9.920	4.025	4.171	9.226	3.941	4.171
3 – 3	10.712	10.222	5.042	5.383	9.966	4.926	5.382
3 – **3**	18.981	11.215	6.940	6.966	10.538	6.923	6.966

Table 5.12 Demonstration of the effects of mesh refinement for MV Derbyshire (bulker structure), all frequencies in rad/s, antisymmetric motion, 184 sections versus 368 sections (shell3d versus beamfd, beam3d).

Element no.		736 elements			1472 elements		
Description (B-T)	shell3d	beamfd		beam3d	beamfd		beam3d
$C_w \neq 0$		$C_w \neq 0$	$C_w = 0$	$C_w = 0$	$C_w \neq 0$	$C_w = 0$	$C_w = 0$
1 – **1**	5.004	4.449	1.480	1.428	4.383	1.472	1.428
2 - 2	5.554	5.912	2.667	2.890	5.852	2.653	2.890
2– **2**	12.629	9.139	3.901	4.171	9.080	3.881	4.170
3 – 3	10.712	9.723	4.870	5.381	9.662	4.842	5.381
3 – **3**	18.981	9.675	6.920	6.966	9.615	6.906	6.966

Table 5.13 Demonstration of the effects of mesh refinement for MV Derbyshire (bulker structure), all frequencies in rad/s, antisymmetric motion, 184 sections versus 368 sections (shell3d versus beamfd, beam3d).

20 elements	50 elements	100 elements	500 elements	1000 elements
1.393	1.392	1.392	1.392	1.392
3.377	3.375	3.374	3.374	3.374
8.049	8.079	8.083	8.085	8.085
10.054	10.051	10.051	10.052	10.052
13.854	14.013	14.035	14.042	14.042

Table 5.14 Demonstration of the effects of mesh refinement for a barge having closed decks, finite difference idealisation, all frequencies in rad/s, coupled horizontal bending and torsion ($C_w \neq 0$).

20 elements	50 elements	100 elements	500 elements	1000 elements
2.815	2.407	2.246	2.114	2.098
4.876	4.387	4.153	3.950	3.924
6.568	6.245	6.161	6.106	6.100
10.728	10.672	10.632	10.592	10.587
16.294	16.306	16.261	16.209	16.202

Table 5.15 Demonstration of the effects of mesh refinement for a barge experiencing deck structural discontinuities (deck 20% closed, 30% open, 10% closed, 30% open, 10%closed), finite difference idealisation, all frequencies in rad/s, coupled horizontal bending and torsion ($C_w \neq 0$).

20 elements	50 elements	100 elements	500 elements	1000 elements
5.527	5.528	5.528	5.528	5.528
11.598	11.661	11.669	11.672	11.672
17.866	18.082	18.113	18.123	18.123
23.702	24.188	24.257	24.279	24.280
29.233	30.131	30.259	30.301	30.302

Table 5.16 Demonstration of the effects of mesh refinement for a barge experiencing deck structural discontinuities (deck 20% closed, 30% open, 10% closed, 30% open, 10%closed), finite difference idealisation, frequencies in rad/s, horizontal bending only ($C_w \neq 0$).

20 elements	50 elements	100 elements	500 elements	1000 elements
3.019	2.580	2.407	2.265	2.247
6.068	5.198	4.855	4.576	4.541
19.934	19.709	19.574	19.445	19.428
26.525	25.941	25.646	25.375	25.339
33.159	32.915	32.579	32.229	32.180

Table 5.17 Demonstration of the effects of accuracy of mesh refinement for a barge experiencing deck structural discontinuities (deck 20% closed, 30% open, 10% closed, 30% open, 10%closed), beamfd idealisation, all frequencies in rad/s, torsion only ($C_w \neq 0$).

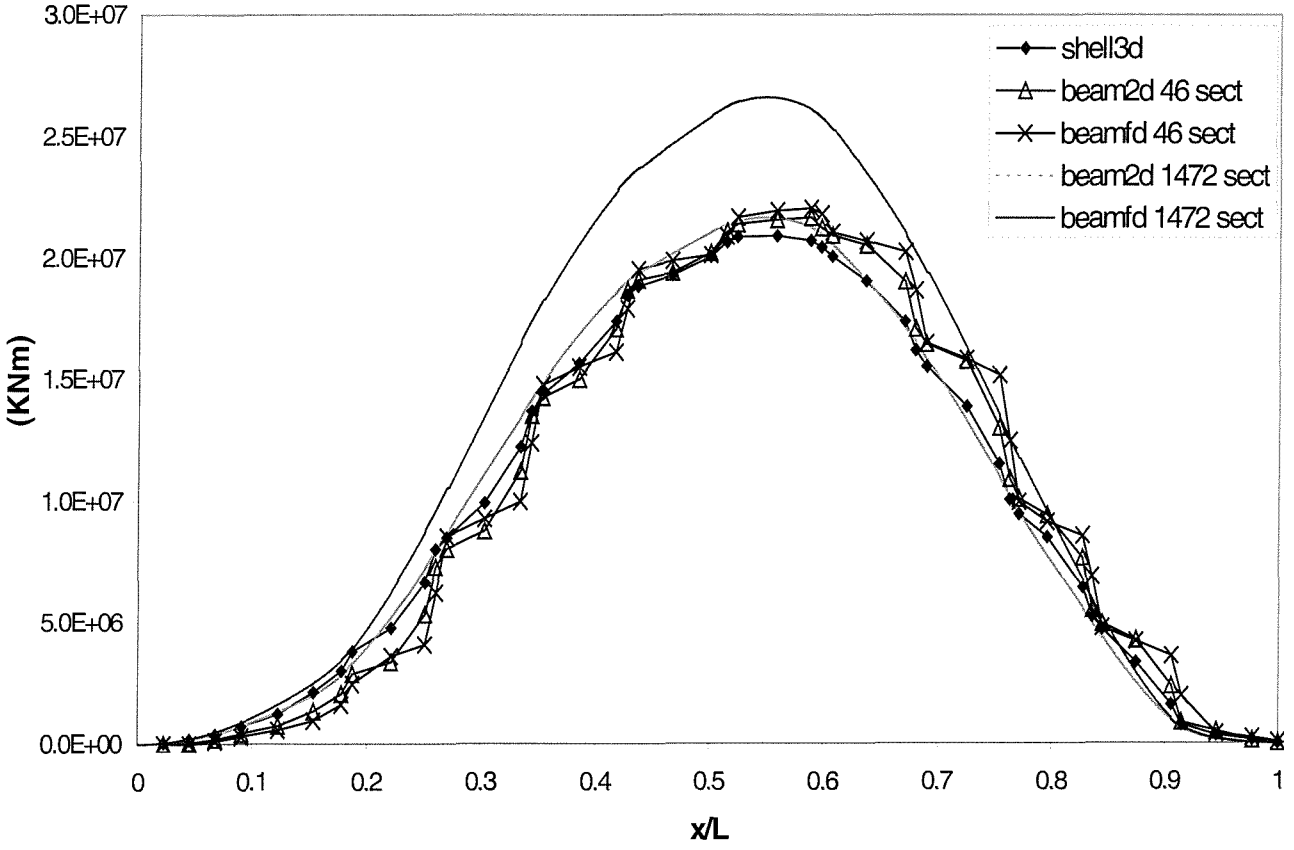

Fig. 5.15 The effects of mesh refinement on symmetric bending moment.

5.7 Further exploration of the effects of warping related hull girder dynamics

There is no doubt that the three-dimensional shell idealisation provides a realistic simulation of the distortions of the ship's structure. In principle, however, it is possible to entertain serious doubts and uncertainties with regards to the values of certain structural data needed in the calculation of antisymmetric distortions by means of a two- or three-dimensional beam like discretisations. Although the hull girder is expected to primarily behave as a beam the identification of the bulker's structural dynamics related parameters in the previous sections has clearly shown that certain deviations from the traditional beam like behaviour take place in antisymmetric motion due to the non-prismatic nature of the hull.

For the case of a bulk carrier there is definitely a point of interest with respect to the role played by the hatch covers. It has to be decided whether or not they form an integral part of the hull so as to contribute significantly to the torsional stiffness. In other words it is a matter of judgement whether the ship is to be treated as a closed or an open type of structure. The point is an important one because results are likely to depend critically on the decision reached. A second and even more important point of discussion arises from the behaviour of the sectorial moment of inertia, which determines the variation of warping stiffness along the hull for an open deck ship [5.9]. In assessing the natural frequencies of antisymmetric motion of the dry hull, the reader should bear these reservations in mind for it is the author's strong belief that further understanding of the effects of warping may lead to significant conclusions with regards to the modal parameter identification of long slender monohulls with large deck openings such as bulkers and containerships.

For the purposes of this investigation two additional shell models were created. One with totally closed decks (shell3dcl) and another one with open decks along the area of the holds (thus ignoring the deck openings between hatch covers) of the vessel (shell3dop) (see figure 5.16). Although the mass properties were kept the same, some of the inertia and structural characteristics of each of these models are different with the saw-tooth variation being no longer valid (see figures 5.17 and 5.18). The terms *tanker-like* (for the closed deck ship) and *container-like* (for the open deck ship) idealisation should be avoided in the sense that engineering practice strictly dictates that each of these vessels have different hull architectural

characteristics. It is true, however, that the following analyses may give some general indication with respect to the global dynamic behaviour of such ship types.

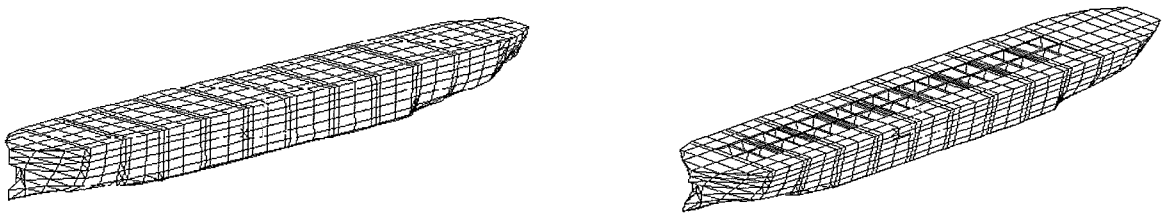

Fig. 5.16 Three-dimensional closed (shell3dcl) and open (shell3dop) ANSYS shell models.

As it becomes obvious from figure 5.17 in the closed deck ship the distance between shear and gravity centers is almost negligible, which leads to the conclusion that for this almost uncoupled ship structure the effects of warping are expected to be minimum. Opposite results are expected for the open ship idealisations (see figure 5.18) where coupling plays a dominant role in the global dynamic behaviour of the structure. Maximum torsional stiffness implies minimum sectorial moment of inertia and vice versa. Like in the case of the typical bulk carrier model the global dynamic characteristics of the both open and closed ship idealisations in two- and three-dimensional space by means of two- and three-dimensional beam and shell elements were explored. For both closed and open ship idealisations 0.23 and 0.28 of the cross-section area was considered to be effective in shear for the symmetric and antisymmetric distortions respectively as for the bulk carrier. This was done to avoid introduction of additional changes in properties and their influences on the in vacuo dynamic analysis.

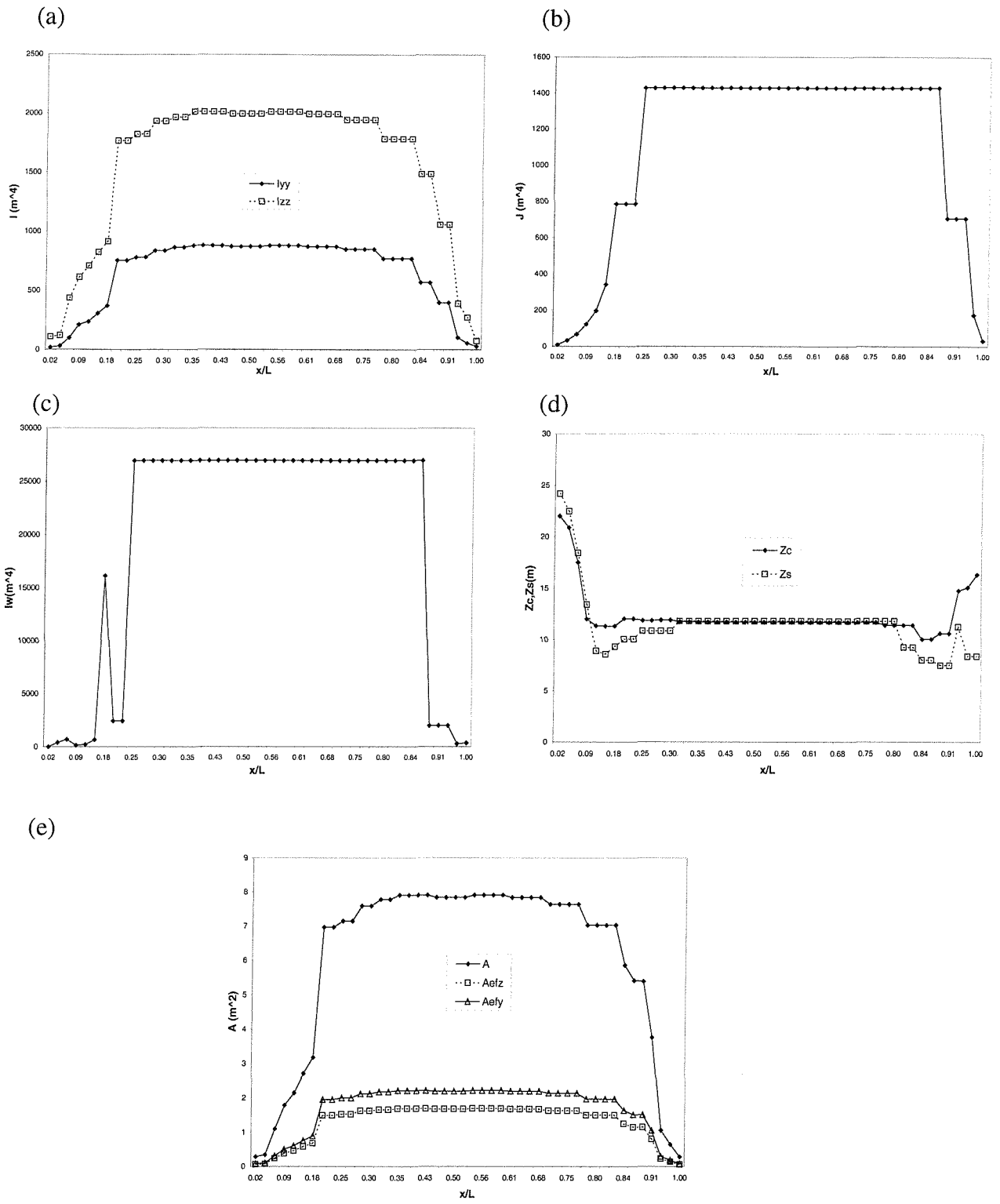

Fig. 5.17 Structural properties along closed ship: (a) Moments of inertia I_{zz} and I_{yy} (m^4); (b) torsional constant (m^4); (c) sectorial moment of inertia (m^6); (d) distances of shear centre (z_s) and centre of gravity (z_c) from keel; (e) cross-section and effective areas (A = sectional area, A_{efz}= symmetric effective shear area, A_{efy}= antisymmetric effective shear area).

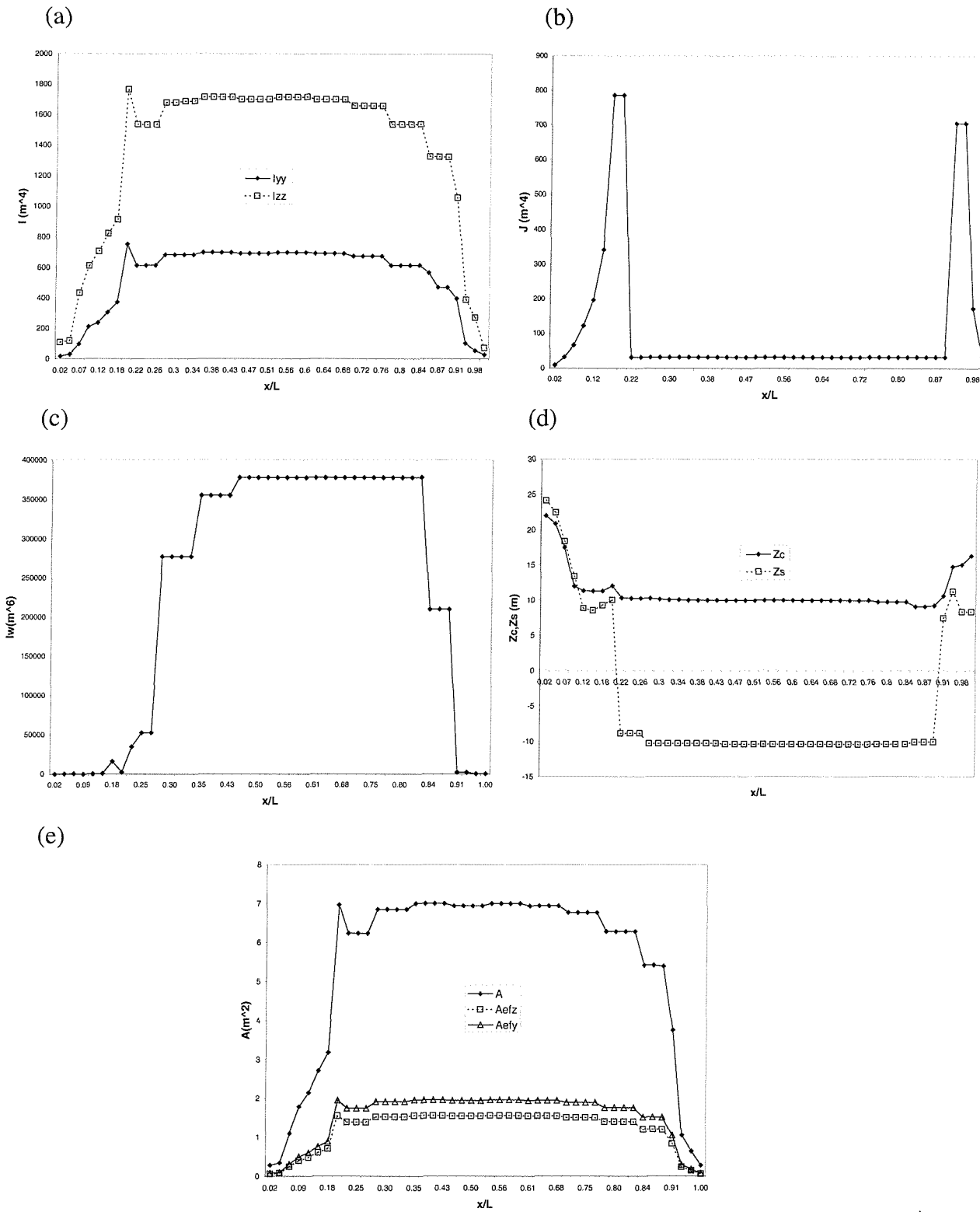

Fig. 5.18 Structural properties along open ship (a) Moments of inertia I_{zz} and I_{yy} (m^4); (b) torsional constant (m^4); (c) sectorial moment of inertia (m^6); (d) distances of shear centre (z_s) and centre of gravity (z_c) from keel; (d) cross-section and effective areas (A = sectional area, A_{efz}= symmetric effective shear area, A_{efy}= antisymmetric effective shear area).

5.7.1 Dynamics of the closed ship

For the closed ship in vertical bending plane the shell idealisation is marginally stiffer than the beam models at lower modes of vibration but is becoming more flexible with increasing modal complexity (see table 5.18). Beamfdcl idealisation appears to be stiffer than the finite element beam2dcl and beam3dcl models only for the 2 noded vertical bending mode and slightly more flexible for higher modes of vertical vibration.

As expected, horizontal bending is more dominant in the antisymmetric vibrations (see figure 5.19). It is commonly assumed in the structural dynamics of ship structures with no deck openings that the effect of warping is negligible [5.10]. This is clearly demonstrated in tables 5.19(a),(b). The shell idealisation is compared not only with the finite difference but also with the three-dimensional, brick like finite element discretisation. Since beam3dcl by definition does not allow for warping stiffness the relevant antiplane effects are quantified, as common practice dictates in most engineering applications of such type [5.10], by increasing the torsional stiffness of the vessel by 10%. In this sense the modal characteristics (eigenvectors, bending moments) of beam3dcl in relation to the beamfdcl and shell3dcl were explored.

Figure 5.20 clearly demonstrates that all numerical models behave similarly for in vacuo symmetric vibrations when normalised for unit displacement at stern (near A.P.; keel center line for model shell3d). The difference between beam2dcl and beam3dcl idealisations could be attributed, as in the case of the original bulker idealisation, to the different displacement functions used by these models. As in the bulker simulation there is some small difference between the two-dimensional beam simulations in comparison to the shell and beam3d idealisations at higher modes of vibration. This could appear because of the fact that the three-dimensional beam and especially shell idealisations are more flexible and more realistic in representing the hull architectural characteristics (e.g. deformations of the double bottom).

The comparison of antisymmetric modal parameters (natural frequencies and eigenvectors) proved to be particularly interesting. The natural frequencies of the shell model are stiffer than those of the beam model (see tables 5.19(a),(b)) since the conservative shear factor of the order of 28% was used to simulate the antisymmetric characteristics of the beam idealisation for reasons of consistency (see sections 5.2,5.3). The implications of this assumption upon the

natural frequencies is further demonstrated in tables 5.20(a),(b) where the shell results are compared with beam models having 90% effective shear area in antisymmetric plane.

At first instance the translations and rotations were extracted as in the case of the bulker idealisation (see section 5.3). From the coupled eigenvector analyses becomes evident that:

- for horizontal bending dominant modes all models are in reasonably good agreement but the rotational term is almost negligible (see figures 5.21(a),(c) and 5.22(b));
- for torsion dominant modes the translation term of all models is negligible and the horizontal displacement of the beam models differs significantly to that of the shell idealisation although the corresponding rotation terms appear to be in good agreement (see figures 5.21(b) and 5.22(a));
- consequently, the generalised masses of all models appear to be in good agreement for symmetric and horizontal dominant antisymmetric distortions but not for torsion dominant modes (see tables 5.21,5.22).

These observations clearly demonstrate that a long slender mono-hull with no deck openings behaves primarily as an 'uncoupled' ship in the antisymmetric plane of vibration. Engineering judgement therefore implies that the eigenvectors, depending on their dominant component (translation or rotation), can be considered as being uncoupled within the context of linear theory (see figure 5.23). This methodology, which normalises rotations to unit twist at stern, has also been successfully followed and implemented by Salas et al [5.11] and was used for the purposes of the current investigation.

The illustration of the direct stress tensors by means of multi-dimensional contours (see figure 5.24) provides an indication of the effects that global symmetric and antisymmetric vibration imposes upon the structure. For pure symmetric distortions (sagging, hogging) the bottom of the vessel amidships appears to be vulnerable to high stresses. Similar behaviour occurs for horizontal bending dominant modes with maximum stresses occurring in the middle of the ship sides. In contrast to the bulk carrier configuration the girder does not appear to experience high stresses at the vicinities where the forward and backward hatch openings with the bow and stern used to be in the original bulk carrier model. This shows that long slender mono hulls without large deck openings do not experience significant antisymmetric direct stresses. For the evaluation of modal actions same methodology to that of the bulk carrier was

followed (see section 5.5). Vertical bending moments and shear forces of all models (beamfdcl, beam2dcl, beam3dcl and shell3dcl along the keel) correlate well, even at higher modes of vibration (see figures 5.25,5.26). In antisymmetric distortions the modal actions (horizontal bending moment, horizontal shear force, torsional moment) of the FD and FE beam models (beamfdcl, beam2dcl, beam3dcl) overestimate those produced by the shell idealisation (shell3dcl along keel) but the results appear to agree much better than in the original bulk carrier configuration. This is expected since the closed ship structure is strictly prismatic and horizontal bending couples weakly with torsion (see figures 5.27,5.28,5.29).

Model / Mode type	shell3dcl	beamfdcl	beam2dcl	beam3dcl
2 node VB	4.866	4.864	4.836	4.835
3 node VB	9.412	9.462	9.480	9.481
4 node VB	13.571	13.848	14.021	14.030
5 node VB	16.204	17.205	17.359	17.362
Longitudinal	18.604	-	18.650	18.661
6 node VB	22.789	23.582	24.078	24.083

Table 5.18 Natural frequencies (rad/s) for symmetric distortions of the dry hull of closed ship (t_{fb} = thickness of fictitious bulkheads, VB = vertical bending).

(a)

Model / mode type	beamfdcl $C_w \neq 0$	shell3dcl $t_{bf} = 0.001$m	beamfdcl $C_w = 0$
2 node **HB** – 1 node T	6.542	6.848	6.541
1 node HB - 1 node **T**	10.217	9.852	10.128
3 node **HB** – 2 node T	11.595	13.716	11.595
2 node HB – 2 node **T**	16.446	18.617	16.433
4 node **HB** – 2 node T	19.724	24.994	19.587

(b)

Model / mode type	beam3dcl $C_w \neq 0$	shell3dcl $t_{bf} = 0.001$m	beam3dcl $C_w = 0$
2 node **HB** – 2 node T	6.541	6.848	6.540
1 node HB – 1 node **T**	8.658	9.852	8.218
3 node **HB** – 2 node T	11.686	13.716	11.068
2 node HB – 2 node **T**	17.720	18.617	17.324
4 node **HB** – 2 node T	20.850	24.994	20.643

Tables 5.19(a),(b). Natural frequencies (rad/s) for antisymmetric distortions of the dry hull of closed ship, $\mathbf{A_{efy}=0.28A}$ (C_w= warping stiffness; HB = horizontal bending; T = torsion; **HB,T** = dominant HB,T).

(a)

Model Mode type ($C_W \neq 0$)	beamfdcl $C_w \neq 0$	shell3dcl $t_{bf} = 0.001$m	beamfdcl $C_w = 0$
2 node **HB** – 1 node T	7.307	6.848	7.305
1 node HB - 1 node **T**	10.520	9.852	10.022
3 node **HB** – 2 node T	15.243	13.716	15.236
2 node HB – 2 node **T**	20.923	18.617	19.945
4 node **HB** – 2 node T	23.97	24.994	23.951

(b)

Model Mode type ($C_W \neq 0$)	beam3dcl $C_w \neq 0$	shell3dcl $t_{bf} = 0.001$m	beam3dcl $C_w = 0$
2 node **HB** – 2 node T	7.383	6.848	7.382
1 node HB - 1 node **T**	8.658	9.852	8.650
3 node **HB** – 2 node T	15.576	13.716	15.067
2 node HB – 2 node **T**	22.335	18.617	22.214
4 node **HB** – 2 node T	24.598	24.994	24.391

Tables 5.20(a),(b). Natural frequencies (rad/s) for antisymmetric distortions of the dry hull of closed ship, $\mathbf{A_{efy}=0.90A}$ (C_w= warping stiffness; HB = horizontal bending; T = torsion; **HB,T** = dominant HB,T).

Mode description	Generalised mass (tonne-m^2)			
	shell3dcl	beam2dcl	beam3dcl	beamfdcl
2 node VB	19359	19438	19424	19336
3 node VB	8544	7959	7949	7661
4 node VB	6248	4199	4187	3875
5 node VB	10897	5368	5398	7052
6 node VB	8580	10046	9886	5203

Table 5.21 Symmetric motion generalised masses for alternative discretisation schemes for the closed ship (VB = vertical bending).

Mode type ($C_W \neq 0$)	Generalised mass (tonne-m^2)		
	shell3dcl	beamfdcl	beam3dcl
2 node **HB** – 1 node T	19125	21527	20721
1 node HB - 1 node **T**	3990541	85749300	21047792
3 node **HB** – 2 node T	7813	11374	10272
2 node HB – 2 node **T**	2784833	1801870	1315125
4 node **HB** – 2 node T	5725	6622	6123

Table 5.22 Anti-symmetric motion generalised masses for alternative discretisation schemes for closed ship (C_w= warping stiffness; HB = horizontal bending; T = torsion; **HB,T** = dominant HB,T).

2 node VB
(ω_r = 4.865 rad/s)

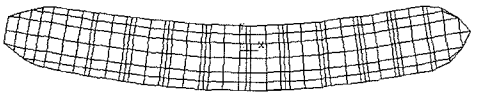

2 node **HB** and 1 node T
(ω_r = 6.848 rad/s)

3 node VB
(ω_r = 9.412 rad/s)

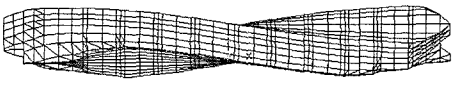

1 node HB and 1 node **T**
(ω_r = 9.852 rad/s)

4 node VB
(ω_r = 13.5716 rad/s)

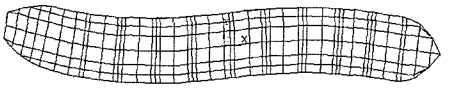

3 node **HB** and 2 node T
(ω_r = 13.716 rad/s)

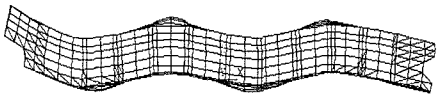

5 node VB
(ω_r = 16.204 rad/s)

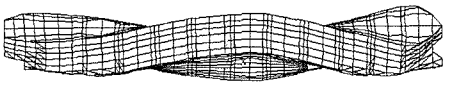

2 node HB and 2 node **T**
(ω_r = 18.617 rad/s)

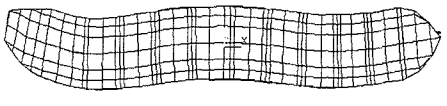

4 node **HB** and 2 node T
(ω_r = 20.489 rad/s)

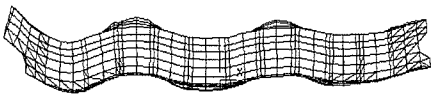

6 node VB
(ω_r = 22.789 rad/s)

Fig. 5.19 Principal mode shapes of model shell3d **for closed ship idealisation** (VB: vertical bending; HB: horizontal bending; T: torsion, **HB,T**: dominant HB,T).

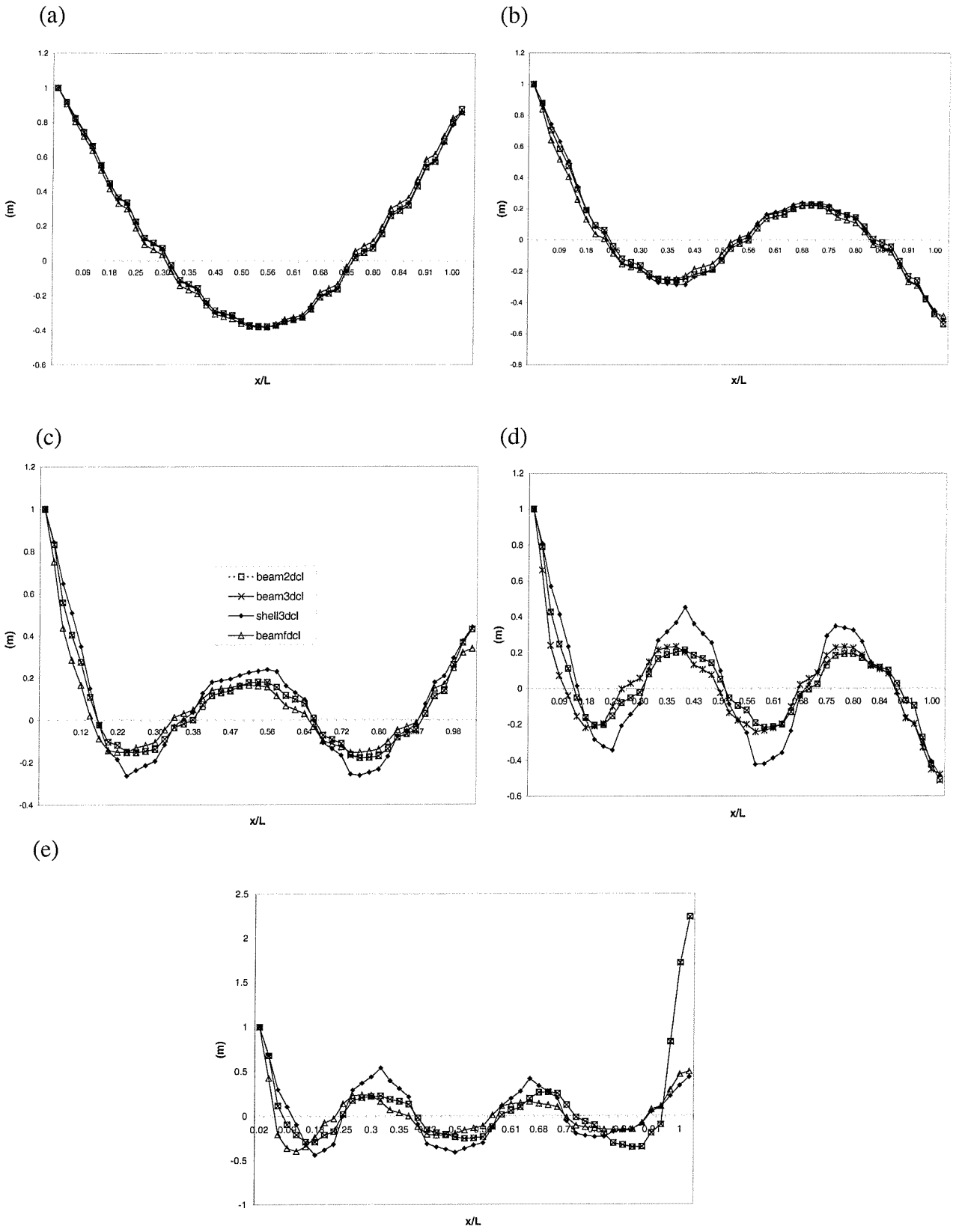

Fig. 5.20 Symmetric mode shapes for all models of closed ship idealisation corresponding to (a) 2 node, (b) 3 node, (c) 4 node, (d) 5 node and (e) 6 node vertical deflections.

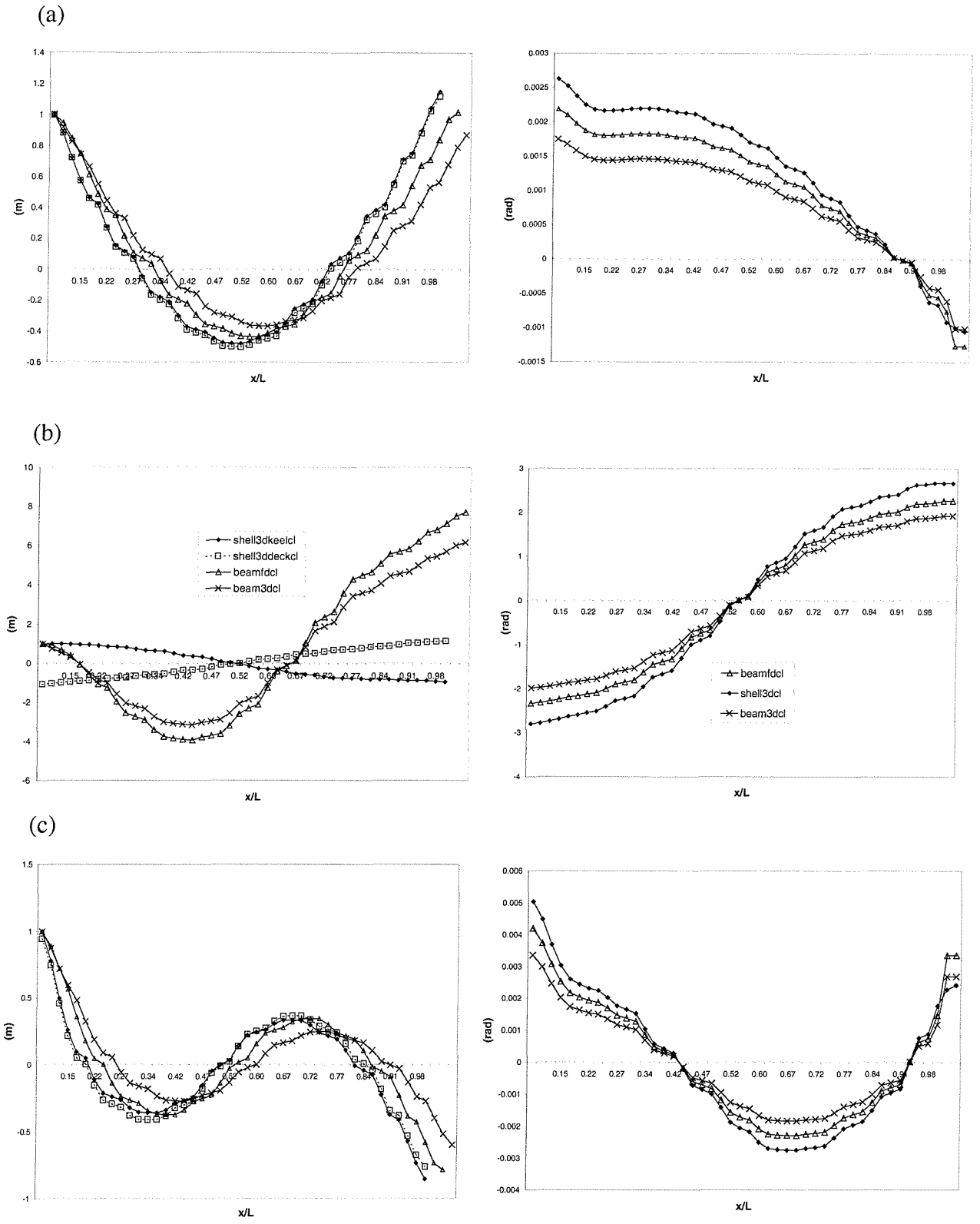

Fig. 5.21 Antisymmetric mode shapes, represented by the horizontal deflection (m) and twist angle (rad) obtained from models beamfd ($C_W \neq 0$), beam3dcl and shell3dcl (keel centre and deck side junction) corresponding to (a) 2 node **HB** 1 node T (b) 2 node HB 1 node **T** (c) 3 node **HB** 2 node T (HB: horizontal bending, T: torsion, **HB,T**: dominant HB,T).

(a)

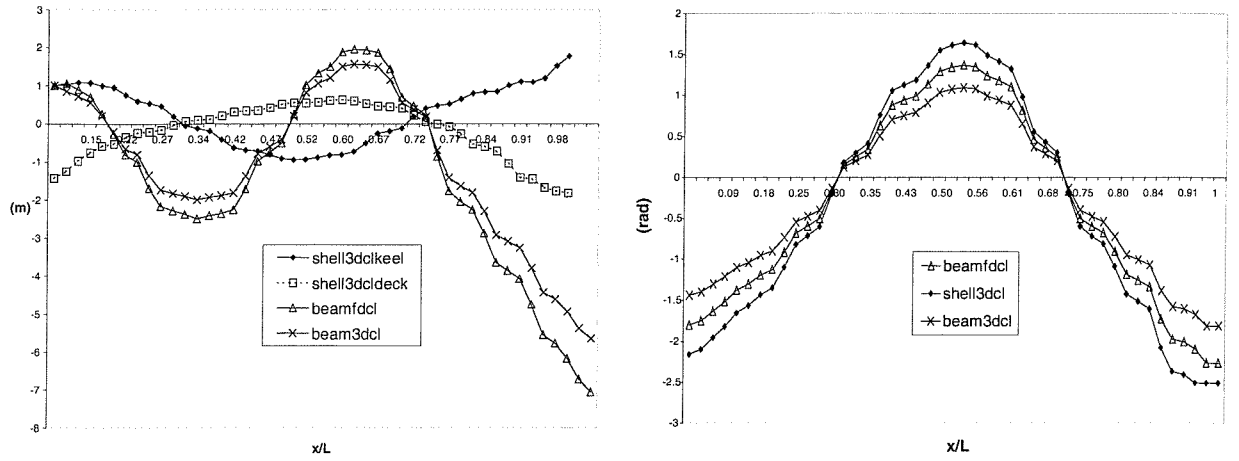

(b)

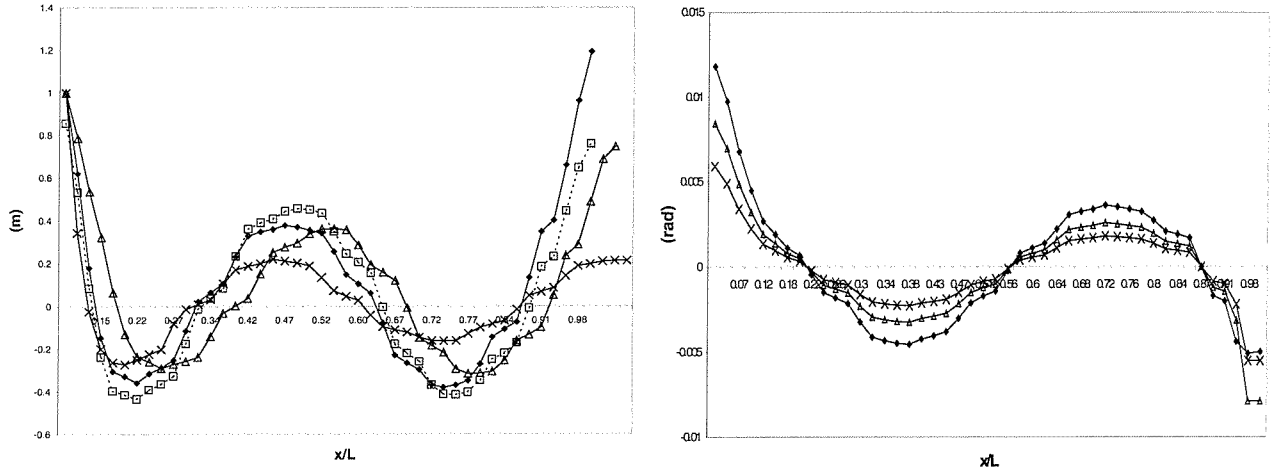

Fig. 5.22 Antisymmetric mode shapes, represented by the horizontal deflection (m) and twist angle (rad), $C_W \neq 0$, obtained from models beamfd ($C_W \neq 0$), beam3dcl and shell3dcl (keel center and deck side junction) corresponding to: (a) 2 node HB 2 node **T**; (b) 4 node **HB** 2 node T (HB: horizontal bending, T: torsion, **HB,T**: dominant HB,T).

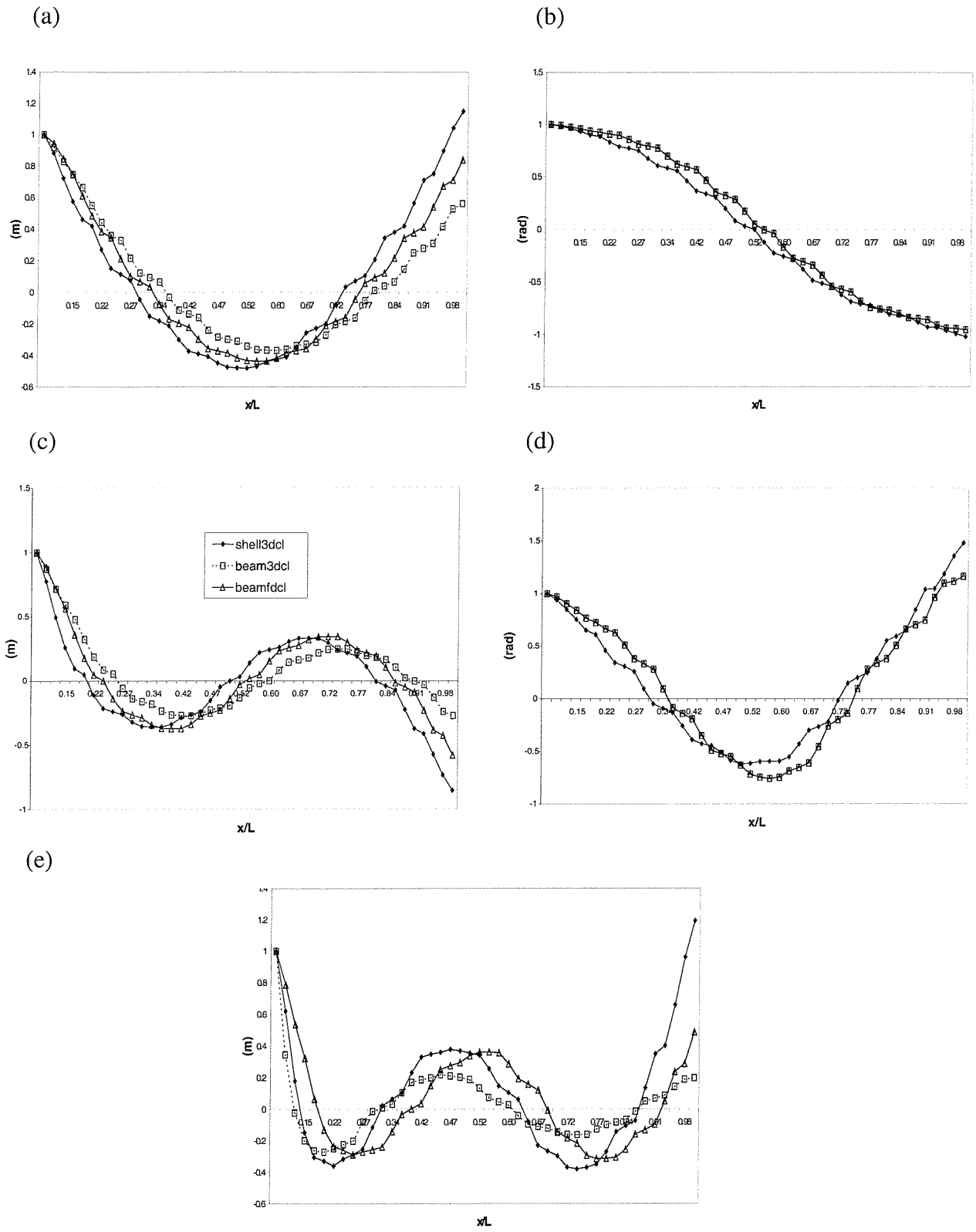

Fig. 5.23 Antisymmetric mode shapes, represented by the 'uncoupled' dominant horizontal deflection (m) or twist angle (rad), $C_W \neq 0$, obtained from models beamfd ($C_W \neq 0$), beam3dcl and shell3dcl (keel center) corresponding to: (a) 2 node **HB**; (b) 1 node **T** (c) 3 node **HB** (d) 2 node **T** (e) 4 node **HB** (**HB**: horizontal bending dominant mode, **T**: torsion dominant mode).

(a)

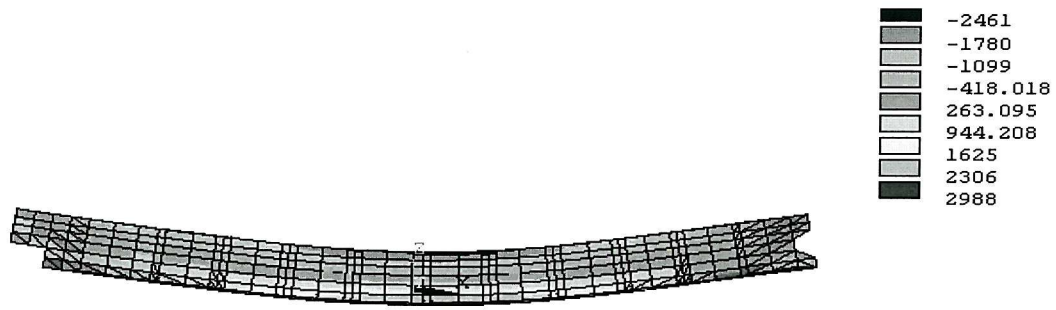

2 node VB
(ω_r = 4.865 rad/s)

(b)

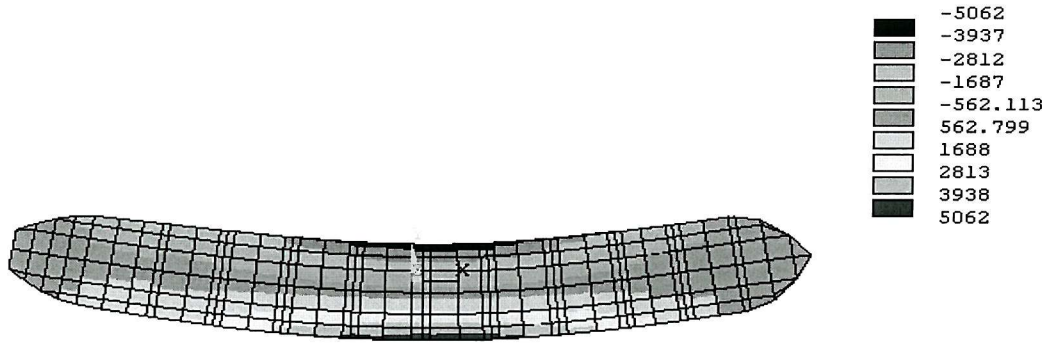

2 node **HB** 2 node T
(ω_r = 6.848 rad/s)

(c)

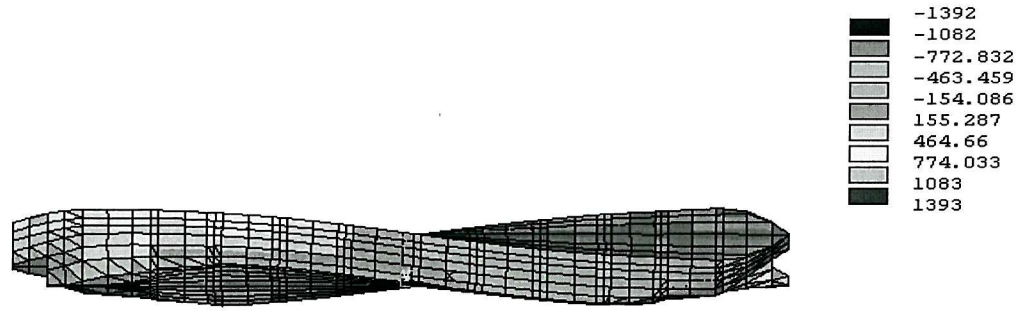

1 node HB 1 node **T**
(ω_r = 9.852 rad/s)

Fig. 5.24 Principal direct modal stresses (KN/m^2) for closed ship idealisation (VB: vertical bending, HB: horizontal bending, T: torsion, **HB,T**: dominant HB,T).

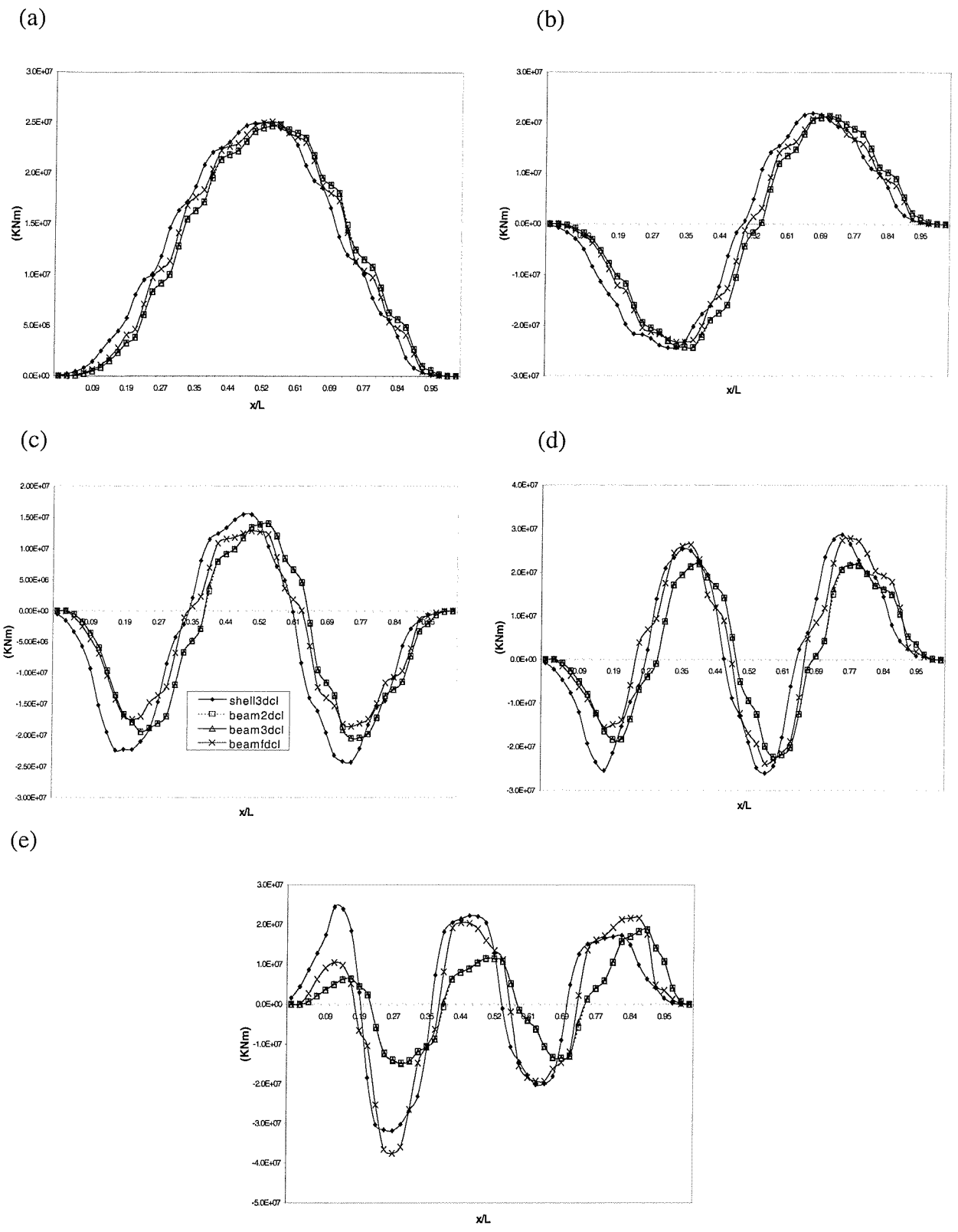

Fig. 5.25 Vertical modal bending moments for closed ship (a) 2 node, (b)3 node, (c)4 node, (d) 5 node, (e)6 node vertical bending.

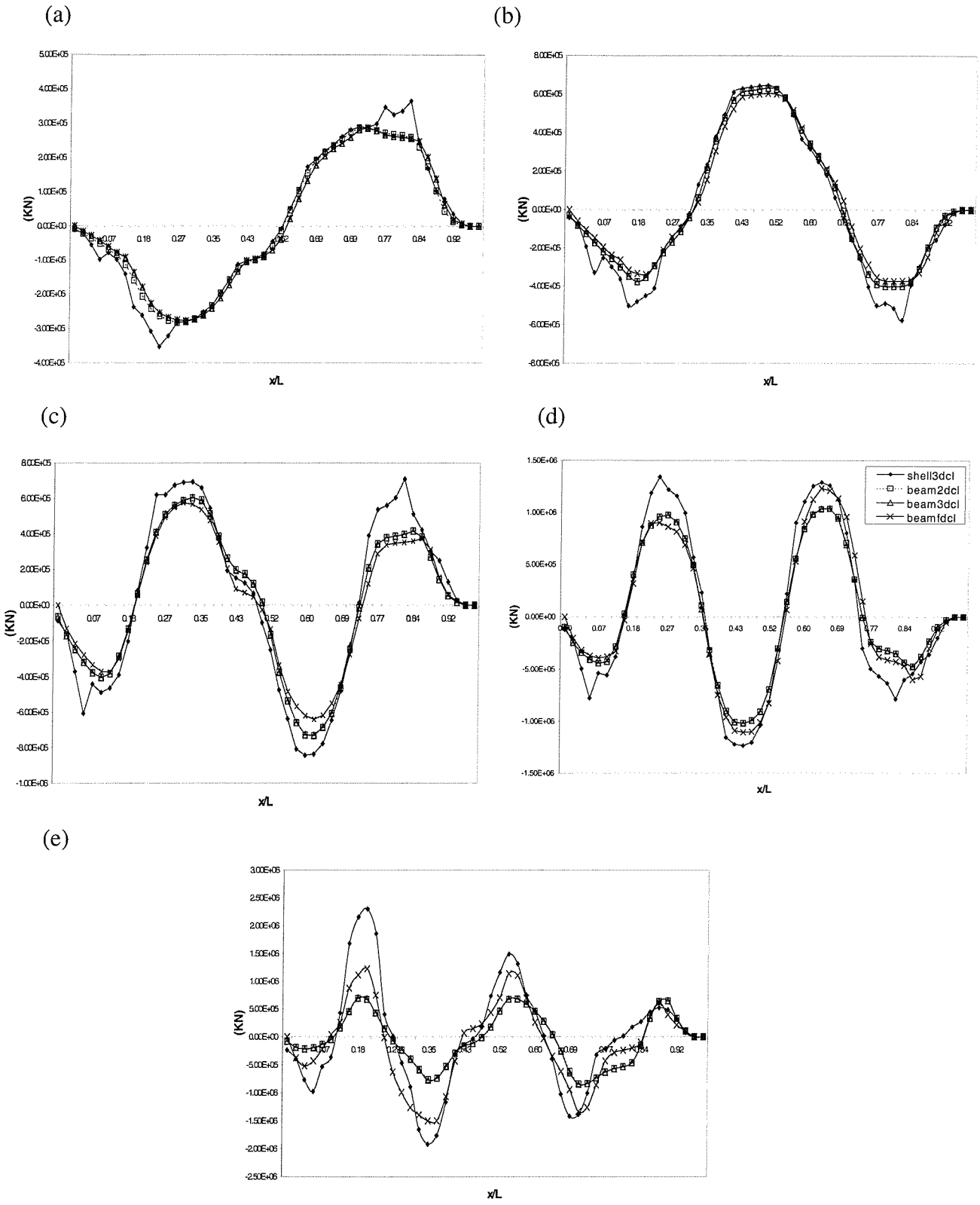

Fig. 5.26 Vertical modal shear forces for closed ship for (a) 2 node, (b)3 node, (c)4 node, (d) 5 node, (e)6 node vertical bending.

(a)

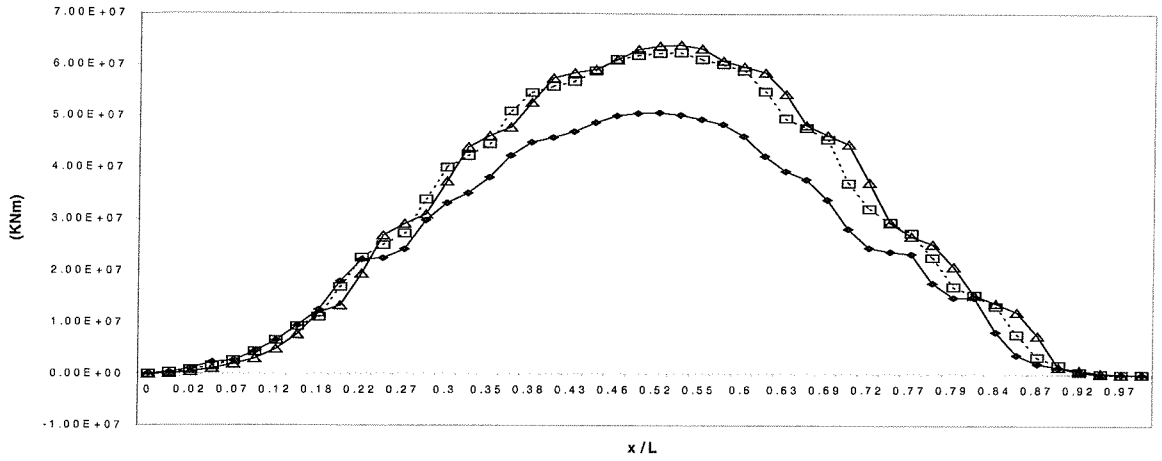

(b)

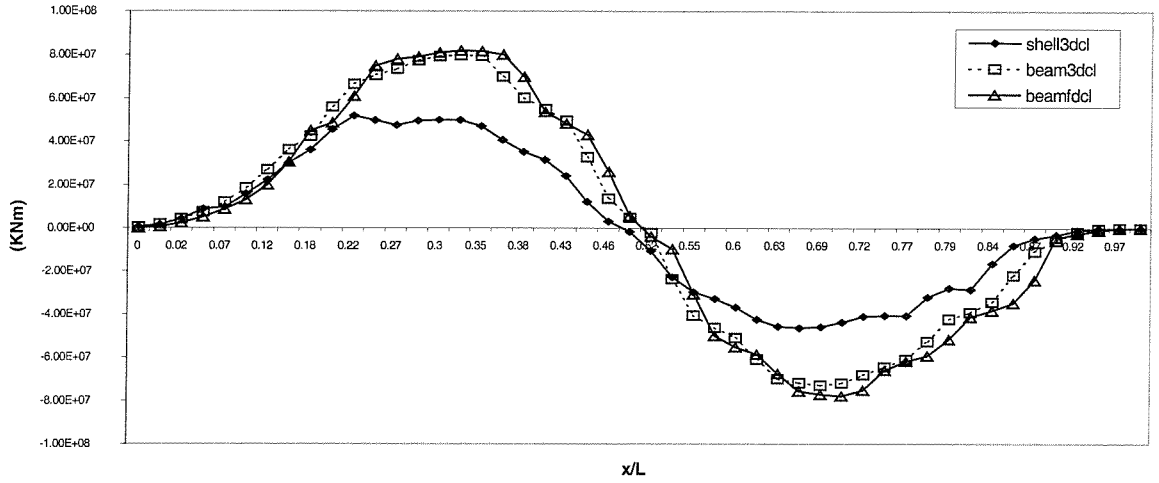

(c)

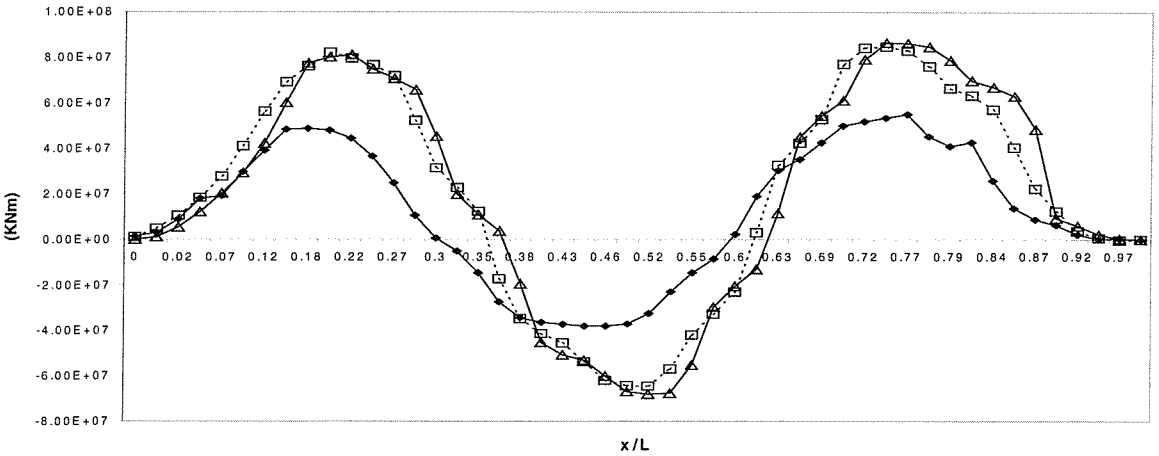

Fig. 5.27 Horizontal modal bending moments corresponding to antisymmetric modes for beamfdcl ($C_W \neq 0$), beam3dcl and shell3dcl idealisations (a) 2 node **HB** 1 node T; (b) 3 node **HB** 2 node T; (c) 4 node **HB** 2 node T (HB: horizontal bending, T: torsion, **HB,T**: dominant HB,T).

(a)

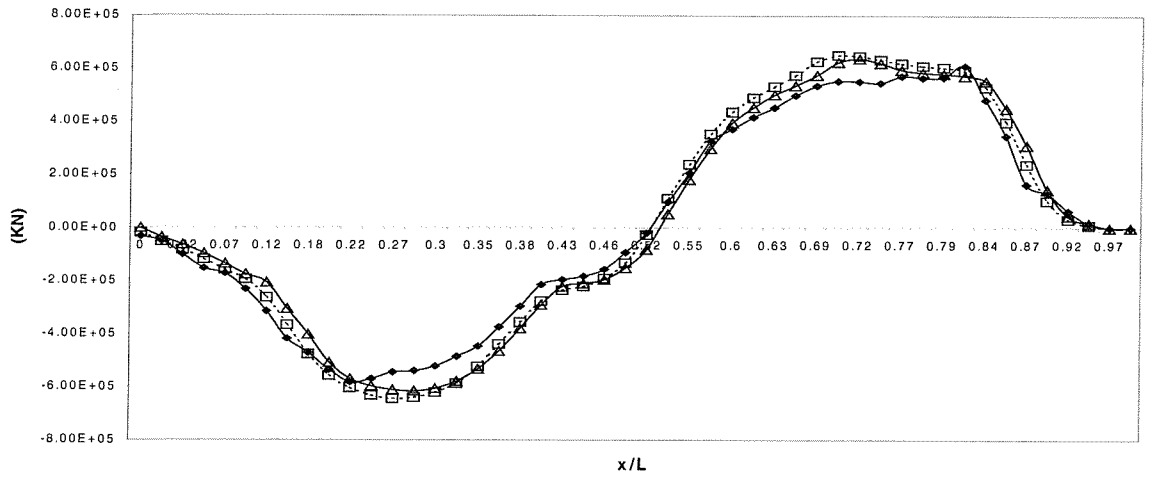

(b)

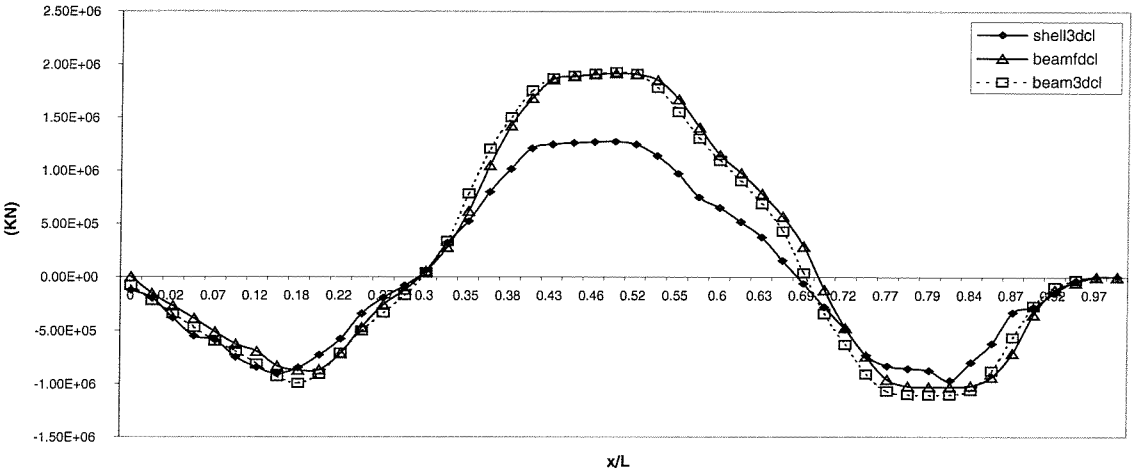

(c)

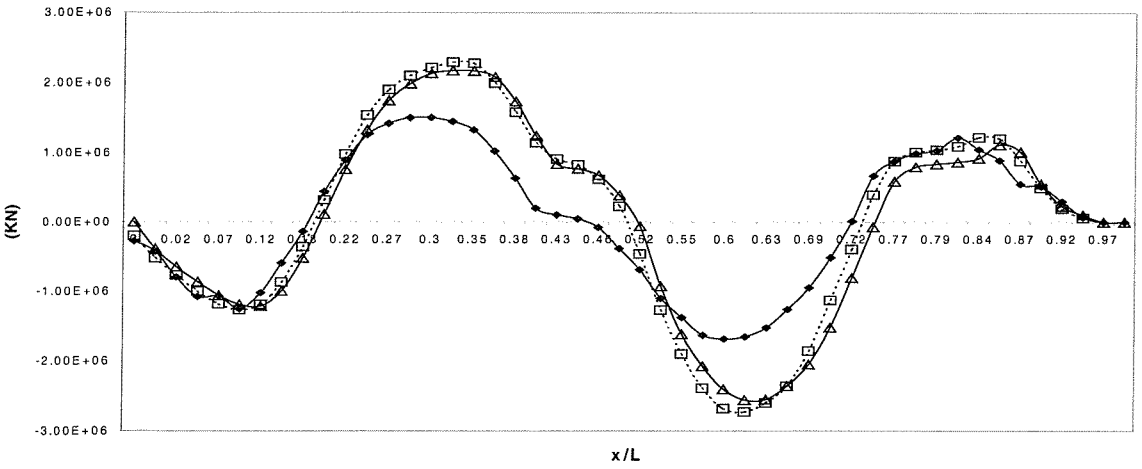

Fig. 5.28 Horizontal shear forces corresponding to antisymmetric modes for beamfdcl ($C_W \neq 0$), beam3dcl and shell3dcl idealisations (a) 2 node **HB** 1 node T; (b) 3 node **HB** 2 node T; (c) 4 node **HB** 2 node T (HB: horizontal bending, T: torsion, **HB,T**: dominant HB,T).

(a)

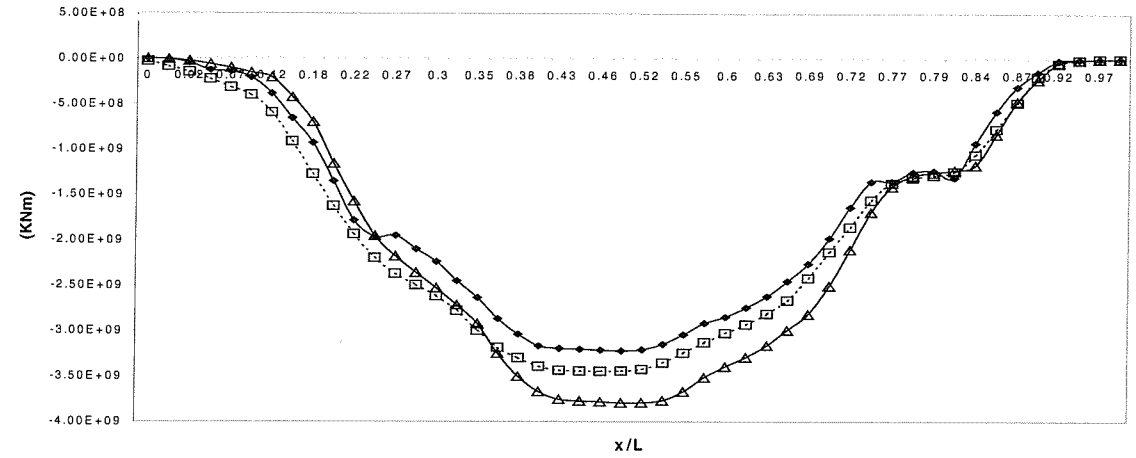

(b)

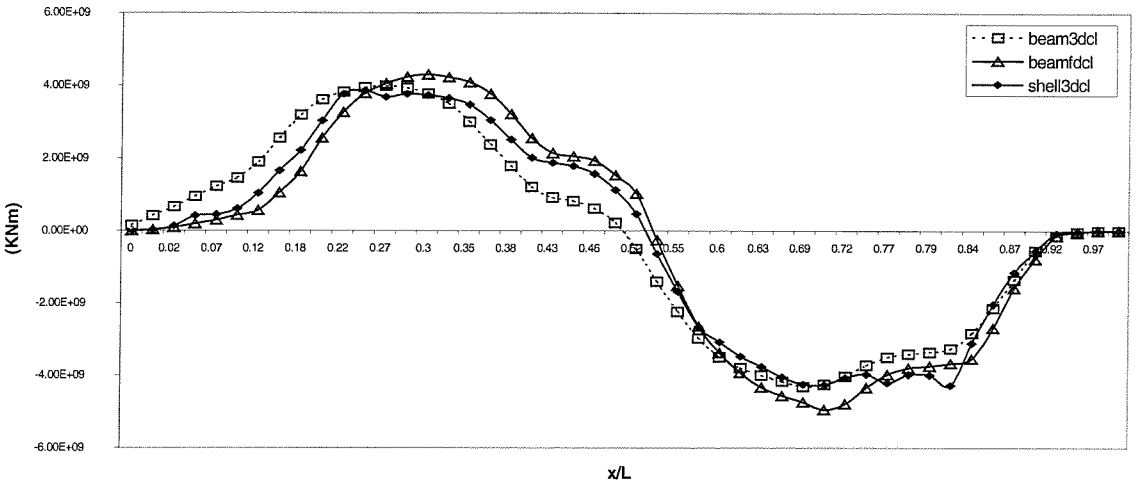

Fig. 5.29 Torsional moments corresponding to antisymmetric modes for beamfdcl ($C_W \neq 0$), beam3dcl and shell3dcl idealisations (a) 2 node HB 1 node **T**; (b) 2 node HB 2 node **T** (HB: horizontal bending, T: torsion, **HB,T**: dominant HB,T).

5.7.2 Dynamics of the open ship

As explained before (see section 5.7) consistency in the analysis implies that for the evaluation of the in vacuo dynamic behaviour of the open ship 0.23 and 0.28 of the cross-section area was considered to be effective in shear for the symmetric and antisymmetric distortions respectively. Generally speaking (see tables 5.23,5.24), in both planes the shell idealisation provides more flexible results than the beam models, for the lower modes of vibration, but this trend is reversed at higher order antisymmetric modes.

It is useful to mention that when the antisymmetric effective cross sectional area is increased from 28 to 90% the finite difference approach (beamfdop) does not appear to be that much affected in comparison to the close ship configuration (beamfdcl) (see tables 5.23,5.24,5.25,5.26). Torsion dominates the antisymmetric motions and warping effects are much more important than those obtained for the case of the closed ship configuration (see tables 5.24,5.25). As in the case of the bulk carrier symmetric and antisymmetric generalised masses appear to be in reasonable good agreement (see tables 5.26, 5.27)

From the eigenvectors of the shell idealisation (shell3dop) becomes also apparent that the open ship structure from dynamics point of view is mostly affected by torsion (see figure 5.30). Figure 5.31 clearly shows that all numerical models behave similarly for in vacuo symmetric vibrations when normalised for unit displacement at stern (near A.P.; keel center line for model shell3dop) for same reasons to those highlighted for the case of the closed ship and bulk carrier structures (see section 5.3). Since warping is significant for such ship structures the antisymmetric eigenvectors behave as in the bulker configuration (compare figures 5.3,5.4 to figures 5.32, 5.33).

The effect of open decks appears to be significant in the distribution of direct stresses along the hull (compare figures 5.3,5.4 to figures 5.32,5.33). Peak stresses appear in the maximum vertical deflection points (along the deck and keel) for symmetric distortions, while for antisymmetric distortions the effect of high stress concentration at hatch opening deck junction is apparent. The vunerability of ship structures with large deck openings to localized direct pressures at the vicinities of the forward and backward hatch openings is once more demonstrated (compare figure 5.6 to figure 5.34).

As in the case of bulker and closed ship idealisations (see sections 5.6,5.7.1) vertical bending moments and shear forces correlate well even at the higher modes of vibration (see figures 5.35,5.36). Comparison of the antisymmetric modal loads (horizontal bending moments, shear forces and torsional moments) shows that, as in the case of the bulker configuration, the beam idealisation overestimates the shell predictions (see figures 5.37,5.38,5.39). Once more it is believed that these deviations appear because of the non-prismatic effects of the hull girder which are of significance at the engine room (sections 8,9) and forward end (sections 43,42)

locations. It is rather interesting to note that the comparison of the relation between beamfd and shell3d for the 2 node horizontal bending dominant mode is better in the case of the bulker than the open ship idealisation (see figures 5.37(b) and 5.10(b). Although at first instance this appears to be surprising in the sense that the global non-prismatic features are less evident in the open ship structure it is expected because of the effects of shear lagging which are less evident for the case of a bulker (see section 5.9).

Model Mode type	shell3dop	beamfdop	beam2dop	beam3dop
2 node VB	4.426	4.424	4.397	4.397
3 node VB	8.809	8.874	8.872	8.878
4 node VB	12.937	13.391	13.483	13.489
5 node VB	15.425	16.624	16.774	16.776
Longitudinal	17.379	-	17.586	27.592
6 node VB	21.727	22.975	23.587	23.592

Table 5.23 Natural frequencies (rad/s) for symmetric distortions of the dry hull of open ship (t_{fb} = thickness of fictitious bulkheads, VB = vertical bending).

Model Mode type ($C_W \neq 0$)	beamfdop $C_w \neq 0$	shell3dop t_{bf} = 0.001m	beamfdop $C_w = 0$
1 node HB – 1 node **T**	2.671	2.576	1.505
2 node **HB** - 2 node T	5.333	4.780	2.100
3 node **HB** – 3 node T	9.572	9.801	3.054
2 node HB – 2 node **T**	10.768	11.259	3.840
3 node HB – 3 node **T**	16.353	17.517	5.170

Table 5.24 Natural frequencies (rad/s) for antisymmetric distortions of the dry hull of open ship, $\mathbf{A_{efy}=0.28A}$ (C_w= warping stiffness; HB = horizontal bending; T = torsion; **HB,T** = dominant HB,T).

Model Mode type($C_W \neq 0$)	beamfdop $C_w \neq 0$	shell3dop $t_{bf} = 0.001$m	beamfdop $C_w = 0$
1 node HB – 1 node **T**	2.872	2.576	1.701
2 node **HB** - 2 node T	5.682	4.780	2.102
3 node **HB** – 3 node T	9.730	9.801	3.080
2 node HB – 2 node **T**	12.752	11.259	3.876
3 node HB – 3 node **T**	20.273	17.517	5.180

Table 5.25 Natural frequencies (rad/s) for antisymmetric distortions of the dry hull of open ship, $\mathbf{A_{efy}=0.90A}$ (C_w= warping stiffness; HB = horizontal bending; T = torsion; **HB,T** = dominant HB,T).

Mode description	Generalised mass (tonne-m^2)			
	shell3dop	beam2dop	beam3dop	beamfdop
2 node VB	19521	19923	19911	19803
3 node VB	9196	9043	9037	8838
4 node VB	7152	4952	4940	4445
5 node VB	9795	4973	4986	6141
6 node VB	10130	7304	7320	5843

Table 5.26 Symmetric distortions generalised masses for alternative discretisation schemes for the open ship (VB = vertical bending).

Mode description($C_W \neq 0$)	Generalised mass (tonne-m^2)	
	shell3dop	beamfdop
1 node HB – 1 node **T**	94963	95302
2 node **HB** – 2 node T	81843	73484
3 node **HB** – 3 node T	17121	21789
2 node HB – 2 node **T**	30393	64756
3 node HB – 3 node **T**	9346	7977

Table 5.27 Anti-symmetric distortions generalised masses for alternative discretisation schemes for the open ship (C_w= warping stiffness; HB = horizontal bending; T = torsion; **HB,T** = dominant HB,T).

1 node HB and 1 node **T**
(ω_r = 2.576 rad/s)

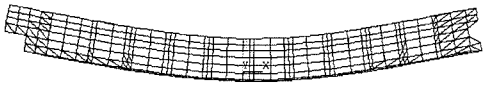

2 node VB
(ω_r = 4.426 rad/s)

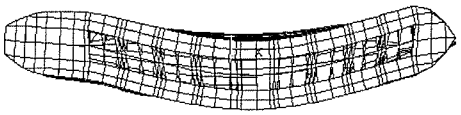

2 node **HB** and 2 node T
(ω_r = 4.780 rad/s)

3 node VB
(ω_r = 8.809 rad/s)

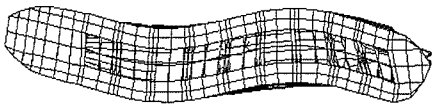

3 node **HB** and 3 node T
(ω_r = 9.801 rad/s)

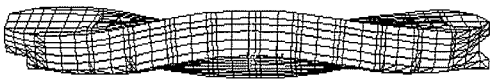

2 node HB and 2 node **T**
(ω_r = 11.259 rad/s)

4 node VB
(ω_r = 12.937 rad/s)

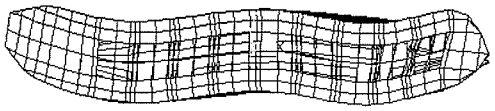

4 node **HB** and 4 node T
(ω_r = 15.393 rad/s)

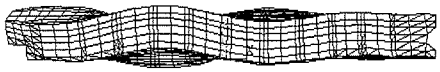

3 node HB and 3 node **T**
(ω_r = 17.517 rad/s)

5 node **HB** and 5 node T
(ω_r = 21.570 rad/s)

Fig. 5.30 Principal mode shapes of model shell3d **for open ship idealisation** (VB : vertical bending ; HB : horizontal bending; T : torsion, **HB,T** : dominant HB,T).

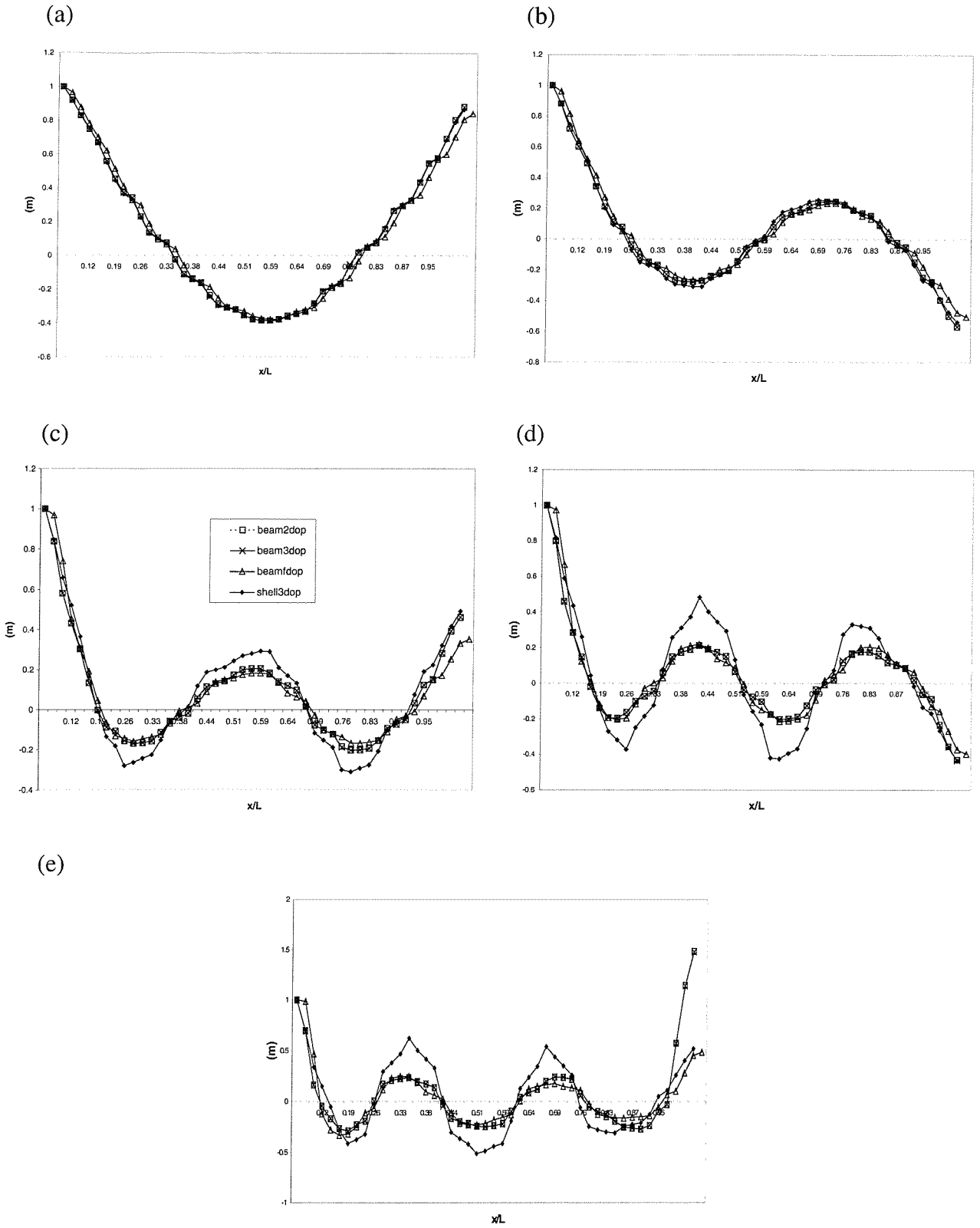

Fig. 5.31 Symmetric mode shapes for all models of open ship idealisation corresponding to (a)2 node, (b)3 node, (c) 4 node, (d) 5 node and (e) 6 node vertical deflections.

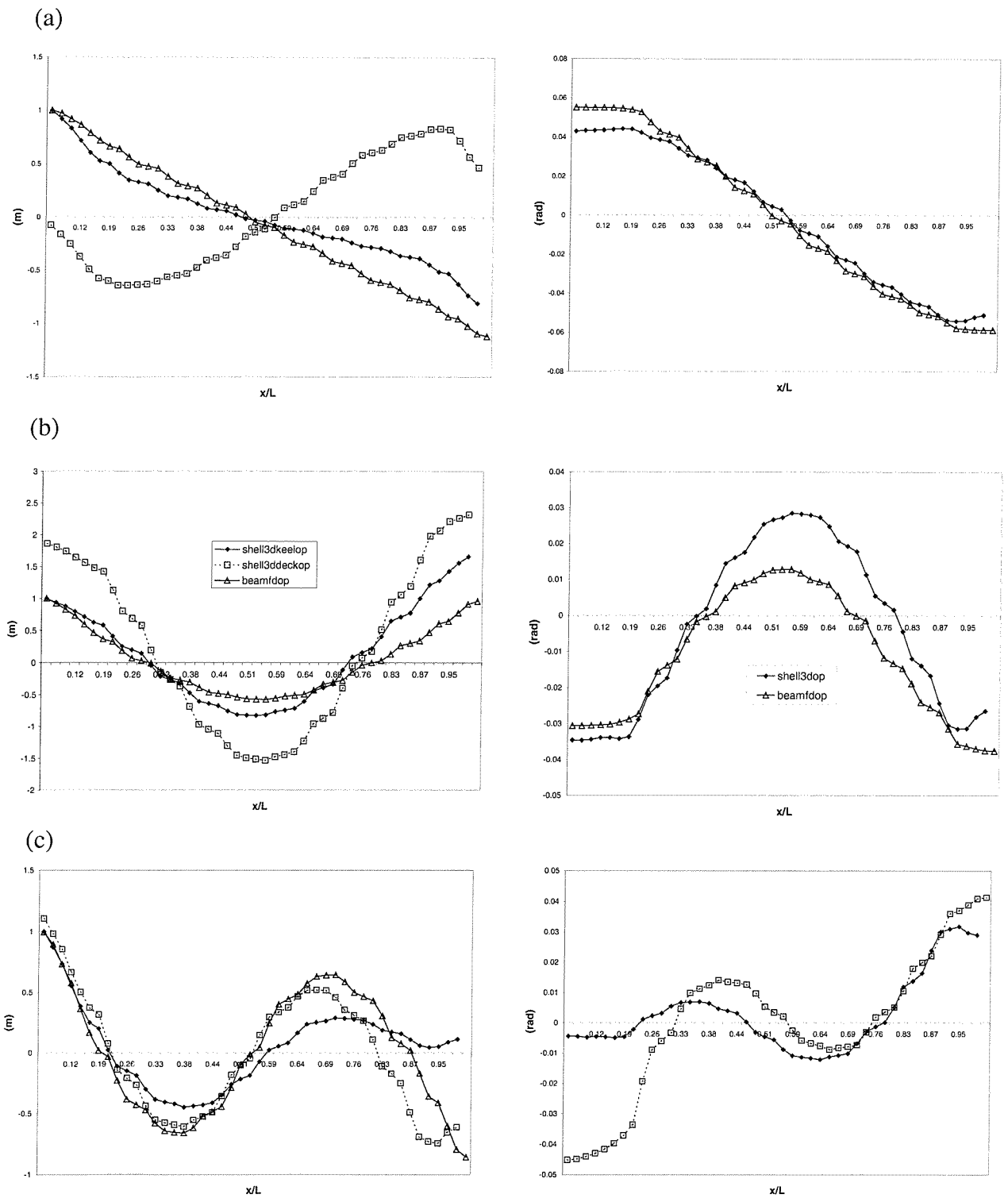

Fig. 5.32 Antisymmetric mode shapes, represented by the horizontal deflection (m) and twist angle (rad), obtained from models beamfdop ($C_W \neq 0$), and shell3dop (keel centre and deck side junction) corresponding to (a) 1 node HB 1 node T; (b) 2 node HB 2 node T; (c) 3 node HB 3 node T (HB: horizontal bending, T: torsion, HB,T: dominant HB,T).

(a)

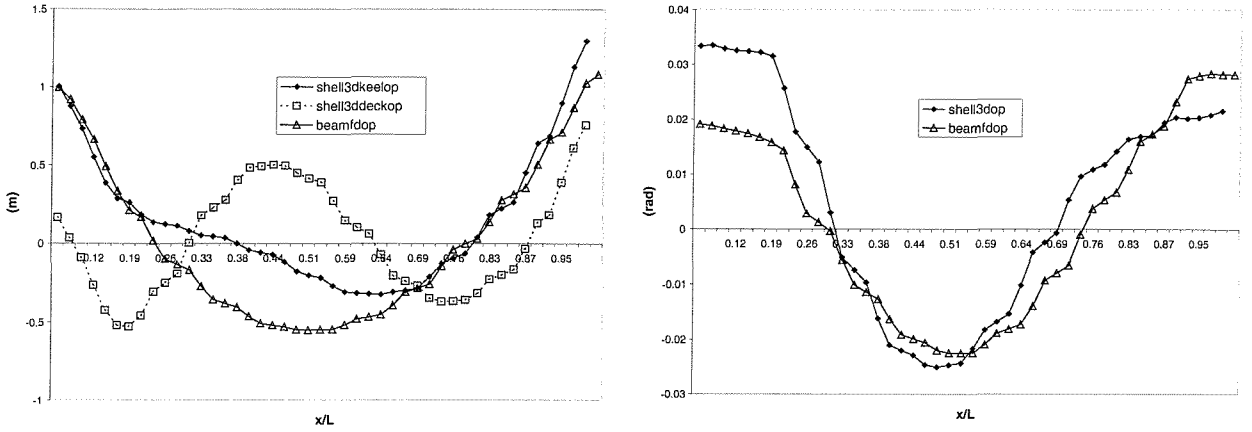

(b)

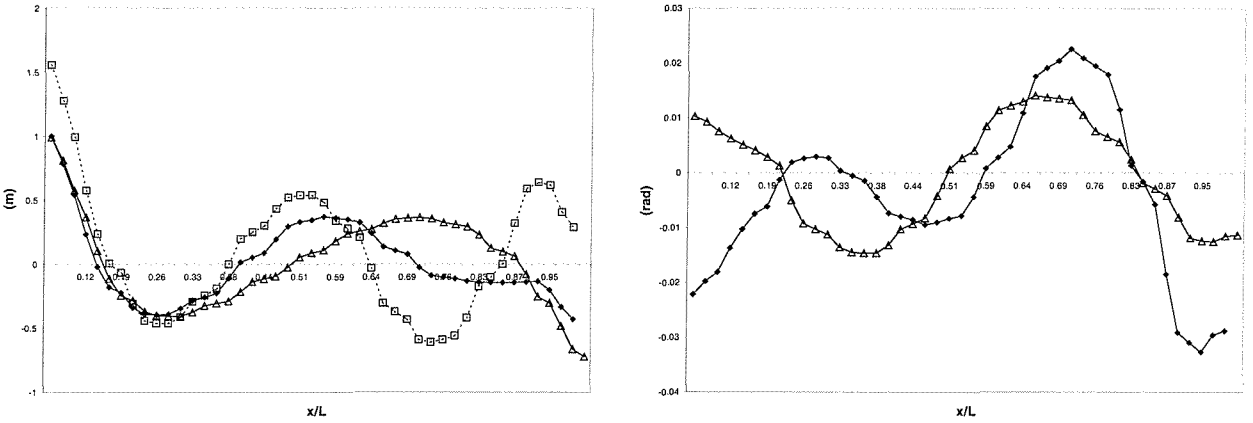

Fig. 5.33 Antisymmetric mode shapes, represented by the horizontal deflection (m) and twist angle (rad), obtained from models beamfdop($C_W \neq 0$), and shell3dop (keel centre and deck side junction) corresponding to: (a) 2 node HB 2 node **T**; (b) 3 node HB 3 node **T** (HB: horizontal bending, T: torsion, **HB,T**: dominant HB,T).

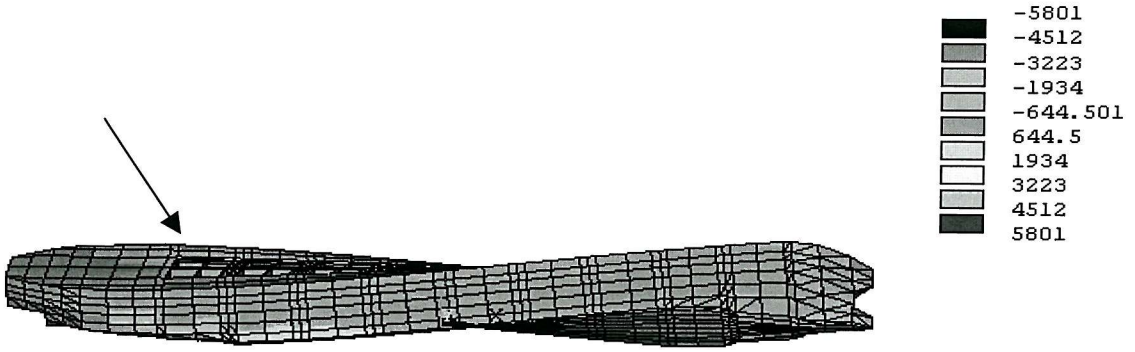

1 node HB 1 node **T**
(ω_r = 2.576 rad/s)

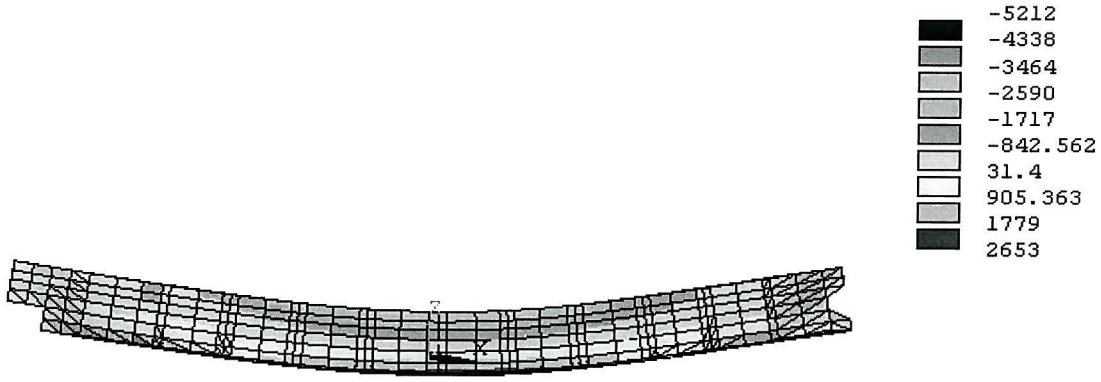

2 node **VB**
(ω_r = 4.426 rad/s)

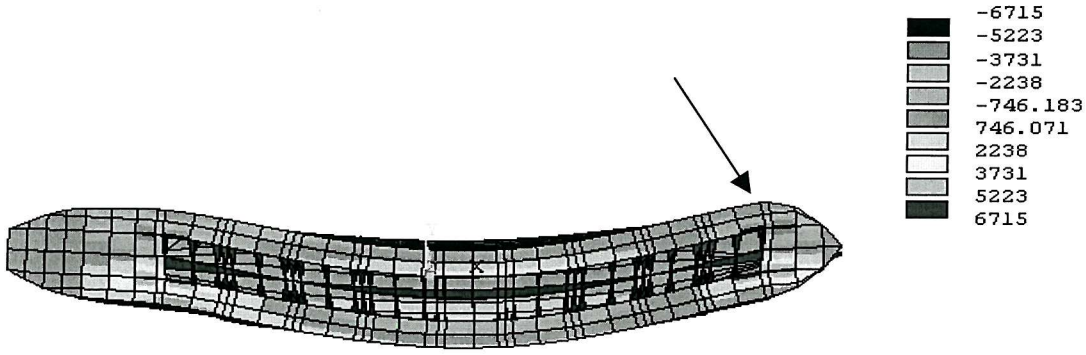

2 node **HB** 2 node T
(ω_r = 4.780 rad/s)

Fig 5.34 Principal direct modal stresses (KN/m^2) for open ship idealisation, arrows indicate possible critical area (VB: vertical bending, HB: horizontal bending, T: torsion, **HB,T**: dominant HB,T).

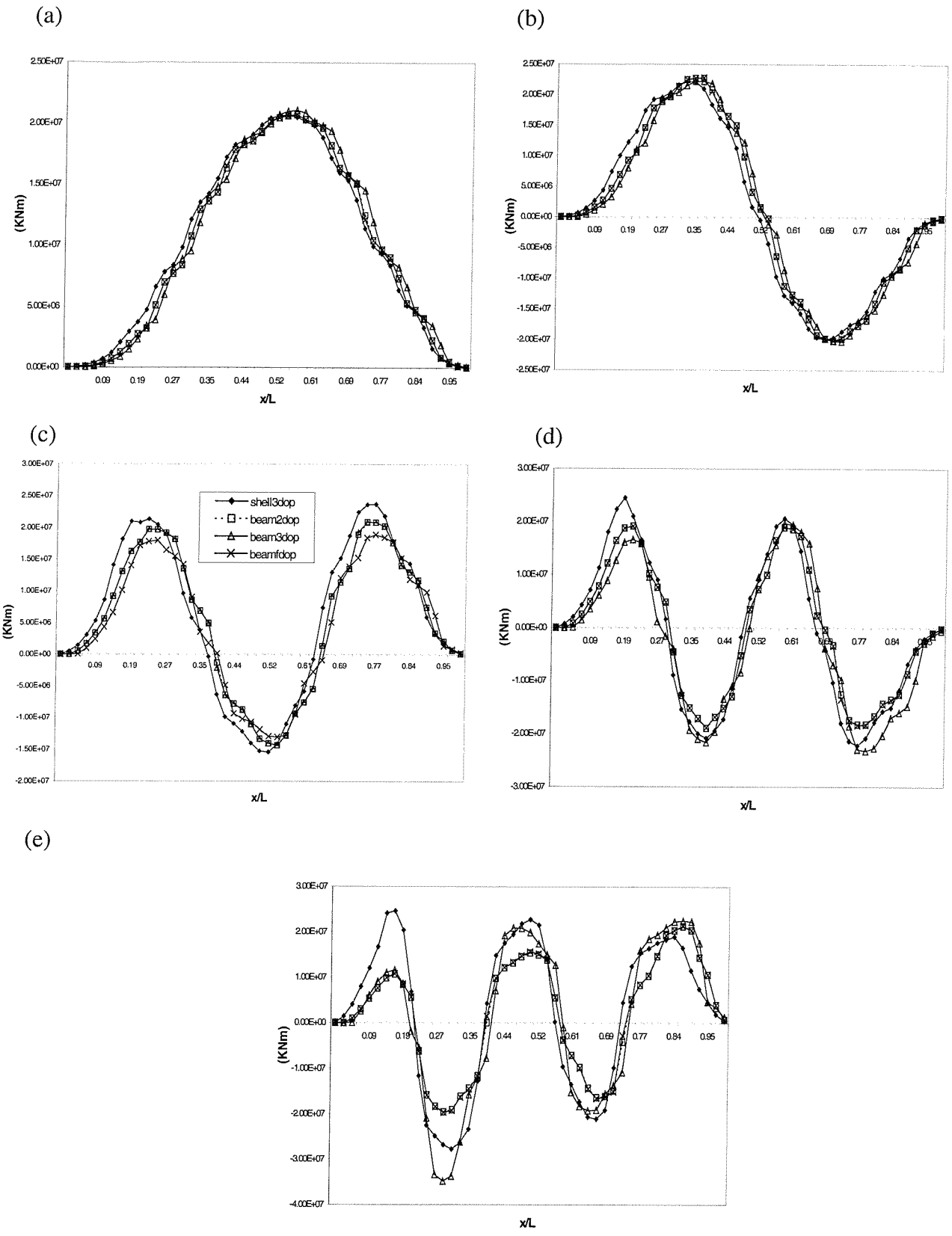

Fig. 5.35 Vertical modal bending moments for open ship for (a) 2 node, (b)3 node, (c)4 node, (d) 5 node, (e)6 node vertical bending.

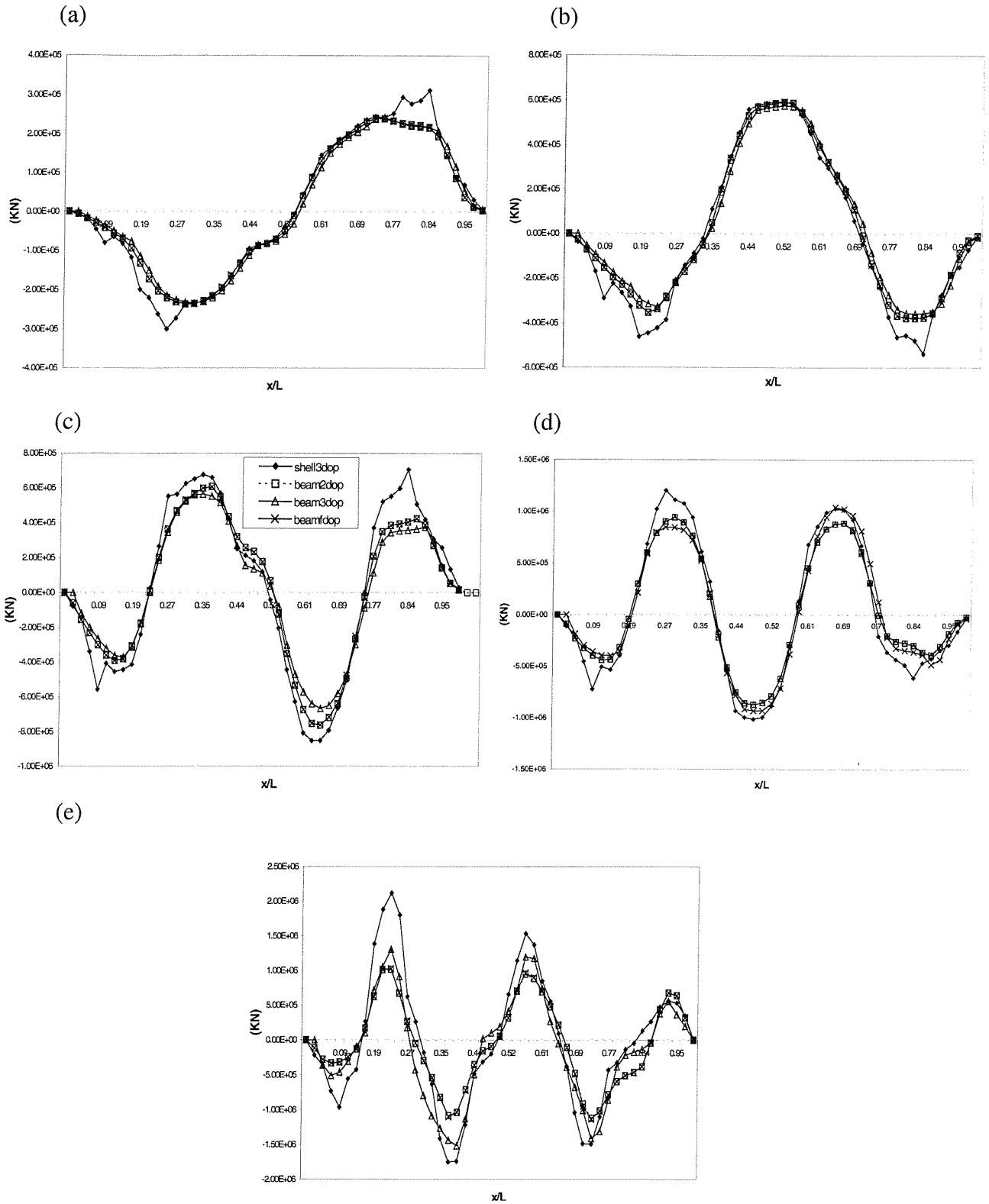

Fig. 5.36 Vertical modal shear forces for open ship for (a) 2 node, (b)3 node, (c)4 node, (d) 5 node, (e)6 node vertical bending.

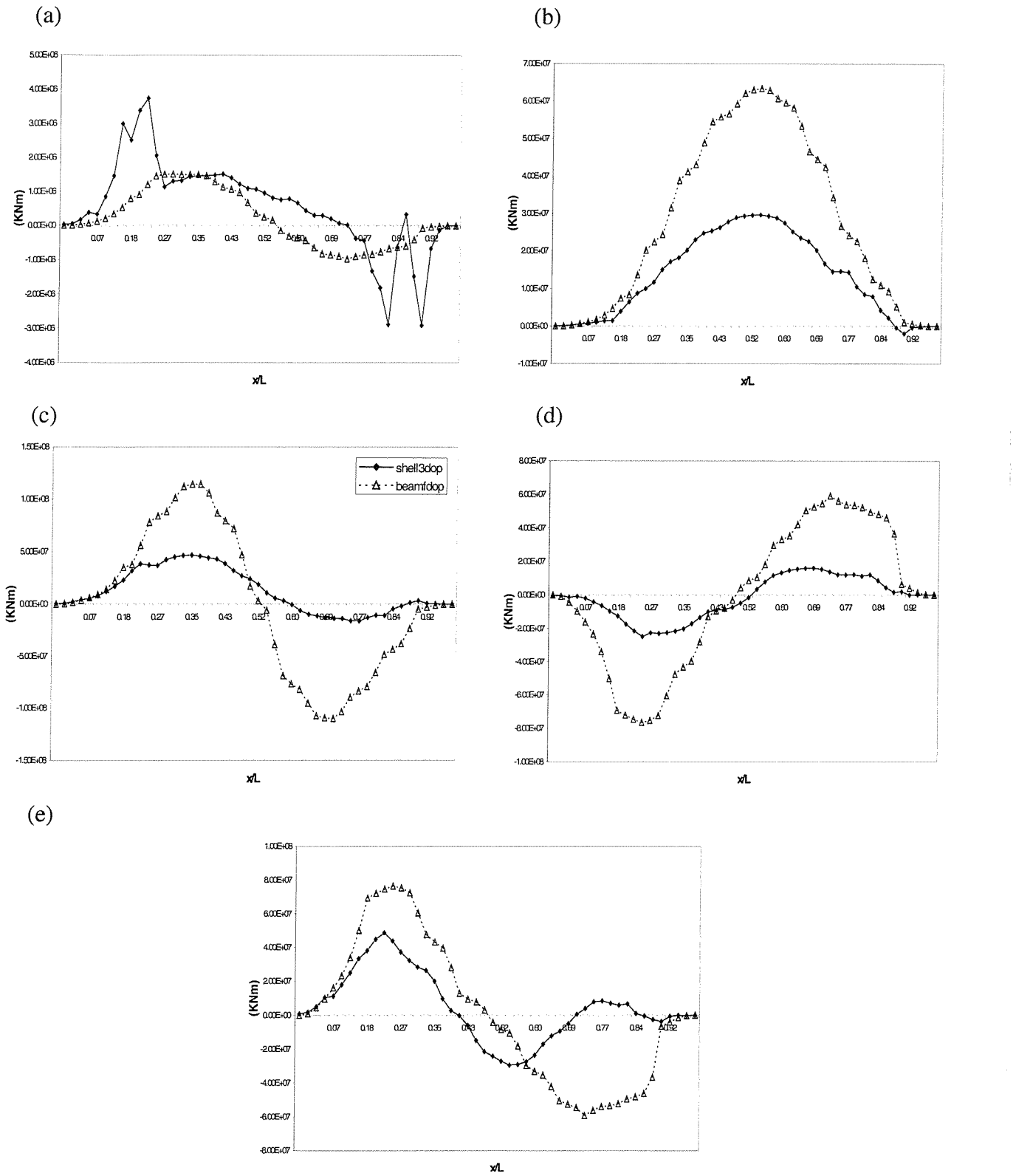

Fig. 5.37 Horizontal modal bending moments corresponding to antisymmetric modes for open ship beamfdop ($C_W \neq 0$), shell3dop idealisations; (a) 1 node HB **1** node **T**; (b) 2 node **HB** 2 node T (c) 2 node HB 2 node **T;** (d) 3 node **HB** 3 node T; (e) 3 node HB 3 node **T** (HB: horizontal bending, T: torsion, **HB,T**: dominant HB,T).

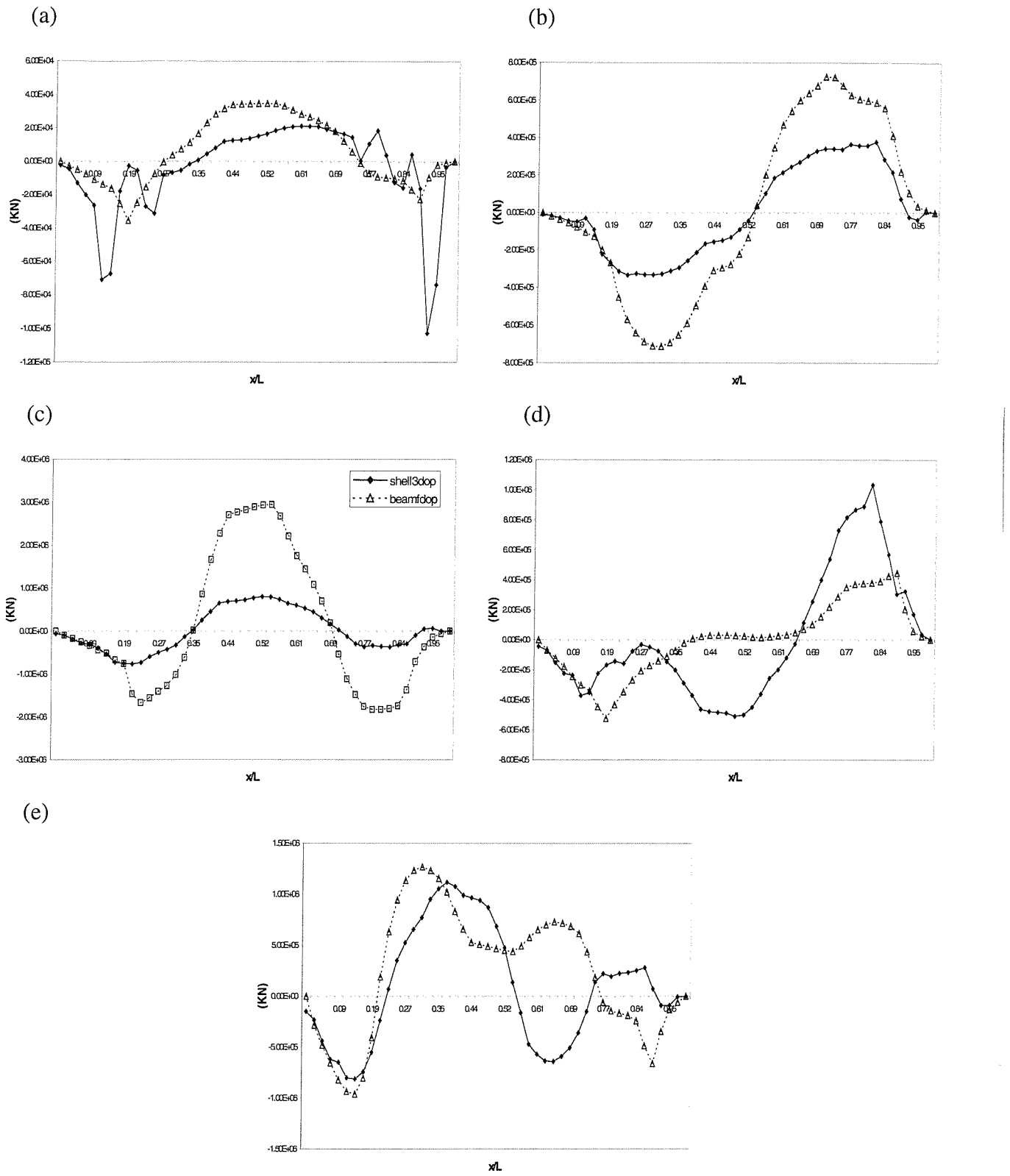

Fig.5.38 Horizontal modal shear forces corresponding to antisymmetric modes for open ship beamfdop ($C_W \neq 0$), shell3dop idealisations; (a) 1 node HB **1** node **T**; (b) 2 node **HB** 2 node T (c) 2 node HB 2 node **T;** (d) 3 node **HB** 3 node T; (e) 3 node HB 3 node **T** (HB: horizontal bending, T: torsion, **HB,T**: dominant HB,T).

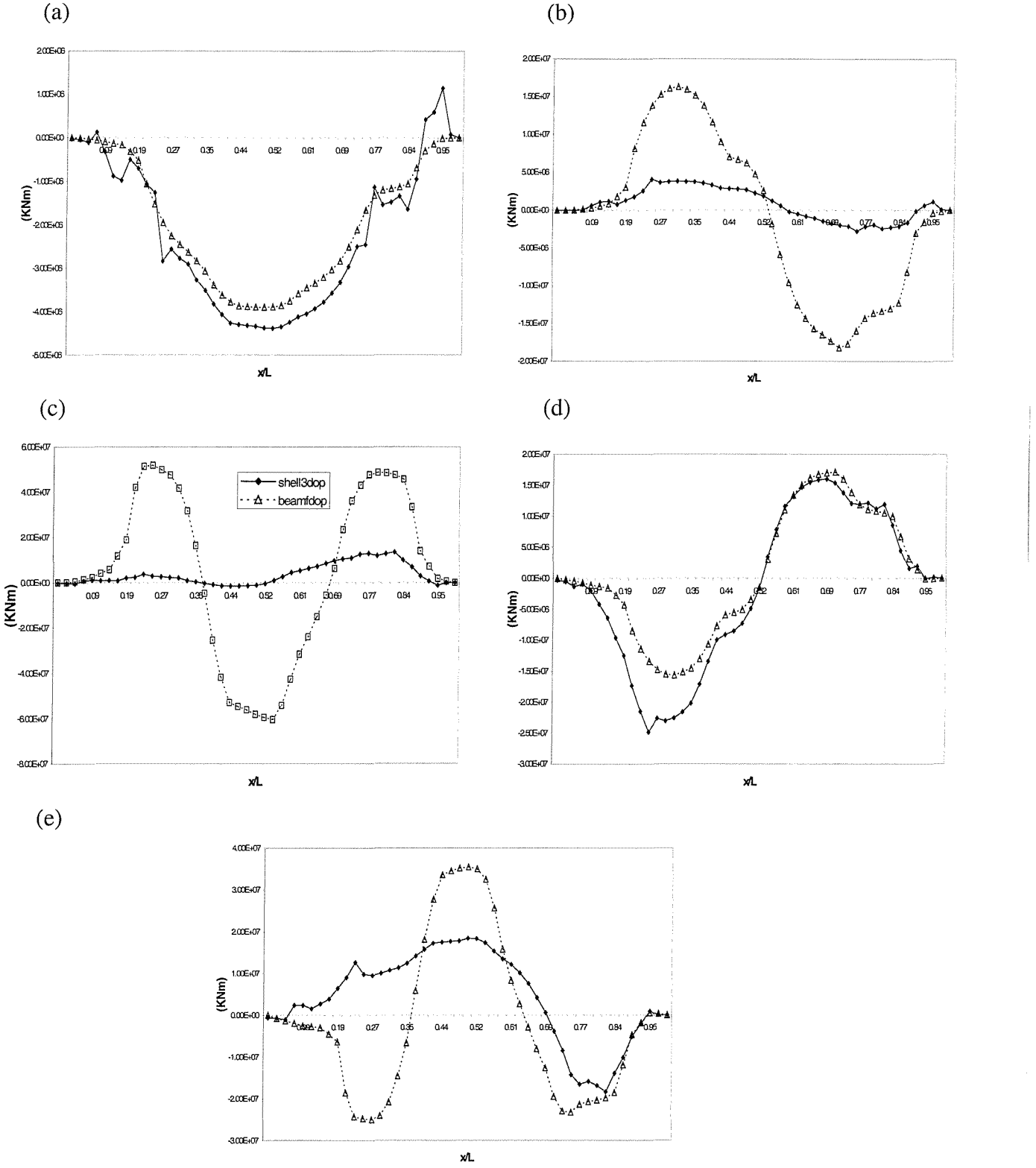

Fig.5.39 Torsional moments corresponding to antisymmetric modes for open ship beamfdop ($C_W \neq 0$), shell3dop idealisations; (a) 1 node HB **1** node **T**; (b) 2 node **HB** 2 node T (c) 2 node HB 2 node **T;** (d) 3 node **HB** 3 node T; (e) 3 node HB 3 node **T** (HB: horizontal bending, T: torsion, **HB**: dominant HB,T).

5.8 Demonstration of the effects of coupling

From the discussion so far it becomes apparent that the coupling of natural frequencies, because of the effects of warping and shear distance, for the case of open and bulker ship configurations is quite significant. This is not so important for the bulk carrier whether equal or unequal spaces are used (see tables 5.28,5.29(a)). Closing the deck of a bulk carrier hull with an equivalent deck and constructing a closed deck ship leads to increase of the natural frequencies (see table 5.29(b)). On the other hand the open deck ship has lower natural frequencies than the closed and bulker configurations, fact which implies that open decks lead to a more flexible structure as a consequence of the increase of the warping stiffness (see table 5.29).

Symmetric		Antisymmetric			Critical ratios
ω_B		ω_T	ω_R		ω_R/ω_B OR ω_R/ω_T
	B	$C_w \neq 0$	$C_w \neq 0$	B-T	$C_w \neq 0$
4.419	**2**	-	5.847	**2** – 2	1.322
-	-	4.908	5.148	1 – **1**	1.048
9.247	**3**	-	11.132	**3** – 3	1.203
-	-	9.716	10.099	2 – **2**	1.039
-	-	13.823	15.385	3 – **3**	1.113
14.237	**4**	-	16.382	**4** – 4	1.151

Table 5.28 Illustration of the effects of coupling on natural frequencies (rad/s) for **MV Derbyshire** – beamfde (**equal** spacing) simulation (ω_B = pure bending, ω_T = pure torsion, ω_R = coupled bending and torsion, B: bending node, **B**: dominant B node, T: torsion node, **T**: dominant T node, C_w= warping constant).

(a)

Symmetric		Antisymmetric			Critical ratios
ω_B		ω_T	ω_R		ω_R/ω_B OR ω_R/ω_T
	B	$C_w \neq 0$	$C_w \neq 0$	B-T	$C_w \neq 0$
6.303	**2**	-	6.261	**2** – 2	0.993
-	-	7.171	5.992	1 – **1**	0.835
11.255	**3**	-	12.656	**3** – 3	1.124
-	-	14.711	10.995	2 – **2**	0.747
16.037	**4**	-	17.086	**4** – 4	1.065
-	**-**	22.152	16.047	3 – **3**	0.724

(b)

Symmetric		Antisymmetric			Critical ratios
ω_B		ω_T	ω_R		ω_R/ω_B OR ω_R/ω_T
	B	$C_w \neq 0$	$C_w \neq 0$	B-T	$C_w \neq 0$
6.538	**2**	-	6.542	**2** – 2	1.001
-	-	10.277	10.217	1 – **1**	0.994
11.586	**3**	-	11.595	**3** – 3	1.001
16.420	**4**	-	19.724	2 – **2**	1.201
-	**-**	20.864	16.446	**4** – 2	0.788

(c)

Symmetric		Antisymmetric			Critical ratios
ω_B		ω_T	ω_R		ω_R/ω_B OR ω_R/ω_T
	B	$C_w \neq 0$	$C_w \neq 0$	B-T	$C_w \neq 0$
-	**-**	2.235	2.671	1 – **1**	1.195
6.098	**2**	-	5.333	**2** – 2	0.874
-	**-**	10.121	10.768	2 – **2**	1.064
10.957	**3**	-	9.572	**3** – 3	0.873
-	**-**	22.636	16.353	3 – **3**	0.722

Table 5.29 Illustration of the effects of coupling on natural frequencies (rad/s) for: (a) **MV Derbyshire**-beamfd (**unequal** spacing) simulation, (b) **closed ship** -beamfdcl simulation, (c) **open ship-** beamfdop simulation (ω_B = pure horizontal bending, ω_T = pure torsion, ω_R = coupled bending and torsion, B: bending node, **B**: dominant B node, T: torsion node, **T**: dominant T node, C_w= warping constant).

5.9 A note on modal shear lag effects

Simple beam theory assumes that plane cross-sections remain plane and therefore the bending stress is directly proportional to the distance from the neutral axis. Thus in any flange and web type of beam this direct stress should be constant across the flanges. However, in most cases the bending is not caused by vertical loads and these loads are absorbed by the webs of the beam and not by the flanges [5.9]. That is, even for a hull girder, in which the vertical loads initially act on the flanges, they are immediately transferred to the webs by transverse beams and frames. The overall result is that the flange undergoes in-plane longitudinal distortion and therefore plane cross-sections do not remain plane when shear stress is present. The most effective aspect of shear distortion is that the central portion of the flange carries less bending stress, and it is therefore less effective than the outer portion. Thus, because of *'shear effects'* the bending stress remote from a web *'lags behind'* the stress near the web. The phenomenon is known as the *shear lag* effect and is considered of being greatly important in beams having very wide flanges and shallow webs (e.g. aircraft wings) while in steel box girders by definition the effect is expected to be only a few percent (see figures 5.40, 5.41(a),(b)) [5.9].

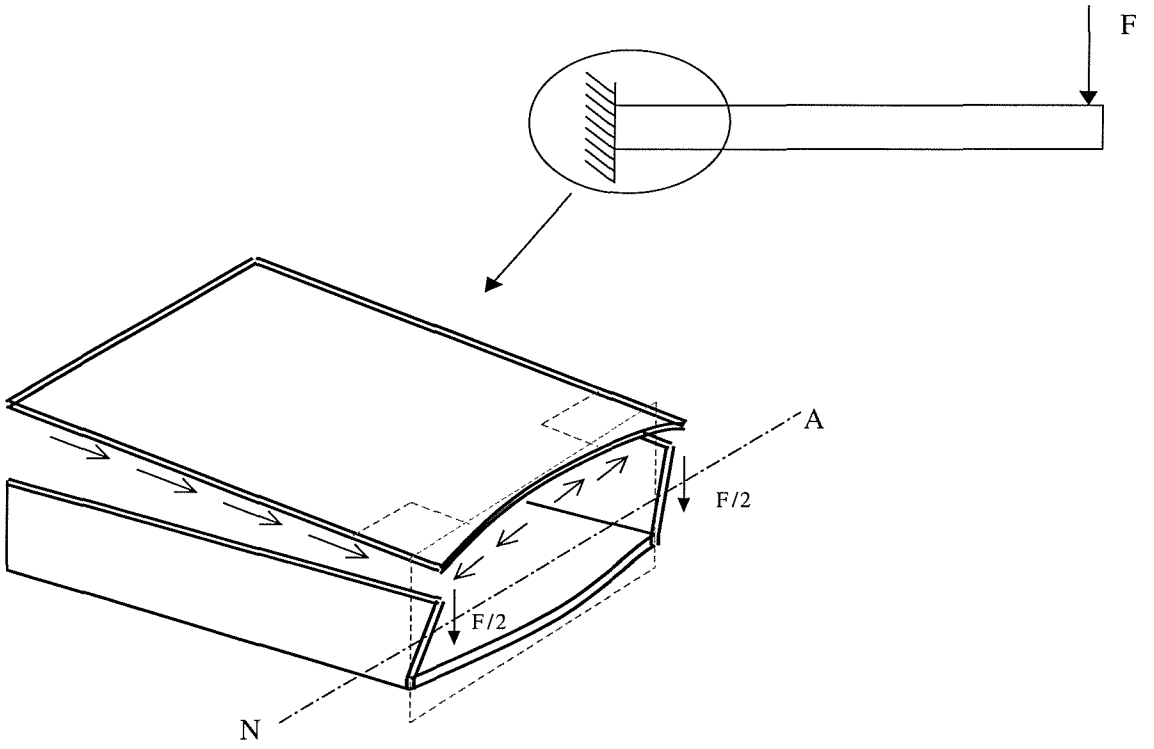

Fig. 5.40 Shear lag in box girders; arrows (→) denote the shear stress distribution (NA: Neutral Axis, F: Force component) [5.9].

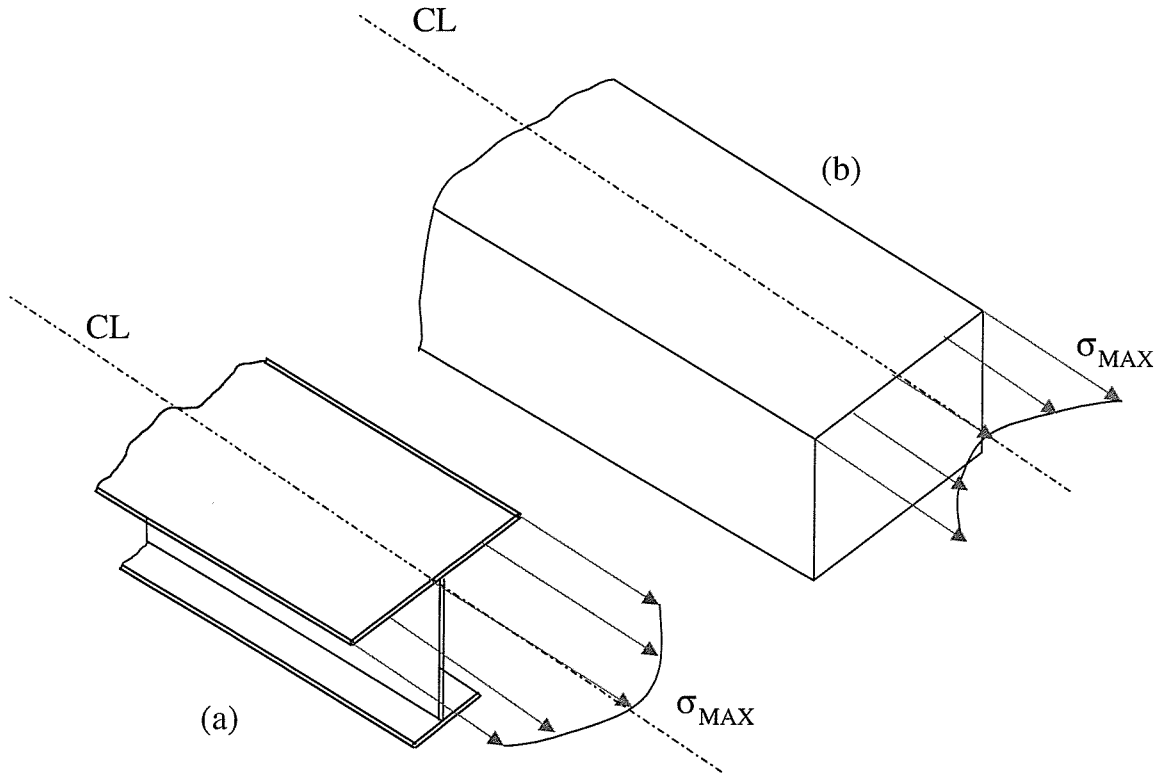

Fig. 5.41 Shear lag in beam flanges; (a) standard single web beam; (b) rectangular beam (σ_{MAX}: maximum stress component, CL: Centre Line) [5.9].

For the purposes of the current investigation the shear lag effect was studied across selected nodal points at 3 alternative positions along the hull namely section 7 (close to stern), 14 (between stern and amidships) and section 23 (amidships) for all types of models (bulker, closed, open). In a way there was no practical reason to study the shear lagging effects forward of section 23 since the distribution of direct stress components (σ_x) is such that, in general, so that maximum values observed in the vicinity of amidships gradually decreasing in magnitude towards the girders' extremities. At first stage the study was based on the direct stresses extracted from the first symmetric mode of vibration. The basics of the methodology described above are an outcome of the detailed modal analysis calculations performed for the bulker (see section 5.5), closed (see section 5.7.1) and open (see section 5.7.2) ship configurations. It was shown that the effects of shear lag are (i) much more important at deck openings and just a few percent for the closed ship type structure, (ii) increased amidships and reduced comparatively at the extremities of the hull (see figures 5.42,5.43,5.44). Maximum shear lag magnitudes always appear across the deck of the structure (see figures 5.42(a),

5.43(a), 5.44(a)). The effects appear to be rather significant across the deck of the open deck structure (see figure 5.44(a)).

(a)

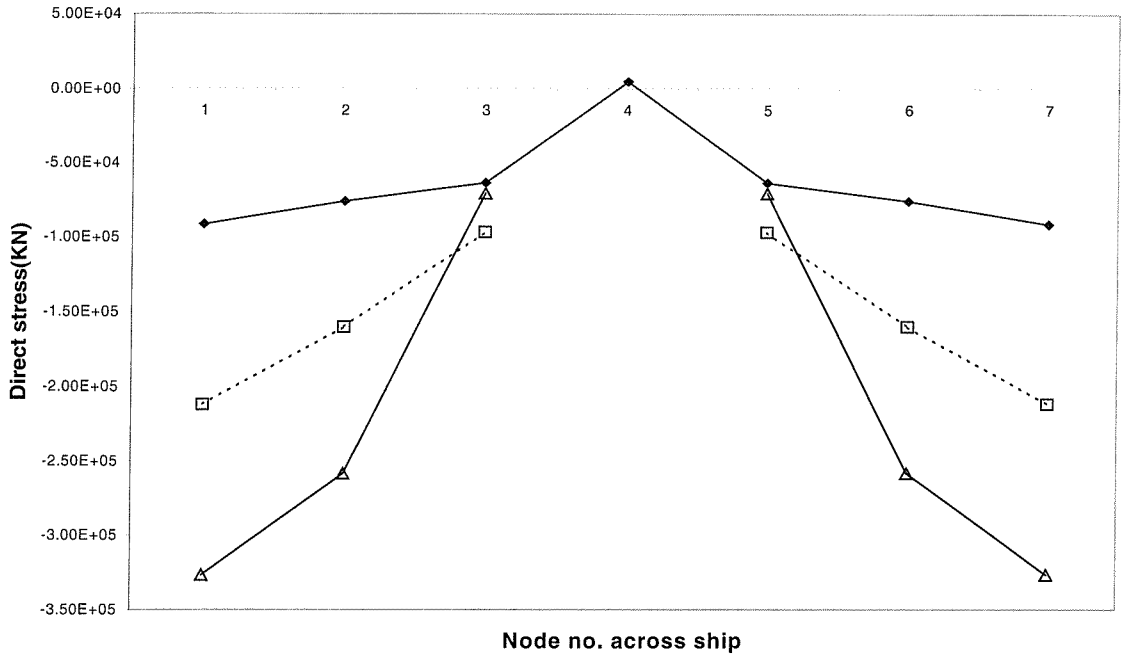

(b)

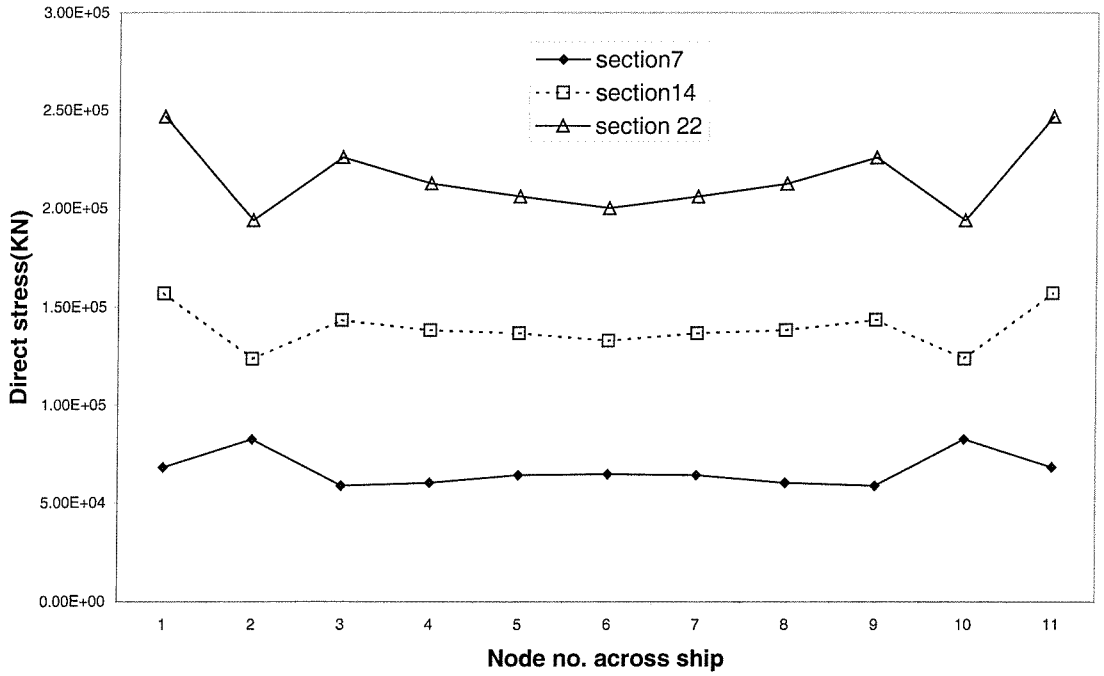

Fig. 5.42 Demonstration of the effects of modal shear lagging of **bulker** across (a) deck (centre line at node 4); (b) bottom (centre line at node 6); modal comparisons are based on the 2 node vertical bending mode.

(a)

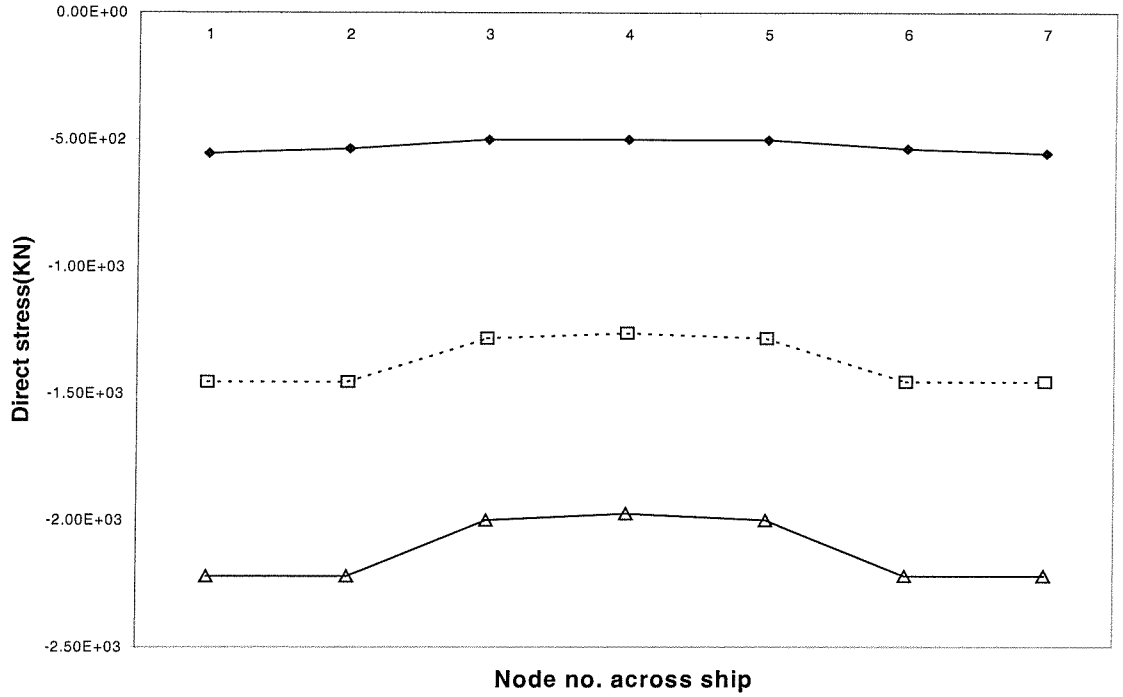

(b)

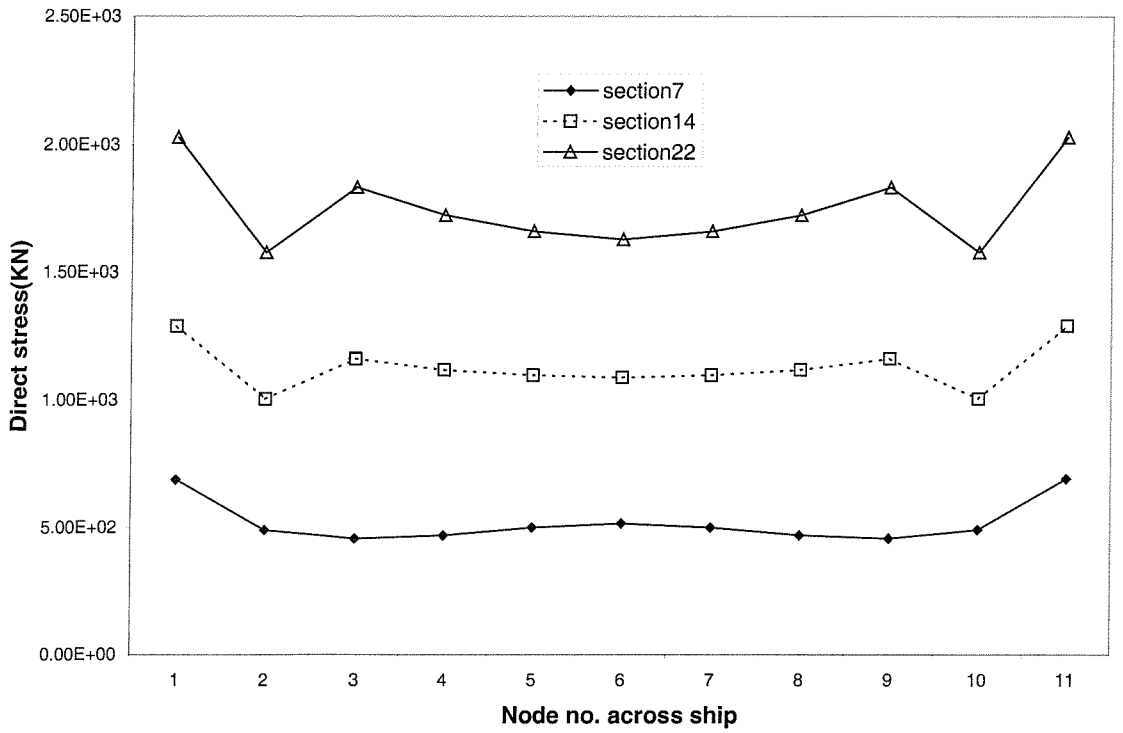

Fig. 5.43 Demonstration of the effects of shear lagging of **closed** ship across (a) deck (centre line at node 4); (b) bottom (centre line at node 6); modal comparisons based on the 2 node vertical bending mode.

(a)

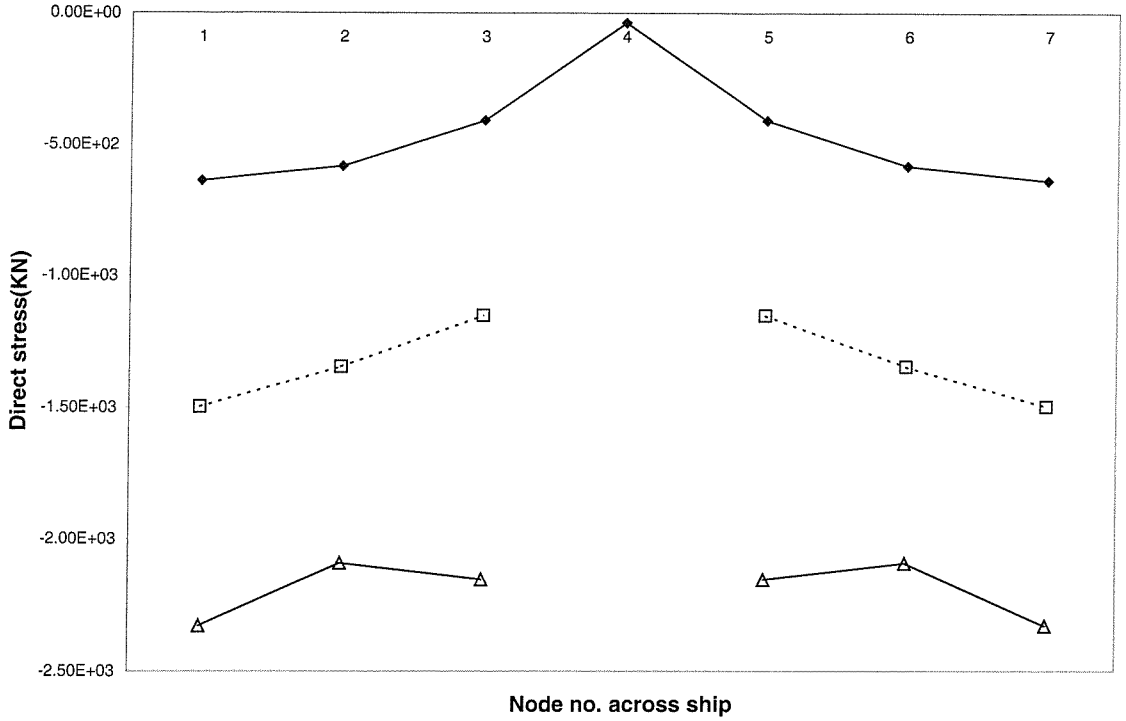

(b)

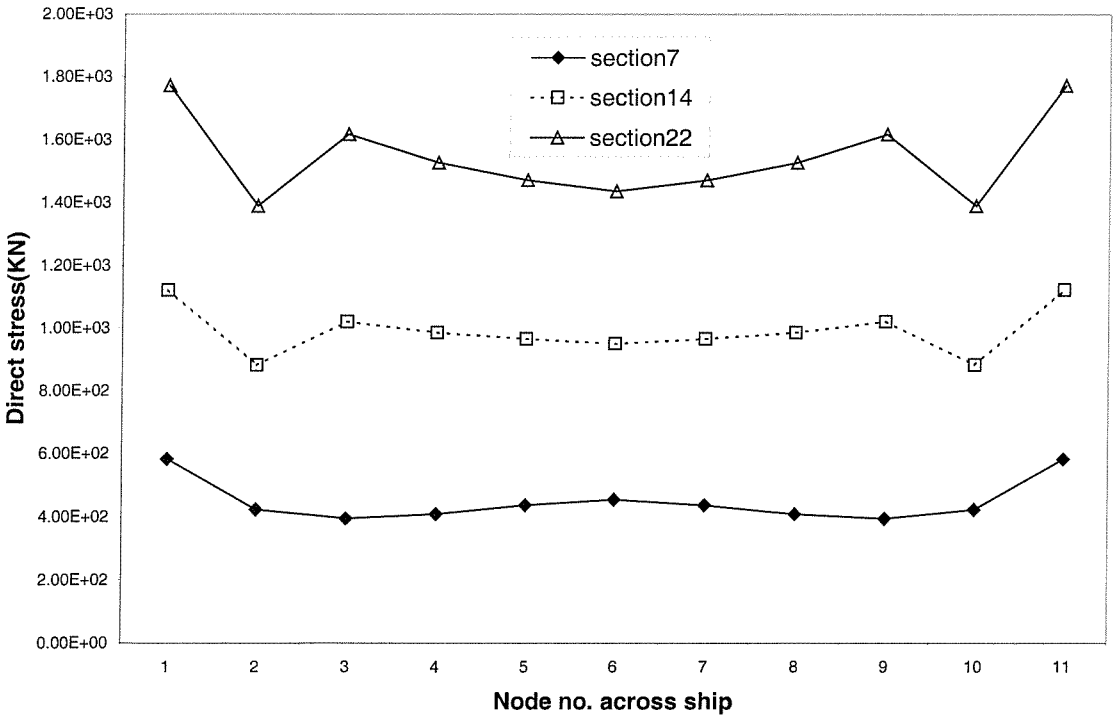

Fig. 5.44 Demonstration of the effects of modal shear lagging of **open** ship across (a) deck (centre line at node 4); (b) bottom (centre line at node 6); modal comparisons based on 2 the node vertical bending mode.

5.10 Conclusions

This chapter focused on the application of the dry analysis module of two- and three-dimensional hydroelasticity theories. The functionality and effects of beam and shell finite idealisations to different levels of ship structural design have been firmly assessed. Particular emphasis was paid upon the in vacuo dynamic behaviour of a bulker structure having similar structural and mass properties to OBO MV Derbyshire. The effects of structural modelling refinement on dry hull natural frequencies and modal characteristics were investigated using two-and three-dimensional beam as well as three-dimensional shell idealisations. From the discussion outlined was shown that the amount of detail incorporated into the structural model could be selected to correspond to various stages of the design process, such as concept and preliminary design. Beam formulations are sufficiently adequate for a preliminary analysis of the dynamic characteristics of a hull form. Shell idealisations are more realistic but time consuming and therefore may be used in the more detailed design stage.

Good overall agreement was obtained between the in vacuo dynamic characteristics (natural frequencies, mode shapes, generalised masses and bending moments) calculated by all models (beamfd,beamfde,beam2d,beam3d,shell3d) for the bulker's symmetric distortions. Some small differences in the eigenvectors predicted from the shell finite element idealisation (shell3d) are becoming evident with increasing modal complexity. Those could be attributed to the ability of this model to simulate realistically the architectural details of the structure (e.g. double bottom).

In antisymmetric plane of vibration the incorporation of the effects of warping in the beam model are important in order to simulate adequately the in vacuo structural dynamics of the ship. Since ANSYS 5.4 software beam finite elements do not account for this only the finite difference beam idealisations beamfd and beamfde were employed and compared against the three dimensional shell model (shell3d). Reasonably good agreement was achieved between the natural frequencies, eigenvalues and generalised masses of all models. However, the predicted modal loads (torsional moments, horizontal bending moments and shear forces) of the beam simulations appear to overestimate those of the shell model. It is thought that this discrepancy could be attributed to the lack of ability of the finite difference scheme to account

for the non-prismatic features of the hull girder whilst accounting for the effects of warping. Although the slenderness ratio of the hull in the antisymmetric plane of vibration is relatively low (L/B=6.7) it should not be considered as a factor affecting the dynamic load deviations between beam and shell idealisations.

Further comparisons between the shell and beam finite element structural models corresponding to two 'artificial' ship models having identical mass distribution to that of the bulker but closed and open decks respectively further validated the bulkers' modal analysis conclusions and the suitability of the overall modelling procedure. Irrespective of the type of idealisation excellent modal agreement was achieved for both closed and open deck ship structures for symmetric distortions. However, whereas for the case of the open-deck vessel significant deviations arise from the predictions of beam and shell models in antisymmetric plane (as in the case of the bulk carrier), a long slender monohull having closed-decks remains 'uncoupled' from torsion since experiences no global structural discontinuities and therefore provides excellent agreement between beam and shell idealisations.

Alternative types of beam idealisations comprising of beams having the same structural and mass properties but being equally (beamfde, beam2de) or unequally discretised (beamfd, beam2d) were compared. It was shown that the methodology of discretisation is not critical for most of the modal characteristics of the ship (i.e. deflections, generalised masses and modal bending moments predicted by beamfd and beamfde models almost agree). Thus, an equally spaced discretisation could be used in the two-dimensional hydroelasticity analysis.

The effects of refinement on the modal characteristics of the finite difference and finite element beam idealisations used were explored in order to validate the choice of 46 sections for the discretisation of the structure. Experience with uniform lightweight barge models has shown that the three-dimensional shell finite element idealisation models sufficiently the dynamics of the structure. For symmetric distortions all beam models (beamfd, beam2d, beam3d) converge well within the allowable numerical error estimates. The finite element beam idealisations have opposite but more rapid convergence trends (i.e. natural frequencies are decreasing with increasing number of elements) in comparison to the finite difference

scheme. In antisymmetric motion the finite difference scheme (beamfd) does not appear to be numerically stable. Experience with uniform beam models incorporating some non prismatic effects (openings) has shown that the numerical instability of beamfd idealisation could be attributed to the violation of compatibility conditions at the locations where structural discontinuities occur.

The effects of modal shear lag were studied for the bulker, closed and open ship configurations (shell3d, shell3dop, shell3dcl) based on the direct longitudinal stresses extracted from first symmetric mode of vibration. It was shown that these effects are (i) much more important at deck openings and just a few percent for the closed ship type structure, (ii) increased amidships and reduced comparatively at the extremities of the hull (iii) maximum shear lagging magnitudes always appear across the deck of the structure.

Following these conclusive remarks in next chapter the steady state hydroelastic behaviour in regular waves of a bulker having similar properties to those of OBO MV Derbyshire is presented by means of two- and three-dimensional flexible fluid-structure interaction models.

5.11 References

[5.1] Hirdaris, S.E., W.G. Price, W.G., & Temarel, P.: Hydroelastic analysis of a bulk carrier (keynote lecture), 13th International Conference on Ship and Shipping Research (NAV00), Hydroelasticity and applications, 1:5.6.1-5.6.12, Venice, Italy, (2000).

[5.2] Hirdaris, S.E., Price, W.G. and Temarel, P.: Symmetric and antisymmetric hydroelastic analysis of a bulker in waves, 8th International Symposium for Practical Design of Ships and other Floating Structures (PRADS01), Structures and Materials-Hydroelasticity, 2:903-910, Shanghai, China, (2001).

[5.3] Bishop, R.E.D. and Price, W.G.: Hydroelasticity of Ships, Cambridge University Press, UK, (1979).

[5.4] Gunnlaugsson, A.G. and Pedersen, P.T.: A finite element formulation for beams with thin walled cross-sections, Computers and Structures, 15:691-699, (1982).

[5.5] Pedersen, P.T.: A beam model for the torsional-bending response of ship hulls; Trans. RINA, 119:171-182, (1983).

[5.6] Pedersen, P.T.: Torsional response of containerships; Journal of Ship Research, 29:194-20, (1985).

[5.7] Pedersen, P.T.: Beam theories for torsional response of ship hulls; Journal of Ship Research, 35:254-265, (1991).

[5.8] Swanson Ltd.: The ANSYS 5.6 users manual, (2000).

[5.9] Hughes, O.F., Ship structural design – A rationally based, Computer aided optimisation approach; The society of Naval Architects and Marine Engineers (SNAME), (1983).

[5.10] Chalmers, D.W.: Design of surface ship structures, Ministry of Defence, England, UK, (1989).

[5.11] Price, W.G., Salas Inzunza, M.A. and Temarel, P.: The dynamic behaviour of a mono-hull in oblique waves using two- and three-dimensional fluid-structure interaction models, Submitted to Trans. RINA, (2000).

Chapter 6

Wet Analyses

6.1 Introduction

In this chapter the calculations related to the symmetric and antisymmetric hydroelastic behaviour of a bulker having similar properties to those of OBO MV Derbyshire are presented by means of two- and three-dimensional flexible fluid-structure interaction (FSI) models. Steady state frequency domain hydroelastic analysis in head, bow quartering and beam waves is performed at the typical bulk carrier speed of 7.463m/s. A set of 8 flexible mode shapes is incorporated in the modelling procedure, in addition to rigid body motions, and the resonance frequencies of the wet hull are identified via examining the variation of the corresponding principal coordinate amplitudes with encounter frequency. Consequently, the effects upon resonant frequencies, dynamic response amplitudes (i.e. principal coordinates) and wave induced dynamic loads of all different fluid-structure interaction models for alternative speeds and headings are highlighted in an attempt to investigate the bulker's strength under alternative operational conditions. A sensitivity analysis is also carried out to assess the influences of damping coefficients and different structural configurations. The latter is achieved by comparing the symmetric and antisymmetric wave induced dynamic response of the bulk carrier against those of open- and a closed-deck vessels along the lines of the dry analyses (see chapter 5). From the investigation it is shown that although the predictions of all alternative fluid-structure interaction models are in good agreement for symmetric motion, for long slender monohulls with large deck openings the antisymmetric dynamic loads predicted by the beam models overestimate those of the shell idealisations. It is thought that these discrepancies are related to the inadequacies of beam models to simulate realistically the highly non-prismatic character of the hull girder, whilst allowing for the effects of warping.

6.2 Summary of wet analyses methodologies

As was explained in chapters 2 and 3 in both two- and three-dimensional unified hydroelasticity theories the analysis is divided into two parts namely wet and dry (see sections 2.6,3.4 and 3.5). In two-dimensional hydroelasticity the vessel is treated as a non-uniform Timoshenko beam, for the dry analysis, and the fluid actions, for the wet analysis, are modelled using a modified strip theory approximation [6.1,6.2] (see section 3.4). Alternatively the generalised three-dimensional hydroelasticity theory relies on a more complex theoretical model able to describe the dynamics of a flexible body of arbitrary shape (e.g. monohull or multihull vessel) travelling in a seaway. Briefly, a finite element discretisation approach (comprising of three-dimensional beams or shell elements) is used to describe the in vacuo, undamped dynamic behaviour of the three-dimensional structure (see section 4.2.8 and chapter 5). The fluid actions associated with the three-dimensional structure (moving with forward speed and undergoing rigid body motions and distortions) are determined from a suitable singularity distribution (e.g. pulsating sources) over the mean wetted surface of the hull (see section 3.5).

Along these lines, for the current investigation the following flexible fluid-structure interaction models, incorporating both symmetric and antisymmetric motions and distortions, are used (see table 6.1):

- **beamfde,** where an in vacuo Timoshenko beam idealisation (including the effects of warping), discretising the ship by 46 sections of equal length, is combined with the modified Salvesen et al strip theory to calculate the hydrodynamic properties of the hull comprising of 'Lewis form' sections swaying, heaving and rolling harmonically at the encounter frequency of the free surface [6.1,6.2]. For this part of the analysis there was no reluctance in employing an equal spacing finite difference disctretisation scheme, since modal analyses have justified that when this idealisation is compared with unequally spaced finite element or difference beam models (beamfd, beam2d, beam3d) it simulates realistically the modal characteristics of the hull (see sections 5.3,5.4).
- **beam3d*** where 952 four-cornered hydropanels, with pulsating sources located at each of their centers, are used to idealise the mean wetted surface of the hull (see figure 6.1). For the symmetric analysis the modal characteristics (natural frequencies, mode shapes, generalised masses) of beam3d dry hull idealisation were employed. The simulation of antisymmetric

effects raises an interesting point of discussion since the ANSYS BEAM4 formulation does not include the effects of warping which are rather important in the antisymmetric plane of vibration (see section 4.2.9). The in vacuo dynamic analysis, however, has shown that the modal characteristics of the finite difference beam (beamfde) and shell idealisations are comparable for the antisymmetric modes. Hence, the behaviour of the finite difference model was assumed to describe adequately that of a finite element idealisation incorporating the effects of warping and it was therefore used as a substitute for the antisymmetric potential flow analysis (see sections 5.3,5.4).

- **shell3d** where a three-dimensional shell finite element idealisation is used in conjunction with a pulsating source distribution over the wetted surface of the hull. As in the case of beam3d model for convenience 952 hydropanels were used with a pulsating source located at their center to idealise the mean wetted surface of the hull (see figure 6.1). However, the in vacuo symmetric and antisymmetric modal characteristics (natural frequencies, mode shapes, generalised masses) of the three-dimensional finite element model (shell3d) were employed in this analysis (see sections 5.3,5.4).

For three-dimensional simulations although wetted surface idealisations with different number of panels were not investigated, the number of panels used is thought to provide a good degree of accuracy based on past experience [6.3]

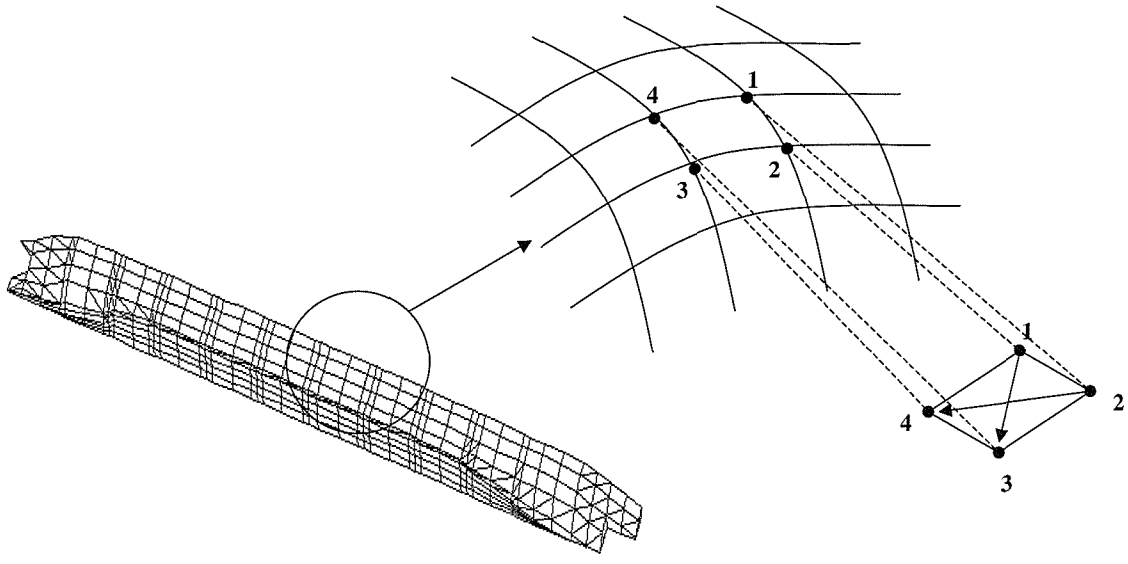

Fig.6.1 Idealisation of the mean wetted surface of OBO MV Derbyshire (952 hydropanels).

MODEL	DRY ANALYSIS		WET ANALYSIS
	Symmetric	*Antisymmetric*	*Symmetric & Antisymmetric*
beamfde	Timoshenko beam (equal spacing)	Timoshenko beam (equal spacing)	Strip theory
beam3d*	FEA beam model (equal spacing)	FEA beam model (unequal spacing)	Pulsating source at panel centres
shell3d	FEA shell model	FEA shell model	Pulsating source at panel centres

Table 6.1 Two- and three- dimensional hydroelasticity analyses.

6.3 Two-dimensional hydroelasticity - Computations

Within the context of linearity, two-dimensional hydroelasticity theory is implemented separately for symmetric and antisymmetric motion (see section 3.4.1). Programme UCLMARS computes the generalised steady state symmetric response of ships in regular waves. At first instance the code evaluates the modal properties (natural frequencies, mode shapes, modal shear forces and bending moments) of an equally spaced Timoshenko beam-like hull by means of the finite difference method. At the second stage, strip theory is used to evaluate the still water distortions, shear forces and bending moments of the vessel for a number of headings and speeds. The two-dimensional hydrodynamic properties for sections heaving in the presence of free surface can be evaluated for a Lewis hull form along with multipole expansion techniques and subsequently the generalised steady state response to regular wave excitation of arbitrary heading is provided [6.1]. If required, the response amplitude operators, bending moments, shear forces and the statistics of the response in regular waves or in irregular seas may be carried out by means of code IRREGULAR. The software performs these computations via modal summation of generalised steady state responses (i.e. principal coordinates) calculated by UCLMARS.

Antisymmetric fluid-structure interaction is carried out in three stages. Programme UCLMOD calculates the natural frequencies and modal characteristics of a non-uniform Timoshenko beam vibrating in vacuo in the absence of structural damping and external force effects (see chapter 5). The finite difference method is used for the discretisation of the hull, which may be divided into an equal or unequal number of sections (see sections 4.2.5, 5.2). As it was outlined in chapters 3 and 4 the software is capable of performing antisymmetric modal analysis (uncoupled lateral bending, uncoupled twisting, coupled lateral bending and twisting) and even

symmetric (uncoupled bending) modal analysis of a dry hull. However, from the hydroelasticity perspective it is used only for the evaluation of antisymmetric hydroelastic responses. Programme UCLATDH calculates the two-dimensional hydrodynamic properties of sections swaying and rolling in the presence of free surface of a fluid using Lewis (or multiparameter, if required) conformal transformation and multipole expansion techniques [6.1]. The calculations are carried out for a range of frequencies characterised by a non-dimensional frequency parameter related to either the beam or draft of the section. The resultant non-dimensionalised hydrodynamic properties (sway added mass and damping, roll added inertia and damping, cross coupled sway/roll added mass and damping) are used as input properties for a strip theory based hydroelastic analysis (see section 3.4.2). At the final stage programme UCLMARA calculates the coupled antisymmetric responses of a flexible ship, which proceeds with a forward speed in oblique sinusoidal waves of given amplitude and arbitrary heading. Distributions of the response amplitudes such as lateral bending displacement, bending moment, lateral shear force and twisting moments along the hull can be obtained.

6.4 Thee-dimensional hydroelasticity – Computations

The three-dimensional hydroelasticity suite also comprises of three individual modules namely P13FLXBD, FLXBD and HYCOF. The first module is a preprocessor generating almost all the data required for programmes FLXBD and HYCOF. It could be applicable to most types of monohull (tanker, bulker, containership etc) or multihull (e.g. trimaran, catamaran) vessels. In its present form the software is capable to process an ANSYS output file but it can be easily modified to read corresponding modal analysis output from other finite element packages such as NASTRAN and ABAQUS. It is assumed that the vessel is port starboard symmetric. In this software the coordinate defined by the user for the dry hull analysis using ANSYS is transformed to a coordinate system Sxyz whose origin is located at the stern of the vessel on the calm water surface. Coordinates of nodes and principal mode shapes are transformed to this system. At the second stage, scanning takes place to identify the elements, which are wholly or partly submerged by using five different artificial 'eyes' located outside to alternative parts of the hull. Although the hydrodynamic panels related to any surface piercing elements are defined based on linear interpolation along the surface piercing edges for the purposes of the current investigation this was not critical as the mean waterline coincides with the nodal lines of the

finite element model shell3d. Quadrilateral panels linked to triangular finite elements have their fourth corner node located as dummy mid-side node along any edge of the triangle. The corresponding degrees of freedom have been obtained by means of linear interpolation between displacements given at the end nodes. This makes such an idealisation of the wetted surface systematic and straightforward procedure.

Programme FLXBD calculates the normal velocity on the wetted surface of a flexible body and the relevant functions needed for evaluating the generalised wave exciting forces and hydrodynamic coefficients. In this sense it acts as a preprocessor to the unified three-dimensional hydroelasticity analysis, performed by HYCOF, in regular waves. The software is capable of calculating the normal velocity of the wetted surface according to two types of structural elements namely a beam-like element or a four nodded quadrilateral shell element. Although P13FLXBD does not act as a preprocessor for beam-like discretisations no panel mapping procedure is considered for such a case and therefore the corresponding FLXBD file can be easily transformed via extracting the corresponding modal properties of the finite element beam modal analysis. A series of ANSYS macro commands can be written for such a purpose, taking advantage of the APDL (Ansys Parametric Design Language). The useful information output by FLXBD concerns panel geometry data, normal displacement and its associated derivatives at panel centers for each principal mode shape, boundary conditions on the radiation potentials and restoring coefficients. Hydrostatic properties are also calculated, based on the input hydrodynamic panels and they were compared with design data so as to check the accuracy of the wet mesh.

The final module of the hydroelastic suite, HYCOF, performs the actual calculation of the potential flow surrounding the flexible body and, in turn, of the radiation, diffraction and wave exciting actions. Operational conditions permitted by the analysis are such that the body moves through regular waves, at an arbitrarily prescribed constant forward speed and heading and in infinitely deep water. Apart from those produced by P13FLXBD additional input data for HYCOF consists of operational parameters (e.g. speed, heading) and structural damping coefficients.

6.5 Unified hydroelasticity analyses in regular head waves

In order to perform an initial comparison between the three described models (beamfd, beam3d* and shell3d), a single condition was selected, corresponding to head waves ($\chi = 180^{O}$) of unit wavelength to ship length amplitude ($L/\lambda=1$) at the typical bulk carrier service speed ($\overline{U}$) of 7.463 m/s (Fn=0.138). For this case antisymmetric motions and distortions are disregarded since no corresponding excitation takes place. Consequently, four symmetric vertical distortions were included in the analysis.

At first instance, the rigid body motions (Response Amplitude Operators – R.A.O.'s) for heave and pitch as well as the diagonal terms of the corresponding hydrodynamic effects (added mass (A_{rr}) and damping (B_{rr}) coefficients) were computed and compared for all three models (see figure 6.2). The following non-dimensionalisation was used:

$$A_{rr}' = \frac{A_{rr}}{\rho \nabla L^2} \tag{6.1}$$

$$B_{rr}' = \frac{B_{rr}\sqrt{L/g}}{\rho \nabla L^2} \tag{6.2}$$

where (ρ) denotes the sea water density; (∇) represents the displacement volume of the ship; (a) the wave amplitude; (L) for convenience is defined as the unit longitude, i.e. L=1m; (g) represents the gravity constant (=9.81m/s^2). As the encounter frequency tends to zero, numerically predicted amplitudes of symmetric heave (P_3) and pitch (P_5) behave as expected, i.e. the former tends to 1.0 whereas the later to 0.0. They both experience a major peak around 0.528rad/s and a secondary peak value at about 3.37 rad/s, which proves their coupling with the first symmetric flexible mode. However, for pitch the strip theory (beamfde) principal coordinate amplitudes overestimate those produced from the pulsating source approaches (beam3d*, shell3d). From graphs 6.2(b) and (c) it also becomes apparent that the rigid body added mass (A_{33}, A_{55}) and fluid damping (B_{33}, B_{55}) coefficients are the same for both three-dimensional models (shell3d and beam3d) but behave slightly differently when the strip theory approach is employed. The differences between strip theory and three-dimensional potential flow analysis predictions appear due to the fact that by contrast to strip theory both pulsating source idealisations (beam3d* and shell3d) use the same wet surface description (952

hydropanels) (see figure 6.1). The variation of hydrodynamic added inertia (A_{rr}) and damping (B_{rr}) coefficients with encounter frequency, for symmetric (r=7,10,13,14) modes was also studied. Trends for the diagonal added mass coefficients are similar to those described for rigid body motions, i.e. the added masses of all three models are in good agreement and generally display asymptotic trends (see figure 6.3). Hydrodynamic damping on the other hand starts from zero value (at zero encounter frequency) and then increases to a large peak before tending asymptotically towards zero (see figure 6.4). Some differences appear between the flexible damping coefficients predicted by the strip theory (beamfde) and potential flow analyses models (beam3d*, shell3d) especially for the higher modes of flexible distortions (see figure 6.4). Most probably these could be attributed to the different hydrodynamic methods employed to solve the problem.

Very little is known about structural damping and its reliable estimation should rely heavily on experimentation. In this case typical damping factors (ν_r) as provided by Bishop and Price [6.1] for long slender monohulls in loaded conditions were used (see table 6.4). The generalised damping matrix (b_{rr}) of the dry structure for the flexible modes is calculated as:

$$b_{rr} = 2\nu_r\omega_r a_{rr} \tag{6.3}$$

where ω_r and a_{rr} are the natural frequency and generalised mass and ν_r is the modal damping factor. The dry hull natural frequencies as well as the corresponding wet resonances obtained from both beam (beamfd, beam3d) as well as the plate (shell3d) models are presented in table 6.1 (see also figure 6.6). From the subsequent analysis it becomes evident that the ratio of the wet resonance to natural frequency aspect ratio (ω_{er}/ω_r) is increasing progressively for higher modes of flexible responses (see table 6.3). Figures 6.5 and 6.6 show the principal coordinate amplitudes (frequency response functions) and their comparisons for all models, for the first four symmetric distortions. Maximum principal coordinate magnitude is obtained for the first symmetric mode (2 node vertical bending). The symmetric principal coordinate amplitudes predicted by all models are comparable in relatively long waves. The difference of resonance encounters could be attributed to the different methods employed (between beamfde and beam3d* and shell3d) and to the differences in the mode shapes, which are increasing for higher eigenvectors (see section 5.2). In addition one should recall that beamfd idealisation performs strip theory analysis for equal section lengths. The generalised masses and in extent

the generalised stiffness of the vessel are affected by such type of discretisation (see section 5.2 and table 6.3).

(a)

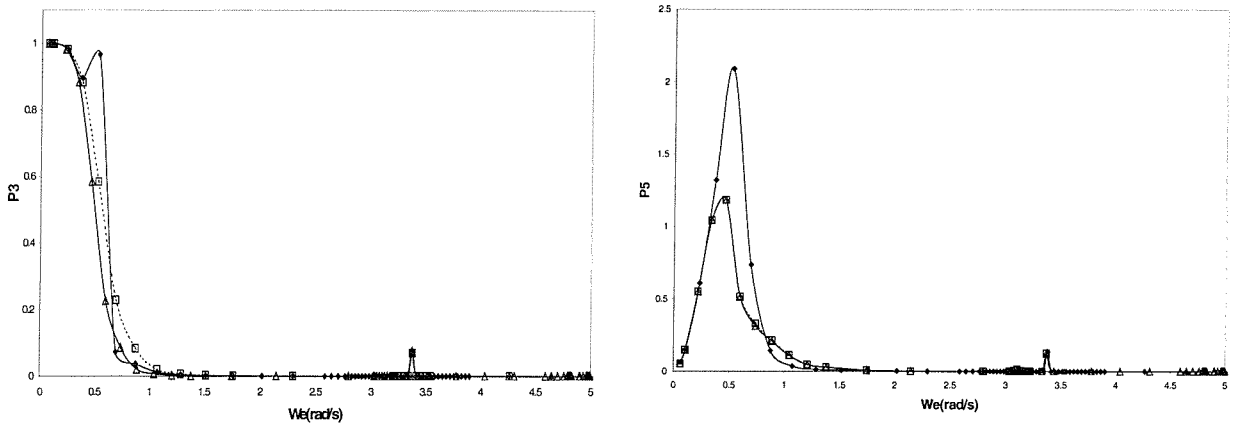

(b)

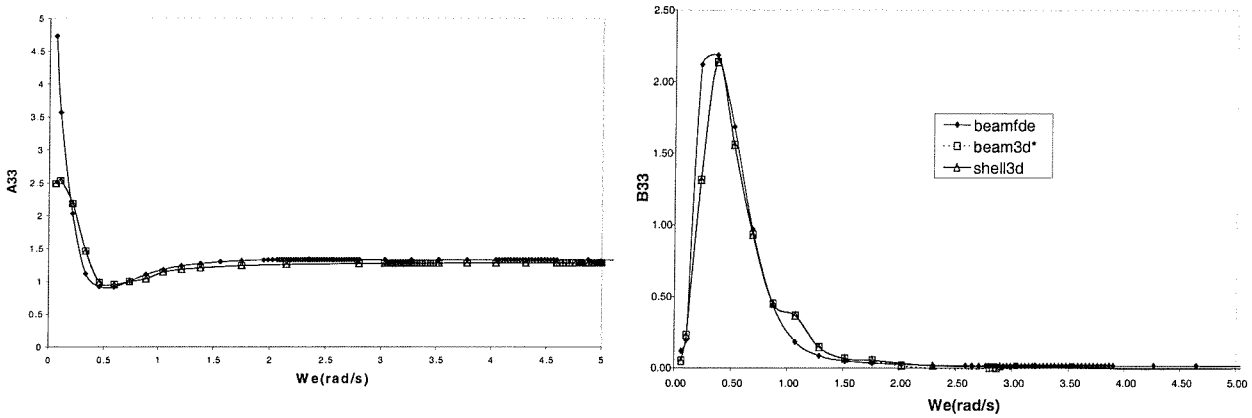

(c)

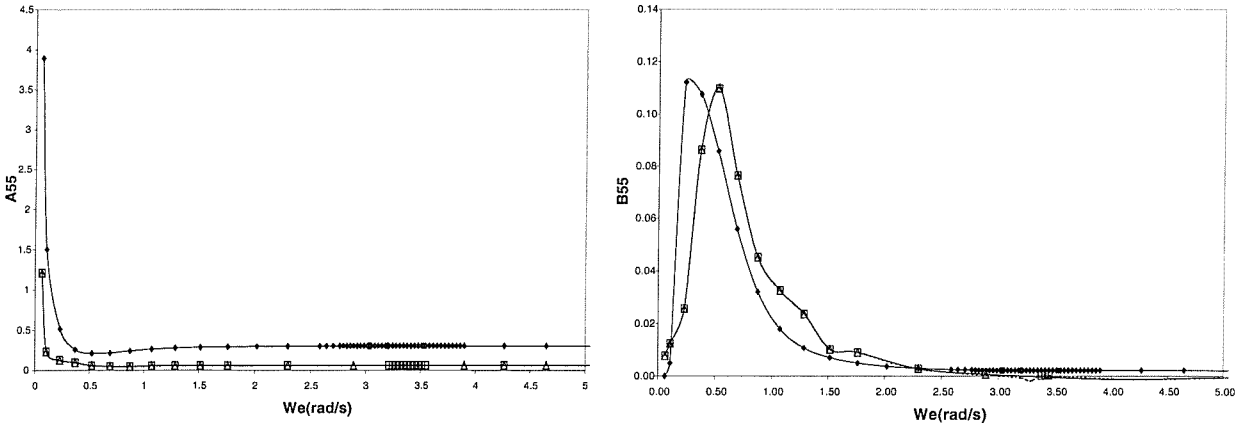

Fig. 6.2 Comparison between R.A.O's and hydrodynamic coefficients at head regular waves conditions for all alternative models (beamfde, beam3d*, shell3d); ($\overline{U}$ = 7.463m/s); (a) heave (P3) and pitch (P5) R.A.O's; (b) added mass and hydrodynamic damping for heave; (c) added mass and hydrodynamic damping for pitch.

Mode type	beamfde		beam3d*		shell3d	
	Dry (ω_r)	Wet (ω_{er})	Dry (ω_r)	Wet (ω_{er})	Dry (ω_r)	Wet (ω_{er})
2 node VB (r=2)	4.42	3.03	4.50	3.11	4.53	3.25
3 node VB (r=3)	9.25	6.33	9.07	6.29	9.01	6.62
4 node VB (r=4)	14.24	9.90	13.74	9.72	13.24	10.20
5 node VB (r=5)	17.62	12.95	17.11	12.65	15.92	12.61

Table 6.2 Dry natural frequencies and wet resonances for symmetric distortions in head sea conditions ($\overline{U}$ = 7.463m/s; VB = vertical bending; r = modal index; ω_r = dry natural frequencies; ω_{er} = wet resonances).

Mode type	beamfde		beam3d*		shell3d	
	ω_{er}/ω_r	GM (tonne-m^2)	ω_{er}/ω_r	GM (tonne-m^2)	ω_{er}/ω_r	GM (tonne-m^2)
2 node VB (r=2)	0.685	24834	0.691	19761	0.717	19364
3 node VB (r=3)	0.685	11082	0.693	8799	0.734	8922
4 node VB (r=4)	0.695	4492	0.707	4778	0.770	6577
5 node VB (r=5)	0.734	3940	0.739	5072	0.792	10036

Table 6.3 Ratio of the wet resonance to natural frequency aspect ratio (ω_{er}/ω_r) for all idealisations (r= modal index; $\overline{U}$ = 7.463m/s; GM = generalised mass; VB = vertical bending; ω_r = dry natural frequencies; ω_{er} = wet resonances).

Symmetric motion	Damping factors	Antisymmetric bending	Damping factors
2 node VB	0.002	1 node HB - 1 node **T**	0.01
3 node VB	0.005	2 node **HB** – 2 node T	0.012
4 node VB	0.008	2 node HB – 2 node **T**	0.015
5 node VB	0.010	3 node **HB** – 3 node T	0.019

Table 6.4 Structural damping factors for a long slender monohull in loaded conditions (VB = vertical bending, HB = horizontal bending; **HB** = HB dominant; T = torsion; **T** = torsion dominant).

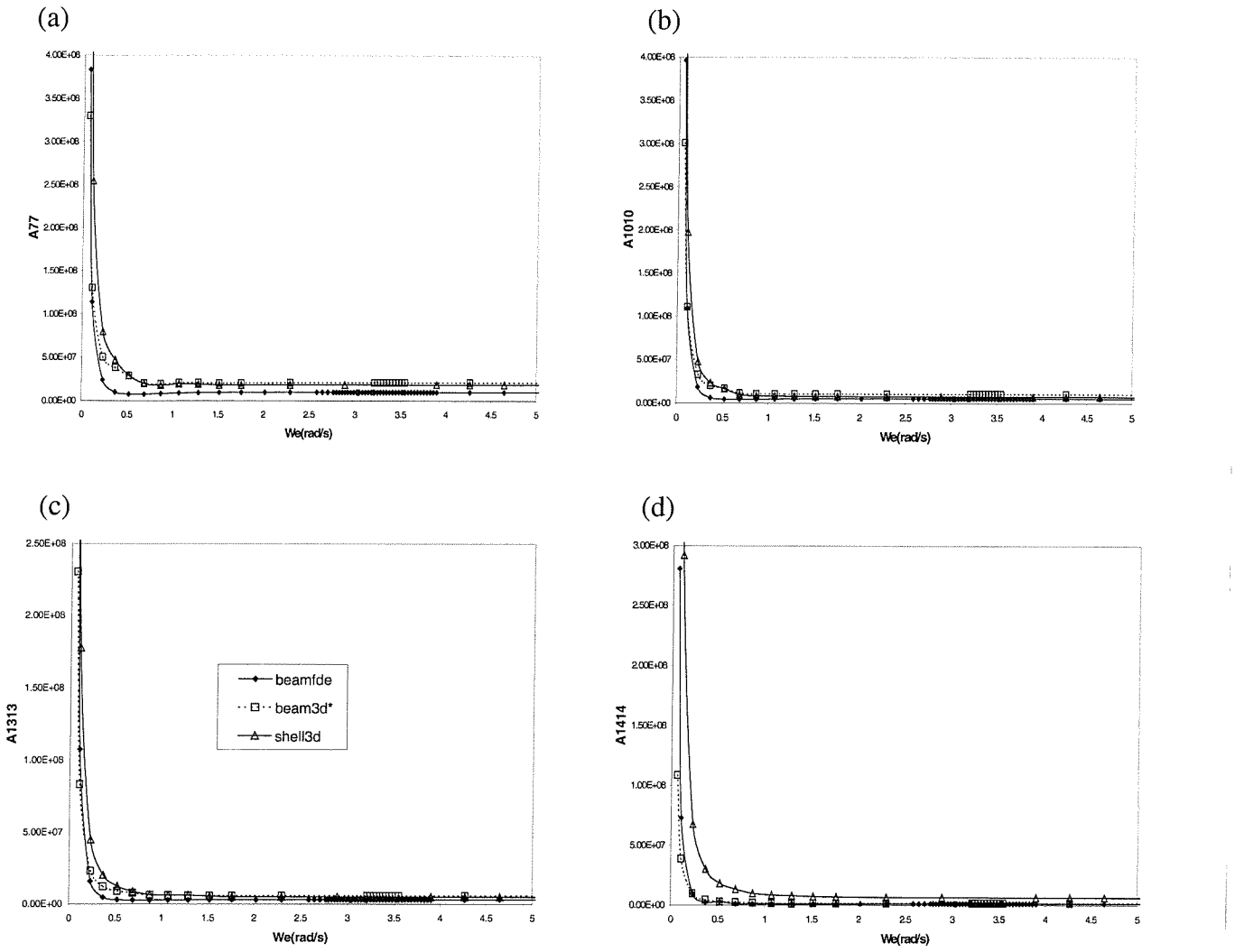

Fig. 6.3 Comparison of hydrodynamic added mass (A_{rr}) coefficients (kgm^2) for symmetric flexible modes of all models (beamfde, beam3d*, shell3d) for head regular waves conditions ($\overline{U}$ = 7.463m/s); (a) 2 node VB; (b) 3 node VB; (c) 4 node VB; (d) 5 node VB (VB: vertical bending).

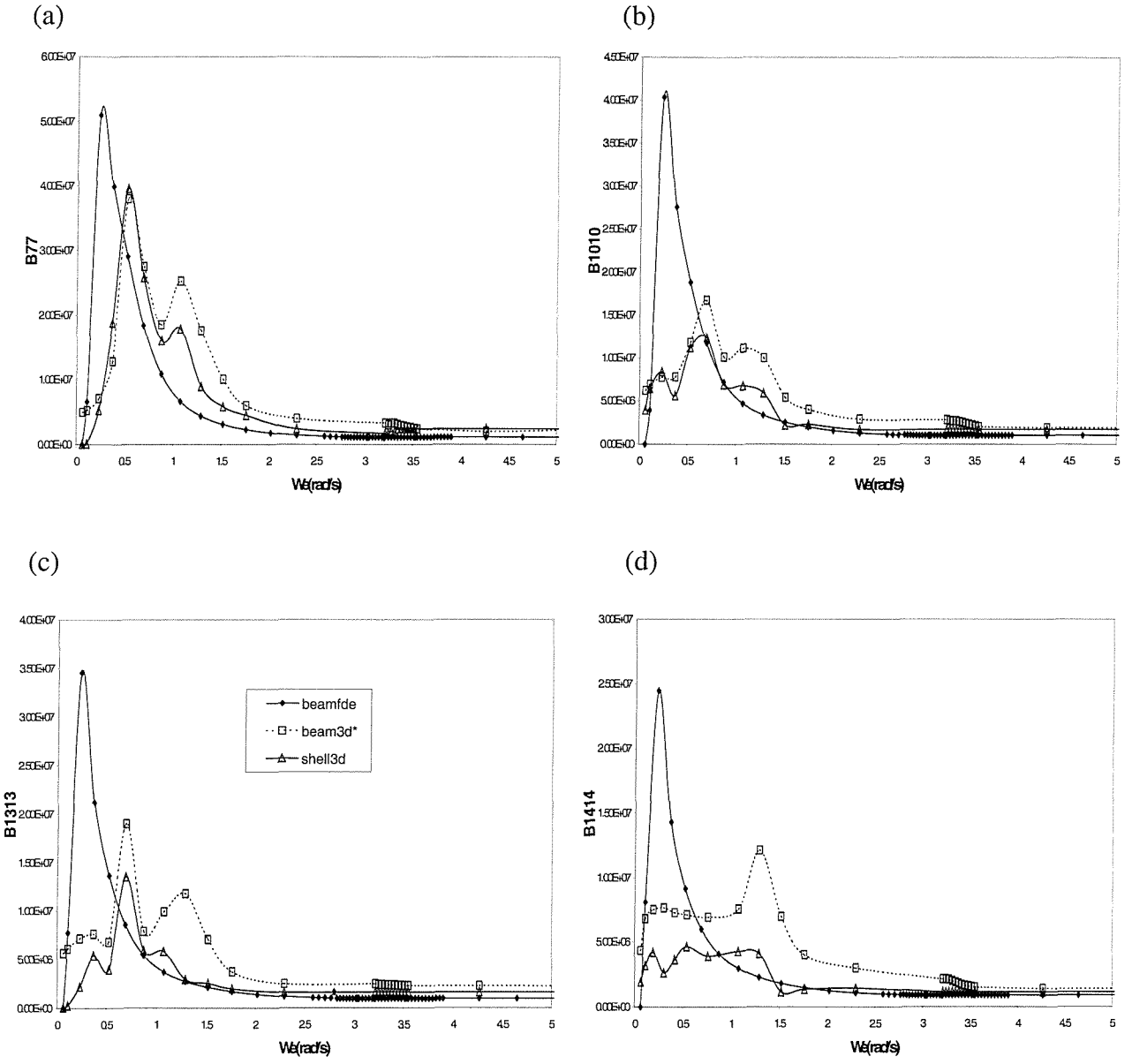

Fig. 6.4 Comparison of hydrodynamic damping (B_{rr}) coefficients (kgm/s) for symmetric flexible modes of all models (beamfd, beam3d, shell3d) for head regular waves conditions ($\overline{U}$ = 7.463m/s); (a) 2 node VB; (b) 3 node VB; (c) 4 node VB; (d) 5 node VB (VB: vertical bending).

(a)

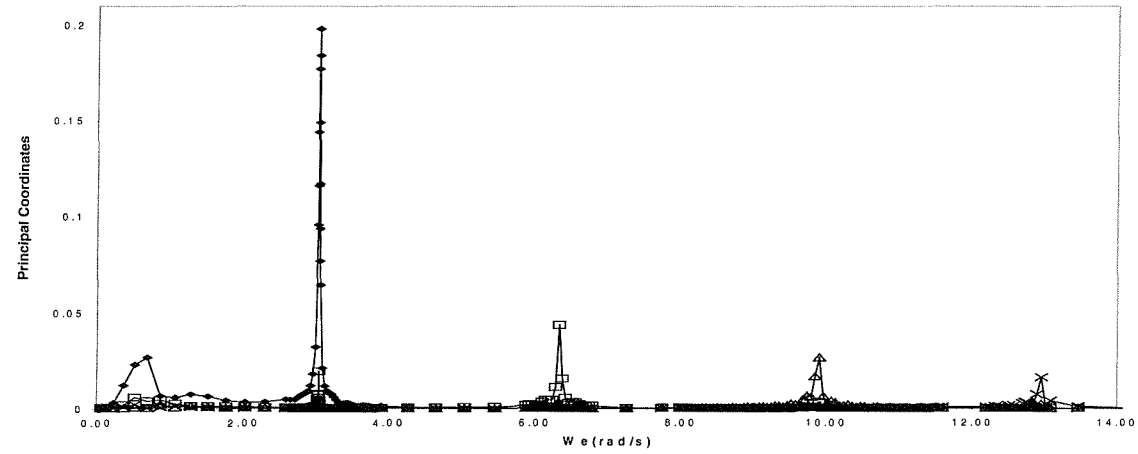

(b)

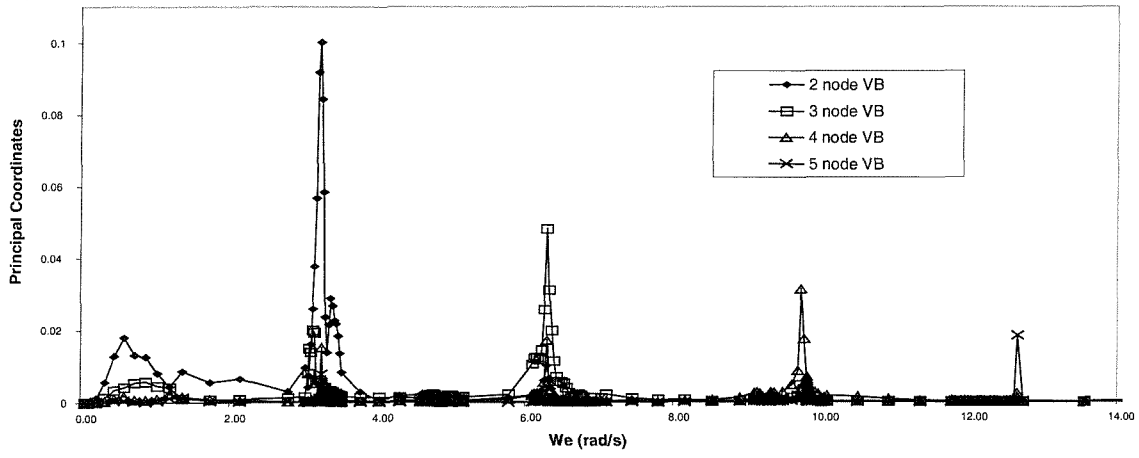

(c)

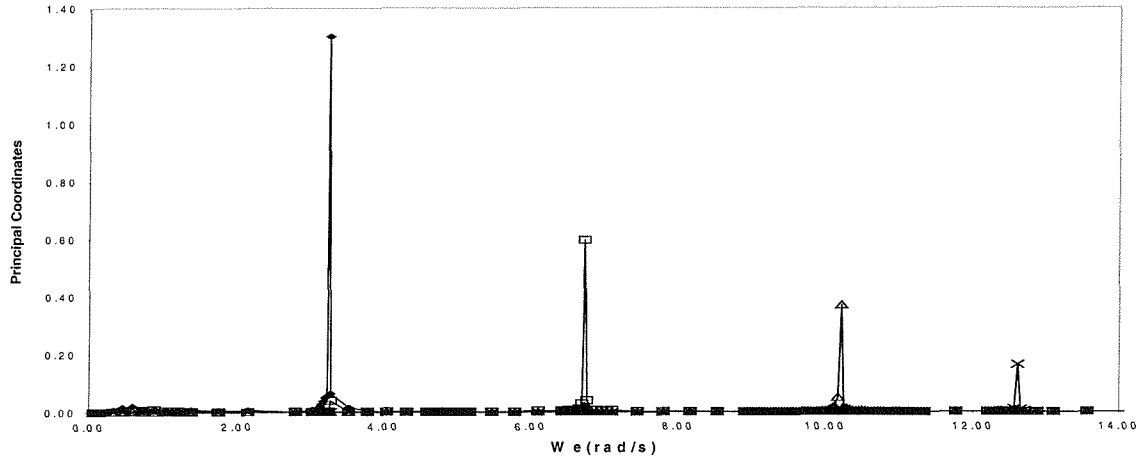

Fig. 6.5 Principal coordinate amplitudes of all models in head regular waves ($\overline{U}$ = 7.463m/s); (a) beamfde; (b) beam3d*; (c) shell3d.

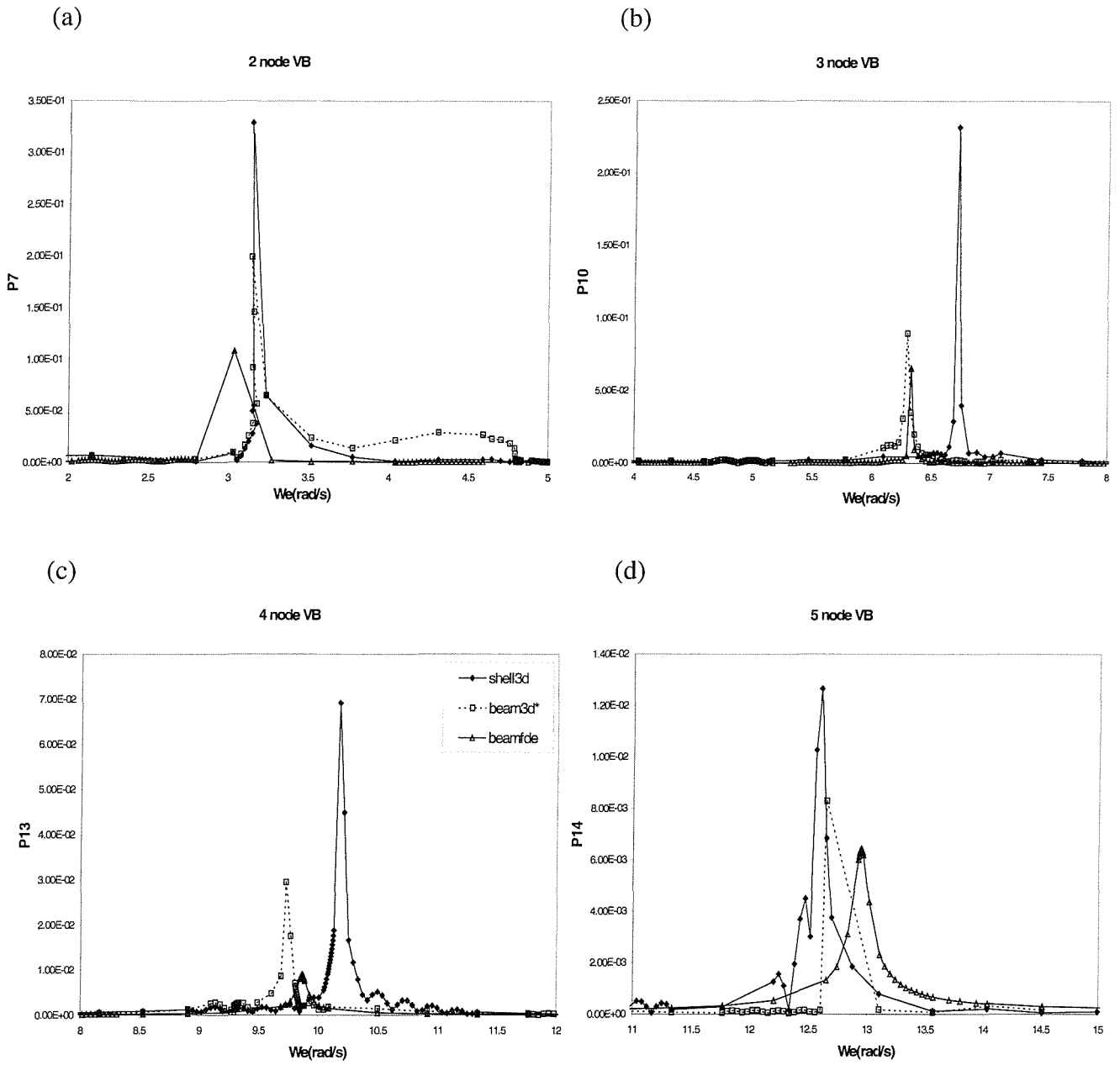

Fig.6.6 Comparison of principal coordinate amplitudes of all models in head regular wave conditions ($\overline{U}$ = 7.463m/s) for; (a) 2 node Vertical bending; (b) 3 node Vertical bending; (c) 4 node Vertical bending; (d) 5 node Vertical bending.

6.6 Steady state vertical bending moments and direct stresses in head waves

As it was demonstrated in chapter 3 (see section 3.4), the wave induced vertical bending moment and shear force at any cross section along the structure can be expressed as a modal summation of the dry flexible bending moments or shear forces of each mode depending on the magnitude of the corresponding principal coordinate, by means of Rayleigh's superposition

method [6.1]. In addition, the direct stresses can also be calculated for the shell model for, say, unit shiplength to wavelength ratio ($L/\lambda=1$). For beam idealisations the evaluation of direct stress components can be obtained at the top or bottom of the ship's structure by dividing the vertical bending moment (VBM) with the corresponding deck (S_{deck}) or keel (S_{keel}) section modulus (see section 3.6). Comparisons of the symmetric steady state wave induced dynamic loads (bending moments and shear forces) proved to be quite interesting. Maximum vertical bending moments are predicted by model beam3d* followed closely by the shell idealisation (see figure 6.7(a)). On the other hand, maximum shear forces given by shell3d model are followed at amidships closely by those of beam3d* model (see figure 6.7 (b)). The dynamic loads predicted by the strip theory idealisation (beamfde) were of slightly lower magnitudes reflecting in this way the behaviour of the principal coordinates (see table 6.5). This is also supported by the fact that although in the dry analyses (see chapter 5):

- the two-node modal vertical bending moment predicted by models beamfde and shell3d were the highest and lowest respectively (see figure 5.8) this does not appear to be the case when the FSI intraction effects are taken under consideration;
- the steady state wave induced shear force of the three-dimensional shell idealisation is magnified around the extremeties (quarter lengths) of the hull, behaving in this way differently to the modal shear force values predicted for model shell3d (see figure 5.9).

The modal stresses of the beam models (beam3d*,beamfde) in turn map the effects of the geometric properties at cross-sections. The direct stresses of the beam models along the top or bottom of the vessel vary in a saw-tooth manner, although the variation of the stresses of the shell model is reasonably smooth. Thus beam3d model stresses appear to produce the maximum amplitudes along the deck edge (beam3d*deck) and keel (beam3d*keel) of the structure. Once more the differences in stress magnitudes between beamfde and beam3d* calculations could be attributed to the different principal coordinates (see table 6.5).

P_R	shell3d	beam3d*	Beamfde
P_7	0.03536	0.03498	0.022000
P_{10}	0.00978	0.00937	0.006530
P_{13}	0.00284	0.00115	0.000173
P_{14}	0.00093	0.00091	0.000224

Table 6.5 Illustration of the magnitude differences between principal coordinate amplitudes (P_r) produced from beam3d*, shell3d (beam and shell potential flow analysis) and beamfde (strip theory) models ($\chi=180^0$, $L/\lambda = 1.0$, $\overline{U} = 7.463$m/s, $\omega_e=0.616$ rad/s).

(a)

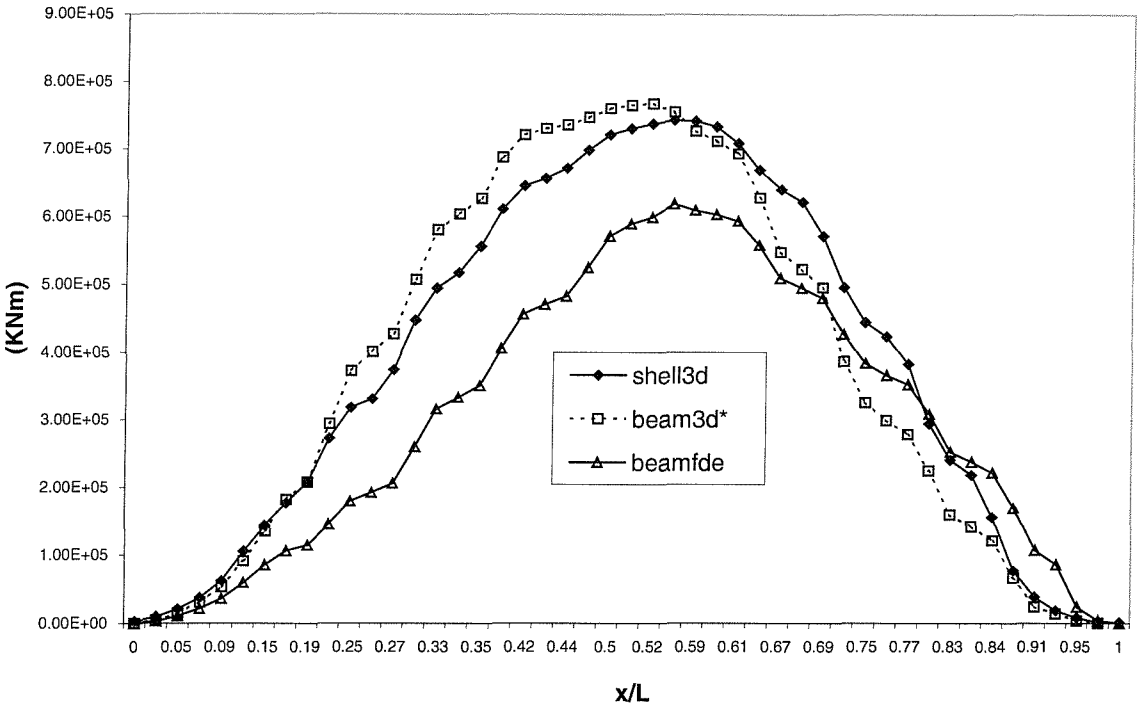

(b)

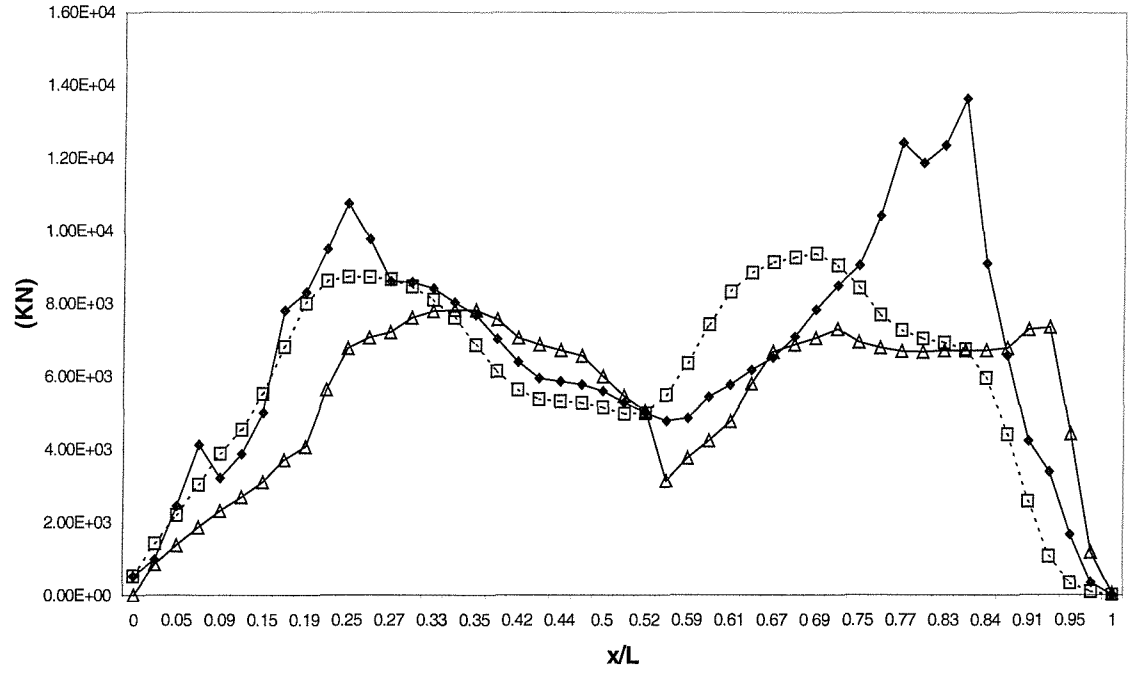

Fig. 6.7 Comparison of the symmetric dynamic loads produced by alternative models in head regular waves (a) vertical bending moment; (b) vertical shear force ($L/\lambda = 1.0$, $\overline{U} = 7.463$m/s, ω_e=0.616rad/s).

(a)

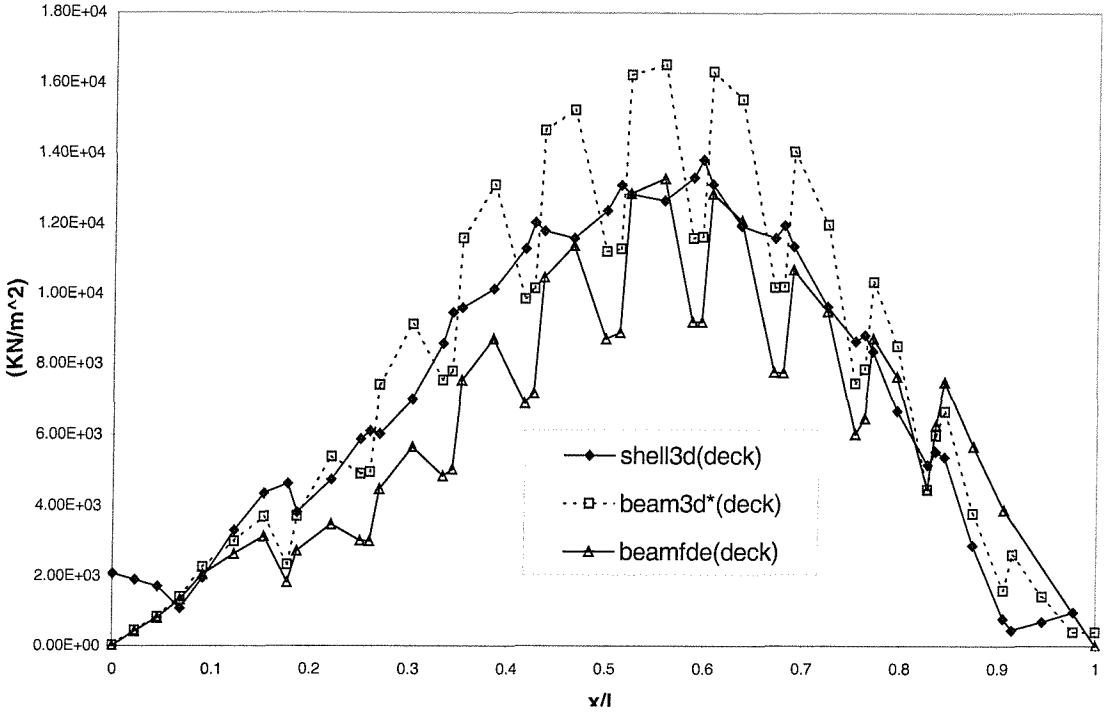

(b)

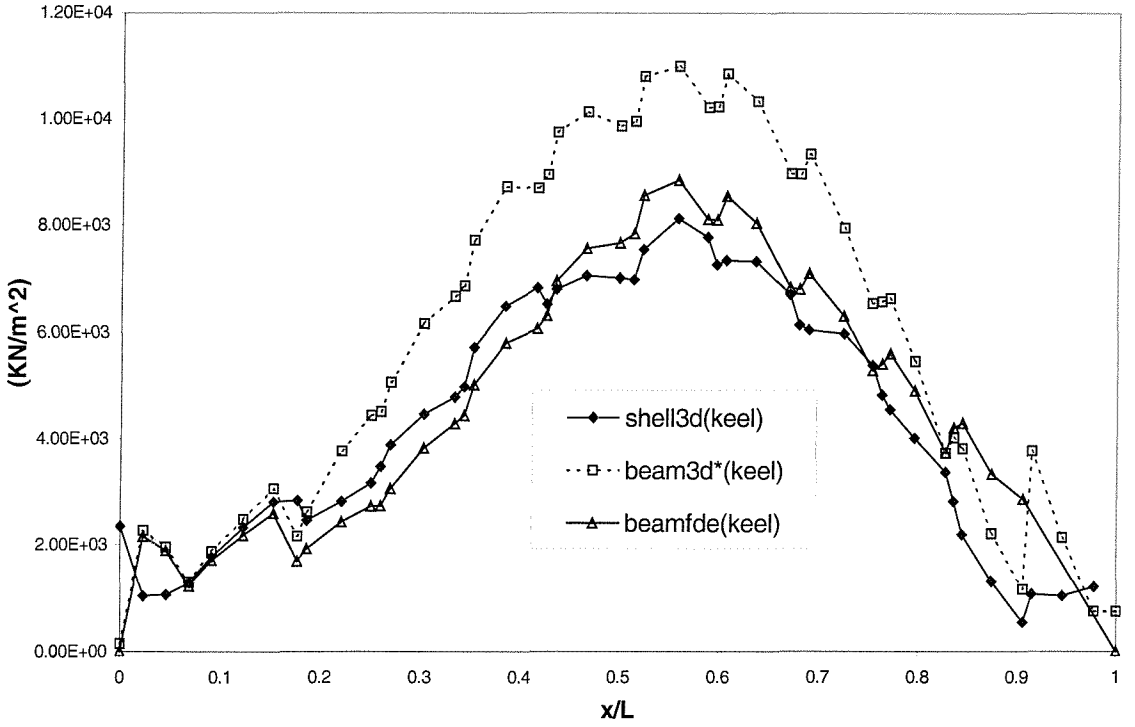

Fig. 6.8 Comparison of the wet symmetric direct stresses predicted by alternative models at head regular waves (L/λ = 1.0, $\overline{U}$ = 7.463m/s, ω_e=0.616rad/s); (a) wet direct stresses along deck; (b) wet direct stresses along keel.

6.7 Unified hydroelasticity analyses in bow quartering and beam waves

Once the behaviour of the three alternative fluid-structure interaction models, for the fundamental case of head waves condition, was established further hydroelasticity studies were carried out in bow quartering (χ=105^0,120^0,135^0,160^0) and beam regular waves (χ=90^0) of unit amplitude, including symmetric and antisymmetric modes. As in the case of head seas the forward speed ($\overline{U}$) of the vessel was at first instance assumed to be 7.463 m/s (Fn=0.138). In the following sections apart form the hydroelastic responses, studied for a variety of headings, principal coordinate amplitudes corresponding to the rigid body motions of heave, roll and pitch are also presented for regular waves of 120^0 heading and unit amplitude. These were computed from a unified analysis, accounting for coupling with eight flexible distortions (4 symmetric and 4 antisymmetric of which 2 are torsion dominant and 2 are horizontal bending dominant), included in the hydroelasticity analyses. Note that the motions and hydrodynamic effects of surge, sway and yaw were not considered to be of direct significance since they are associated with hydrodynamic coefficients and wave excitations influencing the accuracy of the solution through coupling.

6.7.1 Rigid body motions and hydrodynamic characteristics

Variations of heave, roll and pitch rigid body motions (see figure 6.9) as well as the diagonal terms of the corresponding hydrodynamic effects (added mass (A_{rr}) and damping (B_{rr}) coefficients) were computed and compared for all three models (see figures 6.2,6.10). The conclusions of this brief seakeeping analysis were similar to those drawn for head sea conditions (see section 6.5). Once more as the encounter frequency tends to zero, numerically predicted amplitudes of symmetric heave (r=3) and pitch (r=5) responses behave as expected, i.e. the former tends to 1.0 whereas the later tends to zero (see also section 6.5). They both experience a peak around 0.48 rad/s, whereas a second 'weaker' peak is induced through coupling (within the range of 3.0 to 3.25rad/s) with the response in the first symmetric flexible mode (see section 6.7.2). For both heave and pitch the strip theory simulation (beamfde) appears to produce higher magnitude of responses than the three-dimensional potential flow analysis models (beam3d*, shell3d). Starting from zero at zero encounter frequency, the numerically predicted antisymmetric response of roll motion (r=4) undergoes wet resonance at about 0.51 rad/s for beamfde model and 1.04rad/s for the potential flow analysis models

(beam3d*, shell3d). The reader, however, should keep in mind that the meaning of this resonant peak, within the context of potential flow theory, has little significance without accounting for viscous flow effects. Note that alike the secondary peak experienced by symmetric motions, a weaker peak appears within the range of 4.9 to 5.1rad/s as a result of coupling between roll motion (r=4) with the flexible dominant torsion mode 8 (see section 6.7.2).

(a)

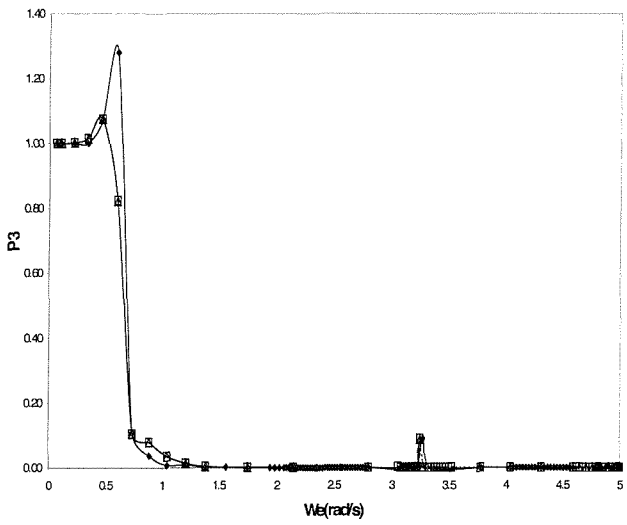

(b)

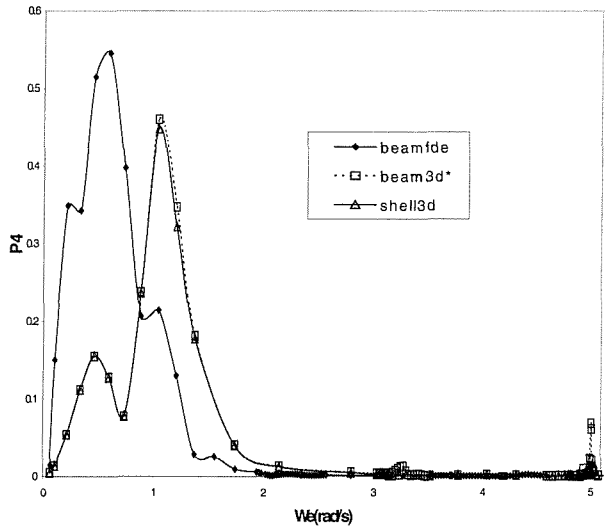

(c)

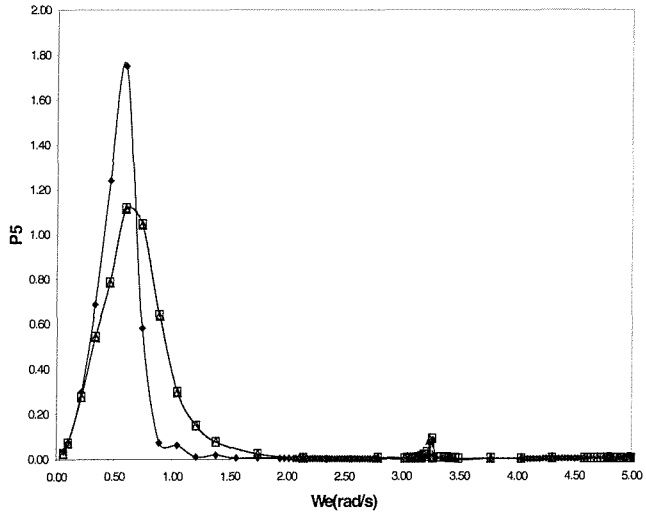

Fig.6.9 Comparison between R.A.O's at bow quartering waves (χ=120^0) for all alternative models (beamfde, beam3d*, shell3d); ($\overline{U}$ = 7.463m/s); (a) heave (P3); (b) roll (P4); (c) pitch (P5).

For the diagonal hydrodynamic added inertia (A_{rr}) and damping (B_{rr}) effects same non-dimensionalisation to that presented for head seas was followed (see equations 6.1, 6.2). Since hydrodynamic effects are functions of encounter frequency and not wave heading the corresponding variations for heave and pitch motions were similar to those demonstrated in figure 6.2(b),(c). Added mass and damping coefficients for roll motion are shown in figure 6.10.

(a) (b)

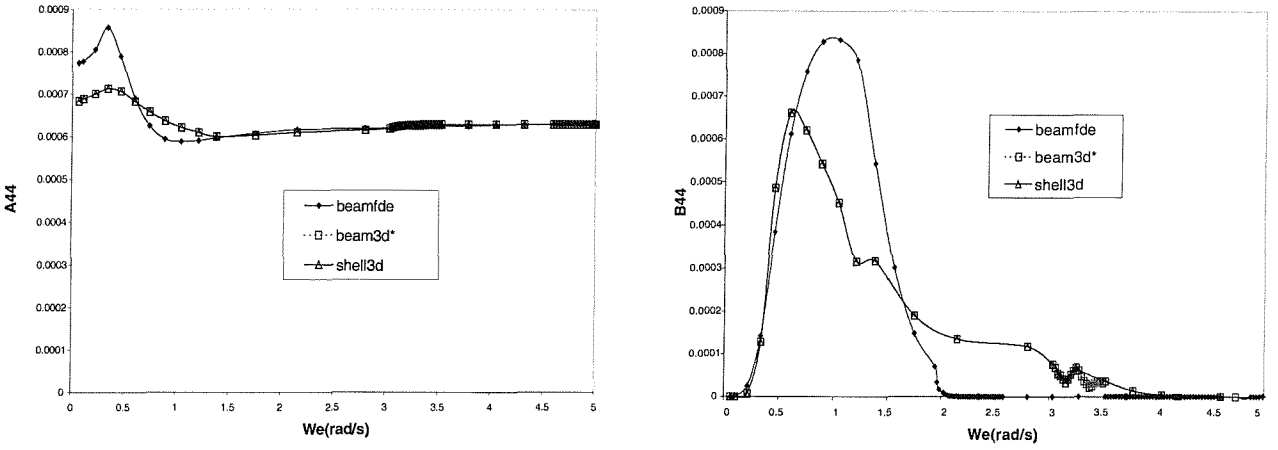

Fig. 6.10 Comparison of hydrodynamic added inertia and damping coefficients for roll motion at bow quartering waves (χ=120^0) for all alternative models (beamfde, beam3d*, shell3d) (a) roll A44; (b) roll (B44).

6.7.2 Flexible responses

As expected the variations of hydrodynamic added inertia and damping coefficients with encounter frequency for the symmetric (r=7,10,13,14) distortions experience similar trends to those shown in figures 6.3 and 6.4. The corresponding hydrodynamic effects for antisymmetric (r=8,9,11,12) modes are shown in figures 6.11 and 6.12. The behaviour of the hydrodynamic damping coefficients expressing the antisymmetric dynamics of the structure (B_{88}, B_{1212}) is quite interesting. Whereas good agreement is achieved between all models for the horizontal bending dominant modes, this is not the case for the torsion dominant modes where the beam simulations (beam3d*,beamfde) appear to significantly overestimate the hydrodynamic damping coefficients produced by the shell model (shell3d). Maybe such discrepancy could be attributed to the not so good agreement between the antisymmetric modal characteristics of the shell and beam structural models (see chapter 5).

Hydroelastic symmetric encounter resonant frequencies having very close magnitudes to those demonstrated in table 6.2 were observed for all headings. The antisymmetric dynamic responses of beam and plate models were also compared. For the reasons explained in section 6.2, beam3d* antisymmetric hydroelasticity analysis was based on the corresponding modal and generalised mass/stiffness characteristics of beamfde idealisation (see table 6.7). The corresponding dry natural frequencies and wet encounter resonances are demonstrated in tables 6.6 and 6.7.

Mode type	beamfde		beam3d*		shell3d	
	Dry (ω_r)	Wet (ω_{er})	Dry (ω_r)	Wet (ω_{er})	Dry (ω_r)	Wet (ω_{er})
1 node HB – 1 node **T** (r=8)	5.15	4.41	5.15	5.0	5.01	4.95
2 node **HB** – 2 node T (r=9)	5.85	4.96	5.85	5.01	5.55	5.02
3 node **HB** – 3 node T (r=11)	10.10	8.71	10.10	9.3	12.63	9.33
2 node HB – 2 node **T** (r=12)	11.13	3.26	11.13	3.26	10.71	9.25

Table 6.6 Dry natural frequencies and wet resonances for antisymmetric distortions in bow quartering waves (r = modal index; $\overline{U}$ = 7.463m/s; HB: horizontal bending; T: torsion; **HB,T**: dominant HB,T; ω_r = dry natural frequency; ω_{er} = wet resonance).

Mode type	beamfde		Beam3d*		shell3d	
	ω_{er}/ω_r	GM (tonne-m^2)	ω_{er}/ω_r	GM (tonne-m^2)	ω_{er}/ω_r	GM (tonne-m^2)
1 node HB – 1 node **T** (r=8)	0.856	84710.95	0.971	84710.95	0.988	81577.10
2 node **HB** – 2 node T (r=9)	0.848	34277.81	0.856	34277.81	0.904	53729.74
2 node HB – 2 node **T** (r =11)	0.862	25142.98	0.920	25142.98	0.738	15313.22
3 node **HB** – 3 node T (r=12)	0.292	51104.78	0.292	51104.78	0.863	40267.67

Table 6.7 Wet resonance to natural frequency aspect ratio (ω_{er}/ω_r) for all idealisations (r = modal index; $\overline{U}$ = 7.463m/s; GM = generalised mass; HB = horizontal bending; T = torsion; **HB,T** = dominant; HB,T; ω_r = dry natural frequencies; ω_{er} = wet resonances).

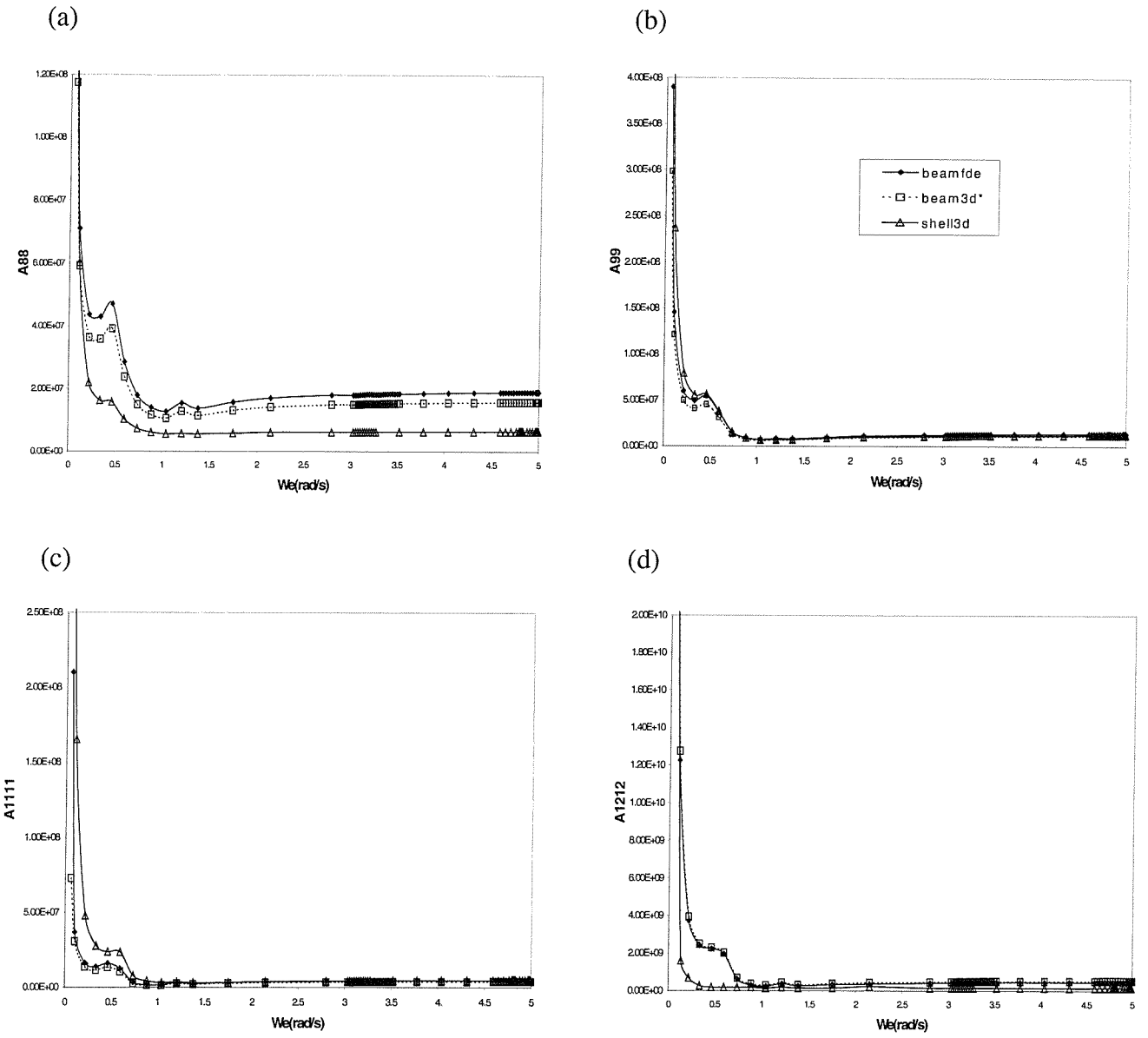

Fig. 6.11 Comparison of hydrodynamic added mass (A_{IT}) coefficients (kgm^2) for antisymmetric flexible modes of all models (beamfde, beam3d*, shell3d) for bow quartering ($\chi=120^0$) regular waves conditions ($\overline{U}$ = 7.463m/s); (a) 1 node HB 1 node **T**; (b) 2 node **HB** 2 node T; (c) 2 node HB 2 node **T**; (d) 3 node **HB** 3 node T (HB = horizontal bending; T = torsion; **HB,T**= HB,T dominant).

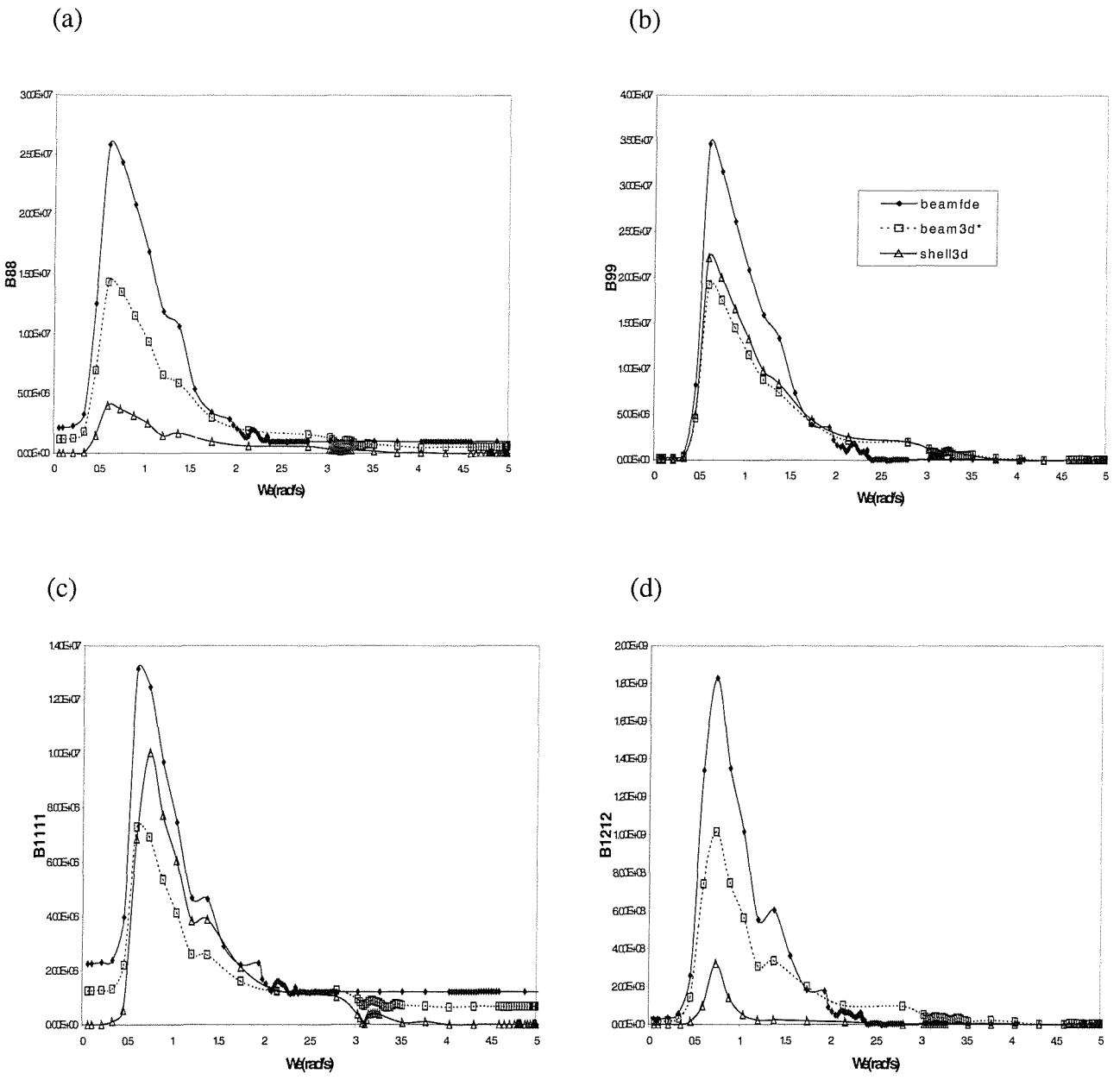

Fig. 6.12 Comparison of hydrodynamic damping (B_{IT}) coefficients (kgm/s) for antisymmetric flexible modes of all models (beamfd, beam3d, shell3d) for head bow quartering (χ=135^0) regular waves conditions ($\overline{U}$ = 7.463m/s); (a) 1 node HB 1 node **T**; (b) 2 node **HB** 2 node T; (c) 3 node **HB** 3 node T; (d) 2 node HB 2 node **T** (HB = horizontal bending; T = torsion; **HB,T**= HB,T dominant).

Maximum principal coordinate amplitudes are observed for the first symmetric (2 node vertical bending) and antisymmetric (1 node horizontal bending 1 node torsion (dominant)) modes of vibration and smaller responses are obtained for the subsequent symmetric and antisymmetric modes (see figures 6.13,6.14). In the relatively long wave region, for symmetric distortions maximum principal coordinate amplitudes are predicted by shell3d model followed by beam3d* and beamfde models (see figure 6.15) for a range of headings. It is worthwhile to mention that the agreement between different idealisations is affected as the heading angle diverts from head to beam seas. Comparative study of the frequency response amplitudes of all models has shown that for symmetric distortions maximum principal coordinates are observed in head waves, with values gradually decreasing as the ship moves towards beam sea conditions (see figure 6.16). Maximum horizontal bending dominant antisymmetric response amplitude is observed at 135^0 (see figures 6.17, 6.18), value which becomes zero as the vessel approaches head sea conditions (for which antisymmetric distortions are irrelevant) and progressively decreases as the vessel approaches beam seas (where roll motion is very significant). Beam3d* idealisation appears to produce even higher responses to those produced by the strip theory model for horizontal bending dominant modes. This is expected, since both beam (beamfde, beam3d*) and shell3d idealisations experience some differences in their generalised mass magnitudes (see table 6.7). For the torsion dominant modes the frequency response function predicted by beamfde idealisation in antisymmetric motion and especially at beam seas appears to have the highest principal coordinates only for the relatively low encounter frequency bandwidth between 0.0 and 2.2 rad/s. This can possibly be considered as being expected due to the fact that the strip theory produces a response of significantly higher amplitude for roll even at bow quartering seas ($\chi=135^0$) (see figures 6.9 and 6.19). Beam3d* idealisation, however, appears to produce responses of lower magnitude than the shell3d predicted values despite the fact that the generalised mass of the two models for torsion dominant modes are in good agreement (see table 6.7). From a general perspective the agreement for different idealisations could be considered as being good for symmetric modes but not so satisfactory for the antisymmetric ones. The dry analyses investigations have proved the weakness of the second order Timoshenko beam theory to simulate reliably the antisymmetric behaviour of the non-prismatic bulk carrier hull. The three-dimensional potential flow analyses idealisations (shell3d,

beam3d*) appear to produce expected results for extreme seakeeping conditions (beam seas) in contrast to the strip theory (beamfde).

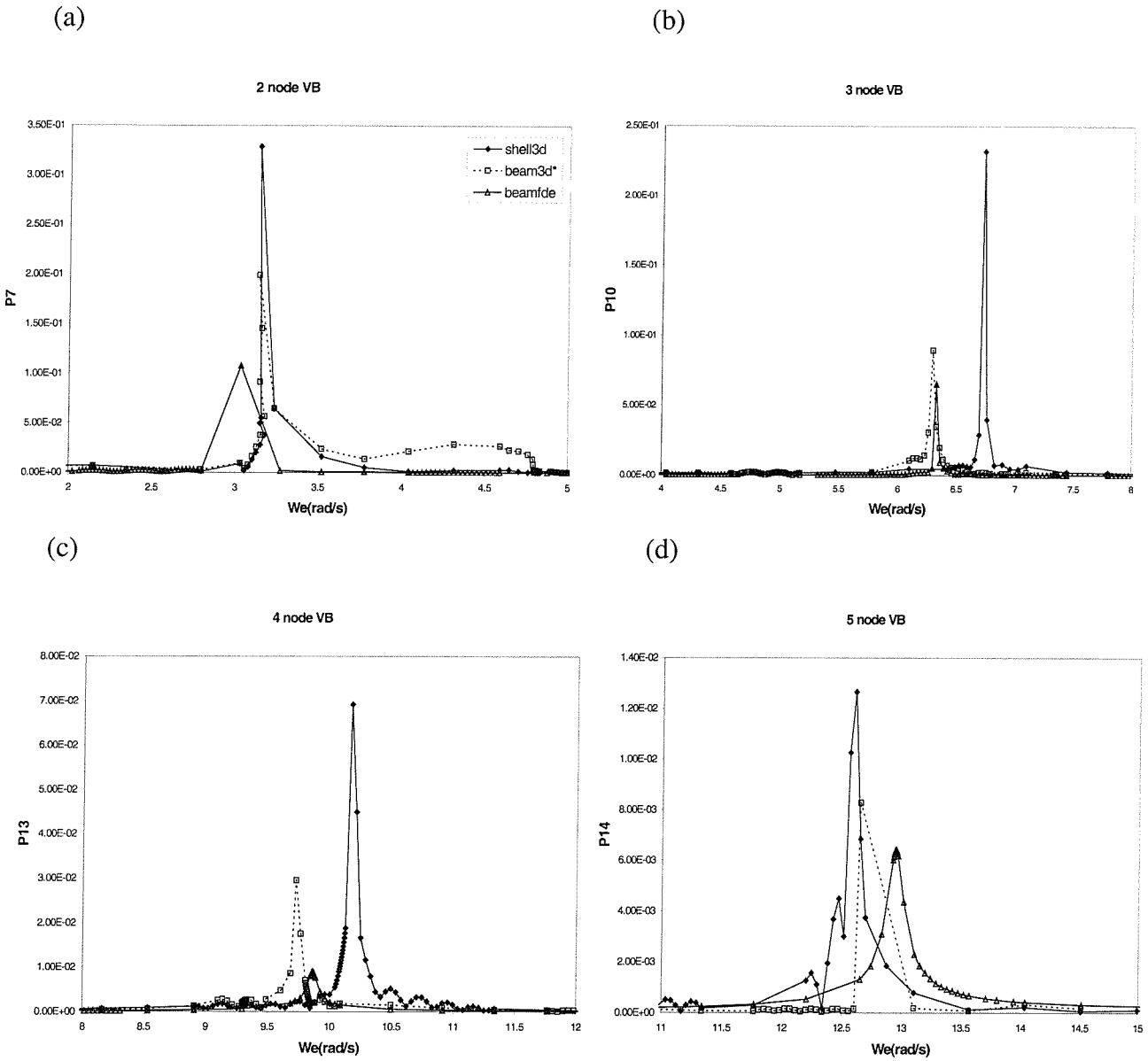

Fig.6.13 Symmetric principal coordinate amplitudes of all idealisations in regular waves of heading 120^0 ($\overline{U}$ =7.463m/s).

(a)

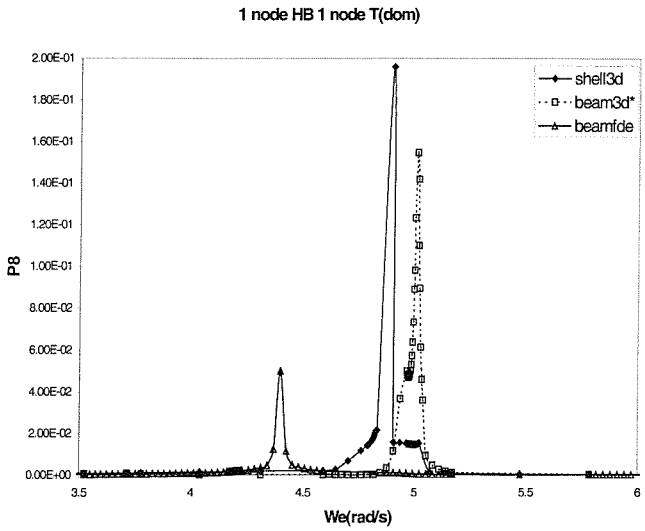

(b)

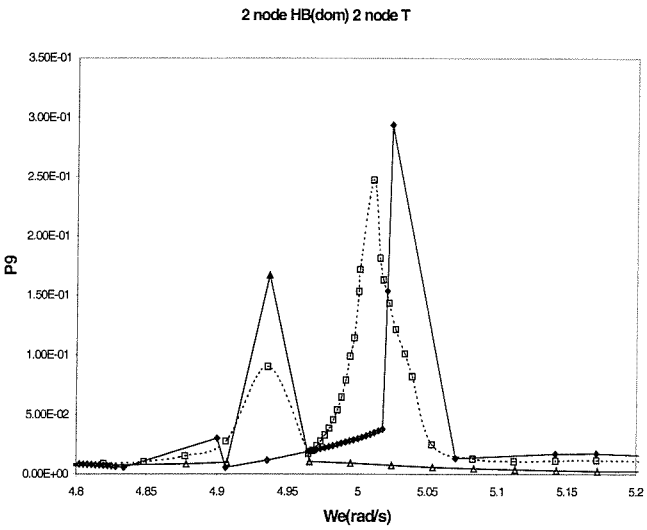

(c)

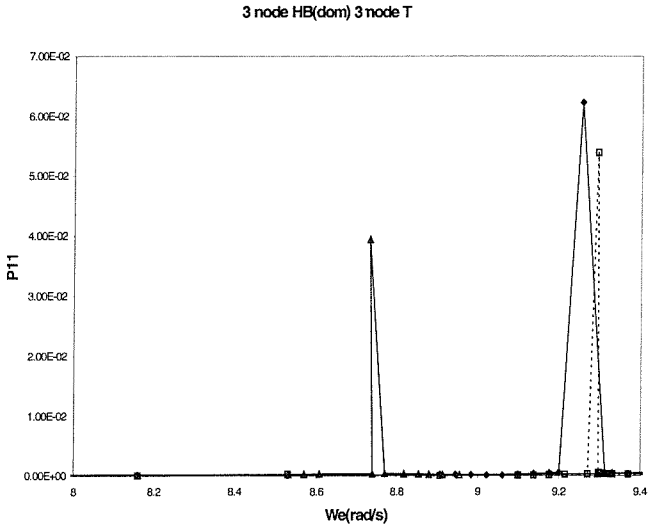

(d)

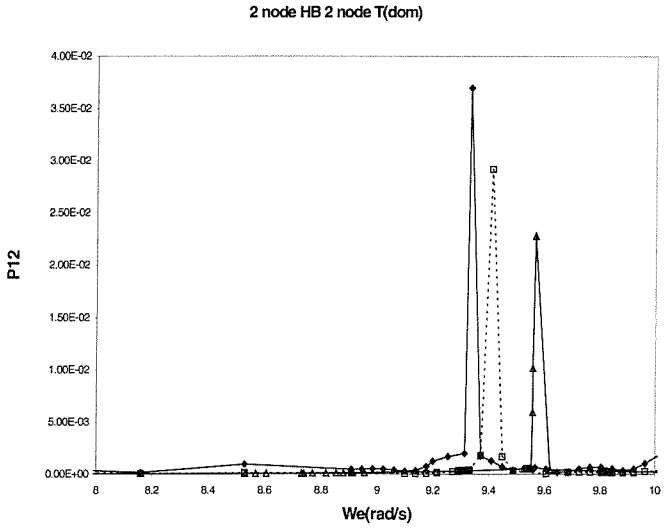

Fig.6.14 Antisymmetric principal coordinate amplitudes of all idealisations at regular waves of heading 120^0 ($\overline{U}$ =7.463m/s)

(a)

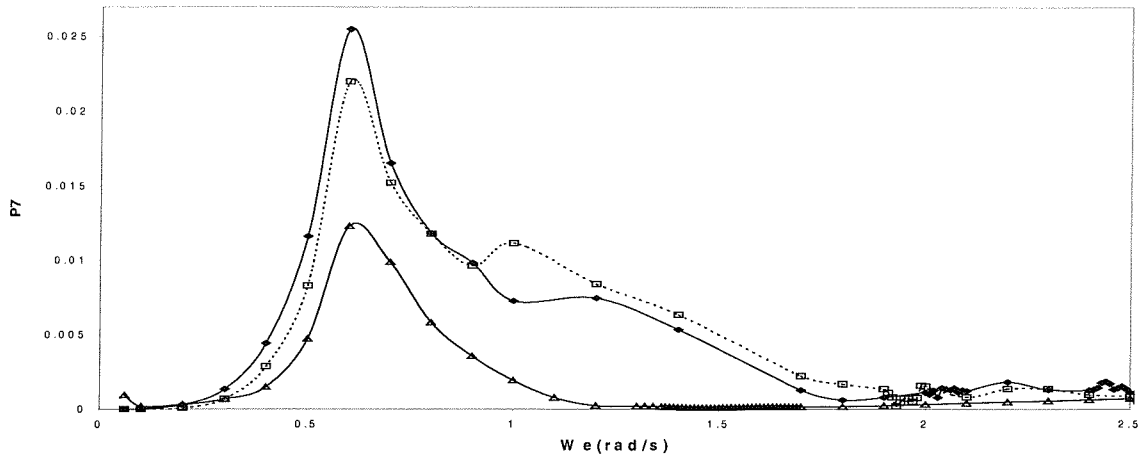

(b)

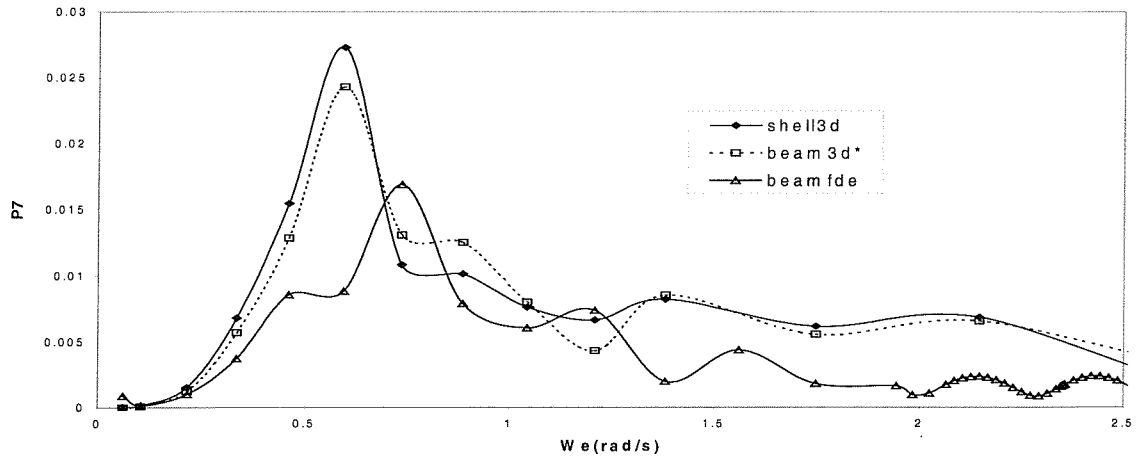

(c)

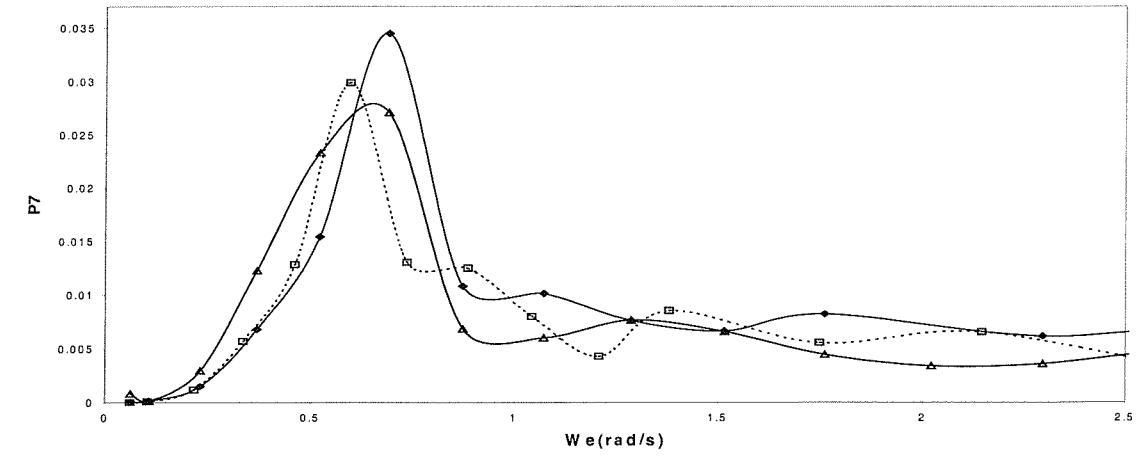

Fig. 6.15 Comparison of the variation of principal coordinate amplitudes of all models for 2 node vertical bending; (a) 90^0; (b) 120^0; (c) 180^0.

(a)

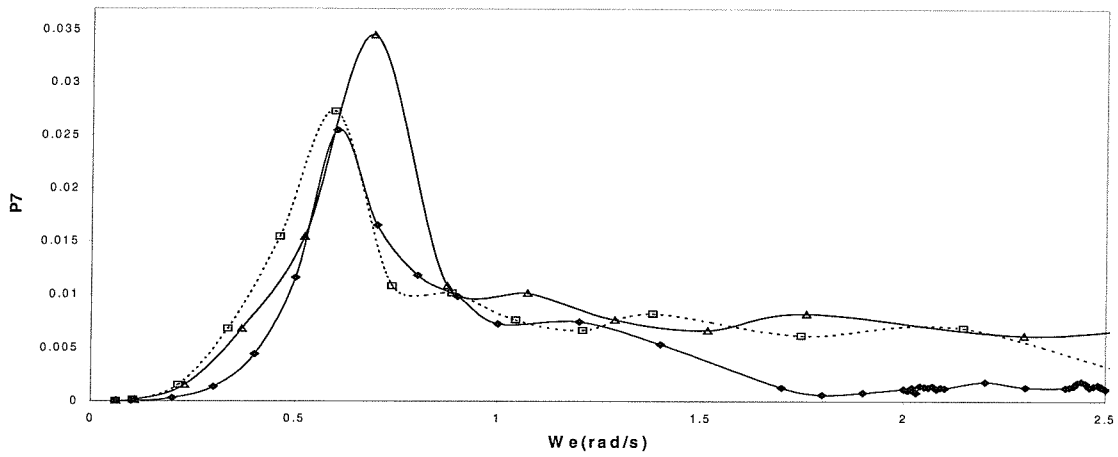

(b)

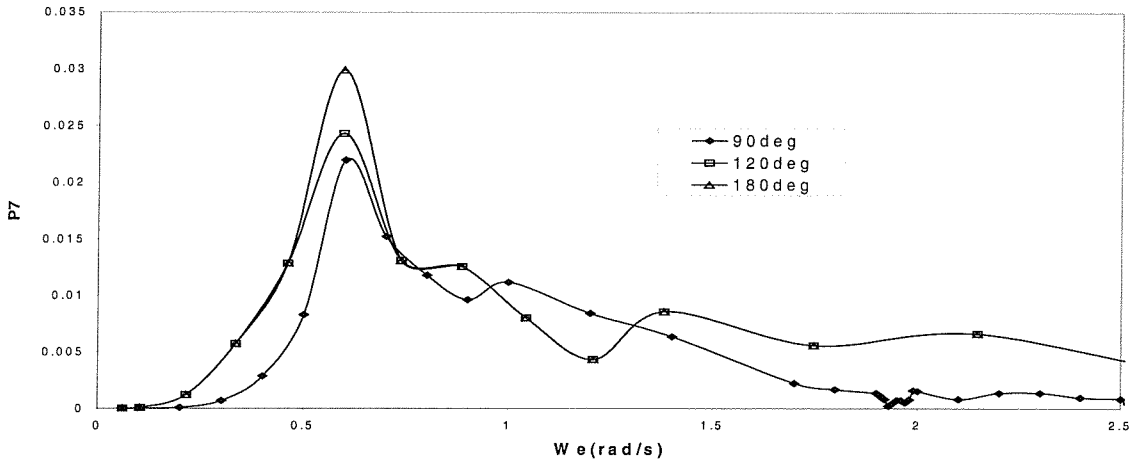

(c)

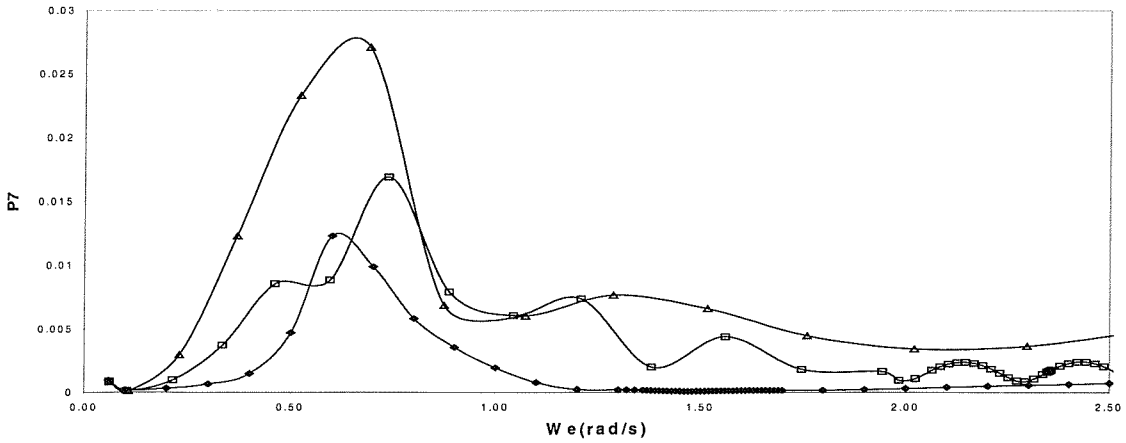

Fig. 6.16 Variation of principal coordinate amplitudes of all models at alternative wave headings for 2 node vertical bending; (a) shell3d; (b) beam3d*; (c) beamfde.

(a)

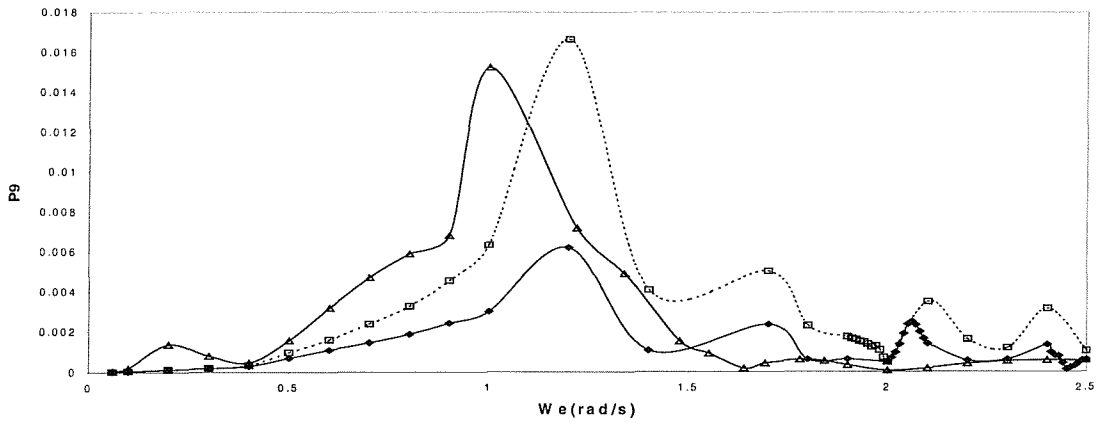

(b)

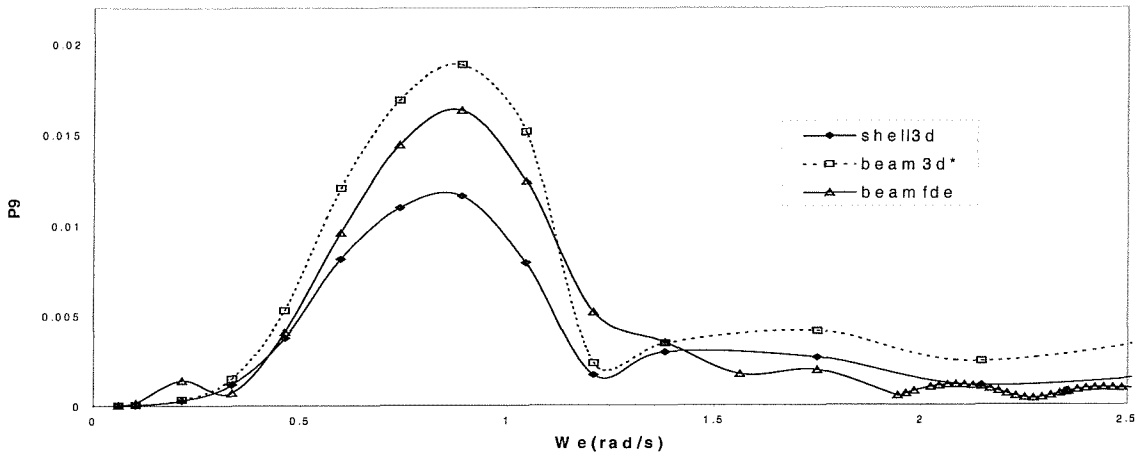

(c)

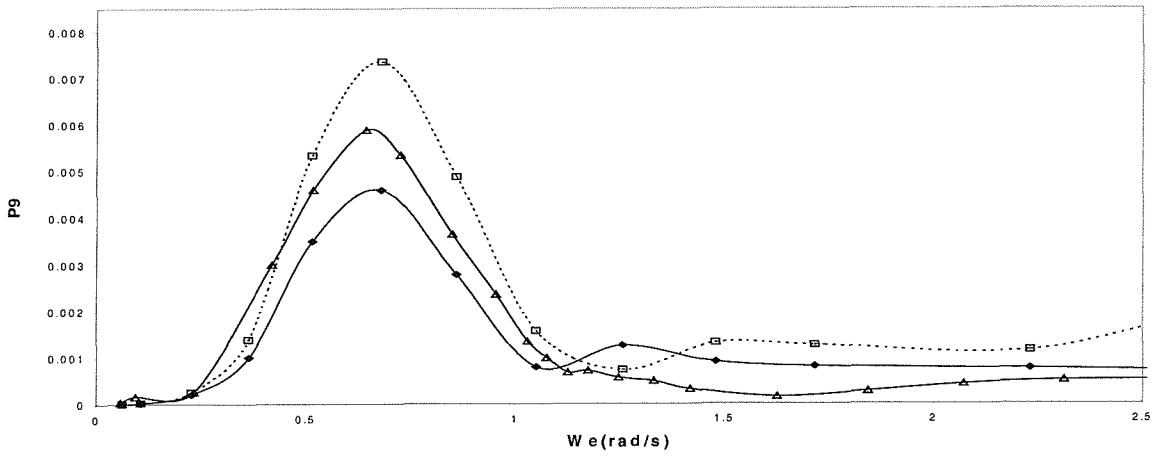

Fig. 6.17 Comparison of the variation of principal coordinate amplitudes of all models for 2 node horizontal bending dominant mode; (a) 90^0; (b) 120^0; (c) 160^0.

(a)

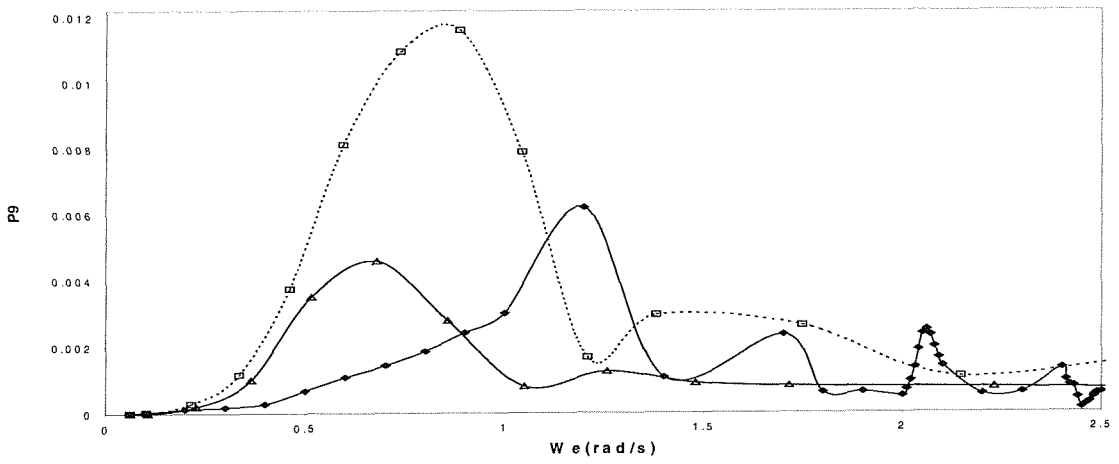

(b)

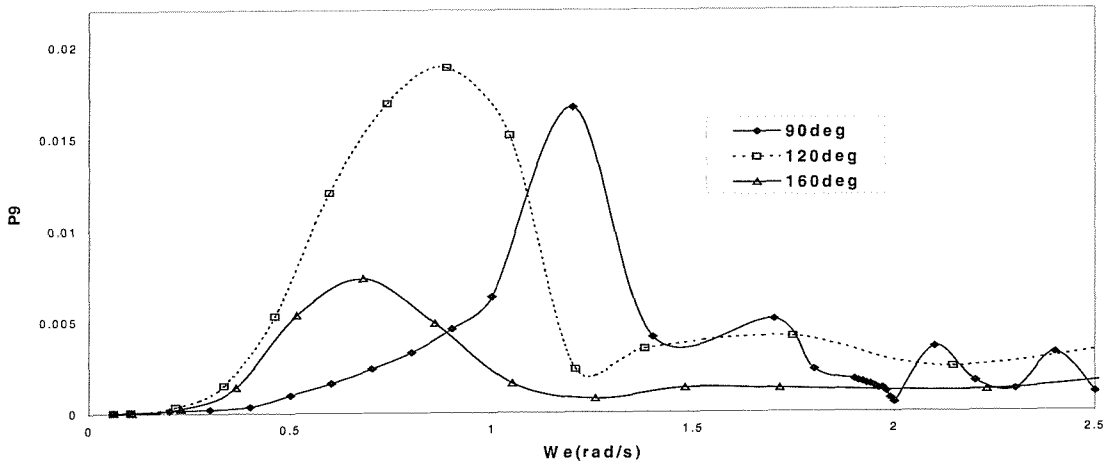

(c)

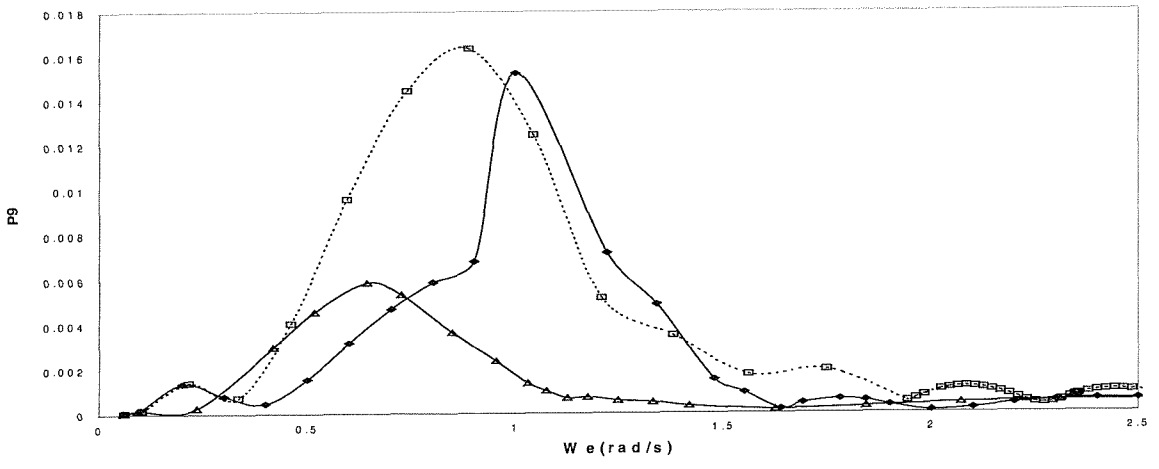

Fig. 6.18 Variation of principal coordinate amplitudes of all models at alternative wave headings for 2 node horizontal bending dominant mode; (a) shell3d; (b) beam3d*; (c) beamfde.

(a)

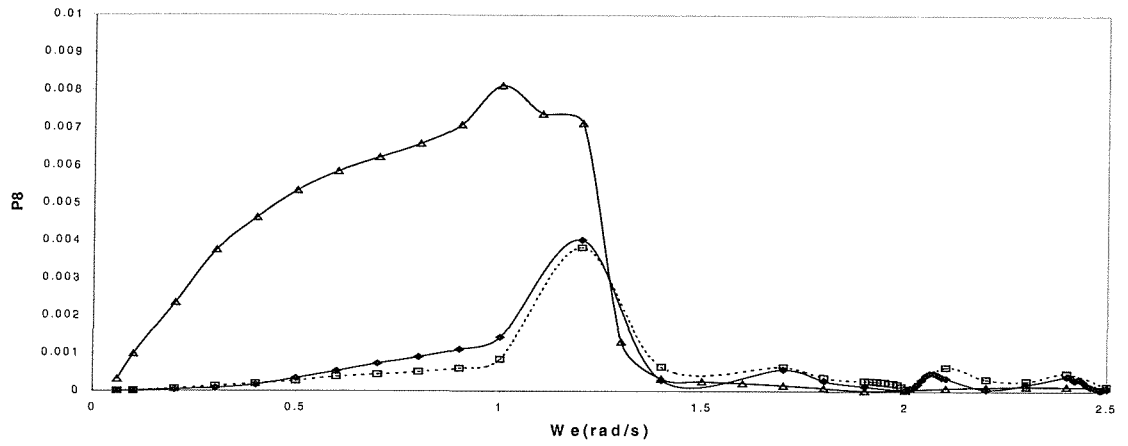

(b)

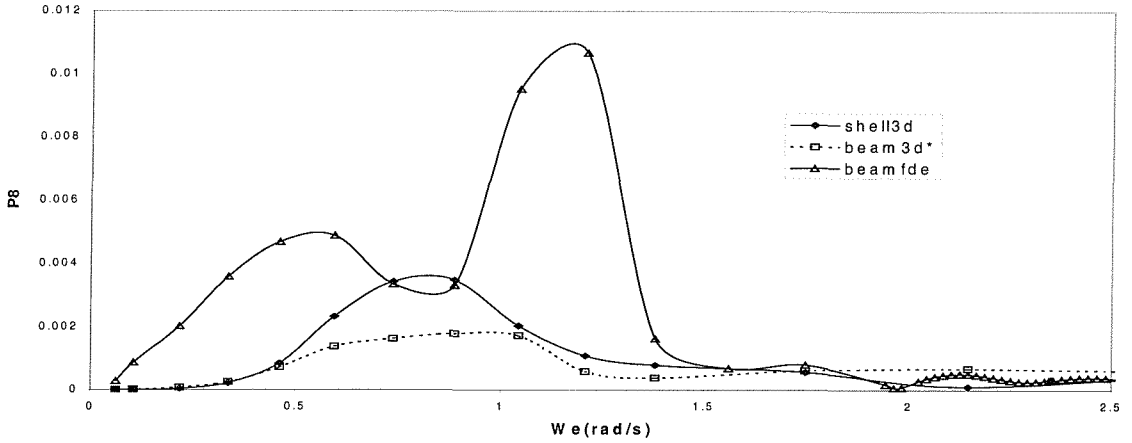

(c)

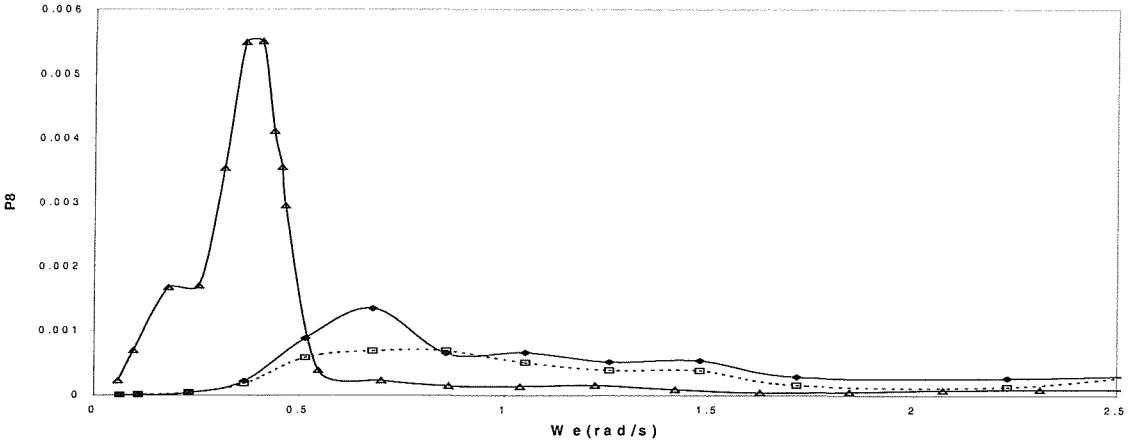

Fig. 6.19 Comparison of the variation of principal coordinate amplitudes of all models for 1 node torsion dominant mode; (a) 90^0; (b) 120^0; (c) 160^0.

(a)

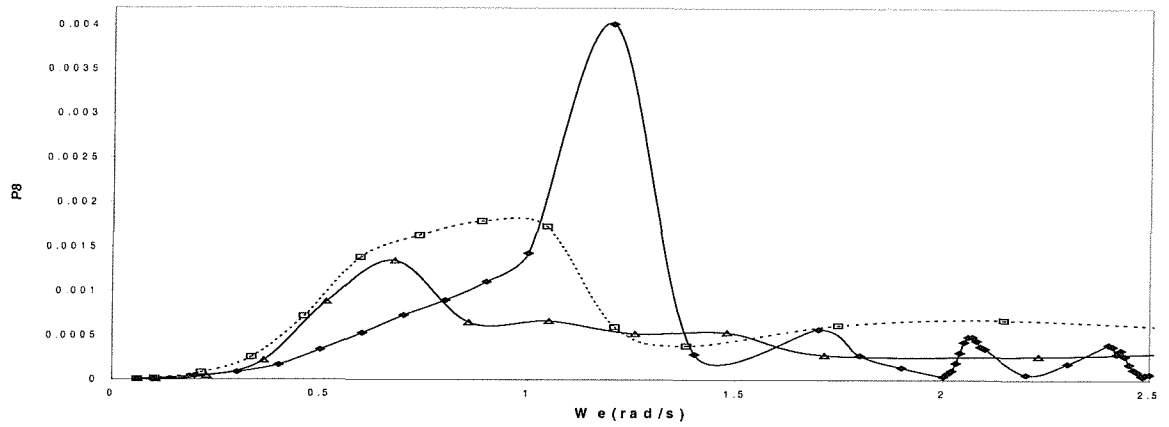

(b)

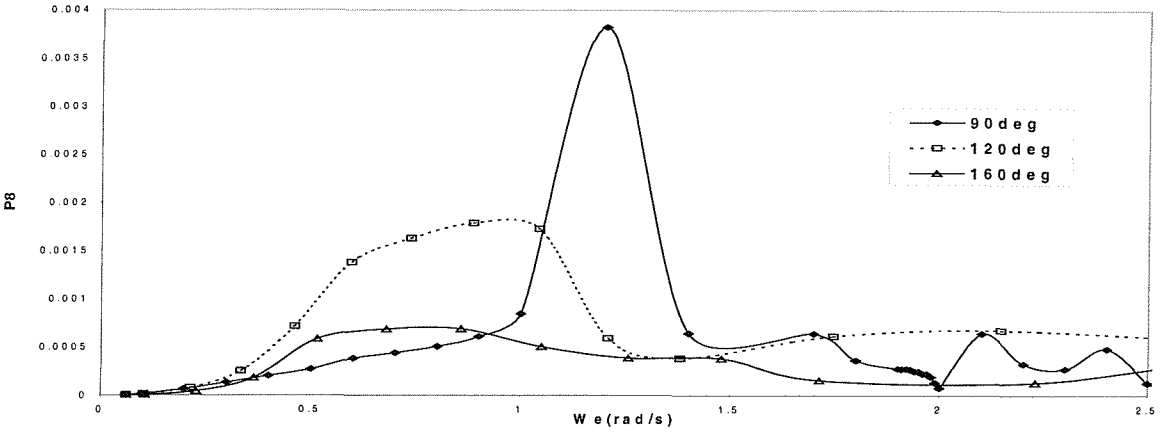

(c)

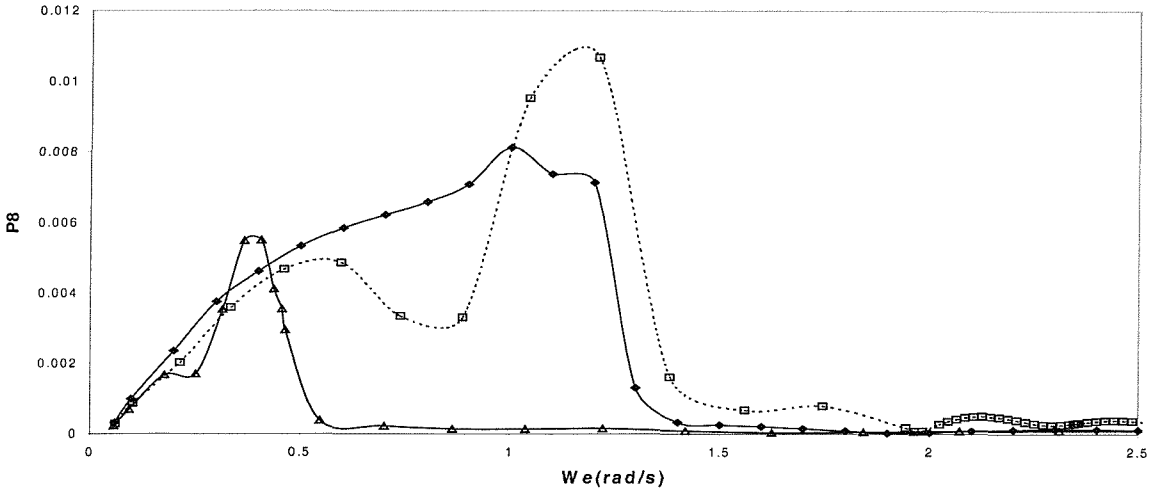

Fig.6.20 Variation of principal coordinate amplitudes of all models at alternative wave headings for 1 node torsion dominant mode; (a) shell3d; (b) beam3d*; (c) beamfde.

6.7.3 Steady-state seaway induced dynamic loads in bow quartering and beam waves

The calculation of the symmetric steady-state wave induced dynamic loads was based upon equations (3.39) and (3.41) respectively (see chapter 3) with the six degrees of freedom representing the rigid body dynamics of the ship as a continuous conservative system, not considered to contribute to the hull girder loading [6.2]. Whereas symmetric modes are important for the vertical bending moment calculations, they are not relevant when calculating horizontal bending moments since they are uncoupled from the antisymmetric modes for a port-starboard symmetric hull. In principle, all flexible modes are considered to contribute to the stress distributions. In two-dimensional hydroelasticity analysis, however, direct stresses, are calculated indirectly from vertical and horizontal bending moments (see equation (3.41)), while in three-dimensional hydroelasticity the corresponding stress components are evaluated as modal summations of the longitudinal direct stresses produced by the symmetric and antisymmetric distortions of the shell finite element model (see sections 3.5 and 6.5).

The methodology followed for the evaluation of the vertical bending moments (VBM) and shear forces (VSF) was identical to the one outlined for head sea conditions (section 6.5). Once more it is worthwhile to stress that the one node longitudinal mode was excluded from the hydroelastic calculations since: (a) despite being a symmetric one, it does not produce any bending moment in beam3d* idealisation; (b) although in shell3d model this mode is coupled with vertical bending, it does not affect the vertical bending moment magnitude (as illustration see figure 6.21). Results of similar nature were obtained in previous studies concerned with the hydroelastic analyses of a mine hunter [6.4].

The contribution of the number of flexible distortions was also examined. Comparison of the variation of all dynamic loads with increasing (2 up to 12) number of symmetric and antisymmetric flexible distortions has shown that 8 flexible modes (4 symmetric and 4 antisymmetric) is adequate to assess accurately the bulker's dynamic strength as shown in figures 6.22, 6.23 using shell3d idealisation.

Study of the relation of the vertical bending moments and shear forces at unit ship length to wavelength ratio and alternative wave headings ($\chi=90^0,105^0,120^0,135^0,160^0,180^0$) has shown

that best agreement between alternative idealisations is achieved at 135^0 heading (see figures 6.24,6.25,6.27) and at unit ship- to wave-length ratio (where ω_e=0.56rad/s). The strip theory predicted bending moment values (beamfde) are always more conservative than the three-dimensional potential flow analysis results (beam3d*,shell3d). It also becomes evident that maximum vertical bending moments are observed along the vessel for head waves and then gradually decrease (see figure 6.26). This mirrors the behaviour of the symmetric principal coordinates (see section 6.5). For head waves maximum vertical bending moment occurs when the ship's length nearly equal to wave-length. This trend is progressively changing near beam seas simply reflecting the fact that at lower frequency regions longer waves are required to produce an increased wave excitation (see figure 6.26). These conclusions are further supported by figures 6.28 and 6.29.

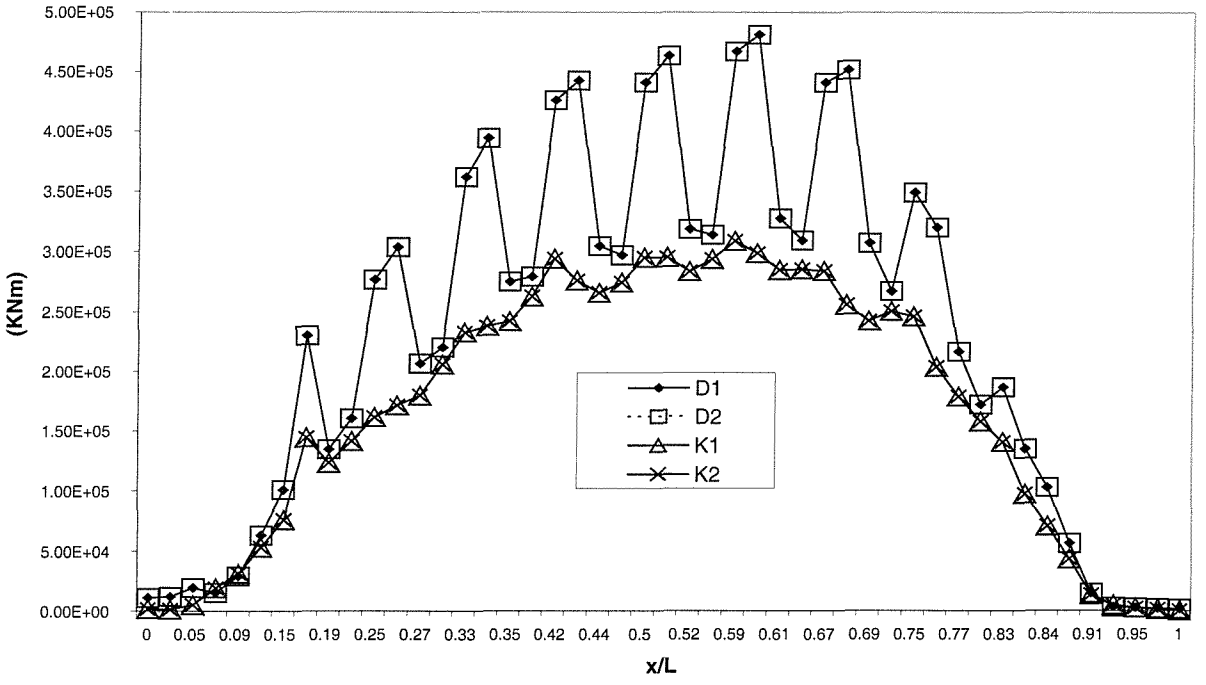

Fig. 6.21 The effects of longitudinal mode on the vertical bending moment (VBM) - (D1: VBM along deck – longitudinal mode excluded; D2: VBM along deck – longitudinal mode included; K1: VBM along keel – longitudinal mode excluded; K2: VBM along deck – longitudinal mode included) – (χ=120^0, U = 7.463m/s, L/λ=1,shell3d idealisation).

(a)

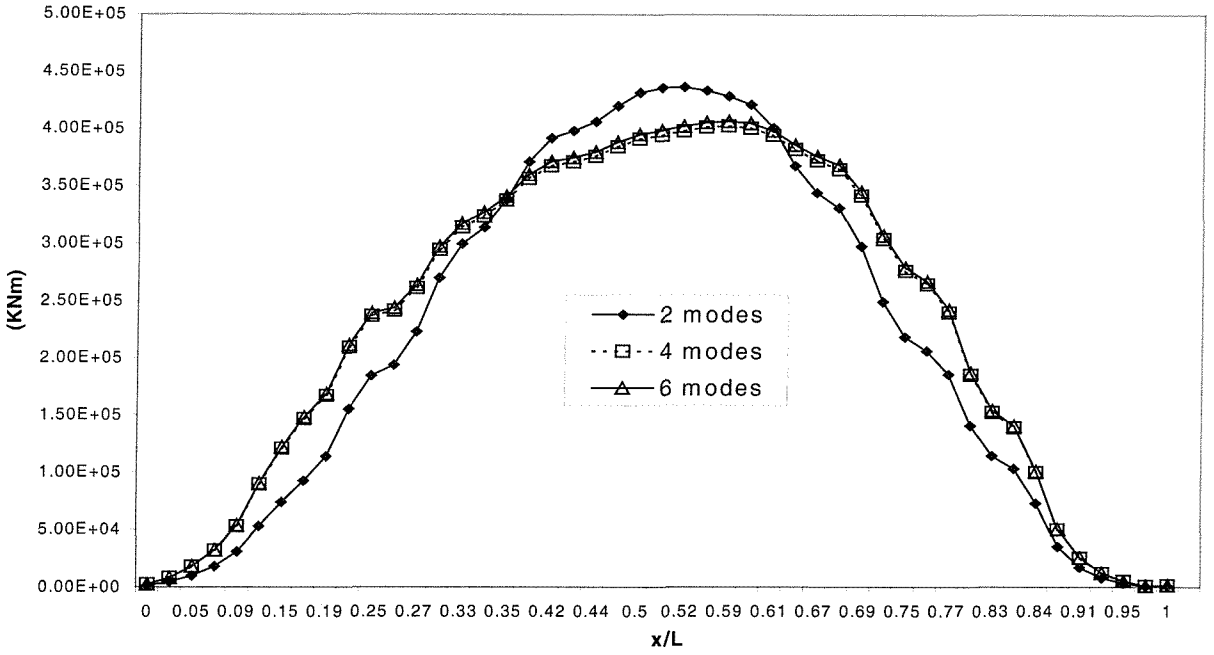

(b)

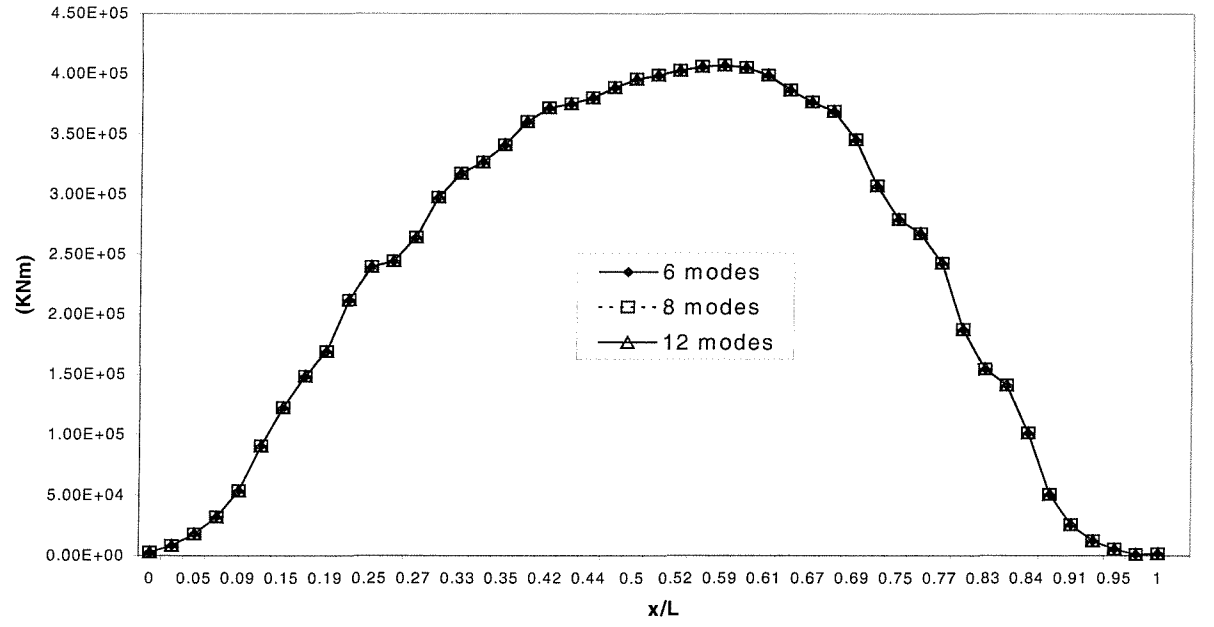

Fig. 6.22 Illustration of the effects of increasing number of flexible bending modes on the computation of VBM and VSF (χ=120^0, $\left(\overline{U}\right)$ = 7.463m/s, L/λ = 1.0, shell3d idealisation); (a) VBM including 2,4,6 symmetric flexible modes; (b) VBM including 6,8,12 symmetric flexible modes.

(a)

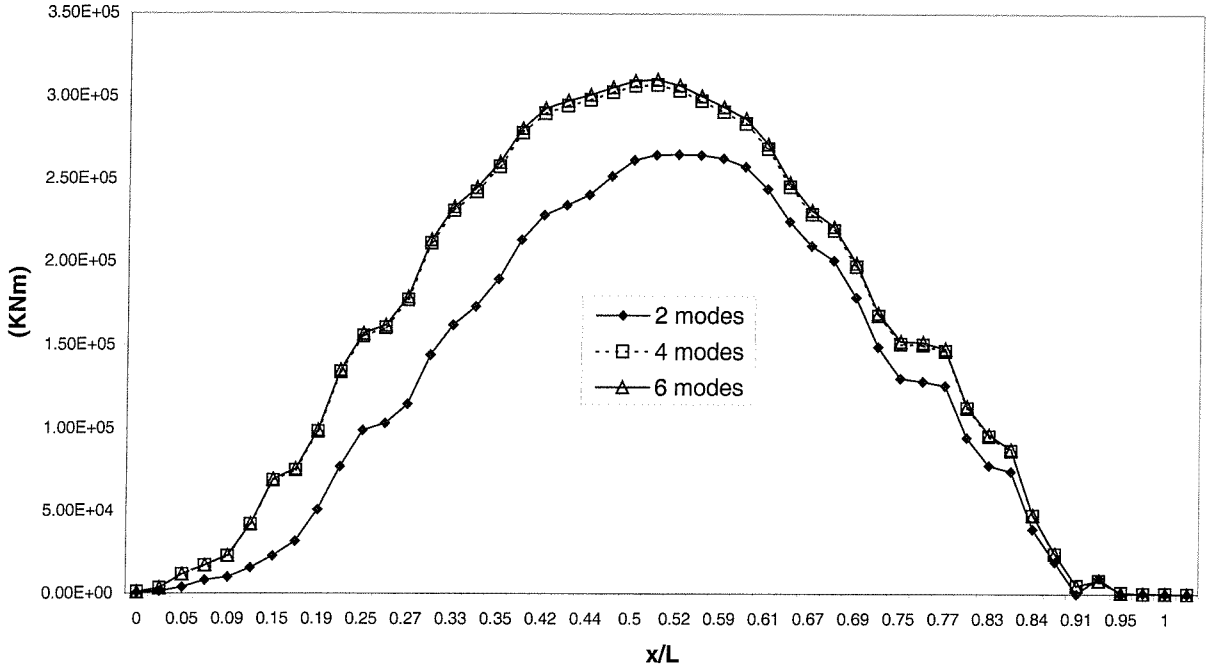

(b)

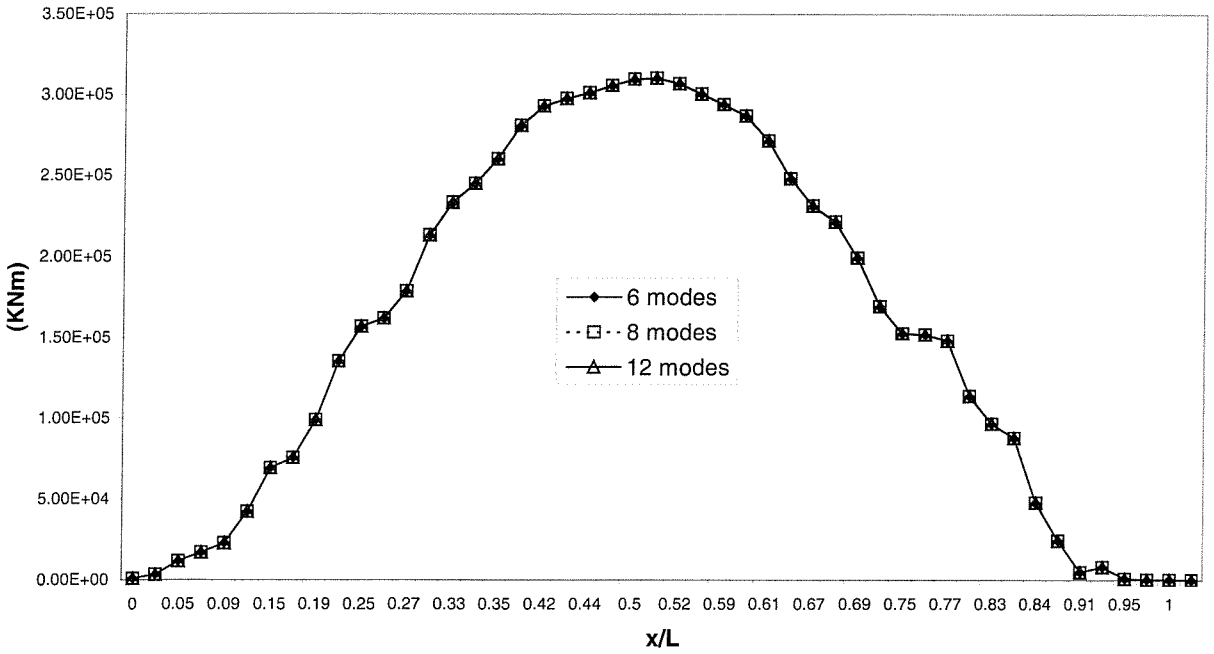

Fig. 6.23 Illustration of the effects of increasing number of flexible bending modes on the computation of HBM and HSF (χ=120^0, $\overline{U}$ = 7.463m/s, L/λ = 1.0, shell3d idealisation); (a) HBM including 2,4,6 antisymmetric flexible modes; (b) HBM including 6,8,12 antisymmetric flexible modes.

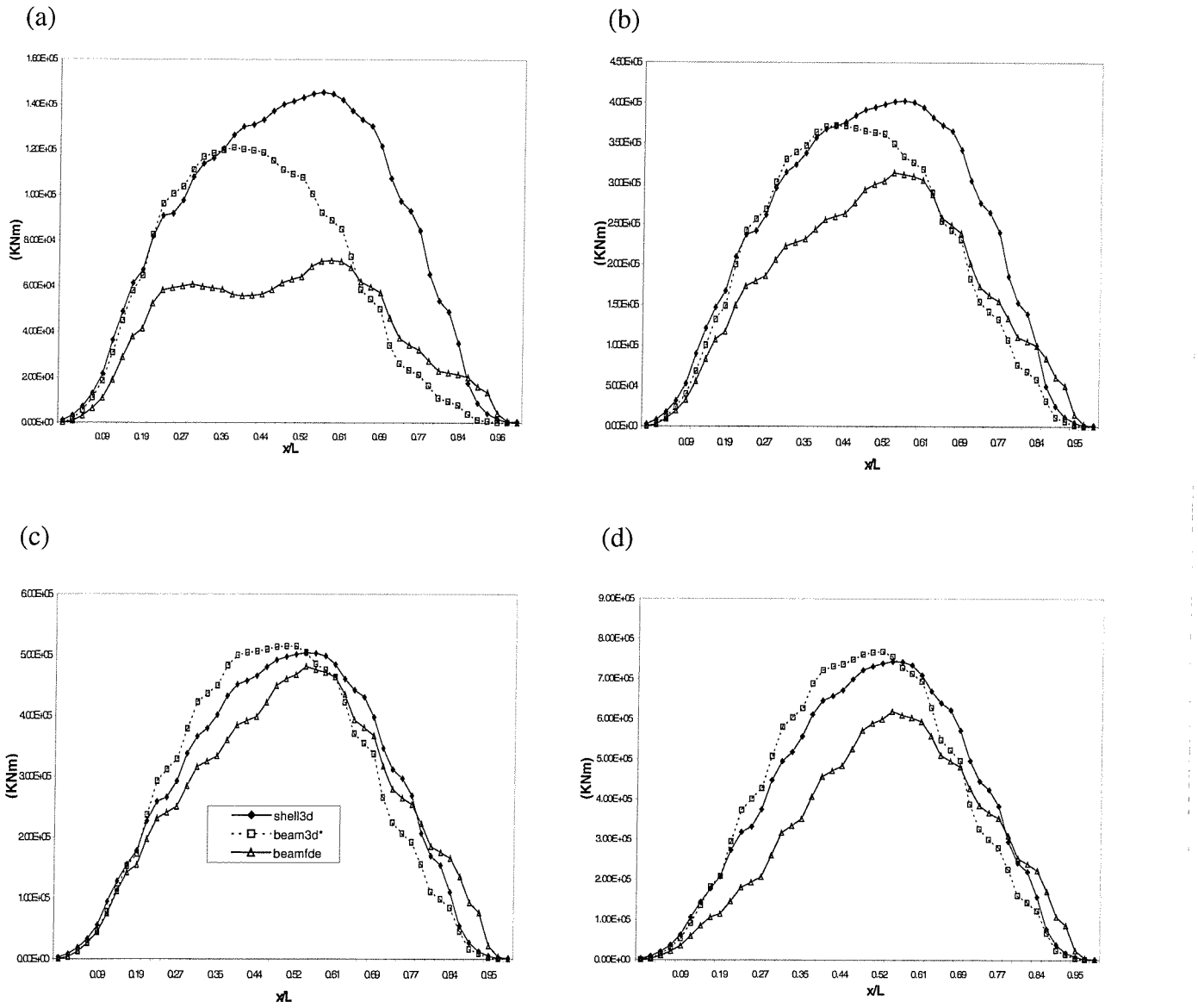

Fig. 6.24 Variation of vertical bending moments (kNm) along the ship obtained from models beamfde, beam3d* and shell3d for a variety of headings – ($L/\lambda = 1.0$, $\overline{U} = 7.463$m/s) – (a) 90^0; (b) 120^0; (c) 135^0; (d) 180^0.

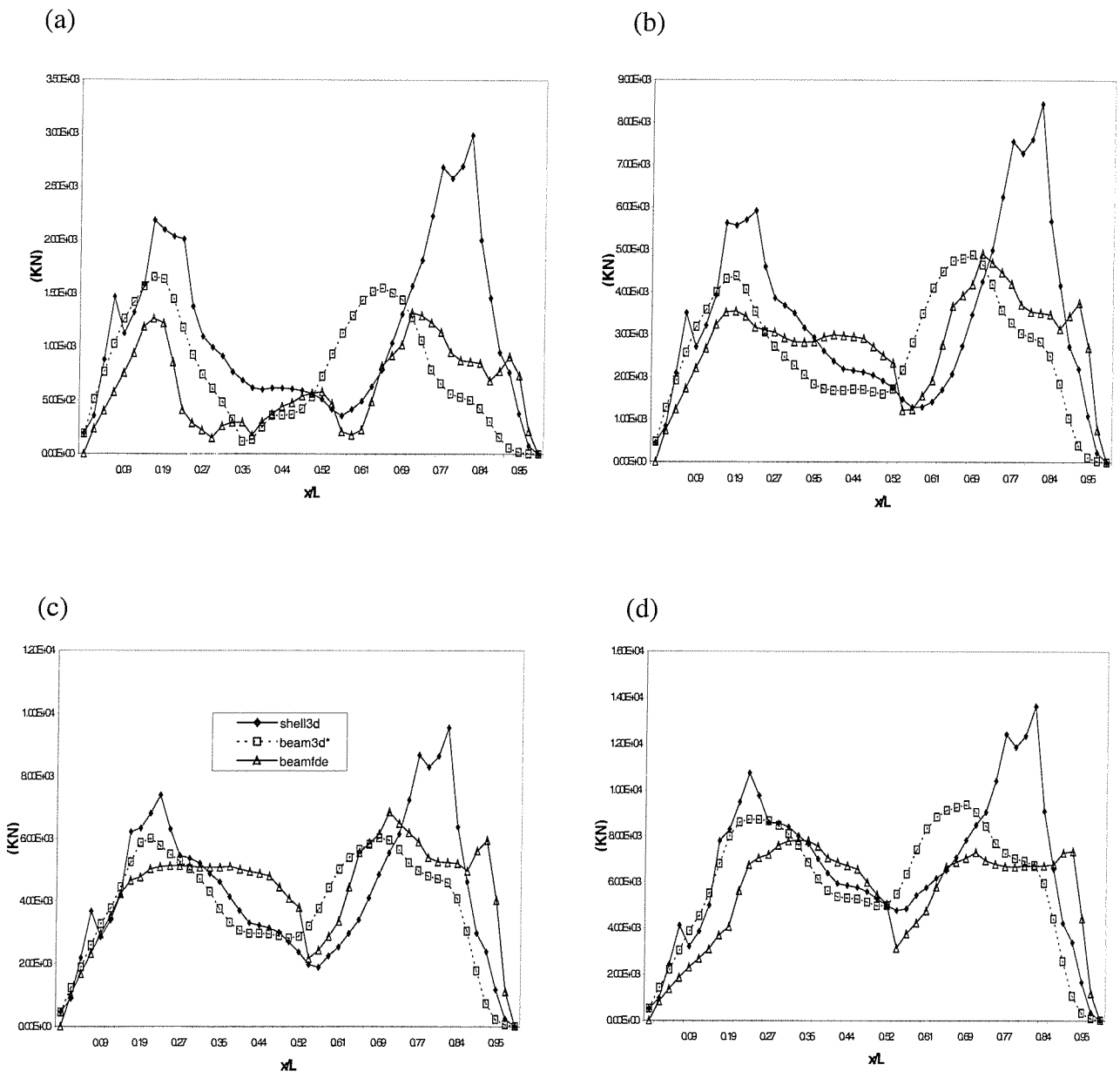

Fig. 6.25 Variation of vertical shear forces (kN) along the ship obtained from models beamfde, beam3d* and shell3d for a variety of headings – ($L/\lambda = 1.0$, $\overline{U} = 7.463$m/s) – (a) 90^0; (b) 120^0; (c) 135^0; (d) 180^0.

(a)

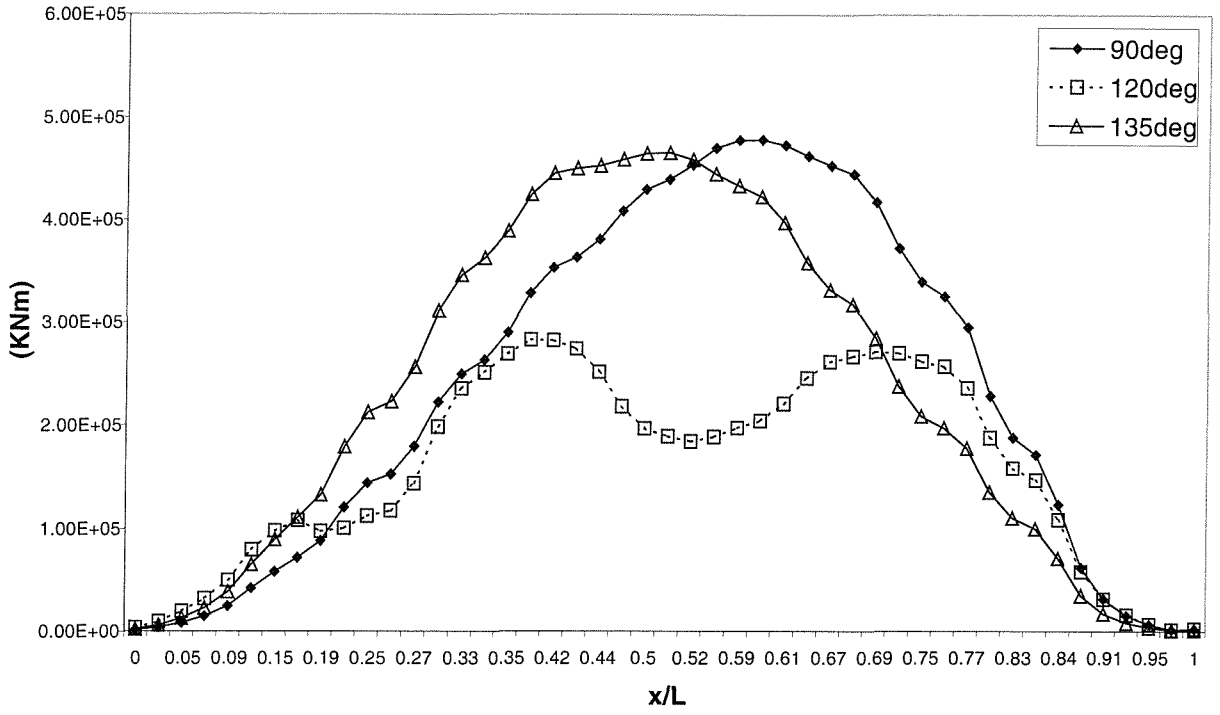

(b)

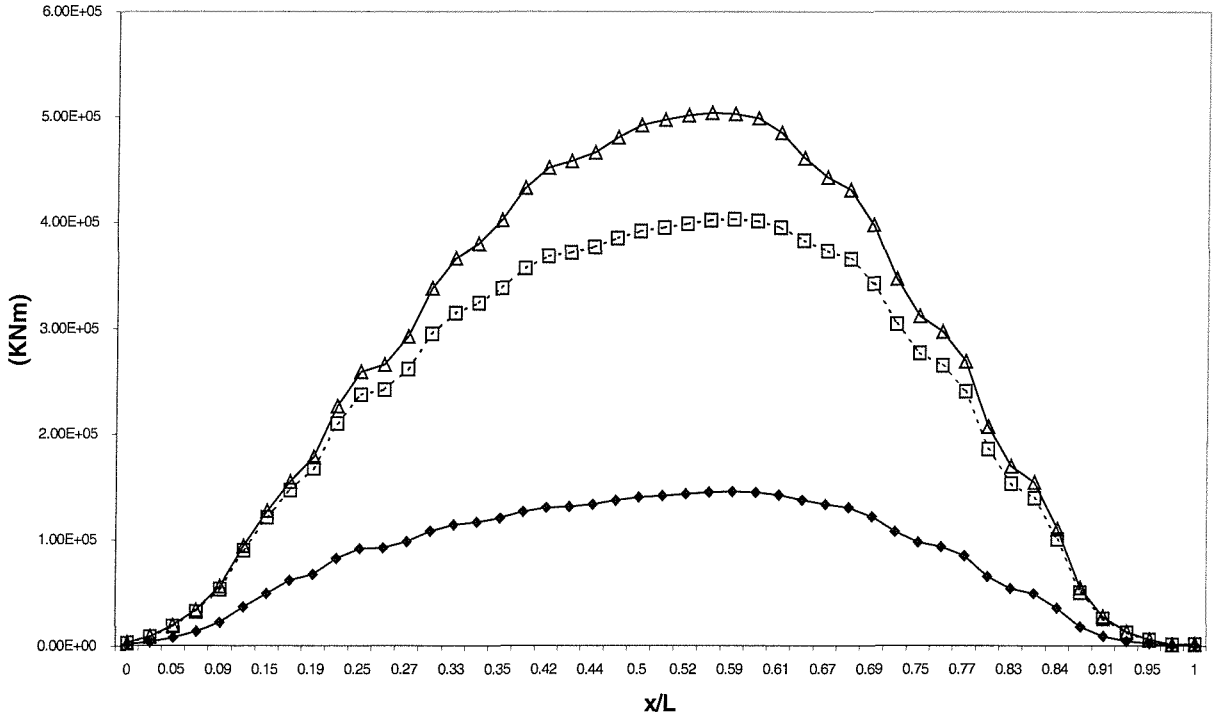

Fig. 6.26 Variation of vertical bending moments (kNm) along the ship obtained at forward speed $(\overline{U})$ of 7.463m/s from model shell3d (a) $L/\lambda = 0.5$; (b) $L/\lambda = 1.0$;

(a)

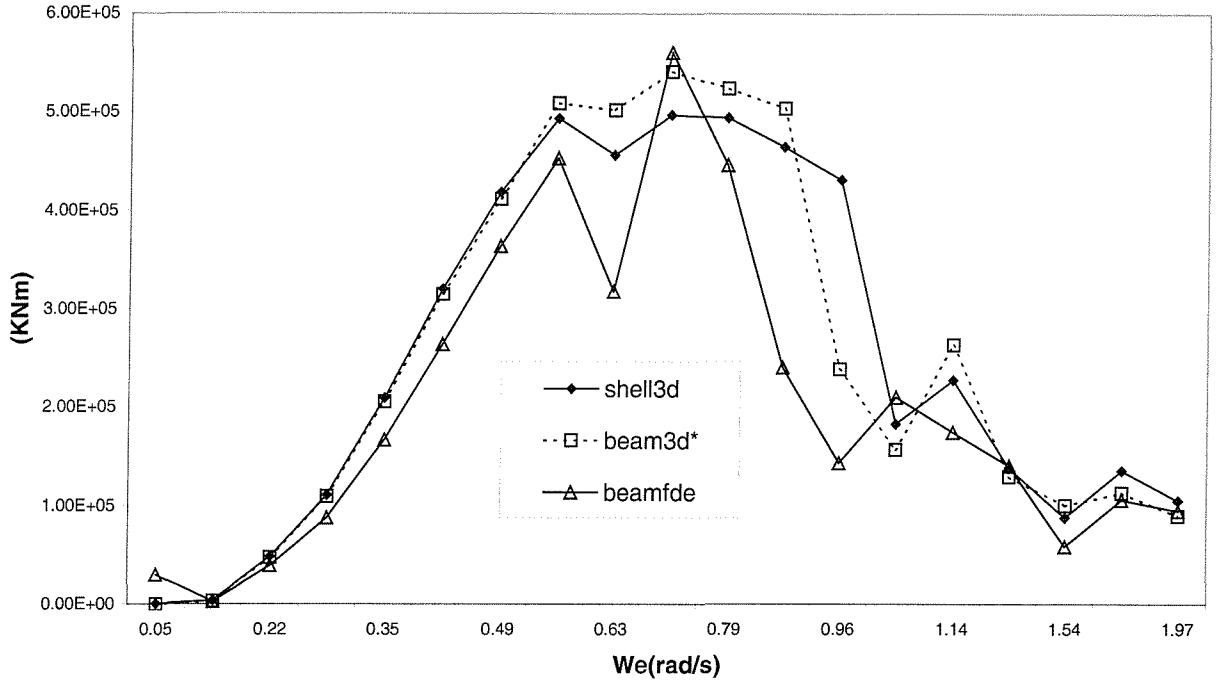

(b)

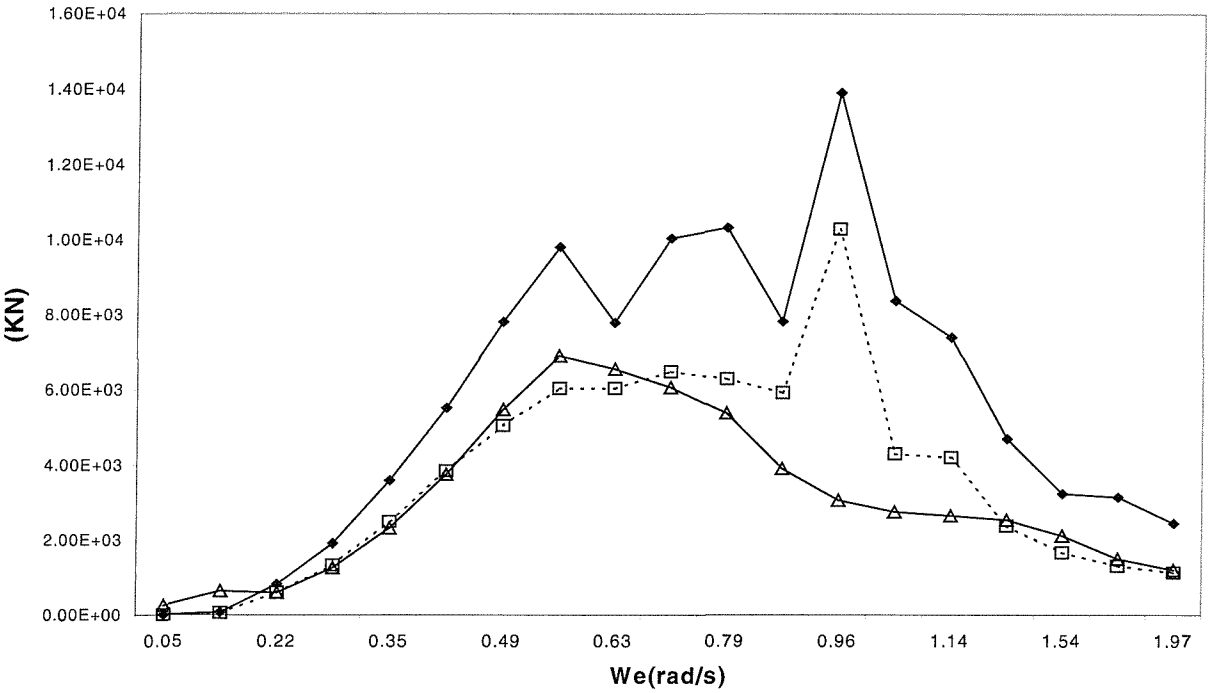

Fig. 6.27 Variation of symmetric dynamic loads with respect to wave encounter ($\overline{U}$=7.463m/s,χ=135^0) for all models (a) Vertical bending moment (kNm); (b) Vertical shear force (kN).

(a)

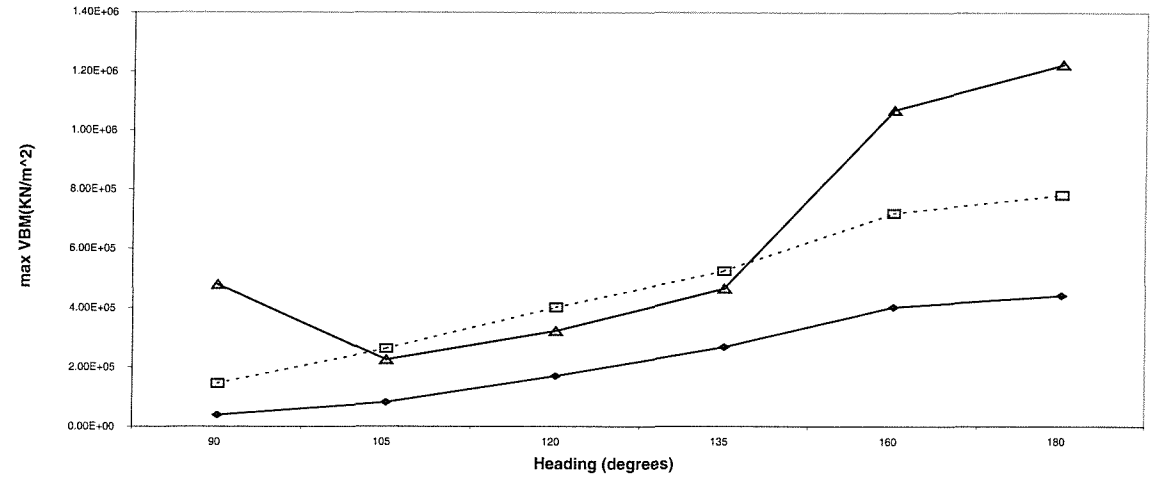

(b)

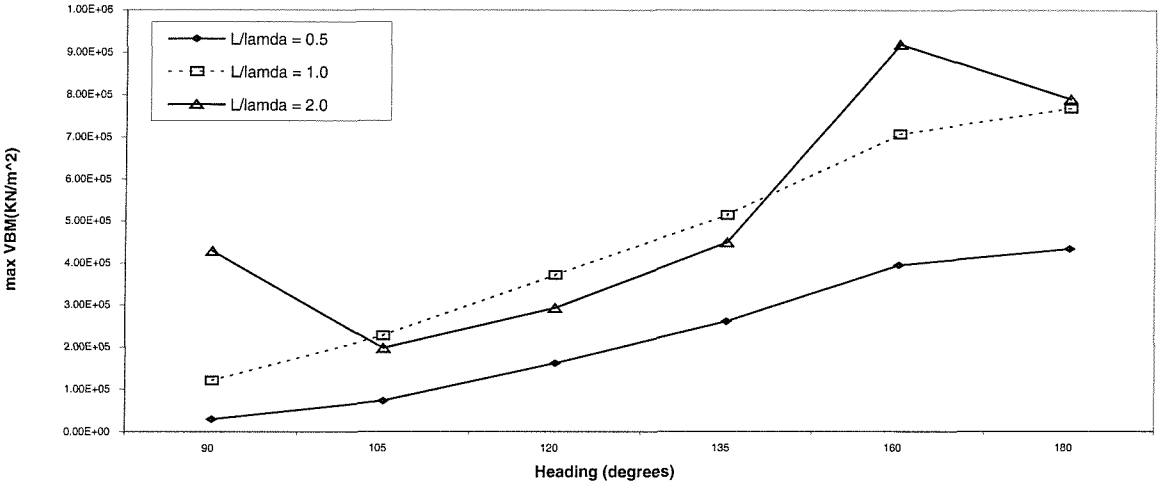

(c)

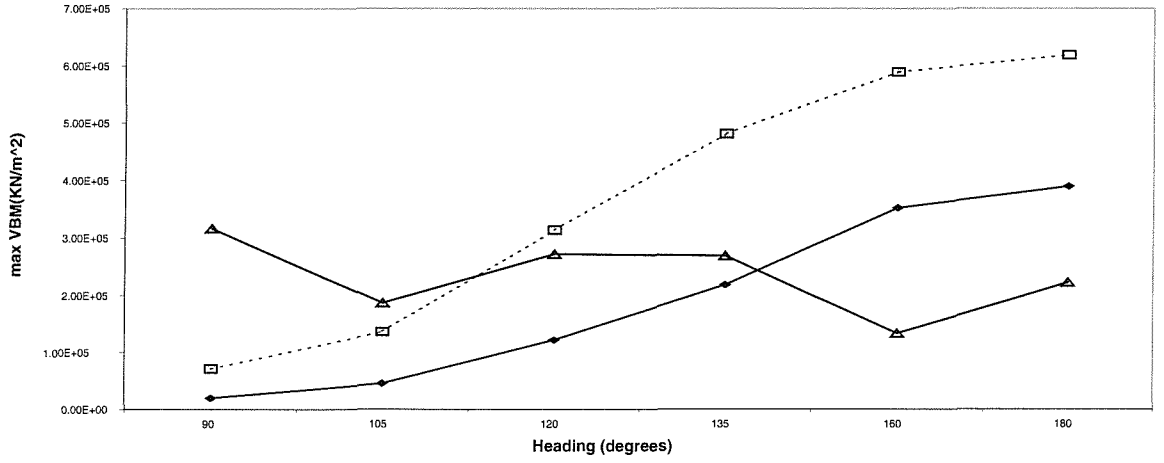

Fig. 6.28 Variation of maximum vertical bending moment amplitudes (kNm) obtained at forward speed $(\overline{U})$ of 7.463m/s for alternative wavelength ratios (a) shell3d; (b) beam3d*; (c) beamfde.

(a)

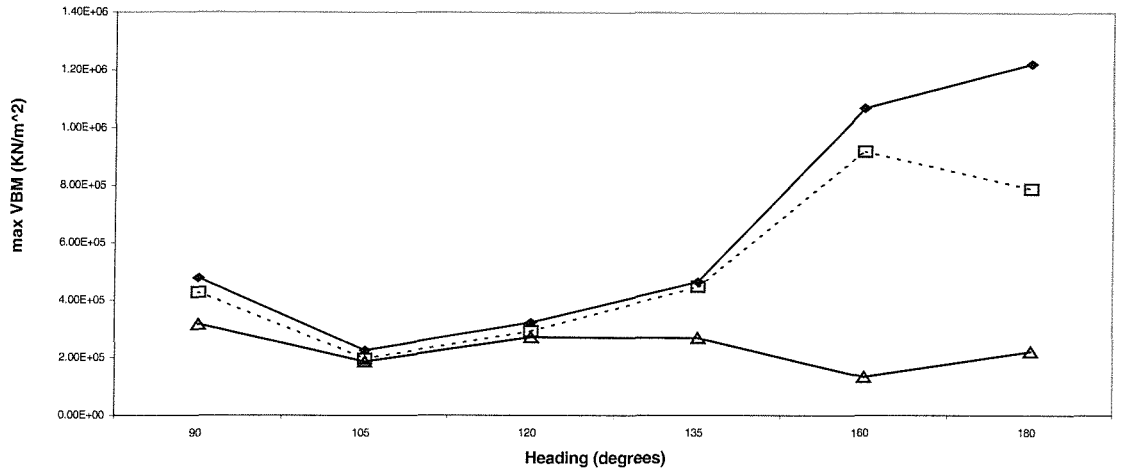

(b)

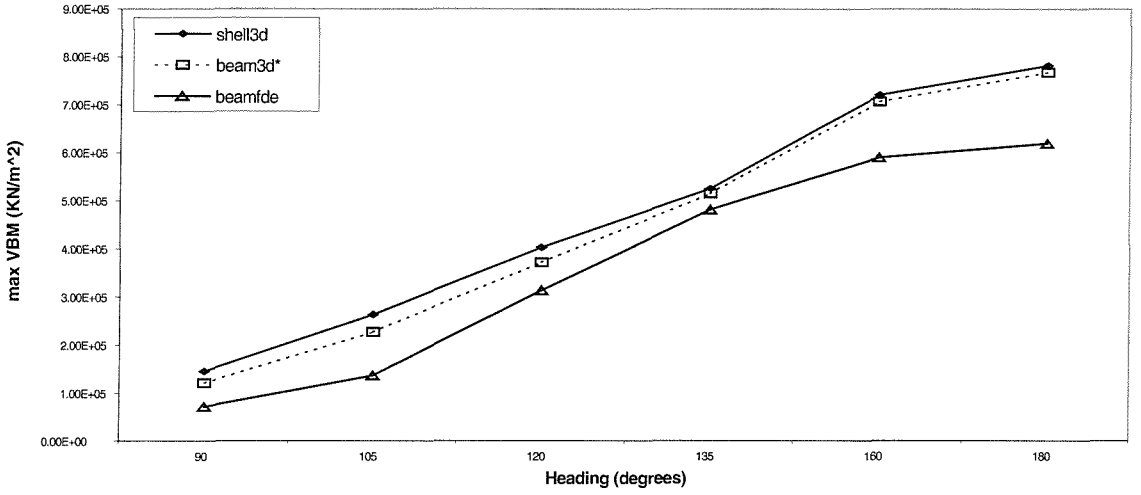

(c)

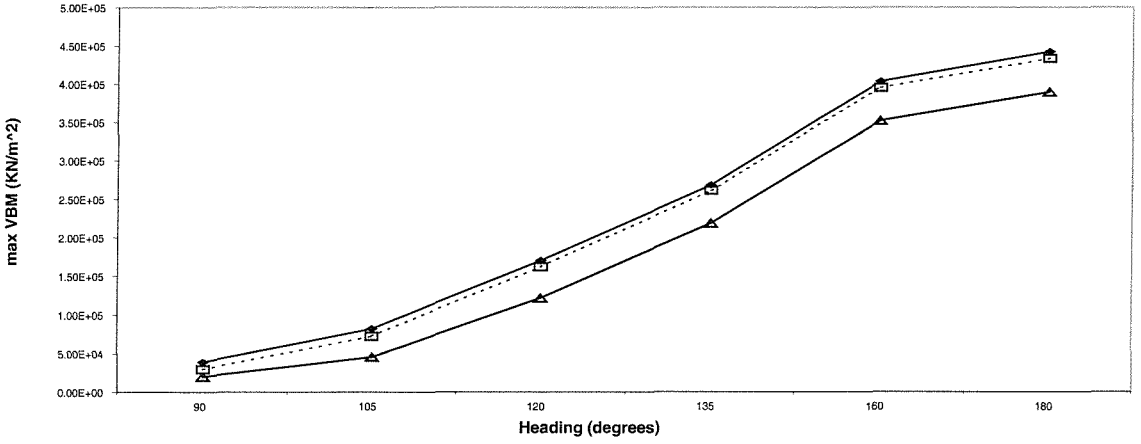

Fig. 6.29 Comparison of the variation of maximum vertical bending moment amplitudes (kNm) obtained at forward speed $(\overline{U})$ of 7.463m/s for alternative models (a) L/λ = 0.5; (b) L/λ=1.0; (c) L/λ = 2.0.

For the antisymmetrically induced dynamic loads (horizontal bending moments, horizontal shear forces and torsional moments) 4 of the eight modes contribute to the final loading. For unit ship-length to wavelength aspect ratio the agreement is not as good between the variations obtained from model shell3d and predictions from beam models (beamfde,beam3d*), the latter being, in general, considerably larger in the vicinity of amidships (see figures 6.30,6.31 and 6.32). This result is expected, since in dry analysis it has been observed that the modal horizontal bending moment magnitudes predicted by the Timoshenko beam idealisation are significantly overestimating the shell3d predictions possibly due to their lack of ability to model the non-prismatic characteristic of the ship structure whilst accounting for the effects of warping (see section 5.5). In addition to that it is worthwhile mentioning that in beam waves the beam3d* approach produces higher horizontal bending and torsional moment amplitudes, since the principal coordinates predicted by the pulsating source methodology are higher than those predicted by beamfde idealisation for horizontal bending dominant modes (see figure 6.17). The big difference of between beam3d and beamfd horizontal bending moments at 135^0 (see figure 6.30(c)) is somehow coincidental and also related to the behaviour of principal coordinates at lower encounter frequency levels (see figures 6.17 to 6.20). Also, from figures 6.30 to 6.32 it becomes evident that irrespective of the model used maximum antisymmetric dynamic loads are observed at 135^0 heading and then gradually decrease becoming eventually zero at head seas. This mirrors the behaviour of the antisymmetric principal coordinates (see section 6.6.2). For bow quartering seas beam3d* idealisation produces higher estimates than beamfde. At beam seas, however, where the effects of roll motion are even more important, this trend is reversed following once more the trend of the principal coordinates of torsion dominant modes (see figure 6.18). Similar parametric study to the one performed for the vertical plane wave induced dynamic loads has shown that maximum horizontal bending moment corresponds to ships' length over wavelength ratio 2.0 with minimum wave induced bending moments appearing at $L/\lambda=0.5$ (see figures 6.34,6.35). As a further comparison, the variation of the wave-induced direct stresses on the deck (junction with side plating) and keel (centre line) are shown in figures 6.36, 6.47 for $L/\lambda=1$. The stresses from the three-dimensional model shell3d were calculated including and excluding the antisymmetric mode shapes, to investigate their contributions. The results were compared against the corresponding direct stresses from the beam idealisation which were evaluated at the keel and deck of the ship's structure by means of

equation (3.41) (i.e. by considering only symmetric modes contributions). The antisymmetric modes contribute negligibly to the stresses on the keel centre line. Nevertheless, they have a significant contribution to the direct stresses obtained at the junction of deck and side plating. The differences observed between two- and three-dimensional direct stresses at keel and deck (see figure 6.36) are similar to those observed for the vertical bending moment in figure 6.24.

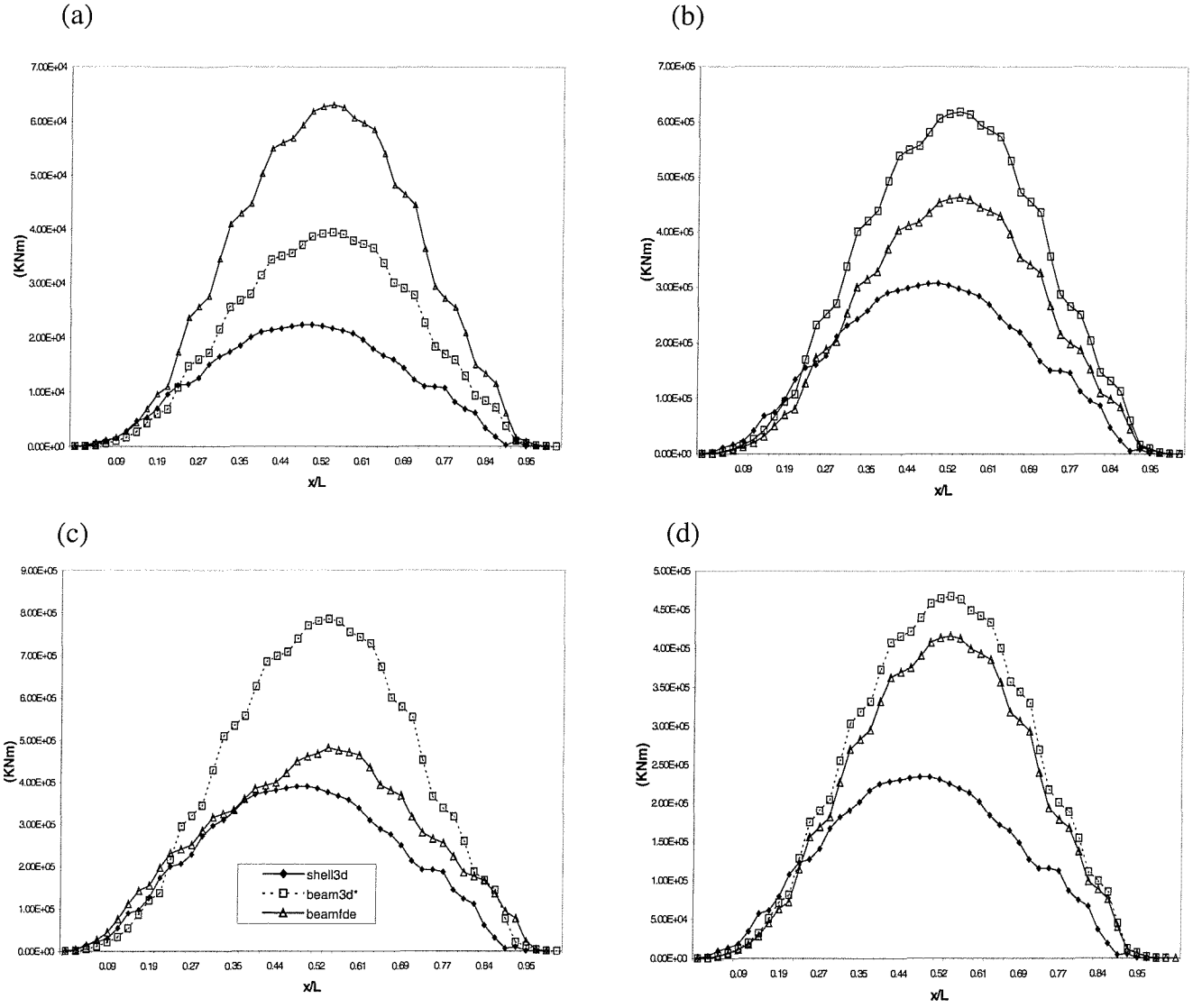

Fig. 6.30 Variation of horizontal bending moments (kNm) along the ship obtained from models beamfd, beam3d* and shell3d for a variety of headings – ($L/\lambda = 1.0$, $\overline{U} = 7.463$m/s) – (a) 90^0; (b) 120^0; (c)135^0; (d)160^0.

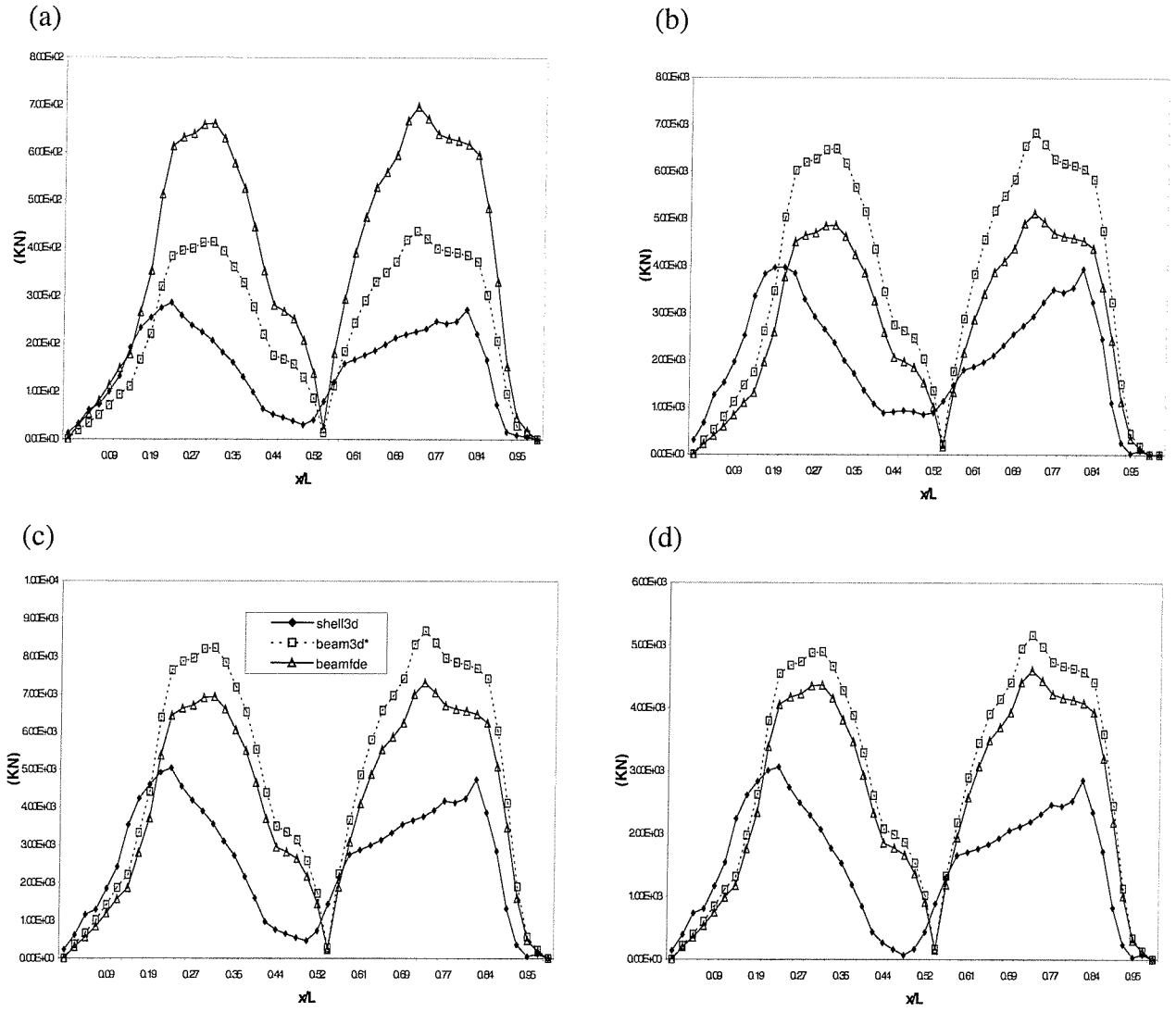

Fig. 6.31 Variation of horizontal shear forces (kN) along the ship obtained from models beamfd, beam3d* and for a variety of headings – ($L/\lambda = 1.0$, $\overline{U} = 7.463$m/s) – (a) 90^0; (b) 120^0; (c)135^0; (d)160^0.

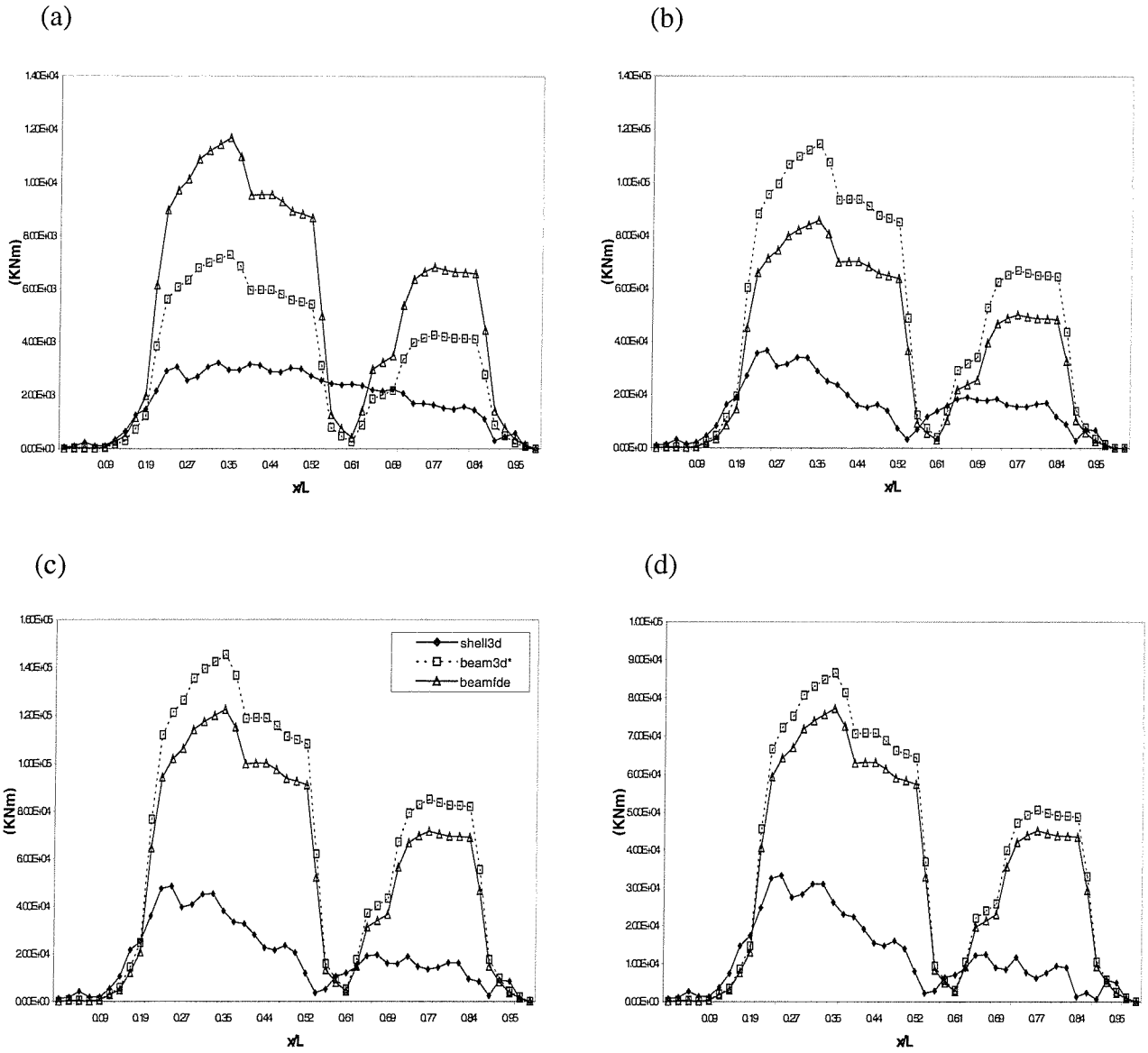

Fig. 6.32 Variation of torsional moments (kNm) along the ship obtained from models beamfd, beam3d* and shell3d for a variety of headings – ($L/\lambda = 1.0$, $\overline{U} = 7.463$m/s) – (a) 90^0; (b) 120^0; (c)135^0; (d)160^0.

(a)

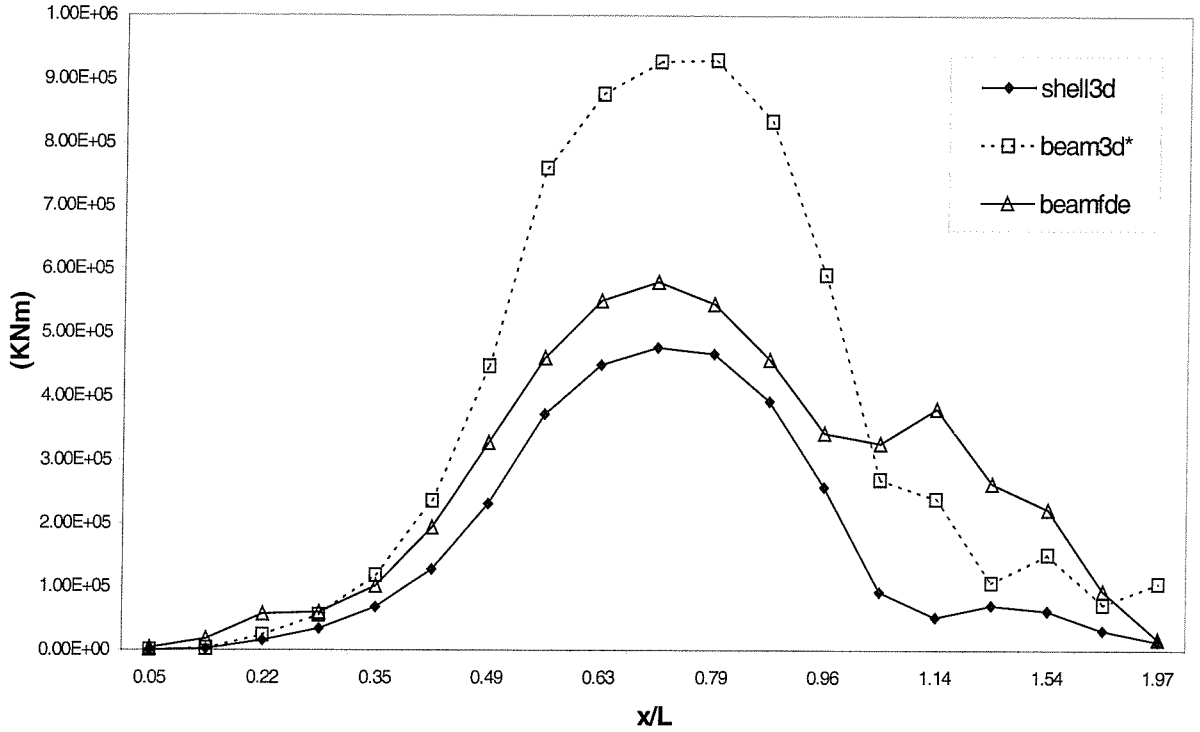

(b)

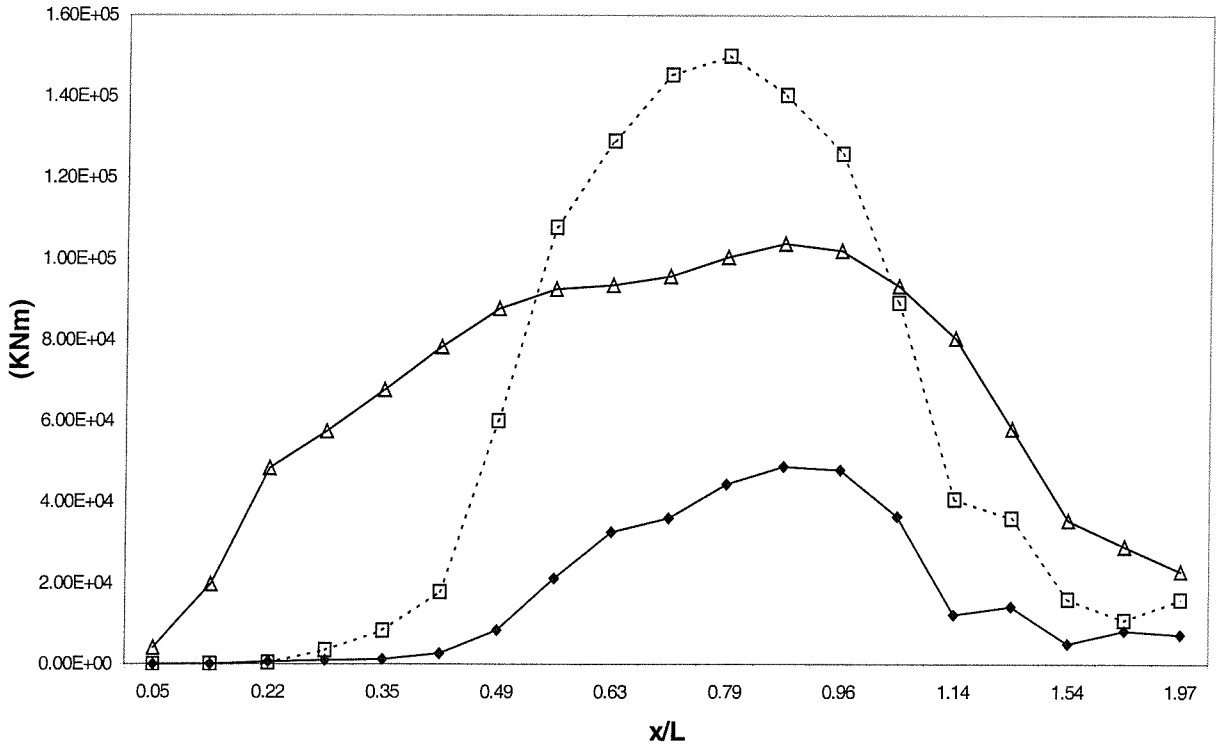

Fig. 6.33 Variation of antisymmetric dynamic loads along the ship ($\overline{U}$=7.463m/s,χ=135^0 L/λ=1.0) for all models (a) horizontal bending moment (kNm); (b) torsional moment (kNm).

(a)

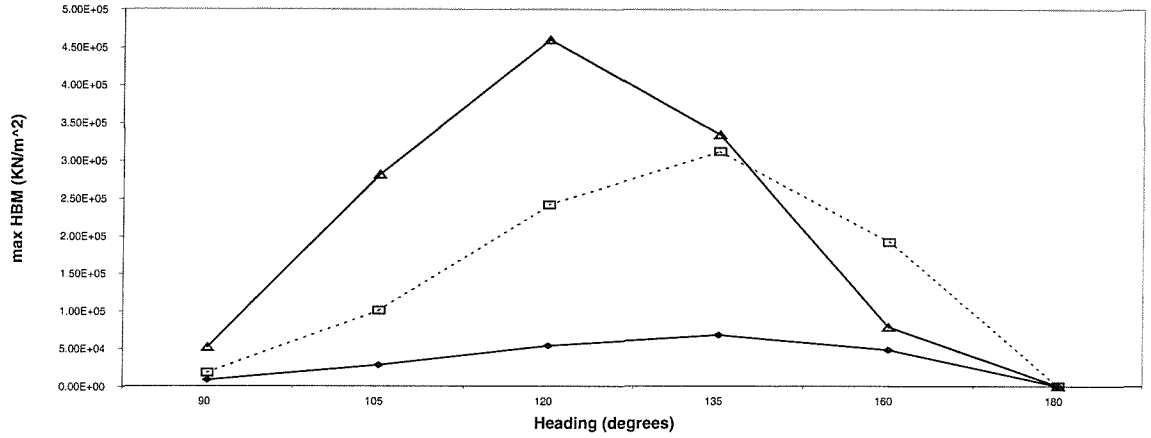

(b)

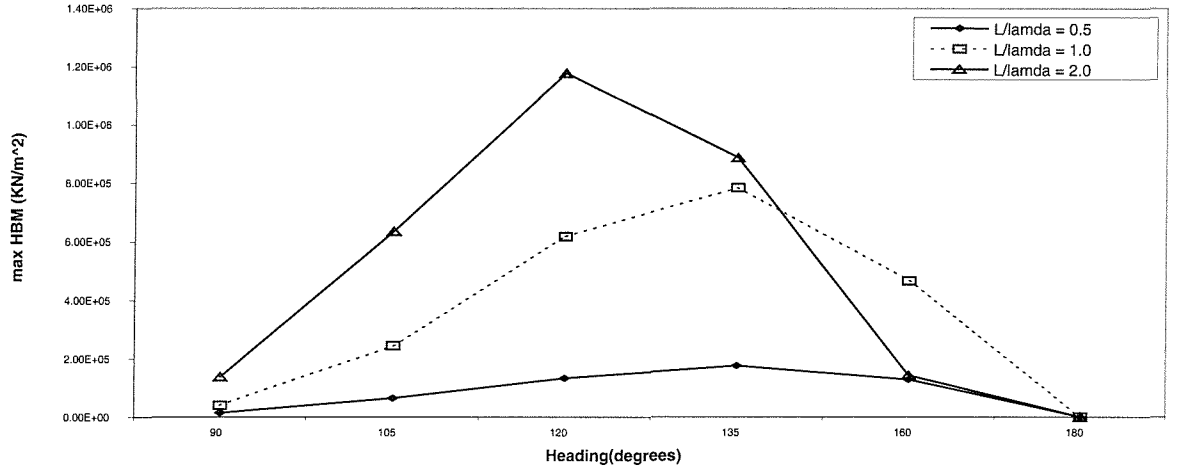

(c)

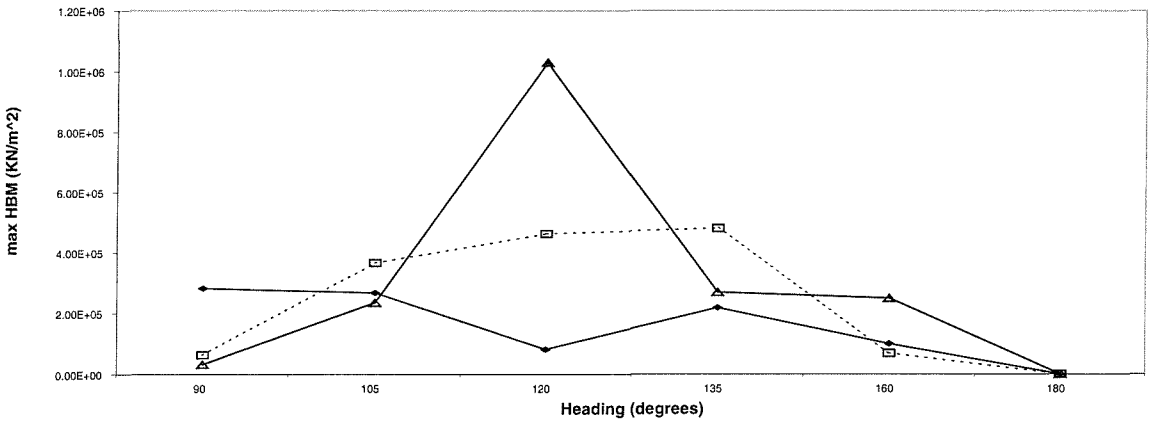

Fig. 6.34 Variation of maximum horizontal bending moments (kNm) obtained at forward speed of 7.463m/s for alternative wavelength ratios (a) shell3d; (b) beam3d*; (c) beamfde.

(a)

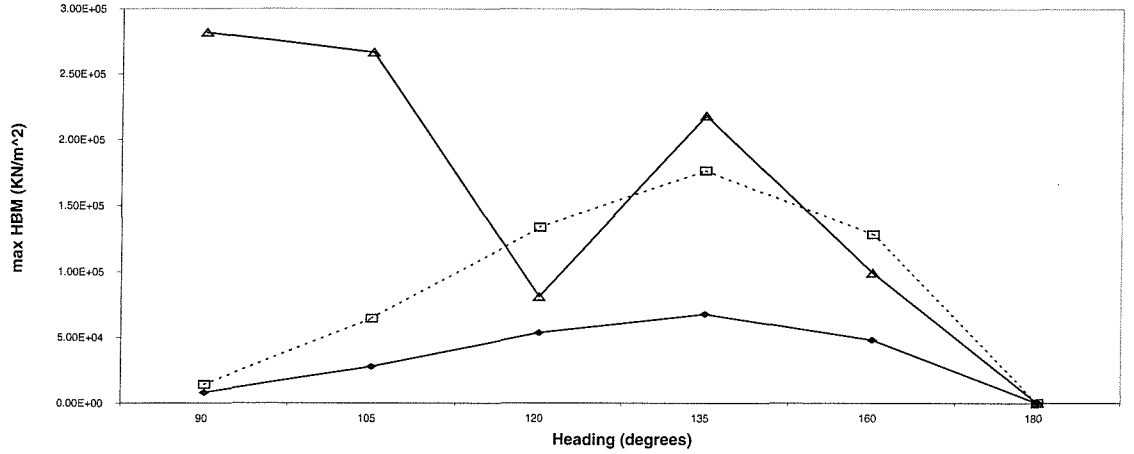

(b)

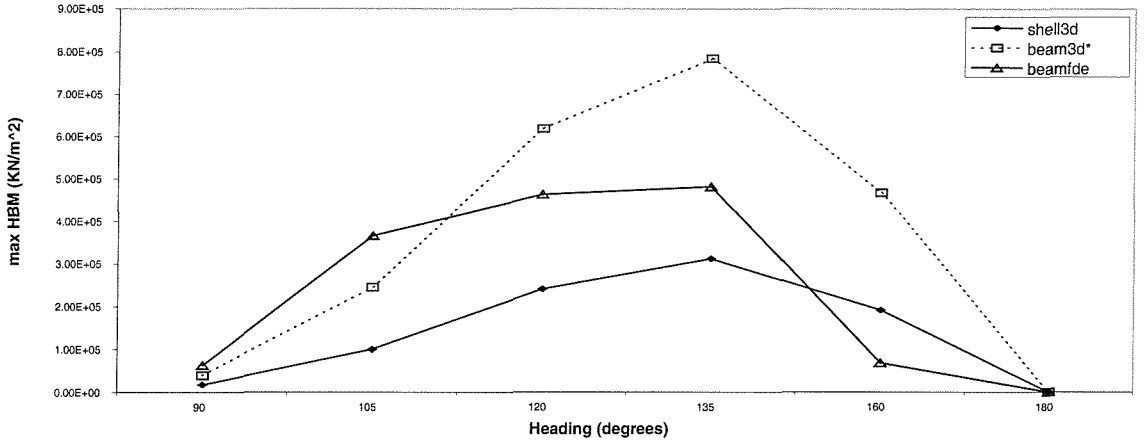

(c)

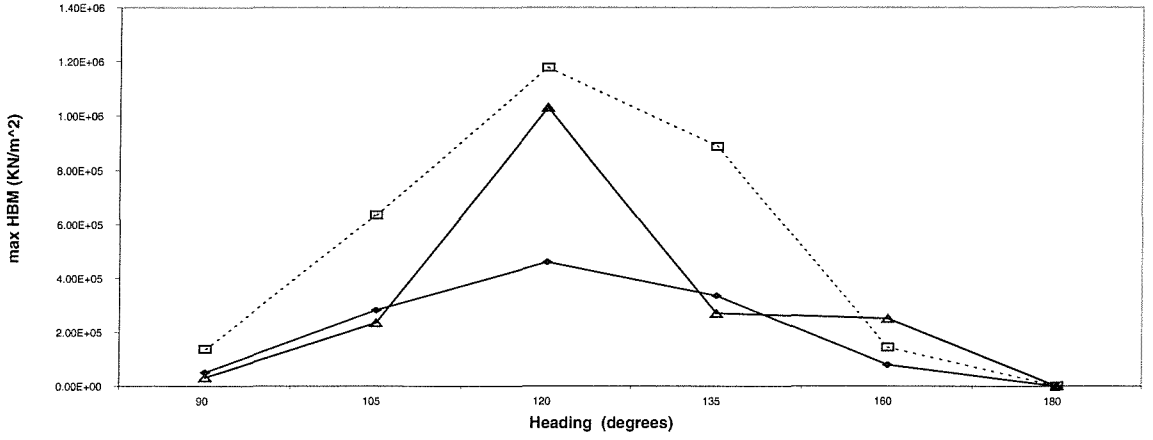

Fig. 6.35 Comparison of the variation of maximum horizontal bending moments (kNm) obtained at forward speed of 7.463m/s for alternative models (a) $L/\lambda = 0.5$; (b) $L/\lambda=1.0$; (c) $L/\lambda = 2.0$.

(a)

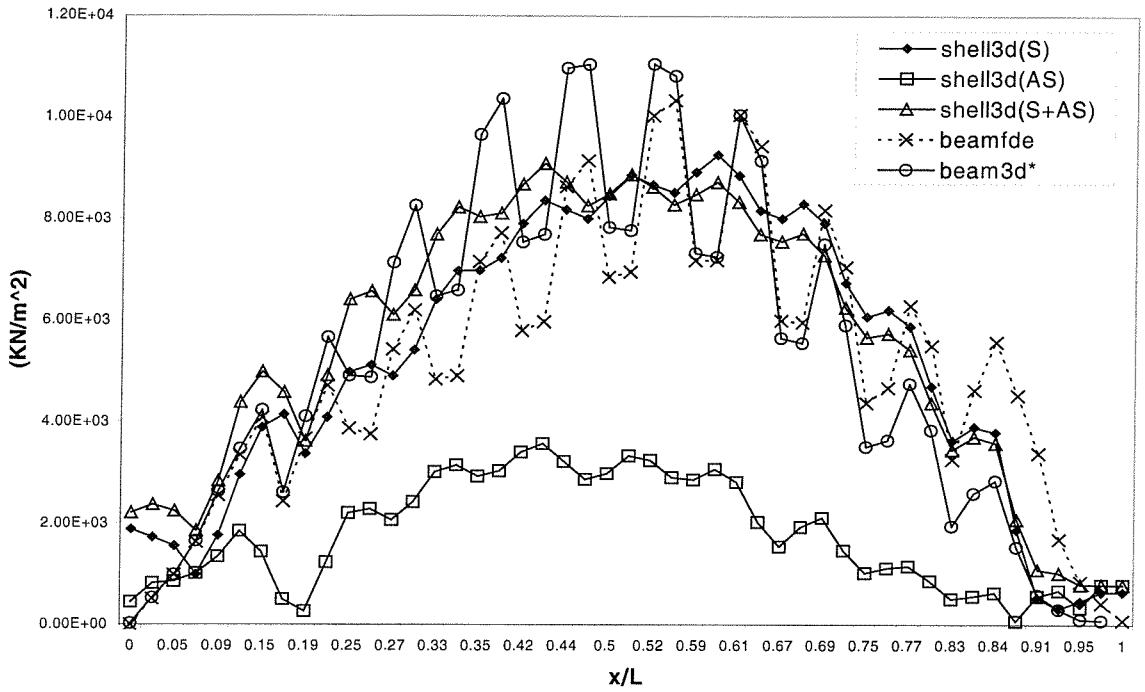

(b)

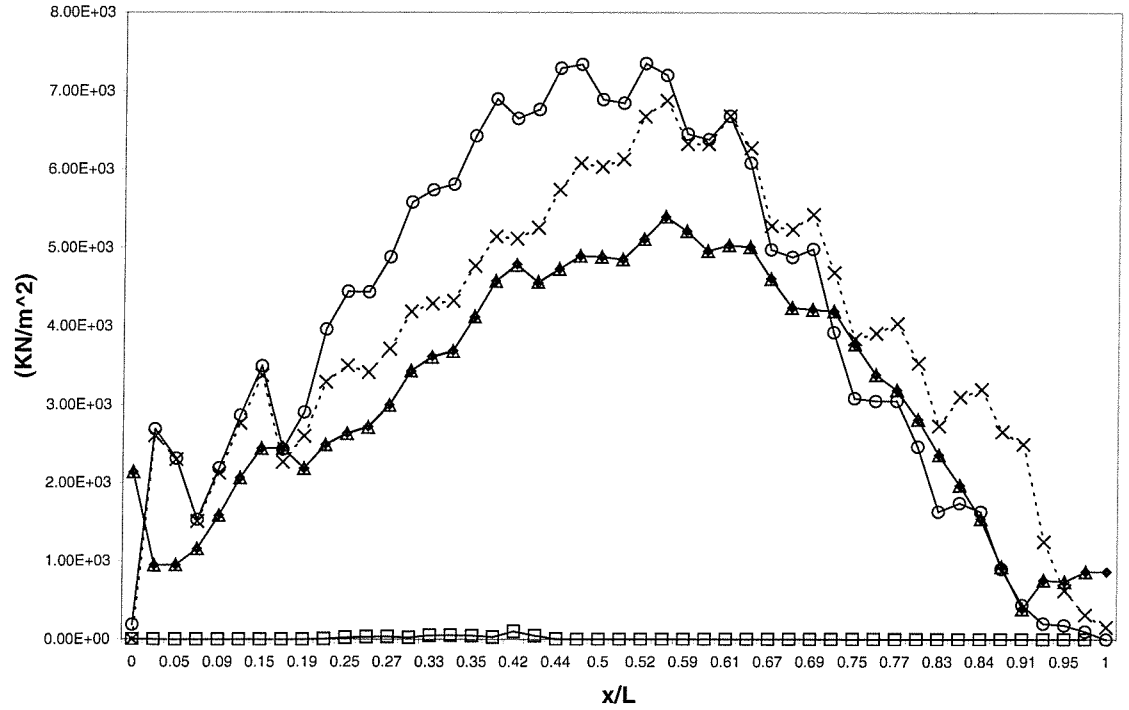

Fig. 6.36 Longitudinal direct stress variations (kN/m^2) along the ship obtained from models beamfd, beam3d* and shell3d when symmetric only (S), symmetric and antisymmetric (S+AS), antisymmetric only (AS) modal stresses are considered ($L/\lambda = 1.0, \overline{U} = 7.463$m/s, $\chi = 135^0$) (a) Direct stress along deck-side junction; (b) Direct stress along keel centerline.

6.8 Further applications

The results predicted from the two- and three-dimensional flexible fluid-structure interaction idealisations presented so far have indicated that the unified hydroelasticity theory can model the steady state dynamic behaviour of a bulker's hull by means of stresses and bending moments. The remaining part of the analysis therefore will be concentrated upon examining the effects of various operational conditions (e.g. incident wave frequency and heading at alternative forward speed levels), the effects of damping as well as the influence of alternative structural configurations on the hull girder strength.

6.8.1 The effects of damping

As expected, the effect of damping on principal coordinates is simply to reduce their resonant magnitude irrespective of the type of idealisation. Figure 6.37 clearly demonstrates this effect for the first symmetric and first antisymmetric response of the vessel. The effect of damping in the amplitude of dynamic response appears to be more significant for the first antisymmetric mode where the structural damping factor is significantly higher (ξ=0.01) than the one used for the symmetric distortions (ξ=0.002) (see table 6.4). Similar type of dynamic response is observed for the higher modes of vibration. Irrespective to the type of idealisation and ship length to wavelength ratio bending moments outside resonances associated with distortions do not appear to change, their trends and magnitudes for alternative headings and wavelengths being identical to those presented in section 6.6.

6.8.2 The effects of operational conditions

The effects of forward speed, upon the dynamic response and strength of the vessel were further explored. Three different forward speed levels were examined, namely $\overline{U}_A$ = 5.0m/s (Fn=0.093), $\overline{U}_B$ = 7.463m/s (Fn=0.138), $\overline{U}_C$ = 9.0m/s (Fn=0.167). As it can be identified from the observed peaks of the principal coordinates, change of the speed level leads to small alteration of the resonant frequencies with corresponding change of the principal coordinate amplitude. Tables 6.8(a),(b),(c) and 6.9(a),(b),(c) illustrate the resonant encounter for alternative speed levels for symmetric and antisymmetric motion respectively. Figure 6.38 illustrates the effects on the rigid body motion related resonant amplitudes for the first symmetric and antisymmetric responses for all three models (similar effects are observed for the frequency domain response of higher

modes). In general, increase of speed leads to increase of the wet encounter with corresponding increase of the principal coordinate amplitude. With increasing speed the magnitude of symmetric and antisymmetric steady state seaway induced dynamic loads is increasing (see figures 6.39 to 6.43). It is quite interesting to note that:

- when the speed is decreasing beamfde and beam3d* antisymmetric dynamic loads are getting closer;
- when the speed is increasing beam3d* and shell3d symmetric loads are getting closer.

6.8.3 The effects of alternative structural configurations

The effects of alternative structural configurations on the prediction of the wave induced dynamic loads were finally explored. Following the extensive dry analyses outlined in chapter 5 (see section 5.7) the hydroelastic behaviour of the bulker was compared against those of an open- and a closed-deck ship (see figures 6.44 to 6.48). All comparisons were performed for bow quartering waves (135^0 heading), unit ship-length to wavelength ratio and speed of 14.5knots (=7.463m/s). Same methodology to the one outlined in section 6.7.3 was followed for the two- and three-dimensional hydroelastic modelling of both open- and closed-deck vessels. Although one can notice differences between various idealisations and structural configurations all FSI models produce very closed symmetric wave induced dynamic loads (see figures 6.43, 6.44). However, the antisymmetrically induced dynamic loads (horizontal bending moments, shear forces and torsional moments) predicted by the alternative beam and shell hydroelastic idealisations do not appear to be in such a good agreement for the models with large deck openings (bulker and open ships) (see figures 6.46(a),(b), 6.47(a),(b), 6.48(a),(b)) where the non-prismatic features of the hull girder (structural discontinuities) are not simulated realistically by the beam idealisations. In this sense, it is clearly demonstrated that:

1. the wave induced dynamic loads predicted by all alternative FSI models map effectively the behaviour of the symmetric wave induced dynamic loads irrespective of the type of structural configuration (i.e. open-deck, closed-deck or bulker vessels);
2. for the case of closed-deck slender monohulls where the effects of coupling are negligible antisymmetric wave induced dynamic loads predicted by two- and three-dimensional FSI models appear to be in good agreement;

3. for the case of long slender monohulls with large deck openings (bulker or open-deck ships) beam FSI models provide not so trustworthy predictions of the antisymmetric wave induced dynamic loads.

6.9 Conclusions

This chapter was focused on the application of the wet analyses module of two- and three-dimensional hydroelasticity theories. Following the dry analyses stage (chapter 5) particular emphasis was paid upon gaining better insight into the hydroelastic behaviour of a bulker having similar structural and mass properties to those of OBO MV Derbyshire.

Three different flexible fluid-structure interaction models (beamfde, beam3d*, shell3d), incorporating both symmetric and antisymmetric motions and distortions, were successfully used to predict and compare the steady state seaway induced dynamic loads of the bulker in regular waves. For two-dimensional hydroelasticity this was achieved by means of model beamfde (equal spacing beam discretisation). Based on past experience [6.3], for the pulsating source models (beam3d*, shell3d) 952 hydropanels were considered adequate to simulate the wetted surface of the hull.

Eight flexible distortions (4 symmetric and 4 antisymmetric of 2 were horizontal bending dominant and 2 torsion dominant) were shown to be adequate in simulating the response of the bulk carrier hull. Resonant encounter frequencies were obtained for all models at various angles of wave incidence (90^0,120^0,135^0,160^0,180^0), at the typical service speed of 7.463m/s (Fn=0.138) and they were found to be in good agreement. The one node longitudinal mode was excluded form the hydroelastic calculations since; (a) despite being a symmetric mode, it does not produce any bending moment in beam3d idealisation; (b) although in shell3d model this mode is coupled with vertical bending, it does not affect the vertical bending moment magnitude.

Principal coordinates and wet encounters calculated for beam3d* and shell3d idealisations are relatively close for all modes. These differ from the principal coordinates of the beamfde model, which show similar trend but lower amplitudes. The differences could be attributed (i) to the alternative wet analysis methodology followed in two-dimensional hydroelasticity, which is

based on a strip theory approach, rather than the potential flow analysis employed by the three-dimensional form of the method; (ii) the relative slenderness of the hull (length to beam ratio 6.68) and (iii) the incapability of Timoshenko beam theory to model, in antisymmetric motion, the non-prismatic features of the bulk carrier hull realistically. The latter problem of course is related to the compatibility of the modal characteristics rather to the wet analysis (see chapter 5). In general the agreement for different idealizations could be considered as being good for symmetric or horizontal bending dominant antisymmetric responses but not so good for the antisymmetric torsion dominant ones.

It was confirmed that the largest magnitude corresponds to the 2 node symmetric mode and much smaller responses are obtained for the subsequent symmetric and antisymmetric modes.

As expected the maximum response for the symmetric two node mode is obtained for head waves, then gradually diminishes as the angle decreases to 90 degrees (beam seas). The principal coordinate corresponding to the 2-node horizontal bending mode is nil for head waves and then grows gradually in magnitude, reaching its maximum at 135^0 heading. The 1 node torsion mode principal coordinate is nil for head waves, then gradually increases reaching its maximum at a heading of 135^0 and once more it is decreasing as the heading angle approaches beam seas.

Longitudinal direct stresses along the deck edge and bottom of the ship's structure were evaluated and compared for all models (beamfde, beam3d*, shell3d) at head ($\chi=180^0$) and bow quartering waves ($\chi=120^0,135^0$). In two-dimensional hydroelasticity analysis, direct wet stresses were calculated indirectly from vertical bending moments (see equation (3.41)), while in three-dimensional hydroelasticity the corresponding stress components were evaluated as modal summations of the longitudinal stresses produced by the symmetric or antisymmetric distortions of the shell finite element model (see sections 3.7 and 6.5). From the analyses it became apparent that maximum stresses are observed along the deck edge of the vessel for head waves and then gradually decrease. This mirrors the behaviour of the symmetric principal coordinates. The contribution of antisymmetric modes to direct stress at the bottom (center plane of symmetry) of shell3d was shown to be negligible.

(a)

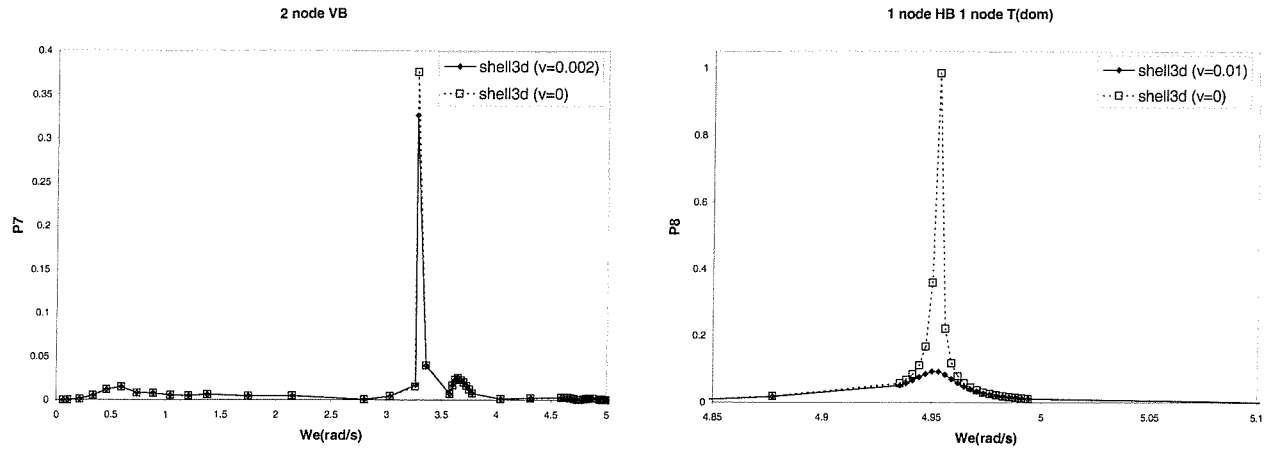

(b)

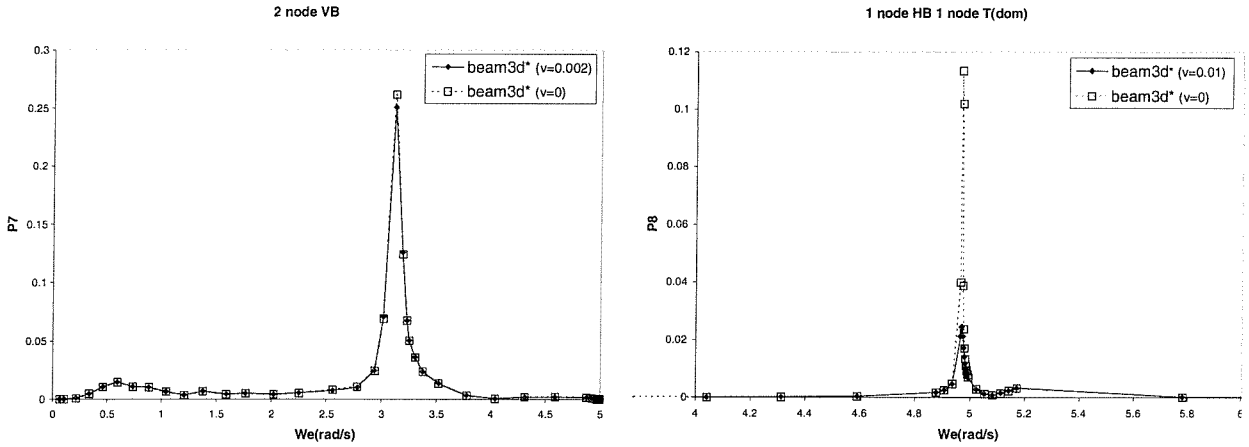

(c)

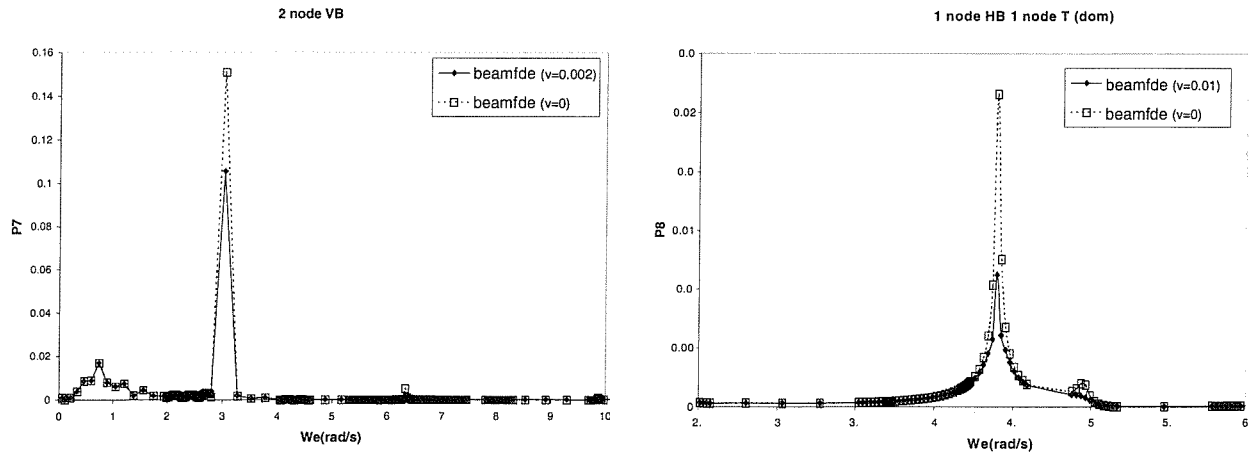

Fig. 6.37 Illustration of the effects of damping on the dynamic response of all idealisations for first symmetric (2 node vertical bending) and first antisymmetric (1 node horizontal bending 1 node torsion dominant) flexible modes (χ=120^0, $\overline{U}$ = 7.463m/s) (a) shell3d; (b) beam3d*; (c) beamfde.

Mode type	beamfde		beam3d*		shell3d	
(a) $\overline{U}_A$ = 5m/s	Dry (ω_r)	Wet (ω_{er})	Dry (ω_r)	Wet (ω_{er})	Dry (ω_r)	Wet (ω_{er})
2 node VB (r=7)	4.42	3.02	4.50	3.10	4.53	3.23
3 node VB (r=10)	9.25	6.37	9.07	6.28	9.01	5.60
4 node VB (r=13)	14.24	9.88	13.74	9.70	13.24	10.07
5 node VB (r=14)	17.62	12.93	17.11	12.63	15.92	12.58

Mode type	beamfde		beam3d*		shell3d	
(b) $\overline{U}_B$ = 7.463m/s	Dry (ω_r)	Wet (ω_{er})	Dry (ω_r)	Wet (ω_{er})	Dry (ω_r)	Wet (ω_{er})
2 node VB (r=7)	4.42	3.03	4.50	3.11	4.53	3.25
3 node VB (r=10)	9.25	6.39	9.07	6.29	9.01	6.62
4 node VB (r=13)	14.24	9.90	13.74	9.72	13.24	10.09
5 node VB (r=14)	17.62	12.95	17.11	12.65	15.92	12.61

Mode type	beamfde		beam3d*		shell3d	
(c) $\overline{U}_C$ = 9m/s	Dry (ω_r)	Wet (ω_{er})	Dry (ω_r)	Wet (ω_{er})	Dry (ω_r)	Wet (ω_{er})
2 node VB (r=7)	4.42	3.04	4.50	3.13	4.53	3.27
3 node VB (r=10)	9.25	6.40	9.07	6.31	9.01	6.64
4 node VB (r=13)	14.24	9.90	13.74	9.73	13.24	10.11
5 node VB (r=14)	17.62	12.95	17.11	12.67	15.92	12.60

Table 6.8 Dry natural frequencies and wet resonance of symmetric distortions heading (VB = vertical bending; ω_r = dry natural frequencies; ω_{er} = wet resonance); (a) for forward speed $\overline{U}_A$ = 5m/s (Fn=0.093); (b) for forward speed $\overline{U}_B$ = 7.463m/s (Fn=0.138); (c) for forward speed $\overline{U}_C$ = 9m/s (Fn=0.167).

Mode type	beamfde		beam3d*		shell3d	
(a) $\overline{U}_A$ = 5m/s	Dry (ω_r)	Wet (ω_{er})	Dry (ω_r)	Wet (ω_{er})	Dry (ω_r)	Wet (ω_{er})
1 node HB - 1 node **T** (r=8)	5.15	4.39	5.15	4.9	5.01	4.94
2 node **HB** – 2 node T (r=9)	5.85	4.94	5.85	4.91	5.55	5.00
3 node **HB** – 3 node T (r=11)	10.10	8.69	10.10	9.2	12.63	9.31
2 node HB – 2 node **T** (r=12)	11.13	3.24	11.13	3.24	10.71	9.23

Mode type	beamfde		beam3d*		shell3d	
(b) $\overline{U}_B$ = 7.463m/s	Dry (ω_r)	Wet (ω_{er})	Dry (ω_r)	Wet (ω_{er})	Dry (ω_r)	Wet (ω_{er})
1 node HB - 1 node **T** (r=8)	5.15	4.41	5.15	5.0	5.01	4.95
2 node **HB** – 2 node T (r=9)	5.85	4.96	5.85	5.01	5.55	5.02
3 node **HB** – 3 node T (r=11)	10.10	8.71	10.10	9.3	12.63	9.33
2 node HB – 2 node **T** (r=12)	11.13	3.26	11.13	3.26	10.71	9.25

Mode type	Beamfde		beam3d*		shell3d	
(c) $\overline{U}_C$ = 9m/s	Dry (ω_r)	Wet (ω_{er})	Dry (ω_r)	Wet (ω_{er})	Dry (ω_r)	Wet (ω_{er})
1 node HB - 1 node **T** (r=8)	5.15	4.43	5.15	5.01	5.01	4.97
2 node **HB** – 2 node T (r=9)	5.85	4.98	5.85	5.02	5.55	5.04
3 node **HB** – 3 node T (r=11)	10.10	8.73	10.10	9.5	12.63	9.35
2 node HB – 2 node **T** (r=12)	11.13	3.28	11.13	3.28	10.71	9.27

Table 6.9 Dry natural frequencies and wet resonances of antisymmetric distortions (VB = vertical bending; ω_r = dry natural frequencies; ω_{er} = wet resonance); (a) for forward speed $\overline{U}_A$ = 5m/s (Fn=0.093); (b) for forward speed $\overline{U}_B$ = 7.463m/s (Fn=0.138); (c) for forward speed $\overline{U}_C$ = 9m/s (Fn=0.167).

(a)

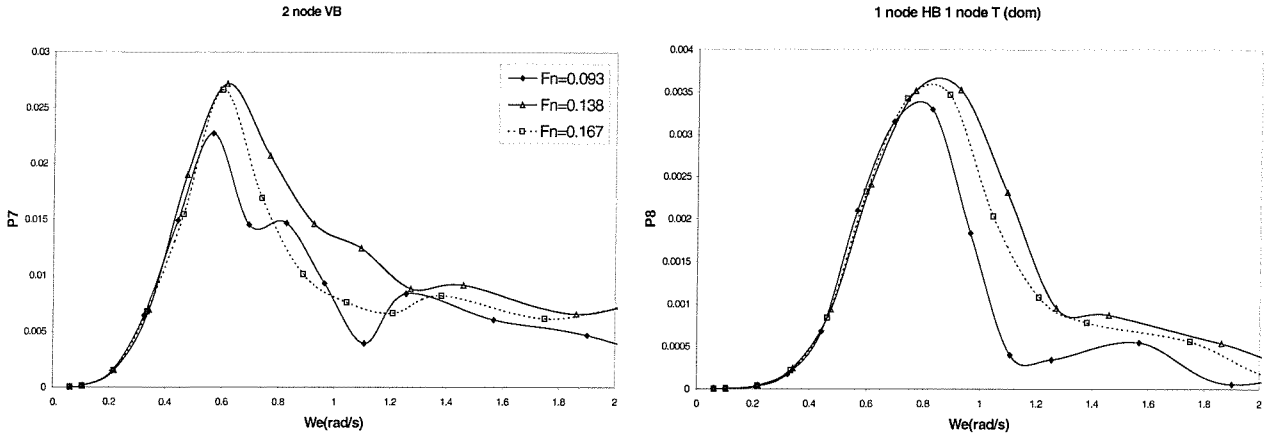

(b)

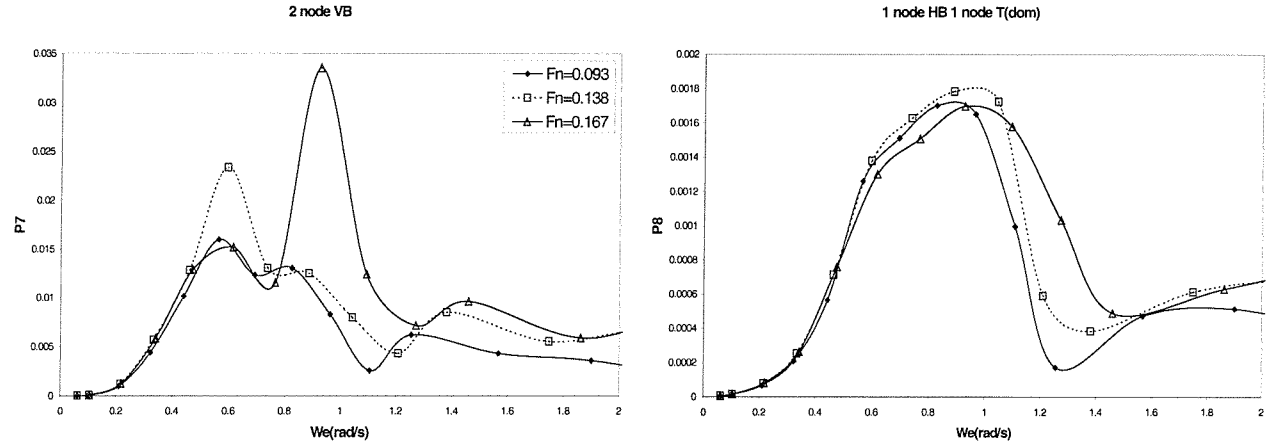

(c)

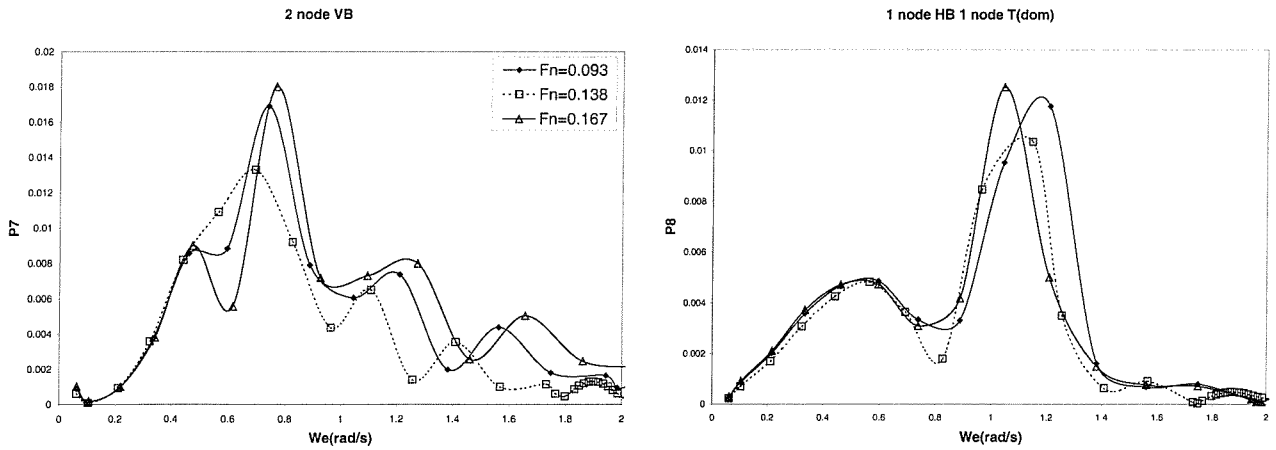

Fig. 6.38 Illustration of the effects of forward speed on the dynamic response of all idealisatons for first symmetric (2 node vertical bending) and first antisymmetric (1 node horizontal bending 1 node torsion dominant) flexible modes (χ=120^0, $\overline{U}$ = 7.463m/s) (a) shell3d; (b) beam3d*; (c) beamfde.

(a)

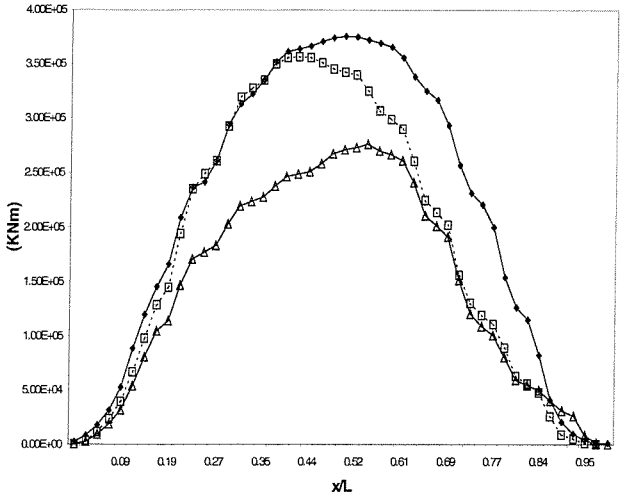

(b)

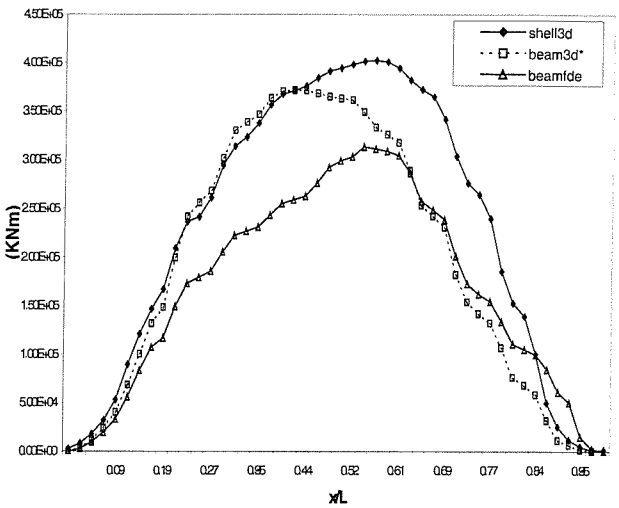

(c)

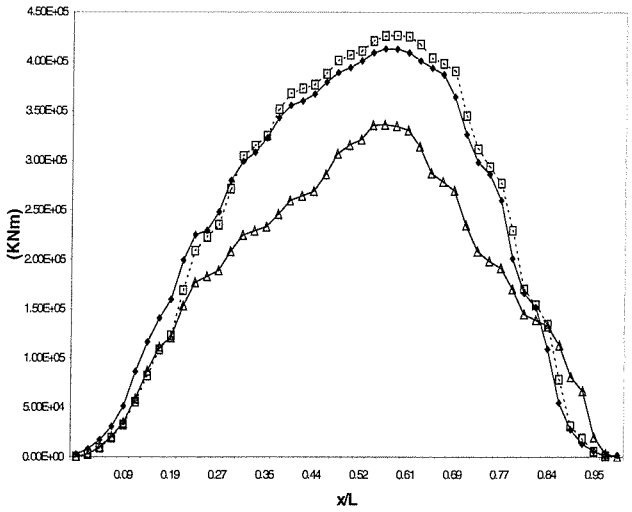

Fig. 6.39 Variation of vertical bending moment at alternative forward speed levels (χ=120^0,L/λ=1.0) – (a) for forward speed $\overline{U}_A$ = 5m/s (Fn=0.093); (b) for forward speed $\overline{U}_B$ = 7.463m/s (Fn=0.138); (c) for forward speed $\overline{U}_C$ = 9m/s (Fn=0.167).

(a)

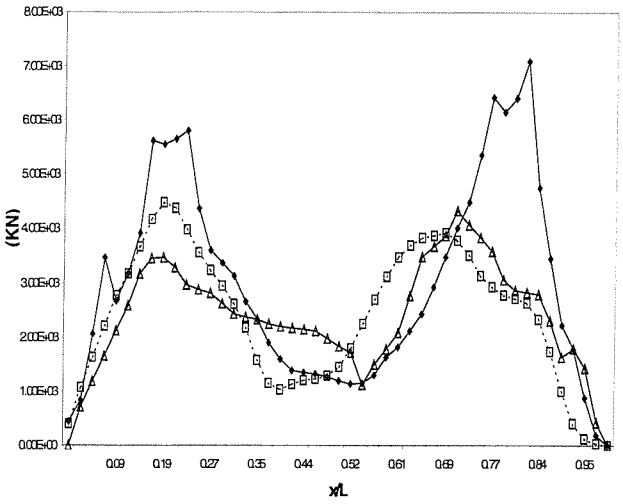

(b)

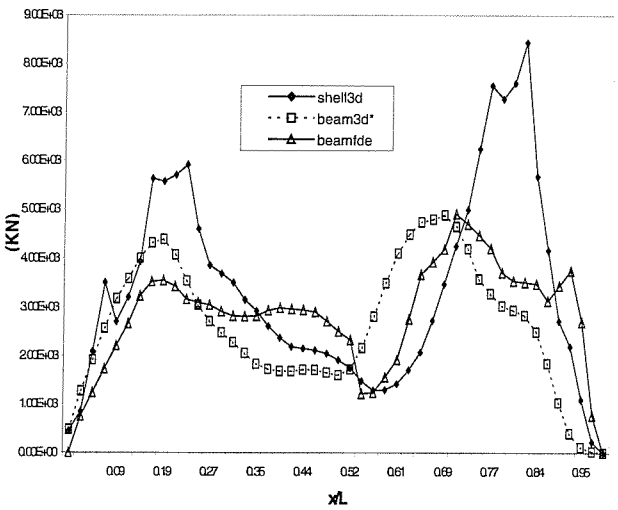

(c)

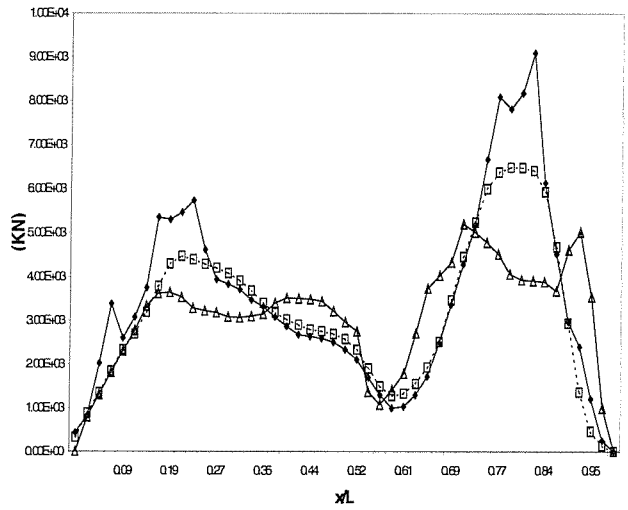

Fig. 6.40 Variation of vertical shear force at alternative forward speed levels (χ=120^0,L/λ=1.0) – (a) for forward speed $\overline{U}_A$ = 5m/s (Fn=0.093); (b) for forward speed $\overline{U}_B$ = 7.463m/s (Fn=0.138); (c) for forward speed $\overline{U}_C$ = 9m/s (Fn=0.167).

(a)

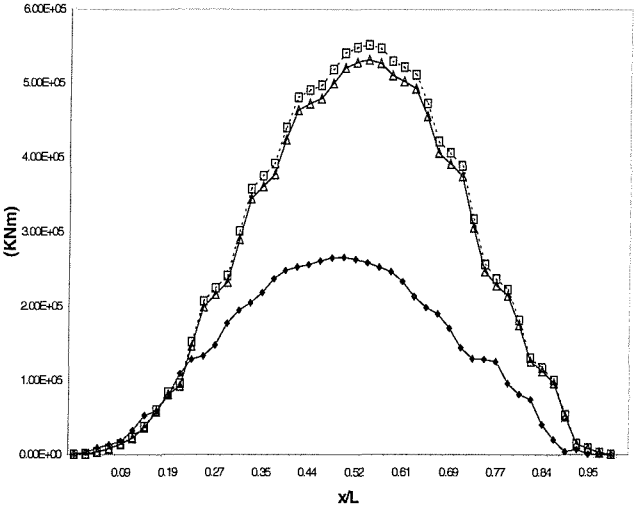

(b)

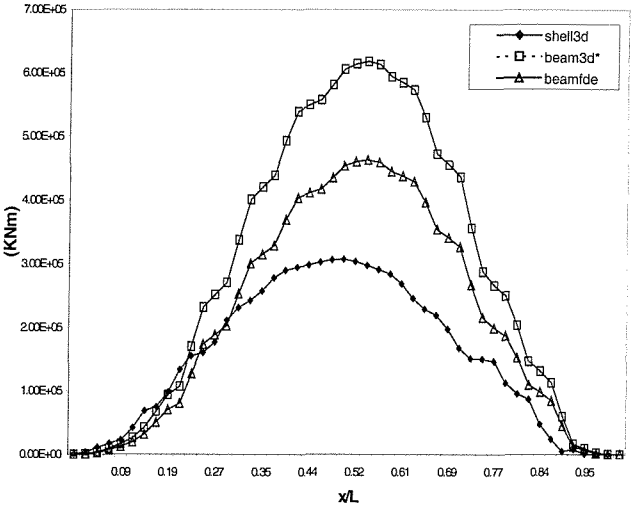

(c)

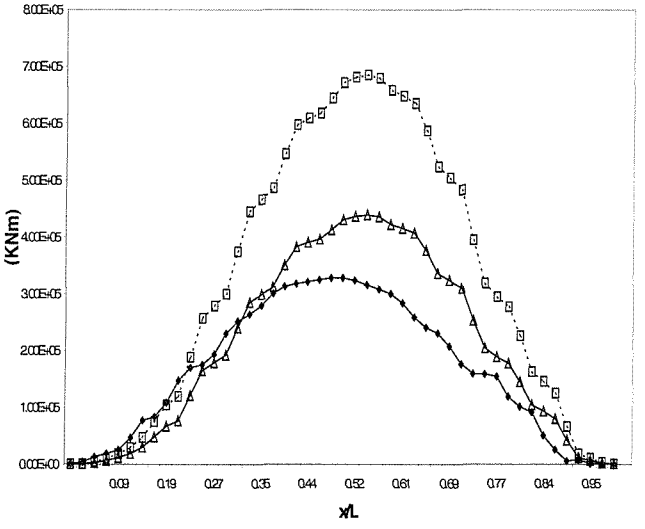

Fig. 6.41 Variation of horizontal bending moment at alternative forward speed levels (χ=120^0,L/λ=1.0) – (a) for forward speed $\overline{U}_A$ = 5m/s (Fn=0.093); (b) for forward speed $\overline{U}_B$ = 7.463m/s (Fn=0.138); (c) for forward speed $\overline{U}_C$ = 9m/s (Fn=0.167).

(a)

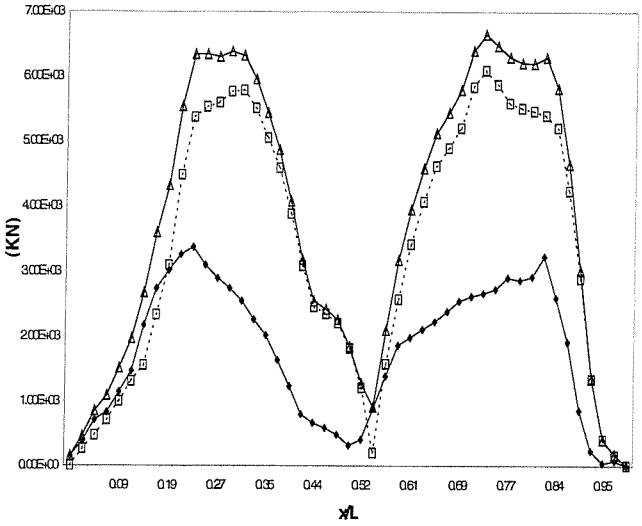

(b)

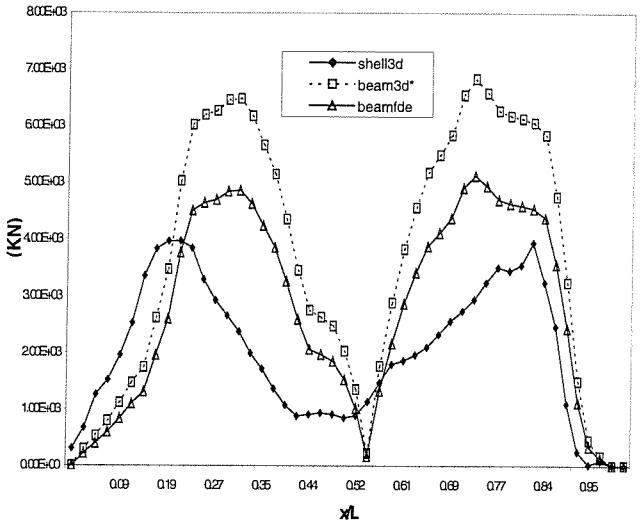

(c)

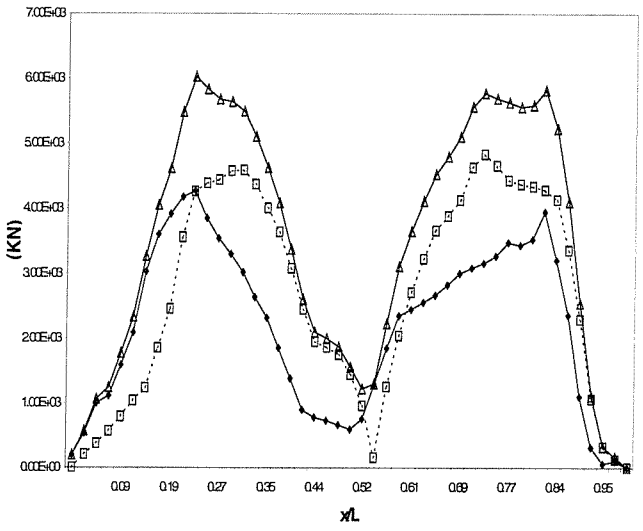

Fig. 6.42 Variation of horizontal shear force at alternative forward speed (U) levels (χ=120^0,L/λ=1.0) – (a) for forward speed $\overline{U}_A$ = 5m/s (Fn=0.093); (b) for forward speed $\overline{U}_B$ = 7.463m/s (Fn=0.138); (c) for forward speed $\overline{U}_C$ = 9m/s (Fn=0.167).

(a)

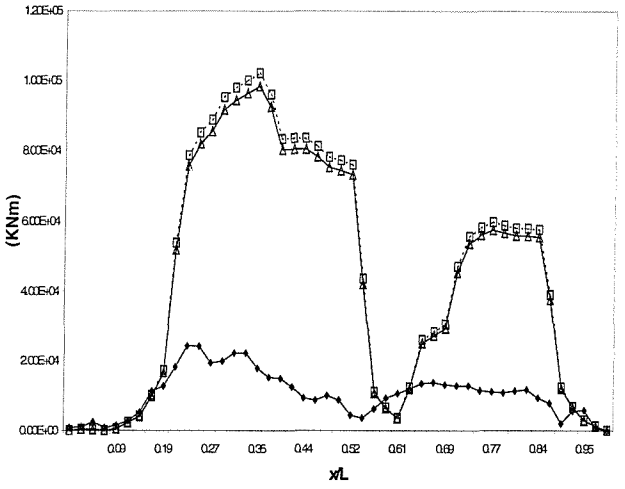

(b)

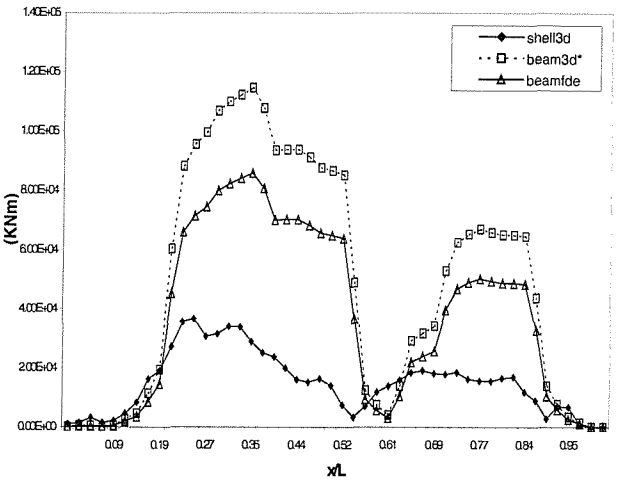

(c)

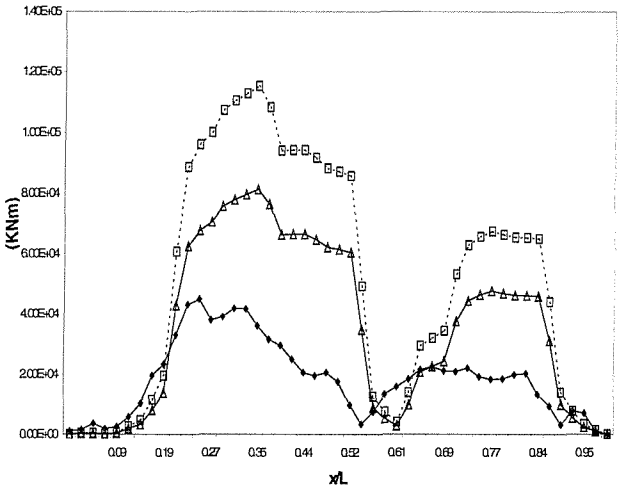

Fig. 6.43 Variation of torsion moments at alternative forward speed levels (χ=120^0,L/λ=1.0) – (a) for forward speed $\overline{U}_A$ = 5m/s (Fn=0.093); (b) for forward speed $\overline{U}_B$ = 7.463m/s (Fn=0.138); (c) for forward speed $\overline{U}_C$ = 9m/s (Fn=0.167).

(a)

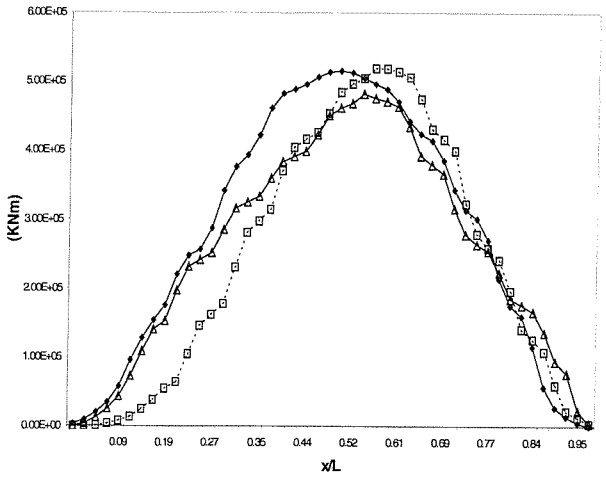

(b)

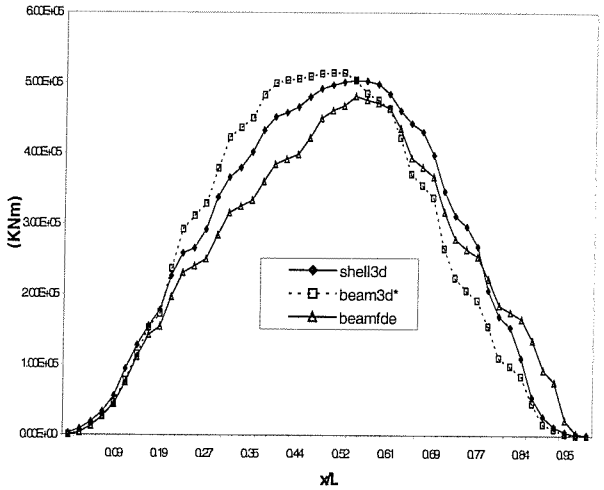

(c)

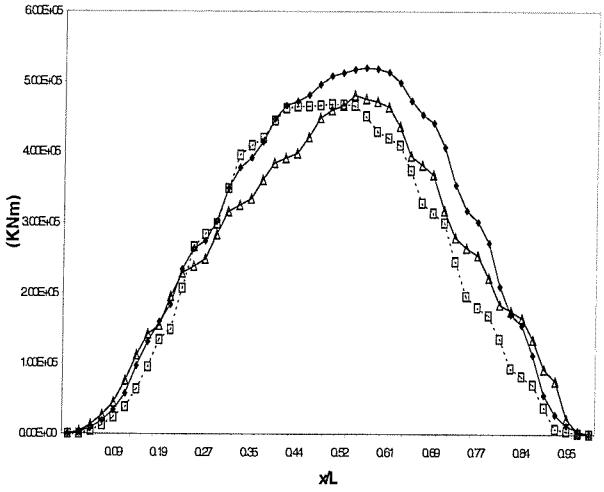

Fig. 6.44 Variation of wave induced vertical bending moments for alternative structural configurations (χ=135^0, $\overline{U}$ = 7.463m/s,L/λ=1.0); (a) open-ship; (b) bulker; (c) closed-ship.

(a)

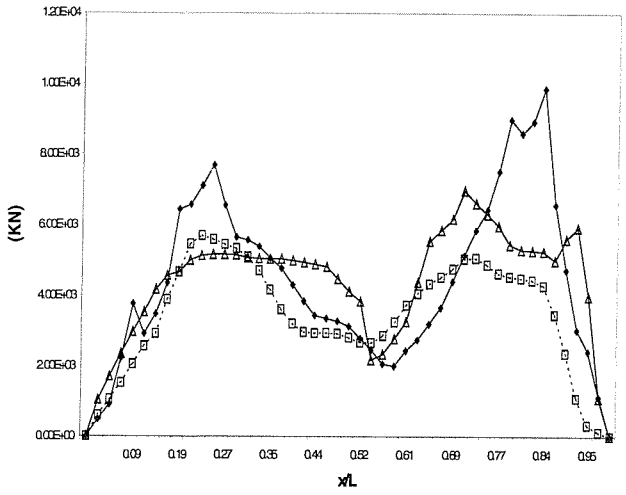

(b)

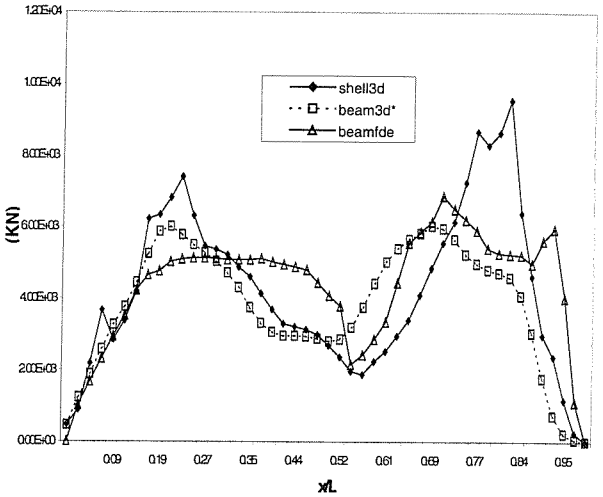

(c)

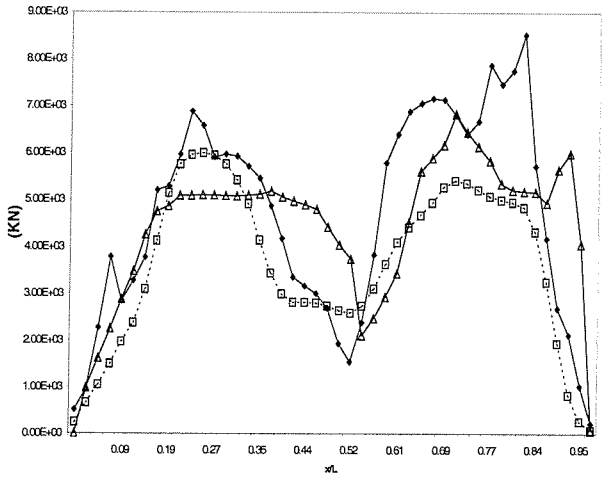

Fig. 6.45 Variation of wave induced vertical shear forces for alternative structural configurations (χ=135^0, $\overline{U}$ = 7.463m/s, L/λ=1.0); (a) open-ship; (b) bulker; (c) closed-ship.

(a)

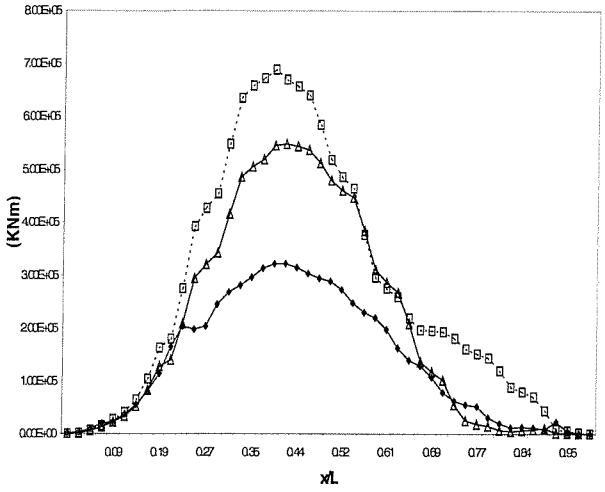

(b)

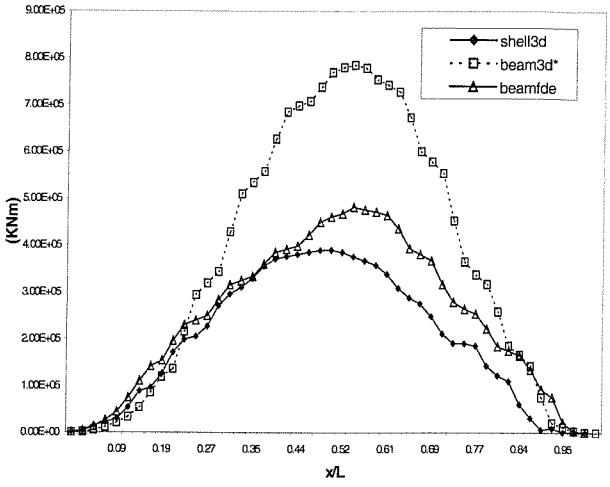

(c)

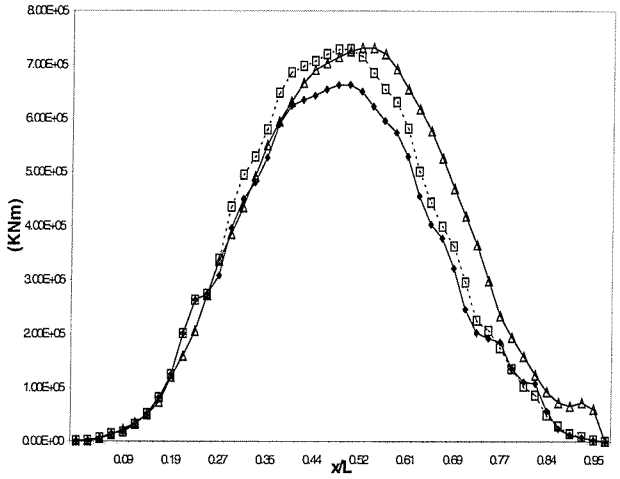

Fig. 6.46 Variation of wave induced horizontal bending moments for alternative structural configurations (χ=135^0, $\overline{U}$ = 7.463m/s, L/λ=1.0); (a) open-ship; (b) bulker; (c) closed-ship.

(a)

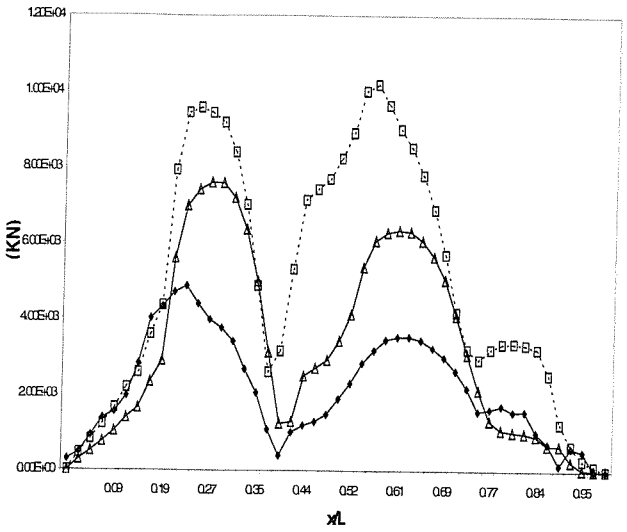

(b)

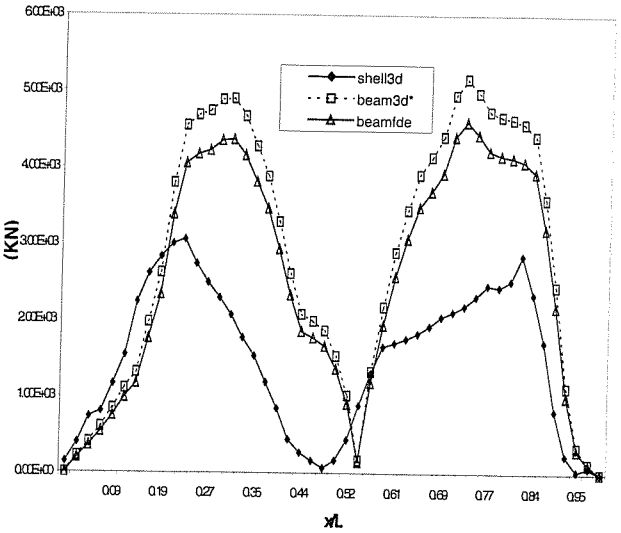

(c)

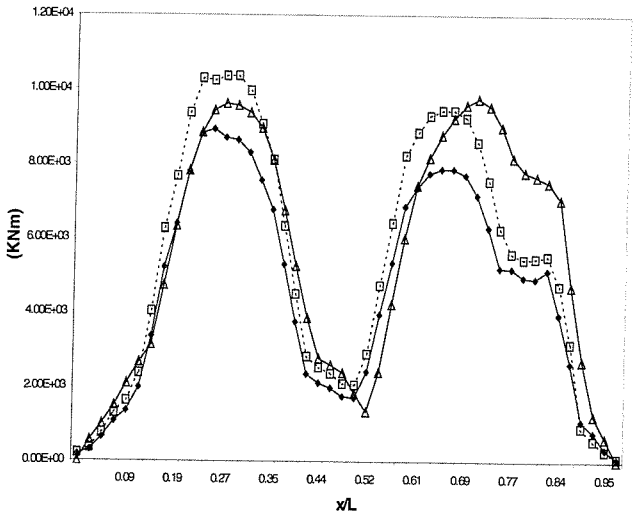

Fig. 6.47 Variation of wave induced horizontal shear forces for alternative structural configurations (χ=135^0, $\overline{U}$ = 7.463m/s, L/λ=1.0); (a) open-ship; (b) bulker; (c) closed-ship.

(a)

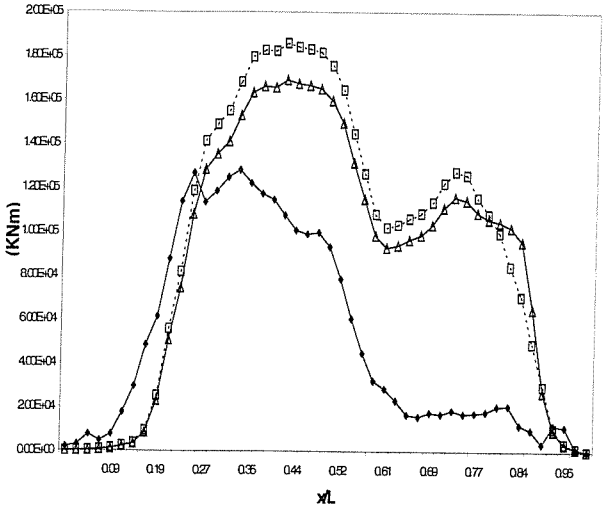

(b)

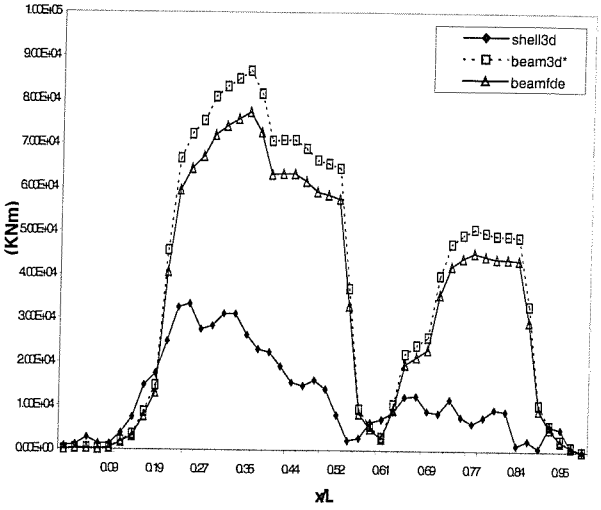

(c)

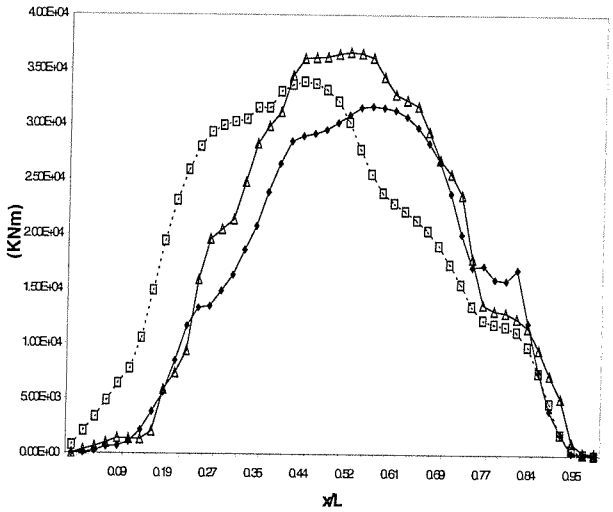

Fig. 6.48 Variation of wave induced torsional moments for alternative structural configurations (χ=135^0, $\overline{U}$ = 7.463m/s, L/λ=1.0); (a) open-ship; (b) bulker; (c) closed-ship.

Vertical bending moments were evaluated and compared for all models (beamfde, beam3d*, shell3d) at different heading angles (90^0,120^0,135^0,160^0,180^0) and alternative wavelength ratios of L/λ=0.5, 1.0 and 2.0. Maximum vertical bending moment and shear force is always observed in head waves and unit wavelength ratio, following the general trend of the principal coordinates. For head or bow quartering seas maximum vertical bending moment corresponds to L/λ=1.0. For near beam seas this is progressively changing simply reflecting that at lower encounter frequencies longer waves are required to produce an increased wave excitation.

For the antisymmetric dynamic loads (horizontal bending moments, horizontal shear forces, torsional moments), only four of the 8 modes contribute in the main to the final loading. Although the general trend of the dynamic loads predicted by beam and shell structural idealisations are similar in shape differences in magnitude arise with the beamfde induced moments being the highest. These differences are in the main related to the fact that the corresponding modal properties are significantly different due to the inadequacy of the Timoshenko beam idealisation to describe the non-prismatic features of the hull in antisymmetric motion (see chapter 5). Maximum antisymmetric dynamic loads (for any idealisation) are for 135^0 heading angle and then gradually decrease towards beam waves and head waves where the antisymmetric dynamics of the vessel are of no significance. Once more this mirrors the behavior of the principal coordinates.

The effects of speed and damping upon the response and hydroelastic loading of the vessel were further explored. Three different forward speed levels were examined, namely U_A=5m/s, U_B=7.463m/s, U_C=9m/s. It has been demonstrated that the effect of damping on the principal coordinates is simply to reduce the level of the principal coordinate of resonant response irrespective of the type of idealisation. Thus, no difference in the wet resonances was observed. On the other hand increasing speed level leads to a slight increase of the resonant frequencies with corresponding alteration of the principal coordinate amplitude. Vertical and horizontal bending moments slightly decrease or increase respectively with decreasing or increasing forward speed respectively.

Irrespective of the structural configuration adopted for a monohull (e.g. bulker, closed-or open-decks ship) beam (beamfde, beam3d*) and shell (shell3d) fluid-structure interaction models appear to have excellent agreement in symmetric motion. However, in the case of ships with large deck openings beam idealisations (beamfde, beam3d*) overestimate the predicted dynamic loads produced by the three-dimensional potential flow analysis (shell3d). This discrepancy is related to the modal rather the wet analysis (see chapter 5) and more specifically to the inadequacy of the modified Timoshenko beam idealisation (including the effects of warping) to simulate the compatibility conditions related to the non-prismatic effects (structural discontinuities) of the hull girder.

Today all leading classification societies evaluate the global antisymmetric dynamic loads by means of quasi-static methodologies having semi-empirical or reliability based character [6.5,6.6,6.7,6.8,6.9] (see section 2.4). However, hull strength assessment should be evaluated on the basis of accurate structural response analysis. In this chapter it has been shown that the unified hydroelasticity theory provides significant insight with regards to the antisymmetric global response of a ship structure with large deck openings. Comparisons against existing rules and regulations, therefore, could shed light towards the accuracy or usefulness of all the alternative current predictions especially at the extremities of the hull where torsion induced dynamic responses appear to be rather significant .

6.10 References

[6.1] Bishop, R.E.D and Price, W.G.: Hydroelasticity of ships, Cambridge university press, London, UK, (1979).

[6.2] Bishop, R.E.D, Price, W.G. and Wu, Y.: A general linear hydroelasticity theory of floating structures moving in a seaway, Phil. Trans. Royal Soc. London, A316: 375-426, (1986).

[6.3] Bailey, P.A., Hudson, D.A., Price W.G. and Temarel, P.: Comparisons between theory and experiment in a seakeeping validations study, Trans. RINA, 143:44-77, (2001).

[6.4] Price, W.G., Salas Inzunza, M.A. and Temarel, P.: The dynamic behaviour of a mono-hull in oblique waves using two- and three-dimensional fluid-structure interaction models, Accepted for publication Trans. RINA, (2001).

[6.5] Class LR, Rules for the classification of ships, Part 3 - Ship structures, Chapter 2 - Longitudinal strength, (2001).

[6.6] Class BV, Rules for the classification of ships, Part B-Hull and stability, Chapter 4 - Longitudinal strength of ocean going vessels, (2002).

[6.7] Class ABS, Rules for the classification of steel vessels, Part 3 - Hull construction and equipment (2002).

[6.8] Class DNV, Rules for the classification of ships, Part3 - Structures and equipment main class, Chapter 1 - Hull structural design for ships of length 100m or above (2002).

[6.9] Class GL, Rules for classification and construction, Part 1 - Seagoing ships, Chapter 1 - hull structures (2000).

Chapter 7

Conclusions & Recommendations

7.1 Conclusions

The alarming rates of bulk carrier casualties in recent years makes this vessel type a suitable example for investigating the influence of the level of hydroelastic modelling (i.e. 2D FSI, 2D structure and 3D fluid interaction or 3D FSI) on predicting wave induced loads and responses. Furthermore, the existence of deck openings in this type of ship and the effects of the structural modelling approach adopted (i.e. bulker, open and closed ship models) on the dynamic characteristics and wave induced loads need to be addressed. In this project, therefore, two- and three-dimensional linear hydroelasticity theories [7.1,7.2] were employed to investigate the steady state dynamic behaviour of a bulker having similar mass and structural properties to OBO MV Derbyshire. All simulations were carried out in regular waves. The analyses were divided into two stages, namely dry and wet, while wide ranging comparisons were carried out with reference to the level of global modelling as well as the structural modelling related to the deck openings.

In dry analyses two- and three-dimensional idealisations were used to determine the symmetric and antisymmetric in vacuo dynamic characteristics of the bulker. Three-dimensional finite element models, using shell-type (shell3d) or brick-type (beam3d) elements, were compared against two-dimensional beam models simulated by means of either finite element (beam2d) or finite difference schemes discretised in equal (beamfde) or unequal (beamfd) spaces. The structural and inertia related properties were distributed, for all models, in 46 sections along the ship. Although constraints of the software used prevented the generation of a more refined shell

model (shell3d) experience with uniform barge models having similar mass and structural properties with the ship studied also validated the convergence and adequacy of the adopted discretisation methodology.

The dynamic characteristics of all idealisations were outlined and found to be in good agreement for symmetric distortions (i.e. vertical bending). No significant deviations were observed between the modal analyses results of the finite difference schemes with equal and unequal intervals (beamfd, beamfde). Further investigation of the effects of refinement has clearly demonstrated that all beam models converge well and the selected level of discretisation describes adequately the symmetric dynamics of the ship structure. The presence of deck openings (i.e. non-prismatic nature of the hull girder) does not appear to unduly influence the dry symmetric dynamic behaviour. This is further confirmed by the similarity of the dry dynamic characteristics between the bulker, open and closed ship configurations.

For the antisymmetric dynamic behaviour, special emphasis was paid upon identifying the influences of hatch openings, shear center and warping rigidity on the dry dynamic characteristics of the structure. Since ANSYS 5.4 beam finite elements (beam2d, beam3d) do not account for the effects of warping, the finite difference beam idealisations (beamfd, beamfde) were employed to simulate the hull girder's two-dimensional dynamics. By following this approach generalised masses, eigenvalues and eigenvectors of all models were found to be in reasonably good agreement. However, horizontal bending moments, shear forces and torsional moments predicted by the beam idealisation overestimated, somehow 'artificially', those of the three-dimensional simulation. Detailed literature review and engineering judgement has led to the conclusion that such deviations could appear because of the inadequacy of the beam model to simulate the non-prismatic nature of the bulker's hull girder whilst allowing for the effects of warping. The latter was further validated by performing extended modal parametric analyses on the open and closed ship configurations having same mass distributions but closed and open decks. For the closed-deck vessel, where structural discontinuities and warping effects are not evident, excellent agreement was achieved between two- and three-dimensional structural models. The beam idealisation of the open-deck vessel, however, appeared to overestimate, as in the case of the bulker, the predicted modal loads compared to

the three-dimensional structural idealisation. Furthermore, a convergence study has also demonstrated that in antisymmetric plane the lack of compatibility conditions at the common nodal locations between the open/closed parts of the hull appears to lead to numerical instability. Further studies with uniform barges have also confirmed this influence of the deck openings.

For the wet analysis the fluid-structure interaction (FSI) was carried out using two-dimensional (Timoshenko beam and strip theory) and three-dimensional (beam and shell finite element idealisations combined with potential flow analysis based on pulsating source distribution over the mean wetted surface) analyses. For the three-dimensional beam (beam3d*) and shell (shell3d) FSI models, 952 hydropanels used to idealise the mean wetted surface of the hull. This idealisation was based on a one-to-one correspondence between shell finite elements on the mean wetted surface and hydropanels. Although wetted surface idealisations with different number of panels were not investigated, the number of panels used is thought to provide a good degree of accuracy based on past experience [7.3].

Eight flexible distortions were shown to be adequate in simulating the response of the hull.

Resonant encounter frequencies were obtained for all models at various angles of wave incidence at the typical service speed of 7.463m/s (Fn=0.138) and they were found to be in good agreement.

From the wet analysis it became evident that the behaviour of symmetric and antisymmetric steady state seaway induced dynamic loads mirrors the behaviour of the principal coordinates and is highly dependent upon the in vacuo modal behaviour of the structure.

Vertical bending moments and shear forces evaluated and compared for all models (namely 2D and 3D FSI models including the bulker, open and closed ship configurations) were found to be in good agreement with maximum values always observed in head waves and unit wavelength ratio.

Maximum antisymmetric wave induced loads occur at 135^0 heading angle and then gradually decrease towards beam waves. Although the general trend of dynamic loads predicted by beam and shell structural idealisations are similar in shape, differences in magnitude were evident. It is believed that these deviations are related to the dry analyses and the inadequacy of the Timoshenko beam idealisation to describe the non-prismatic features of the hull in antisymmetric motion. As in the dry analysis stage, this was also confirmed by the wave induced loads (i.e. horizontal bending moment, horizontal shear force, and torsional moment) predicted by the open and closed deck configurations. For the former (open deck) the differences between the loads predicted when using the two- and three-dimensional structural idealisations are similar to the bulker. For the latter (closed deck) there is good agreement between loads predicted using either two- or three-dimensional FSI models.

Longitudinal direct stresses along the deck edge and bottom of the ship's structure were evaluated and compared for all models in head and bow quartering waves. In two-dimensional hydroelasticity analysis stresses were calculated indirectly from vertical bending moments while in three-dimensional hydroelasticity the corresponding stresses were readily available from the modal analysis. In any case, maximum stresses were observed along the deck edge of the vessel for head waves. The contribution of antisymmetric modes to direct stress along the deck edge of the shell (in non-head waves) model were shown to be important.

From the analyses become apparent that the level of agreement between various FSI models shows a degree of discrepancy on heading. The effects of speed and structural damping upon the response and hydroelastic loading of the vessel were further explored. It was shown that the effect of structural damping on the principal coordinates is, as expected, in the form of reducing the magnitude of the principal coordinates at resonance, irrespective of the type of idealisation used. On the other hand, increasing speed level leads to a slight increase in the resonant frequencies with consequent increases of the principal coordinate amplitude and the wave induced loads.

The current investigation shows that two- and three-dimensional fluid-structure interaction models have different degrees of complexity and associated data requirements. The former

could be, in general, suitable for the concept design stage, where the performance of design variants can be assessed using acceptable engineering approximations. The latter could be, in general, far more suitable in predicting or confirming the dynamic performance of a detailed design. This notwithstanding this work assesses the degree of confidence that can be placed on hydroelastic predictions obtained from two-dimensional models by comparison to three-dimensional models where structural features, such as deck openings, double bottoms, transverse bulkheads etc, are modelled more explicitly.

7.2 Suggestions for further research

Bearing in mind that it is in the nature of research to be an ongoing, endless and challenging process some suggestions for further investigations follow:

- At first instance a more detailed three-dimensional shell model including stiffeners and transverse frames could be created to examine the effects of such refinement upon (e.g. usage of fictitious bulkheads) the prediction of dynamic characteristics and wave induced loads;

- It could be of interest to consider how the results obtained from the global three-dimensional structural model can be used in order to examine in more detail the behaviour of a specific area of the ship (e.g. bow, stern or mid-ship section). This could be achieved by using nodal displacements based on the wet analysis of the global model as loading conditions on the refined localised finite element model;

- Although bulkers proceed in the seaway with slow or moderate speeds, regarding the potential flow model the use of translating pulsating, as opposed to simply pulsating sources could be investigated as a more rigorous theoretical solution. The work by Du et al [7.4] could be used as a reference point for such investigation;

- One of the main conclusions of the current investigation was that the Bishop et al [7.1] mathematical model does not account for the compatibility conditions at the common nodal locations between the closed and open parts of the hull girder. In the author's opinion this

theoretical model should be updated by means of suitable correction factors such as those suggested by Pedersen [7.5,7.6].

- A comparison with the dynamic loads predicted by quasi-static and rigid body hydrodynamic theories could be particularly useful in the sense that it would highlight the possible limitations, advantages or practical adequacy of such theories over hydroelasticity. Some preliminary work based for the case of a trimaran warship has demonstrated the significance of such investigations [7.7]. Further comparisons against the existent classification societies rules [7.8,7.9,7.10,7.11,7.12] could shed light towards the accuracy or usefulness of hydroelastic predictions especially at the extremities ship hulls with large deck openings where torsion induced dynamic responses appear to be rather significant.

- Frequency domain results could be used as a basis for a time domain simulation in realistic seaways, also including slamming loads and responses. During such an analysis it would be useful to compare two- and three-dimensional hydroelasticity theories. The preliminary work by Salas [7.13] for the case of a mine-hunter could be used as a reference point;

- Following such theoretical investigations experimental and full scale measurements would come as a desirable means of validating the mathematical model operating under steady state or transient conditions. In hydroelasticity studies there is a clear need for further experimental validations along the lines followed by Taggart et al [7.14] for the case of a frigate model in severe seas.

7.3 References

[7.1] Bishop, R.E.D. and Price, W.G.: Hydroelasticity of Ships, Cambridge University Press, UK (1979).

[7.2] Bishop, R.E.D, Price, W.G. and Wu, Y.: A general linear hydroelasticity theory of floating structures moving in a seaway, Phil. Trans. Royal Soc. London, A316: 375-426, (1986).

[7.3] Bailey, P.A., Hudson, D.A., Price W.G. and Temarel, P.: Comparisons between theory and experiment in a seakeeping validations study, Trans. RINA, 143:44-77, (2001).

[7.4] Du, S.X., Wu, Y. and Price W.G.: Forward speed effect on the structural responses of a ship travelling in waves, Proceedings of the 2nd international conference of hydroelasticity in marine technology, 1:401-410 (1998).

[7.5] Pedersen, P.T.: Torsional response of containerships; Journal of Ship Research, 29:194-20, (1985).

[7.6] Pedersen, P.T.: Beam theories for torsional response of ship hulls; Journal of Ship Research, 35:254-265, (1991).

[7.7] Bingham, A.E., Hampshire, J.K., Miao, S.H. and Temarel, P.: Motions and loads of a trimaran travelling in regular waves, The 6th international conference on fast ship transportation, 2:167-176, Southampton, UK (2001).

[7.8] Class LR, Rules for the classification of ships, Part 3 - Ship structures, Chapter 2 - Longitudinal strength, (2001).

[7.9] Class BV, Rules for the classification of ships, Part B-Hull and stability, Chapter 4 - Longitudinal strength of ocean going vessels, (2002).

[7.10] Class ABS, Rules for the classification of steel vessels, Part 3 - Hull construction and equipment (2002).

[7.11] Class DNV, Rules for the classification of ships, Part3 - Structures and equipment main class, Chapter 1 - Hull structural design for ships of length 100m or above (2002).

[7.12] Class GL, Rules for classification and construction, Part 1 - Seagoing ships, Chapter 1 - hull structures (2000).

[7.13] Salas Inzunza, M.A.: Two- and three-dimensional hydroelastic analyses of a composite monohull in waves, Ph.D. thesis, University of Southampton, (1999).

[7.14] McTaggart, K., Datta, I., Stirling, A., Gibson, S., Glen, I.: Motions and loads of a hydroelastic frigate model in severe seas, Journal of Ship Research, 105:427-453, (1997).

Appendix 1

- Scantlings for OBO MV Derbyshire
- Sectional data for OBO MV Derbyshire
- Sectional data for closed ship
- Sectional data for open ship
- General arrangement plan for OBO MV Derbyshire
- Shipshape lines plan for OBO MV Derbyshire
- Simplified mid ship section for OBO MV Derbyshire

SCANTLINGS

OBO MV Derbyshire

Section no.	Upper Deck	Outer Side shell (1) (upper part)	Outer Side shell (2) (middle part + inner bottom)
1	0.00295	0.004	0.006775
2	0.00295	0.004	0.006775

	Bottom shell
1	0.0049
2	0.0049

	Upper Deck	Outer Side shell (1) (upper part)	Outer Side shell (2) (middle part + inner bottom)
3	0.01534	0.0066	0.01117875

	Bottom shell	Outer Side shell (1) (lower part)
3	0.011025	0.0066

	Upper Deck	Outer Side shell (1) (upper part)	Outer Side shell (2) (middle part + inner bottom)
4	0.01534	0.0066	0.01117875
5	0.01475	0.01	0.0169375
6	0.019175	0.0112	0.01897
7	0.0236	0.0112	0.01930875

	Outer Side shell (1) (lower part)	Inner bottom	Bottom shell
4	0.0066	0.0111375	0.011025
5	0.01	0.0111375	0.011025
6	0.0112	0.01485	0.0147
7	0.0114	0.0185625	0.018375

	Bottom Girder1	Bottom Girder2	Bottom Girder3
4	0.00792	0.0144	0.0216
5	0.008745	0.0159	0.02385
6	0.00924	0.0168	0.0252
7	0.009405	0.0171	0.02565

	Bottom Girder4 (central girder)
4	
5	0.0585
6	0.06552
7	0.06552

	Upper Deck	*For - aft hatch coaming*	*Diaphgram*
8	0.04071	0.0369248	0.02365495
9	0.04071	0.0369248	0.02365495
10	0.040415	0.0366176	0.02345815
11	0.04071	0.0369248	0.02365495
12	0.045135	0.03848	0.02465125
13	0.04543	0.038816	0.0248665
14	0.045135	0.03848	0.02465125
15	0.045135	0.03848	0.02465125
16	0.045725	0.03904	0.02501
17	0.045725	0.03904	0.02501
18	0.045725	0.03904	0.02501
19	0.045725	0.03904	0.02501
20	0.0452235	0.03872	0.024805
21	0.0452235	0.03872	0.024805
22	0.0452235	0.03872	0.024805
23	0.0452235	0.03872	0.024805
24	0.045725	0.03904	0.02501
25	0.045725	0.03904	0.02501
26	0.045725	0.03904	0.02501
27	0.045725	0.03904	0.02501
28	0.0452235	0.03872	0.024805
29	0.0452235	0.03872	0.024805
30	0.0452235	0.03872	0.024805
31	0.0452235	0.03872	0.024805
32	0.043955	0.037792	0.0242105
33	0.043955	0.037792	0.0242105

34	0.043955	0.037792	0.0242105
35	0.043955	0.037792	0.0242105
36	0.03776	0.0355424	0.02276935
37	0.03776	0.0355424	0.02276935
38	0.03776	0.0355424	0.02276935
39	0.03776	0.0355424	0.02276935
40	0.019175	0.0348064	0.02229785
41	0.019175	0.0348064	0.02229785
42	0.0197945	0.034944	0.022386

	Topside tank sloping bulkhead plating	*Outer Side shell (1) (upper part)*	*Outer Side shell (2) (middle part + inner bottom)*
8	0.01742389	0.023078	0.039088363
9	0.01742389	0.023078	0.039088363
10	0.01727893	0.022886	0.038763163
11	0.01742389	0.023078	0.039088363
12	0.01815775	0.02405	0.040734688
13	0.0183163	0.02426	0.041090375
14	0.01815775	0.02405	0.040734688
15	0.01815775	0.02405	0.040734688
16	0.018422	0.0244	0.0413275
17	0.018422	0.0244	0.0413275
18	0.018422	0.0244	0.0413275
19	0.018422	0.0244	0.0413275
20	0.018271	0.0242	0.04098875
21	0.018271	0.0242	0.04098875
22	0.018271	0.0242	0.04098875
23	0.018271	0.0242	0.04098875
24	0.018422	0.0244	0.0413275
25	0.018422	0.0244	0.0413275
26	0.018422	0.0244	0.0413275
27	0.018422	0.0244	0.0413275
28	0.018271	0.0242	0.04098875
29	0.018271	0.0242	0.04098875

30	0.018271	0.0242	0.04098875
31	0.018271	0.0242	0.04098875
32	0.0178331	0.02362	0.040006375
33	0.0178331	0.02362	0.040006375
34	0.0178331	0.02362	0.040006375
35	0.0178331	0.02362	0.040006375
36	0.01677157	0.022214	0.037624963
37	0.01677157	0.022214	0.037624963
38	0.01677157	0.022214	0.037624963
39	0.01677157	0.022214	0.037624963
40	0.01642427	0.021754	0.036845838
41	0.01642427	0.021754	0.036845838
42	0.0164892	0.02184	0.0369915

	Outer Side shell (1) (lower part)	*Hopper tank sloping plating*	*Inner bottom*
8	0.023078	0.022693367	0.028559025
9	0.023078	0.022693367	0.028559025
10	0.022886	0.022504567	0.028321425
11	0.023078	0.022693367	0.028559025
12	0.02405	0.023649167	0.029761875
13	0.02426	0.023855667	0.03002175
14	0.02405	0.023649167	0.029761875
15	0.02405	0.023649167	0.029761875
16	0.0244	0.023993333	0.030195
17	0.0244	0.023993333	0.030195
18	0.0244	0.023993333	0.030195
19	0.0244	0.023993333	0.030195
20	0.0242	0.023796667	0.0299475
21	0.0242	0.023796667	0.0299475
22	0.0242	0.023796667	0.0299475
23	0.0242	0.023796667	0.0299475
24	0.0244	0.023993333	0.030195
25	0.0244	0.023993333	0.030195

26	0.0244	0.023993333	0.030195
27	0.0244	0.023993333	0.030195
28	0.0242	0.023796667	0.0299475
29	0.0242	0.023796667	0.0299475
30	0.0242	0.023796667	0.0299475
31	0.0242	0.023796667	0.0299475
32	0.02362	0.023226333	0.02922975
33	0.02362	0.023226333	0.02922975
34	0.02362	0.023226333	0.02922975
35	0.02362	0.023226333	0.02922975
36	0.022214	0.021843767	0.027489825
37	0.022214	0.021843767	0.027489825
38	0.022214	0.021843767	0.027489825
39	0.022214	0.021843767	0.027489825
40	0.021754	0.021391433	0.026920575
41	0.021754	0.021391433	0.026920575
42	0.02184	0.021476	0.027027

	Bottom shell	***Bottom Girder1***	***Bottom Girder2***
8	0.02827055	0.01903935	0.034617
9	0.02827055	0.01903935	0.034617
10	0.02803535	0.01888095	0.034329
11	0.02827055	0.01903935	0.034617
12	0.02946125	0.01984125	0.036075
13	0.0297185	0.0200145	0.03639
14	0.02946125	0.01984125	0.036075
15	0.02946125	0.01984125	0.036075
16	0.02989	0.02013	0.0366
17	0.02989	0.02013	0.0366
18	0.02989	0.02013	0.0366
19	0.02989	0.02013	0.0366
20	0.029645	0.019965	0.0363
21	0.029645	0.019965	0.0363

22	0.029645	0.019965	0.0363
23	0.029645	0.019965	0.0363
24	0.02989	0.02013	0.0366
25	0.02989	0.02013	0.0366
26	0.02989	0.02013	0.0366
27	0.02989	0.02013	0.0366
28	0.029645	0.019965	0.0363
29	0.029645	0.019965	0.0363
30	0.029645	0.019965	0.0363
31	0.029645	0.019965	0.0363
32	0.0289345	0.0194865	0.03543
33	0.0289345	0.0194865	0.03543
34	0.0289345	0.0194865	0.03543
35	0.0289345	0.0194865	0.03543
36	0.02721215	0.01832655	0.033321
37	0.02721215	0.01832655	0.033321
38	0.02721215	0.01832655	0.033321
39	0.02721215	0.01832655	0.033321
40	0.02664865	0.01794705	0.032631
41	0.02664865	0.01794705	0.032631
42	0.026754	0.018018	0.03276

	Bottom Girder3	***Bottom Girder4 (central girder)***
8	0.0519255	0.1350063
9	0.0519255	0.1350063
10	0.0514935	0.1338831
11	0.0519255	0.1350063
12	0.0541125	0.1406925
13	0.054585	0.141921
14	0.0541125	0.1406925
15	0.0541125	0.1406925
16	0.0549	0.14274
17	0.0549	0.14274

18	0.0549	0.14274
19	0.0549	0.14274
20	0.05445	0.14157
21	0.05445	0.14157
22	0.05445	0.14157
23	0.05445	0.14157
24	0.0549	0.14274
25	0.0549	0.14274
26	0.0549	0.14274
27	0.0549	0.14274
28	0.05445	0.14157
29	0.05445	0.14157
30	0.05445	0.14157
31	0.05445	0.14157
32	0.053145	0.138177
33	0.053145	0.138177
34	0.053145	0.138177
35	0.053145	0.138177
36	0.0499815	0.1299519
37	0.0499815	0.1299519
38	0.0499815	0.1299519
39	0.0499815	0.1299519
40	0.0489465	0.1272609
41	0.0489465	0.1272609
42	0.04914	0.127764

	Upper Deck	*Outer Side shell (1) (upper part)*	*Outer Side shell (2) (middle part + inner bottom)*
43	0.0197945	0.02184	0.0369915
	Outer Side shell (1) (lower part)	***Bottom shell***	***Bottom Girder1***
43	0.02184	0.026754	0.018018
	Bottom Girder2	***Bottom Girder3***	***Bottom Girder4 (central girder)***
43	0.03276	0.04914	0.127764

	Upper Deck	*Outer Side shell (1) (upper part)*	*Outer Side shell (2) (middle part + inner bottom)*
44	0.00885	0.008	0.01355
45	0.0059	0.006	0.0101625

	Outer Side shell (1) (lower part)	*Bottom shell*
44	0.008	0.0098
45	0.006	0.00735

	Upper Deck	*Outer Side shell (1) (upper part)*	*Outer Side shell (1) (lower part)*
46	0.00295	0.004	0.00748

	Bottom shell
46	0.0049

Sectlonal data
OBO MV Derbyshire

	L	A	Mass	Izz	Iyy	Jxx =rho(Izz+Iyy)	It	Iw	C.G.	S.C.	Aefz	Aefy
	(m)	(m^2)	(tonne)	(m^4)	(m^4)	tonne m	m^4	m^6	(m)	(m)	(m^2)	(m^2)
Section												
1	6.6840	0.2849	692.3289	18.1838	109.2092	46307.8867	9.2140	4.7900	22.0210	24.2000	0.0607	0.0798
2	13.3680	0.3426	610.5533	29.3874	120.0052	39836.5200	32.2363	406.2300	20.9045	22.5000	0.0730	0.0959
3	20.0520	1.1023	777.4935	97.7562	434.2393	56140.4525	67.0775	692.0000	17.5258	18.4300	0.2348	0.3086
4	26.7360	1.7835	1043.2742	210.1891	610.4927	71824.2532	122.9768	149.0000	12.0058	13.4200	0.3799	0.4994
5	36.0500	2.1471	1206.7881	236.5421	707.5872	56973.3675	197.0681	211.2600	11.3474	8.8900	0.4573	0.6012
6	45.0500	2.7109	1156.8555	306.8430	823.2387	53582.9124	341.9629	660.5400	11.3062	8.5760	0.5774	0.7591
7	52.1378	3.1816	4668.8439	371.8307	914.5573	266335.0526	786.2577	16133.0000	11.3114	9.3150	0.6777	0.8908
8	54.9378	6.9657	5763.6924	755.0324	1766.3005	745093.2442	786.2577	2416.1800	12.0416	10.0450	1.4837	1.9504
9	65.0500	6.2390	6950.4889	614.2985	1536.8046	236982.9694	31.8991	34754.0000	10.3574	-8.8800	1.3289	1.7469
10	73.7378	6.2339	6436.7875	614.2840	1533.0504	255208.8719	31.8991	52577.0000	10.2839	-8.8670	1.3278	1.7455
11	76.5378	7.1457	6095.5927	781.6972	1821.6320	793130.6941	1429.0789	75123.0000	11.8652	10.8500	1.5220	2.0008
12	79.3378	7.5877	4695.3071	836.9602	1931.3566	611804.7823	1429.9219	75123.0000	11.9054	10.8500	1.6162	2.1245
13	89.0500	6.8515	2868.5941	683.6548	1679.3359	101866.1219	31.8991	277182.0000	10.1476	-10.3000	1.4594	1.9184
14	98.1378	6.8473	2982.0542	683.6426	1687.0000	113606.9234	31.8991	277182.0000	10.0746	-10.3000	1.4585	1.9172
15	100.9378	7.7798	3627.0543	865.1340	1965.6215	471333.1539	1429.0789	26957.0000	11.7406	11.8000	1.6571	2.1784
16	103.7378	7.9073	5397.1665	879.5665	2012.6730	705038.4348	1429.9219	26957.0000	11.7101	11.8000	1.6843	2.2140
17	113.0500	7.0014	6883.7081	698.8626	1714.6870	254824.1435	31.8991	355152.0000	9.9906	-10.3000	1.4913	1.9604
18	122.5378	7.0014	6581.9296	698.8626	1714.6870	239143.2543	31.8991	355152.0000	9.9906	-10.3000	1.4913	1.9604
19	125.3378	7.9073	5616.5772	879.5665	2012.6730	733700.3314	1429.0789	26957.0000	11.7101	11.8000	1.6843	2.2140
20	128.1380	7.8369	4231.0923	871.3715	1994.5379	552560.6743	1429.9219	26957.0000	11.7007	11.8000	1.6693	2.1943
21	137.0500	6.9410	683.5484	692.4435	1699.8201	26435.2525	31.8991	377832.0000	9.9839	-10.4200	1.4784	1.9435
22	146.9378	6.9410	788.3135	692.4435	1699.8201	27478.2269	31.8991	377832.0000	9.9839	-10.4200	1.4784	1.9435
23	151.1010	7.8369	2327.1111	871.3715	1994.5379	204411.9869	1429.0789	22700.6000	11.7007	11.8000	1.6693	2.1943
24	153.9010	7.9073	3571.1772	879.5665	2012.6730	466507.2276	1429.9219	22700.6000	11.7101	11.8000	1.6843	2.2140
25	164.0500	7.0014	6968.1069	698.8626	1714.6870	236680.2268	31.8991	377832.0000	9.9906	-10.4200	1.4913	1.9604
26	172.7010	7.0014	6947.9724	698.8626	1714.6870	276861.2621	31.8991	377832.0000	9.9906	-10.4200	1.4913	1.9604
27	175.5010	7.9073	6829.6317	879.5665	2012.6730	892163.1147	1429.0789	22700.6000	11.7101	11.8000	1.6843	2.2140
28	178.3010	7.8369	5994.3276	871.3715	1994.5379	782886.7845	1429.9219	22700.6000	11.7007	11.8000	1.6693	2.1943
29	187.0500	6.9410	3692.5559	692.4435	1699.8201	145464.8511	31.8991	377832.0000	9.9839	-10.4200	1.4784	1.9435
30	197.1010	6.9410	3639.9253	692.4435	1699.8201	124816.6725	31.8991	377832.0000	9.9839	-10.4200	1.4784	1.9435
31	199.9010	7.8369	3716.4231	871.3715	1994.5379	485381.9697	1429.0789	22700.6000	11.7007	11.8000	1.6693	2.1943
32	202.7010	7.6410	4833.0580	849.0490	1944.3544	631028.0514	1429.9219	22700.6000	11.6865	11.8000	1.6275	2.1395

33	213.0500	6.7701	7077.9944	674.8401	1657.9034	235657.3752	31.8991	377832.0000	9.9740	-10.4200	1.4420	1.8956
34	221.5010	6.7701	7015.1414	674.8401	1657.9034	286020.7503	31.8991	377832.0000	9.9740	-10.4200	1.4420	1.8956
35	224.3010	7.6410	6701.0706	849.0490	1944.3544	874925.0510	1429.0789	22700.6000	11.6865	11.8000	1.6275	2.1395
36	226.7120	7.0287	6056.3064	769.9746	1782.2611	912130.9708	1429.9219	22700.6000	11.3883	11.8000	1.4971	1.9680
37	234.0500	6.2806	1958.0634	614.8573	1536.1823	91389.7095	31.8991	377832.0000	9.7669	-10.4200	1.3378	1.7586
38	243.2120	6.2806	499.4871	614.8573	1536.1823	18671.6324	31.8991	377832.0000	9.7669	-10.4200	1.3378	1.7586
39	245.6370	7.0287	473.8024	769.9746	1782.2611	70946.6868	1429.0789	5181.0000	11.3883	9.2500	1.4971	1.9680
40	248.2800	5.8590	1192.7041	567.0202	1483.0547	157898.9678	1429.9219	5181.0000	10.0359	8.0200	1.2480	1.6405
41	257.0500	5.4136	5599.1978	470.6981	1324.3617	211699.1319	31.8991	210000.0000	9.1072	-10.1000	1.1531	1.5158
42	266.2880	5.3872	5823.7503	470.7298	1321.9728	209783.2399	31.8991	210000.0000	9.2489	-10.1000	1.1475	1.5084
43	268.9540	3.7575	5570.7477	395.7387	1057.2311	808003.1678	706.4171	1976.0000	10.6171	7.5000	0.8003	1.0521
44	278.0500	1.0550	3170.6617	102.8910	388.9297	162495.4595	706.4171	1976.0000	14.7671	11.2500	0.2247	0.2954
45	287.4160	0.6424	705.1173	53.6933	271.3470	38094.5745	173.3208	272.0000	15.0862	8.4000	0.1368	0.1799
46	294.1000	0.2783	392.3000	27.1958	73.1412	21157.8724	31.7895	339.9400	16.3320	8.4000	0.0593	0.0779

Sectional data
CLOSED SHIP

	L	A	Mass	Izz	Iyy	Jxx =rho(Izz+Iyy)	It	Iw	C.G.	S.C.	Aefz	Aefy
	(m)	(m^2)	(tonne)	(m^4)	(m^4)	tonne m	m^4	m^6	(m)	(m)	(m^2)	(m^2)
Section												
1	6.684	0.2849	692.3289	18.1838	109.2092	46307.8867	9.2140	4.7900	22.0210	24.2000	0.0610	0.0798
2	13.368	0.3426	610.5533	29.3874	120.0052	39836.5200	32.2363	406.2300	20.9045	22.5000	0.0734	0.0959
3	20.052	1.1023	777.4935	97.7562	434.2393	56140.4525	67.0775	692.0000	17.5258	18.4300	0.2360	0.3086
4	26.736	1.7835	1043.2742	210.1891	610.4927	71824.2532	122.9768	149.0000	12.0058	13.4200	0.3819	0.4994
5	36.05	2.1471	1206.7881	236.5421	707.5872	56973.3675	197.0681	211.2600	11.3474	8.8900	0.4598	0.6012
6	45.05	2.7109	1156.8555	306.8430	823.2387	53582.9124	341.9629	660.5400	11.3062	8.5760	0.5805	0.7591
7	52.1378	3.1816	4668.8439	371.8307	914.5573	266335.0526	786.2577	16133.0000	11.3114	9.3150	0.6813	0.8908
8	54.9378	6.9657	5763.6924	755.0324	1766.3005	745093.2442	786.2577	2416.1800	12.0416	10.0450	1.4916	1.9504
9	65.05	6.9657	6950.4889	755.0324	1766.3005	248792.6623	786.2577	2416.1800	12.0416	10.0450	1.4916	1.9504
10	73.7378	7.1457	6436.7875	781.6972	1821.6320	269926.9263	1429.0789	26957.0000	11.8652	10.8500	1.5301	2.0008
11	76.5378	7.1457	6095.5927	781.6972	1821.6320	793130.6941	1429.0789	26957.0000	11.8652	10.8500	1.5301	2.0008
12	79.3378	7.5877	4695.3071	836.9602	1931.3566	611804.7823	1429.0789	26957.0000	11.9054	10.8500	1.6247	2.1245
13	89.05	7.5877	2868.5941	836.9602	1931.3566	107760.1981	1429.0789	26957.0000	11.9054	10.8500	1.6247	2.1245
14	98.1378	7.7798	2982.0542	865.1340	1965.6215	119395.7162	1429.0789	26957.0000	11.7406	11.8000	1.6659	2.1784
15	100.9378	7.7798	3627.0543	865.1340	1965.6215	471333.1539	1429.0789	26957.0000	11.7406	11.8000	1.6659	2.1784
16	103.7378	7.9073	5397.1665	879.5665	2012.6730	705038.4348	1429.0789	26957.0000	11.7101	11.8000	1.6932	2.2140
17	113.05	7.9073	6883.7081	879.5665	2012.6730	270380.3727	1429.0789	26957.0000	11.7101	11.8000	1.6932	2.2140
18	122.5378	7.9073	6581.9296	879.5665	2012.6730	253742.2136	1429.0789	26957.0000	11.7101	11.8000	1.6932	2.2140
19	125.3378	7.9073	5616.5772	879.5665	2012.6730	733700.3314	1429.0789	26957.0000	11.7101	11.8000	1.6932	2.2140
20	128.138	7.8369	4231.0923	871.3715	1994.5379	552560.6743	1429.0789	26957.0000	11.7007	11.8000	1.6781	2.1943
21	137.05	7.8369	683.5484	871.3715	1994.5379	28048.5608	1429.0789	26957.0000	11.7007	11.8000	1.6781	2.1943
22	146.9378	7.8369	788.3135	871.3715	1994.5379	29155.1866	1429.0789	26957.0000	11.7007	11.8000	1.6781	2.1943
23	151.101	7.8369	2327.1111	871.3715	1994.5379	204411.9869	1429.0789	26957.0000	11.7007	11.8000	1.6781	2.1943
24	153.901	7.9073	3571.1772	879.5665	2012.6730	466507.2276	1429.0789	26957.0000	11.7101	11.8000	1.6932	2.2140
25	164.05	7.9073	6968.1069	879.5665	2012.6730	251128.8259	1429.0789	26957.0000	11.7101	11.8000	1.6932	2.2140
26	172.701	7.9073	6947.9724	879.5665	2012.6730	293762.7896	1429.0789	26957.0000	11.7101	11.8000	1.6932	2.2140
27	175.501	7.9073	6829.6317	879.5665	2012.6730	892163.1147	1429.0789	26957.0000	11.7101	11.8000	1.6932	2.2140
28	178.301	7.8369	5994.3276	871.3715	1994.5379	782886.7845	1429.0789	26957.0000	11.7007	11.8000	1.6781	2.1943
29	187.05	7.8369	3692.5559	871.3715	1994.5379	154342.3775	1429.0789	26957.0000	11.7007	11.8000	1.6781	2.1943
30	197.101	7.8369	3639.9253	871.3715	1994.5379	132434.0680	1429.0789	26957.0000	11.7007	11.8000	1.6781	2.1943
31	199.901	7.8369	3716.4231	871.3715	1994.5379	485381.9697	1429.0789	26957.0000	11.7007	11.8000	1.6781	2.1943
32	202.701	7.6410	4833.0580	849.0490	1944.3544	631028.0514	1429.0789	26957.0000	11.6865	11.8000	1.6362	2.1395

33	213.05	7.6410	7077.9944	849.0490	1944.3544	250032.5311	1429.0789	26957.0000	11.6865	11.8000	1.6362	2.1395
34	221.501	7.6410	7015.1414	849.0490	1944.3544	303468.0841	1429.0789	26957.0000	11.6865	11.8000	1.6362	2.1395
35	224.301	7.6410	6701.0706	849.0490	1944.3544	874925.0510	1429.0789	26957.0000	11.6865	11.8000	1.6362	2.1395
36	226.712	7.0287	6056.3064	769.9746	1782.2611	912130.9708	1429.0789	26957.0000	11.3883	11.8000	1.5051	1.9680
37	234.05	7.0287	1958.0634	769.9746	1782.2611	96893.7166	1429.0789	26957.0000	11.3883	11.8000	1.5051	1.9680
38	243.212	7.0287	499.4871	769.9746	1782.2611	19796.1441	1429.0789	26957.0000	11.3883	9.2500	1.5051	1.9680
39	245.637	7.0287	473.8024	769.9746	1782.2611	70946.6868	1429.0789	26957.0000	11.3883	9.2500	1.5051	1.9680
40	248.28	5.8590	1192.7041	567.0202	1483.0547	157898.9678	1429.0789	26957.0000	10.0359	8.0200	1.2546	1.6405
41	257.05	5.4136	5599.1978	567.0202	1483.0547	241774.1607	1429.0789	26957.0000	10.0359	8.0200	1.1592	1.5158
42	266.288	5.3872	5823.7503	395.7387	1057.2311	170027.4876	706.4171	1976.0000	10.6171	7.5000	1.1536	1.5084
43	268.954	3.7575	5570.7477	395.7387	1057.2311	808003.1678	706.4171	1976.0000	10.6171	7.5000	0.8046	1.0521
44	278.05	1.0550	3170.6617	102.8910	388.9297	162495.4595	706.4171	1976.0000	14.7671	11.2500	0.2259	0.2954
45	287.416	0.6424	705.1173	53.6933	271.3470	38094.5745	173.3208	272.0000	15.0862	8.4000	0.1375	0.1799
46	294.1	0.2783	392.3000	27.1958	73.1412	21157.8724	31.7895	339.9400	16.3320	8.4000	0.0596	0.0779

Sectional data
OPEN SHIP

	L	A	Mass	Izz	Iyy	Jxx =rho(Izz+Iyy)	It	Iw	C.G.	S.C.	Aefz	Aefy
	(m)	(m^2)	(tonne)	(m^4)	(m^4)	tonne m	m^4	m^6	(m)	(m)	(m^2)	(m^2)
Section												
1	6.684	0.2849	692.3289	18.1838	109.2092	46307.8867	9.2140	4.7900	22.0210	24.2000	0.0635	0.0798
2	13.368	0.3426	610.5533	29.3874	120.0052	39836.5200	32.2363	406.2300	20.9045	22.5000	0.0764	0.0959
3	20.052	1.1023	777.4935	97.7562	434.2393	56140.4525	67.0775	692.0000	17.5258	18.4300	0.2458	0.3086
4	26.736	1.7835	1043.2742	210.1891	610.4927	71824.2532	122.9768	149.0000	12.0058	13.4200	0.3977	0.4994
5	36.05	2.1471	1206.7881	236.5421	707.5872	56973.3675	197.0681	211.2600	11.3474	8.8900	0.4788	0.6012
6	45.05	2.7109	1156.8555	306.8430	823.2387	53582.9124	341.9629	660.5400	11.3062	8.5760	0.6045	0.7591
7	52.1378	3.1816	4668.8439	371.8307	914.5573	266335.0526	786.2577	16133.0000	11.3114	9.3150	0.7095	0.8908
8	54.9378	6.9657	5763.6924	755.0324	1766.3005	745093.2442	786.2577	2416.1800	12.0416	10.0450	1.5533	1.9504
9	65.05	6.2390	6950.4889	614.2985	1536.8046	236982.9694	31.8991	34754.0000	10.3574	-8.8800	1.3913	1.7469
10	73.7378	6.2339	6436.7875	614.2840	1533.0504	255208.8719	31.8991	52577.0000	10.2839	-8.8670	1.3902	1.7455
11	76.5378	6.2339	6095.5927	614.2840	1533.0504	749884.3946	31.8991	52577.0000	10.2839	-8.8670	1.3902	1.7455
12	79.3378	6.8515	4695.3071	683.6548	1679.3359	578341.3694	31.8991	277182.0000	10.2839	-10.3000	1.5279	1.9184
13	89.05	6.8515	2868.5941	683.6548	1679.3359	101866.1219	31.8991	277182.0000	10.1476	-10.3000	1.5279	1.9184
14	98.1378	6.8473	2982.0542	683.6426	1687.0000	113606.9234	31.8991	277182.0000	10.0746	-10.3000	1.5269	1.9172
15	100.9378	6.8473	3627.0543	683.6426	1687.0000	448480.9940	31.8991	277182.0000	10.0746	-10.3000	1.5269	1.9172
16	103.7378	7.0014	5397.1665	698.8626	1714.6870	664474.3234	31.8991	355152.0000	9.9906	-10.3000	1.5613	1.9604
17	113.05	7.0014	6883.7081	698.8626	1714.6870	254824.1435	31.8991	355152.0000	9.9906	-10.3000	1.5613	1.9604
18	122.5378	7.0014	6581.9296	698.8626	1714.6870	239143.2543	31.8991	355152.0000	9.9906	-10.3000	1.5613	1.9604
19	125.3378	7.0014	5616.5772	698.8626	1714.6870	691487.1690	31.8991	355152.0000	9.9906	-10.3000	1.5613	1.9604
20	128.138	6.9410	4231.0923	692.4435	1699.8201	520778.2694	31.8991	377832.0000	9.9839	-10.4200	1.5478	1.9435
21	137.05	6.9410	683.5484	692.4435	1699.8201	26435.2525	31.8991	377832.0000	9.9839	-10.4200	1.5478	1.9435
22	146.9378	6.9410	788.3135	692.4435	1699.8201	27478.2269	31.8991	377832.0000	9.9839	-10.4200	1.5478	1.9435
23	151.101	6.9410	2327.1111	692.4435	1699.8201	192654.5368	31.8991	377832.0000	9.9839	-10.4200	1.5478	1.9435
24	153.901	7.0014	3571.1772	698.8626	1714.6870	439666.9162	31.8991	377832.0000	9.9906	-10.4200	1.5613	1.9604
25	164.05	7.0014	6968.1069	698.8626	1714.6870	236680.2268	31.8991	377832.0000	9.9906	-10.4200	1.5613	1.9604
26	172.701	7.0014	6947.9724	698.8626	1714.6870	276861.2621	31.8991	377832.0000	9.9906	-10.4200	1.5613	1.9604
27	175.501	7.0014	6829.6317	698.8626	1714.6870	840832.8579	31.8991	377832.0000	9.9906	-10.4200	1.5613	1.9604
28	178.301	6.9410	5994.3276	692.4435	1699.8201	737856.3906	31.8991	377832.0000	9.9839	-10.4200	1.5478	1.9435
29	187.05	6.9410	3692.5559	692.4435	1699.8201	145464.8511	31.8991	377832.0000	9.9839	-10.4200	1.5478	1.9435
30	197.101	6.9410	3639.9253	692.4435	1699.8201	124816.6725	31.8991	377832.0000	9.9839	-10.4200	1.5478	1.9435
31	199.901	6.9410	3716.4231	692.4435	1699.8201	457463.5762	31.8991	377832.0000	9.9839	-10.4200	1.5478	1.9435
32	202.701	6.7701	4833.0580	674.8401	1657.9034	594748.2657	31.8991	377832.0000	9.9740	-10.4200	1.5097	1.8956

33	213.05	6.7701	7077.9944	674.8401	1657.9034	235657.3752	31.8991	377832.0000	9.9740	-10.4200	1.5097	1.8956
34	221.501	6.7701	7015.1414	674.8401	1657.9034	286020.7503	31.8991	377832.0000	9.9740	-10.4200	1.5097	1.8956
35	224.301	6.7701	6701.0706	674.8401	1657.9034	824622.8604	31.8991	377832.0000	9.9740	-10.4200	1.5097	1.8956
36	226.712	6.2806	6056.3064	614.8573	1536.1823	860317.7526	31.8991	377832.0000	9.7669	-10.4200	1.4006	1.7586
37	234.05	6.2806	1958.0634	614.8573	1536.1823	91389.7095	31.8991	377832.0000	9.7669	-10.4200	1.4006	1.7586
38	243.212	6.2806	499.4871	614.8573	1536.1823	18671.6324	31.8991	377832.0000	9.7669	-10.4200	1.4006	1.7586
39	245.637	6.2806	473.8024	614.8573	1536.1823	66916.5899	31.8991	377832.0000	9.7669	-10.4200	1.4006	1.7586
40	248.28	5.4136	1192.7041	567.0202	1324.3617	157662.6109	31.8991	210000.0000	9.1072	-10.1000	1.2072	1.5158
41	257.05	5.4136	5599.1978	470.6981	1324.3617	211699.1319	31.8991	210000.0000	9.1072	-10.1000	1.2072	1.5158
42	266.288	5.3872	5823.7503	470.7298	1321.9728	209783.2399	31.8991	210000.0000	9.2489	-10.1000	1.2013	1.5084
43	268.954	3.7575	5570.7477	395.7387	1057.2311	808003.1678	706.4171	1976.0000	10.6171	7.5000	0.8379	1.0521
44	278.05	1.0550	3170.6617	102.8910	388.9297	162495.4595	706.4171	1976.0000	14.7671	11.2500	0.2353	0.2954
45	287.416	0.6424	705.1173	53.6933	271.3470	38094.5745	173.3208	272.0000	15.0862	8.4000	0.1432	0.1799
46	294.1	0.2783	392.3000	27.1958	73.1412	21157.8724	31.7895	339.9400	16.3320	8.4000	0.0621	0.0779

M.V. LIVERPOOL BRIDGE

(Re-named M.V. DERBYSHIRE)

CAPACITY PLAN

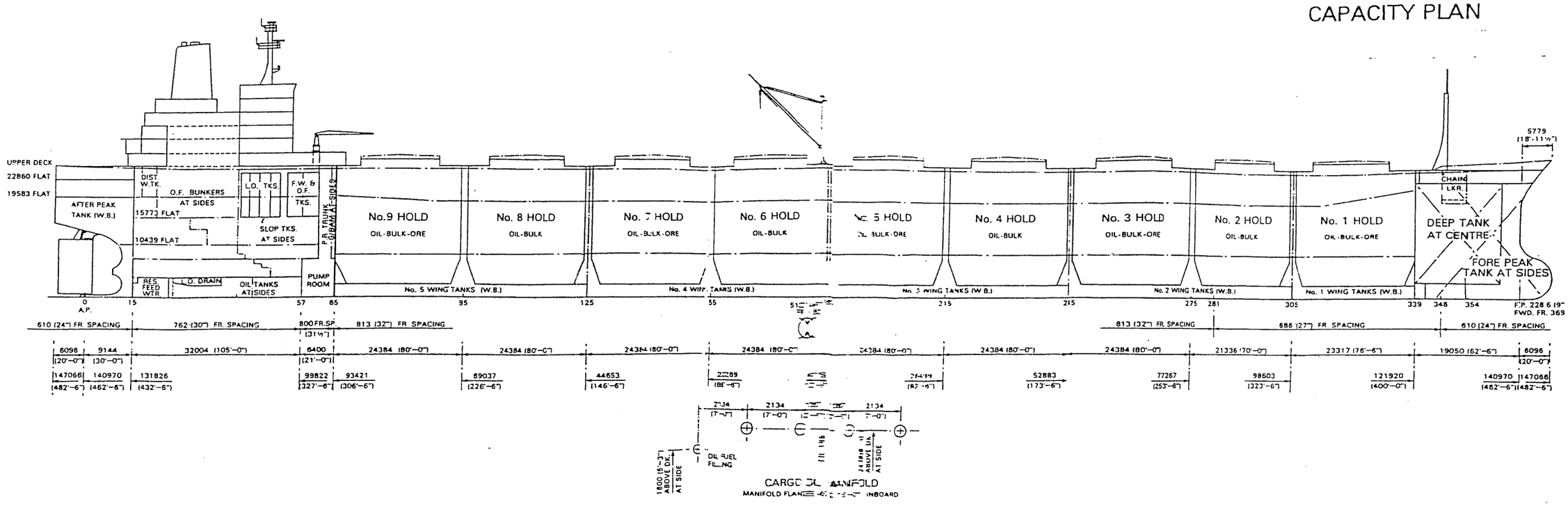

BODY PLAN

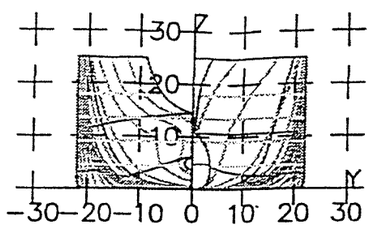

PRINCIPAL PARTICULARS OF MV DERBYSHIRE

LENGTH (OA) = 294.1 m
BREADTH MOULDED = 44 m
DEPTH MOULDED = 24.99 m
DRAUGHT AMIDSHIPS = 17.885 m
DISPLACEMENT = 192065 tonne
BLOCK COEFFICIENT = 0.84
LCB = 3.412 m
WETTED AREA = 20575.09 mò

SHEER PLAN

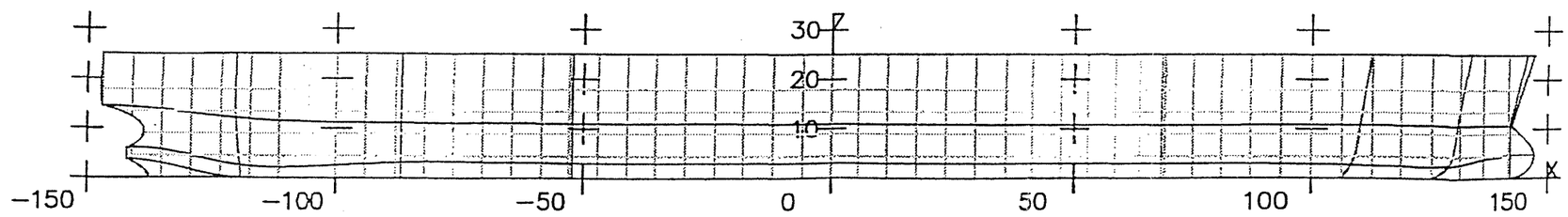

BREADTH PLAN

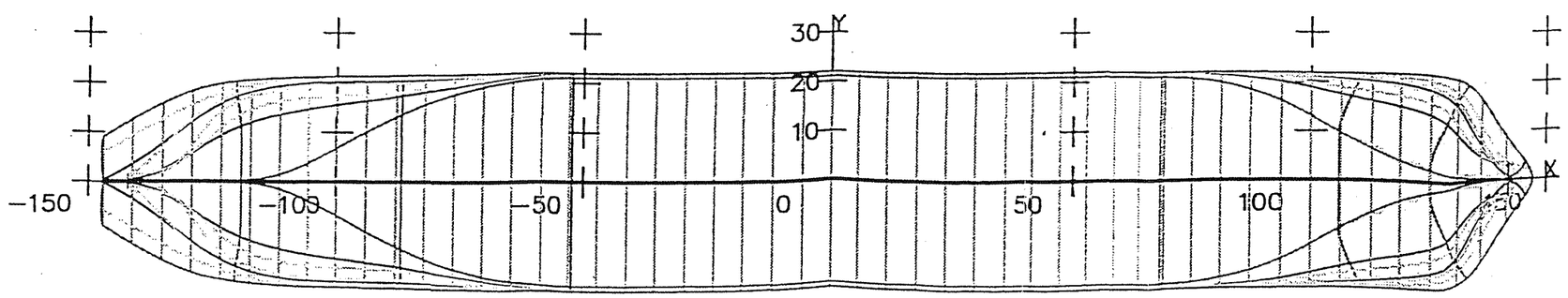

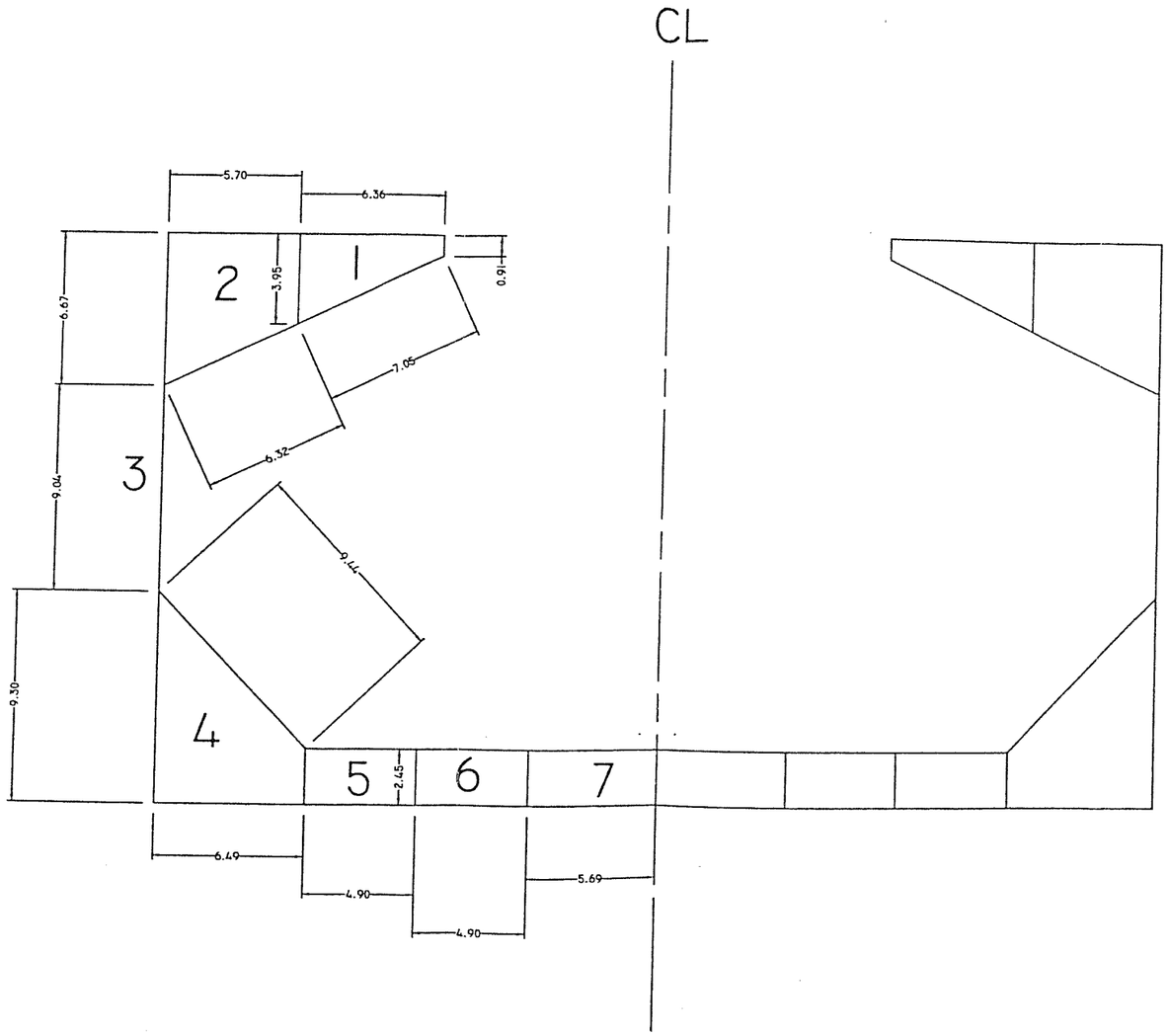

SIMPLIFIED MID-SHIP SECTION FOR MV DERBYSHIRE

Appendix 2

- The finite difference method
- The finite element method in 2D & 3D hydroelasticity analyses
- The finite element method as a measure of dynamic strength
- Mass matrix entries for a typical Przemieniecki finite element

- **The finite difference method**

The finite difference (FD) method is the oldest finite discretisation technique. Since its introduction by Euler in the 18th century it has been widely employed for the numerical solution of partial differential equations (PDE's) by several engineers and mathematicians worldwide [1,2,3]. Although in principle it can be applied in any mesh type most of the applications are related to structured grids of one- two- or three-dimensional form.

The grid lines serve as local coordinate lines. In principle Taylor series expansion or polynomial fitting is used to obtain approximations to the first and second derivatives of the variables with respect to the coordinates. At each point, the differential equation is approximated via replacing the partial derivatives in terms of the nodal values of the functions as:

$$\left(\frac{\partial \Psi}{\partial x}\right)_{x_i} = \lim_{\Delta x \to 0} \frac{\Psi(x_i + \Delta x) - \Psi(x_i)}{\Delta x} \qquad (1)$$

A geometrical interpretation is shown in figure 4.5. The first derivative $\partial\Psi/\partial x$ at a point is simply the slope of the tangent to the curve $\Psi(x)$ (line marked as exact in figure 1).

Three alternative discretisation schemes namely forward, backward and central are widely used depending on the dimensionality and complexity of the problem. In hydroelasticity studies it has been customary to use one dimensional line grid functioning according to the so-called central finite difference scheme. This methodology uses the slope of a line passing through two points lying at opposite sides of the point at which the derivative is approximated.

Since the function $\Psi(x)$ represents a second or even higher order polynomial (depending on the degree modal complexity) mapping the internal modal actions of the structure this numerical approach can be considered as quite accurate and close to the analytical solution of the Bishop et al mathematical model describing the symmetric or antisymmetric in vacuo vibrations of the hull girder (see chapter 3, equations 3.13, 3.14).

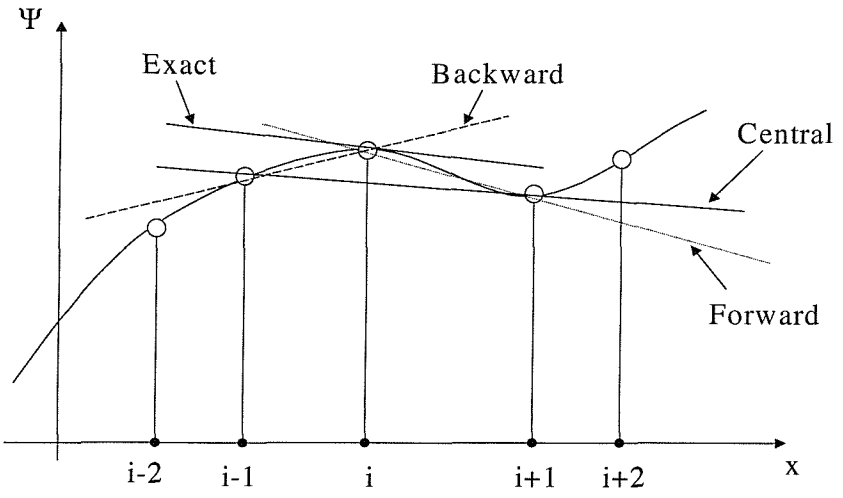

Fig. 1 Alternative FD discretisation schemes

- **The finite element method in 2D & 3D hydroelasticity analyses**

The basic ideas of the finite element method were originated from the advances in aircraft structural analysis, based on the finite difference method. The key feature of the finite element method and the point of departure from FD and matrix frame analyses is the use of two- as well as three-dimensional elements for the discrete representation of a continuum. The first paper to clearly and fully implement this idea was presented in 1956 by Turner et al [4]. It should however be mentioned that some of the basic features of the method had appeared before this in papers by Courant [5], McHerny [6], Hrenikoff [7], and others. There followed many other contributions by many authors, including a series of papers on matrix structural analysis by Argyris and his collaborators, beginning in 1954 and culminating in a monograph by Argyris and Kelsey in 1960 [8]. These initial investigations were focussed on structural plane stress applications, buckling, material and geometric non-linearities. However, the term finite elements was initially coined and used by Clough in 1960's and the first book on the method was published by Zienkiewitcz and Chung in 1967, leading to serious investigation of stress analysis, fluid flow, heat transfer and non-linear problems, whose formulations were combined to the mathematical foundations of the process in 1970 [1].

In FEA structural analysis a complex region defining a continuum of abrupt form, is discretised into areas or volumes known as elements having boundaries defined by nodal points. The

material properties and governing relationships are considered over these elements and expressed in terms of unknown values at element corners. An assembly process, duly considering the loading and constraints results into a system of matrix equations to represent the stiffness and mass effects and thus predict the approximate behaviour of the continuum. The theoretical concepts of the method have been well established in literature [1,2]. In the following section some information related to the importance of FEA in dynamics is outlined.

- **The finite element method as a measure of dynamic strength**

The application of a cyclic load with frequency less than one third of a structure's lowest natural frequency of vibration can be considered as static. However, if the load has a higher frequency, or varies randomly or is applied suddenly, a dynamic analysis is required which implies the existence of inertia effects and sometimes damping in addition to the usual stiffness effects expressing the potential energy stored into a static structure.

The basic difference between static and dynamic modelling is based on the effects exerted by the inertia. For vibrations to occur, the structure must possess inertia so that when it reaches a position of equilibrium the corresponding force causes it to overshoot. Since this term is proportional to the acceleration of the structure, and the constant of proportionality is the mass, which stores kinetic energy, the additional effects are expressed by the so-called mass matrix. This methodology manifests the dynamic strength of a ship on the basis of interchange between potential and kinetic energies.

For a vibrating solid body with distributed mass like a ship structure, overall potential and kinetic effects may be considered as the summation of the corresponding energies of the individual finite elements. For an element (e) of volume (V_e), surface (S_e) and distributed mass (see figure 2), the potential energy (Π_e) is formulated as the sum of the total strain energy and work potential:

$$\Pi_e = \frac{1}{2}\int_v \sigma^T e dV - \int_v u^T f dV - \int_s u^T T ds - \sum u_i^T P_i \qquad (2)$$

where (σ) is the stress tensor, (u) is the displacement vector, (f) is the body force, (T) is the traction force and (P_i) is the point load. The elemental kinetic energy (T_e) is given by:

$$T_e = \frac{1}{2}\int_V \dot{u}^T \rho \dot{u} dV \tag{3}$$

where (ρ) is the density and $(\dot{u})$is the velocity vector at a point. Since in FEA the body is discretised, the displacement (u) may be expressed in terms of a nodal displacement (q) using interpolation functions (N) (also known as shape functions) in the form:

$$u = Nq \tag{4}$$

Accordingly, the velocity vector is expressed by the formulae:

$$\dot{u} = N\dot{q} \tag{5}$$

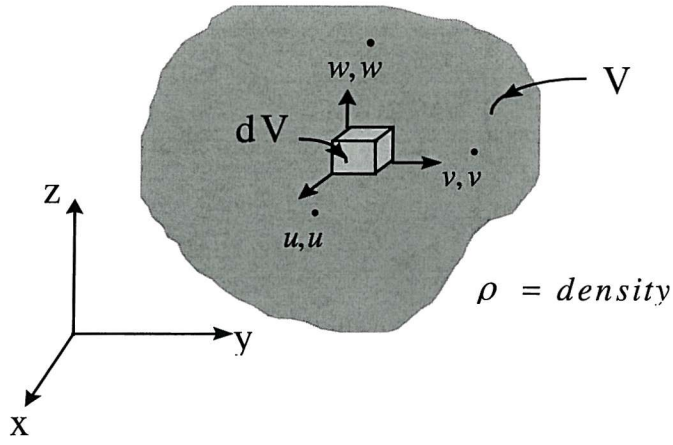

Fig. 2 Body with distributed mass

Substitution of (4.12) into (4.10) leads to the expression:

$$T_e = \frac{1}{2}\dot{q}^T\left[\int_v \rho N^T N dV\right]\dot{q} \tag{6}$$

where the bracketed expression is the element mass matrix and on taking the summation of all the elements the total kinetic energy (T) becomes:

$$T = \sum T_e = \frac{1}{2}\dot{Q}^T M \dot{Q} \tag{7}$$

Similarly, the total potential energy (Π) after considering free vibration (i.e. neglecting the terms (f),(T) and (P_i) of equation 2) becomes equivalent to the summation of the internal strain energies of each of the elements of the overall system:

$$\Pi = \sum \Pi_e = \frac{1}{2}\sum\left[\int_e \sigma^T E A dx\right] = \frac{1}{2}\sum\left[\int_e q^T B^T E B q A dx\right] = \frac{1}{2}\sum q^T\left[\int_e B^T E B A dx\right] q \qquad (8)$$

Considering that the last bracketed expression is the stiffness matrix the potential energy of the system becomes equivalent to:

$$\Pi = \frac{1}{2} Q^T K Q \qquad (9)$$

According to Hamilton's principle for an arbitrary time interval from t_1 to t_2 [1], the state of motion of a body maximises the functional $\Re = \int_{t_1}^{t_2} L dt$ and if $(\Re)$ can be expressed in terms of the generalised variables (q), then the equations of motion are given by Lagrange's expression:

$$\frac{d}{dt}\left(\frac{\partial \Re}{\partial \dot{q}_i}\right) - \frac{\partial \Re}{\partial q_i}\Big|_{i=1}^{i=n\in N} = 0 \qquad (10)$$

The Lagrangean transformation $\Re$=**T**-Π leads to the well known equation of motion for an undamped, freely vibrating structure:

$$M\ddot{Q}(t) + KQ(t) = 0 \qquad (11)$$

This is known as the equation of motion for a free vibrating linear conservative system (see also chapter 3, equation 3.24) from which the eigenvalues of the vibrating structure may be derived and consists the basis of analysis for the dry module of both two- and three-dimensional hydroelasticity theories (see chapter 3, section 3.6).

- **Mass matrix entries for a typical Przemieniecki finite element**

According to Thomas et al [9,10], the first formulation of a simple beam element was given by Mc Calley [11,12] and was extended to the more general case of a tapered beam by Archer [13]. Przemieniecki [14], gave detailed derivation for a uniform beam of the mass and stiffness matrices given by McCalley and Archer by deriving the stiffness and mass matrices reffered to the displacement vector ($w_1,\theta_1,w_2,\theta_2$) (where w_1,w_2 denote the transverse displacements at nodes 1,2 and ,θ_1,θ_2 are the cross-section rotations) denoted as:

$$k = \frac{EI}{L^3(1+\Phi)}\begin{bmatrix} 12 & 6L & -12 & 6L \\ 6L & L^2(4+\Phi) & -6L & L^2(2-\Phi) \\ -12 & -6L & 12 & -6L \\ 6L & L^2(2-\Phi) & -6L & L^2(4+\Phi) \end{bmatrix} \qquad \text{where } \Phi = \frac{12EI}{GkAL^2}$$

$$m = \frac{\rho AL}{(1+\Phi)^2}\begin{bmatrix} m_1 & m_2 & m_3 & m_4 \\ m_2 & m_5 & -m_4 & m_6 \\ m_3 & -m_4 & m_1 & -m_2 \\ m_4 & m_6 & -m_2 & m_5 \end{bmatrix} + \frac{\rho AL}{(1+\Phi)^2}\left(\frac{r}{L}\right)^2\begin{bmatrix} m_7 & m_8 & -m_7 & m_8 \\ m_8 & m_9 & -m_8 & m_{10} \\ -m_7 & -m_8 & m_7 & -m_8 \\ m_8 & m_{10} & -m_8 & m_9 \end{bmatrix}$$

where:

$$m_1 = \frac{13}{35} + \frac{7\Phi}{10} + \frac{\Phi^2}{3}$$

$$m_2 = \left(\frac{11}{210} + \frac{11\Phi}{120} + \frac{\Phi^2}{24}\right)L$$

$$m_3 = \frac{9}{70} + \frac{3\Phi}{10} + \frac{\Phi^2}{6}$$

$$m_4 = -\left(\frac{13}{420} + \frac{3\Phi}{40} + \frac{\Phi^2}{24}\right)L$$

$$m_5 = \left(\frac{1}{105} + \frac{\Phi}{60} + \frac{\Phi^2}{120}\right)L^2$$

$$m_6 = -\left(\frac{1}{140} + \frac{\Phi}{60} + \frac{\Phi^2}{120}\right)L^2$$

$$m_7 = \frac{6}{5}$$

$$m_8 = \left(\frac{1}{10} - \frac{\Phi}{2}\right)L$$

$$m_9 = \left(\frac{2}{15} + \frac{\Phi}{6} + \frac{\Phi^2}{3}\right)L^2$$

$$m_{10} = \left(-\frac{1}{30} - \frac{\Phi}{6} + \frac{\Phi^2}{6}\right)L^2$$

- **References**

[1] Zienkiewicz, O.C., Taylor, R.L.: The finite element method, McGraw Hill, New York, USA ,(1979).

[2] Bathe, K.J.: Finite element procedures, Prentice Hall, New Jersey, USA, (1996).

[3] Ferziger, J.H., Peric, M: Computational methods for fluid dynamics, Springer, Berlin, Germany, (1997).

[4] Turner, M, Clough, R., Martin, H. and Topp, L.: Stiffness and deflection analysis of complex structures, Journal of Aerospace Science, 23:805-823, (1956).

[5] Courant, R.: Variational methods for the solution of problems of equilibrium and vibration, Bulletin of the American Mathematical Society, 49:1-43, (1943).

[6] McHerny, D.: A lattice method for the solution of plane stress problems, Journal of Institution of Civil Engineers, 21:59-82, (1943).

[7] Hrenikoff, A.: Solution problems in elasticity by the framework method, Journal of Applied Mechanics, 8:169-175, (1941).

[8] Argyris, J, Kesley, S.: Energy theorems and structural analysis, Butterworth Scientific Publications, London, (1960).

[9] Thomas, D.L., Wilson, J.M. and Wilson, R.R.: Timoshenko beam finite elements, Journal of sound and vibration, 33:315-330, (1975).

[10] Lees, A.W. and Tomas, D.L.: A unified Timoshenko beam finite element, Journal of sound and vibration, 80:335-366, (1982).

[11] McCalley, R.B.: Mass lumping for beams, General Electric Knolls Atomic Power Laboratory, Schenectady, New York, Report DIG/SA 63-68, (1963).

[12] Archer, J.S.: Consistent matrix formulations for structural analysis using finite element techniques, Journal of the American Institute of Aeronautics and Astronautics, 3:234-245, (1968).

[13] Przemieniecki, J.S.: Theory of matrix structural analysis, 2nd edition, McGraw Hill, New York, USA, (1970).

Appendix 3

1st Conference Publication (keynote lecture)

Hirdaris, S.E., Price, W.G. and Temarel, P.; Hydroelastic analysis of a bulk carrier (Keynote lecture); *13th International Conference on Ship and Shipping Research (NAV00)*; Vol.1, Hydroelasticity and applications, pp.5.6.1 - 5.6.12, Venice, Italy (2000).

HYDROELASTIC ANALYSIS OF A BULK CARRIER

S.E. Hirdaris, W.G. Price and P.Temarel

Ship Science,
School of Engineering Sciences,
University of Southampton,
Southampton, SO17 1BJ,
United Kingdom.

ABSTRACT

Bulk carrier losses since the beginning of the 1980s are in excess of 150 and account for the loss of more than 1200 lives. Many of those are attributed to causes such as hull girder failure, loss of stability and loss of reserve buoyancy. The remainder are unexplained losses. Seaway induced dynamic loads and their consequences may be able to shed light in explaining such disasters. Hydroelasticity theory provides a description of the mechanisms for the fluid-flexible structure interaction and the evaluation of these dynamic loads.

In this paper, two- and three- dimensional hydroelasticity theories are applied to determine the dynamic characteristics of a bulk carrier, representing the structure of MV Derbyshire. The structure is modeled using two different types of idealisation. Namely, a three-dimensional finite element model using shell elements and two-dimensional models using beam elements. The generation of the structural idealisation is described and modelling issues are discussed. Both symmetric and antisymmetric distortions are included in the *dry* or *in vacuo* analysis. The *in vacuo* dynamic characteristics (i.e. natural frequencies and mode shapes) of all models are discussed and compared with particular emphasis on the effects of modelling hatch openings, shear centre and warping.

1. INTRODUCTION

Bulk carriers today comprise 33% of the world's merchant fleet. Of these 72% are Handysize, 19% Panamax and 9% Capesize. The age of the current fleet is between 10 and 15 years [1]. Casualty statistics for the period between 1990 and 1997, as assessed by the Baltic and International Maritime Council (BIMCO), indicate that 25 bulk carriers, totaling 1,847,174 DWT, and 572 lives were lost. Of these casualties 40% correspond to Handysize, 12% to Panamax and 48% to Capesize ship types [2]. Since the beginning of the eighties, according to Lloyd's Register of Shipping, more than 57 bulk carriers have been lost at sea and a further 61 incurred damage to such an extent that their loss was narrowly averted [3]. Although these statistics provide just a general overview of the situation a number of points should be noted [3]:

- The rate of known or possible structural failures increased dramatically between 1989 and 1994, 1991 being the worst year with 11 ships lost and 14 occurrences of serious structural failure ;
- The average age of ships lost in this period was 17.5 years;
- The majority of the casualties occurred midway between special surveys;
- The number of losses for vessels carrying steel/iron may be considered rather high as these products account only for 7% of the dry bulk trade [2].

The bulk carrier industry today is recognised as the workhorse of the world's merchant fleet. Research undertaken by IMO and IACS suggests that some of the possible causes for 90% of the losses could be hull girder failure, loss of stability and loss of reserve buoyancy [4]. However there still remains 10% unexplained disasters, which could be attributed to structural failure, although concrete evidence is hard to procure. Seaway induced dynamic loads and their consequences may be able to shed light in explaining these disasters. Hydroelasticity theory, unlike empirical and quasi-static methods, provides a rigorous analysis whereby the fluid-flexible structure interaction is formulated and the wave induced dynamic loads and responses (e.g. stresses, bending moments, etc) are evaluated. Accordingly, this theory was applied to investigate the losses of the bulk carrier Onomichi Maru [5] and the OBO Derbyshire and the failures suffered by her sister ships [6].

The objectives of current investigations are to examine the influence of three-dimensional structural modelling on the dynamic behaviour of slender beamlike vessels in waves and, in particular, the antisymmetric dynamic behaviour of vessels with large deck openings. Along these lines the *dry* or *in vacuo* dynamic characteristics of a vessel with principal dimensions similar to those of MV Derbyshire are presented in this paper. The structure is modelled using two-dimensional beam and three-dimensional (shell finite element) idealisations. The emphasis in all structural models is on retaining structural/geometric (e.g. hatch openings, hold configurations) and physical (e.g. mass distribution) characteristics. Modal analyses are carried out for both symmetric and antisymmetric distortions. The natural frequencies and mode shapes of all models are compared with particular emphasis on the effects of modelling hatch openings, shear centre (thus, coupling between horizontal bending and torsion) and warping. The implications of this investigation, in terms of modal characteristics predicted by different models, are of significance

for the accurate prediction of wave-induced dynamic loads, since these characteristics are the fundamental building blocks of hydroelasticity theory.

2. THE UNIFIED HYDROELASTICITY THEORY

Hydroelasticity theory aims at modelling the fundamental physical characteristics of fluid-flexible structure interactions. The two-stage approach of *dry* or *in vacuo* and *wet* analyses leads to a direct evaluation of dynamic loads and responses (e.g. stresses, bending moments, shear forces, torsional moments) for a vessel travelling at arbitrary heading in regular waves and irregular seaways. This theory is unified in the sense that it incorporates rigid body motions (i.e. conventional seakeeping) as well as distortions. The concept of hydroelasticity theory gained significant momentum in the mid-seventies, when Bishop and Price established the basic principles of a theory for flexible beam-like hulls subject to steady state or transient (e.g. slamming) wave-induced loads, combining Timoshenko beam and strip theories [7]. The method was applied successfully to a variety of beamlike merchant and naval ships and its capabilities in simulating symmetric, antisymmetric and unsymmetric dynamic behaviour in waves was demonstrated [7, 8]. Comparisons with available experimental and full-scale measurements, such as those by Bishop et al [9] and Aksu et al [10], confirmed the validity of the hydroelastic approach.

The three-dimensional hydroelasticity theory was developed to simulate the wave-induced dynamic behaviour of non-beamlike vessels in waves [11]. This analysis makes use of a two- or three-dimensional finite element model of the structure and a singularity distribution (such as pulsating source) over its wetted surface. The application to SWATHs, using crude and refined structural models, has demonstrated the versatility and potential of this method [11,12]. Recent applications to trimarans showed good agreement with flexible model experiments for wave induced loads, such as prying moment, for a range of speeds and headings [13]. Applications to non-slender, mono-hulled vessels, such as sailing yachts, showed that the method is capable of simulating accurately the dynamic behaviour of such vessels and identifying correctly areas where structural problems may arise [14]. The analysis has also been applied to beamlike mono-hulls (without any significant deck openings), showing good agreement between wave-induced loads and responses predicted by two- and three-dimensional models [15].

3. STRUCTURAL MODELLING

Two- and three-dimensional structural models were generated to idealize the structural and inertia characteristics of a vessel based on the OBO Derbyshire. The length of this vessel is L_{OA}=294m (L=L_{BP}=282m) and the remaining dimensions and properties can be found in papers and reports by Bishop et al [6,16]. Shell finite elements were used to incorporate major structural elements such as deck, side, inner/outer bottom, hopper spaces, bulkheads, major longitudinal girders etc. in this three-dimensional idealisation

of the structure [17]. The two-dimensional (beamlike) idealisation was obtained using uniaxial beam finite elements with non-uniform length [17], as well as a non-uniform beam idealisation, based on a finite difference formulation of Timoshenko beam theory, using beams of equal length [7]. The latter method was required due to the unavailability of a beam element capable of coupled horizontal bending and torsion (including the effects of warping) in ANSYS 5.4 finite element library [17].

3.1. Three - dimensional model *shell3d*

The midship section (in the vicinity of a hatch opening) was generated in the first instance with sufficient detail to model the inner bottom using seven longitudinal girders and hopper spaces. The material contributions of other longitudinal stiffeners and transverse frames were subsumed into the properties of adjacent shell elements. Although this modelling approach, which can be seen in Fig.1(a), may be perceived as relatively crude, it is firmly believed that all elements necessary for an accurate idealisation of the dynamic behaviour of this vessel, in vertical bending and coupled horizontal bending and torsion, are incorporated. The midship section was, subsequently, incorporated into the parallel body and the idealisation was extended through the length of this vessel including transverse bulkheads and hatch openings where appropriate. Particular care was paid to the structural configurations at the stern and bow, including the bulbous bow. For simplicity of modelling the superstructure as well as the stiffness of the hatch covers were not included. The resultant model consists entirely of shell elements representing deck, side, inner/outer bottom, hopper and bulkhead plating (incorporating the adjacent transverse frames and longitudinal stiffeners) and inner bottom girders. SHELL63, an element with four nodes, six degrees of freedom per node and, thus, capable of membrane as well as bending deformations, was selected as a suitable element for the dynamic analysis, neglecting bending deformation effects [17]. Corresponding triangular elements were used in areas of large curvature, such as the bilge and the side shell in the vicinities of bow and stern, where the warpage (due to the four nodes of the shell element not being on a flat plane) was outside acceptable limits.

The three-dimensional FE model, shown in Fig.1(b), is in the form of 46 sections along the vessel. This facilitates the determination of the mass distribution along the vessel by manipulating the mass density of elements in a section, as well as the acquisition of properties required for the beam models. This method was preferred to using lump mass elements so that relevant numerical problems during modal analysis can be avoided [12]. The omission of transverse frames and longitudinal stiffeners from structural idealisations of mono- and multi-hulled vessels has been dealt successfully in the past by incorporating *fictitious* bulkheads where appropriate [13 - 15]. Omission of such elements results in mode shapes containing localised distortions, which are not physically representative of the dynamic behaviour of the vessel. These localised distortions can be avoided via the use of *fictitious* bulkheads, of negligible mass and thickness, which act as anchors, so to speak, to nodes of

elements not otherwise connected to other elements in a direction normal to their plane. Adopting the same approach, transverse and longitudinal *fictitious* bulkheads were incorporated in the structural model shown in Figs. 1(a) and (b). The degree of refinement adopted in this model would have resulted in a large number of shell elements to idealise the transverse bulkheads. Consequently, the *fan* shape form, seen in Fig.1(a), was adopted for both actual and fictitious transverse bulkheads used in the idealisation. The structural model, which can be seen in Fig.1(b), consists of 6439 nodes and 3673 shell elements.

3.2. Two-dimensional beam models – *beam2d, beamfd*

BEAM4 was selected for the beam finite element idealisation of the vessel (beam2d), using 46 beam elements of non-uniform length [17]. This is a uniaxial two-noded element with six degrees of freedom per node, thus including bending (in both directions), torsion as well as tension/compression capabilities. However, this element has shortcomings in simulating the coupling between horizontal bending and torsion for this type of vessel with large deck openings as there is no distinction between the centroid and shear centre. In addition, where torsion is concerned, warping of a cross section is neglected, which is again unsuitable for ships with large deck openings. It is believed that newer versions of ANSYS, such as 5.6, may contain elements which incorporate some of these effects. A finite difference formulation for a non-uniform Timoshenko beam (beamfd) was also used to provide a comparator for the three-dimensional model [7]. This method, however, is based on a discretisation of sections of uniform length along the vessel.

The lengthwise variation of structural and inertia properties for the beam models were calculated using the three-dimensional model, to allow for meaningful comparisons between the idealisations used. Properties such as mass, moments of inertia, second moments of area, effective shear areas, torsional stiffness (or torsional constant), warping stiffness (or sectorial second moment of area) were evaluated at every section of the three-dimensional shell model. A selection of these properties is shown in Fig.2. These properties have been checked against available data [6,16]. The only difference between past applications and the current analysis, as far as the beam idealisation is concerned, is the saw - tooth variation of structural properties, clearly seen in Fig.2, due to the deck openings. The longitudinal variation of the inertia properties is the same as in past applications, with the saw - tooth character being the result of the loading condition [6]. The same structural and inertia properties were used for both beam models, for convenience. This implies that the finite difference model (beamfd) has some small differences in the longitudinal variations of these properties by comparison to the other two models. Nevertheless, the influence of these differences appears to be small, as can be seen from Table 1 and Fig. 4.

The influence of the effective shear area is very important when determining the natural frequencies and modal characteristics. It is common practice to determine this property, which is rather difficult to evaluate, as a fraction of the (longitudinally effective) cross section area [18]. In the current analysis this

fraction was adjusted by comparing the natural frequencies obtained, for the two-noded symmetric and antisymmetric (horizontal bending dominated) mode shapes, from the three-dimensional shell and beam models. This resulted in 0.28 and 0.23 of the cross-section area being considered effective in shear for the symmetric and antisymmetric distortions, respectively.

4. IN VACUO DYNAMIC ANALYSIS

The subspace reduction method was selected to obtain the eigenvalues and eigenvectors of this vessel in vacuo for the numerical models shell3d and beam2d constructed using shell and beam finite elements, respectively. The finite difference scheme was adopted for the second beam model (beamfd), based on Timoshenko beam theory [7].

An overview of the natural frequencies and corresponding mode shapes, in ascending order, obtained for model shell3d are shown in Fig.3. As this vessel is assumed to be port-starboard symmetric the principal mode shapes were classified as symmetric (vertical bending) and antisymmetric (coupled horizontal bending and torsion). The corresponding natural frequencies are shown in Tables 1 and 2, respectively, including a brief description of the type of mode shape. The results obtained using model shell3d are compared with those from both beam models beam2d and beamfd for the symmetric modal analysis and only model beamfd for the antisymmetric analysis. This is due to the lack of coupling between horizontal bending and torsion and the omission of warping effects in the BEAM4 finite element used in model beam2d. Two sets of natural frequencies were calculated for model shell3d, corresponding to thicknesses t_{fb}=1 mm and 5mm for the *fictitious* bulkheads used. This was done in order to assess the influence of these bulkheads on the modal characteristics. It was observed that values of t_{fb}<1 mm resulted in the emergence of localised distortions in the mode shapes obtained, whilst for values of t_{fb}>5 mm eigenvector stiffening occurred. In other words 1mm is the minimum thickness that can be assigned to the *fictitious* bulkheads of this structural idealisation in order to obtain realistic mode shapes. The natural frequencies increase with increasing values of t_{fb}, as can be seen from Tables 1 and 2, due to increasing stiffness but not mass.

For the first few symmetric mode shapes the natural frequencies obtained from model shell3d (t_{fb}=1mm) are, in general, lower than those calculated for both beam models. The natural frequencies for model beam2d are closer to those obtained for the shell3d model, by comparison to the beamfd model. This is attributed to the one-to-one correspondence between the beam elements of beam2d and sections of shell3d models. Both finite element models also predict a longitudinal mode shape which is not included in the formulation of model beamfd. The vertical deflections, normalised to unit vertical displacement at the stern (near A.P.; keel centre line for model shell3d) are shown for all three models in Fig.4 for the first few symmetric mode shapes. In this figure only the vertical displacement at keel (centre line) is shown for model shell3d. Nevertheless, it should be noted that for these mode shapes the vertical deflection at the deck is very close to that of the keel, confirming the beamlike

symmetric dynamic behaviour of this vessel. There is good agreement between the mode shapes obtained from all three models. However, as the complexity of the mode shape increases (e.g. 5 nodes) so do the differences between both beam and shell3d models.

The antisymmetric natural frequencies calculated using model shell3d (t_{fb}=1mm) are lower than the corresponding predictions from model beamfd (accounting for the effects of warping) for its first three mode shapes, but higher for the remaining few, as can be seen from Table 2. It can also be observed from Table 2 that the antisymmetric dynamic behaviour of this vessel is driven by the influence of warping, i.e. the natural frequencies calculated from model beamfd ignoring the effects of warping (assuming zero warping stiffness) are very low and,in the main, dominated by torsion. In this respect, one should note that the maximum value for the warping stiffness (or sectorial second moment of area) corresponds to a minimum value of torsional stiffness (or torsional constant) and occurs at sections with hatch openings as can be seen from Fig.2. The first few antisymmetric mode shapes, normalised to unit horizontal displacement at the stern (near A.P.; keel centre line for model shell3d), are shown in Fig.5. The mode shapes are represented by the horizontal displacement (at shear centre) and the angle of twist for model beamfd. The horizontal displacements v_k and v_d, at keel (centre line) and deck (junction of side and deck shells) respectively, are used for model shell3d. The corresponding angle of twist is calculated as $\tan^{-1}[(v_k - v_d)/D]$, where D represents the vertical distance between deck and keel. Comparison of antisymmetric mode shapes obtained using models beamfd and shell3d is rather difficult. The horizontal deflections at keel and deck of model shell3d are very close to each other for horizontal bending dominated modes, e.g. see Fig.5(b). On the other hand, the horizontal deflections at deck and keel are different for the torsion dominated modes, e.g. see Figs. 5(a) and (c). This difference can sometimes result in horizontal deflections with different number of nodes for the keel and deck, as can be seen in Fig.5(c). In spite of these difficulties, the agreement between the mode shapes obtained from models shell3d and beamfd is reasonably good for the first few mode shapes. One should note, however, that identification of number of nodes for the mode shapes obtained from model shell3d is rather difficult, as explained previously. The node numbers quoted in Table 2 are with reference to both models, as can be verified from Figs. 3 and 5. It should be noted, from Table 2, that for the 2-node and 3-node torsion dominant modes the natural frequencies do not follow the ascending order for model shell3d.

5. CONCLUSIONS AND RECOMMENDATIONS

- This paper focuses on the application of hydroelasticity theory (*dry hull* analysis) to different levels of refinement in structural modelling for ships with large deck openings, such as bulk carriers, containerships, LNG carriers etc. The effects of structural modelling refinement on *dry hull* natural frequencies and modal characteristics was investigated for a bulk carrier using two-dimensional beam and three-dimensional shell idealisations.

- The amount of detail incorporated into the structural model can be selected to correspond to various stages of the design process, such as concept and preliminary design.
- Good overall agreement has been obtained between the *in vacuo* or *dry* hull dynamic characteristics (natural frequencies and mode shapes) calculated by all models for both symmetric and antisymmetric distortions.
- The generated three-dimensional structural model shell3d, incorporating deck openings, is capable of describing the effects of coupling between horizontal bending and torsion (through the shear centre) and warping. These effects **must** be included in a corresponding beam idealisation to obtain comparable dynamic characteristics.
- Furthermore the three-dimensional model is also capable of describing the effects of shear deformation for both symmetric and antisymmetric dynamic behaviour. These effects **must** also be incorporated into the equivalent beam idealization, which can be done through the use of effective shear area.
- The use of *fictitious* bulkheads in the three-dimensional structural model appears to have, once again, worked well; thus, resulting in a model with a reasonably small number of elements and degrees of freedom. It will be interesting, nevertheless, to make comparisons with a more refined three-dimensional model, incorporating longitudinal and transverse stiffeners rather than fictitious bulkheads, to further validate their use.
- The antisymmetric dry hull analysis also merits further investigation in order to derive better understanding of the influence of deck openings and the comparison of mode shapes between two- and three-dimensional structural models. To this end the sensitivity of the modal analysis to the deck openings and , in particular, shear centre merit further investigation.
- The next stage of this investigation will comprise the *wet* analysis, whereby loads such as vertical and horizontal bending moments and shear forces, torsional moments, stresses etc in regular head and oblique waves are predicted and compared using different structural models.

REFERENCES

[1] Mathiesen, T.C. : Safety of new and existing bulk carriers, International association of Classification Societies studies and conclusions, *RINA International Conference on the Design and Operation of Bulk Carriers*, 23-27, London, (1998).

[2] BIMCO : Bulk carrier safety – the view and role of an industry organisation, *RINA International Conference on the Design and Operation of Bulk Carriers*, 1-12, London, (1998).

[3] Tustin, R.D. : Existing bulk carrier safety – on the evaluation of the foremost hold structure under conditions of hold flooding, *RINA International Conference on the Design and Operation of Bulk carriers*, 48-68, London, (1998).

[4] IACS : Bulk carriers – guidance and information on bulk cargo loading and discharging to reduce the likelihood of over-stressing the hull structure, *IACS publications*, London, (1997).

[5] Bishop, R.E.D., Price, W.G., and Temarel, P. : A hypothesis concerning the disastrous failure of the Onomichi – Maru, *Trans. RINA*, 127:169-186, (1985).
[6] Bishop, R.E.D., Price, W.G., and Temarel, P. : A theory on the loss of MV Derbyshire, *Trans. RINA*, 127:169-186, (1991).
[7] Bishop, R.E.D. and Price, W.G. : Hydroelasticity of Ships, *Cambridge University Press*, UK, (1979).
[8] Bishop, R.E.D., Chalmers, D.W., Price, W.G. and Temarel, P. : The dynamic characteristics of unsymmetrical ship structures, *Trans. RINA*, 128:205 - 215, (1986).
[9] Bishop, R.E.D. Clarke, J.D., and Price, W.G. : Comparison of full scale and predicted responses of two frigates in severe weather trial, *Trans. RINA*, 126:153 - 166, (1984).
[10] Aksu, S, Price, W.G., Suhrbier, K.R. and P. Temarel, P. : A comparative study of the dynamic behavior of a fast patrol boat travelling in rough seas, *Journal of Marine Structures*, 6:421-441, (1993).
[11] Bishop, R.E.D, Price, W.G. and Wu, Y. : A general linear hydroelasticity theory of floating structures moving in a seaway, *Phil. Trans. Royal Soc. London*, A316:375-426, (1986).
[12] Price, W.G., Temarel, P. and Keane, A.J. : Hydroelastic analysis of a SWATH in waves, *In International Conference of Hydroelasticity in Marine Technology*, 231-243, Trondheim, Norway, (1994).
[13] Miao, S.H., Price, W.G. and Temarel, P. : The hydroelastic behaviour of multi hulls travelling in a seaway, *Proceedings 3rd International Conference Advances in Marine Structures*, Dunfermline, (1997).
[14] Louarn, F.H. and Temarel, P. : An investigation of the structural dynamics of a racing yacht, *In Proceedings of the 14th Chesapeake Sailing Yacht Symposium*, 123-142, USA, (1999).
[15] Price, W.G., Salas Inzunza, M.A. and Temarel, P. : The dynamic behaviour of a mono-hull in oblique waves using two- and three-dimensional fluid-structure interaction models, *Submitted to RINA*, (2000).
[16] Bishop, R.E.D., Price, W.G. and Temarel, P. : Derbyshire - A design review, *Report to Dept. of Transport, UK,* (1984).
[17] Swanson Ltd : The ANSYS 5.4 users manual, (1999).
[18] Chalmers, D.W. and Price, W.G. : On the effective shear area of ship sections, *Trans. RINA*, 122: 245-252, (1980).

Model Mode type	Beamfd	Beam2d	shell3d t_{fb} = 0.001m	shell3d t_{fb} = 0.005m
2 node VB	4.419	4.527	4.529	4.598
3 node VB	9.247	9.192	9.010	9.343
4 node VB	14.236	14.000	13.236	14.999
5 node VB	17.615	17.498	15.915	17.567
Longitudinal	-	17.831	17.932	18.208
6 node VB	25.019	24.586	24.586	25.250

Table 1. Natural frequencies (rad/s) for symmetric distortions of the dry hull (t_{fb} = thickness of fictitious bulkheads, VB = vertical bending).

Model Mode type	beamfd $C_w \neq 0$	Shell3d t_{bf} = 0.001m	shell3d t_{bf} = 0.005m	beamfd $C_w = 0$
1 node HB – 1 node **T**	5.148	5.004	5.390	1.655
2 node **HB** - 2 node T	5.847	5.554	5.727	2.933
2 node HB – 2 node **T**	10.099	12.629	12.993	4.523
3 node **HB** – 3 node T	11.132	10.712	11.045	5.392
3 node HB – 3 node **T**	15.385	18.981	19.440	6.770
4 node **HB** – 4 node T	16.382	16.286	16.725	7.773

Table 2. Natural frequencies (rad/s) for antisymmetric distortions of the dry hull (HB = horizontal bending, **HB** = dominant HB, T = torsion, **T** = dominant T, C_w.= warping stiffness).

(a) (b)

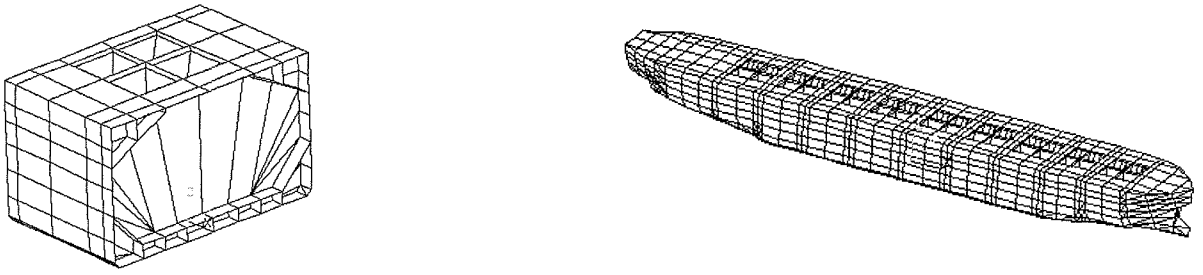

Fig.1 Finite element idealisation for model shell3d : (a) Transverse cross-section in the parallel body ; (b) Three dimensional view of the entire vessel.

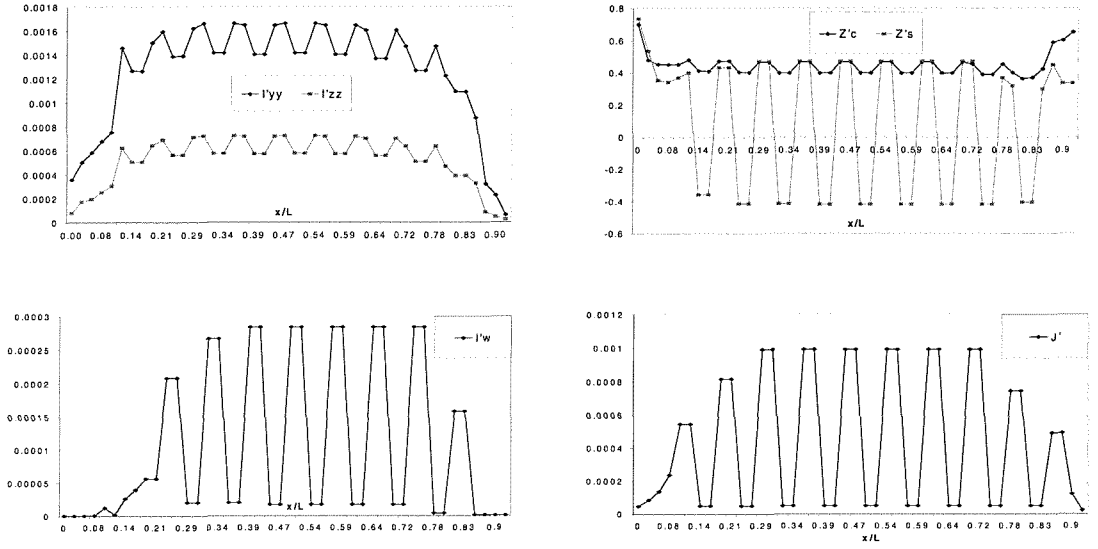

Fig.2 Variation of selected (non- dimensional) structural properties along the vessel. $I'_{yy} = I_{yy}/(D^2B^2)$, $I'_{zz} = I_{zz}/(D^2B^2)$, $z'_s = z_s/D$, $z'_c = z_c/D$, $I'_w = I_w/(D^3B^3)$, $J' = J/(D^2B^2)$; {I_{yy}, I_{zz} : second moments of area; z_c,z_s : distance of centroid and shear center from keel (+ve upwards); I_w : sectorial second moment of area; J : torsional constant; D : depth; B : beam; L : length; x : distance along the hull measured from A.P.}.

2 node VB
(ω_r = 4.529 rad/s)

1 node HB and 1 node **T**
(ω_r = 5.004 rad/s)

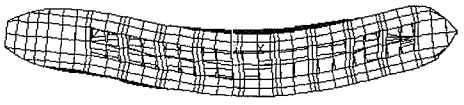

2 node **HB** and 2 node T
(ω_r = 5.554 rad/s)

3 node VB
(ω_r = 9.010 rad/s)

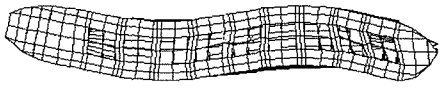

3 node **HB** and 3 node T
(ω_r = 10.712 rad/s)

2 node HB and 2 node **T**
(ω_r = 12.629 rad/s)

4 node VB
(ω_r = 13.236rad/s)

5 node VB
(ω_r = 15.915 rad/s)

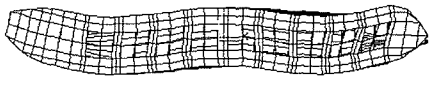

4 node **HB** and 4 node T
(ω_r = 16.286 rad/s)

3 node HB and 3 node **T**
(ω_r = 18.981 rad/s)

Fig.3 Principal mode shapes of model shell3d (VB : vertical bending ; HB : horizontal bending; T : torsion, **HB** : dominant HB, **T** : dominant T).

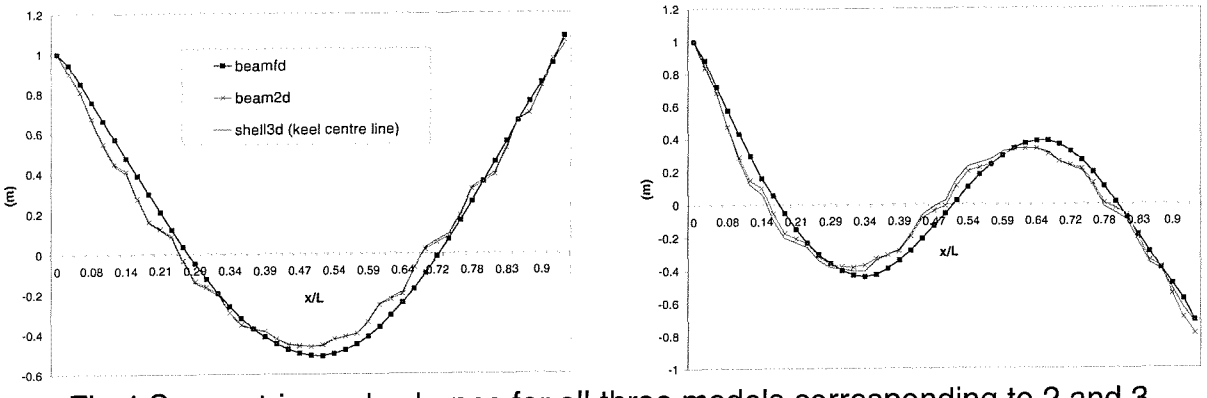

Fig.4 Symmetric mode shapes for all three models corresponding to 2 and 3 node deflections.

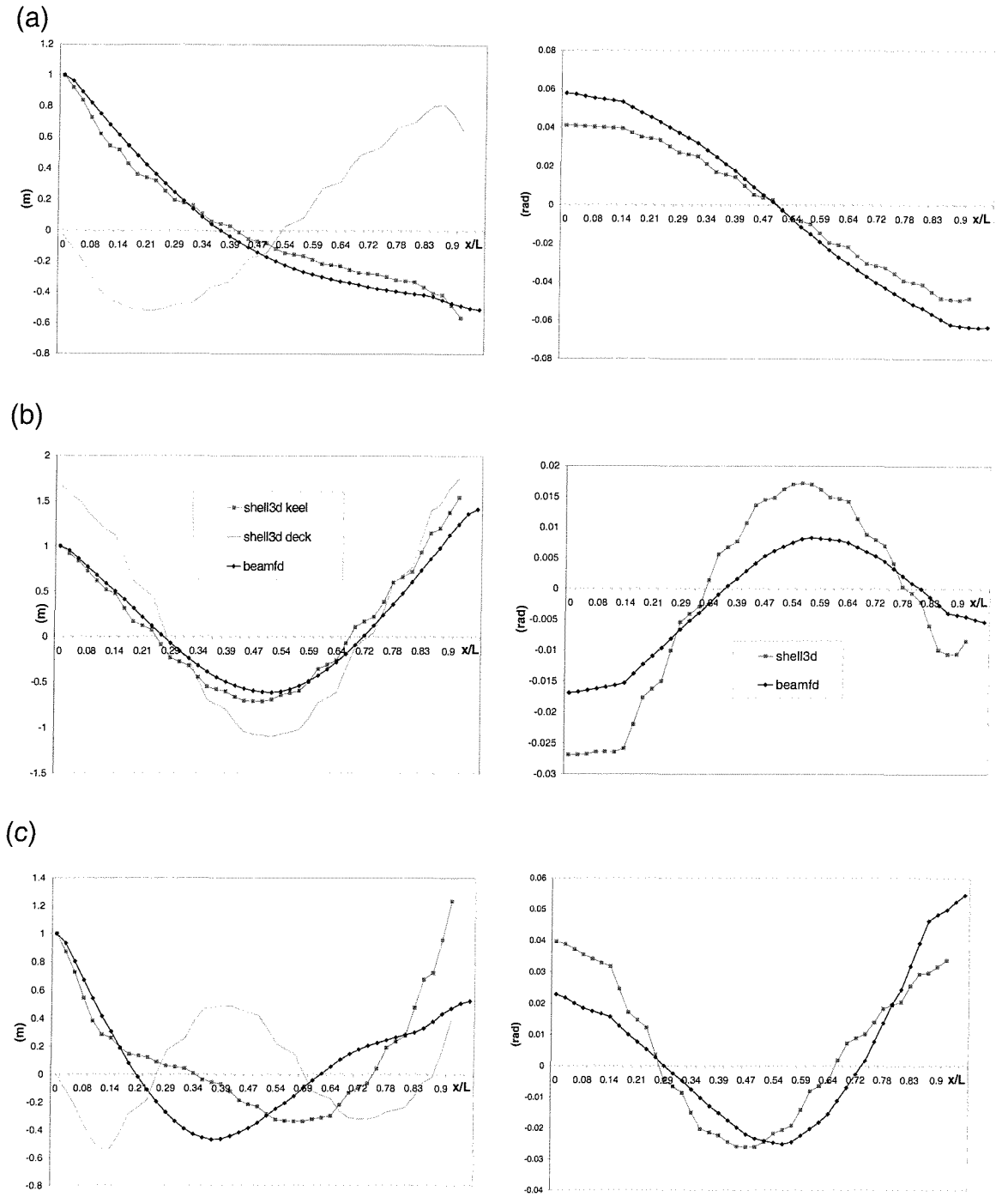

Fig.5 Antisymmetric mode shapes, represented by the horizontal deflection (m) and twist angle (rad), obtained from models beamfd and shell3d (keel centre and deck side junction) corresponding to : (a) 1 node torsion dominant; (b) 2 node horizontal bending dominant; (c) 2 node torsion dominant.

Appendix 4

2nd Conference Publication

Hirdaris, S.E., Price, W.G. and Temarel, P.; Symmetric and antisymmetric hydroelastic analysis of a bulker in waves; *8th International Symposium for Practical Design of Ships and other Floating Structures (PRADS01)*; Vol. 2, Structures and Materials-Hydroelasticity, pp. 903-910, Shanghai, China (2001).

SYMMETRIC AND ANTISYMMETRIC HYDROELASTIC ANALYSIS OF A BULKER IN WAVES

S.E. Hirdaris, W.G. Price and P.Temarel

School of Engineering Sciences, Ship Science, University of Southampton,
Southampton, SO17 IBJ, UK

ABSTRACT

The influence of structural configurations (such as large deck openings and double skins encountered in containerships, bulk carriers and LNG carriers) on predicting the global dynamic behaviour of these flexible vessels in waves is of particular interest. This is due to the options available for structural modelling, namely two-dimensional beam and three-dimensional FE idelisations. Two-dimensional idealisations offer a fast and efficient means of simulating the dynamic behaviour in waves whilst three-dimensional models are time and effort consuming, even when a relatively simple idelisation is used. The high rate of bulk carrier casualties in recent years makes this type of vessel a suitable example for investigating the influence of modelling on the fluid structure interactions and subsequent loads and responses in waves. Therefore, in this paper two- and three-dimensional hydroelasticity theories are applied to predict and compare the dynamic behaviour of a bulk carrier hull in regular oblique waves. Both symmetric and antisymmetric distortions are incorporated in these investigations.

KEYWORDS

Bulk carriers, dynamic loads, FE idealisation, hydroelasticity, wave-induced dynamic response

INTRODUCTION

The evaluation of wave-induced motions and loads are two of the most important aspects in ship design. Traditionally, prediction of wave-induced loads, in the main, relies on quasi-static and/or empirical methods. Overall, such methods proved to be quite adequate over the years with problems arising dealt by relying on accumulated experience. Nevertheless, the international amendments for bulkers, tankers and LNG carriers brought about by IACS and IMO are a measure of the concern related to the behaviour of such vessels and associated risks involving loss of human life, environmental pollution etc. (IACS 1997; Tustin 1998).

During the past ten years, more than 700 crewmen have died as a result of bulk carrier casualties. Following a rush of 25 bulk carrier losses in 1990 and 1991 five more bulk carriers and 74 lives were lost in 1993, followed, in 1994, by the tragic loss of six bulkers and 100 lives (IACS 1997; Tustin 1998). Research undertaken by IMO and IACS suggests that some of the possible causes for 90% of the losses could be hull girder failure, loss of stability and loss of reserve buoyancy (IACS 1997). However there still remains 10% unexplained disasters, which could be attributed to structural failure, although concrete evidence is hard to come by. The accurate prediction of seaway induced dynamic loads and their consequences may be able to shed light in explaining these disasters.

Hydroelasticity theory, unlike empirical and quasi-static methods, provides a rigorous analysis whereby the fluid-flexible structure interaction is formulated and the wave induced dynamic loads and responses (e.g. stresses, bending moments, etc) are evaluated. The two-stage approach of *dry* or *in vacuo* and *wet* analyses leads to a direct evaluation of dynamic loads and responses for a vessel travelling at arbitrary heading in regular waves and irregular seaways. This theory is unified in the sense that it incorporates rigid body motions (i.e. conventional seakeeping) as well as distortions. The concept of hydroelasticity theory gained significant momentum in the mid-seventies, when Bishop and Price (1979) established the basic principles of a theory for flexible beam-like hulls subject to steady state or transient (e.g. slamming) wave-induced loads, combining *Timoshenko beam* and *strip* theories. The method was applied successfully to a variety of beamlike merchant and naval ships and its capabilities in simulating symmetric, antisymmetric and unsymmetric dynamic behaviour in waves was demonstrated. Comparisons with available experimental and full-scale measurements, such as those by Bishop et al (1984) and Aksu et al (1993), confirmed the validity of the hydroelastic approach. The three-dimensional hydroelasticity theory was developed to simulate the wave-induced dynamic behaviour of non-beamlike vessels in waves (Bishop et al 1986). This analysis makes use of two- or three-dimensional finite element models of the structure and a singularity distribution (such as pulsating source) over its wetted surface. The application to SWATHs, using crude and refined structural models, has demonstrated the versatility and potential of this method (Bishop et al 1986, Price et al 1994). Recent applications to trimarans showed good agreement with flexible model experiments for wave induced loads, such as prying moment, for a range of speeds and headings (Miao et al 1997). Applications to non-slender, mono-hulled vessels, such as sailing yachts, showed that the method is capable of simulating accurately the dynamic behaviour of such vessels and identifying correctly areas where structural problems may arise (Louarn et al 1999). The analysis has also been applied to beamlike mono-hulls (neglecting any small deck openings), showing good agreement between wave-induced loads and responses predicted by two- and three-dimensional models (Price et al 2001).

The objectives of the current investigations are to examine the influence of three-dimensional structural modelling on the dynamic behaviour of slender beamlike vessels in regular waves and, in particular, vessels with large deck openings. Along these lines a vessel with principal dimensions and characteristics similar to those of MV Derbyshire is used in this paper (Bishop et al 1991; Hirdaris et al 2000). Two fluid-structure interaction models, incorporating both symmetric and antisymmetric motions and distortions, are used, namely (i) **beamfd** where Timoshenko beam idealisation is combined with a suitable strip theory (Bishop and Price 1979) and (ii) **shell3d** where a shell FE idealisation is used in conjunction with a three-dimensional pulsating source distribution over the wetted surface of the hull. Comparisons between the *dry* and *wet* hull characteristics, such as principal mode shapes, natural frequencies and wet resonance frequencies, and wave induced loads in oblique regular waves predicted by these models are presented.

FLUID-STRUCTURE INTERACTION MODELLING

Two- and three-dimensional structural models were generated to idealize the structural and inertia characteristics of a vessel based on the OBO MV Derbyshire. The length of this vessel is L_{OA}=294m (L=L_{BP}=282m) and the remaining dimensions and properties can be found in Bishop et al (1991).

For the three-dimensional model (shell3d) shell finite elements were used to incorporate major structural elements such as deck, side, inner/outer bottom, hopper spaces, bulkheads, major longitudinal girders etc. The material contributions of other stiffeners and transverse frames were subsumed into the properties of adjacent shell elements. For simplicity of modelling the superstructure as well as the stiffness of the hatch covers were not included, thus resulting in a deck with a number of large openings. Element SHELL63 with four nodes and six degrees of freedom per node was selected, considering only membrane deformations (Swanson Ltd. 2000). The three-dimensional FE model, shown in Fig.1(a), consists of 6439 nodes and 3673 shell elements and is in the form of 46 sections along the vessel. This facilitates the determination of the mass distribution along the vessel, by manipulating the mass density of elements in a section, as well as the acquisition of properties required for the beam model. This method was preferred to using lump mass elements so that relevant numerical problems during modal analysis, as noted by Price et al (1994), can be avoided. The omission of transverse frames and longitudinal stiffeners from structural idealisations of mono- and multi-hulled vessels has been dealt successfully in the past, as illustrated for example by Miao et al (1997), Louarn et al (1999) and Price et al (2001), by incorporating *fictitious* bulkheads of negligible mass and thickness (e.g. 1mm for the current application), where appropriate. Omission of such elements results in mode shapes containing localised distortions, which are not physically representative of the global dynamic behaviour of the vessel. A *fan* shape form, clearly seen in the detail of the FE model shown in Fig.1(b), was adopted for all actual and fictitious transverse bulkheads to avoid using excessive number of elements.

A finite difference formulation for a non-uniform Timoshenko beam (beamfd) was used to provide a comparator for the three-dimensional model (shell3d). The lengthwise variations of structural and inertia properties for the beam model were calculated from model shell3d, to allow for meaningful comparisons between the two idealisations. Properties such as mass, moments of inertia, second moments of area, effective shear areas, torsional stiffness, warping stiffness, shear centre were evaluated at every section of model shell3d, with the saw-tooth character being a result of the loading condition (for mass properties) and the large deck openings (for structural properties). These properties were illustrated by Hirdaris et al (2000) and, hence, not repeated here. However, the section moduli at deck and keel, relating to vertical bending, and at side, relating to horizontal bending, are shown in Fig.1(c), as they are used when comparing wave-induced loads. Previous two-dimensional structural models (e.g. Bishop et al 1991) adopted smooth variations of structural characteristics. It should be noted that although the 46 sections along the shell3d model are of unequal length, as seen in Fig.1(a), beamfd model was discretised using sections of equal length along the hull.

The mean wetted surface of the vessel, shown in Fig.1(d), is idealised using 952 four-cornered panels. For convenience a one-to-one correspondence between shell finite elements and panels on the mean wetted surface has been adopted. This implies that triangular elements, used to overcome warpage constraints (i.e. limitations imposed on four nodes of an element being coplanar), are also idealised as four-cornered panels with, for example, one node assigned to two corners. A pulsating source is allocated to each panel.

DRY AND WET ANALYSES

The *dry* hull natural frequencies obtained from models beamfd and shell3d are shown in Tables 1(a) and 1(b), for the symmetric and antisymmetric modes respectively. The dominant distortions of antisymmetric principal modes are highlighted. Views of the first few principal mode shapes obtained from the shell3d model are shown in Fig.2, highlighting the dominant distortion. The vertical deflections for the first two symmetric mode shapes are shown in Figs.3(a,b). The first antisymmetric (torsion dominant) and second antisymmetric (bending dominant) mode shapes are shown in Figs.3(c,d,e,f), represented by the horizontal deflection and the twist, respectively. For the shell3d model the horizontal deflections at both deck (junction with side plating) and keel (centreline) are used. From Figs.3(a-f) and Tables 1(a) and 1(b) it can be seen that there is good overall agreement between the two structural models used, in terms of natural frequencies and mode shapes, for the first few mode shapes. Nevertheless as the complexity of the mode shapes increases so do the differences. It should be noted that inclusion of warping effects in the beamfd model is essential for agreement in the antisymmetric modes.

The calculations in regular waves were carried out for the bulker proceeding at 7.41 m/s in regular waves encountered at a heading of $\chi = 135^{O}$, thus allowing inclusion of both symmetric and antisymmetric mode shapes. For the preliminary investigation a set of 8 flexible mode shapes, shown in Tables 1(a) and 1(b), was included in the wet analysis. The resonance frequencies for the *wet* hull can be identified by examining the variation of corresponding principal coordinate amplitudes with encounter frequency ω_e. The differences between the (wet) resonance frequencies predicted by two- and three-dimensional fluid-structure interaction models, also shown in Tables 1(a) and 1(b), follow, in general, the same trends as the dry hull natural frequencies.

The modal internal actions and wave-induced loads are obtained in the form of bending moments, shear forces and torsional moment for the beamfd and in the form of direct and shear stress components for the shell3d model. Vertical and horizontal bending moments and longitudinal direct stress can be related, for a beamlike vessel, using the following relationships:

$$\sigma_{deck} = \frac{VBM}{S_{deck}} \quad or \quad \sigma_{keel} = \frac{VBM}{S_{keel}} \quad and \quad \sigma_{side} = \frac{HBM}{S_{side}} \tag{1}$$

where S_{deck}, S_{keel} and S_{side} denote the corresponding section moduli, shown in Figure 1(c).The vertical and horizontal bending moments obtained directly from model beamfd and from the relevant stresses of model shell3d using the above relationships are shown in Figs.4(a) and 4(b), respectively, for $L/\lambda=1$, λ denoting the length of the ship. Contributions from symmetric modal direct stresses only were used for the vertical bending moment and antisymmetric modes only for the horizontal bending moment to allow for direct comparisons with the relevant bending moments obtained from model beamfd. There are some differences between the vertical bending moment obtained from the direct stresses on the deck (junction with side plating) and keel (centreline). Nevertheless, there is good overall agreement between the two models for the vertical bending moment magnitudes along the vessel. The agreement is not as good between the horizontal bending moment variation along the hull obtained from model shell3d using direct stresses on the side plating, either at nodes near the centroid or the junction with deck, and predictions from beamfd, the latter being considerably larger in the vicinity of amidships. It has been observed that the horizontal bending moment magnitudes predicted by model beamfd are

rather sensitive to the values of torsional moment of inertia (per unit length). This discrepancy is under further investigation.

As a further comparison, the variation of the wave-induced direct stresses on the deck (junction with side plating) and keel (centre line) are shown in Figs.5(a,b) for $L/\lambda=1$. The stresses from the three-dimensional model shell3d were calculated including and excluding the antisymmetric mode shapes, to investigate their contributions. Comparisons are also made with corresponding stresses obtained from model beamfd using the relationships of equation (1). As expected the antisymmetric modes contribute negligibly to the stresses on the keel centre line. Nevertheless, they have a significant contribution to the direct stresses obtained at the junction of deck and side plating. The differences observed between two- and three-dimensional direct stresses at keel and deck are similar to those observed for the vertical bending moment in Fig.4(a).

CONCLUSIONS

- This paper focuses on comparing the influences of different levels of refinement in fluid-structure interaction modelling on the dry hull dynamic characteristics and wave-induced loads and stresses for ships with large deck openings, such as bulk carriers, containerships, LNG carriers etc.. The results of this investigation are important from the point of view of selecting the detail to be incorporated into a model when working at various stages of the design process, such as concept and preliminary design.
- The dry hull analysis showed good overall agreement between beamfd and shell3d models for the first few symmetric and antisymmetric mode shapes; however, differences increase with modal complexity.
- The wave-induced vertical bending moment and direct stress show good overall agreement between the two models, taking into account the saw-toothlike nature of relevant second moment of area and section moduli. However, the agreement is not good between the horizontal bending moment values predicted by both models. The contributions from antisymmetric modes to stresses on the deck, at the junction with side plating, are noted.
- Further investigations are required to assess the influence of structural properties with saw-toothlike variation, a consequence of the large deck openings, on the dry hull characteristics and, consequently, wave-induced loads. The effects of wetted surface idealisation on wave-induce loads also merit further investigation.

REFERENCES

Aksu, S, Price, W.G., Suhrbier, K.R. and P. Temarel, P. (1993). A comparative study of the dynamic behaviour of a fast patrol boat travelling in rough seas, *Journal of Marine Structures* **6,** 421 - 441.

Bishop, R.E.D. Clarke, J.D., and Price, W.G. (1984). Comparison of full scale and predicted responses of two frigates in severe weather trial, *Trans. RINA* **126,** 153 - 166.

Bishop, R.E.D. and Price, W.G. (1979). Hydroelasticity of Ships, *Cambridge University Press*, UK.

Bishop, R.E.D., Price, W.G., and Temarel, P. (1991). A theory on the loss of MV Derbyshire, *Trans. RINA* **127,** 169-186.

Bishop, R.E.D, Price, W.G. and Wu, Y. (1986). A general linear hydroelasticity theory of floating structures moving in a seaway, *Phil. Trans. Royal Soc. London* **316:A,** 375 - 426.

Hirdaris, S.E., Price, W.G. and Temarel, P. (2000). Hydroelastic analysis of a bulk carrier, (keynote lecture), *International Conference on Ship and Shipping Research NAV2000,* **1**, 5.6.1 - 5.6.12, Venice, Italy.

IACS (1997). Bulk carriers - guidance and information on bulk cargo loading and discharging to reduce the likelihood of over-stressing the hull structure, *IACS publications*, London, UK.

Louarn, F.H. and Temarel, P. (1999). An investigation of the structural dynamics of a racing yacht, *In Proceedings of the 14th Chesapeake Sailing Yacht Symposium*, 123-142, USA.

Miao, S.H., Price, W.G. and Temarel, P. (1997). The hydroelastic behaviour of multi hulls travelling in a seaway, *Proceedings of the 3rd International Conference for Advances in Marine Structures*, Dunfermline.

Price, W.G., Temarel, P. and Keane, A.J. (1994). Hydroelastic analysis of a SWATH in waves, *In International Conference of Hydroelasticity in Marine Technology*, 231 - 243, Trondheim, Norway.

Price, W.G., Salas Inzunza, M.A. and Temarel, P. (2001). The dynamic behaviour of a mono-hull in oblique waves using two- and three-dimensional fluid-structure interaction models, *Accepted for publication RINA.*

Swanson Ltd. (2000). The ANSYS 5.6 users manual.

Tustin, R.D. (1998). Existing bulk carrier safety – on the evaluation of the foremost hold structure under conditions of hold flooding, *RINA International Conference on the Design and Operation of Bulk Carriers*, 48 - 68, London, UK.

TABLE 1

DRY HULL NATURAL (ω_r) AND WET RESONANCE (ω_{er}) FREQUENCIES (RAD/S) FOR (a) SYMMETRIC AND (b) ANTISYMMETRIC DISTORTIONS

(VB = VERTICAL BENDING; HB = HORIZONTAL BENDING; T = TORSION; **HB,T** = DOMINANT HB, T)

(a) Mode type	beamfd		shell3d	
	ω_r	ω_{er}	ω_r	ω_{er}
2 node VB	4.42	3.03	4.53	3.25
3 node VB	9.25	6.62	9.01	6.62
4 node VB	14.24	9.03	13.24	10.09
5 node VB	17.62	12.76	15.92	12.61

(b) Mode type	beamfd		shell3d	
	ω_r	ω_{er}	ω_r	ω_{er}
1 node HB – 1 node **T**	5.22	4.41	5.00	4.97
2 node **HB** - 2 node T	5.86	4.96	5.55	5.01
2 node HB – 2 node **T**	10.51	8.71	12.63	9.30
3 node **HB** – 3 node T	11.14	9.58	10.71	9.11

(a)

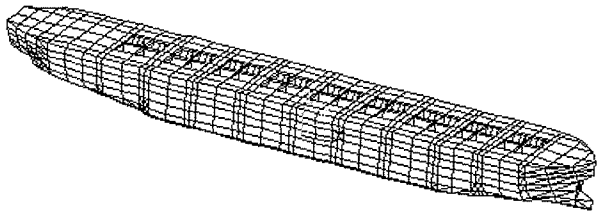

(b)

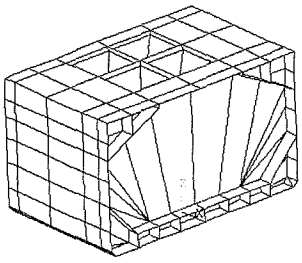

(c)

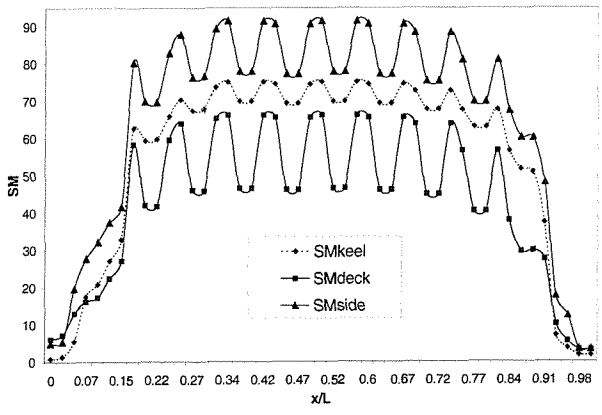

(d)

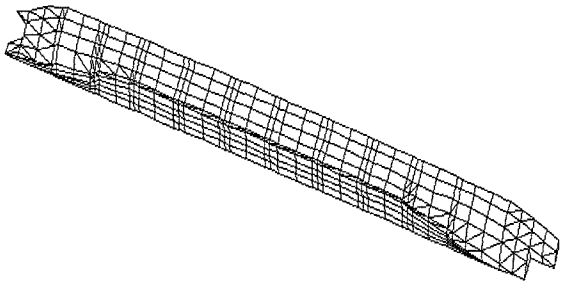

Fig.1 (a) Three dimensional FE model ; (b) Transverse cross-section in the parallel body ; (c) Section modulus (m^3) variation along deck, keel and side of the vessel ; (d) Idealisation of the mean wetted surface.

2 node VB

1 node HB and 1 node **T**

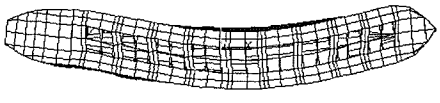

2 node **HB** and 2 node T

3 node VB

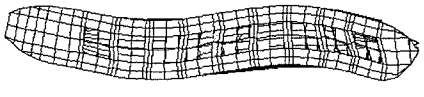

3 node **HB** and 3 node T

2 node HB and 2 node **T**

Fig.2 Principal mode shapes of model shell3d (VB: vertical bending; HB: horizontal bending; T: torsion, **HB,T**: dominant HB, T).

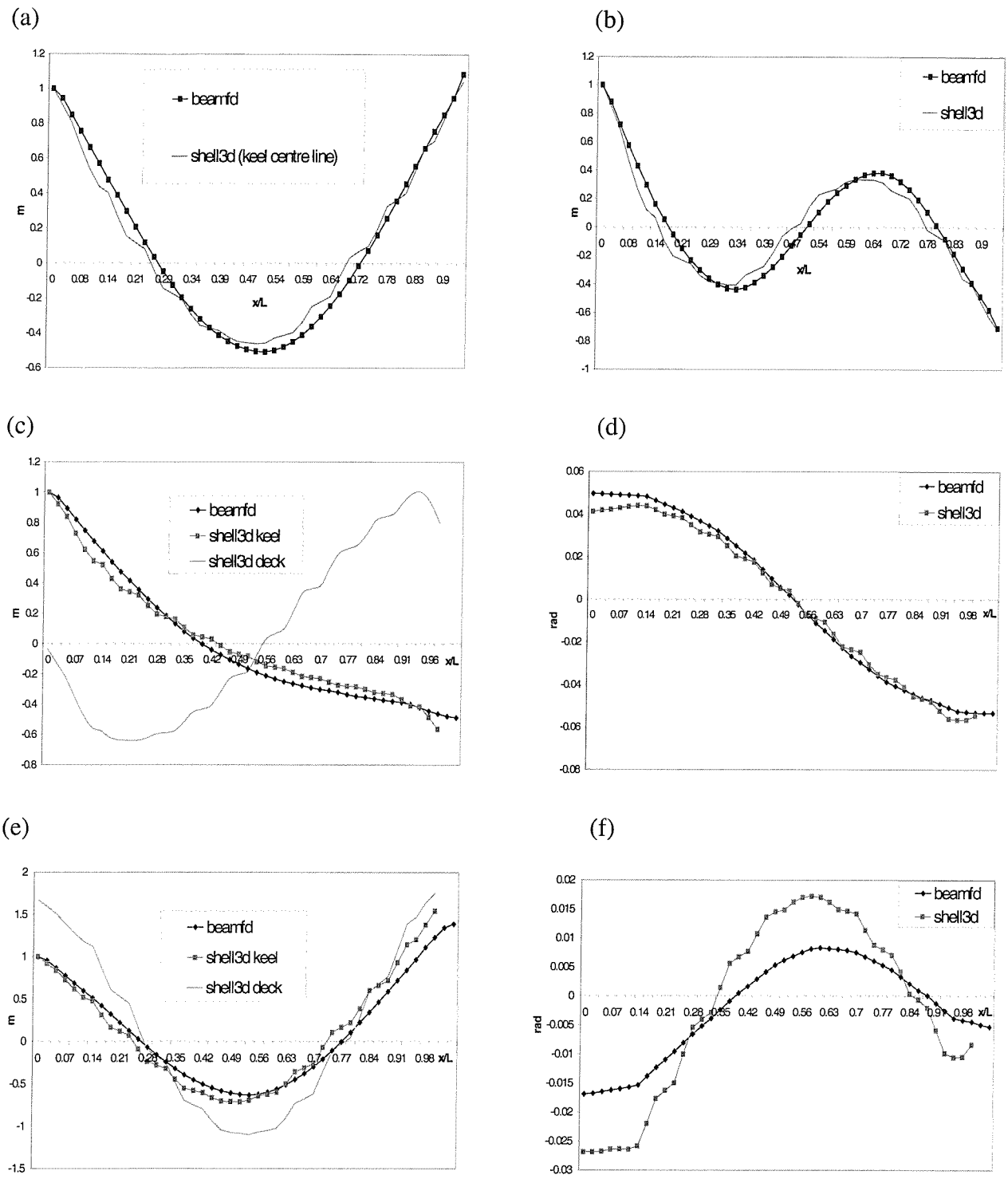

Fig.3 Principal mode shapes for: (a,b) 2 and 3-node symmetric vertical deflections ; (c,e) 1 and 2-node horizontal deflections (keel centerline and deck side junction for shell3d) and (d,f) twist angles for 1-node torsion dominant and 2-node HB dominant antisymmetric modes, respectively.

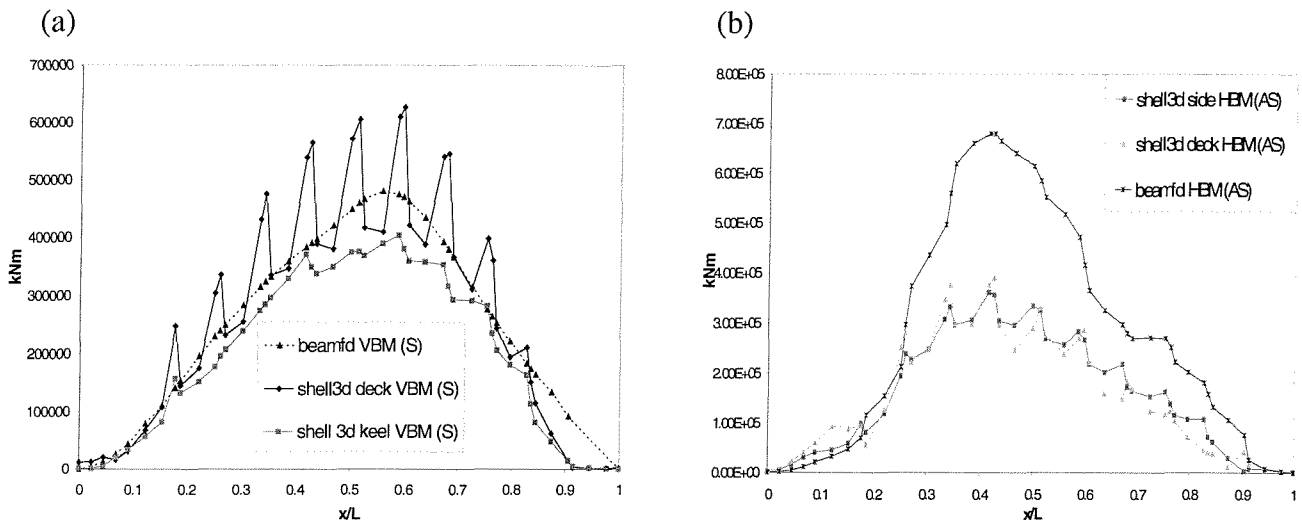

Fig.4 Variation of (a) vertical and (b) horizontal bending moments (kNm) along the ship obtained from models beamfd and shell3d (keel centre and deck side junction) when symmetric modal stresses (S) and antisymmetric modal stresses (AS) are taken into account, for $L/\lambda = 1.0$.

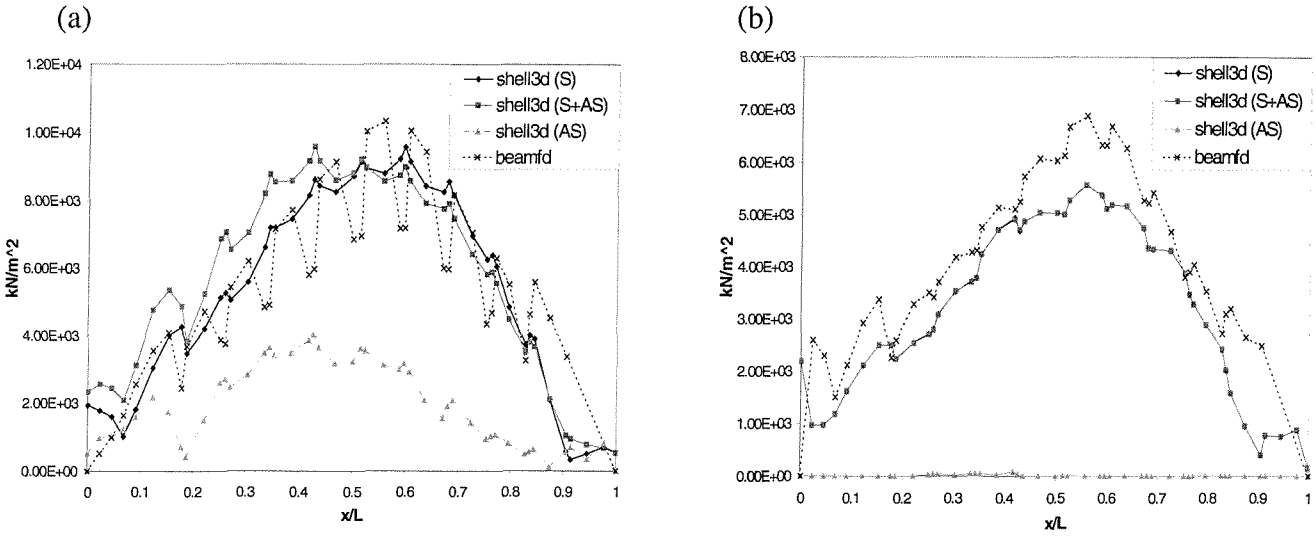

Fig.5 Longitudinal direct stress variations (kN/m^2) along the ship obtained from models beamfd and shell3d when symmetric only (S), symmetric and antisymmetric (S+AS), antisymmetric only (AS) modal stresses are considered for $L/\lambda = 1.0$ (a) Direct stress along deck-side junction; (b) Direct stress along keel centerline.

Appendix 5

Journal publication (under review)

Hirdaris, S.E., Price, W.G. and Temarel, P.; Two- and three-dimensional hydroelastic modelling of a bulker in regular waves, *Marine Structures*, Special issue on bulk carriers (2002).

Marine Structures, Elsevier Science AA (2002) 1-32

Two- and three-dimensional hydroelastic modelling of a bulker in regular waves

S.E. Hirdaris, W.G. Price, P. Temarel*

School of Engineering Sciences, Ship Science, University of Southampton, Highfield, Southampton, SO17 1BJ,UK

Abstract

The relatively high rates of bulk carrier casualties in recent years, as well as structural features such as large deck openings, make this vessel type a suitable example for investigating the influence of hydroelastic modelling on predicting wave-induced loads and responses. Two- and three-dimensional fluid-flexible structure interaction models, due to their different degree of complexity and associated data requirements, can be used at different stages of the design process when estimating wave-induced loads, namely preliminary and detailed design stages respectively.

In this paper, therefore, two- and three-dimensional hydroelasticity theories are applied to predict and compare the dynamic behaviour of a bulk carrier hull, based on OBO MV Derbyshire, in waves. Both symmetric and antisymmetric motions and distortions are incorporated in these investigations. The three-dimensional structural model consists entirely of shell finite elements, representing all major external and internal structural components, whilst the two-dimensional model is generated using Timoshenko beam finite element and finite difference discretisations. Issues relevant to the structural modelling stage, for both idealisations, are discussed. The in vacuo dynamic characteristics are compared for all models, with particular emphasis on the influence of hatch openings, shear center and warping on the antisymmetric dynamics of the structure. For the wet analysis the fluid-flexible structure interaction is carried out using two-dimensional (Timoshenko beam and strip theory) and three-dimensional (beam and shell finite element idealisations combined with potential flow analysis based on pulsating source distribution over the mean wetted surface) analyses. Comparisons are made between steady state responses predicted by two- and three-dimensional models in bow quartering regular waves.

It is shown that whereas the predicted symmetric dynamic responses obtained from two- and three-dimensional models are in good agreement, differences are observed for the antisymmetric dynamic characteristics. It is thought that this may be due to inadequacies in the beam models employed when simulating the global dynamic behaviour of this highly non-prismatic hull girder whilst allowing for the effects of warping.

Keywords: Bulk carriers, dynamic loads, FE idealisation, hydroelasticity, wave-induced dynamic response

* Corresponding author. Tel.: +023-80-59-38-66; fax: +023-80-59-32-99
E-mail address: penny@ship.soton.ac.uk (P. Temarel)

Nomenclature

English Symbols

A	cross-sectional area
A_{efy}	effective shear area for horizontal bending and shear
A_{efz}	effective shear area for vertical bending and shear
[A]	generalised hydrodynamic added mass matrix
[a]	generalised structural mass matrix
a_{rr}	element of generalised structural mass matrix
[B]	generalised hydrodynamic damping matrix
[b]	generalised structural damping matrix
b_{rr}	element of generalised structural damping matrix
[C]	generalised fluid stiffness (restoring) matrix
[c]	generalised stiffness matrix
c_{rr}	element of generalised stiffness matrix
C	torsional rigidity
C_W	warping stiffness
E	Young's modulus
G	shear modulus
I_w	sectorial moment of inertia
I_{yy}	moment of inertia (2^{nd} moment of area) about horizontal axis
I_{zz}	moment of inertia (2^{nd} moment of area) about vertical axis
L	ship length
M_y	vertical bending moment
M_{yr}	modal vertical bending moment
N	highest distortion mode admitted in the analysis
n	N+6
{p(t)}	principal coordinate vector
{p}	principal coordinate amplitude vector
p_r	element of {p}
r	modal index
s	position vector
S_{deck}	deck section modulus
S_{keel}	keel section modulus
t	time
U	forward speed
w	vertical displacement
w_r	modal vertical displacement
(x,y,z)	Cartesian coordinate system; x longitudinal, y horizontal and z vertical axes
z_C	distance of centre of gravity from keel
z_S	distance of shear centre from keel

Greek symbols

λ	wave length
ν_r	modal damping factor
$\{\Xi\}$	wave excitation vector
σ_x	longitudinal direct stress
σ_{xr}	modal direct stress

χ	heading angle
ω	wave frequency
ω_e	encounter frequency
ω_r	natural frequency (dry hull)
ω_{er}	wet resonance frequency

1. Introduction

The evaluation of wave-induced motions and loads are two of the most important aspects in ship design. Traditionally, prediction of wave-induced loads, in the main, relies on quasi-static and/or empirical methods [1]. Overall, such methods proved to be quite adequate over the years with problems arising dealt by relying on accumulated experience. Nevertheless, the international amendments for bulkers, tankers and LNG carriers brought about by the International Association of Classification Societies (IACS) and the International Maritime Organisation (IMO) are a measure of the concern related to the behaviour of such vessels and associated risks involving loss of human life, environmental pollution etc [2,3].

Bulk carriers, based on statistics collated in 1997, comprise 33% of the world's merchant fleet. Of these 72% are Handysize, 19% Panamax and 9% Capesize. The age of the current fleet is between 10 and 15 years [2]. Casualty statistics for the period between 1990 and 1997, as assessed by the Baltic and International Maritime Council (BIMCO), indicate that 25 bulk carriers, totaling 1,847,174 DWT, and 572 lives were lost. Of these casualties 40% correspond to Handysize, 12% to Panamax and 48% to Capesize ship types [4]. Since the beginning of the eighties, according to Lloyd's Register of Shipping, more than 57 bulk carriers have been lost at sea and a further 61 incurred damage to such an extent that their loss was narrowly averted [3]. Although these statistics provide only a general overview of the situation a number of points should be noted:

- The rate of known or possible structural failures increased dramatically between 1989 and 1994, 1991 being the worst year with 11 ships lost and 14 occurrences of serious structural failure [3];
- The average age of ships lost in this period was 17.5 years [3];
- The majority of the casualties occurred midway between special surveys [3];
- The number of losses for vessels carrying steel/iron may be considered rather high as these products account only for 7% of the dry bulk trade [4].

Research undertaken by IMO and IACS suggests that possible causes for 90% of the losses relate, by and large, to hull girder failure, loss of stability and loss of reserve buoyancy [4]. The remaining 10% are unexplained disasters which can be attributed to structural failure, although concrete evidence is hard to procure. Seaway induced dynamic loads and their consequences may be able to shed light in explaining these. Hydroelasticity theory, unlike empirical and quasi-static methods, provides a rigorous analysis whereby the fluid-flexible structure interaction is formulated and the wave induced dynamic loads and responses (e.g. stresses, bending and torsional moments etc) are evaluated [5,6].

In the early 1990s hydroelasticty theory was applied to investigate failures experienced by bulk carriers, such as the Onomichi Maru and OBO MV Derbyshire [7,8]. These investigations on the dynamic behaviour of bulk carriers in a seaway, including steady state as well as transient (i.e. slamming) loads and responses, focussed on the symmetric dynamic behaviour and the two-dimensional hydroelasticity theory. This research showed that significant wave-induced global

stresses (steady state and transient) occur not only at amidships but also at the extremities of the hull, namely 15-20% of hull's length from either end [9,10].

The objectives of the current investigations are to examine the influence of three-dimensional structural modelling on the dynamic behaviour of slender beamlike vessels with large deck openings in regular waves [11,12]. Previous investigations comparing two- and three-dimensional hydroelasticity theories dealt with a uniform rectangular barge and a vessel without any significant deck openings [13,14]. The two-dimensional hydroelasticity employs a Timoshenko beam idealisation of the structure combined with a strip theory representation of the fluid-structure interaction. A beam or three-dimensional FE structural idealisation in conjunction with three-dimensional potential flow analysis can be adopted for the three-dimensional hydroelasticity. It should be noted that the beam idealisations employed, based on mathematical formulations which assume slow variation of properties along the structure, may be inadequate in dealing with discontinuities occurring at the transition between closed- and open-deck regions of vessels with large deck openings [15-17]. This is particularly important when investigating antisymmetric (coupled horizontal bending and torsion) distortions.

In this paper the steady state hydroelastic behaviour of a vessel with principal dimensions, structural and mass characteristics similar to those of OBO MV Derbyshire in regular waves is carried out. Predictions from two- and three-dimensional fluid-flexible structure interaction methods and relevant models are presented and compared with reference to *dry* and *wet* hull characteristics (e.g. principal mode shapes, natural frequencies and wet resonance frequencies) and wave induced loads (e.g. bending moments, shear forces, torsional moment and direct stresses). A typical loaded operational condition for the vessel travelling at 14.5 knots in regular bow quartering regular waves is considered.

This investigation assesses the degree of confidence that can be placed on predictions obtained from two-dimensional models by comparison to three-dimensional models where detailed structural features (e.g. deck openings, double bottoms, transverse bulkheads etc) are modelled more explicitly.

2. Theoretical Background

2.1 Development of Hydroelasticity Theory

The fact that floating structures are flexible has probably been intuitively accepted since ancient times. The assumption that ships are rigid structures is a relatively modern simplification in an attempt to bring some understanding into ship motions in waves. Although the term *Hydroelasticity* appeared for first time in technical literature in 1959 as the naval counterpart to aeroelasticity [18], the study of hydroelasticity of ships traveling in waves did not gain significant momentum until the mid seventies when Bishop and Price established the basic principles of a theory for flexible beamlike hulls subject to steady state or transient wave induced loads, combining Timoshenko beam and strip theories [5]. The two-stage approach of *dry* or *in vacuo* and *wet* analyses adopted leads to a direct evaluation of dynamic loads and responses (e.g. stresses, bending moments etc) for a vessel travelling at arbitrary heading in regular waves and irregular seaways. The theory is unified in the sense that it incorporates rigid body motions (i.e. conventional seakeeping) as well as distortions.

The two-dimensional hydroelasticity theory was applied successfully to a variety of beamlike merchant and naval ships in order to demonstrate its suitability to simulate symmetric, antisymmetric and unsymmetric steady state dynamic behaviour in waves [5,19,20]. It was also extended to the prediction of transient responses due to bottom and flare slamming, using impact and momentum slamming theories, in head regular waves and irregular seaways making use of time domain simulation techniques [21-23].

The beamlike hull idealisation is not suitable for non-beamlike structures, such as multi-hulled vessels, semi-submersibles etc. The three-dimensional hydroelasticity theory overcomes these limitations and is able to simulate the wave-induced dynamic behaviour of non-beam like, as well as beamlike, vessels in waves [6]. This analysis makes use of a three-dimensional finite element modelling of the structure (*dry* analysis) and a pulsating source distribution over the mean wetted surface (*wet* analysis). Du et al extended this theory using translating, pulsating source distribution over the mean wetted surface area of the vessel [24]. This singularity satisfies a speed dependent linearised free surface boundary condition and is, therefore, more rigorous in accounting for forward speed effects and more suitable for high speed mono- and multi-hulled vessels.

The three-dimensional hydroelasticity theory has been applied to a variety of structures such as SWATHs [6,25], a dry dock [26], jack-up rig transportation [27], a cylindrical shell representative of a submarine [28] and a non-slender mono-hull [14]. Further applications of interest include a sailing yacht where the fluid-flexible structure interaction model included, in addition to the canoe body, the rig, keel and bulb and areas where structural problems arise have been identified from the predictions obtained [29].

Verification studies have also been carried out, in parallel to expanding the range of applicability of hydroelasticity theory as illustrated in the aforementioned examples. Validation of theoretical predictions obtained using hydroelasticity theory against experimental measurements and/or full-scale data were carried out for a fast patrol boat and two frigates travelling in rough seas [22,30], a SWATH [31] and a dry dock [26]. Recent applications to trimarans also indicate good agreement with flexible model experiments for wave induced loads, such as prying moment, for a range of speeds and headings [32].

2.2 *Equations of Motion*

The equations of motion for a flexible structure travelling with forward speed U in regular waves of frequency ω encountered at arbitrary heading χ can be written as [5,6]:

$$[[a]+[A(\omega_e)]]\{\ddot{p}(t)\}+[[b]+[B(\omega_e)]]\{\dot{p}(t)\}+[[c]+[C]]\{p(t)\}=\{\Xi\ (\omega,\omega_e)\}\ e^{i\omega e t} \qquad (1)$$

where [a], [b] and [c] denote the n×n generalised mass, structural damping and stiffness matrices and [A], [B] and [C] the n×n generalised added inertia, hydrodynamic damping and fluid restoring matrices, respectively. $\{\Xi\}$ denotes the n×1 generalised wave excitation vector, containing both incident wave and wave diffraction contribution. $\{p(t)\}=\{p\}\exp(i\omega_e t)$ is the n×1 principal coordinate vector, with $\{p\}$ containing the complex principal coordinate amplitudes and ω_e denoting the wave encounter frequency. The total number of modes allowed in the analysis is defined as n=6+N, where N corresponds to the number of distortional modes included in the analysis. Therefore, it can be seen that this system of equations of motion is *unified* in the sense that it allows for both rigid body motions and distortions which are coupled through the effects of the fluid actions. This can be seen in the make-up of the generalised matrices of structural origin, shown in eq.(1),

$$[a]=\begin{bmatrix}[a_R] & 0\\ 0 & [a_D]\end{bmatrix}\ ,\quad [b]=\begin{bmatrix}0 & 0\\ 0 & [b_D]\end{bmatrix}\ ,\quad [c]=\begin{bmatrix}0 & 0\\ 0 & [c_D]\end{bmatrix} \qquad (2)$$

where the indices R and D denote rigid and distortional modes, respectively. The generalised structural damping and stiffness matrices have no contributions from the rigid body modes and are diagonal. An element of the diagonal generalised stiffness matrix is $c_{rr}=\omega_r^2 a_{rr}$, for r=7,....N. The generalised structural damping is assumed diagonal such that $b_{rr}=2\ \omega_r \nu_r a_{rr}$, for r=7,...N, where ν_r denotes the structural damping factor. As far as the generalised mass matrix is concerned the 6×6 symmetric matrix $[a_R]$ contains mass, moments of mass and moments and products of inertia corresponding to the six rigid body motions of surge (r=1), sway (r=2), heave (r=3), roll (r=4), pitch (r=5) and yaw (r=6). The diagonal matrix $[a_D]$ contains the generalised massess a_{rr} (for r=7,...N) for the distortional mode shapes.

It should be noted that when investigating the linear dynamic behaviour of vessels with port-starboard symmetry the symmetric (surge, heave and pitch motions and distortions in the vertical plane of symmetry) and antisymmetric (sway, roll and yaw motions and distortions involving horizontal deflection and twisting) dynamic behaviour is uncoupled. As a result the two-dimensional hydroelasticity theory was developed separately for these two cases, ignoring surge, when considering symmetric motions and distortions [5]. This is a matter of convenience and it does not affect the wave-induced loads and stresses discussed in this paper.

To obtain the natural frequencies, principal mode shapes, modal internal actions (i.e. modal vertical and horizontal bending moments and shear forces, torsional moment and stresses) and generalised masses the hull is assumed to freely vibrate *in vacuo*, in the absence of any external excitation and structural damping. In two-dimensional hydroelasticity theory the hull is modelled as a non-uniform Timoshenko beam for this *dry* analysis stage. For the antisymmetric vibrations the beam theory includes the effects of shear centre and warping requisite for the analysis of coupled horizontal bending and torsional which are important for vessels with large deck openings [5,19]. The dry hull analysis for the three-dimensional hydroelasticity theory is, in general, carried out by modelling the hull using suitable finite elements, such as beam and shell elements.

To obtain the generalised fluid-flexible structure interaction characteristics, such as the generalised added inertia, during the *wet* analysis stage strip theory is used for the two-dimensional hydroelasticity theory with suitable conformal mapping techniques to represent the shape of the strips under the mean waterline [5,33]. The mean wetted surface for the three dimensional analysis is discretised using four-cornered panels in order to attain a pulsating source distribution over this surface [6].

Having obtained the principal coordinates in requlars waves, distortions and internal actions, such as bending moments and stresses, are obtained using modal summation. In generic terms, for example, the vertical displacement (including rigid body motion and distortion) is

$$w(s;t) = \sum_{r=1}^{n} p_r(t)\, w_r(s) \tag{3}$$

the vertical distortion is

$$w(s;t) = \sum_{r=7}^{n} p_r(t)\, w_r(s) \tag{4}$$

the vertical bending moment is

$$M_y(x;t) = \sum_{r=7}^{n} p_r(t)\, M_{yr}(x) \tag{5}$$

and the longitudinal direct stress is

$$\sigma_x(s;t) = \sum_{r=7}^{n} p_r(t)\,\sigma_{xr}(s) \tag{6}$$

In these expressions w_r , M_{yr} and σ_{xr} are the modal vertical displacement, vertical bending moment and direct stress, respectively for the rth mode shape with the corresponding principal coordinate p_r evaluated in regular waves from eq.(1). The position on the vessel is defined as $s \equiv (x,y,z)$ for three dimensional structural models, whilst s denotes the position along the vessel for beam models. It should be noted, however, that in beam models stresses vary within a cross section in accordance with the beam theory assumptions. It can also be seen, from eqs.(5,6) that rigid body modes do not contribute to internal actions, such as bending moments and stresses.

3. Modelling

Two- and three-dimensional structural models were generated to idealize the structural and inertia characteristics of a vessel, based on the OBO MV Derbyshire, whose principal characteristics are summarised in Table 1. The lines plan, shown in Fig.1(a), was generated using the Wolfson Unit ShipShape v3.2 software [34] and with reference to hydrostatic properties available from previous investigations [8,35]. Draught and displacement correspond to a typical loaded condition.

The three-dimensional structural model (**shell3d**) was generated to begin with using suitable shell finite elements (see Figs.1(b,c)), available in the ANSYS 5.4 software, to incorporate major structural components such as deck, side, inner/outer bottom, hopper spaces, bulkheads, major longitudinal girders etc [36]. Various methodologies and idealisations were used for the modelling of the structure as a beam, namely : (i) uniaxial three-dimensional beam finite elements of non-uniform length (**beamfe3d**) and a Timoshenko beam idealisation, implemented through a finite difference scheme, using a lengthwise discretisation of (ii) equal (**beamfde**) and (iii) unequal (**beamfd**) intervals. There are several reasons for using different beam idealisations namely, additional verification, suitability of current beam finite elements and issues relating to data generation for the beam models. These will be clarified in sections 3.2 and 3.3.

3.1 Three-dimensional FE modelling of the structure

The midship section (in the vicinity of a hatch opening) was generated in the first instance with sufficient detail to model the deck, side, inner/outer bottom and hopper space plating. In addition major longitudinal girders in inner bottom and hopper spaces were incorporated. Although this modelling approach, shown in Fig.1(b), may be perceived as relatively crude, it is firmly believed that all elements necessary for an accurate idealisation of the dynamic behaviour of this vessel, in vertical bending and coupled horizontal bending and torsion, are incorporated.

The midship section formed the parallel body and the idealisation was extended over the ship's length including transverse bulkheads and hatch openings where appropriate. Particular care was paid to the stern and bow structural configurations, including the bulbous bow. For simplicity of modelling the superstructure and the hatch covers were not included. The resultant model consists entirely of shell elements representing deck, side, inner/outer bottom, hopper and bulkhead plating and inner bottom and hopper space girders. The contributions from other longitudinal stiffeners, transverse frames and other stiffeners were subsumed into the properties of adjacent shell elements.

Element SHELL63 was selected for the structural model. This is a general purpose multiplex shell element with four nodes, six degrees of freedom (three translations and three rotations) per node [36]. The nodal rotations normal to the element plane were neglected as these elements

primarily behave as membranes in the structural model generated. Corresponding triangular elements were used in areas of large curvature, such as the bilge and the side shell in the vicinities of bow and stern, where the warpage (due to the four nodes of a shell element not being on a flat plane) was outside prescribed limits. The three-dimensional FE model, shown in Fig.1(c), consists of 6439 nodes and 3673 shell elements distributed over 46 sections, of unequal length, along the ship. Such a distribution fits in with the general arrangement of this vessel and facilitates the determination of mass distribution by manipulating the mass density of elements in a section, as well as the acquisition of properties required for the beam models. Based on past experience, this method was preferred to using lump mass elements in order to avoid numerical problems that may arise during modal analysis [25].

The omission of transverse frames and longitudinal stiffeners from structural idealisations of mono- and multi-hulled vessels has been dealt successfully in the past by incorporating *fictitious* bulkheads where appropriate [14,29]. Omission of such elements results in mode shapes containing localised distortions, which are not physically representative of the dynamic behaviour of the vessel. Such spurious distortions can be avoided via the use of *fictitious* bulkheads, of negligible mass and thickness, which act as 'anchors' to nodes of elements not otherwise connected to, and hence supported by, other elements in a direction normal to their plane. Adopting the same approach, transverse and longitudinal *fictitious* bulkheads were incorporated in the structural model, as shown in figures 1(b,c). The *fan* shape form used to idealise both real and fictitious transverse bulkheads, seen in figure 1(b), was adopted in order to reduce the number of corresponding shell elements.

Structural cross-section properties and inertia related properties were evaluated at each of the 46 sections of this three-dimensional FE model in order to provide the longitudinal variation of properties required for the beam models of the structure. These properties, shown in Fig.2, were compared with data available from previous investigations [8,35].

3.2 Beam modelling of the structure

BEAM4 elements were selected for the finite element idealisation (**beamfe3d**) of the vessel's structure using 46 elements of unequal length along the vessel. BEAM4 is a uniaxial element with two nodes and six degrees of freedom per node, namely three translations and three rotations [36]. It has bending (in both directions), torsion as well as tension/compression capabilities and incorporates the effects of shear deformation and rotatory inertia. However, this element has shortcomings in simulating the coupling between horizontal bending and torsion, important for this type of vessel with large deck openings, as there is no distinction between the centroid and shear centre. In addition, where torsion is concerned, the warping of cross sections is neglected, which is again unsuitable for ships with large deck openings. Use of this element, therefore, can only provide verification for the symmetric dry and wet analyses only.

Previous applications of the two-dimensional hydroelasticity, for both dry and wet analyses, were carried out using a discretisation based on equal intervals along the ship, i.e. sections or strips of equal length. Such a scheme is convenient and practical as it corresponds to the distribution of stations along a vessel, where hydrostatic and other data are available. The structural and inertia related properties obtained from the shell3d model are based on 46 sections of unequal length. Accordingly two finite difference formulations for a non-uniform Timoshenko beam discretised using 46 intervals (or sections) of equal (**beamfde**) and unequal (**beamfd**) length were employed, the latter requiring modifications to the available scheme [11,12]. It should be noted that the adopted beam formulation, for either idealisation, includes the influence

of shear centre, thus being suitable for coupled horizontal bending and torsional, and the effects of warping [5,19].

Longitudinal variation of mass, moments of inertia, second moments of area, effective shear areas, torsional rigidity (C=G J), warping stiffness (C_w=E 1_w), centroid and shear centre were evaluated at every section of model shell3d. These properties, shown in Fig.2, were used for all beam models. This implies that model beamfde has some small differences in the longitudinal variations of these properties by comparison to the other two models. As can be seen from Fig.2, all structural properties display a saw tooth-like variation, denoting where the hatch openings are. The locations of the hatch openings corresponds to the bottom value of all structural properties but one, namely the warping stiffness which is negligible for closed sections. Naturally, the maximum of warping stiffness correspond to a minimum in torsional rigidity. This is the major difference between the current analysis and past investigations, where only the mass related properties displayed an oscillatory variation along the vessel – as seen in Figures 2(a and h) [8,35]. The influence of the effective shear area is very important when determining the natural frequencies and modal characteristics. It is common practice to estimate this property, which is rather difficult to evaluate, as a fraction of the (longitudinally effective) cross section area [37]. In the current analysis this fraction was adjusted by comparing the natural frequencies obtained from models shell3d and beamfd for the two-noded symmetric and the first antisymmetric mode shapes. This resulted in 0.23 and 0.28 of the cross-section area being considered effective in shear for the symmetric and antisymmetric distortions, respectively (see figure 2(f)). Same factors were used for model beamfde for consistency in the analysis.

3.3 Fluid-structure interaction modelling

Three models were generated to provide comparisons for the wave-induced loads and responses. The aim of these comparisons were to ascertain the influences of beam structural modelling for ships with large deck openings as well as to observe the effects of three-dimensional flow. Accordingly the beam structural model was combined, so to speak, with two- as well as three-dimensional potential flow analyses. The following models were employed:

- **shell3d** where the three-dimensional shell finite element idealisation is used in conjunction with a pulsating source distribution over the mean wetted surface of the hull, which is discretised using 952 four-cornered hydropanels, as shown in Fig.1(d). A one-to-one correspondence between shell elements on the mean wetted surface and hydropanels was adopted for convenience.
- **beamfde,** where the Timoshenko finite difference beam idealisation, with 46 equal sections along the ship, is used in conjunction with the modified strip theory by Salvesen et al [33] discretising the ship with 46 strips of equal length. The 'Lewis form' conformal mapping is employed to evaluate hydrodynamic properties of swaying, heaving and rolling sections. The use of a longitudinal distribution based on equal sections or strips is justifiable from the comparison of the dry hull characteristics (e.g. natural frequencies and mode shapes) obtained from idealisations using sections of equal and unequal length, discussed in section 4.
- **beam3d** where the Timoshenko beam idealisation is used in conjunction with a pulsating source distribution over the mean wetted surface of the hull, which is also discretised using 952 four-cornered hydropanels, as shown in Fig.1(d). The modal characteristics of model beamfde, which has a longitudinal distribution of 46 sections of equal length, were employed since the finite element beam idealisation is not capable of coupled horizontal bending and torsion and does not include the effects of warping.

4. In vacuo or dry analysis

4.1 Natural frequencies and principal mode shapes

The subspace reduction method was selected to obtain the eigenvalues and eigenvectors (i.e. natural frequncies and mode shapes) of the vessel freely vibrating in vacuo for models shell3d and beam3d constructed using shell and beam finite elements [36,38]. The Prohl-Myklestad finite difference scheme was adopted for both models beamfd and beamfde, based on Timoshenko beam theory incorporating the effects of warping [5].

As this vessel is port-starboard symmetric the principal mode shapes, shown in figure 3 for model shell3d, were classified as symmetric (vertical bending) and antisymmetric (coupled horizontal bending and torsion). The corresponding natural frequencies are shown in Tables 2 and 3 with the mode shapes identified by the number of nodes in vertical deflection and horizontal deflection and twist, respectively. It can be seen that two sets of natural frequencies were calculated for model shell3d, corresponding to thicknesses t_{fb}=1 mm and 5mm for the *fictitious* bulkheads used, whilst maintaining the same mass. This was done in order to assess the influence of these bulkheads on the modal characteristics. It was observed that values of t_{fb}<1 mm resulted in the emergence of localised distortions in the mode shapes obtained, whilst for values of t_{fb}>5 mm eigenvector stiffening occurred [11,12]. In other words 1mm is the minimum thickness that can be assigned to the *fictitious* bulkheads of this structural idealisation so as to obtain realistic mode shapes. The natural frequencies increase, for either symmetric or antisymmetric modes, with increasing values of t_{fb} because of increasing stiffness (but not mass), as can be seen in tables 2 and 3.

For the first few symmetric mode shapes (except the 2-node mode) the natural frequencies obtained from model shell3d (t_{fb}=1mm) are, in general, lower than those calculated from all beam models, as seen in table 2. Both finite element models predict a longitudinal mode shape that is not included in the finite difference formulations. Furthermore, the natural frequencies for models beamfe3d and beamfd are closer to those obtained from the shell3d model, by comparison to the beamfde model which, in general, appears to be the model with the largest overall stiffness. This is attributed to the one-to-one correspondence between the sections of shell3d , beamfe3d and beamfd models.

The variation of the vertical deflections along the vessel, normalised to unit vertical displacement at the stern (keel centre line for model shell3d) are shown in fig.4. In these figures only the vertical deflection at keel (centre line) is shown for model shell3d. Nevertheless, it should be noted that for the symmetric mode shapes the vertical deflection at the deck is very close to that of the keel, confirming the beamlike symmetric dynamic behaviour of this vessel. There is good overall agreement between the mode shapes obtained from all models. However, as the complexity of the mode shape increases (e.g. 5 nodes, shown in Fig.4(d)) so do the differences between various beam and shell3d models. This could be attributed to the fact that shell3d model provides a dynamic behaviour based on more realistic description of the hull girder (e.g. double bottom effects). It is also worth noting that the vertical deflections obtained from beamfde model compare well against all other models based on unequal section distribution along the vessel. Furthermore these deflections are quite smooth by comparison to those predicted by the other models, as a result, it is believed, of the equal discretisation adopted in model beamfde, as can be seen from Fig.4.

The comparison for the antisymmetric modal characteristics is limited to beam idealisations using finite difference scheme (beamfd and beamfde) and the three-dimensional shell FE model shell3d. This, as explained in section 3.2, is due to the unavailability of suitable beam finite

elements in the software version used [36]. Model beamfde appears to be stiffer than models beamfd and shell3d, as seen in Table 3, for the same reasons mentioned above. It should be noted that the natural frequencies in Table 3 are arranged in ascending order of the predictions obtained from the beam models. Overall, the antisymmetric natural frequencies for the first few mode shapes calculated using model shell3d (t_{fb}=1mm) are lower than the corresponding predictions obtained using either of the finite difference models (accounting for the effects of warping), but higher for the remaining few shown in Table 3. It can also be observed that the antisymmetric dynamic behaviour of this vessel is driven by the influence of warping. This is illustrated by the low natural frequencies calculated from model beamfd ignoring the effects of warping (i.e. assuming zero warping stiffness) which are, in the main, dominated by torsion (see last column of Table 3).

The first few antisymmetric mode shapes, normalised to unit horizontal displacement at the stern (keel centre line for model shell3d),are shown in Fig.5. Comparison of horizontal deflections between beam and shell3d models is rather difficult. The mode shapes for either beamfd or beamfde models are represented by two variables, namely the horizontal deflection (assumed at the shear centre) and the angle of twist [5,19]. On the other hand horizontal nodal deflections, obtained for a set of nodes along model shell3d, contain the effects of twist, to a small or large extent depending on whether the mode shape is horizontal bending or torsion dominant. This is a consequence of the strong coupling between horizontal bending and torsion experienced by vessels with large deck openings. There is not, therefore, a unique horizontal deflection comparable with that obtained from beam models. The horizontal displacements v_k and v_d, at keel (centre line) and deck (junction of side and deck plating) respectively, are used for model shell3d. The corresponding angle of twist is calculated as $\tan^{-1}[(v_k - v_d)/D]$, where D represents the vertical distance between deck and keel. The horizontal deflections at keel and deck calculated by model shell3d are close to each other, as well as those obtained from models beamfd and beamfde, for horizontal bending dominant modes, as seen in Fig. 5(c), as a result of the small amount of twist angle. On the other hand, the horizontal deflections for the shell3d model at deck and keel are out of phase for the torsion dominant modes, as shown in Figs.5(a,e). This effect can be appreciated by examining the relevant three-dimensional mode shape, shown in Fig.3. In spite of these differences, the overall agreement between the mode shapes obtained from three-dimensional shell FE and finite difference beam models is reasonably good for the first few mode shapes, but as the modal complexity increases so do the differences between models beamfd and beamfde and models beamfd and shell3d.

The generalised masses, shown in Tables 4 and 5 for the symmetric and antisymmetric mode shapes respectively, are an important modal characteristic as can be seen by their influence on the equations of motion (1). All generalised masses have been obtained for mode shapes normalised to unit deflection at stern, as mentioned before. Generalised masses calculated from model beamfde differ the most from other models for the first few symmetric and antisymmetric mode shapes. The increased numerical differences with increasing modal complexity follow similar trends to those observed in natural frequencies and mode shapes. Overall the differences observed in the antisymmetric generalised masses calculated from the various models are larger than those observed in the symmetric mode shapes

4.2 Modal internal actions

For model shell3d the modal internal actions are provided in terms of direct and shear stresses at the nodes. By contrast for the beam structural models the modal internal actions are readily available in the form of Vertical and horizontal bending moments and shear forces and torsional moment, as well as axial force for beam FE models, at the nodes. The following

relationships between longitudinal direct stresses and bending moments are valid in any cross section of a beam, namely the direct stresses on the deck or keel due to a vertical bending moment M_y are

$$\sigma_{x\,deck} = \frac{M_y}{S_{deck}} \quad and \quad \sigma_{x\,keel} = \frac{M_y}{S_{keel}}, \tag{7}$$

where S_{deck} and S_{keel} denote the section moduli at keel and deck, respectively, shown in Fig.2(g). According to beam theory the direct stresses have a linear distribution about the centroid and are assumed to be constant across the deck or keel.

The modal vertical bending moments (VMB), corresponding to 2-node symmetric mode shape are shown in Fig.6(a) and 7(a) for all structural models used. In fig.6(a) the vertical bending moments for the shell3d model were obtained using eq.(7) and direct stresses along deck edge (deck/side junction) and the keel centreline, denoted by shell3d deck and keel, respectively. It should be noted that no meaningful longitudinal direct stress variation along deck centreline can be obtained due to the presence of the hatch openings. There are two important characteristics for the modal vertical bending moments derived from the shell3d model in this manner, i.e. using eq.(7). The first relates to the saw tooth variation of the VBM along the ship, especially that obtained using the stresses along the deck/side junction. This is due to the saw tooth variation of the corresponding section moduli, a result of modelling the hatch openings. The second remark relates to the comparative values of these modal VBM with reference to the beam structural models; the VBM obtained from the deck edge stress straddles the predictions from the beam models whilst that obtained from the keel stresses is lower than these, providing, so to sepeak, a lower envelope to the VBM obtained from the deck edge stresses. Another, and more accurate, way of obtaining modal bending moments (either vertical or horizontal) in three-dimensional shell FE models involves the use of the direct stress distribution in the entire cross section Accordingly longitudinal forces, arising from the longitudinal direct stresses, are calculated for each element appearing in the cross-section. Subsequently the moments of these longitudinal forces, about the centroid, are summed up for all the elements, providing the required bending moment [32]. The resultant modal VBM for the shell3d model, for 2- and 3-node symmetric mode shapes are shown in Figs.7(a,b), respectively, together with modal VBM obtained from all the beam models. It can now be seen that all the modal VBM are in close agreement. The conclusion that can be drawn from this exercise is that the direct stress distribution along the depth of model shell3d has some differences compared to beam models, although the resultant bending moments are in good agreement. This can be further illustrated in the modal direct stress variation along the deck (deck/side junction for model shell3d) and keel (centreline for model shell3d) for the 2-node mode shape, shown in Fig.6(b). In this figure the stresses for model beamfd were obtained using eq.(7), whilst those for shell3d are readily available from stress data at the relevant nodes. It can be seen that whilst the stresses from model shell3d display a relatively smooth variation, those from beamfd are saw-tooth like, due to the corresponding deck and keel section moduli. The vertical modal shear forces for all models are shown in figs7(c,d), for 2- and 3-node symmetric mode shapes, respectively. It should be noted that the modal VSF for the shell3d model were evaluated using the shear stress distribution over each cross section [32]. There is a close agreement between all models, although small differences are observed for the shell3d model at quarter-length positions. Once again predictions obtained from model beamfde are smoother than the rest, as can be seen from Fig.7. The differences between the modal symmetric internal actions obtained from various models increase with increasing modal complexity, in line with differences observed in the mode shapes.

For the antisymmetric modes the resultant modal horizontal bending moment (HBM) for the shell3d model was evaluated in the same manner as for the modal VBM, namely using the longitudinal direct stress distribution for the entire cross-section, rather than only the direct stress

on the side [32]. These modal HBM are shown in Figs.7(a,c,e), for the first three antisymmetric mode shapes, and are compared with the readily available modal HBM obtained from models beamfd and beamfde. As can be seen from these figures the finite difference models are close to each other and overestimate the modal HBM by comparison to the shell3d results, especially for horizontal bending dominant modes (see figure 7 (b)). This is a trend that has been observed in higher modes, not presented in this paper. The modal torsional moments for the shell3d model were evaluated using the relevant shear stresses in each element and taking moments of the resultant forces about the centroid and summing up these moments to produce a resultant torsional moment at each cross section along the vessel. The modal torsional moments are readily available for the beam models and are shown in Figs.7(b,d,f) for the first three antisymmetric mode shapes. Once again it can be seen that the modal torsional moments predicted by the beam models, using the finite difference scheme, are larger by comparison to those obtained from model shell3d.

The differences between models shell3d and beamfd or beamfde, observed in Fig.7, raise some interesting points for discussion. The beam theory used for the description of torsion accounts for the influences of warping on the torsional moment, but the effect of the warping induced longitudinal direct stresses are not accounted for. That is to say the modal horizontal bending moment obtained from models beamfd and beamfde assume linear variation of these direct stresses with horizontal distance to the centre line, with constant direct stress distribution along the vertical sides of any cross section. Investigation of the variation of the direct stresses along the side shell, at a cross section in way of the hatchways, of model shell3d revealed differences between their values on the deck/side junction and the vicinity of the centroid. These differences indicate an influence from warping induced direct stresses. They do not appear, however, to be large enough to explain the differences observed in Fig.7. These contribution from these direct stresses is, usually referred to as the bimoment [15-17,39]. These differences imply that when comparing modal horizontal bending moments, as well as torsional moments, obtained by beamfd or beamfde and shell3d models one may not be comparing like with like. The global dynamic analysis was carried out for a highly non-prismatic hull girder, as can be seen from Figs.1(b) and 2. This has had small effects on the symmetric dynamic behaviour of this non-uniform beamlike vessel. The saw-tooth like extreme variations of warping rigidity and torsional stiffness, seen in Figs.2(c,d), may, however, be more problematic. That is to say for two adjacent sections with completely different warping characteristics (e.g. open- and closed-deck) a geometric compatibility mapping the alternative warping functions at the common interface may be required [15-17]. In other words at the interface (or node) joining the two adjacent sections the common value of the angle of twist produces two alternative and incompatible distributions of warping, implying a discontinuity of longitudinal warping displacement. This matter requires further investigation, for example using the bulk carrier with the deck opening extending the whole length of the hold area.

5. Wet analysis

Symmetric and antisymmetric motions and distortions of the vessel were evaluated for a typical forward speed of 7.463 m/s (Fn=0.138) and bow quartering regular waves (χ=135^0) of unit amplitude. Along with the distortional responses principal coordinate amplitudes corresponding to the rigid body motions were also evaluated. These were computed from a unified analysis, accounting for coupling between the rigid body modes and the first eight distortional modes, namely the first 4 symmetric (see Table 2) and the first 4 antisymmetric of which 2 are torsion dominant and 2 are horizontal bending dominant (see Table 3). The rigid body motions are not discussed in this paper as it focuses on the distortions and loads which, as

illustrated in eqs.(4-6), are not contributed to by the rigid body motions. Although little is known about structural damping, typical structural damping factors provided by Bishop and Price for long slender monohulls were adopted and are shown in Table 6 [5].

5.1 Steady state principal coordinates

A selection of principal coordinate amplitudes for the first few distortion modes are shown in Fig.9 as a function of the wave encounter frequency. A principal coordinate can be though of as a factor controlling the contribution of corresponding principal mode shape on the vessel's response (e.g. distortion, bending moment, stress etc) at a particular frequency. At low wave frequencies, the principal coordinates associated with rigid body motions are dominant but the principal coordinates associated with distortions are also excited. At shorter wave lengths a principal coordinate will, in general, display a large peak (as assumed structural damping is light) corresponding to its resonance as well as smaller peaks at resonances associated with other mode shapes as a result of hydrodynamic coupling. The resonant wet encounter frequencies ω_{er}, identified in this manner, for all models are shown in tables 7 and 8, for symmetric and antisymmetric distortion modes allowed in the hydroelastic analysis, respectively. In these tables the corresponding dry hull natural frequencies are also quoted as a reference. The structure, therefore, flexes in all wavelengths and, thus, distortions are not confined in the vicinity of resonances associated with distortional modes. For both symmetric and antisymmetric mode shapes, in general, resonances predicted by the two-dimensional beamfde model are lower than those predicted by the other two models. Furthermore, for the first two antisymmetric mode shapes (r=8 and 9) the wet resonance frequencies predicted by models beam3d and shell3d are very close, albeit lower, to the corresponding dry hull natural frequencies. This can be attributed to the different generalised masses (see Table 5) and their relationship to the generalised added masses. In general, the three-dimensional fluid-structure interaction models, either using beam or shell FE structural idealisations, appear to be in closer agreement. It can be noted that both beam structural models (beamfde and beam3d) indicate the presence of a relatively low wet resonance frequency at 3.26 rad/s for antisymmetric principal coordinates as can be seen in Figs.9(b,c). This resonance is associated with the 2-node torsion dominant mode (r=12). The ratio between wet resonance and dry natural frequencies appears to be rather low for this mode shape, as a result of a rather large generalised added mass. This occurrence requires further investigation.

5.2 Steady state dynamic loads

Vertical bending moment and shear force, horizontal bending and torsional moments variations along the bulk carrier travelling in regular waves (heading 135^{o}) of wavelength equal to ship length ($L/\lambda=1$, $\omega_e=0.56$ rad/s) are shown in Fig.10. These were evaluated according to eq.(4) and using the modal characteristics shown in Figs.7 and 8. It should be noted that only contributions from symmetric and antisymmetric mode shapes were included, respectively, when evaluating the vertical bending moment and shear force and the horizontal bending and torsional moments. This approach was adopted for all models used, as there is no coupling between symmetric and antisymmetric mode shapes for this port/starboard symmetric vessel. There is good overall agreement for the symmetric wave-induced loads, as can be seen from Figs.10(a,b). The vertical bending moment values predicted by model beam3d, for this frequency, are a little larger than predictions by other models over the aft half of the vessel. Predictions obtained by model shell3d, over the same part of the vessel, fall in between the predictions from the two beam structural idealisations beamfde and beam3d. The sharpness of the shear force peaks predicted by model shell3d at the quarter lengths is also noted. The differences observed in the antisymmetric

responses are larger, as can be seen from Figs. 10(c,d), with the horizontal bending and torsional moment values predicted by model shell3d, being the smallest. There is closer agreement between the two beam structural models for the torsional moment; however, horizontal bending moment predictions obtained from models shell3d and beamfde are, in general, closer. The reasons for the differences lie in the respective differences observed for the modal horizontal bending and torsional moments, discussed in section 4.2. Nevertheless one can also observe the differences attributable to the fluid-structure interaction modelling by comparing the predictions obtained by models beam3d and beamfde, with essentially the same modal characteristics.

It has been observed that frequency and heading variations affect the predicted loads, especially the antisymmetric ones. Variation of vertical bending moment and shear force, horizontal bending and torsional moment at amidships, for the same operational conditions, as a function of encounter frequency are shown in Fig.11. The frequency range adopted is well below the first resonance associated with distortion modes. As it can be seen, at this relatively low frequency region the amidships vertical bending moment and shear force predictions obtained by the three-dimensional models beam3d and shell3d are, in general, in closer agreement. Nevertheless, symmetric wave-induced loads predicted by all three models are in good overall agreement and exhibit similar trends with encounter frequency. The observations made for horizontal bending and torsional moments for $L/\lambda=1$ are also valid for this range of relatively low frequencies, e.g. the amidships horizontal bending moment variations with encounter frequency predicted by models shell3d and beamfde are in close agreement.

As a further comparison, the variation of the wave-induced direct stresses along the deck (deck/side junction) and keel (centre line) for $L/\lambda=1$ are shown in Figs.12(a,b). The stresses predicted by model shell3d were evaluated using eq.(6) whilst those for the beam structural models using eq.(7). The comparisons between all models conform to the behaviour of the modal direct stresses for 2-node symmetric mode, discussed in section 4.2. That is to say the deck/side junction stresses predicted by model shell3d (contributions from symmetric modes only) are rather smooth and, in general, appear as the mean to the saw tooth like variations of stresses predicted by beam3d and beamfde models. On the other hand the keel stresses predicted by either model beam3d or beamfde are larger than the smoother stress variation obtained from model shell3d, with model beam3d providing the largest prediction. For model shell 3d the predictions were carried out both including and excluding the contributions from antisymmetric mode shapes, in order to assess their influence. As expected the antisymmetric modes contribute negligibly to the stresses on the keel centre line. Nevertheless, they have a sizeable contribution to the direct stresses obtained at the junction of deck and side plating, as can be seen in Fig.12(a).

6. Conclusions and Recommendations

- This paper focuses on comparing the influences of different levels of refinement in fluid-structure interaction modelling on the dry hull dynamic characteristics and wave-induced loads and stresses for ships with large deck openings, such as bulk carriers, containerships, LNG carriers etc. The results of this investigation are important from the point of view of selecting the detail to be incorporated into a model when working at various stages of the design process, such as concept and preliminary design. This investigation also assesses the degree of confidence that can be placed on the relatively easier two-dimensional fluid-flexible structure interaction modelling both for symmetric and antisymmetric dynamic behaviour in waves.
- The use of shell finite elements to model internal and external plating, transverse bulkheads and major longitudinals together with the use of *fictitious* bulkheads in the three-dimensional structural model shell3d appears to have worked well; thus, resulting in a structural

idealisation with a reasonably small number of elements and degrees of freedom. This model is capable of allowing for the effects of shear deformation along with the effects of coupling between horizontal bending and torsion and warping. It will be interesting, nevertheless, to make comparisons with a more refined three-dimensional model, incorporating transverse frames and other longitudinal and transverse stiffeners rather than fictitious bulkheads, to further validate their use.

- The dry hull analysis showed good overall agreement between beam and three-dimensional structural models for the first few symmetric and antisymmetric mode shapes; however, differences increase with modal complexity.
- Comparison of internal actions obtained from beam and three-dimensional structural models is not straightforward and requires careful consideration when relating bending moments to direct stresses and shear forces and torsional moments to shear stresses.
- The modal vertical bending moment and shear forces obtained by beam and three-dimensional structural models are in good agreement for the first few mode shapes. The discontinuities arising from the hatch openings, in general, do not appear to affect the comparisons. Nevertheless the modal direct stresses at deck and keel show some differences as a result of these discontinuities and the ensuing highly non-prismatic nature of this structure.
- The modal internal actions for the antisymmetric mode shapes (e.g. horizontal bending and torsional moments) show differences between the predictions obtained from beam and three-dimensional structural models. It is thought that this is due to the highly non-prismatic character of this vessel and the influence of the discontinuities between regions with open and closed deck. Further investigations are required in this respect to assess the influence of a geometric compatibility condition with reference to these discontinuities and warping
- The dynamic behaviour of the various models in waves also reveal differences between two- and three-dimensional modelling of fluid actions, as seen when comparing the responses obtained from fluid-structure interaction models beamfde and beam3d.
- The wave-induced vertical bending moment and direct stress show good overall agreement between the all three models, taking into account the saw-toothlike nature of relevant moments of inertia and section moduli. However, the agreement is not, in general, good between horizontal bending and torsional moment values predicted by models using beam and three-dimensional structural idealisations. This is, mainly, a consequence of the differences observed in the antisymmetric modal characteristics.
- In oblique and beam waves the antisymmetric modes contribute to the stresses on the deck, at the junction with side plating.
- Further investigations are required, using structural models with closed deck and open deck throughout the length of the holds, to assess the influence of structural modelling on both the symmetric and antisymmetric dynamic behaviour in waves.

References

[1] Report of Committee II.1: Quasi-static response, 14th International Ship and Offshore Structures Congress, Japan (2000).

[2] IACS: Bulk carriers – guidance and information on bulk cargo loading and discharging to reduce the likelihood of over-stressing the hull structure, IACS Publications, London (1997).

[3] Tustin, R.D.: Existing bulk carrier safety – on the evaluation of the foremost hold structure under conditions of hold flooding, RINA International Conference on the Design and Operation of Bulk carriers, 48-68, London, (1998).

[4] BIMCO: Bulk carrier safety – the view and role of an industry organisation, RINA International Conference on the Design and Operation of Bulk Carriers, 1-12, London, (1998).
[5] Bishop, R.E.D. and Price, W.G.: Hydroelasticity of Ships, Cambridge University Press, UK (1979).
[6] Bishop, R.E.D, Price, W.G. and Wu, Y.: A general linear hydroelasticity theory of floating structures moving in a seaway, Phil. Trans. Royal Soc. London, A316: 375-426, (1986).
[7] Bishop, R.E.D., Price, W.G., and Temarel, P.: A hypothesis concerning the disastrous failure of the Onomichi – Maru, Trans. RINA, 127:169-186, (1985).
[8] Bishop, R.E.D., Price, W.G., and Temarel, P.: A theory on the loss of MV Derbyshire, Trans. RINA, 127:169-186, (1991).
[9] Bishop, R.E.D., Houot, J.P., Price, W.G., and Temarel, P.: On the distribution of symmetric shearing force and bending moment in hulls, Trans. RINA, 128:205-215 (1984).
[10] Aksu, S., Price, W.G. and Temarel, P.: Steady state and transient responses of bulk carriers and tankers in random seas, Trans. RINA, 138:72-102 (1996).
[11] Hirdaris, S.E., Price, W.G. and Temarel, P.: Hydroelastic analysis of a bulk carrier (Keynote lecture), 13th International Conference on Ship and Shipping Research NAV'00, 1:5.6.1 - 5.6.12, Italy (2000).
[12] Hirdaris, S.E., Price, W.G. and Temarel, P.: Symmetric and antisymmetric hydroelastic analysis of a bulker in waves; 8th International Symposium for Practical Design of Ships and other Floating Structures PRADS'01, 2:903-910, China (2001).
[13] Aksu, S., Price, W.G and Temarel, P.: A comparison of two-dimensional and three-dimensional hydroelasticity theories including the effects of slamming, Proceedings of IMechE, 205:3-15 (1991).
[14] Price, W.G., Salas Inzunza, M.A. and Temarel, P.: The dynamic behaviour of a mono-hull in oblique waves using two- and three-dimensional fluid-structure interaction models, to appear Trans. RINA (2002).
[15] Pedersen, P.T.: A beam model for the torsional-bending response of ship hulls, Trans. RINA, 125: 171-182 (1983).
[16] Pedersen, P.T.: Torsional response of containerships, Journal of Ship Research, 29:194-205 (1985).
[17] Pedersen, P.T.: Beam theories for torsional-bending response of ship hulls, Trans. SNAME, 35:254-265 (1991).
[18] Heller, S.R and Ambramson, H.N.: Hydroelasticity - a new naval science, Journal of the American Society of Naval Engineers, 71:205-209 (1959).
[19] Bishop, R.E.D., Price, W.G. and Temarel, P.: A unified dynamical analysis of antisymmetric ship response to waves, Trans. RINA, 122:349-365 (1980).
[20] Bishop, R.E.D., Chalmers, D.W., Price, W.G. and Temarel, P.: The dynamic characteristics of unsymmetrical ship structures, Trans. RINA, 128:205-215, (1986).
[21] Belik, O., Bishop, R.E.D. and Price, W.G.: A simulation of ship responses due to slamming in irregular head waves, Trans. RINA, 125:237-253 (1983).
[22] Bishop, R.E.D., Clarke, J.D. and Price, W.G.: Comparison of full scale and predicted responses of two frigates in severe weather trial, Trans. RINA, 126:123-166 (1984).
[23] Belik, O., Bishop, R.E.D. and Price, W.G.: Influence of bottom and flare slamming on structural responses, Trans. RINA, 130:261-275 (1988).
[24] Du, S.X., Wu, Y. and Price W.G.: Forward speed effect on the structural responses of a ship travelling in waves, Proceedings of the 2nd International Conference on Hydroelasticity in Marine Technology, 1:401-410, Japan (1998).

[25] Price, W.G., Temarel, P. and Keane, A.J.: Hydroelastic analysis of a SWATH in waves, Proceedings of the 1st International Conference on Hydroelasticity in Marine Technology, 231-243, Norway, (1994).
[26] Lundgen, J., Price, W.G. and Wu, Y.: A hydroelastic investigation into the behaviour of a floating dry dock in waves, Trans. RINA, 131:213-231 (1989).
[27] Fu, Y., Price, W.G. and Temarel, P. : The 'Dry and Wet' towage of a jack-up in regular and irregular waves, Trans. RINA, 129:147-159 (1987).
[28] Ergin, A., Price, W.G., Randall, R. and Temarel, P.: Dynamic characteristics of a submerged, flexible cylinder vibrating in finite water depths, Journal of Ship Research, 36:154-167 (1992).
[29] Louarn, F.H. and Temarel, P.: An investigation of the structural dynamics of a racing yacht, Proceedings of the 14th Chesapeake Sailing Yacht Symposium, 123-142, USA (1999).
[30] Aksu, S., Price, W.G., Suhrbier, K.R. and Temarel, P.: A comparative study of the dynamic behaviour of a fast patrol boat travelling in rough seas, Marine Structures, 6:421-441 (1993).
[31] Qian, J.Y. and Li, Q.H.: The theoretical and experimental study on the hydroelastic behaviour of a SWATH travelling in waves, Proceedings of the 2nd National Conference on Marine Technology, China (1996).
[32] Bingham, A.E., Hampshire, J.K., Miao, S.H. and Temarel, P.: Motions and loads of a trimaran travelling in regular waves, Proceedings 6th International Conference on Fast Ship Transportation FAST'01, 2:167-176, Southampton, UK (2001).
[33] Salvesen, N., Tuck, E.O. and Faltinsen, O.: Ship motions and sea loads, Trans. SNAME, 78:250-287 (1970).
[34] WUMTIA : Manual for ShipShape, University of Southampton (1992)
[35] Bishop, R.E.D., Price, W.G. and Temarel, P.: Derbyshire - A design review, Report to Dept. of Transport, UK (1984).
[36] Swanson Ltd : The ANSYS 5.4 users manual (1999).
[37] Chalmers, D.W. and Price, W.G.: On the effective shear area of ship sections, Trans. RINA, 122: 245-252 (1980).
[38] Bathe, K.J. : Finite Element Procedures, Prentice Hall, USA (1996).
[39] Papangelis, J. and Hancock, G.J. : Computer analysis of thin walled structural members, Computers and Structures, 56:157-176 (1995).

Length over all (m)	L_{OA}	294.1
Length between perpendiculars (m)	L_{BP}	281.94
Beam moulded (m)	B	44.2
Draught (m)	T	17.04
Depth moulded (m)	D	24.99
Displacement (tonnes)	Δ	186,028
Longitudinal centre of gravity from A.P. (m)	LCG	147.5
Block coefficient (m)	C_B	0.861

Table 1. Principal particulars of Bulk Carrier used in the investigation.

Model Mode type	beamfde	beamfd	beamfe3d	shell3d t_{fb} = 0.001m	shell3d t_{fb} = 0.005m
2 node VB	4.419	4.527	4.502	4.529	4.598
3 node VB	9.247	9.060	9.072	9.010	9.343
4 node VB	14.236	13.632	13.741	13.236	14.999
5 node VB	17.615	16.954	17.106	15.915	17.567
Longitudinal	-	-	17.831	17.932	18.208
6 node VB	25.019	23.363	23.989	24.586	25.250

Table 2. Natural frequencies (rad/s) for symmetric distortions of the dry hull (t_{fb} = thickness of fictitious bulkheads, VB = vertical bending).

Model Mode type	beamfd $C_w \neq 0$	beamfde $C_W \neq 0$	shell3d t_{bf} = 0.001m	shell3d t_{bf} = 0.005m		beamfd $C_W = 0$
1 node HB – 1 node **T**	5.992	5.148	5.004	5.390		1.797
2 node **HB** – 2 node T	6.261	5.847	5.554	5.727		3.189
2 node HB – 2 node **T**	10.995	10.099	12.629	12.993		4.622
3 node **HB** – 3 node T	12.656	11.132	10.712	11.045		5.856
3 node HB – 3 node **T**	16.047	15.385	18.981	19.440		7.077
4 node **HB** – 4 node T	17.086	16.382	16.286	16.725		8.080

Table 3. Natural frequencies (rad/s) for antisymmetric distortions of the dry hull (t_{fb} = thickness of fictitious bulkheads, HB = horizontal bending, **HB** = HB dominant, T = torsion, **T** = T dominant, C_w= warping stiffness).

Mode description	Generalised mass (tonne m^2)			
	shell3d	beamfe3d	beamfd	beamfde
2 node VB	19364	19761	19648	24834
3 node VB	8922	8799	8591	11082
4 node VB	6577	4778	4308	4492
5 node VB	10036	5072	6268	3940
6 node VB	8854	7343	5868	3984

Table 4. Generalised masses of the symmetric mode shapes.

Mode description	Generalised mass (tonne m^2)		
	shell3d	beamfd	beamfde
1 node HB – 1 node **T**	81577	84711	95684
2 node **HB** – 2 node T	53730	34278	40727
2 node HB – 2 node **T**	15313	25143	14117
3 node **HB** – 3 node T	40268	51105	37140
3 node HB – 3 node **T**	8288	13185	7447
4 node **HB** – 4 node T	18828	17879	15382

Table 5. Generalised masses of the antisymmetric mode shapes.

Symmetric motion	Damping factors	Antisymmetric bending	Damping factors
2 node VB	0.002	1 node HB - 1 node **T**	0.01
3 node VB	0.005	2 node **HB** – 2 node T	0.012
4 node VB	0.008	2 node HB – 2 node **T**	0.015
5 node VB	0.010	3 node **HB** – 3 node T	0.019

Table 6. Structural damping factors used in all fluid-structure interaction models (VB = vertical bending, HB = horizontal bending; **HB** = HB dominant; T = torsion; **T** = T dominant).

Mode type	beamfde		beam3d		shell3d	
	Dry (ω_r)	Wet (ω_{er})	Dry (ω_r)	Wet (ω_{er})	Dry (ω_r)	Wet (ω_{er})
2 node VB(r=7)	4.42	3.03	4.50	3.11	4.53	3.25
3 node VB (r=10)	9.25	6.33	9.07	6.29	9.01	6.62
4 node VB (r=13)	14.24	9.90	13.74	9.72	13.24	10.20
5 node VB(r=14)	17.62	12.95	17.11	12.65	15.92	12.61

Table 7. Dry natural and wet resonance frequencies (rad/s) for symmetric mode shapes for the bulk carrier travelling at U = 7.463m/s in bow quartering waves, $\chi = 135^o$ (VB = vertical bending; ω_r = dry natural frequency; ω_{er} = wet resonance frequency and r denotes the modal index).

Mode type	beamfde		beam3d		shell3d	
	Dry (ω_r)	Wet (ω_{er})	Dry (ω_r)	Wet (ω_{er})	Dry (ω_r)	Wet (ω_{er})
1 node HB – 1 node **T** (r=8)	5.15	4.41	5.15	5.0	5.01	4.95
2 node **HB** – 2 node T (r=9)	5.85	4.96	5.85	5.01	5.55	5.02
3 node **HB** – 3 node T (r=11)	10.10	8.71	10.10	9.3	12.63	9.33
2 node HB – 2 node **T** (r=12)	11.13	3.26	11.13	3.26	10.71	9.25

Table 8. Dry natural and wet resonance frequencies (rad/s) for antisymmetric mode shapes for the bulk carrier travelling at U = 7.463m/s in bow quartering waves, $\chi = 135^o$ (HB = horizontal bending; **HB** = HB dominant; T = torsion; **T** = T dominant; ω_r = dry natural frequency; ω_{er} = wet resonance frequency and r denotes the modal index).

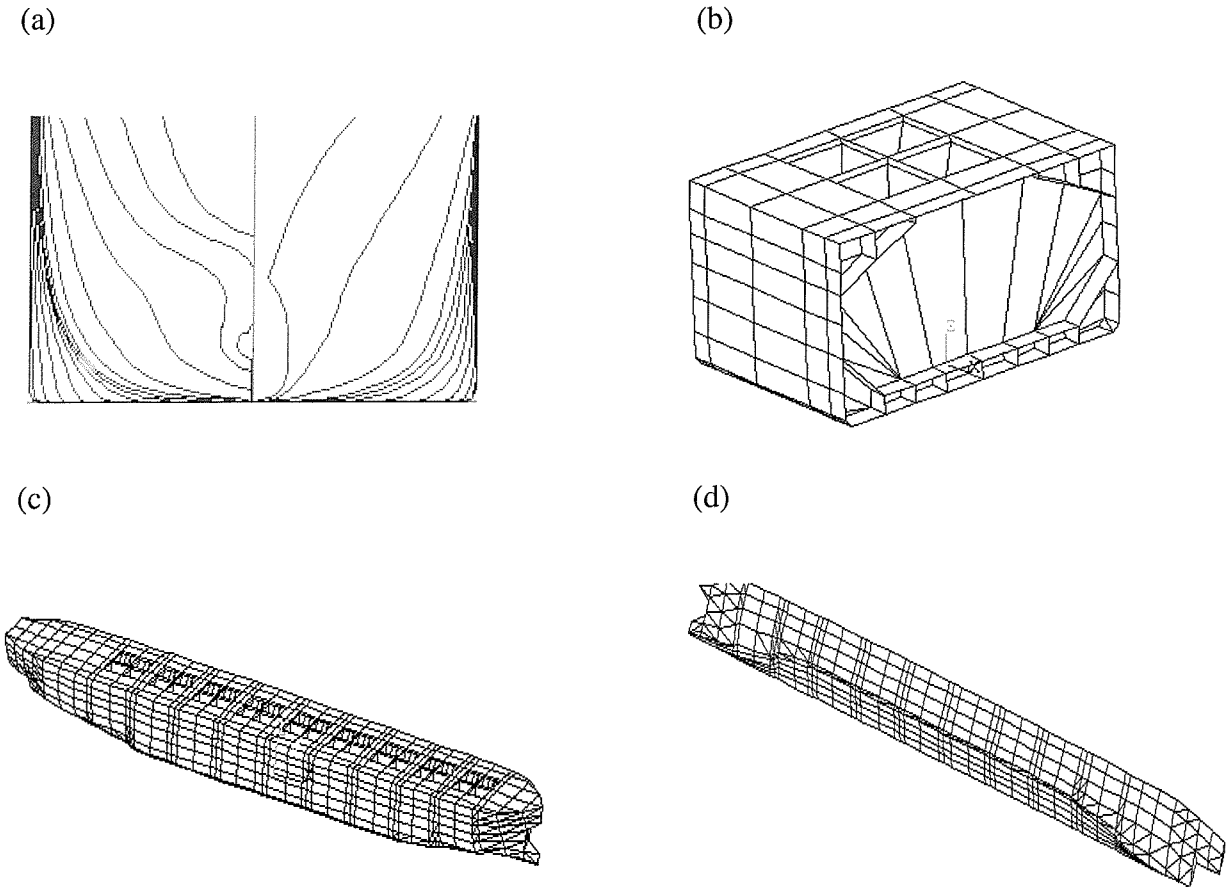

Fig. 1. Hull shape and structural idealisation of the bulk carrier; (a) Body plan, (b) Transverse section in the parallel body region; (c) Three-dimensional FE model shell3d; (d) Idealisation of the mean wetted surface for three-dimensional analyses.

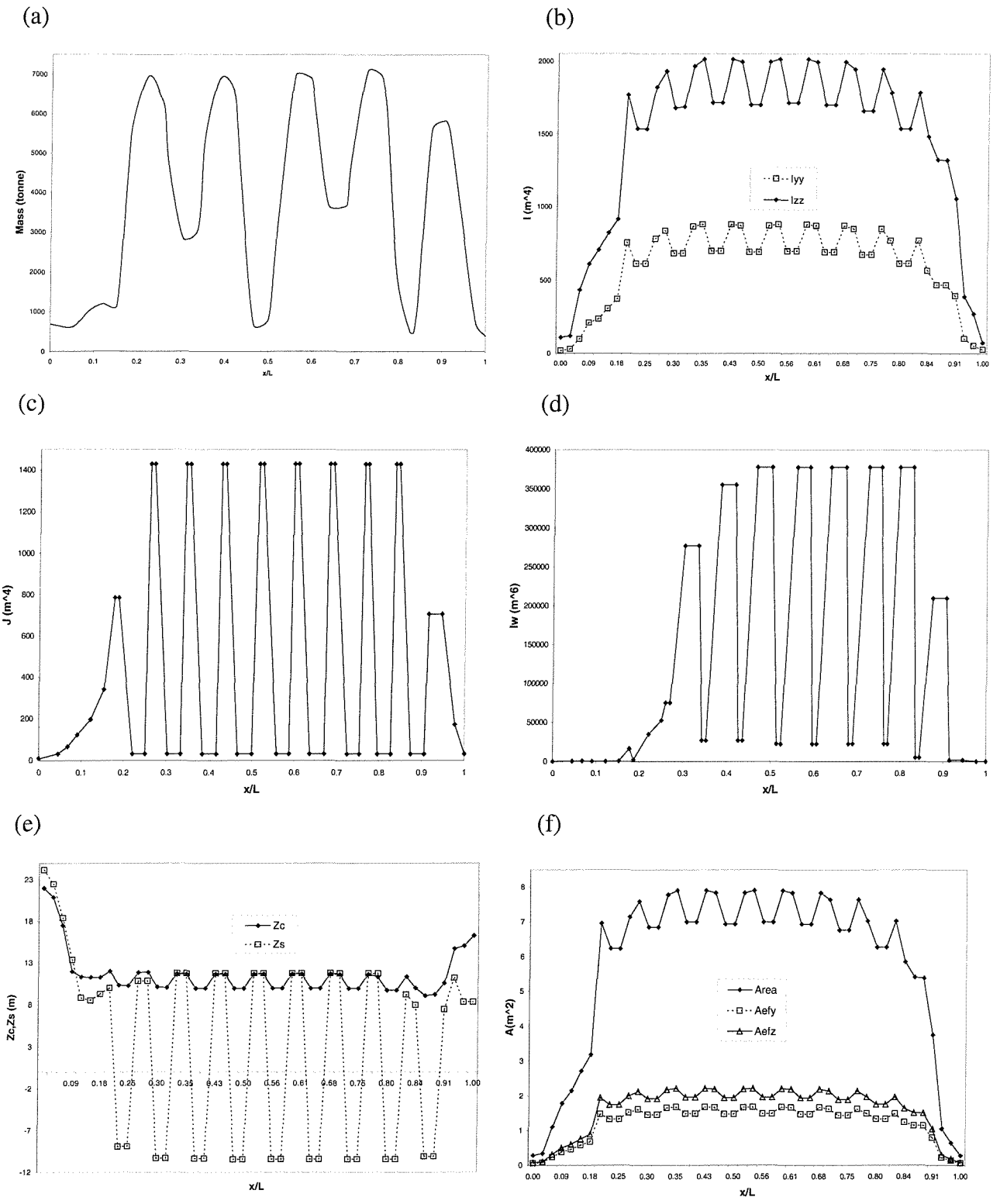

Fig. 2. Variation of mass and structural properties along the bulk carrier; (a) Mass (tonnes); (b) Moments of inertia I_{zz} and I_{yy} (m^4); (c) Torsional constant J (m^4); (d) Sectorial moment of inertia I_w (m^6); (e) distances of shear centre z_s and centre of gravity z_c from keel (m); (f) cross-section A and effective shear areas A_{efz} and A_{efy} (m^2); (g) Deck and keel section moduli S_{deck} and S_{keel} (m^3); (h)Torsional moment of inertia about centre of gravity (tonne m^2).
Apologies in 2(f) Aefy and Aefz are the wrong way round – will be corrected.

(g)

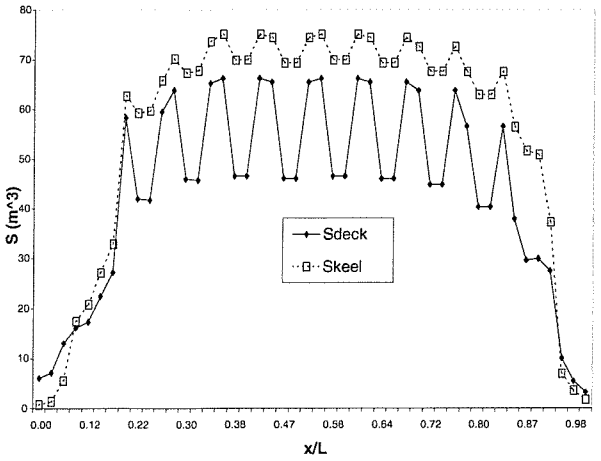

(h)

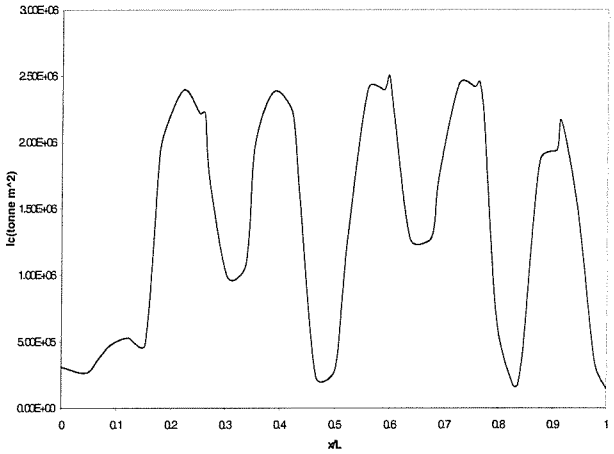

Fig.2 continued

2 node VB

1 node HB and 1 node **T**

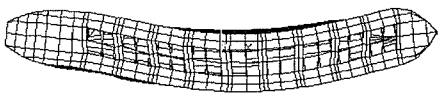

2 node **HB** and 2 node T

3 node VB

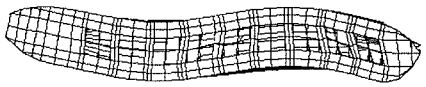

3 node **HB** and 3 node T

2 node HB and 2 node **T**

4 node VB

5 node VB

Fig. 3. Selection of principal mode shapes obtained from model shell3d (VB: vertical bending; HB: horizontal bending; T: torsion, **HB, T**: HB,T dominant).

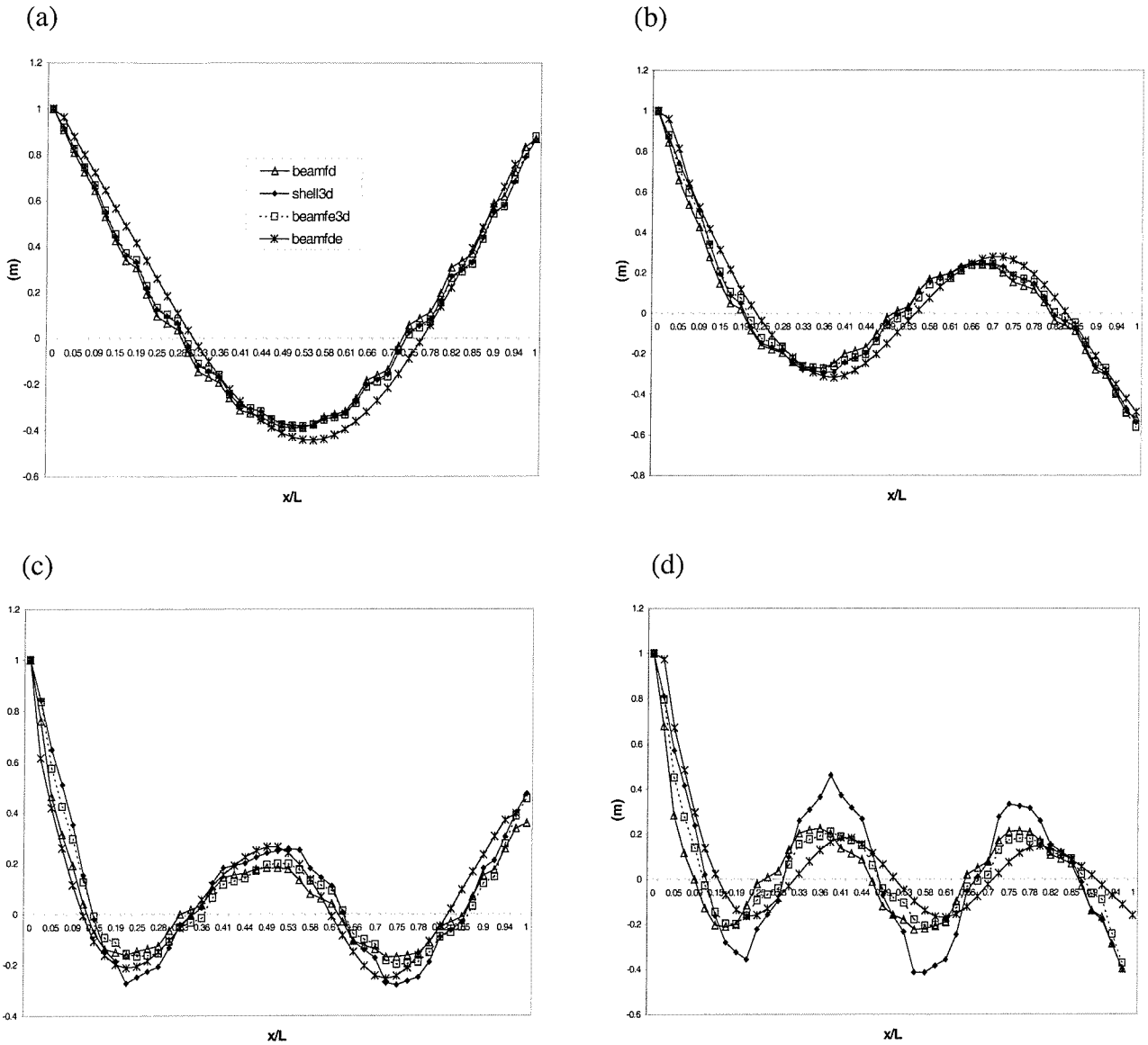

Fig. 4. Symmetric mode shapes for models beamfd, beamfde, beamfe3d and shell3d corresponding to: (a) 2, (b) 3, (c) 4 and (d) 5 node vertical deflections.

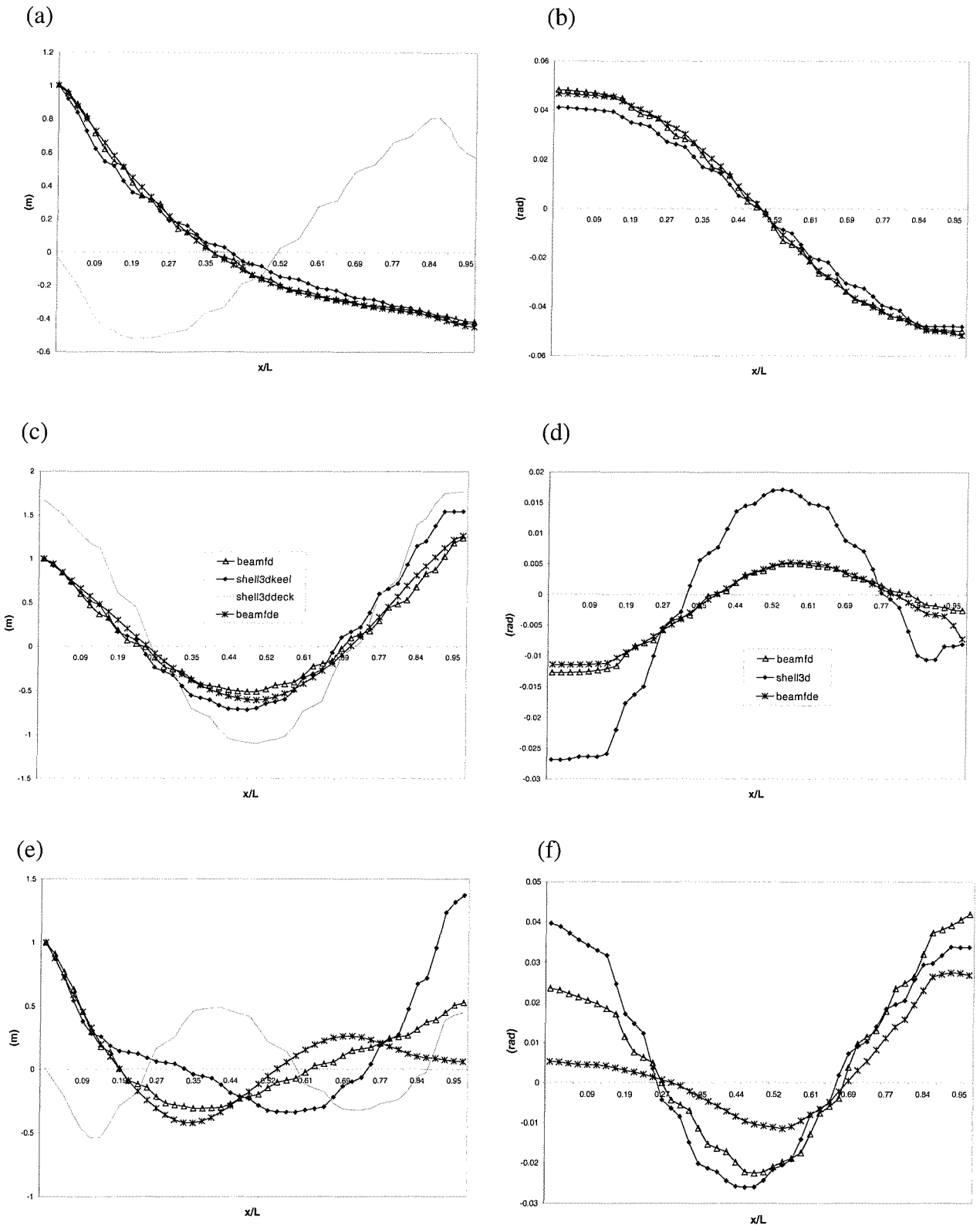

Fig. 5. Antisymmetric mode shapes, represented by the horizontal deflection (m) and twist angle (rad), obtained from models beamfd, beamfde and shell3d corresponding to: (a,b) 1 node HB 1 node **T**, (c,d) 2 node **HB** 2 node T and (e,f) 2 node HB 2 node **T** modes. Note that for model shell3d horizontal deflections at keel (centre line) and deck /side junction are shown.(HB: horizontal bending, T: torsion, **HB,T**: HB,T dominant)

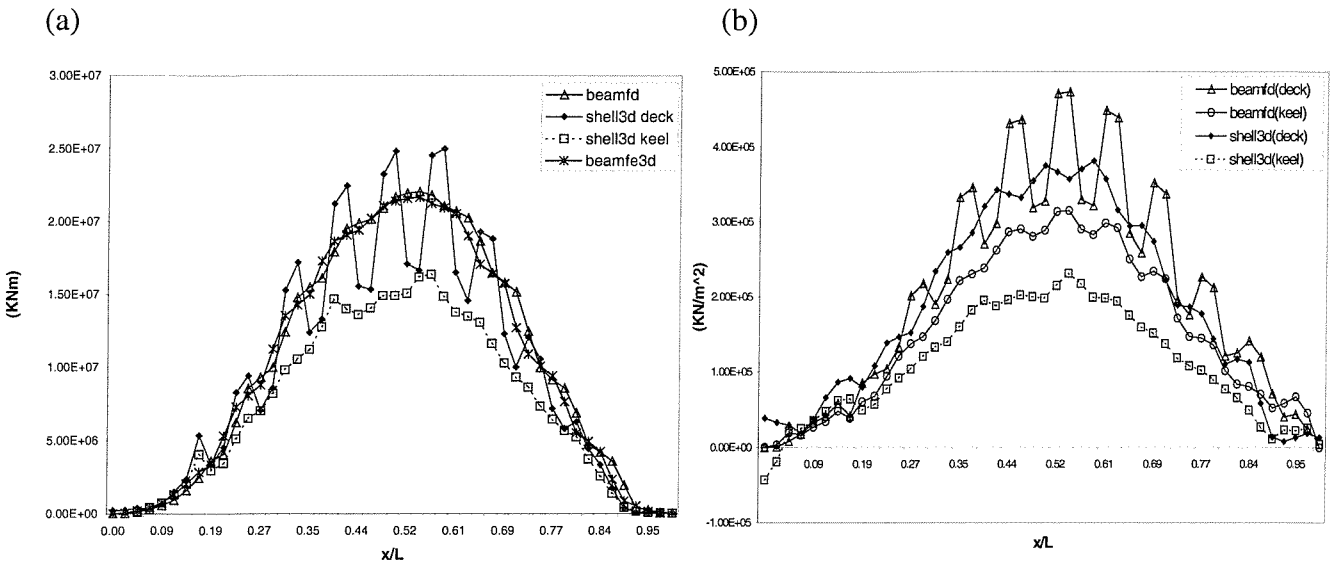

Fig.6 Variation of modal internal actions for 2 node symmetric mode shape along various structural models; (a) Modal vertical bending moment (kNm); (b) Modal direct stress on deck and keel (kN m^2). Note that the vertical bending moment for model shell3d and the direct stresses for model beamfd were evaluated using eq. (7). Also note that for model shell3d the direct stresses are on keel centre line and deck/side junction.

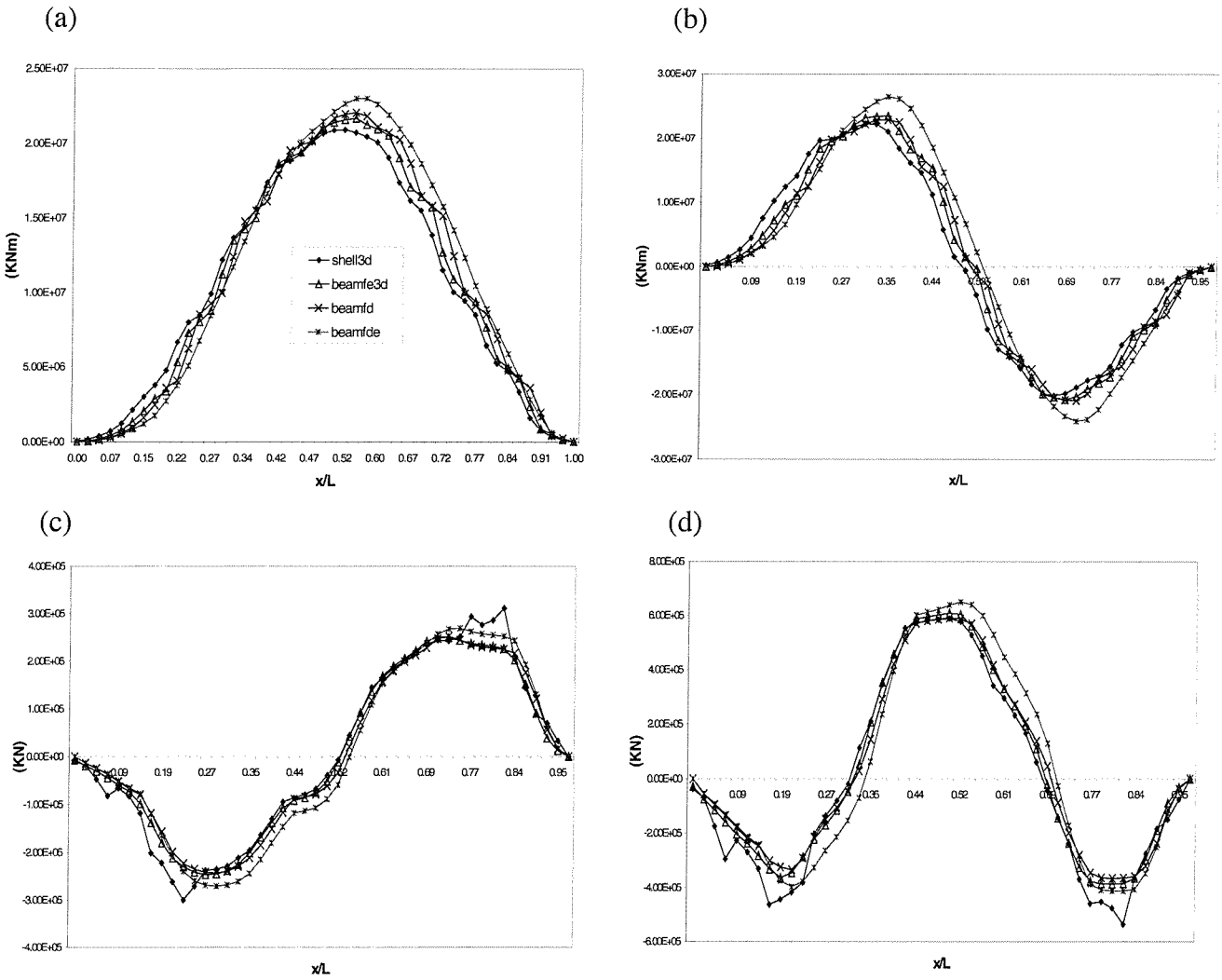

Fig.7 Variation of modal vertical bending moments (VBM kNm) and shear forces (VSF kN) along models shell3d, beamfd, beamfde and beamfe3d; (a) 2 node VBM; (b) 3 node VBM; (c) 2 node VSF; (d) 3 node VSF. Note that VBM and VSF for model shell3d were evaluated using the relevant stress distributions over respective cross-sections.

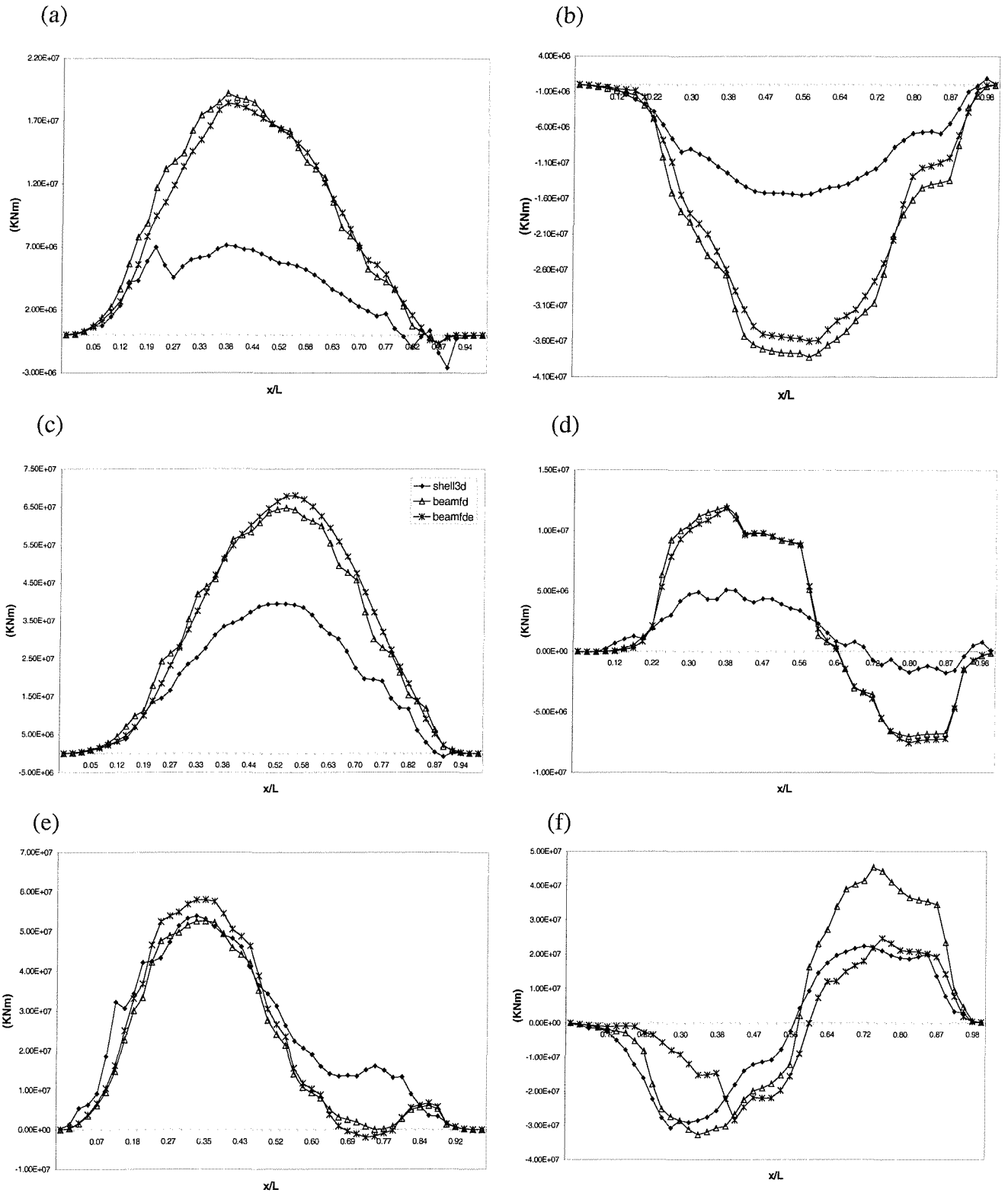

Fig.8 Variation of modal (a), (c), (e) Horizontal bending (kNm) and (b), (d), (f) Torsional moments (kNm) along models beamfd, beamfde and shell3d for antisymmetric mode shapes: (a,b) 1 node HB 1 node **T**; (c,d) 2 node **HB** 2 node T; (e,f) 2 node HB 2 node **T**. Note that horizontal bending and torsional moments for model shell3d were evaluated using the relevant stress distributions over respective cross-sections. (HB: horizontal bending, T: torsion, **HB,T**: HB,T dominant).

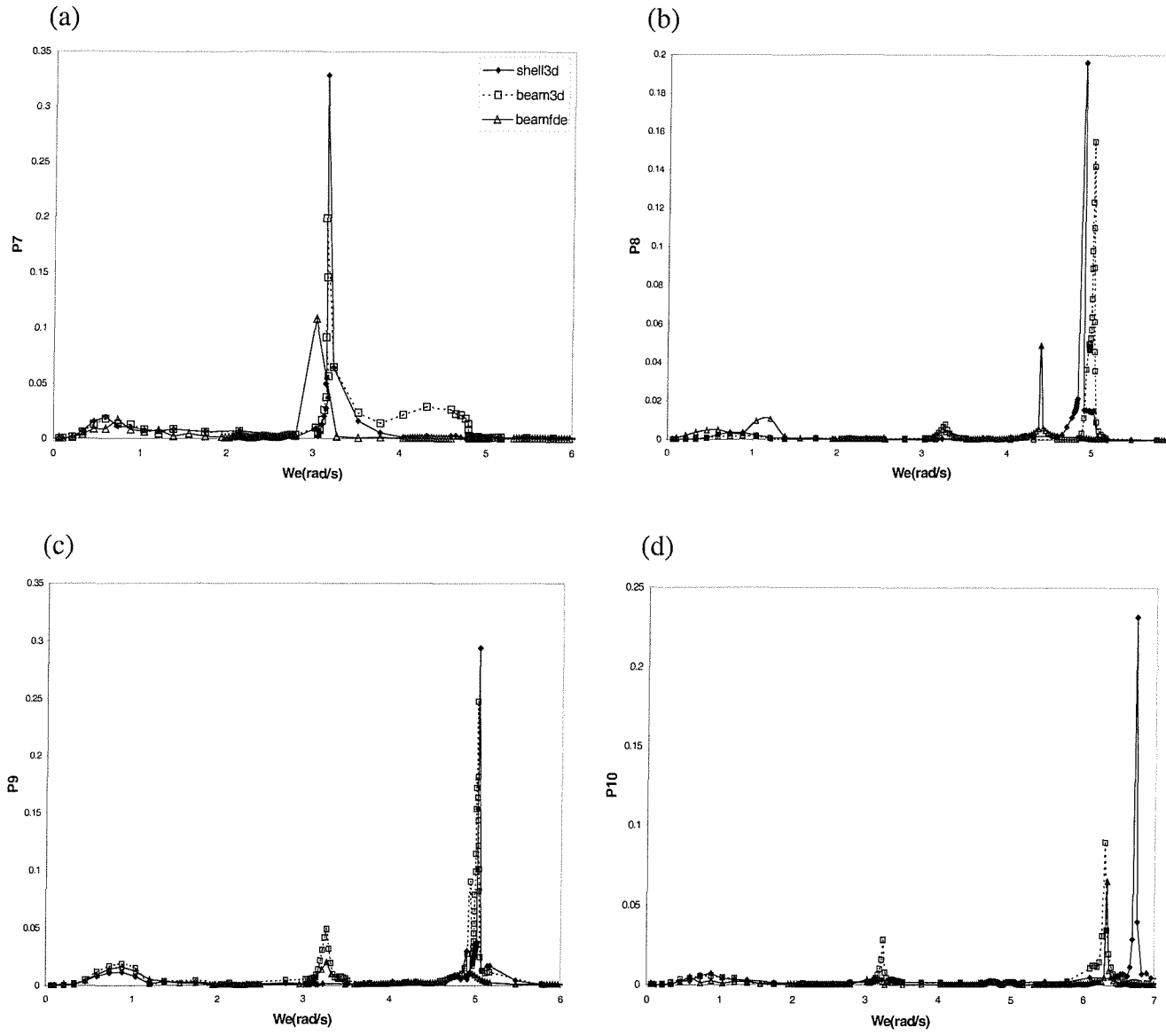

Fig. 9. Variation of principal coordinate amplitudes with encounter frequency predicted from models beamfde, beam3d and shell3d for the bulk carrier travelling at U=7.463 m/s in bow quartering regular waves (χ=135^0) of unit amplitude; (a) r=7, 2 node VB; (b) r=8, 1 node HB 1 node **T**; (c) r=9, 2 node **HB** 2 node T; (d) r=10, 3 node VB. (VB: vertical bending, HB: horizontal bending, T: torsion, **HB,T**: HB,T dominant).

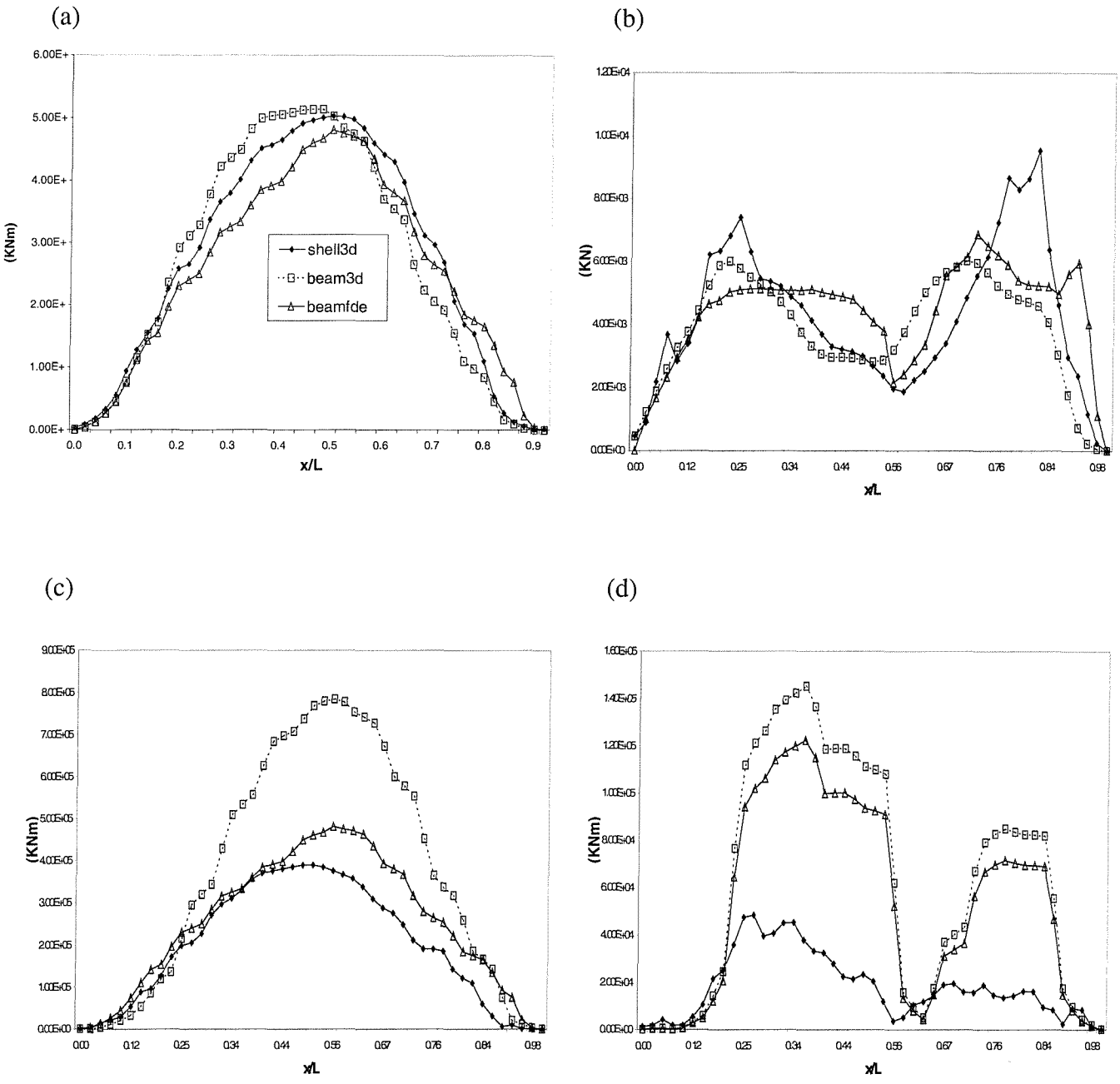

Fig. 10. Variation of wave-induced loads along models beamfde, beam3d and shell3d for the bulk carrier travelling at U=7.463 m/s in bow quartering regular waves (χ=135^0) of unit amplitude and L/λ=1; (a) vertical bending moment (kNm); (b) vertical shear force (kN); (c) horizontal bending moment (kNm); (d) torsional moment (kNm).

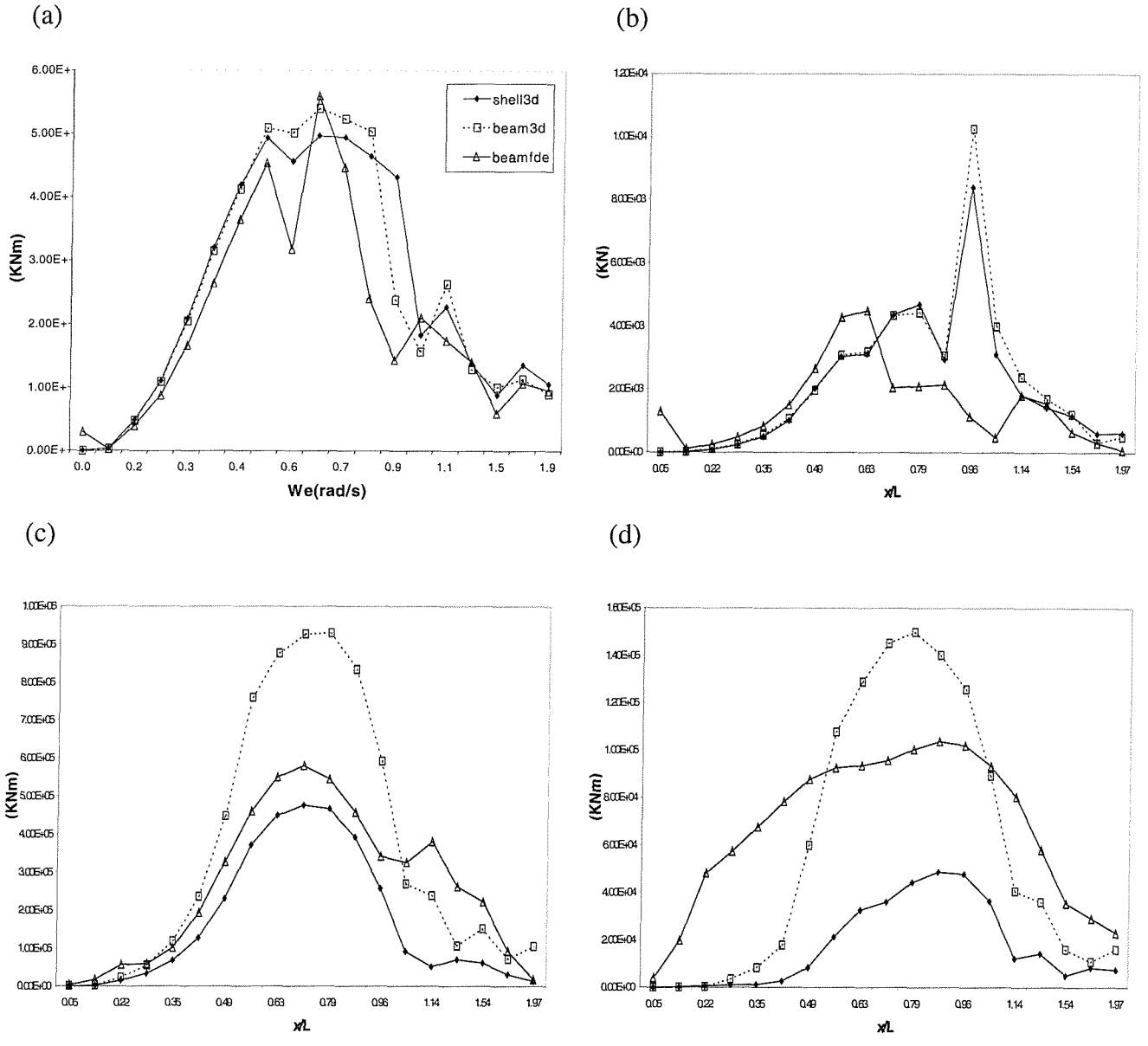

Fig. 11. Variation of amidships wave-induced loads with encounter frequency predicted by models beamfde, beam3d and shell3d for the bulk carrier travelling at U=7.463 m/s in bow quartering regular waves (χ=135^0) of unit amplitude; (a) vertical bending moment (kNm); (b) vertical shear force (kN); (c) horizontal bending moment (kNm); (d) torsional moment (kNm).

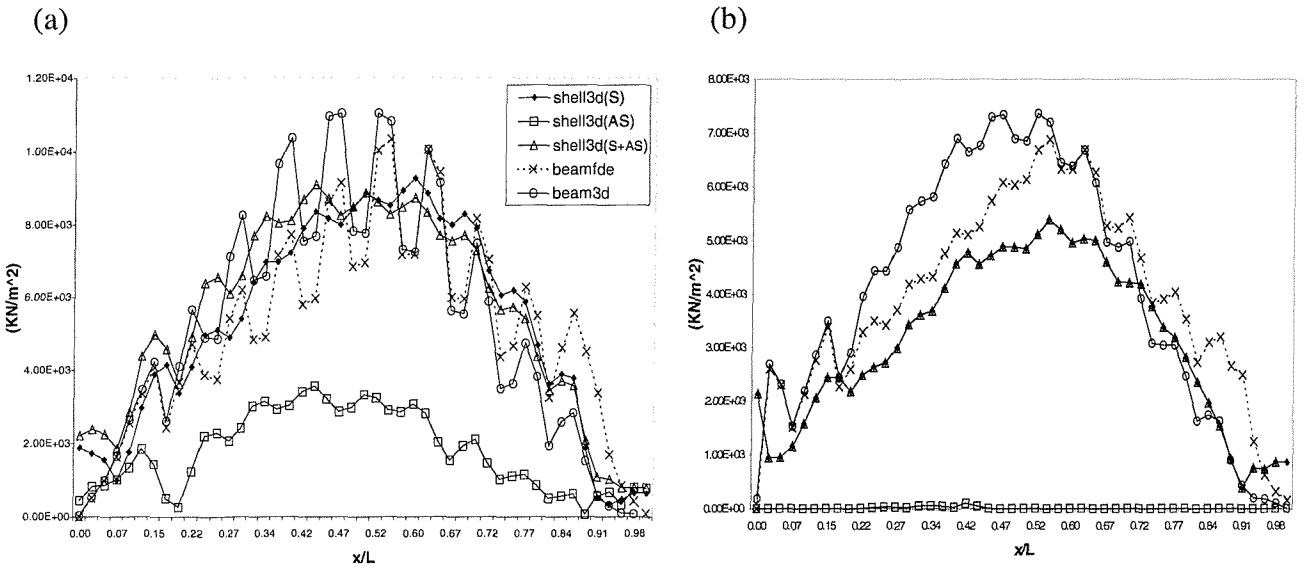

Fig. 12 Variation of longitudinal direct stress (kN/m^2) along (a) deck and (b) keel predicted from models beamfde, beam3d and shell3d for the bulk carrier travelling at U=7.463 m/s in bow quartering regular waves (χ=135^0) of unit amplitude and L/λ=1. Note that for model shell3d the direct stresses are obtained along deck/side junction and keel centre line. Also note that for model shell3d (S), (AS) and (S+AS) denote that contributions from symmetric modes only, antisymmetric modes only and symmetric and antisymmetric modes, respectively, were included in the modal summation of eq.(6).